HYDROCHEMICAL AND ISOTOPIC CHARACTERIZATION OF AQUIFERS IN THE LOWER TANO RIVER BASIN, GHANA, WEST AFRICA.

BY

ADWOBA EDJAH

(10359157)

THIS THESIS IS SUBMITTED TO UNIVERSITY OF GHANA, LEGON IN PARTIAL FULFILMENT OF THE REQUIREMENT FOR THE AWARD OF DOCTOR OF PHILOSOPHY IN EARTH SCIENCES

JULY 2020

DECLARATION

This is to certify that this Thesis is entirely my original work and does not contain any previously published materials except where due reference has been duly made in the text. This Thesis has also not been previously submitted to any other University for the purpose of the award of a Doctor of Philosophy degree. However, portions of this thesis have been published in international Scopus journals.

Signature: ..... Date..... 23/01/2023

Adwoba Kua-Manza Edjah (10359157)

(Candidate)

Signature: ..... Date..... 23/01/2023

Naa Prof. Bruce Kofi Banoeng-Yakubo

(Principal Supervisor)

Signature: ..... Date..... 23-01-2023

Dr. Thomas Tetteh Akiti

(Co-Supervisor)

Signature: ..... Date..... 23-01-2023

Prof. Sandow Mark Yidana

(Co-Supervisor)

Signature: ..... Date..... 23/01/2023

Prof. Lary Pax Chegbeleh

(Co-Supervisor)

ABSTRACT

The Lower Tano River basin is one of the basins endowed with minerals, oil, and gas resources in West –Africa. It covers 104,000 km^2, and the major riparian countries are Ghana and Ivory Coast. The basin, underlain by the Birimian supergroup rocks and the rocks of the Apollonian has enough surface water resources to meet current water demands, but there are many challenges including high population growth rate (due to influx of oil and gas industrial workers), land degradation, mining activities, climate change etc. These challenges have put immense pressure on the groundwater resources in the basin. Also, the surface water is unreliable to meet the basin's water demand for socio-economic development. This therefore makes groundwater the most cost effective and preferred means of supplying water to the dispersed population and rural settlements across the basin. One probable requirement for a sustainable and efficient management of groundwater is the characterization of aquifers in terms of its quantity, quality, and quantification of the recharge sources. Hence in this study, the aquifer hydraulic parameters were estimated, the overall quality of groundwater including the level of trace elements contamination, and its suitability for domestic and agricultural purposes was assessed, the hydrogeochemical processes that produces the chemical characteristics or compositions of the aquifer system was determined, the sources of recharge to the aquifer was investigated and the ages of groundwater was determined. The methodology used involved pumping tests carried out on 55 boreholes drilled across the basin, yearly sampling of surface water and groundwater resources, measurement of cations, anions, trace elements, stable isotopes of deuterium (δ^2 H), oxygen-18 (δ^{18} O), tritium (^{3}H) and measurement of silica. Pumping test together with Theis (1934) graphical method was used to estimate the aquifer hydraulic parameters (transmissivity, hydraulic conductivity, and specific capacity). From the estimation of the aquifer hydraulic parameters, it was observed that the mean transmissivity, hydraulic conductivity, and specific capacity

values were 5.96 m^2/day, 5.70 m/day and 18.80 L/min/m, respectively. The cations (calcium, sodium, potassium, magnesium) and anions (chloride, bicarbonate, nitrate, and sulphate) show that the aquifer of the Apollonian formation and the Birimian super group produces fresh groundwater with most being soft and few being moderately hard and hard. Na^+ and SO_4^{2-} were the dominant cation and anion in the surface water and ground water sampled in 2016. Likewise, Na^+ and HCO_3^- were the dominant cation and anion in the surface water sampled in 2017, the groundwater sampled from 2013 to 2015, and the hand dug wells sampled in 2017. The boreholes sampled in 2017 had Na^+ and SO_4^{2-} as the dominant cation and anion, respectively. All the measured ions (bicarbonates, sulphate, chloride, nitrate, calcium, magnesium, sodium, potassium) in most of the surface water and groundwater sampled from the rocks of the Apollonian and the Birimian supergroup were within the WHO (2011) allowable limits for drinking water. The results of the measured trace elements that is Fe, Pb, Cd, Ni, As, and Al were high in most of the surface water samples. Also, the results of Cu, Cd, Zn, Cr, Fe, Ni, Mn, Co, Pb, As and Al in most groundwater especially those sampled from the aquifer of the Apollonian formation were higher than the WHO (2011) permissible limits for drinking water. The elevated concentrations of trace elements in the surface water and the groundwater were mostly related to geogenic sources. Based on water quality index (WQI) results, it was observed that majority of the groundwater sampled from the aquifer of the Apollonian formation were unsuitable for drinking whiles most groundwater samples taken from the aquifer of the Birimian supergroup were suitable for drinking. As per sodium adsorption ratio (SAR), 99% of the groundwater sampled from both aquifer of the Apollonian formation and the Birimian supergroup were suitable for irrigation. The sodium percent classification indicates that, minority of the groundwater sampled from the aquifer of the Apollonian formation and the Birimian supergroup falls under excellent category for irrigation. Wilcox diagram and magnesium hazard classification indicate that majority of the groundwater especially those sampled from the aquifer of the Apollonian formation gave out

excellent to good water for irrigation. The residual sodium carbonate and Permeability index classification specify that all the sampled groundwater from the aquifer of the Apollonian formation and the Birimian supergroup were suitable for irrigation. The chlorinity index classification indicates that the aquifer of the Apollonian formation and the Birimian super group produce groundwater that were suitable for irrigation. Graphical including hydrogeochemical modelling and statistical approaches applied in the delineation of the major factors influencing the evolution of groundwater and the general hydrochemical characteristics revealed that the chemistry of groundwater in the Apollonian formation aquifer and the aquifer of the Birimian supergroup was mainly rock weathering and rainfall. In addition, ion exchange processes, rock-water interaction and incongruent dissolution were the major natural factors governing the formation of the groundwater chemistry in the Lower Tano River Basin. However, the occurrence of sulphate implies that sulphide mineral (pyrites, arsenopyrites and chalcopyrite) oxidation or mobilization and mining activities including illegal and legal small-scale mining possibly have an impact on the groundwater chemistry in the Lower Tano River Basin. The hydrochemistry of the sampled groundwater transited from Ca-HCO^{-}_{3} to Na-Cl water type along a flow direction for the groundwater samples taken from 2014 to 2015 and 2017. For the groundwater sampled in 2016, the hydrochemistry evolved from Ca-HCO_3^- to Ca-SO_4^{2-} water type and then to NaCl water type along the flow direction. The evolution was influenced by ion exchange processes and rock-water interaction. Based on mineral stability diagram, most groundwater in the aquifer of the Apollonian formation and the aquifer of the Birimian super group appears to be stable within the Kaolinite field suggesting ion exchange processes. Stable isotope composition ($\delta^{18}O$ and $\delta^{2}H$) of rainwater indicates that the rainwater was not highly evaporated. Also, the slope and intercept of the rainfall regression lines obtained for this study were slightly similar to the local meteoric water line for Ghana and the global meteoric water line. Stable isotope composition ($\delta^{18}O$ and

δ^2H) of surface water (rivers, streams, lagoon, and seawater) and groundwater (hand dug wells and boreholes) reveal that the mechanism of recharge to the aquifer of the Apollonian formation and the Birimian supergroup was rapid with the source being meteoric. Also, the surface water (rivers and streams) contributed to the groundwater recharge of the Lower Tano River Basin. Tritium in rainfall ranges from 1.27 to 10.11 TU. That of the rivers ranges from 2.04 to 3.08 TU and that of the groundwater ranges from 0.99 to 6.78 TU. The tritium results revealed that groundwater from the aquifer of the Apollonian formation and the Birimian supergroup were young, of modern recharge with short residence time. Also, the groundwater was recharged between 1960- 1965 and 1965 – 1970. The outcome of this study has added to the current hydrogeological knowledge about Lower Tano River Basin. It has also added to the characteristics of semi-confined and unconfined aquifers.

DEDICATION

THIS WORK IS DEDICATED

TO

MY DAD (ING, KWASI ASEMONE EDJAH) AND MY CHILDREN, KWAW (Junior)

KOJO AND NANA YAW (MY THREE ISOTOPES).

ACKNOWLEDGEMENT

I wish to express my profound gratitude to ICTP (The Abdus Salam, International center for theoretical physics), IAEA (International Atomic Energy Agency), and GETFUND (Ghana Educational Trust Fund) for financial assistance for this PhD Programme. I am indeed, invaluably grateful to Prof Barbara Stenni, Giuliano Dreossi (PhD), Giulio Cozzic (PhD), Clara Turetta (PhD), all of Ca Foscari University of Venice Italy and Prof Covelli Stefano of the Department of Mathematics and Geology, University of Trieste, Italy for their strict supervision, untiring efforts, and encouragements throughout my PhD studies. My profound gratitude also goes to Naa Prof Bruce Kofi Banoeng Yakubo, Dr Thomas Tetteh Akiti, and Prof Sandow Mark Yidana, all of University of Ghana for their constructive criticisms and encouragement throughout the studies. My heartfelt appreciation also goes to Prof. Kwabena Doku- Amponsah (Department of Statistics, UG), who took care of my kids whiles analyzing my samples in Italy. I also wish to thank the lecturers and staff of the Department of Environment, Statistics, and Informatics, Ca Foscari University of Venice, Italy, and Daniele Karlicek (PhD) of the Isotope geochemistry laboratory, University of Trieste as well as staff of the Department of Mathematics and Geology, University of Trieste, Italy. I am also grateful to Dr Ofosu (Director, NNRI, GAEC), Dr Dennis Adotey, Prof Shiloh Osae (Deputy Director General, GAEC), Dr Daniel Gyingiri Achel (Deputy Director, RAMSRI), Prof. Daniel Asiedu (Provost, UG), Dr Thomas Armah, Prof Patrick Sakyi, Prof. David Atta-Peters, All of the Department of Earth Science, UG, Dr Kippo (CEO, of Heisa Engineering,) Sir Nash Bentil (Principal Technologist, GAEC), George Crabbe(Senior Technologist, GAEC), Hendrick, Nana Bonsu,Kwabina Ibrahim(UG), Godfred Ayanu (Senior Technologist, GAEC), Edward Awuku Kaka (Research Scientist,GAEC), Michael A. Owusu (Catholic Priest, St Patrick Parish, Half Assini) and Dennis Mensah (Farmer, Esiama) for their technical assistance and helpful guidance. I also wish to acknowledge the priceless efforts of Mr. Eric Kufuor, a Senior Driver at the Transport Section of the Ghana Atomic Energy Commission, and all staff of Heisa Engineering.

TABLE OF CONTENTS

LIST OF TABLES

LIST OF FIGURES

LIST OF ABBREVIATIONS

AAS	Atomic Absorption Spectrophotoscopy
ACi	Groundwater Acidification
AMD	Acid Mine Drainage
ANC	Acid Neutralizing Capacity
CAI	Chloro alkaline Indices
CWSA	Community Water and Sanitation Agency
EDTA	Ethylene diamine tetracetic acid
GAEC	Ghana Atomic Energy Commission
GMWL	Global Meteoric Water Line
IAEA	International Atomic Energy Agency
ICP-MS	Inductively coupled plasma mass spectrometry
LMWL	Local Meteoric Water Line
NANC	Net Acid Neutralizing Capacity
NE	North East
NNRI	National Nuclear Research Institiute
NW	North West
RAMSRI	Radiological and Medical Sciences Research Institute
SE	South East
SI	Saturation Indices
SW	South West
WHO	World Health Organization
WRC	Water Resources Commission

CHAPTER ONE

INTRODUCTION

1.1 Background

Groundwater resources accessed through hand dug wells and boreholes are the major sources of water supply for all socio-economic activities in the Lower Tano River Basin of Ghana. In the basin, almost 80% of the citizens depend solely on hand dug wells and mechanized boreholes or hand pump fitted boreholes for their daily water supply, while the remaining 20% depends on rainwater, rivers, and streams {WRC (Water Research Commission), 2012}, but most of these surface water bodies have issues with colour and turbidity as shown in Figure 1.1. The change in colour and the turbidity might be resulting from human activities and that might give rise to water borne diseases such as typhoid fever, bilharzia, and other carcinogenic diseases etc. (WHO, 2011). Since groundwater is believed to be of a better quality (Anim- Gyampo et al., 2019; Ewusi et al., 2017; Asante Annor & Ewusi, 2016; Atta-Darkwa, 2016; Affum et al., 2015; Nyarko et al., 2015; Edjah et al., 2015) and requires little or no treatment, it is chosen by most policy makers in charge of water resources as the best source of potable water. This is the case of the Lower Tano River Basin where non-governmental agencies like Tullow oil and Christian organizations have made it their aim to provide mechanized and boreholes fitted with hand pump to supply quality water for the service of the communities. The development of hand dug wells, boreholes and other groundwater access infrastructure within the basin started well before Ghana gained independence. However, it is worth noting that there are now over 600 of such facilities in the area (Unpublished reports from Community water and sanitation agency (CWSA, 2013).

The involvement of organized non-governmental agencies, churches, and the central government agencies in the development of groundwater resources in the Lower Tano River Basin in recent times has not led to improvement in the generation of reasonably good datasets

such as the lithological data, water quality data, and aquifer hydraulic parameter data etc. This is due to lack of organized data. If the above data were organized and adequately processed, the hydrogeological conditions of the rocks would have been characterized and that would have led to prudent management of groundwater resources in the Lower Tano River Basin. In general, even though, the aquifers in the basin produce groundwater of acceptable quality for most uses (Edjah et al., 2015), there are some communities where the quality is hampered by elevated concentrations of trace elements (Edjah, 2012; Doyi et al., 2018). These trace elements are mostly believed to be of geogenic and/or anthropogenic origin. However, it is not known the extent to which each of these two factors has contributed to the current state of groundwater quality in the area. Increasing anthropogenic activities and the rise in demand for groundwater resources implies that concerns about the resource quality will even increase in the future. Though it is part of the drilling protocol {Rural Water Supply Network (RWSN), 2010} to assess the quality of water before its use, little attempt has been made to monitor changes in the ground water quality. Moreover, a holistic assessment of the hydraulic properties of the groundwater bearing units within the basin, the general factors influencing groundwater hydrochemistry and quality, the mode, spatial and temporal distribution of groundwater recharge are required to form the basis for prudent management of the resource to ensure sustainability. The present study therefore seeks to fill the above knowledge gaps by using pumping test data, hydrochemical and isotope data to characterize various aspects of the hydrogeological conditions and general groundwater resources occurrence in the Lower Tano River Basin. This will facilitate decision making on groundwater resource allocation and it will add to the current baseline information about the aquifers in the Tano Bain. The outcome of this study will contribute to the appropriate development of future groundwater systems within the basin.

1.2 Statement of the Problem

The Lower Tano River Basin with its numerous rivers is located along the coast in southwestern Ghana and it is occupied by three districts, namely Ellembelle, Jomoro and Nzema East. The basin is endowed with minerals such as gold, kaolin, limestones etc. The basin is the hub for oil and gas industries as well as mining including legal and illegal small-scale mining. These two has increased the population due to influx of industrial workers and migration of people. In 2010 population census, approximately 298,436 (60, 828 for Nzema East, 87,501 for Ellembelle and 150.107 for Jomoro districts) people were counted (Ghana Statistical service, 2012). The endlessly growing population over the years will put immerse pressure on the available groundwater resources leading to high demand for groundwater. Sustainable development goal (SDG) 6 states that "portable water must be provided for all citizens". However, this goal is somewhat challenging to attain with respect to the Lower Tano River Basin as there is limited information on the available borehole logs. As a result, most agencies develop boreholes with inadequate processed data on the quantity of water the aquifer yields and the quality. To achieve SDG (6), broad and in-depth knowledge of the Lower Tano River basin dynamics of water use and availability is necessary. Current exploitation and sustainable management of groundwater are only possible with a deep knowledge of the complex dynamics that locally characterize the aquifers of the Lower Tano River Basin.

1.3 Justification

Knowledge of aquifer hydraulic parameters, groundwater quality, hydrogeochemistry, groundwater recharge and abstraction levels has become one of the essential issues to safe guard the sustainable use of groundwater resources in the Lower Tano River Basin. Understanding the above are of crucial importance for an effective development and management of groundwater resources within the Tano Basin (WRC, 2012).

In the Lower Tano River Basin, estimating the aquifer hydraulic parameters will deliver a quantitative prediction for aquifer response to recharge and groundwater abstraction. One

of the suitable methods used in calculating the aquifer hydraulic parameters is pumping test (Hasan et al., 2018 b). The use of Pumping test as a method to estimate the aquifer hydraulic parameters is limited in the study area due to lack of pumping test data. This has made it difficult to predict future groundwater availability. For proper development of any groundwater resource, an understanding of the aquifer hydraulic parameters is important. This is because, when the parameters are understood, the success rate of groundwater development increases. Likewise, when the aquifer hydraulic parameters are known, it is very easy for policy makers and scientists to locate suitable sites for groundwater development. Several authors across the globe have suggested that the estimation of aquifer hydraulic parameters can be highly valuable (Purvance & Andricevic, 2000; Chen & Hubbard et al., 2001; Soupios et al., 2007; Sinha et al., 2009; Batte et al., 2010; Majumdar & Das, 2011; Niwas & Celik, 2012; Sikandar & Christen, 2012; Ugada et al., 2013b; Attwa et al., 2014; Sattar et al., 2016; Hasan et al., 2018b, etc.), since the parameters depend on heterogeneity and pore-space structures.

Information on the aquifer quality will not only sustain human and aquatic life but it will contribute to the suitability of groundwater for socio-economic uses. An aquifer is often threatened by population growth, change in land use, agriculture and change in climate. Apart from the above, mining is another contributor, which is rampant in the Lower Tano River Basin. Many studies in Ghana have shown a direct link between mining and trace elements contamination in groundwater (Doyi et al., 2018; Ewusi et al., 2017; Asare – Donkor et al., 2016; Antwi-Agyei et al., 2009; Asanti et al., 2007, etc.).

Sulphide bearing rocks which contain gold ore are extensive in the Lower Tano River Basin (Luebe et al., 1990). These rocks frequently contain pyrite and arsenopyrites (Smedley et al., 1995). Exposure of these rocks to the atmosphere habitually results in the generation of acid-mine drainage. When these rocks are in contact with the atmosphere, there is high proportions of toxic trace element mobilization in the aquifer.

The indiscriminate use of mercury and other chemicals during mining operations, which are harmful to human health (WHO, 2011), is another problem confronting the water resources within the basin. This is because during mining operations, the miners use simple methods to extract and process the gold (Esdaile & Chalker, 2018). Waste water or effluents from their activities might leach into the aquifer through natural processes like rainfall and that could possibly elevate some trace elements contents in the aquifers and the surrounding surface water bodies.

In the Lower Tano River Basin most mining operations especially illegal small-scale mining is usually located along the banks of most rivers and streams and their activities have great impacts on these rivers and streams, polluting the groundwater through leaching (Karmakar et al., 2012; Dorleku et al., 2018). For instance, 80% of water samples collected and analysed from some communities within the Lower Tano River Basin, precisely Ellembelle district by Edjah (2012) and Doyi et al. (2018) contained heavy metal (Pb, Cd, Fe, Mn, and As) concentrations significantly above the drinking water standards of WHO (2011). The presence of these trace metals in the groundwater is a threat to human health. Despite previous research on the susceptibility of groundwater to contamination, the results obtained are difficult to interpret due to the limited study area in which the studies covered. Subsequently, due to fewer literatures in the Tano basin especially in the Lower Tano River Basin about groundwater quality and its suitability for socio-economic uses, it has become difficult to obtain a clear understanding of the groundwater quality.

In general, aquifers are becoming more important and critical to human and aquatic life (Olago, 2018). However, inadequate knowledge of the aquifer characteristics and sources (Banoeng-Yakubo et al., 2011; Olago, 2018) means that groundwater is being over exploited under growing uncertain regimes (McDonald & Roger, 2009). With restricted evidence, it is impossible to achieve safe water for rural settlement (Yan et al., 2016). This is the case of the Lower Tano River basin, where the aquifers are strongly dependent on rainwater and surface

water for recharge (WRC, 2012) but the aquifer is not characterized. In order to describe the aquifer, there is a need for sufficient evidence based on the understanding of the hydrogeology. This will give a better understanding of the aquifer potential for a sustainable supply of safe water for various uses under rapidly climatic change and groundwater development. Although the Lower Tano River basin depends largely on groundwater, limited comprehensive hydrogeochemical studies have also been carried out. Apart from Edjah et al. (2015) and Edjah et al. (2019) who worked in the Lower part of the Tano Basin, there have not been any detailed studies on the hydrogeochemistry of the aquifer systems. An adequate and a fellow up knowledge on the aquifer hydrogeochemistry are important for proper aquifer characterization and management.

Although isotopic research has been conducted in different locations across the basin by Edjah et al.(2015, 2019), a distinct quantification of aquifer recharge especially from local precipitation has not been conducted as well as the ages of groundwater.

It is therefore important to understand the aquifer system by combining pumping test data, hydrochemical data, and isotopic data to the current methods used in characterizing an aquifer. To describe the aquifer in the Lower Tano River Basin, new boreholes will be drilled, pumping test will be carried out, samples will be collected from the new boreholes and existing groundwater (hand dug wells and boreholes), the samples will be analyzed in various laboratories in Ghana and beyond and the results will be interpreted with the help of software tools like Aquachem, ArcGIS 10.5 software, AquaSolve, and Phreeqc. Findings of this research after a successful completion will (a) assist policy makers to evaluate old sites and seek new sites for the development of groundwater resources (b) it will help policy makers to evaluate various strategies for water resource planning, development, and management (c) will expand the knowledge of hydrogeology and the application of isotopes in the Tano Basin (d) evaluate various strategies for groundwater management and pollution control.

Figure 1. 1 The Tano River at Elubo within the basin, serving as a source of water to the citizens.

1.4 Aim and Objectives

The broader goal of this project is to contribute to the hydrogeology of the Lower Tano River Basin in South-Western Ghana, to assist in optimal decision-making regarding groundwater resources management to ensure sustainability. This overarching objective includes groundwater quality and quantity issues in the terrain. The specific objectives of this study are to:

1. Estimate aquifer hydraulic parameters;
2. Assess the overall quality of groundwater including the level of trace elements contamination, and its suitability for domestic and agricultural purposes;
3. Determine the hydrogeochemical processes that produces the chemical characteristics or compositions of the aquifers;
4. Investigate the sources of recharge to the aquifers;
5. Determine the ages (residence time) of groundwater.

1.5. The Area of Study

1.5.1. Study Location

The Lower Tano river basin carved out of the Tano Basin is in the South Western zone of Ghana, approximately 260 km west of the capital Accra. The basin lies within latitude 4°40' and 5°20' north of the equator and longitude 2°05' and 2°35' west of the Greenwich meridian (Fig 1.2). The basin is accessed from Accra by driving 200 km on the main coast high way to Cape Coast and from Cape Coast to Takoradi, and from there to a further 80 km on a paved road to the villages in Axim all the way to Elubo and 8 km from Esiama to Bomuakpole and a further 7 km of unpaved road from the villages of Teleku-bokazo to Salman. The catchment area covers a total of 2812 sq. Km, which constitute about 6.8% of the total land, mass of the Western Region of Ghana {GSS (Ghana Statistical Service), 2010} and extends beneath a coastal ridge from Ankobra Township towards the Ivory-Coast boundary. From the map of Ghana (Figure 1.2), it is observed that the Lower Tano River Basin is in a deposition environment.

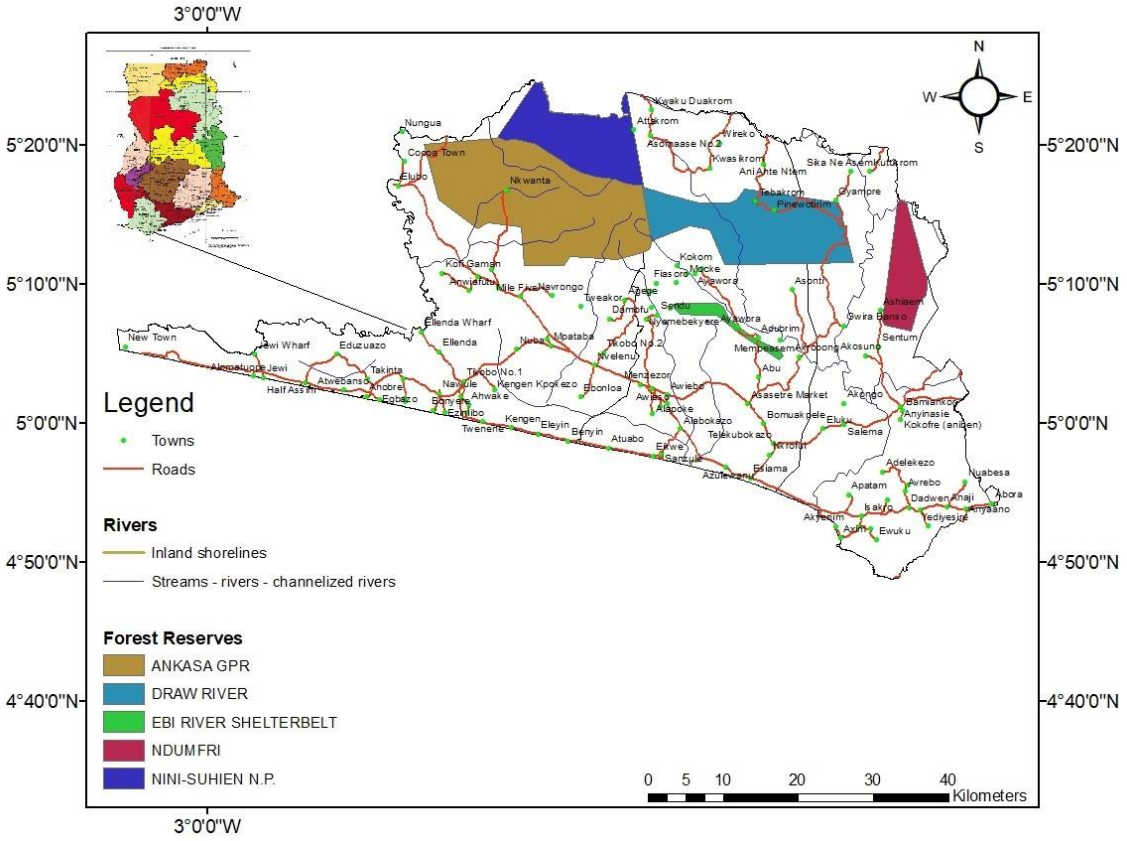

Figure 1.2: Map of the Lower Tano River Basin (Modified after Ghana Geological Survey Authority, (GSSA, 2010)

1.5.2. Topography, Relief and Drainage System

The topography of the study region is characterized by relatively flat land in the coastal zone, which gives way to few peaks in the middle to northern sections of the basin. The highest elevations are in the northern parts and the environs of the eastern parts. In the coastal terrain of the study catchment, altitudes range between zero at the boundary with the Gulf of Guinea to about 150 m above mean sea level. Similarly, the study area lies within the wet evergreen (southeast) and the moist-semi-deciduous agro-ecological zones (AEZ) of Ghana (Ghana Geological Survey Department (GGS, 2009). The southern part of the basin has the thickest vegetation, which appears largely continuous. About 60% of the land cover is enclosed by forests, which are largely protected areas (forest reserves). In the wet evergreen forest area is the Ankasa Resource Reserve. In the middle to northern halves of the basin, the forest cover is relatively sparse and much more scattered. In addition, several rivers and streams drain across the basin and noticeable among them is the Ankobra River and the Amanzure River. The major tributaries of the Amanzura River are Ahama River, the Nwini River, the Ankasa River, the Draw River and the Tano River. In the basin, the Amanzura river and some minor rivers and streams allow flow of water throughout the year. These streams and rivers exhibit a dendritic outline that forms the Lower Tano river basin (Ghana Geological Survey Department (GGS), 2009).

1.5.3. Climate

The Climate of the study area is sub-equatorial wet (WRC, 2012) with two rainfall seasons. The wettest months are May to July and September to October. The drier period is from December to February.

Data obtained from the Ghana Meteorological Agency (GMA) indicates that the total annual amount of rainfall from 2006 to 2017 is 6443.8 mm. Additionally, the annual rainfall pattern ranges from 32.8 mm to 87.2 mm (Figure 1.3) in Axim, whiles that of Elubo varies from 22.1

mm to 46.6 mm (Figure 1.4). In Half Assini, the annual rainfall patterns vary from 19.1 to 116.8 mm (Figure 1.5) and in Nkroful, it ranges from 33.4 to 78.7 mm (Figure 1.6). The monthly mean minimum temperature ranges from 22.6 °C to 25.9 °C (Figure 1.7) whiles the mean monthly maximum temperatures range from 27.3 ° C to 31.9 ° C (Figure 1.8).

The coldest month happens in June, while the hottest month occurs in December to March. The basin is moist and warm with comparative humidity between 75 % - 85 % throughout the year. The mean yearly potential evapo- transpiration is about 1322 mm. Two wind systems are experienced in the basin and these are the southwestern monsoon and dry harmattan winds.

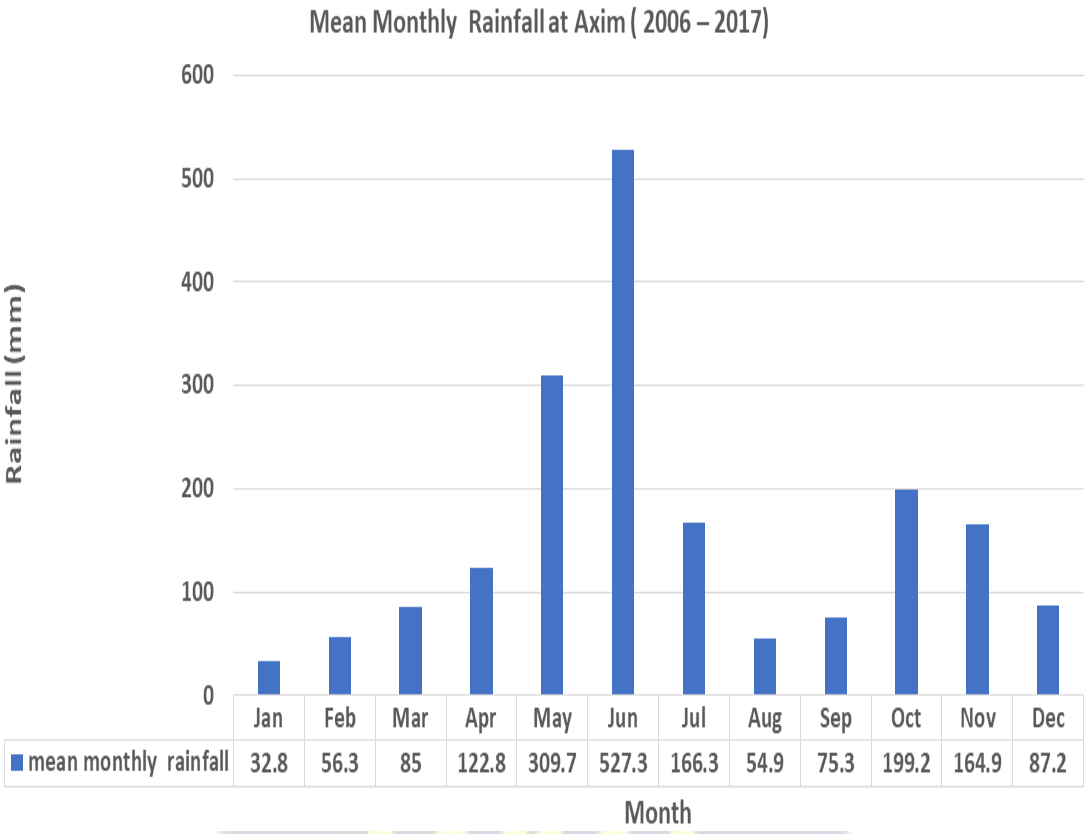

Figure 1.3: Mean Monthly Rainfall (mm) from 2006 to 2007 in Axim (Data Source: Ghana Meteorological Station)

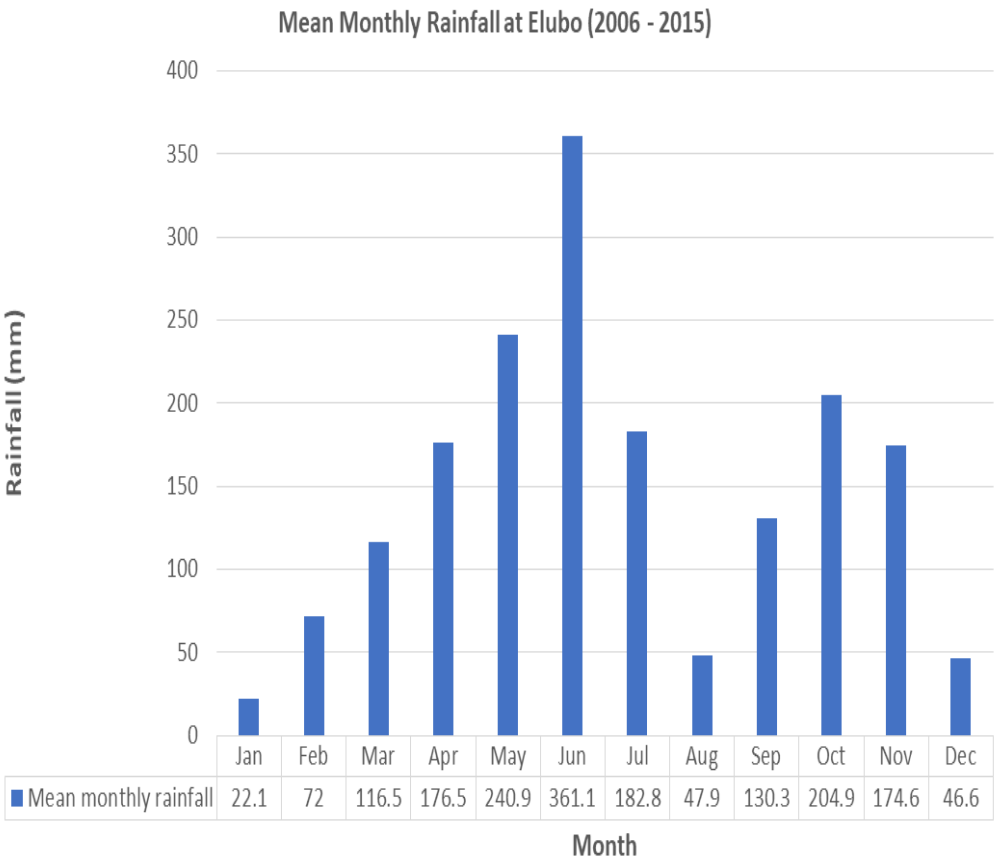

Figure 1. 4: Mean Monthly Rainfall (mm) from 2006 to 2015 in Elubo (Data Source: Ghana Meteorological Station)

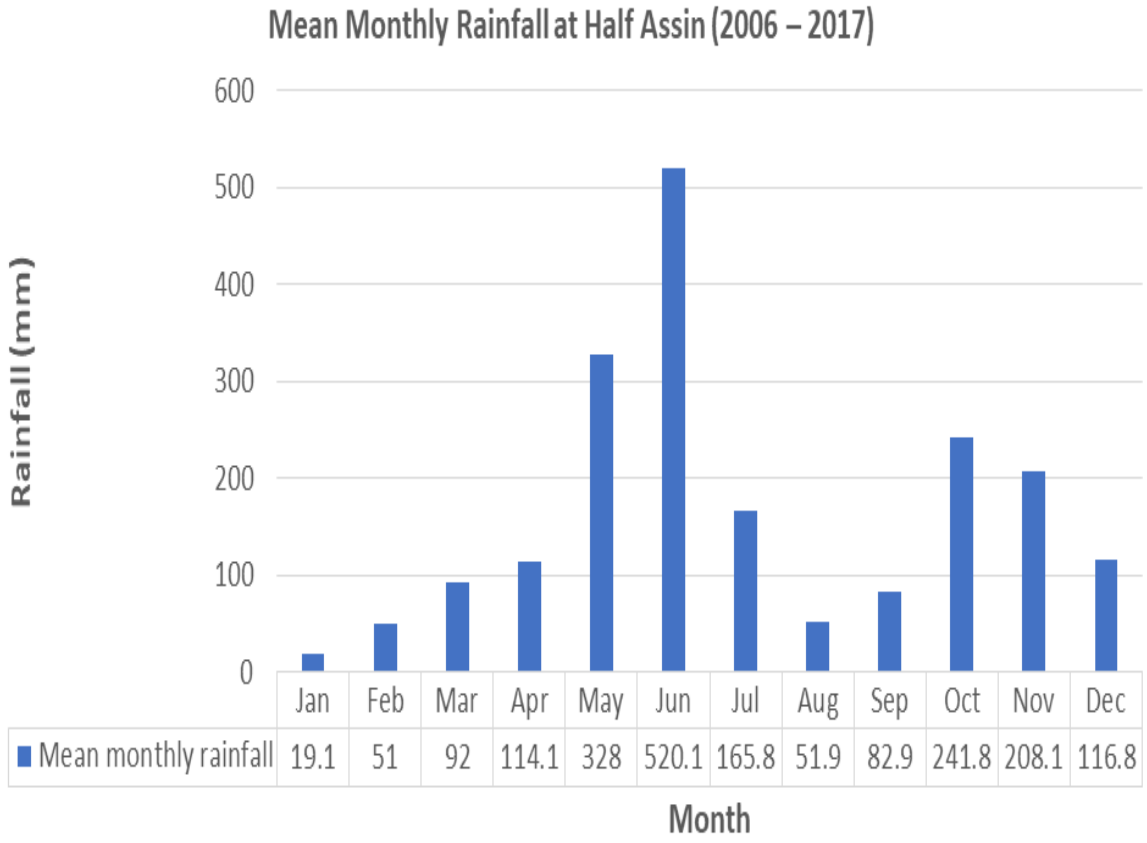

Figure 1. 5: Mean Monthly Rainfall (mm) from 2006 to 2017 in Half Assini (Data Source: Ghana Meteorological Station)

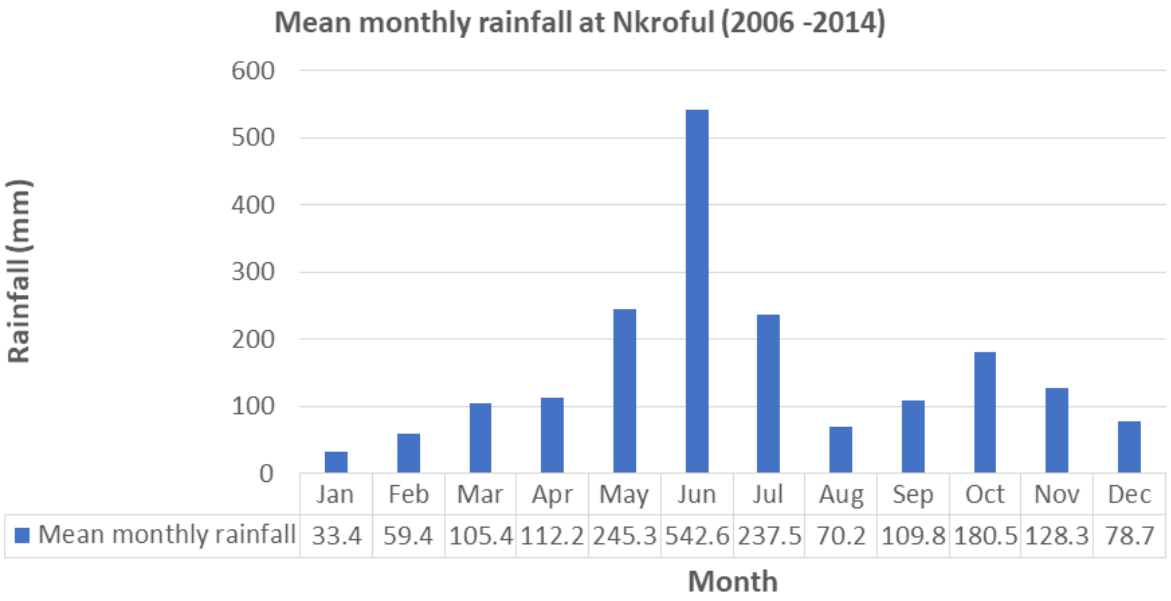

Figure 1. 6: Mean Monthly Rainfall (mm) from 2006 to 2014 in Nkroful (Data Source: Ghana Meteorological station)

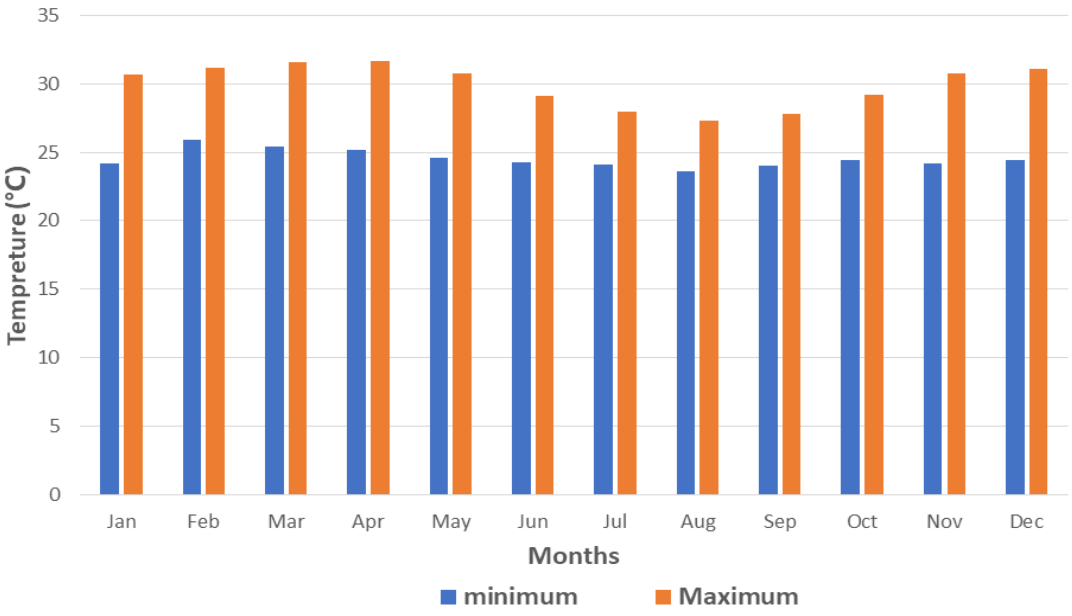

Figure 1. 7: Average Monthly Minimum and Maximum Temperature from 2006 to 2017 (Data Source: Ghana Meteorological Station).

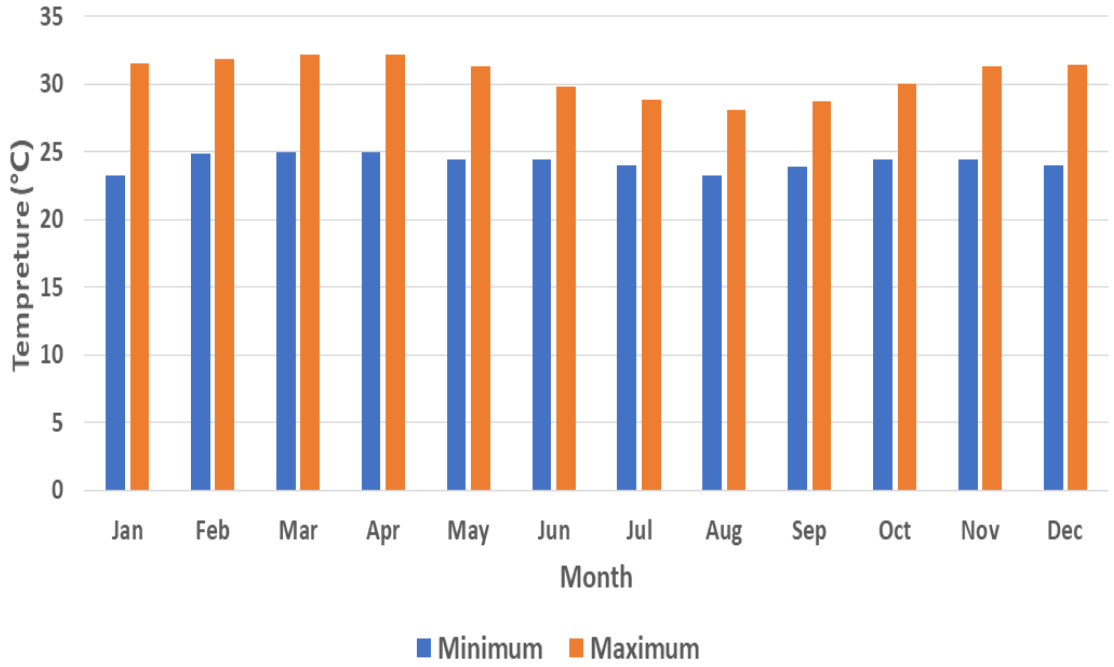

Figure 1. 8: Average Monthly Minimum and Maximum Temperature from 2006 to 2017 (Data Source: Ghana Meteorological Station).

1.5.4. Land use and Vegetation

In the study area, agricultural with extensive cocoa farming is practiced mostly in the forest areas (Figure 1.9). Within the forest belt, logging is another important industry and it is mostly carried out in concessions granted to timber companies. Fuel obtained from wood is the main source of energy for the inhabitants and this is harvested mainly from the forests. This has considerably reduced the forest cover since 1960 (Ahn PM, 1961; GSD 2009). Currently, the existence of agriculture (50 %), human settlements (urban and suburban developed lands) (10 %), and forest (40 %), are the estimated major land use types in the study area (Ghana Statistical Service (GSS, 2012).

The main vegetation as described by Ghana survey department (GSD, 2009) and Water Resources Commission (WRC, 2012), is coastal and wet semi – deciduous rain forest. The wet semi – deciduous rain forest can be seen in the northern part of the study area but as one travels southward, it turns into secondary forest and it is characterized by tall trees with grass cover, shrubs, and soft woody types. In addition, rattan and bamboo are some of the non-timber forest

products that can be seen and several timber species can be found in the study area. The Savanna vegetation is also situated along the coastline, which is approximately 140 km.

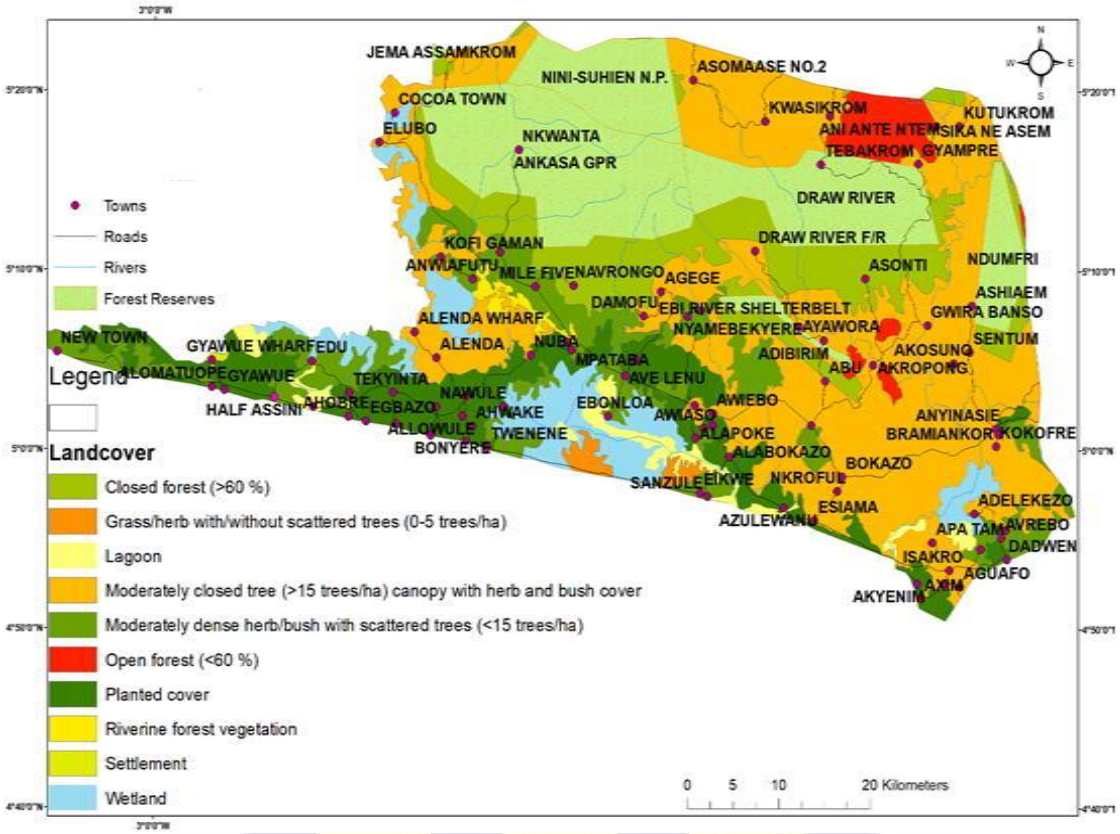

Figure 1. 9: Location Map of the Lower Tano River Basin (Modified after Ghana Geological Survey Authority, (GSSA, 2010)

1.5.5. Soil Type

The soils in the basin consist of five groups. These are the forest lithosols, regosols, podsols, alluviusols, and forest oxysols (Brammer, 1962). The location of the forest lithosols develops on steep slopes and have extensive exposure of hard rock and iron pan. The soils are shallow or brushy and have very little agricultural significance. The soil covers a wide area within the basin, mostly the forest and savannah belts. The forest belt is seen in the northern part of the study area and the Savanna belt is found along the coast. The Savanna belt stretches from Kikam to Half Assini.

The forest oxysols occur normally in high rain forest zones. They are deeply weathered to a depth of approximately 4 m (Ahn PM, 1961). They are mostly orange brown to yellowish brown. Organic matter concentration in the forest zones is described to be moderately low but

more intensely distributed (Brummer, 1962). Further, these soils are highly leached due to high rainfall amount, thereby reducing their nutritional contents. Though the forest oxysols have good physical characteristics, their use in the production of crops is limited due to the strong acidic reaction in the soil. As such plantations like oil palm, coconut, rubber, and coffee that are acid tolerant are mainly grown in such soils. In the study area, the forest oxysols cover all areas of the basin including the coastal belt and they occur in the hinterlands of the basin thus from Sanwoma through to Elubo.

The regosols are limited to a thin strip along the coastal zone of Ghana. They are deep sands established in an outward costal ridge land scape. The regosols are extremely acidic and deprived of nutrients. They contain quartzite and they support good coconut plantations due to the high quantity of rain. The texture of their sands offers good rooting condition for the growth of the coconut palm that has wide roots. In the basin, the regosols can be found along the coast.

In old in-filled lagoons, the groundwater podsols are developed. They can locally be identified along the seashore. The profile consists of humus, which is approximately 5 cm in depth, and stained sand, which is approximately 60 cm in depth. The profile of the podsol also consist of bleached sand that is abruptly underlain by a dark brown organic pan. Beneath the pan, gray to brown sandy soils can be seen. Subsequently, the soils belong to the Atuabo series and the groundwater podsols is found in Atuabo through to Twenen in the southwestern part of the basin (Ahn PM, 1961).

In the basin, alluvisols border a network of most rivers and streams (Ahn PM, 1961). The top soils of alluvial sediments are mostly sandy, loamy, or clayey textured. In addition, their lithology is discontinued and likely consist of buried horizons. Their locations in flood plains limit their agricultural use. Locally, they are used for the cultivation of sugar cane. In areas that fall under alluvisols, the dry season vegetable garden is common. Hence, in the study area, alluvisols cover areas from Aniwafutu to Elubo. The soils from the alluvial deposits in the basin

belongs to the Fredericksburg association, Tikobo association, and Ankasa association (Ahn PM, 1961).

1.5.6. *Geology*

The Geological Survey Department (GSD) of Ghana, in partnership with Bundesanstalt fur Geowissenchaften and Rohstoffe, Hannover, Federal Republic of Germany have come out with a new Geological Map of Ghana that talks about four major rock complexes namely:

i. Paleoproterozoic Supracrustal and intrusive rocks made up of Birimian Supergroup, Tarkwaian Group, Tamnean Plutonic Suite and the Eburnean Plutonic Suite. These groups of rocks are described to be formed between 2195 Ma and 2072 Ma.
ii. Neoproterozoic to Early Cambrian, comprising the Voltaian Supergroup, Bombouaka Group, Oti-Pendjari Group and the Obusum Group at the top.
iii. Pan African Dahomeyide orogenic belt consisting of the Togo Structural Unit, a variety of gneisses of the Dahomeyan Supergroup and the Buem Structural Unit.
iv. Coastal Sedimentary Basins of Ordovician to Cretaceous age comprising Sekondian Group, Accraian Group, Amisian Group and Apollonian Group.

From the above, the geological formation underlying the upper part of the Lower Tano River basin is the Paleoproterozoic Supracrustals and Intrusive rocks made up of the Birimian Super group rocks and the Tarkwain formations (Figure 1.10). In addition, the geological formation underlying the Lower Part of the basin is the Coastal Sedimentary Basin of Ordovician to Cretaceous age, comprising of the rocks of the Apollonian formations (Figure 1.10).

The Birimian Super group rocks which dominates the hinterland of the study area appears to be folded with a dominant northeast trend and are interfered by granitoids, greywacke, interbedded greywacke-phyllite, undifferentiated Biotite (± hornblende, ± muscovite), gneiss, Muscovite, Hornblende – biotite granitoid etc. (Kesse, 1985; Leube et al., 1990; Hirdes et al., 1992; Taylor et al., 1992). The rocks of the Birimian Super group are strongly foliated, and

jointed with connected intense weathering along with weak zones and fractures (Kesse, 1985; Leube et al., 1990; Hirdes et al., 1992; Taylor et al., 1992). The structure can enable percolation of water to improve the storage of groundwater (Kesse, 1985; Leube et al., 1990; Hirdes et al., 1992; Taylor et al., 1992). In addition, the Birimian Supergroup is characterized by isoclinally folded and thickly-bedded metavolcanic rocks and metasedimentary rocks. The metavolcanic rocks overly the metasedimentary rocks and contain generally rocks from volcanic origin, which are dominated by lavas and tuffs and pyroclastics rocks. The metasedimentary rocks form the basement of the Birimian Supergroup and are mainly composed of phyllite, schist, and slate (Dapaah-Siakwan, 2003).

The Tarkwaian Supergroup, which is the deficient suit of rocks in the study area displays synclinal structures. It is mainly composed of coarse-grained young sedimentary rocks that have undergone low-grade metamorphism. Consequently, the metasedimentary arrangements in the Tarkwaian Supergroup consist of quartzites, phyllites, conglomerates, sandstones, etc. that are interrupted by igneous rocks such as quartz, porphyry gabbro, dolerite, felsite etc. in some places (Kesse, 1985; Leube et al., 1990; Hirdes et al., 1992; Taylor et al., 1992). Additionally, the Tarkwaian Supergroup has a tectonic connection with the Birimian Supergroup, which is revealed by elevated degree of cropping along the contact zones with most of the crop-related gold deposits hosted in these zones (Junner et al., 1942). Kesse (1985), and Hirdes and Luebe (1989), summarized the literature on the Tarkwaian formation up through the mid-1980's. More recent data is also presented in Eisenlohr & Hirdes, 1992; Oberthur, 1994. Additionally, the rocks of the Tarkwaian formations represent erosional products of the Birimian Super group rocks and are dominated by coarse clastic sediments. They are slightly folded and metamorphosed with some level of openings along the joints, and that makes the Tarkwaian formation permeable for groundwater development and storage (Eisenlohr & Hirdes, 1992; Oberthur, 1994).

The rocks of the Apollonian formation which dominates the coastal zone of the study area consist of clay (SiO2 and Al_2 O_3), fossiliferous sandy limestone interbedded with limestone, sandstone, marl (CaCO3), siltstone, and shale with basal conglomerates (Figure 1.11 and Kesse, 1985). This group forms part of the Coastal Sedimentary Basin and their Basement rocks belong to the Pre-Cambrian metamorphosed rocks of the Birimian Super group. Kitson, 1928 reported that "the rocks of the Lower Tano River Basin are part of the Apollonian System of Cretaceous age and consist mainly of alternating clays and sands with limestones. The limestones within the basin are fossiliferous and are inter bedded with clay (Junner, 1940; Cox, 1952). This clay forms a continuous crest that rises from the beach of Keegan and run in a north-westward direction to the north of Nawuley and north of the Tano River in Ekpu. The coastal zone of the Lower Tano River Basin consists of tertiary deposits of clays, laterite and sands and these overlain the inter bedded and fossiliferous limestones (Cox, 1952). In addition, nodules of pyrite or marcasite in the clays and shales of the Apollonian formations was discovered by Atta-Peters et al. (2014)

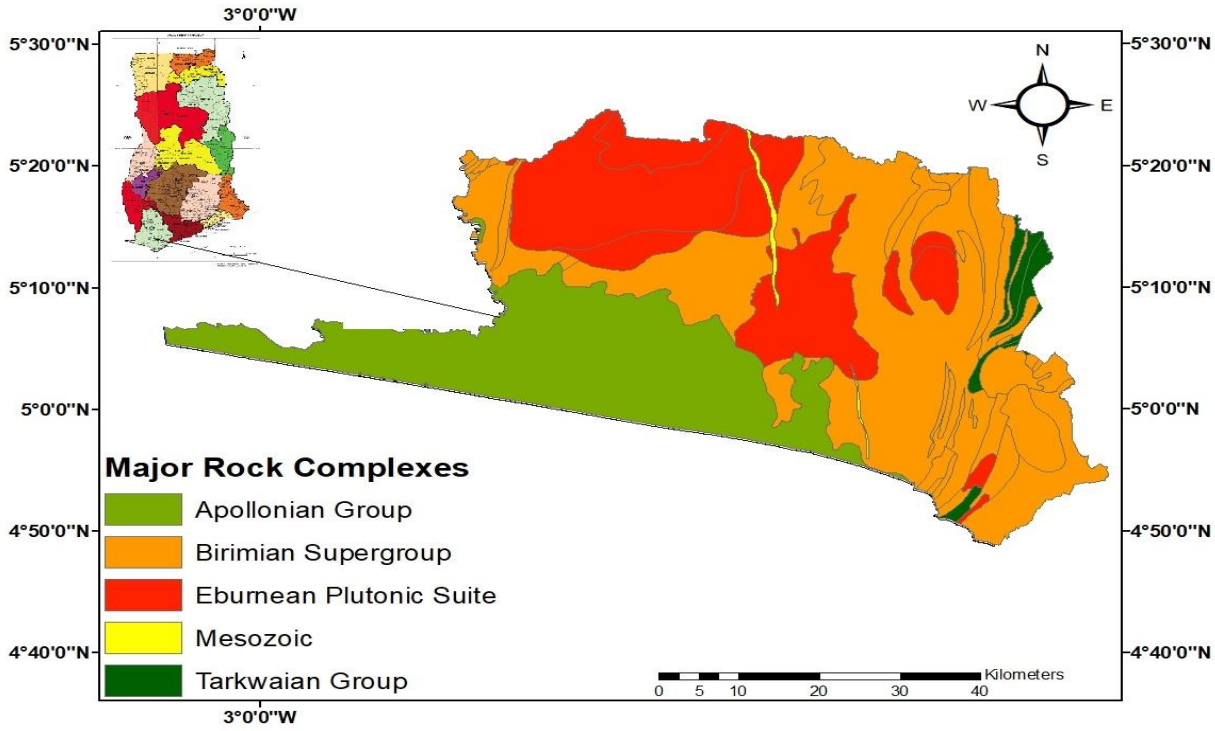

Figure 1. 10: Geological Map of the Lower Tano River Basin with the major rock complexes (Modified after Ghana Geological Survey Authority, (GSSA, 2010)

1.5.7. Stratigraphy

In the Tano basin, deposition of rocks started throughout the Aptian ages of early cretaceous era (Luebe et al., 1990). This agrees to the period of continental rifting between the African plate and the South American plate, which lead to the creation of the Tano basin inside the Atlantic Ocean. The above makes the Lower Tano River basin a region of focus for the deposition of clastic sediment from the African continent. A Palynostratigraphical study carried out by Amoo (2014) and Atta-Peters (2013) to determine the stratigraphy of the Tano basin using oil wells indicate that the stratigraphy started with the deposition of sandstone during the early Aptian age with a mix of shale which formed the basement rocks, with a depth of 7000 ft to 9000 ft. One of the earlier studies conducted by Khan (1974), on a borehole in the Lower Tano River basin revealed the following, that is (a) The sedimentary rocks within the basin has a maximum thickness of 3048 m or more along the coast and towards the border of Côte d'Ivoire, (b) The oldest rocks encountered during the study was of middle Cretaceous age, (c) The maximum depth of 1768 m was found in the marine rocks, (d) An angular discordance separated the non-marine stratigraphy from the marine stratigraphy (e) Two horizons with signs of oil were seen. One was near the surface of the Nauli (Nawulley) Limestone Horizon and the other was the Black-Shale Horizon which had the highest depth.

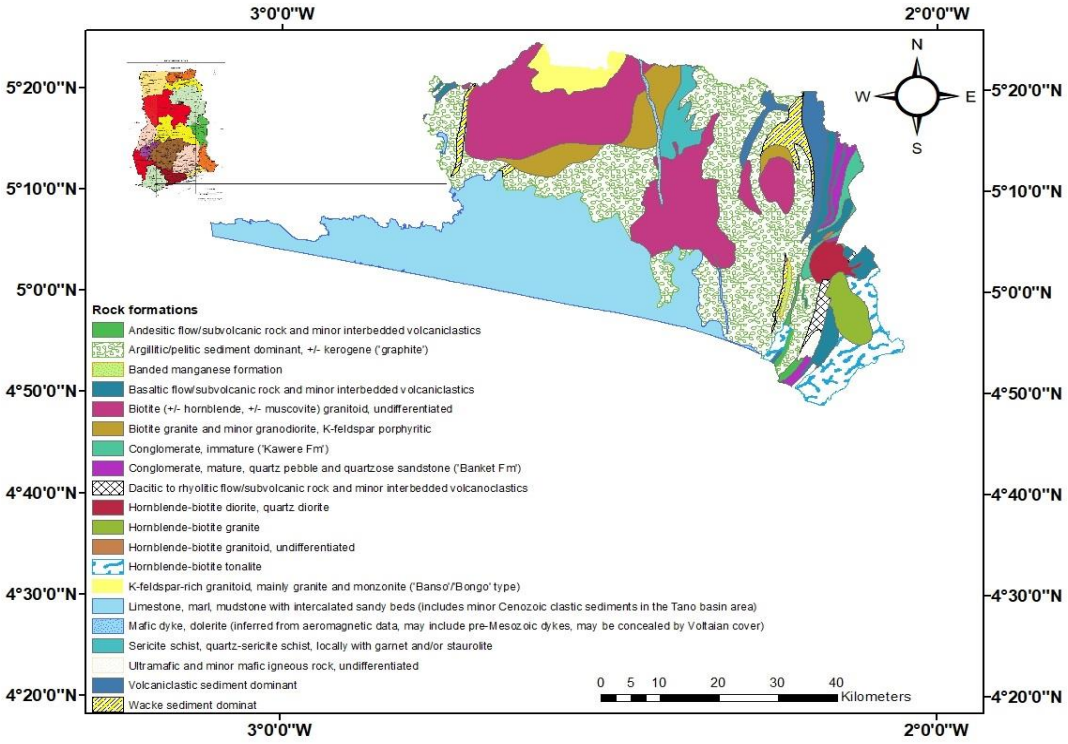

Figure 1. 11: A map showing the rock formations of the study catchment (Modified after Ghana Geological Survey Authority, (GSSA, 2010)

1.5.8. Hydrogeology

Sufficient hydrogeological information could not be obtained from the Tano Basin to enable describe the hydrogeology of the Lower Tano River basin. This is due to available borehole records being scanty and unavailability of detailed pumping test records. However, a baseline study carried out by WRC (2012) in the Tano Basin indicates that, the rocks of the Apollonian contains alluvial material, which forms part of the isotropic and heterogeneous unconfined aquifer. They also identified hydrogeological features similar to those of the Pra Basin with transmissivity values ranging from 5.7 m^2 /day to 799 m^2/day, and the yields ranging from 37.5 L/min to 200 L/min.

For a generalized idea about the hydrogeology of the Lower Tano River Basin, borehole records and pumping test results will be obtained from this study through drilling. The methodology to be used will be discussed in chapter 3 and the results obtained from the pumping test data will be used to compute the aquifer hydraulic parameters and that will be discussed in my first specific objective.

1.5.9. Socio-economic Activities

In the study area, the main occupation of the citizens is fishing and this takes 40 % of the labour force. In addition, 20% of the labour force are into agriculture particularly cocoa, rubber farm, cassava, oil palm, cocoyam, coconut, and plantain. Most farming is done on a small scale mainly for household consumption and the excess are sold for extra income. Forests within the basin make significant contribution to employment, rural income, and trade. This is done through Non-timber Forest Products (NTFPs). Other rural employment generated for the inhabitants include self-employment and jobs generated from timber processing factories. The transportation and manufacturing sector provides an average of 8% employment to the citizens. Also, about 12 % of the citizens are involved in menial daily jobs which include illegal small-scale mining activities. Equally, the mining industries absorb 10 % of the citizens and the oil and gas industries absorbs the remaining 10 % (Ghana Statistical Service, 2012).

CHAPTER TWO

LITERATURE REVIEW

2.1 Introduction

The literature review in this section provides a broad coverage of subjects related to the thesis topic. The review considers (a) the estimation of aquifer hydraulic parameters using pumping test, (b) assessing the overall quality of groundwater including the level of trace elements contamination, and its suitability for domestic and agricultural purposes, (c) determining the hydrogeochemical processes that produces the chemical characteristics or compositions of an aquifer, (d) Investigating the sources of recharge to an aquifer system and (e) Determine the ages of groundwater to understand the levels of abstraction. Each of the above represents an integral part in defining the overall aim of this research work.

2.1.1 *Estimation of Aquifer Hydraulic Parameters using Pumping Tests.*

Pumping test method is commonly used for computing aquifer hydraulic parameters (Todd, 1980) though other methods such as bail tests, slug tests, and tracer tests are employed for this purpose. The normal practice in a pumping test is to pump a borehole at a specified discharge rate and observe the draw down recovery rate in an observation well located at some distance from the pumping borehole. The obtained drawdown data can then be used to estimate the aquifer hydraulic parameters by employing Theis (1934) method, Cooper-Jacob's (1946) methods and other methods. One of the challenges encountered when conducting a pumping test is keeping the discharge rate constant. This is because the discharge rate tends to vary slightly when there is (a) an increase in discharge head, (b) fluctuations in electric power supply to the pump motor and (c) fluctuations in voltage.

Across the globe, (Boulton, 1954, 1963; Prickett, 1965; Neuman, 1972, 1974; Neuman, 1975; Nwankwor et al., 1992, ; Moench, 1995; Heidari & Moench, 1997; Chen & Ayers, 1998; Meier et al.(1998); Grimestad, 2002; Zhan & Zlotnik, 2002; Wu et al., 2005; Kollet & Zlotnik, 2005;

Hunt, 2006; Tartakovsky & Neuman, 2007; Akaha & Promise, 2008; Ishaku et al., 2009; Attwa et al., 2014; Rao et al., 2015; Hamidu et al., 2016; Akhter & Hasan, 2016; Okon et al., 2018; Hasan et al., 2020; Suprapti & Pongmanda, 2020), various methods including pumping test have been used to estimate the aquifer hydraulic parameters for efficient groundwater development and management.

Across Ghana, especially in the rocks of the Birimian formations, Yidana et al. (2013) used steady state numerical groundwater flow model to estimate the aquifer hydraulic parameters in a crystalline aquifer system in Southern Ghana. The outcome of the author's research provided a general framework for understanding the hydrogeology of Southern Ghana.

Also, in the Tolon and Wa districts of Northern Ghana, Abdul-Ganiyu et al. (2017) used Theis (1934) graphical type curve method to estimate the transmissivity of two boreholes. The authors monitored the pumping tests, barometric and absolute pressures using non- vented water level sensors for a one-year period (2015 to 2016). Their results indicate that the aquifer in the Wa district is of granitoid intrusions while that of the Tolon district is of Voltaian province. Their estimated transmissivity values for both Wa and Tolon districts were $0.5 m^2$/day and, $0.8 m^2$/day respectively. They also concluded that the yields for both boreholes were enough for domestic water supply.

Asante-Annor (2018) used Cooper-Jacob (1946) graphical method for unsteady state flow graphical test method to estimate the hydraulic conductivity, transmissivity, and specific capacity in Assin and Biriman districts of Ghana. Their results show a strong positive correlation between specific capacity and hydraulic parameters (transmissivity and hydraulic conductivity).

In this study, Theis (1934) curve matching method will be used to estimate the aquifer hydraulic parameters. To do this, a plot will be assumed on a semi-logarithmic paper including the relationship between the residual drawdown ($\Delta s'$) and (t/t') and the fitted straight line passing

through the plotted points. t is the time in minutes including the recovery time period and the total pumping period, t' is the time of recovery (min) that is the time in which the pumping process was stopped. The transmissivity of the aquifers will be determined by

$$T = \frac{2.3\ Q}{4\pi\Delta s'}$$

From the equation above, the residual drawdown difference measured in meter per log cycle of t/t' is characterized by Δs' and Q is the discharge rate. The above equation reflects accuracy when calculating the aquifer hydraulic parameters. This is because the level of water in the borehole becomes normal and prevents fluctuation of the borehole water during pumping. In this study, the aquifer of the Apollonian is assumed to be unconfined and that of the Birimian is assumed to be confined. Since the aquifer of the Apollonian is assumed to be unconfined, the obtained drawdown data would have to be corrected using the equation:

$$S' = S - \frac{S^2}{2h}$$

Where S is the recorded drawdown and h is the aquifer saturated thickness. The above equation will be used based on the above assumptions. Hence to account for the change in transmissivity that occurs in both aquifers, especially the aquifer of the Apollonian formation, the drawdown must be corrected from the above equation.

Estimating the aquifer hydraulic parameters in this study will be the first of its kind in the Lower Tano River Basin and the outcome will add to the current knowledge about the hydrogeology of the Lower Tano River Basin.

2.1.2 Assessing the overall Quality of Groundwater including the level of Trace Element Contamination, and its Suitability for Domestic and Agricultural purposes.

2.1.2.1 Groundwater Quality and its suitability for domestic and agricultural purposes

In evaluating and classifying the quality of both surface water and groundwater, the characteristics of chemical and trace element concentrations play an important role. This may reveal immense information regarding the environments through which the water resources have circulated (Appelo & Postma, 1999). During the past decade, various geochemical methods, and chemical indices {water quality index (WQI), Sodium adsorption ratio (SAR)}, Percent sodium, Magnesium hazard (MH), Kelly ratio (KR), Wilcox diagram} have been effectively used to evaluate the quality of groundwater and its suitability for irrigation and domestic purposes (Pazand & Javanshir, 2014; Fijani et al., 2016; Barzegar et al., 2016; Kavurmac & Ustun, 2016).

In Ghana, particularly in the Birimian supergroup, Yidana et al. (2012), applied spatial analytical and multivariate statistical techniques to hydrochemical data to aid in the classification of groundwater quality control parameters in the Voltaian and Birimian aquifers in northern Ghana. They determined groundwater suitability for commercial, domestic, and irrigation uses. The findings of Yidana et al. indicated that, the Birimian aquifer is more suitable for irrigation due to generally low salinities.

Also, in southwestern and coastal basins of Ghana, Darko et al. (2013) used water quality index (WQI) based on chemical and microbiological data to classify the overall ambient water quality at 19 different stations. The obtained results indicated that most groundwater in southwestern and coastal basins in Ghana were good for drinking and domestic purposes.

In the near shore coastal zone of Accra, Nyarko et al. (2015) applied WQI, based on chemical and microbiological data to assess the quality of groundwater. Their results suggest that

groundwater in the coastal zone of Accra were poor to grossly polluted and not suitable for aquatic life and recreation.

Affum et al. (2015) applied hydrochemical data to explain the quality of groundwater in parts of the Western Region of Ghana. They reported hardness, salinity pollution, and toxic elements as the key factors affecting groundwater quality. Also, according to the authors, 79% of arsenic concentration and 43% of cadmium content exceeded the WHO guidelines of 0.01 mg/L and 0.03 mg/L for suitability.

Atta-Darkwa (2016), investigated the quality of groundwater for irrigation in Ejisu- Besease in the Oda River Basin. The author analyzed physicochemical parameters and interpreted the result with Percent sodium, sodium adsorption ratio, Kelly ratio, and Magnesium hazard. Result obtained indicated that EC ranges from 186 to 638 µS/cm, TDS was less than 500 mg/L, Na% varied from 20.55 to 44.09%, SAR values ranged from 0.34 to 0.86 meq/L, KR content varied from 0.13 to 0.44 and MH values ranged between 25.86% to 55.29%. The application of Wilcox, 1955 diagram and USSL, 1954 diagram in the study revealed groundwater in the Oda River Basin was of good quality for irrigation.

In the Lambussie-Karni District of Ghana Annor et al. (2018) investigated the suitability of groundwater for irrigation. In their works, sixteen boreholes were sampled and sodium adsorption ratio (SAR), residual sodium carbonate (RSC), sodium percentage (Na %), permeability index (PI) and irrigation quality water index (IQWI), was used to classify the suitability of groundwater for irrigation. Results of the chemical indices indicated that groundwater in Lambussie-Karni District of Ghana was generally suitable for irrigation.

Further, in the Atankwidi catchment of the White Volta Basin in Ghana, Anim-Gyampo et al. (2019) investigated the suitability of groundwater for drinking and irrigational purposes. In their study, twenty-six boreholes were sampled, and heavy metal concentrations, and physicochemical constituents were determined. Chemical indices such as water quality index,

salinity, chlorinity, sodium adsorption ratio, residual bicarbonates, magnesium hazards, and permeability indices were employed by the authors. The authors also estimated the hazard index, hazard quotient, and cancer risk of the analyzed heavy metals. The estimation was done to assess the potential carcinogenic risk to human health. According to the authors, 80% of groundwater in the Atankwidi catchment was potable and suitable for irrigation.

Apart from the above authors, a lot of studies to investigate the quality of groundwater and its suitability for socio-economic uses have been carried out across Ghana (Ackah et al., 2011; Salifu et al., 2017; Agyemang, 2019; Chegbeleh et al., 2020).

2.1.2.2 Trace Elements Contamination in Groundwater

The occurrence of trace elements contamination in groundwater has become a problem of increasing concern. This situation has arisen because of increasing population, migration, expansion of industries, exploitation of natural resources, modern agricultural practices, and abuse of environmental regulations. Trace elements have some relationship between public health and the composition of water, which may be related to neither natural condition nor contamination (Karanth, 1987). Additionally, trace elements contribute to groundwater quality from a variety of anthropogenic and natural geogenic sources (Ramessur, 2000; Newcomba et al., 2002; Abollino et al., 2004; Leung & Jiao, 2006).

Problems associated with trace metal contamination in water were first emphasised in countries with advanced industries due to their huge industrial discharges (Kurland et al., 1960; Goldberg 1976). After, various studies have focused on analyzing the normal trace element concentrations in groundwater in order to separate natural as well as anthropogenic causes that disturb the groundwater quality and also define the interactions that occur in an aquifer (Hussain et al., 2008; Shahab et al., 2016; Mahmood et al., 2015; Okogbue et al. 2012; Aghazadeh & Mogaddam, 2010; Kord et al., 2013; Narany et al., 2014; Masoud, 2014; Uddameri et al., 2013; Yadav et al., 2014; Sarikhani et al., 2015; Qing et al., 2015; Golchin

& Azhdary Moghaddam, 2016; Cao et al., 2016; Ehya & Marbouti, 2016 Sethy et al., 2016; Jacintha et al., 2016; Rehman et al., 2018; Peng et al., 2019; Gu et al., 2020).

In Ghana, in spite of the relatively low level of industrial activities, there is nevertheless a growing awareness on the need for sustainable groundwater development and management. This becomes even more important in view of rampant small-scale mining (legal and illegal). Existing information on various groundwater contamination in Ghana showed that most surface water and groundwater are contaminated with trace elements (Tay & Momade, 2006; Ato et al., 2010; Obiri-Danso et al., 2009; Tiimub et al., 2012; Bempa, 2014; Cobbina et al., 015); Amu-Mensah et al., 2019). However, information on groundwater contamination in the Lower Tano River Basin is limited. This therefore demonstrates the need for a more precise, and specific review of the occurrence of trace metals in various aquifers within the basin. This will aid to the understanding of trace element loads and its distribution from geogenic and anthropogenic sources into the aquifer - for an effective management especially the quantities, qualities and pollution control.

The need to assess the level of trace metal contamination in groundwater in the rocks of the Birimian supergroup of Ghana in which the basin lies has led to the initiation of several research work in various universities and scientific institutions across Ghana. Hence, the decision to review trace metal contamination in groundwater in the aquifer of the Birimian supergroup and the Apollonian formation is as a result of the need to have a holistic approach that could influence future control strategies in the Lower Tano River Basin.

In the Birimian supergroup, one of the earliest studies carried out by Amasa (1975) examined trace elements content in drinking water within the Obuasi gold mining area and found high levels of Arsenic (As) concentrations in groundwater.

This was followed up by Akoto Bamford et al. (1990). According to the authors, heavy metal pollution (Mn, Fe, Cr, Cu, Zn, As, Pb, Rb, Sr, Y, Zr and Nb) in gold ore tailings and sediments was in a range of 0.08 to 49000 μg/g, whereas Zn and Fe was detected in water at levels of 0.08–2.4 μg/ml.

Pelig Ba et al. (1991) assessed the level of groundwater contamination from the Accra plains and the upper regions of Ghana and found groundwater with elevated Pb, Cr and Fe concentrations.

Pelig Ba, (1998) also analyzed groundwater from some crystalline rocks in the Upper Region of Ghana and identified Al, Fe, Zn, Sr, and Ba to be excessively higher in natural water systems.

Tay, (2006) conducted a survey on the levels of trace elements (Cu, Hg, Ni, Pb, Fe, Mn, Fe, Zn, Cr, Cd, Mg and Ca) content in surface water and groundwater in the Northern parts of the Ashanti gold belt. According to the author, correlation between trace elements revealed expected process-based relationship derived mainly from the geochemical and biochemical processes within the aquifer system.

Armah et al. (2011) spatially assessed the distribution of heavy metals in surface water and groundwater within the study catchment of the Tarkwa mining area using interpolation techniques in a geographical information system environment. According to the authors, most of the surface water and groundwater had high levels of As, Pb, Cd, Mn and Fe.

Edjah (2012) found high concentrations of Pb, Fe, Mn and Cd in groundwater in some communities within the Lower Tano River Basin.

Anim –Gyampo et al. (2014) reported high levels of Pb and Cd in groundwater of the Bunpkurugu-yunyo district of Ghana.

Boateng et al. (2015) used multivariate statistical model and pollution evaluation indices as a complementary tool to identify the various possible sources of pollution that influence the quality of groundwater.

Tay et al. (2016), reported high values of Aluminum, selenium, cadmium, lead, iron, manganese, and mercury in groundwater located in the Lower Pra River basin of Ghana.

Doyi et al. (2018) reported high values of lead, cadmium and nickel in groundwater and zinc, cadmium and Iron in soil located in some communities within the Lower Tano River Basin.

2.1.2.3 Sources of Trace Element concentration in groundwater

Trace metals enter the aquifer system through natural (geogenic) and anthropogenic sources. Entry may be because of direct discharges into surface water bodies that leaches into the aquifer systems by natural processes. Another way of entry is through indirect directions such as wet and dry deposition as well as runoff. In view of the toxicity of trace metals, it is important to understand their sources and its effects on an aquifer.

Some anthropogenic sources of trace metal contamination in groundwater includes effluents from mining, domestic, industries, storm water runoff, leaching of metals from garbage and solid waste dump sites, burning of fossil fuels, industrial emissions, incineration of wastes and activities from petroleum industries.

2.1.2.4 Effects of Trace Elements contamination in groundwater

Trace metals such as Fe, Mn, Zn, and Cu are essential for the growth and well-being of humans (WHO, 2011). However, they are likely to show poisonous effects when humans and living beings are exposed to levels higher than the normal requirements of WHO. Other elements such as Pb, Hg and Cd are not essential for metabolic activities but exhibit carcinogenic properties (WHO, 2011). Most published data on the effects of trace metals on human health report adverse effects at concentrations (Boateng et al., 2015; Hadzi et al., 2015; Adewoyin et

al., 2019; Tay et al., 2019; Anim-Gyampo et al., 2019) higher than WHO. The WHO has produced water quality criteria for drinking water for several chemicals including trace elements since 1984 to 2017.

From the above, it is perceived that, water quality research in Ghana especially areas underlain by the Birimian super group rocks like the area under study focused mainly on surface water and groundwater. In addition, the above studies were restricted to only few sites with most communities not having issues of mineral mining. Unfortunately, small scale gold mining is gradually increasing in southwestern Ghana due to the geology being rich in sulphide minerals (arsenopyrite, chalcopyrite and pyrite) Luebe et al. (1990). Yet the impact of small-scale mining in most communities within southwestern Ghana especially the Lower Tano River Basin has not received the fullest attention. Apart from Edjah (2012) and Doyi et al. (2018), no studies have been conducted to investigate the quality of groundwater with respect to trace elements. Hence the results of this study will define the sources of aquifer contamination with respect to trace elements and that will add to the current literature on aquifer hydrochemistry and its suitability for socio-economic purposes.

2.1.3 Determination of the Hydrogeochemical processes that produces the Chemical Characteristics or Compositions of an aquifer system

Hydrogeochemical processes refers to the correlation between water-rock chemistry, groundwater movement and the origin of the chemical composition of groundwater (Appelo & Postma, 1999). A change in the chemical composition of groundwater is principally a function of the interaction between the groundwater and the mineral composition of the aquifer materials through which it moves (Appelo & Postma, 1999). Hydrochemical processes such as precipitation, ion exchange, weathering, dissolution, etc. coupled with groundwater residence time along a flow-path control the changes in chemical composition of groundwater (Apodaca et al., 2002). Besides, the chemical composition of groundwater is controlled by several factors

and groundwater has a distinct chemistry or chemical characteristics due to chemical variation of rainfall recharging an aquifer (Drever, 1988; Hem, 1991). In any environment, groundwater has a unique chemistry due to several processes like groundwater flow and rock- water interaction during recharge, dissolution of minerals and prolonged storage in the aquifer (Hem, 1986).

In the early times of hydrogeochemical studies, some scientists reported the importance of hydrogeochemical processes in groundwater (Moller et al., 2007; Devadas et al., 2007; Tesoriero et al., 2004; Elango et.al., 2003; Apodaca et al., 2002; Sikdar et.al., 2001). The studies of the above-mentioned authors and other water scientists in the past years have aided in the creation of suitable management plans for aquifer protection and remedial measures for aquifer contamination.

To overcome aquifer related issues, a detailed knowledge about the hydrogeochemical processes regulating its chemistry is required. This can be achieved with the help of computerized geochemical models such as Durov (1948), Piper (1944), Stiff (1951), Gibbs, (1970), saturation indices, and mineral stability diagrams (Edmunds et al., 2001; Appelo & Postma, 1999; Sahib et al., 2016). To understand the chemical state of groundwater and predict the various water types as well as the factors controlling the chemistry of an aquifer, the above-mentioned models are the most powerful tools to use.

Parkhurst et al. (1995), Felmy et al. (1984), Wolery ,1979, Spostigo et al. (1979), Shannon et al. (1977), Plummer et al. (1976), Helgeson et al. (1970) and other scientists across the globe have established different geochemical models for assuming and describing the chemical character of mixed plus complex water. Plummer et al. (1990), Plummer et al. (1983), Jenne (1981), Runnels (1978) and Nordstrom et al. (1979) gave a brief review of this geochemical models.

Numerous researchers have also used geochemical models for groundwater solubility equation study (Murphy & Schramke, 1998; Deutsch, 1997; Elangovan, 1997; Tamata, 1990; Wolery, 1983; Wolery, 1979). Worldwide approaches to groundwater problems and the significance of geochemical modelling are discussed in detail by Jenne, 1981.

Currently, across the globe, the temporal and seasonal changes of the hydrogeochemical processes of groundwater are observed by different researchers (Kumar et al., 2006; Halima et al., 2010; Mahato et al., 2016; Abdelshafy et al., 2019; Akoachere et al., 2019) and statistical methods such as factor analysis, multivariate analysis, principal component analysis, correlation matrix, histograms and semi-logarithmic have been used by several researchers across the world for data analysis and interpretation (Banoeng –Yakubo et al., 2009; Gakin & Happell, 2014; Jacintha et al., 2016; Tatou et al., 2017; Baghdadl et al., 2019; Kumar, 2020). The above-mentioned statistical methods are a good way of organizing sets of data to make useful generalizations and understanding of aquifer chemistry. Likewise, the above-mentioned statistical tools can be used to classify groundwater, investigate and interpretate hydrochemical facies of groundwater (Lawrence & Upchurch, 1983).

In Ghana, some researchers have similarly carried out investigations about hydrogeochemical processes using geochemical models and statistical tools. For example:

Akiti (1980), being one of the early water scientists in Ghana studied the hydrogeochemistry of groundwater in the Accra plains of Ghana. The author applied hydrochemical data and identified three major hydrochemical facies ($NaHCO_3$, NaCl, and $MgCl_2$) for groundwater in the Accra plains. The results indicate NaCl as the dominant water type in parts of the Accra plains.

Follow up to Akiti's work, Kortatsi (2006 a) in some parts of the Accra plains applied mass balance techniques in studying the hydrochemistry of groundwater. The author related the

hydrochemistry of groundwater in the Accra plains to the weathering of the host rocks, cation-exchange reaction, evaporative concentration of some solutes and seawater intrusion.

In the Ankobra basin, Kortasi, (2006b) used hydrochemical data to establish the hydrochemistry of groundwater. According to the author, groundwater in the Ankobra basin is mildly acidic with low conductivity and under - saturated with carbonate minerals. The author indicated silicate weathering as the main hydrochemical processes controlling the chemistry of groundwater in the Ankobra basin.

Using Q - mode mass balance methods and multivariate techniques, Helsrup et al. (2007) attributed the hydrochemistry of groundwater from some sedimentary aquifers in Togo and southern Ghana to silicate mineral weathering, carbonate equilibria, effects of seawater intrusion and ion exchange processes.

In the Southern Voltaian sedimentary aquifers in Ghana, Yidana et al. (2008) used mass balance methods to describe the hydrochemistry of groundwater. Their results suggest weathering of silicate minerals as the likely dominating factor influencing the hydrochemistry of aquifers in Southern Voltaian aquifer.

Banoeng-Yakubo et al. (2009) determine the main controls on the hydrochemistry of groundwater in some Birimian aquifers of the Birim River basin. In their studies, mass balance modelling was used simultaneously with multivariate R-mode hierarchical cluster analysis to determine the important sources of variations in the hydrochemistry of groundwater. In addition, they identified two water types, thus water influenced by silicate weathering and anthropogenic activities. Mineral speciation and silicate mineral stability diagrams generated from their data indicate montmorillonite, probably derived from the incongruent dissolution of feldspars and micas, as the most stable silicate phase in the groundwater. They also suggest cation exchange processes as one of the hydrogeochemical processes playing minor roles in the hydrochemistry of some areas underlain by the Birimian Supergroup rocks.

In the Densu River Basin, Fianko et al. (2009 a) studied the hydrochemistry of groundwater with multipurpose approaches. According to the authors, the analytical results of groundwater was acidic and moderately mineralized. The Chemical constituents they observed were Na^{+}> Ca^{2+} > Mg^{2+} > K^{+} and Cl^{-} > $HCO3^{-}$> $SO4^{2-}$> $NO3^{-}$. The main water types they identified were Ca–Mg–HCO_3, Mg–Ca–Cl, Na–Cl, and mixed waters (neither a particular cation nor anion dominates). The authors also reported that the influence of different anthropogenic activities have an impact on ground water resources within their study catchment.

Edjah et al. (2015), studied the hydrogeochemistry of groundwater in some communities within the Lower Tano River basin and identified rock weathering as the dominant processes controlling the chemistry of groundwater and identified NaCl water as the dominant water within the study catchment.

In the Lower Pra River basin, Tay et al. (2017) investigated the hydrogeochemical processes and the anthropogenic impact that influence groundwater resources. The hydrochemical results show that, the major processes responsible for chemical evolution of groundwater include silicate weathering, ion- exchange processes, sea aerosol spray, and the weathering of biotite, chlorite, and actinolite from the source rock. Hydrochemical facies of their results delineated two main water types, i.e., Na-HCO3 and Ca-Mg-HCO3 water types, with Na-Cl and Ca-Mg-Cl as minor water types. Using Q-mode Hierarchical Cluster Analyses (HCA), surface water and groundwater within the basin were characterized into four (4) water groups and five (5) subgroups. Results from the hydrochemical data suggest that groundwater within the basin was mainly undergoing the process of recharge, which involves the mixing of freshwater with geochemically different ionic signatures than processes involving saline-freshwater mixing. According to the authors, the use of Principal Component Analysis (PCA) together with Varimax with Kaiser Normalization for component matrix delineated three main processes in their study region and these processes are biochemical (water-soil-rock interactions), natural

geochemical, incongruent dissolution of silicates/aluminosilicates, and pollution of the water resources principally from agricultural inputs.

In the Central Region of Ghana, Ganyaglo (2015) studied the hydrogeochemical processes occurring in some parts of the region in order to determine the origin of groundwater salinity. The hydrochemical results from his work identified Ca-Mg-HCO_3, Na-Cl, Ca-Mg-Cl-SO_4, and non-dominant water types as the hydrochemical facies of the Central Region. The author concluded that groundwater salinization in the coastal zone of the Central Region was caused largely by halite dissolution and to a minor extent silicate weathering. Also, seawater intrusion played a minimal role in controlling the chemistry of groundwater in parts of central region.

Review from the above studies shows that most authors focused mainly on groundwater potential assessment, groundwater quality and its suitability for domestic and agricultural purposes, and the hydrogeochemical processes controlling the chemistry of groundwater

It is apparent that the hydrogeochemistry of groundwater in most communities within the Lower Tano River Basin have not been intensively studied for comparisons, monitoring, and sustainable management of the resource. However, this study being an addition to the previous studies carried out by Edjah et al. (2015) intend using a four-year groundwater hydrochemical data to estimate the hydrogeochemistry of groundwater with the help of statistical tools and hydrogeochemical modelling. Hydrogeochemical modelling which is a very useful tool will be used to evaluate the aquifer chemistry and to see if the aquifers within the basin are controlled by equilibrium with solid phases (Appelo & Postma, 1996). Equally, calcium, magnesium, sodium, and potassium aluminosilicate stability diagrams, and saturation indices for some primary silicate minerals will aid in describing the control on the composition of groundwater within the basin. ArcGIS 10.5 software will help in the production of groundwater quality maps and hydrogeochemical maps of the Lower Tano River Basin. The outcome of this

study will add to the current literature on the hydrogeochemical studies of groundwater in the Tano Basin.

2.1.4 Sources of Recharge to the Aquifer System using oxygen-18 (δ^{18} O) and deuterium (δ^{2}H).

Isotopes are used to investigate the inter-relationships between the components of the water cycle such as rainfall, run-off, plant transpiration, and evaporation (Clark & Fritz, 1997). This is done using oxygen-18 (δ^{18}O) and deuterium (δ^{2}H). In addition, these isotopes are used to evaluate recharge, flow direction and mixing conditions as well as trace the origin of groundwater sources (Zaharin et al., 2008).

In a particular environment, estimating groundwater recharge or origin comes with a characteristic isotopic signature, most often permitting the separation of water from different environments (Clark & Fritz, 1997). Isotopes are routinely used in hydrogeological investigations to complement physical hydrology and geochemistry due to their ability to provide information about recharge, geochemical evolution, and water- rock interactions, etc. (Clark & Fritz, 1997; Kendall & McDonnell, 1998; Cook & Herezeg, 2000).

In Ghana, Akiti (1980) was the first researcher that used environmental isotopes (δ^{18}O, δ^{2}H,), to estimate groundwater recharge in some parts of the Afram plains. He developed a local meteoric water line from δ^{18}O and δ^{2}H in rainfall data. The author's line is currently used as the local meteoric water line (LMWL) in Ghana and other sub - Saharan African nations. The equation of his line was in the form: $\delta^{2}H‰ = 7.86\delta^{18}O‰ + 13.61$. The equation reflects the relatively high humidity in the Accra plains. The slope of the author's line was slightly close to that of the global meteoric water line of $\delta^{2}H‰ = 8\delta^{18}O + 10$. In addition, he used environmental isotopes (δ^{18}O, δ^{2}H) in groundwater to trace the sources of recharge in parts of the Accra plains of Ghana.

In the Upper East, Upper West, and parts of the Accra plains of Ghana, Pelig-Ba et al. (1990) carried out a similar work like Akiti (1980). Their study showed that groundwater in the three regions was recharged predominantly from precipitation.

Armah (2002), conducted similar environmental stable isotope studies in the Awutu-Senya District and some communities within the Central Region of Ghana. The author's study showed a close correlation of the isotopic data to the Global Meteoric Water Line (GMWL) data. According to the author, the origin of groundwater in the Awutu-Senya District is of meteoric origin and not marine.

In the Densu River basin, stable isotopes (δ^{18} O and δ^{2}H) from depth profiles were used to estimate groundwater recharge by Adomako et al. (2010). The obtained results suggested recharge in some parts of the Densu River basin to be between 94 and 182 mm/year.

Using environmental isotopes (δ^{18}O and δ^{2}H), Kaka et al. (2011), estimated groundwater recharge in the southwestern margin of the Volta Lake in Ghana. Their results suggested meteoric origin of recharge to groundwater in the Volta Lake area.

In the same way, Saka et al. (2013), assessed groundwater recharge in the Ga East Municipal area using environmental isotopes (δ^{18} O and δ^{2}H). In their study, the isotopic compositions suggest groundwater recharge to be from meteoric origin.

In the Lower Pra River Basin of Ghana, Tay, 2015 used isotopes (δ^{18}O and δ^{2}H) to investigate groundwater recharge. The author's results indicated that groundwater recharge in the Lower Pra River Basin was of meteoric origin with evaporation playing a significant role on the infiltrating water.

Using isotopes (δ^{18}O and δ^{2}H), Egbi et al. (2018) estimated groundwater recharge in the Lower Volta River Basin of Ghana. Results obtained from their work indicated that groundwater recharge was from direct infiltration of rainwater with minimal evaporation.

Using $\delta^{18}O$ and $\delta^{2}H$, Edjah (2012) estimated groundwater recharge in the Lower Tano River Basin and results obtained indicated that the source of groundwater was from direct rainfall infiltration.

Comparison between stable isotopes (δ^{18} O and $\delta^{2}H$) from the above studies as well as those carried out in the Southern Voltaian Sedimentary basin (Acheampong, 1996; Kortatsi & Sekpey, 1993; Jorgensen & Banoeng-Yakubu, 2001) showed that the isotopes of δ^{18} O and δ^{2} H in groundwater follow one trend, that is, they all cluster along the global meteoric water line (GMWL), suggesting rapid recharge from rainwater with little or no isotopic evaporation.

In this study the use of environmental isotopes ($\delta^{18}O$, $\delta^{2}H$) for estimating groundwater recharge will follow the trend carried out by Akiti,1987. Rainfall samples will be collected for 2 years and the results computed to obtain a rainfall regression line for the study area. This research being the first of its kind will give a general rainfall regression line for the Lower Tano River Basin, since the rainfall regression line for Akiti,1987 did not cover the southwestern part of Ghana. Also, the outcome of this research will add to the current studies on groundwater recharge using environmental isotopes ($\delta^{18}O$, $\delta^{2}H$) in south western Ghana and the Birimian Supergroup rocks of Ghana.

2.1.5 Groundwater Age (residence time) Determination

The age of groundwater is a vital parameter for understanding the dynamics of groundwater and the contaminants that travels with it (MacDonald et al., 2003). Identification of the age of water and transit times, allows easy determination of delayed impacts of present and past environmental practices on the quality of water (McGuire et al., 2002; MacDonald et al., 2002; Katz et al., 2004; Moore et al., 2006) and for determining the anthropogenic or geogenic effects on the quality (Morgenstern & Daughney, 2012).

Ages of groundwater is also described by the groundwater transit time through regions or catchments and it's important for conceptual understanding of recharge sources (McGuire & McDonnell, 2006; Stewart et al., 2010; Morgenstern et al., 2010, 2012; Cartwright & Morgenstern, 2012).

The age of groundwater, which is related directly to fluid flux is also very valuable for calibrating mathematical groundwater transport models (Burton et al., 2002; Molson & Frind, 2005; Bethke & Johnson, 2008) and the age also gives essential information on contamination and water quality of drinking water (Morris et al., 2005; New Zealand ministry of Health, 2008).

Hydrochemical evolution resulting from rock-water interaction can be quantified using groundwater age measurements (Burns et al., 2003; Glynn & Plummer, 2005; Daughney et al., 2010; Beyer et al., 2014).

In all the above-mentioned applications, it is vital to constrain not only the average age of groundwater, but also the age distribution within the groundwater discharge sampling point.

Tritium (^{3}H) with a half-life of 12.43 years is the only radioactive isotope of hydrogen (Unterweger et al., 1980). Thermonuclear testing in the 1950's and 1960's introduced large amount of tritium into the hydrological cycle. This provided a useful environmental tracer for groundwater originating from this period (Solomon & Cook, 2000). The unit of tritium content in water is usually computed in tritium units (TU) also known as tritium ratio (TR) (Taylor & Roether, 1982).

2.1.5.1 Sources of Tritium (^{3}H)

The only source of tritium in rainfall prior to 1950 was from natural production in the upper atmosphere. This was generally through the bombardments of nitrogen by the flux of neutrons in cosmic radiation. Across the world, atmospheric thermonuclear testing

which occurred in 1952 elevated the tritium content in precipitation. This created a natural cause which was used to identify precipitation from 1952.

Between October 1952 to December 1953 approximately 600 kg of tritium (^3H) was introduced into the atmosphere by thermonuclear test carried out by UK, USA, and USSR (Araguas et al., 1996). The tritium content in rainfall has decreased after the atmospheric test ban treaty of 1963. After the ban, French and China continued with the thermonuclear testing until 1980 thus producing smaller quantities of tritium into the atmosphere (Weiss et al., 1979). Currently, significant amounts of tritium are released into the atmosphere from nuclear fuel reprocessing facilities and nuclear power plants (Kim et al., 1998)). Additionally, little amounts of tritium are released from compasses, exist signs and luminous watches. Globally the averaged production rate of tritium (^3H) in the Earth's atmosphere from galactic cosmic rays has been estimated between 0.19 and 0.29 atoms $cm^{\cdot 2}s^{\cdot 1}$. Production of tritium is more at higher geomagnetic latitudes (Masarik & Reedy, 1995). The mean global list before the advent of thermonuclear testing has been estimated to be 1.3 x 1018 Bq (35 MCi, or 3.6 kg of ^3H) (O'Brien, 1979).

The normal level of tritium in rainfall was determined from measurements on vintage wines to be 3-6 TU in North America and Europe (Kaufman & Libby, 1954; Roether, 1967), and 1-3 TU in South Australia (Allison & Hughes, 1977). Thermonuclear tritium content in precipitation has been determined by direct measurement, and indirect measurement from surface water, groundwater, tree ring cellulose and wine samples. Regular measurement of tritium in rainwater began in 1953 in Ottawa, Canada. Since 1961, tritium concentrations in monthly precipitation samples have been measured at a global network of stations (IAEA, 1992). At numerous northern hemisphere stations during the early 1960's, the average monthly concentrations in excess of 5000 TU were recorded. This follows the 1961- 1962 Soviet testing series in the Arctic. Much lower tritium contents were recorded in the southern hemisphere due to more nuclear tests conducted in the northern hemisphere. In both hemispheres, a strong

dependence on latitude was detected, with little tritium concentrations nearer to the equator. Precipitated water re-evaporation instigated higher tritium concentrations at continental stations, relative to those at oceanic stations at similar latitude. Spatial differences in tritium fall out can be read from Gat (1980), Weiss and Roether. (1980), and Eriksson, (1983).

2.1.5.2 Understanding groundwater recharge sources in Ghana using tritium (^3H).

In Ghana, few studies have tried using tritium to study groundwater age or residence time for groundwater management.

In the Accra plains of Ghana, Akiti, 1987 obtained tritium values of 15 TU to 27 TU (tritium units) in groundwater, suggesting that the groundwater in parts of the Accra plains was young water or of modern recharge or have not been overly abstracted.

In the Voltaian Sedimentary basin of Ghana, Acheampong and Hess (2000), recorded tritium values of 1TU and 7.2 TU indicating young water.

Adomako et al. (2011), reported tritium values of 5 TU and 12 TU for groundwater in the Densu River basin, suggesting young or modern recharge.

Ganyaglo, (2017) reported tritium values ranging from 0.05±0.07 TU to 4.75±0.16 TU in the Central Region of Ghana suggesting young or modern recharge. In addition, he recorded low tritium content in three boreholes at Ekumfi Asokwa suggesting an old water.

From the above studies, the tritium values revealed short residence time for most groundwater in Ghana. The groundwater residence time in the Lower Tano River basin is unknown. Hence, to have a generalized idea about the residence time, this study intends measuring tritium values in surface water and groundwater and this being the first of its kind in the Basin will add to literature on groundwater age determination in Ghana.

CHAPTER THREE

METHODOLOGY

Under this chapter, the approach and procedures used for Desk study, Field work, Sample preparation, Laboratory analysis, Data validation, Data treatment, Data interpretation and Spatial distribution maps are described.

3.1. Desk Study

To achieve the objectives of this study, a desk study was conducted to assess the general hydrogeology and the hydrochemical settings prevailing in the various lithologies of the study area. This involved available literature review, collection of topographical, geological, and hydrogeological maps from the Survey Department (SD) and, Ghana Geological Survey Authority (GGSA), Community Water and Sanitation Agency (CWSA, Takoradi), respectively. Based on the available records (borehole records, topographical, hydrogeological, and geological maps), sampling sites were selected, and fieldwork embarked.

3.2 Field work

3.2.1. *Geophysical Sitting*

In 2013 and from 2014 to 2015, 30 and 18 vertical electrical soundings (VESs) were carried out, respectively using Schlumberger configuration at various communities across the study area. This was done to identify potential aquifers for borehole drilling and development. Resistivity measurement was carried out with SAS 1000 Terrameter apparatus and the obtained resistivity data was reversed and interpreted using Van Der Velpen (1988) software. The software aided in the identification of different geoelectric units as well as aquifer saturated thicknesses and true resistivity units. Potential drilling sites were selected based on VES curve interpretations (Figure 3.1), which were related to the general geology of the Lower Tano River Basin.

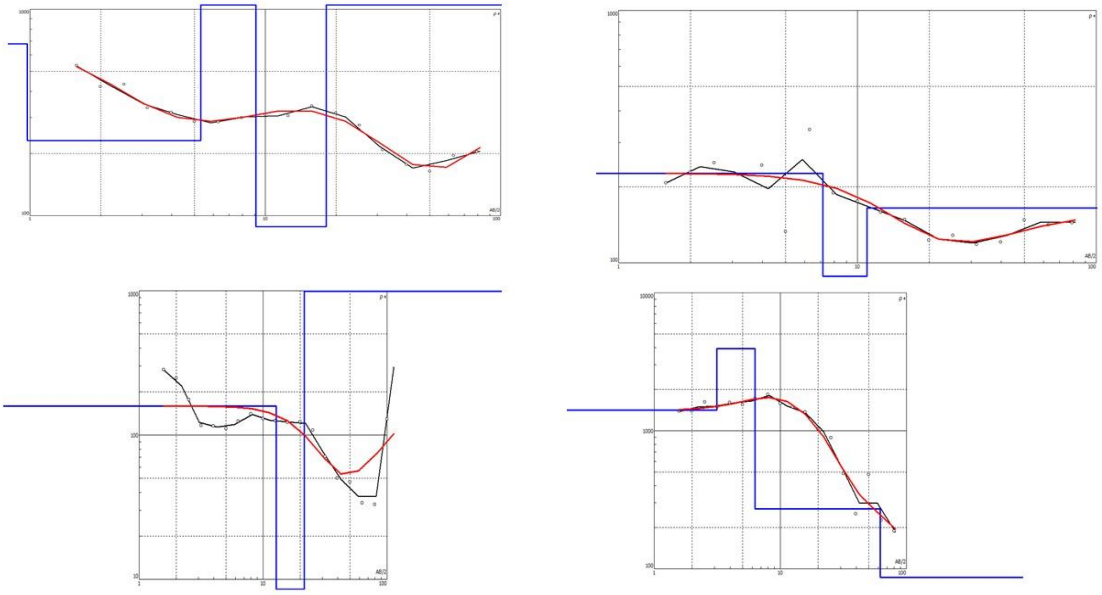

Figure 3.1: VES sounding curves generated as model curves that suit the apparent resistivity values (field curves) for selected sites in the Lower Tano River Basin.

3.2.2. Borehole Drilling and Development

After the geophysical siting, a total number of 30 and 18 boreholes were drilled (Figure 3.2), across the basin in 2013 and from 2014 to 2015, respectively. Reports on the borehole logs, type of drilling cuttings, penetration rate, rock types, geological structures (bedding plane, joints, and fractures), thickness of the saturated zones, drilling and developmental yields were recorded for each drilled borehole. The number of drilling rods used during drilling determined the depth of each borehole, and each successful drilled borehole was cased and screened at water bearing zones. The rocks encountered during drilling belonged mostly to the Apollonian formation with few from the Birimian Supergroup rocks.

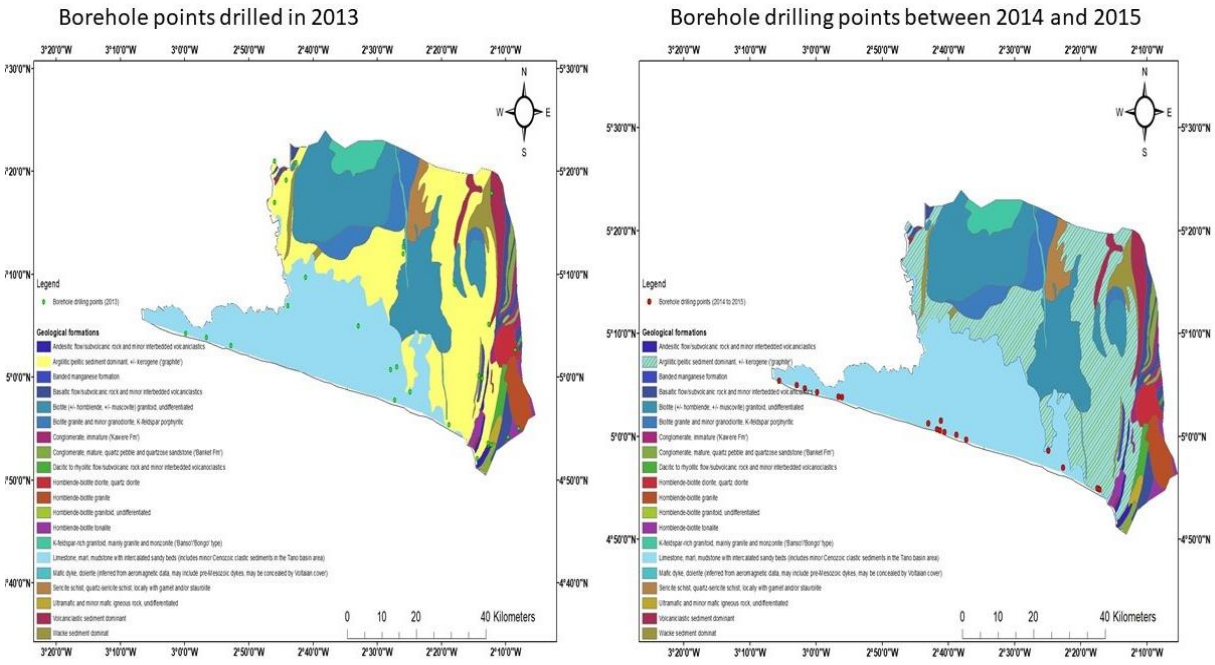

Figure 3. 2: Geological map of the study catchment with the borehole drilling points (2013 and 2014 to 2015).

3.2.3. Pumping Test

Six to twelve hours constant discharge test on a single well pumping test method (Todd, 1980) was adapted for the generation of pumping test data. This method was used due to the high-recorded borehole drilling yields.

Prior to pumping, the wellhead of the borehole was opened, and the static water level was measured using a calibrated water level meter. A pump with the specific horsepower per the developmental yield for each drilled borehole was dropped to a substantial depth in the borehole, whiles connected to a source of power. A calibrated 80 litre bucket was set in place to collect the discharge water, and a stopwatch was set to zero as the start time. As pumping started, the drawdown was measured based on the scheduled times on the data sheet. The water level drawdown and the time was simultaneously measured and recorded. The exercise was done in two phases specifically discharge and recovery phase. During the discharge stage, the borehole was pumped at a constant rate and the water level was measured at intervals in the same pumped borehole.

In the recovery stage, the borehole was allowed to recover and the water level in the same borehole was measured at the same intervals as that of the discharge. The recovery and time drawdown curves were plotted for each drilled borehole using Theis (1934) solution model. This model was used due to it most simplifying expectations and in using the model, the type curves (mathematical models) to water level changes (response data) were fitted by a curve matching method. The curve matching technique of a computer software known as AQTESOLV 4.0 was employed. The drawdowns according to Theis (1934) model were calculated using the equation:

$$S = \frac{Q}{4\Pi T}(-0.5772\ \frac{\log_e r^2 S}{4\Pi T})\ldots\ldots\ldots\ldots \text{ Eq 3.1}$$

The residual drawdown "s" that is the difference between the drawdown component due to continues pumping and the recovery component due to recharge were given by the formula:

$$S = \frac{Q}{4\Pi T}\ [(\log_e(\frac{4Tt}{r2wS}) - \log_e(\frac{4Tt\prime}{r2W})]\ldots\ldots\ldots \text{ Eq 3.2}$$

Where

S =storage coefficient

Q = discharge (m^3/ day)

rw = effective radius of the borehole, in which the water recovery is measured

T = time since pumping started

t' = time since pumping stopped

s = drawdown (m).

3.2.4. Sample Collection

3.2.4.1. Surface water and groundwater sampling for chemical and trace element analysis

For this study, 30 and 18 boreholes drilled across the basin in 2013, and from 2014 to 2015 were sampled, respectively (Figure 3.2). Monthly rainfall, 9 rivers, 15 streams, 3 lagoons, 3 seawater, 36 hand dug wells and 44 boreholes were sampled during the rainy season in 2016

(Figure 3.3). Additionally, during the dry season in 2017, monthly rainfall, 14 rivers, 13 streams, 3 lagoon, 9 sea water, 30 hand dug wells and 54 boreholes were sampled across the study catchment (Figure 3.4).

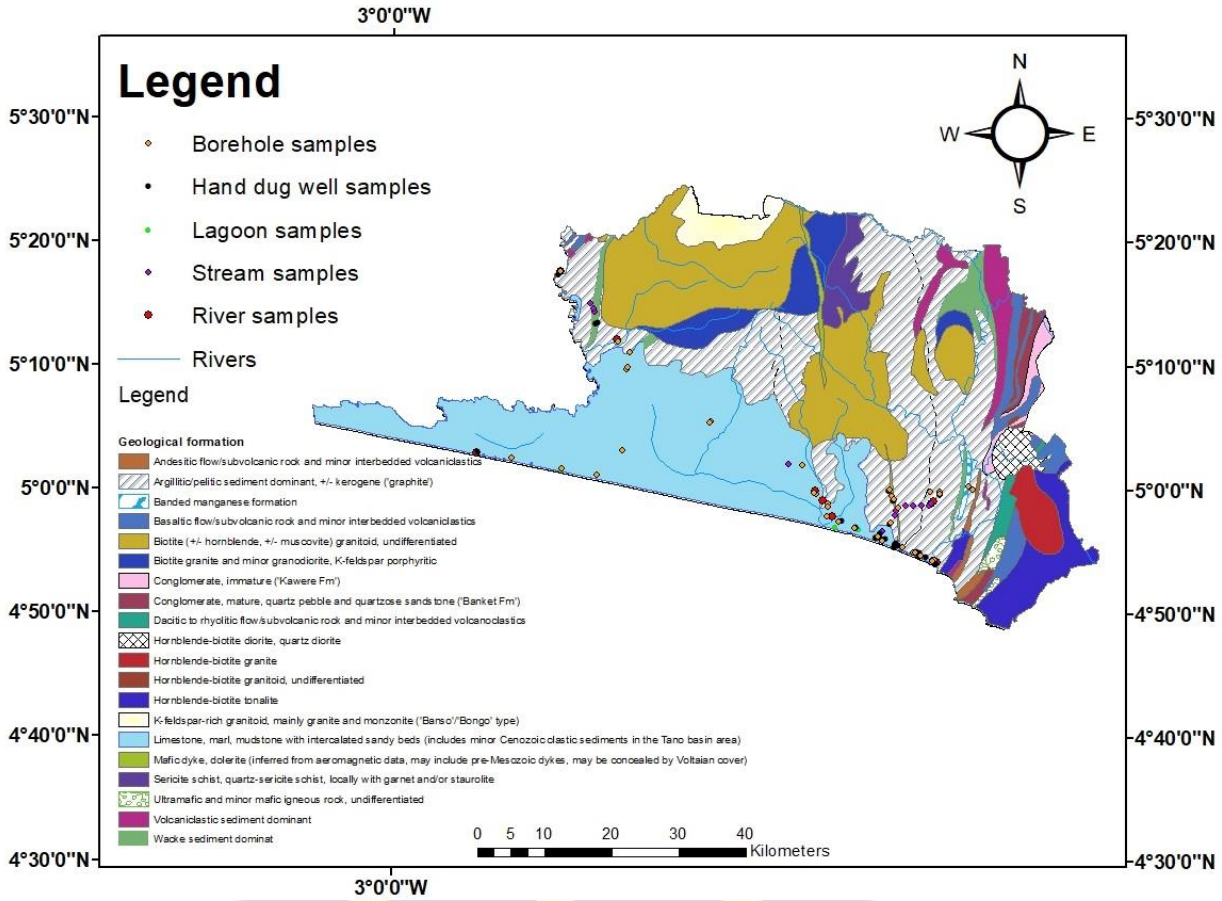

Figure 3. 3: Geological map of the study catchment with surface water and groundwater sampling points (2016)

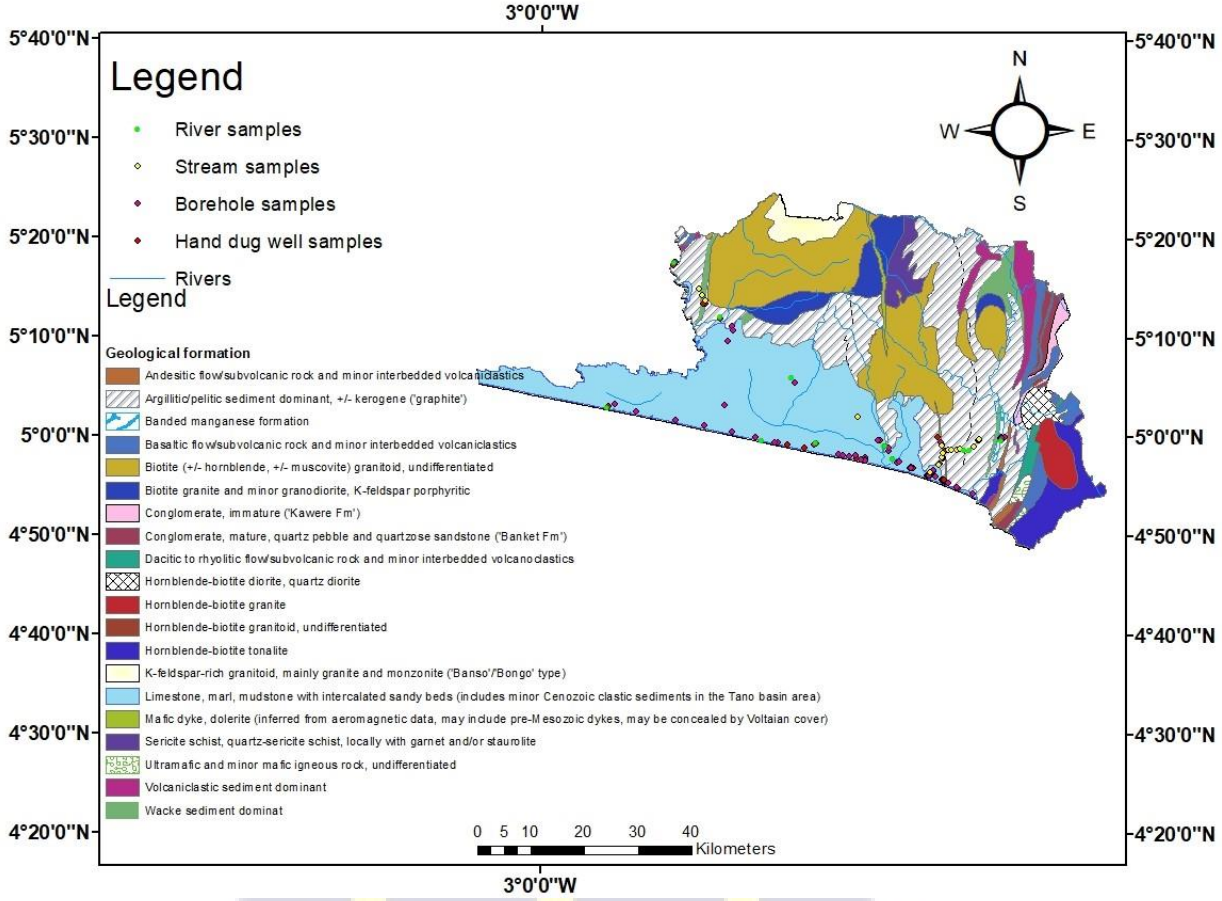

Figure 3. 4: Geological map of the study catchment with surface water and groundwater sampling points (2017).

Before the sampling of the surface water and groundwater, a detergent was used to wash the HDPE (high-density polyethylene) bottles. After, the bottles were rinsed thoroughly with distilled water to remove contaminants from the bottles. The bottles were then washed with 10% nitric acid in order to pre-condition the HDPE bottles.

For the sampling of the streams, rivers, lagoons and seawater, a dip sampler was used to collect the water from a downstream direction to upstream direction and placed in a 250 ml pre-condition HDPE bottles. The samples were taken from downstream direction to an upstream direction in order to avoid the minor inclusion of disturbed sediments. The HDPE bottles with the sampled rivers, streams, lagoon, and seawater together with duplicate samples were labelled silica, anions, cations, and trace elements. The bottles labelled anions, silica and trace elements with its duplicates were acidified with 0.2M HNO_3. This was done to keep the ions in solution. The sampled streams, rivers, lagoon, and seawater in the HDPE bottles were tightly capped

and placed in an ice chest with ice blocks and transported to the various laboratories for analysis. Similar procedures were applied to the sampling of the hand dug wells and the boreholes. The only thing that was done differently was how the groundwater samples were taken. For instance, in the sampling of the hand dug wells, the static water level was first measured, after much water was pumped out for 30 minutes before sampling was done. This was done to purge the aquifer and remove all stagnant water from the hand dug wells. For the sampling of the borehole water, the boreholes drilled in 2013 and 2014 to 2015 were sampled after each pumping test. For the existing boreholes, the hand pump on each borehole was dismantled. After, the static water levels were taken, and the hand pump was rearranged and pumped for 30 minutes in order to purge the aquifer and empty stagnant water from the casing. The purging for both hand dug wells and boreholes were done to get a typical sample of groundwater in-situ. After, groundwater samples were collected with a sterilized bucket. Part of the water in the sterilized bucket was used to rinse the sample bottles thrice before filling. This was done in accordance with Weaver (2007).

3.2.4.2. Rainfall, Surface water and groundwater sampling for stable isotope compositions ($\delta^{18}O$ and $\delta^{2}H$)

Rainfall samples were collected monthly from 1st January 2016 to 1st January 2018. A rainfall collector donated by the International Atomic Energy Agency (IAEA) as shown in Figure 3.5 was mounted at Edjah Villa near the coast of Esiama (002˚21.130´W0456.032´N). Another rain gauge fabricated by the author and Staff of Nuclear Chemistry and Environmental Research Centre of the Ghana Atomic Energy Commission as shown in Figure 3.6 was mounted at St Patrick Catholic Church in Half Assini (002°53.103´W0502.981N). The fabricated rainfall collector was built per IAEA specification (www.iaea.org/water). The rain collector consisted of a funnel, a measuring tube, and an outer cylinder. All the rain collectors were mounted at both sites on the 29th of December 2015. Both collectors were placed 30 to 50 cm above the ground to avoid splashes. Processing of the collected rainfall samples consisted of rainwater

transfer from the rain collectors using a wide funnel into a 2000 ml plastic granulated cylinder. The amount of every monthly rainfall collected was measured and recorded on site. After, the rainwater was poured into 50 ml and 500 ml HDPE bottles for the analysis of chemistry, stable isotope compositions and tritium. Both bottles were capped to prevent air bubbles and placed in a cool dry box. It was then transported to the laboratories of Ghana Atomic Energy Commission for preservation.

Surface water (rivers, lagoon, streams, and seawater) and groundwater sampled in 2016 and 2017 for isotopic composition measurements, followed the method outline under 3.2.4.1. The only difference was that, the sampled surface water and groundwater were filled directly into a 50 ml HDPE bottles and capped to prevent air bubbles. Surface water including rainfall and groundwater sampling for isotopic composition measurement was done in accordance to the procedures outlined by Boghici (2003) and IAEA, 2000 (www.iaea.org/water).

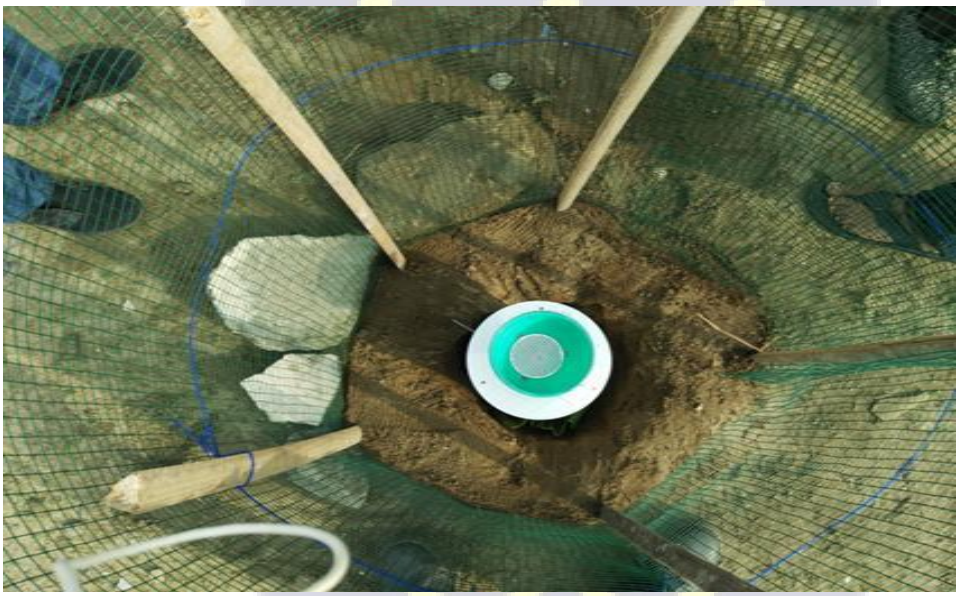

Figure 3. 5: IAEA donated rain collector mounted at Edjah Villa in Esiama

Figure 3. 6: A fabricated rainfall collector mounted at St Patrick Catholic Church in Half Assini.

3.2.4.3 Rainfall, Surface water and groundwater sampling for Tritium analysis

Sampling of rainfall, surface water (rivers and streams) and groundwater for Tritium analysis does not require any special methodology. But in this study, a 500 ml HDPE bottles donated by IAEA were rinsed thoroughly with some of the rainwater, rivers, streams, hand dug wells and boreholes at each sampling point. The bottles were filled with some of the surface water and groundwater samples. After, the bottles were tightly sealed to prevent contact with air. In all, 57 water samples including rainwater, rivers, hand dug wells and boreholes were sampled for tritium analysis. The selection was done based on proximity of the hand dug wells and boreholes to the rivers and streams.

After sampling of the surface water and groundwater for hydrochemical and stable isotope measurements, each sample bottle was given an identification label. Each label consisted of the sample location, date of sampling, record of any stability preservative treatment and prevailing weather condition at the time of sampling. After, the surface water and groundwater samples were preserved at 4° C until laboratory analyses were performed. This was done in order to limit the degradation of nitrate, sulphate, phosphate, and bacterial activity.

3.2.5. Measurements of Field Parameters

The geochemistry of the sampled water is centered on the analysis of inorganic ions in water as well as series of physico-chemical parameters controlling the interaction of these ions (Appelo & Postma, 1999). The parameters that control the interaction of these ions are alkalinity, electrical conductivity (EC), oxidation-reduction potential (Eh), pH, temperature, and total dissolved solids (TDS).

For all thermodynamic calculations, temperature is one of the fundamental keys required (Appelo & Postma, 1999). In addition, it is needed for modifying pH and electrical conductivity measurements. In this study, the temperature was measured as close to in situ settings using a temperature probe which was a component of the pH meter used.

Electrical Conductivity (EC) is relative to the number of dissolved ions present in solution and provides a general idea of the total dissolved solids (TDS) (Appelo & Postma, 1999). EC is normally measured in milli siemens per meter ($1mSm^{-1} = 10\mu Scm^{-1} = 10\mu mhoscm^{-1}$) but for this study, EC values were recorded in μScm^{-1} and TDS was recorded in milligram per liter using TDS/EC probe.

One of the most essential field parameters is pH. This is because it controls most of the organic and inorganic constituents in water and it is expressed as:

$pH = - \log (H^{+})$ ……. Eq (3.3) (Fisher, 2002).

pH measurements come in different methods and some of these methods are electronic meters, pH indicator paper, and liquid calorimetric indicators. In this research, a more complex meter designed for conductivity, temperature, salinity, and pH measurement was used. This meter attains an accuracy of ±0. 002 pH units. pH is essential because it will help identify the primary aggressive nature of the groundwater during chemical weathering of the underlying rocks (Hem, 2002). Hem (2002) recognizes the reaction of dissolved carbon dioxide with water as

one of the most important processes in establishing the pH of natural water. The author represented this with a three-step reaction expressed as:

H_2CO_3 (aq) ↔ CO_2(g) + HO(1) E q (3.4)

H^+(aq) + HCO_3^- (aq) ↔ H_2CO_3 Eq (3.5)

H^+(aq) +CO_3^{2-} (aq) ↔ HCO_3^- (aq) E q (3.6)

Equations (3.5) and (3.6) produce H^+ which influences the groundwater pH.

Prior to sampling, the probes used for measurement of the pH, temperature, salinity, electrical conductivity (EC), and total dissolved solids (TDS) were calibrated with a standard solution. A reference buffer solution of pH 4 and 7 was used to calibrate the pH meter. The conductivity probe was also calibrated against a standard solution made up of KCl of value 1480 µS/cm. The probe was calibrated each morning before field measurement. In addition, alkalinity (as bicarbonate) was determined on the field by titrimetric method (Figure 3.7 and Appelo & Postma, 1999) and the procedure used are outlined below. That is:

1. At each sampling point, 100 ml of the sampled water was transferred with a volumetric pipette into a conical flask.
2. Two to three drops of phenolphthalein and methyl orange indicator was added to the water sample in the conical flask and shaken.
3. During shaking, the water sample that turned red or pink had its alkalinity to phenolphthalein determined by titrating that sample against hydrochloric acid until the colour disappears.
4. In the same way, the water sample that turned orange during shaking, without the addition of hydrochloric acid, had its total alkalinity zeroed.
5. The water sample that turned yellow during shaking had the resulting solution titrated against hydrochloric acid until the first noticeable colour changed to orange.

Figure 3. 7: Determination of alkalinity (as HCO_3^-) on the field by titrimetric method

Equation of reactions occurring during titration was expressed as:

$HCl(aq) + HCO_3^{-1}(aq) \leftrightarrow CO_2(g) + H_2O(l) + Cl^-(aq)$ ……. Eq (3.7) {Appelo and Postma, (1999)}

From the equation above, 1 mole of HCl^- reacts with 1 mole of $HCO3^-$.

The mole ratio was 1:1. Hence, the concentration of $HCO3^-$ in millimol/l was obtained from the equation:

$$[HCO_3^-] = \frac{V_{T(HCL)}}{a} \times \frac{M_{(HCL)}}{a} \times 1000$$ Eq (3.8) {Appelo and Postma, (1999)}

Where $V_{T(HCL)}$ = total volume of HCl^- needed to titrate to a pH of 4.4

$M_{(HCL)}$ = Molarity of HCL

a = aliquot of extract in ml

The Molar Mass of HCO_3^- = 61

Hence $[HCO_3^-] = \frac{V_{T(HCL)}}{a} \times \frac{M_{(HCL)}}{a} \times 1000 \times 61$

$$= \frac{V_{T(HCL)} \times M_{(HCL)} \times 6100}{a}$$ Eq (3.9)

For quality control (QC) and quality assurance (QA) for the measurement of alkalinity on the field, a duplicate water sample was prepared and taken through the same mentioned procedures above after every 10 sampling points. The end point of the duplicate water sample was within plus or minus 0.1 ml. In addition, a control standard of 50 mg of $NaCO_3$/L was prepared and analyzed together with the water samples. The value of the control standard was plotted on a control chart after a day's work. From the charts, the values that fell outside the action limits (±α), were reanalyzed by visiting the site and resampling.

Calculation of results:

Phenolphthalein alkalinity as $CaCO_3$ (P) = $\frac{50{,}000 \times A \times N}{V}$ mg/L …….. Eq (3.10)

Total alkalinity as $CaCO_3$ (T) = $\frac{50{,}000 \times B \times N}{V}$ mg/L ……. Eq (3.11)

If, Phenolphthalein alkalinity (P) = 0, then, bicarbonate (HCO^-_3) is total alkalinity (T)

If, Phenolphthalein alkalinity (P) < ½ T, then, HCO_3^- equals the difference between total alkalinity (T) and 2 × Phenolphthalein alkalinity (P) (i.e. HCO_3^- = T-2P).

If, Phenolphthalein alkalinity (P) = ½ T, T or > ½ T, then, HCO_3^- = 0

Where, A = ml of hydrochloric acid solution added to obtain the phenolphthalein end-point of 8.3,

B = ml of hydrochloric acid solution added to obtain the methyl orange end-point of 4.5 pH

N = Normality of the mineral acid,

V = volume of water sample used.

3.2.6. Laboratory Analysis

3.2.6.1. Measurement of Calcium by EDTA (ethylenediaminetetraacetic acid or its salts) titrimetric method at the Laboratory of Nuclear Chemistry and Environmental Research Center, Ghana Atomic Energy Commission.

When EDTA (ethylenediaminetetracacetic acid or its salts) is added to water containing both calcium (Ca^{2+}) and magnesium (Mg^{2+}), it combines first with calcium and then determined directly with EDTA when the pH is made sufficiently high so that magnesium is largely precipitated as hydroxide. Several indicators that combine with calcium only gives colour change when all the calcium has been complexed by EDTA at a pH of 12 to 13.

For the determination of calcium in the surface water and groundwater samples using EDTA, titrimetric method, the following procedures were followed and that is:

1. The water samples were diluted to 50 ml, such that the concentration of calcium was about 5 to 10 mg.
2. 2.0 ml of NaOH solution was added to produce enough pH of 12.
3. 0.1 g of $CaCO_3$ indicator mixture was added to the solution.
4. The EDTA titrant was slowly added to the solution with continuous shaking until the colour changed from salmon to orchid purple.
5. The end point was checked by adding one or two drops of titrant in excess to make sure that no further colour change was observed.

In accordance to APHA, 2012, the concentrations of calcium in the water samples using EDTA was calculated as:

$$\text{Ca (mg/)} = \frac{A \times B \times 400.8}{ml \text{ of sample}} \quad \ldots\ldots\ldots\ldots\ldots\ldots \quad \text{Eq (3.12)}$$

Where A = ml of EDTA titrant used

$$B = ml \text{ of standard cacium soution} = \frac{ml \text{ of standard cacium soution}}{ml\ of\ EDTA\ titrant} \quad \ldots\ldots\ldots\ldots\ldots \quad \text{(Eq 3.13)}$$

For Quality assurance and quality control (QA/QC),

6. Blanks were analyzed after every batch of five water samples. Also, a control standard of 10 mg/l of Ca^{2+} was prepared and analyzed together with the water samples.
7. The values of the control standard were plotted on a control chart. From the chart, a fresh control standard was prepared and water samples with calcium content outside the action limit of ±3α was reanalyzed.

3.2.6.2. Measurement of Magnesium (Mg^{2+}) using Atomic Absorption Spectrometric (AAS) Method at the Laboratory of Nuclear Chemistry and Environmental Research Center, Ghana Atomic Energy Commission.

For the measurement of magnesium in the surface water and groundwater samples the following procedures were used:

1. The samples were first digested before using AAS to analyze the samples.

To digest the sample,

2. 5 ml of the water sample was measured in three replicates into TFM Teflon vessels of a microwave digester (ETHOS 900).
3. 6 ml of 65% concentrated HNO_3, 3 ml of 35% HCl and 0.25% H_2O_2 were added to each vessel containing the water samples.
4. The vessel was swirled gently to mix.
5. After the vessel was fitted vertically into a microwave digester and digested for 20 mins.
6. Once digestion was completed, the vessel containing the samples cooled in a water bath for 20 mins to reduce high temperature and pressure build up within the vessel.

To measure the surface water and groundwater samples using AAS,

7. The mixture in the vessel was transferred quantitatively into a volumetric flask and diluted to 20 ml with deionized water.

8. Each mixture was analyzed using VARIAN AA240FS Flame Atomic Absorption Spectrometer. This instrument searches for a particular element by focusing a beam of ultraviolet light at a specific wavelength through a flame and onto a detector.
9. The mixture was aspirated into a flame, followed by a light absorbance thus reducing its intensity.
10. The instrument measured change in intensity which was later converted to absorbance with the aid of a computer data system.
11. The amount of light absorbed was proportional to the number of atoms in the flame hence, the number of Magnesium ions in solution

For QA/QC,

12. The quality of the obtained results was assessed by checking the linearity of the Mg^{2+} calibration lines for the prepared standards.
13. Under ideal condition, a perfect correlation should be observed and a correlation of r^2 = 0.92 was observed for the surfaced water and groundwater samples.
14. A reagent blank ($HNO_3/HClO_4/H_2O_2$) was used to establish the method detection limit (MDL) for the water samples. In the analyses, seven replicates of the water samples were measured for Mg^{2+} content. Since the values for water blank was below the detection limits for magnesium, the detection limits of the instrument were taken as the detection limit for magnesium concentration (Table 3.1).

Table 3. 1: MDL for water sample

	Detection Limits	
Element	IDLs* (mg/L)	MDLs*water (mg/L)
Mg^{2+}	0.002	0.002

IDLs and MDLs water are the instrumental detection limit and method detection limit of the water samples, respectively.

The correctness of the methodology used was checked with Fluka, which is an analytical certified reference material (CRM) produced and certified in accordance with ISO/IEC 17025 and ISO Guide 34.

3.2.6.3. Measurement of Total Hardness by Ethylenediaminetetraacetic acid (EDTA) titrimetric method at the Laboratory of Nuclear Chemistry and Environmental Research Center, Ghana Atomic Energy Commission.

1. 25 ml of each surface water and groundwater sample was diluted to 50 ml using distilled water.
2. 1 ml of buffer solution was added to the diluted water sample.
3. Two drops of murexide indicator were added.
4. This turned the water to wine red colour.
5. The resulting solution was titrated instantly against EDTA.
6. The titration was carried out slowly with continuous stirring until the last colour (wine red) disappeared from the water

Calculation:

Total Hardness ($CaCO_3$) = $\frac{V1 \times S \times 1000}{V}\ mg/L$ ……. Eq (3.14)

Where,

S = mg $CaCO_3$ equivalent to 1 ml of EDTA titrant = 1mg $CaCO_3$

V = volume of the water sample in Ml

V_1 = Volume of the added EDTA.

For QA/QC procedures, please refer to QA/QC under calcium determination in the previous chapter.

3.2.6.4. Measurement of sodium and potassium using flame photometric method at the Laboratory of Nuclear Chemistry and Environmental Research Center, Ghana Atomic Energy Commission.

The levels of Na^+ and K^+ in the surface water and groundwater samples were determined by the flame photometric method, using the Sherwood 420 Flame Photometer (Sherwood, UK).

Preparation of the Masking agent

7. 100 mg L^{-1} Li (lithium) solution (masking solution) was prepared by dissolving 6.941 g of $Li_2SO_4 \cdot H_2O$ in double distilled water and diluted to the 1000 mL mark of a volumetric flask.

The masking solution is important because Na^+, K^+ and Li are Group one elements. Hence the addition of Li is to mask other Group one elements [Rubidium (Rb), Cesium (Cs) and Francium (Fr)] that may be present in the water samples except Na^+ and K^+.

To prepare standard (*Mixed Na/K calibration standard) solution*

8. A 100 mg L-1 mixed Na^+ and K^+ calibration standard was prepared by pipetting 1 mL of commercially-available stock Na standard and 1 mL of commercially-available stock K^+ standard in a 10 mL volumetric flask and then diluted to the 1000 ml mark of a volumetric flask.

To calibration the flame photometer

9. 2 mL volume of the masking solution was added to 5 mL of the mixed Na^+ and K^+ standard and mixed thoroughly by swirling.
10. The combined solution was aspirated into a liquefied petroleum gas (LPG)-fed flame of the Sherwood 420 Flame Photometer.
11. The concentrations of Na^+ and K^+ were respectively read.
12. This was followed by the analysis of the blank solution and the water samples subsequently.

To analysis the water samples

13. A blank solution made up of 5 ml of doubled distilled water and 2 ml of masking solution were aspirated with a liquefied petroleum gas (LPG)-fed flame of the Sherwood 420 Flame Photometer.
14. After analysis of the blank, Na^+ and K^+ contents in the water samples were determined through the procedure below.

The procedure for the analysis of the water samples are as follows:

15. 5 mL volume of the water samples were transferred into 10 mL test tube and 2 ml of masking solution was added.
16. The mixture was homogenized by shaking for about one minute.
17. The homogenized solution was aspirated into the flame of the photometer.
18. Na^+ and K^+ content was read and recorded.
19. In instances where Na^+ or K^+ content is high and had to be diluted, the results was calculated as:

K^+ or Na^+(mg/L) = (mg/L K^+ or Na^+ aliquots) * D …… Eq (3.15)

Where D= dilution ratio expressed as

$$\frac{ml\ of\ sample + distilled\ water}{ml\ of\ sample} \quad \text{……..Eq (3.16)}$$

For QA/QC,

20. Duplicate water samples were analyzed after every batch of five water samples.
21. The prepared standard for sodium and potassium and the masking solution were read after every batch of five samples.
22. 5 mg/L of Na^+ or K^+ control standards were prepared and analyzed together with the water samples.
23. The value of the control standard was plotted on a control chart, and the values that fell outside the action limits (±3σ), were reanalyzed by preparing a fresh control standard.

3.2.6.5. Measurement of Chloride (Cl^-) by MOHR Ajentometric Method at the Laboratory of Nuclear Chemistry and Environmental Research Center, Ghana Atomic Energy Commission.

In neutral or slightly alkaline solution, potassium chromate can indicate the endpoint of silver nitrate titration of chloride. Silver chloride is precipitated quantitatively before red silver chromate is formed.

$AgNO_3 + NaCl \rightarrow AgCl + NaNO_3$……. Eq (3.17)

$AgNO_3 + K_2CrO_4 \rightarrow Ag_2CrO_4 + KNO_3$……. Eq (3.18)

For the determination of chloride content in the surface water and groundwater samples the following was used:

1. 25 ml of the water sample was filtered into a conical flask.
2. 2 drops of potassium chromate indicator (K_2CrO_4) were added and titrated against 0.0141 molar of $AgNO_3^-$ solution until an endpoint was reached where the colour changed from yellow to reddish brown.
3. In accordance with APHA 2012, the chloride ion concentration in the water sample was calculated as:

Cl^- (mg/L) = ((A-B)×N×35.450)/(mL of the water sample)……..Eq (3.19)

Where,

A = ml titration of the sample

B = ml titration of blank

N = Molarity of AgNO3

For quality control (QC) and quality assurance (QA), the following procedure was used:

4. Duplicate water samples were analyzed after every batch of five samples.
5. The end point of the duplicate water sample was within ± 0.1 ml.

6. The water samples were analyzed together with a control standard of 20 mg/L prepared from NaCl stock solution.
7. The value of the control standard was plotted on a control chart and the values that fell outside the action limits (±3σ) were reanalyzed by preparing a fresh control standard.

3.2.6.6. Measurement of Phosphate using a UV –visible Spectrophotometer at the Laboratory of Nuclear Chemistry and Environmental Research Center, Ghana Atomic Energy Commission.

In this study, the phosphate content in the water sample was measured using a Shimadzu UV-1201 UV- Visible Spectrophotometer with a wave length of 880 nm. The methodology used for the determination of Phosphate was based on the Official Method 4500-P E (Ascorbic acid method) in the Association of Official Analytical Chemists (AOAC International, 2007).

Principle

Potassium antimonyl tartrate and ammonium molybdate react in an acid medium with orthophosphate to form antimonyl-phosphomolybdate complex. This is reduced to intensely coloured molybdenum blue by ascorbic acid. The absorbance of the molybdenum blue is measured at a wavelength of 880 nm on a UV-visible spectrophotometer.

Instrumentation

A Shimadzu UV-1201 UV-visible Spectrophotometer (Japan) with 1 cm matching quartz cells was used for phosphate absorbance measurements.

Chemicals Used

Ammonium heptamolybdate [$(NH4)_6Mo_7O_{24}\cdot 4H_2O$], Potassium antimonyl tartrate [$K(SbO)C_4H_4O_6.5H_2O$], Sulphuric acid (96% H_2SO_4) and Ascorbic acid.

Reagents

Potassium antimony tartrate [$K(SbO)C_4H_4O_6$ ½H_2O].

Procedure Used

1. 500ml potassium antimony tartrate solution was prepared by dissolving 1.375 g of $K(SbO)C_4H_4O_6$ ½H_2O in about 400ml double distilled water and diluted to 500ml.
2. The solution was stored in a glass-stoppered bottle.
3. 500 ml ammonium molybdate [$(NH_4)_6Mo_7O_{24}$ ·$4H_2O$] solution was prepared by dissolving 20 g of ammonium molybdate in double distilled water and then diluted to the 500 ml mark of the conical flask.
4. 0.1 M ascorbic acid solution was prepared by dissolving 1.76 g ascorbic acid in double distilled water and diluted to the 100 ml mark of a conical flask.

Since ascorbic acid solutions are not stable for longer periods of time at room temperature, it is advisable to always prepare them fresh due to its stability for four hours.

5. 100 ml combined reagent consisting of an acidic (H_2SO_4) solution of potassium antimony tartrate, ammonium molybdate and ascorbic acid was freshly prepared by adding 50 ml of 5 M H_2SO_4 to a mixture of 5 ml potassium antimony tartrate, 15 mL of ammonium molybdate and 30 mL of ascorbic acid.
6. The mixture was allowed to attain room temperature after which it was vigorously mixed and stored in a plastic bottle.
7. After, a stock standard phosphate solution of 50 mg/L was prepared by dissolving 219.5 g of oven-dried potassium dihydrogen phosphate (KH_2PO_4) in double distilled water to make 1000 ml of stock solution.
8. Working solutions of 0.2, 0.4, 0.6, 0.8, and 1.0 mg/L were prepared daily by suitable dilution of the stock solution.
9. After, 10 ml aliquot of the calibrated stock solution was poured separately into 20 ml test tubes.
10. For each test tube with the calibrated solution, 2 mL of the combined reagent was added and then left for about 5 minutes.

11. During the 5 minutes, a blue colour was formed and that revealed the presence of antimonyl-phosphomolybdate complex.
12. Appropriate aliquot of each blue-coloured solution in each test tube was transferred into a 1 ml cuvette.
13. The cuvette with the solution was inserted into the spectrophotometer and set at a wave length of 800 nm.
14. The absorbance was measured against a reagent blank.
15. A calibration graph of absorbance against phosphate concentration in each calibrant solution was plotted. The concentration of phosphate in the water samples were deduced from a calibration graph.

For Quality assurance and Quality control (QA/QC) measurement for phosphate in the water samples the following procedures were used:

16. A control standard of 1 mg/L of phosphate was prepared and analyzed together with the duplicate water samples after every batch of five water samples.
17. The value of the control standard was plotted on a control chart, and a fresh control standard was prepared for re-analysis of samples that fell outside the action limits ($\pm 3\sigma$).

3.2.6.7. Measurement of Sulphate using a UV –visible Spectrophotometer at the Laboratory of Nuclear Chemistry and Environmental Research Center, Ghana Atomic Energy Commission.

Principle

The method used is based on the reaction of sulphate ion with barium chloride ($BaCl_2$) under acidic conditions to precipitate to barium sulphate (BaSO4). The absorbance of the white BaSO4 suspension is measured at a wavelength of 420 nm on a UV-visible spectrophotometer. Official Method 4500-SO_4^{2-} E (Turbidimetric method) is used for the determination of sulphate (AOAC International, 2007).

Instrumentation

A Shimadzu UV-1201 UV-visible Spectrophotometer (Japan) with 1 cm matching quartz cells was used for absorbance measurements.

Chemicals

Barium chloride ($BaCl_2$, 99.999%), Sodium chloride (NaCl), Hydrochloric acid (HCl), Sodium sulphate (Na_2SO_4) and Glycerol.

Reagents

For the preparation of acid salt solution, the following procedures were used:

1. 60 g of NaCl was dissolved in 5 ml of 37% HCl and diluted to 250 ml mark of a volumetric flask with double-distilled water.

For the preparation of sulphate standard, the following were used:

2. 100 mg/L stock standard sulphate solution was prepared by dissolving 0.1479 g of anhydrous Na_2SO_4 in double distilled water to 1000 ml.
3. Working solutions of 15, 20, 25, 30 and 35 mg/L concentrations was prepared daily by appropriate dilution of the stock.

For calibration the following were used:

4. 10 ml of the standard sulphate calibrants solutions was quantitatively transferred into separate test tubes.
5. To each test tube, 1 ml of acid salt solution, 0.5 ml of concentrated glycerol solution and 0.5 g $BaCl_2$ were added.
6. The resulting cloudy solution was shaken for 60 seconds and left for 5 minutes.
7. Appropriate aliquot of the cloudy solution was transferred into 1 cm cell and the absorbance of the coloured solution was measured at a wavelength of 420 nm on the UV-visible spectrophotometer.

8. The absorbance of each calibrant solution was plotted against the concentration of the calibrants.
9. A straight-line graph was obtained.
10. The concentration of the water samples was deduced from the graph after measurement of the absorbance of each water sample at a wavelength of 420 nm on the UV-visible spectrophotometer

For the Measurement of Sulphate in the surface water and groundwater samples, the following was used:

11. 10 ml aliquot of the water sample was transferred into a 20 ml test tube and the same procedure as used for the establishment of the calibration graph was followed to obtain the absorbance of each water sample at a wavelength of 420 nm on the UV-visible spectrophotometer. The sulphate concentration of the water samples was deduced from the graph after measurement of the absorbance of each water sample at a wavelength of 420 nm on the UV-visible spectrophotometer.

For QA/QC measurement:

12. Duplicate water samples were analyzed after every batch of five water samples.
13. A control standard of 10 mg/L SO_4^{2-} was prepared and analyzed together with the samples.
14. The value of the control standard was plotted on the control chart and the values that fall outside the action limits (±3σ) was reanalyzed with a fresh control standard.

3.2.6.8. Determination of Nitrate (NO_3^-) at the Laboratory of Nuclear Chemistry and Environmental Research center, Ghana Atomic Energy Commission.

Principle

The method used is based on the reaction of the nitrate ion with brucine sulfate in a H_2SO_4 solution at a temperature of 100 °C. The yellow colour of the resulting complex is measured

at a wavelength of 410 nm. Nitrate was determined using AOAC Official Method 973.50 (AOAC International, 2007).

Preparation of standards

A stock standard nitrate solution of concentration 100 mg/L was prepared by dissolving 0.7218 g of KNO_3 (pre-oven dried at 105 ºC for 24 hours) in double distilled water to make 1000 ml of solution. The stock solution was preserved with 2 mL $CHCl_3$. Working calibrant solutions of concentrations 0.2, 0.4, 0.6, 0.8, and 1.0 mg L-1 were prepared daily by the appropriate dilution of the stock.

Preparation of reagents (Brucine-sulfanilic acid reagent)

1. 1 g of brucine sulfate $[(C_{23}H_{26}N_2O_4)_2H_2SO_4\ 7H_2O]$ and 0.1 g sulfanilic acid ($NH_2C_6H_4SO_3H\ H_2O$) were dissolved in 70 mL warm double distilled water.
2. 3 ml concentrated hydrochloric acid was added.
3. The resulting solution was cooled and diluted with double distilled water to 100 ml mark of a conical flask.
4. The prepared reagent was stored in a dark bottle at 5 °C.

Calibration

7. 5 ml of each calibrant solution was pipetted into separate 20 mL test tubes.
8. To each test tube, 1 ml of 30% NaCl was added, followed by the addition of 5 ml of 6.5 M of H_2SO_4.
9. The test tubes with the solution were swirled to ensure thorough mixing of the reagents.
10. 0.5 ml of brucine-sulfanilic acid reagent was added to the content of each tube (except blank)
11. The test tubes with the solution were placed on a rack and lowered into a water bath at 95 ºC for 25 minutes.

12. An appropriate aliquot of the yellow coloured calibrant solutions was transferred into a 1 cm cell.
13. The cell was placed into the spectrophotometer and the absorbance of the solution was measured at a wavelength of 410 nm.
14. A standard graph of absorbance of standards against concentration of standards was plotted.

Measurement of Nitrate in the water samples

15. 5 ml aliquot of the water samples were transferred into separate 20 ml test tube and the same procedure as used for the establishment of the calibration curve was followed in order to obtain the absorbance of each water sample at a wavelength of 410 nm on the UV-visible spectrophotometer.
16. The concentration of nitrate in each water sample was deduced from the calibration graph.

The concentration of nitrate was calculated from the relation:

$$C_{NO_3^-} = C_{Calib.} \cdot D_f \quad \text{Eq (3.20)}$$

Where: $C_{NO_3^-}$ is the nitrate concentration, $C_{Calib.}$ is the concentration from the calibration curve and D_f is the dilution factor.

Measurement of QA/QC

17. Duplicate water samples were analyzed after every batch of five water samples.
18. A control standard of 0.5 mg/L nitrate was prepared and analyzed together with the samples. The value of the control standard was plotted on the control chart and those that fell outside the action limits (±3σ) were reanalyzed with a fresh prepared control standard.

3.2.6.9. Measurement of Silica in surface water and groundwater at SGS Laboratory in Tema, Ghana

1. 2 ml ammonium molybdate reagent and 1.0 ml 1-1 HCl were added to 50 ml of the water sample in rapid succession.
2. This was mixed by reversing at least six times and allowed to stand for five to ten minutes.
3. 2 ml oxalic acid solution was added and mixed thoroughly.
4. The colour was read after 2 minutes at a wave length of 410 nm.
5. To correct for turbidity and colour, a blank was prepared by adding hydrochloric acid and oxalic acid without the addition of molybdate reagent.
6. Thermo Scientific* Aquakem 250 Photometric analyzer was adjusted to zero absorbance with the blank containing no molybdate before reading absorbance of molybdate-treated samples.
7. Silica concentration in the water sample was directly determined from the calibration curve of the photometer.

For quality control (QC) and quality assurance (QA), blanks were analyzed after every batch of 5 water samples. Additionally, a control standard of 10 mg/L of Silica was prepared and analyzed together with the samples.

3.2.6.10. Measurement of Arsenic (As) in the water samples at the Laboratory of Nuclear Chemistry and Environmental Research Center, Ghana Atomic Energy Commission.

Instrumentation for Arsenic (As) measurement in the water samples

Total arsenic (As) was determined using the HG-AAS technique. The HG-AAS system consist of an AA 240FS fast sequential Atomic Absorption Spectrometer (with a deuterium background corrector) equipped with a VGA-77 vapor generator (Varian, Australia). The Varian's Vapor Generation Accessory (VGA-77) employs a peristaltic pump to provide

continuous generation of flow vapor. The radiation sources involve the hollow cathode lamp of As (wavelength 193.7 nm; spectral slit width 0.5 nm; lamp current 10 mA) and the hollow cathode lamp of Hg (wavelength 253.7 nm; spectral slit width 0.5 nm; lamp current 4 mA) (Varian, Australia). ETHOS 900 microwave digester (Milestone, USA) is used for the sample water digestion.

Chemicals and Reagents for As measurement in the surface water and groundwater samples

All solutions was prepared from analytical reagent grade chemicals: Commercially available stock standard solution [(1000 ± 4 mg As L^{-1} in 2% (w/w) HNO_3, Trace CERT®, Fluka Chemie, Switzerland)], Commercially available stock standard solution [(999 ± 4 µg Hg ml in 1.4% (w/w) HNO_3, Spectrascan, Teknolab AB, Sweden], Sodium borohydride ($NaBH_4$), Sodium hydroxide (NaOH), Nitric acid (65% HNO_3), Hydrochloric acid (37 % HCl), Hydrogen peroxide (30%, H_2O_2).

Reagents

1. For As determination, hydride generation was performed with a 0.6% (w/v) $NaBH_4$ in 0.5% (w/v) NaOH as the reductive solution with 6 M HCl as the carrier solution.

Standards

Calibration standards for As (0.2, 0.4, 0.6 mg L^{-1}) was prepared daily by appropriate dilution of the respective commercial stock standard solutions for As. Digestion of the water samples for As measurement was done in accordance with standard procedures setup by Hoeing et al. (1998).

Experimental procedure

Digestion

Digestion of water samples was done according to the procedure described by Hoeing et al. (1998) and below is an outline of the procedures.

2. 6 ml of HNO_3 (65%), 3 mL of HCl (37%) and 0.25 ml of H_2O_2 (30%) were added to 5 ml of the water sample in a Teflon digestion tubes.
3. The tubes were covered tightly and placed in an ETHOS 900 microwave digester.
4. The water samples were digested using a four-step digestion procedure (Table 3.2).
5. At the end of the digetion, the digested water samples were cooled and transferred into a clean 25 ml volumetric flask.
6. The digested samples were diluted to 20 ml with double-distilled water.
7. To reduce all As^{5+} to As^{3+}, 4 ml of freshly prepared 5 M KI was added to the digested water samples
8. .This was followed by hydride generation and subsequent measurements using the Atomic Absorption Spectroscopy.

Table 3.2: Microwave digestion programme used for the digestion of the water samples

Digestion Step	Digestion Time (min)	Microwave			
		Power (W)	Pressure (bar)	Temperature 1 (°C)	Temperature 2 (°C)
1	5	250	100	400	500
2	1	0	100	400	500
3	10	250	100	400	500
4	5	450	100	400	500

Temperature 1 and temperature 2 represent, the initial and final digestion temperatures

Reduction of As^{5+} to As^{3+}

To reduce all As^{5+} to As^{3+},

9. 4 mL of freshly prepared 5 M KI was added to the digested solution.
10. This was followed by hydride generation and measurement by the atomic absorption spectroscopy.

Calibration

11. The HG-AAS system was calibrated with As standard calibrants (0.2, 0.4, 0.6 mg As L^{-1}) and the obtained absorbance were used for linear regression analysis (plot of absorbance against the concentration of the calibrants).
12. The concentration of As was deduced from the equation of the regression line.

Hydride generation and atomic absorption measurement

13. The continuous flow approach of an HG-AAS system was used to merge the water samples and the reagents.
14. The sample solution (flow rate 5 mL/45 sec) was mixed in a PEEK (polyetheretherketone) cross connector with both HCl (flow rate 5 mL/45 sec) and $NaBH_4$ (flow rate 5 mL/45 sec) solutions (both solutions pumped and added with the peristaltic pump) and pumped into the reaction coil.
15. During mixing, the tetrahydroborate ion, BH_4^- converts As (III) into a hydride (AsH_3).
16. The tetraborohydrate was hydrolyzed in the presence of HCl producing considerable hydrogen.
17. The gaseous hydride formed together with the hydrogen gas generated were separated from the liquid in the A-shaped gas-liquid separator component of the vapour generator, and then transferred with a flow of argon gas into a Perma-pure dryer and dried by a stream of nitrogen gas.
18. The liquid was released as waste and the gaseous hydride and excess hydrogen formed were swept out of the vapour generation vessel by an argon gas (flow rate 13.5 mL min^{-1}) into the AAS detection system.
19. In the detection system, AsH_3 was atomized in the air-acetylene flame (also fed by the excess hydrogen generated) aligned in the light path of As lamp in the atomic absorption spectrometer.

20. Absorbance measurements were recorded, and the concentration deduced from the regression line.

Calculation of Arsenic concentration

The concentration of As in each water sample was obtained from the equation of the regression line. The concentration of As in the water sample (mg L^{-1}) was done using the relation;

$$Conc_{As} = Conc_{calib} \times D_f \quad \text{Eq (3.21)}$$

Where: D_f is dilution factor, and $Conc_{calib}$ is the concentration from the calibration curve.

Where: D_f is dilution factor, and $Conc_{calib}$ is the concentration from the calibration curve. To ensure quality control (QC) and quality assurance (QA), blanks were prepared using the same procedure above.

3.2.6.11 Measurement of trace elements (Cu, Cd, Zn, Cr, Fe, Ni, Mn, Co, Pb, As and Al) in the water samples at the Laboratory of Nuclear Chemistry and Environmental Research center, Ghana Atomic Energy Commission.

Instrumentation, Chemicals and Standards

Instrumentation

Fast Sequential Atomic absorption spectrometer (VARIAN, AA 250 FS, Australia) was used for atomic absorption measurement (Fig 3.8) of trace elements in the water samples.

Figure 3.8: Fast Sequential Atomic absorption spectrometer (VARIAN, AA 250 FS, Australia) used for the analysis of trace elements.

Chemicals

The under-listed commercially available stock standard solutions of Cd, Cr, Cu and Fe were used: 1000 ± 4 mg Cd L^{-1} in 2% (w/w) HNO3, 1000 ± 4 mg Cr L^{-1} in 2% (w/w) HNO_3, 1000 ± 4 mg Cu L^{-1} in 2% (w/w) HNO_3, and 1000 ± 4 mg Fe L^{-1} in 2% (w/w) HNO_3 (Trace CERT®, Fluka, Chemie, Switzerland).

Atomic Absorption Measurement

The instrumental conditions used for flame atomic absorption spectrometric determination of Cd, Cr, Cu, Fe, Co, Pb, Ni and Zn were as follows:

1. the air-acetylene flame atomizer was made up of air as oxidant (flow rate: 13.50 L/min) and acetylene as fuel (flow rate: 2 L/min).

Calibration of atomic absorption spectrometer

2. The atomic absorption spectrometer was calibrated with calibration standards for the above-mention trace element.
3. The absorbances obtained were used to plot calibration graphs for each trace element.
4. After calibration, each element was determined by measurement of absorbances of the surface water and groundwater samples aspirated into the absorption cell.

Calculation of concentration

5. The concentration of each analyte in the water samples was calculated from the calibration curve for the analyte.
6. In cases where there was a dilution of water sample, the concentration deduced from the calibration graph was multiplied by a dilution factor to give the actual concentration of the analyte in the surface water and groundwater sample.

Quality Control and Quality Assurance

Validation of the analytical technique

Calibration Procedure

AAS as an analytical method for the measurement of trace metals is affected by many factors including the calibration and standards preparations procedure. The quality of the results obtained was assessed by checking the linearity for the calibration lines for standards prepared (Table 3.3). Under ideal condition this was supposed to give a correlation of unity($r^2 = 1$) each, but due to systematic and random errors encountered during measurements, the correlation of unity could not be perfectly met.

Table 3.3: The correlation coefficient of the calibration lines of the trace elements

Metal	r^2 (coefficient of correlation)
Fe	0.93
Cu	0.95
Zn	0.94
Pb	0.99
Cr	0.93
Cd	0.92
As	0.96
Mn	0.94

Analytical Method Detection Limit

Method detection limit (MDL) is the minimum concentration of analyte that can be recognized, measured and reported with 99% confidence that the analyte concentration is greater than zero. MDLs for trace metals varies based on the wavelength selected, the spectrometer configuration and operating conditions.

Reagent blank ($HNO_3/HClO_4/H_2O_2$) was used to establish the MDLs for each surface water and groundwaterwater sample. In the analyses, seven replicates of both samples were measured for each trace metal. Since the values for water blank was below the detection limits for the metals, the detection limits of the instrument for each trace metal was taken as detection limit for the metals (Table 3.4)

Table 3.4: MDLs for the water samples

	Detection Limits	
Element	IDLs* (mg/L)	MDLs*water (mg/L)
Fe	0.006	0.006
Cu	0.003	0.003
Zn	0.001	0.001
Pb	0.001	0.001
Cr	0.001	0.001
Cd	0.002	0.002
As	0.001	0.001
Mn	0.002	0.002

IDLs and MDLs of water are the instrumental detection limit and method detection limit of water respectively.

Validation with Reference Material

Fluka· Analytical is a certified reference material (CRM) produced and certified in accordance with ISO/IEC 17025 and ISO Guide 34. This CRM is used to check for the correctness of the methodology.

Recovery Test

For environmental studies, recoveries are expected to fall within the range of 80 to 115%, and the results obtained fell in this range (table 3.5). Thus, the recoveries range between 85.44 to 105.00%.

Table 3. 5: Percentage recoveries of the various metals analysed

Metal	CRM number for metals	Std.CRM* (mg/L)	Amount Recovered (mg/L) 1	2	3	Mean	Recovery (%)
Fe	16596	2.000	1.962	1.968	1.983	1.971	98.55
Cu	38996	2.000	1.978	1.980	1.989	1.982	99.12
Zn	18827	0.300	0.255	0.256	0.258	0.256	85.44
Pb	16595	1.000	1.936	1.900	1.908	1.915	95.73
Cr	02733	1.000	0.989	0.952	0.974	0.972	97.17
Cd	51994	0.500	0.498	0.490	0.502	0.497	99.33

CRM is standard solutions from the CRM (Fluka· Analytical) of each metal.

3.2.6.12 Measurement of trace elements (Cu, Cd, Zn, Cr, Fe, Ni, Mn, Co, Pb, As and Al) in the water samples at the Laboratory of Environmental, Informatics and Statistics, Ca Foscari University of Venice, Italy.

Instrumentation

Measurement of trace element in the water samples were also performed using ICP- MS (PerkinElmer® Optima™ 7000 DV ICP-OES instrument, Inc. Shelton, CT, USA) instrument equipped with winLab 32 for ICP Version 4.0 software for simultaneous measurement of all selected trace element wavelengths (Fig 3.9).

Figure 3. 9: ICP-MS used for the measurement of trace elements in the water samples.

Standards, chemicals and Certified Reference Material (CRM)

Working standards were prepared by using PerkinElmer NIST® traceable quality control standards for ICP or ICP-MS (N9300235, N9300233 and N9300234) as the stock standards. Calibration was done using three standards with each trace element represented by one standard. The calibration blank consists of ASTM® type one, acidified with nitric acid.

Two QC samples consisting of a continuing calibration blank (CCB) was prepared at the midpoint of each calibration. This was run to monitor the long-term solidity of the instrument and it was done after drawing of the calibration curves.

Preparation of standards were done in ASTM® type I water and Suprapur® nitric acid (Merck®, Germany) was used for the acidification of the standard. PerkinElmer Quality Control Check standards for ICP/ICP-MS (N9300233, N9300234 & N9300235) was used to prepare the quality control check standard solution. On a daily bases, working standards were prepared in polypropylene vials. This was done on the basis of volume-by-volume dilution. The solution was pipetted using Micro pipettes (Eppendorf®, Germany) with disposable tips. The above method was validated using several certified surface water and groundwater reference materials from high purity standards.

Internal Standards

2.5 mm Y was used to spike all solutions. A single element stock solution of Y 1000 ppm was used to make the spiking solution.

Sample Preparation

All the water samples were filtered through acid treated 0.45 µm mesh millipore disposable filters, into a pre-conditioned polyethylene – terephthalate (PET) bottle. The filtered water samples were acidified to pH less than 2 with ultra-purified 6mol/ L of HNO_3. It is then preserved at a temperature of 4°C. The concentration of the dissolved trace elements was analysed using ICP-MS.

QA/QC

Quality control standards were used to produce calibration curves, and the curves were used to evaluate the data for each surface water and groundwater sample. Blanks, reagents, and water samples were parallel measured six times. The average of the last three values were employed because the first three values were used to clean the pipe in order to prevent contamination by

the last water sample. Relative standard deviation (RSD) of the three results was computed and were seen to be less than 5% of all the analysed trace element content in the water samples.

3.2.6.13 Measurement of Stable Isotopes of Water (δ^{18} O and δ^{2} H) using Los Gatos Research instrument at the National Isotope Hydrology Laboratory of the Ghana Atomic Energy Commission.

Instrumentation

Determination of stable isotopes (δ^{2}H and δ^{18}O) composition in the water samples was accomplished using the Los Gatos DLT-100 Liquid-water Stable Isotope Analyzer [off-axis integrated cavity output spectroscopy (OA-ICOS) via laser absorption] (Los Gatos, CA, USA) (Fig 3.10). The equipment was made up of a laser analysis system, an internal computer, a CTC LC-PAL liquid autosampler (Sigma-Aldrich, USA), a small membrane vacuum pump, and a room air intake line that passes air through a Drierite column for moisture removal. The autosampler and the DLT-100 was connected to a ~1 m long polytetrafluoroethylene (PTFE) transfer line. A 1.2 µL microliter syringe (Model 7701.2N, Hamilton) was used to inject 0.75 µL of sample through a PTFE septum in the autosampler.

Figure 3. 10: Isotopic composition analysis (δ^{2} H and δ^{18} O) of the water samples using Los Gatos DLT-100 Liquid-water Stable Isotope Analyzer.

Reference Material

The validity of the isotopic composition analysis (δ^2 H and δ^{18} O) using the liquid-water stable isotope analyser was checked using the analysis of International Atomic Energy Agency (IAEA) reference material, GISP [(Water) (δ^2H VSMOW and δ^{18}O VSMOW)]. This reference material is also known as NIST RM 8536 and it is developed by the IAEA in cooperation with the United States National Institute of Standards and Technology (NIST).

Standards

Three secondary standards were used for the analysis: two calibration standards [prepared from IAEA reference material, GISP (Water; δ^2H VSMOW and δ^{18}O VSMOW)], and a control standard ('in-house' prepared).

Calibration standard 1: STD1 (WS1)-enriched: δ^2H = 2.10 ± 0.3Hg and δ^{18} O = 0.24 ± 0.03.

Calibration standard 2: STD2 (WS2)-depleted: δ^2H = -117.00 ± 1.0 and δ^{18} O = -15.55 ± 0.1.

Control standard 3: STD3 (CS2)-control: δ^2 H = -68.78 ± 0.6 and δ^{18} O = -9.6 ± 0.8.

Experimental procedure

The experimental procedure is according to the methods prescribed in the IAEA training course series 35 [IAEA laser spectroscopic analysis of liquid samples for stable hydrogen and oxygen isotopes], (IAEA, 2009). The procedure is as follows:

1. About 1 mL aliquot of each standard (in-house, working and control) and 1 mL aliquot of the water sample were quantitatively transferred into 1.5 mL autosampler glass vials using the 1000 µL Eppendorf disposable tip pipette.
2. 1.5 mL autosampler glass vials were capped with PTFE septum caps.
3. The samples and standards were arranged on a CTC LC PAL autosampler.

The arrangement of the samples and the standards on the autosampler was done with respect to the following procedure (IAEA, 2009):

4. A dummy sample (de-ionized water or tap water) was placed in the first position to prime the flow line.
5. The dummy vial was followed by three secondary standards (two calibration standards and a control standard); five water samples, followed by another set of the three standards.
6. The array of standards and water samples were repeated up to a maximum of six times (30 water samples) for a single run.
7. Each standard and sample were individually measured with six injections lasting about 25 minutes.
8. Measurement for each batch of 30 samples lasted for a period of 20 hours.
9. The measurement results for the last four of the six injections from each vial was averaged.
10. The measured and known δ values of calibration standards before and after each batch of five water samples was used for a linear regression to convert absolute isotope ratios to δ values.
11. The instrument was prone to give erratic results during the start of a run, the dummy sample used allowed the system to stabilize before the first standards were run on the liquid-water analyser (IAEA, 2009).
12. The arrangement of the vials in the CTC LC PAL autosampler was designed to overcome the effects of instrumental drift which could be significant during a daily run (IAEA, 2009).
13. The first two injections were disregarded because they were often less stable and the injections with the most potential for carrying a memory effect from the previous sample (IAEA, 2009).

3.2.6.14 Picarro Cavity ringdown spectrometer instrument for the measurements of stable isotopes ($\delta^{18}O$ and $\delta^{2}H$) at the Laboratories of Environmental, Statistics and Informatics, Ca Foscari University of Vernice, Italy.

Instrumentation and procedures

The instrument used was the Picarro L2130-I cavity ringdown spectrometer (Fig 3.11). The instrument was based on wavelength-scanned cavity ring down spectroscopy, and it was equipped with an autosampler. In this technology, light re-circulates severally through the sample, forming a very long operational path length of the water sample to work together with the light. The principle behind the instrument is that, it adopts time- based optical absorption spectroscopy of target gasses for the determination of $\delta^{18}O$ and δ^{2} H in the water samples. The isotopic standards used included SLAP2 (Standard Light Antarctic Precipitation- 2) and the isotopic reference standards VSMOW- 2 (Vienna Standard Mean Ocean Water- 2) obtained from NIST (National Institute of Standards and Technology) and IAEA (International Atomic Energy Agency). In obtaining the standards, all measurements were calibrated and normalized to VSMOW. The instrument had a precision of approximately ±0. 5‰ VSMOW for $\delta^{2}H$ and ±0. 10‰ VSMOW for $\delta^{18}O$.

For sample preparation, 2 ml of each surface water and groundwater sample was transferred into vials which had caps with a septa appropriate for use with the auto- sampler syringe. The transfer was done using a clean dry pasteur pipette. 2 µL of n- methyl-2 pyrrolidone (NMP) wash solvent, 2µL deionized water and 2µL of the water samples were used to wash the syringe once the autosampler is set. This is done before active measurement of each vial was taken. Also, six separate 2µL injection of the water samples in the vials were analysed after rinsing. The first three injection data were thrown away to reduce any probable contamination from previous water samples. This resulted in three isotopic measurements for each vial. The analytical method involved 25 vials (one for each water sample), a consistency standard in the middle enclosed by international standards, as well as the consistency standards. All these

formed the calibration line. Measurement of the water samples were fitted to the corresponding line for each group of 25 samples, one each for $\delta^{18}O$ and $\delta^{2}H$ measurements, creating the calibrated measurements. To assess variance and increase analytical confidence, a number of water samples were reanalysed. Standard deviations for each triplicate analysis were calculated using the equation:

$$SD = \sqrt{\sum \frac{(X-\mathcal{X})^2}{(n-1)}} \text{..... Eq (22)}$$

Where X is each measurement of the set, $\mathcal{X}$ is the statistical mean of the set, n is the number of samples. Dixons Q- test with 90% confidence level ($CL_{90\%}$) was used to evaluate possible data outliers and it's given by;

$$Qexp = \frac{X_2 - X_1}{X_n - X_1} \text{..... Eq(23)}$$

$Q_{exp} > Q_{crit}$ (reject outlier)

Where X_1 is the suspect value, X_2 is the closest value to the suspect, and $X_n - X_1$ is the range of the data.

Figure 3. 11: Picarro L2130-i used for the measurement of $\delta^{18}O$ and $\delta^{2}H$ in the water samples with its auto sampler.

The obtained isotopic composition values in the surface water and groundwater samples were passed through, a post-processing procedure expressed as:

$\delta=((Rs-Rstd)/Rstd) \times 1000$ ……. Eq 3.24

where Rs = the isotope ratio ($^{2}H/^{1}H$, $^{18}O/^{16}O$) of the sample

Rstd = the isotope ratio ($^{2}H/^{1}H$ or $^{18}O/^{16}O$) of the standard.

The above equation was used to compute the delta-scale (δ) values and it was done in accordance with Vienna Standard Mean Ocean Water (VSMOW). Delta values were expressed in parts per thousand (per mil ‰) deviation from the standard, however the global adopted standard for the measurements of deuterium and oxygen-18 was SMOW (Standard Mean Ocean Water) which later became the Vienna-SMOW (V-SMOW).

The oxygen-18 for V-SMOW is similar to that of SMOW but the deuterium content is 0.2‰ lesser. Thus, for all practical uses, SMOW and V-SMOW are considered identical since the accuracy of measurements is usually 1‰ and 0.1‰ for deuterium ($\delta^{2}H$) and oxygen- 18 ($\delta^{18}O$), respectively. When water changes state through vaporisation and condensation, isotopic fractionation occurs due to differences in vapour pressures and diffusion velocities in air of the different isotopic species of water (Sidle, 1998). The degree of isotopic fractionation is contrariwise in relation to temperature. There is seasonal change in the stable isotopic compositions of rainfall at a given area, with more depleted values occurring in the colder months. More depleted values are also seen at upper latitudes. Rainfall falling at higher elevations are more depleted than those falling at lower elevations; this final property is of specific utility in the hydrological cycle. Rainfall at continental locations is more depleted than those that fall nearer to the coast (Fritz & Fontes, 1980; Clark & Fritz, 1997). Under equilibrium condition, evaporation does not take place, that is in contrast to the condensation process. Also, the actual fractionation features are greater than the equilibrium values. When water undergoes evaporation, the lighter isotopic species ($1H^{2}$, ^{18}O) specially leave the surface, so the remaining

water becomes enriched in the heavier isotopic species ($1H^2$ ^{18}O or ^1H ^2H ^{18}O) (Kendal & McDonnell, 1998; Singh & Kumar, 2005).

The degree of enrichment depends on the relative humidity of the atmosphere, the temperature, and the hydrological balance of the surface water. The enrichment of $\delta^{18}O$ is about one order of magnitude less than that of δ^2H. An important process which controls the enrichment of the surface water is molecular exchange, which occurs between the atmospheric water vapour and the surface water. The δ^2H and $\delta^{18}O$ values of natural waters obey the general relation:

$\delta^2 H = a\delta^{18} O + d$ after (Criag, 1961b) ……. Eq 3.25.

For water which have not been subjected to evaporation, the value of a‘is 8 and the average global value of d for precipitation is 10. The deuterium excess (d), the intercept of the Global meteoric water line (GMWL) is defined as:

$d = \delta^2 H - 8\delta^{18}O$ (Dansgaard, 1964) ……. Eq 3.26

Therefore, in this study, the results of the isotopic composition of rainfall samples were separated into dry season samples and wet season samples, and regression lines for each season was obtained using eq 3.18. The regression line for each season was used as reference lines in discussing the isotopic composition in both surface water and groundwater on the $\delta^2H/\delta^{18}O$ diagram illustrated in chapter 4.

3.2.6.15. Measurements of Tritium (^3H) in the water samples conducted at the Laboratory of Geology, University of Trieste, Italy.

Tritium activity measurement involves two major parts. In the first part, tritium in the water samples was pre-concentrated using electrolytic enrichment. After, the samples were distilled to a conductivity value of 25 µS/cm. The distillation was done to remove impurities which may cause corrosion of the electrodes. During the electrolytic process, which was the second part, two grams (2g) of peroxide were added to the water samples in 500 ml standard glass flask.

After, the solution was poured into an electrolytic cell, weighed and the initial mass of water (Wi) recorded. After, the electrolytic cell with the solution was subjected to electrolysis resulting in the release of O_2 and H_2 at the cathode and anode, respectively. After electrolysis, the cells were weighed, and the final mass of water was recorded as Wf. Subsequently, the samples were transferred from the cell into a distillation flask, neutralized with 8g of $PbCl_2$, and subjected to final distillation. A mixture between the final distillates and a cocktail was poured into polyethylene vials. The vials, together with two dead water (water without tritium) and two standards were placed on the Liquid Scintillation Counter (LSC) for tritium activity measurement. This was done to estimate the tritium enrichment parameter and the calibration of the equipment. All the tritium samples, numbering 57 was analyzed at the Department of Geology, University of Trieste, Italy.

The above methodology for the measurement of tritium in the water samples was illustrated below:

$$Wi = Wcf - Wce \quad \ldots\ldots\ldots\ldots \quad \text{Eq 3.27.}$$

Where W_i = initial weight of the sampled water

W_{cf} = weight of the empty cell plus the sampled water

W_{ce} = weight of the empty cell

During electrolysis of the empty cell plus the sampled water, the reactions taking place at the various electrodes are expressed as:

Anode: $2OH^- \rightarrow H_2O + 2e + 1/2\ O_2$ ..... Eq 3.28

Cathode: $2H_2O + 2e \rightarrow 2OH^- + H_2$ ..... Eq 3.29

Overall reaction: $2H_2O \rightarrow 2H_2 + O_2$ ..... Eq 3.30

After electrolysis, the final weight of the cell plus water was expressed as:

$W_f = W_{cf} - W_{ce}$ ..... Eq 3.31

The enrichment parameter (P-Factor) was expressed as;

$$P = \frac{(Wi-Wf)\ In\ (E)}{\frac{Q}{2.975}\ In\ (\frac{Wi}{Wf})} \quad \text{…….. Eq 3.32}$$

Where P = average of spike values

E = enrichment factor

Q = total charge in Ah.

The enrichment factor for the tritium is expressed as:

$$E = \exp\left(\frac{P'avg}{Wi-Wf}\right) In\ (\frac{Wi}{Wf}) \quad \text{…… Eq 3.33}$$

3.2.7. Validation of Data

Prior to data analysis, an ionic balance of each water sample was evaluated for checking the analytical results. The ionic balance equation per Freeze and Cherry (1979) was given as:

$$Ionic\ Balance = \frac{(Sum\ of\ cations - Sum\ of\ anions)}{(Sum\ of\ cations + Sum\ of\ anions)} \times 100 \text{ ……..} \quad \text{Eq (3.34)}$$

IBE (Ionic balance error) for the groundwater in the study area was calculated on the bases of ions expressed in mill equivalent per liter for analytical precision for cations and anions measurement. The calculated IBE values for each sampled groundwater are shown in Appendix 15 to 19. The IBE value of the sampled groundwater was within a limit of ±15 % and this was probably due to the omission of constituents such as nutrients, organic anions, and trace elements. These constituents might possibly be a contributing factor to the higher ionic balances (Hem, 1985) recorded in fewer groundwater samples.

3.2.7.1 Treatment of Data

The data obtained from the laboratory analyses were examined using different statistical methods like standard deviation, skewness, kurtosis and mean. The skewness and kurtosis analyses were done to assess whether the sampled surface water and groundwater came from a normal distribution. Based on the skewness and the kurtosis, the statistical content found outside the range of -2 to + 2 and -7 to + 7, respectively were considered to depart significantly from normality.

The results of the field parameters, chemical data and trace element concentrations were compared to WHO (2011) guidelines for drinking water quality: First Addendum to the third Edition.

Pearson correlation between the measured cations, anions and trace elements in the surface water and groundwater were computed to know whether there was any significant linkage, which might reveal strong homology between the ions.

Principal Component Analysis (PCA) was not used to demonstrate the relationship between the cations, anions and trace elements in the water samples due to the limited data set for each sampling year. Gorsuch, 1983 recommended at least 100 samples for PCA analysis, and Hatcher, 1994 recommended that the sample size should be larger than five times the number of variables (p) for PCA analysis. Hence, instead of using PCA on the data set, Pearson correlation matrix, bivariate plots and other hydrogeochemical models were employed.

The spatial distribution of the physical data, hydrochemical data, trace elemental data and isotopic data were analysed and drawn using ArcGis 10.5 software and the drawing was done based on the topographical map of the study catchment. In addition, the static water levels were computed using Surfer 16.5 software. This was done to identify the general groundwater flow direction. Statistical data analyses performed on all measured variables in the dataset was done using Microsoft excel 2016 version.

3.2.7.2. Data analysis and interpretation

This section highlights the statistical analysis and various graphical forms used for the interpretation of the data set. The main analytical error determined was the charge balance error, which had been discussed in previous chapters. The statistical analyses used comprise minimum, maximum, mean, median etc. The major graphical forms used in the interpretation of the results were the chemical indices {water quality index, sodium absorption ratio (SAR), percent sodium (% Na), Wilcox diagram etc.} Ficklin diagram (Manjo et al., 2012;

Piper, 1944), diagram (Stiff, 1951), diagram (Gibbs, 1970) plots (Durov, 1948) diagram and mineral stability diagrams.

3.2.7.3. Spatial interpolation methods

Spatial interpolation is a numerical model that changes attribute dataset of sampling point into a surface map. This map replicates the spatial changes in a dataset throughout a study catchment. This model used in the generation of maps is a useful tool, which provides sensitive information for decision makers. In this model, there are several computational methods such as inverse distance weighted (IDW), Kriging, natural neighbour spine etc. Nevertheless, the IDW and the Kriging is the interpolation model used mostly in environmental studies. Hence, in this study, the most suitable interpolation tool that reflect the quantity and quality of water in the aquifer system was the IDW model. This was due to variability in the data set, distance between the sampling points and the number of surface water and groundwater available in the study area. Also comparing the performance parameters vis RMSE, R^2, RSS for both IDW and Kriging, it was seen that IDW gave a better idea of the prediction accuracy. The IDW model was therefore used to generate spatial interpolation maps for surface water and groundwater in this study.

3.3. Limitation of the Study

- This study should have covered the entire Tano Basin for all-inclusive and complete approach towards the characterization of the aquifers to aid in the understanding of the hydrogeology but due to limited funding, this PhD was restricted to the Lower Tano River Basin.
- The study could not access the ionic balances for the boreholes drilled in 2013. This is as a result of unavailability of equipment for the measurements of some hydrochemical parameters hence limiting the discussions for 2013 borehole samples.
- Due to limited funding, rainfall sampling was carried out from 2016 to 2018.

- Due to limited funding, measurement of silica in groundwater was carried out in few selected groundwater samples with respect to their closeness and sampling was done from 2014 to 2015, 2016 and 2017.
- Due to inadequate funding, Tritium measurement in the water samples was limited to few surface water and groundwater samples based on the basin topography.
- Due to inadequate maintenance, some of the boreholes which were sampled initially could not be sampled during subsequent field sampling. This was because the boreholes had collapsed and some were out of order.

CHAPTER FOUR

RESULTS AND DISCUSSIONS

In this section, the results for each specific objective are discussed.

4.1 Estimation of Aquifer Hydraulic Parameters

In this study, the first specific objective was to estimate the aquifer hydraulic parameters, but the depths and the yields are firstly discussed under this section. Table 4.1 contains descriptive statistics of the depths, yields and the computed aquifer hydraulic parameters of the boreholes developed across the Lower Tano River Basin from 2013 to 2015.

Table 4. 1: Descriptive statistics of aquifer parameters within the Lower Tano River Basin

Parameters	SC	b	K	SWL	T	D	Y
Number of samples	55	55	55	55	55	55	55
Mean	18.80	45.45	5.70	5.17	205.96	37.67	205.33
Standard Error	5.65	2.13	1.66	0.40	50.03	2.14	25.75
Median	7.47	48.50	2.00	4.09	84.13	41.50	155.00
Mode	N/A	53.50	N/A	18.50	N/A	20.00	300.00
Standard Deviation	30.41	11.46	8.91	4.26	269.41	15.42	185.71
Sample Variance	924.68	131.31	79.44	18.14	72580.75	237.75	34489.17
Kurtosis	7.48	**-0.07**	12.54	3.07	6.34	**-1.68**	2.73
Skewness	2.76	**-0.96**	3.17	1.70	2.28	**0.04**	1.56
Minimum	0.72	19.00	0.04	-0.80	1.73	18.00	10.00
Maximum	122.24	59.00	44.35	20.70	1219.70	62.00	800.00
Sum	545.28	1318.00	165.39	599.72	5972.91	1959.00	10677.00
Confidence Level (95.0%)	11.57	4.36	3.39	0.78	102.48	4.29	51.70

SC- Specific Capacity (L/min/m), b – Aquifer saturated thickness (m), K – Hydraulic conductivity (m/day), SWL – Static Water level (a.m.s.l), T – Transmissivity (m^2/day), D – Depth (m), Y – Yield (L/min).

4.1.1 Borehole depths

The depths of the newly developed boreholes range from 18 m to 62 m with a mean of 37.67 m. The shallowest depth is measured for a borehole developed at Bankanta, Twene and Agyeza in the aquifer of the Apollonian formation. The deepest depth is recorded for a borehole developed at Bamiankor in the aquifer of the Birimian Supergroup. A spatial distribution map of the borehole depths in the study area is drawn using Inverse distance Weighting (IDW) interpolation in ArcGIS 10.5 software (GIS Geography, 2020). From the interpolated map (Fig

4.1), it is observed that the deeper boreholes represented by shades of red is mostly found in the aquifer of the Birimian Supergroup with fewer representations in the aquifer of the Apollonian formation. The shallowest boreholes represented by shades of blue is dominant in the aquifer of the Apollonian formation. From figure 4.1, it is also seen that the depth (18 to 49.62) of the boreholes developed in the aquifer of the Apollonian formation were shallower than those developed in the aquifer of the Birimian supergroup.

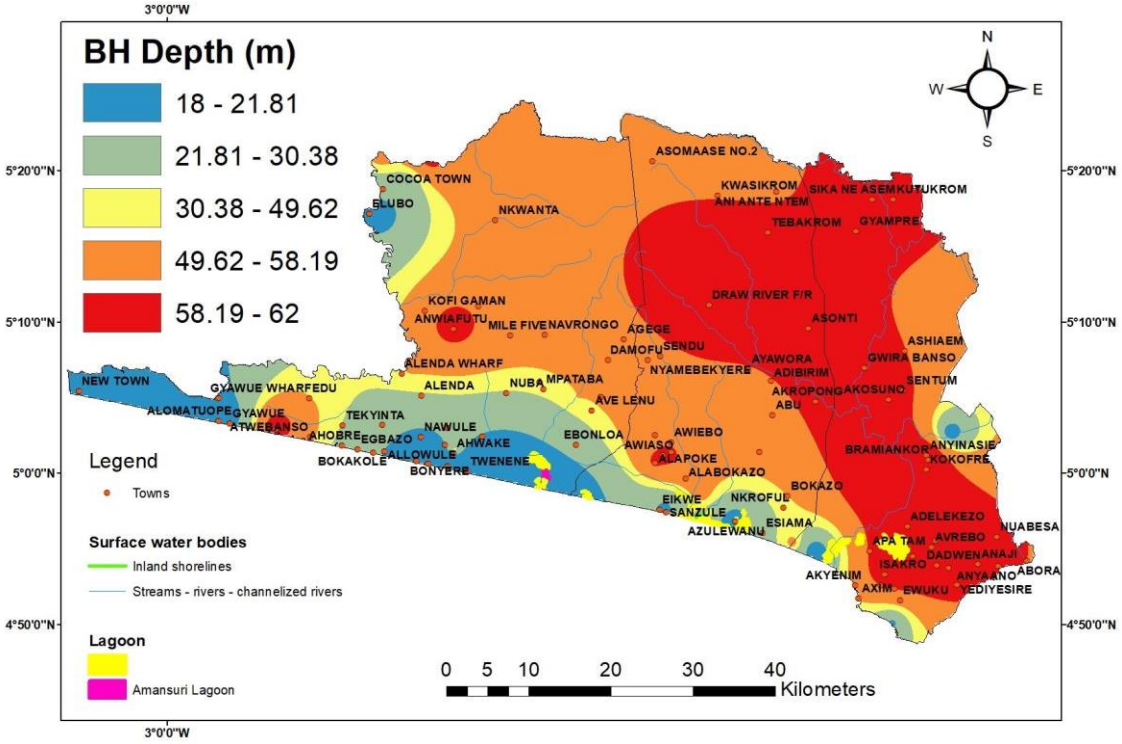

Figure 4. 1: Spatial distribution map of the borehole depths drawn using ArcGIS 10.5 Software.

4.1.2 Borehole Yields

The yields of the boreholes range from 10 l/min to 800 l/min with a mean of 205.33 l/min. The minimum yield of 10 l/min occurs in a borehole developed at Sameye Barrier 2 in the aquifer of the Birimian Supergroup and the maximum yield of 800 l/m happens in a borehole developed at Keenen and New town, both in the aquifer of the Apollonian formation. The yields of the boreholes in the study area are grouped into three yielding aquifers in accordance with Dike (1960) classification scheme. The aquifers are classified into low, medium, and high. The low yielding aquifer is described as an aquifer that can produce water between 10 l/min

to 50 l/min. Such an aquifer is characterized as extensively thick and inadequate for agricultural and industrial usage. The medium yielding aquifer is classified as an aquifer that has the capability of producing water between 50 l/min and 100 l/min. Such an aquifer is described as moderately thick and wide. Additionally, the zone of high yielding aquifer is defined as an aquifer that can produce water between 100 l/min and 300 l/min or more. Such an aquifer is categorized as thick and extensive. In accordance with the above classification, 17.65% (n=55) of the developed boreholes fall in the zone of low yielding aquifer and about 11.76% (n=55) of the developed boreholes falls in the zone of the medium yielding aquifer. The remaining 29.41% of the developed boreholes falls in the zone of high yielding aquifer.

From the above classification, it is established that the low yielding aquifer has unproductive bedrock and these are seen mostly in the aquifer of the Birimian Supergroup (Fig 4.2). The medium zone is a good aquifer whose bedrock is moderately productive, and this aquifer is possibly a characteristic of the Birimian Supergroup aquifer (Fig 4.2). This is possible because the rocks of the Birimian are highly fractured with low permeability and porosity. The zone of high yielding aquifer is described as an excellent aquifer with highly productive bedrock. This kind of aquifer is a characteristic of the Apollonian formation aquifer (Fig 4.2). The rocks of the Apollonian are unconsolidated, highly porous, and permeable.

The depths of the borehole are plotted against the yields (Fig.4.3) and the graph indicate that the depth of the boreholes developed in the aquifer of the Apollonian formation, and the Birimian supergroup are dependent on the yields.

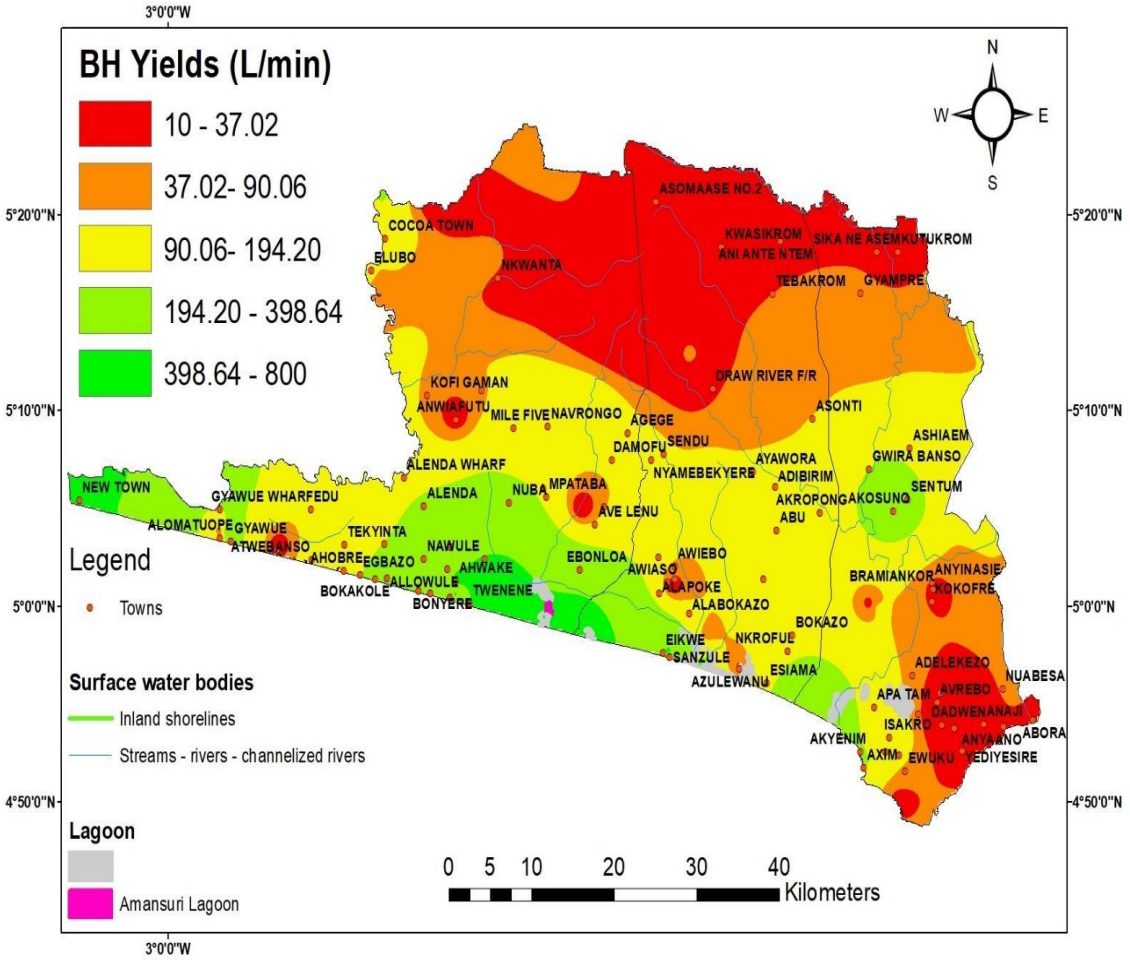

Figure 4. 2: Spatial distribution map of the borehole yields drawn using ArcGIS 10.5 software.

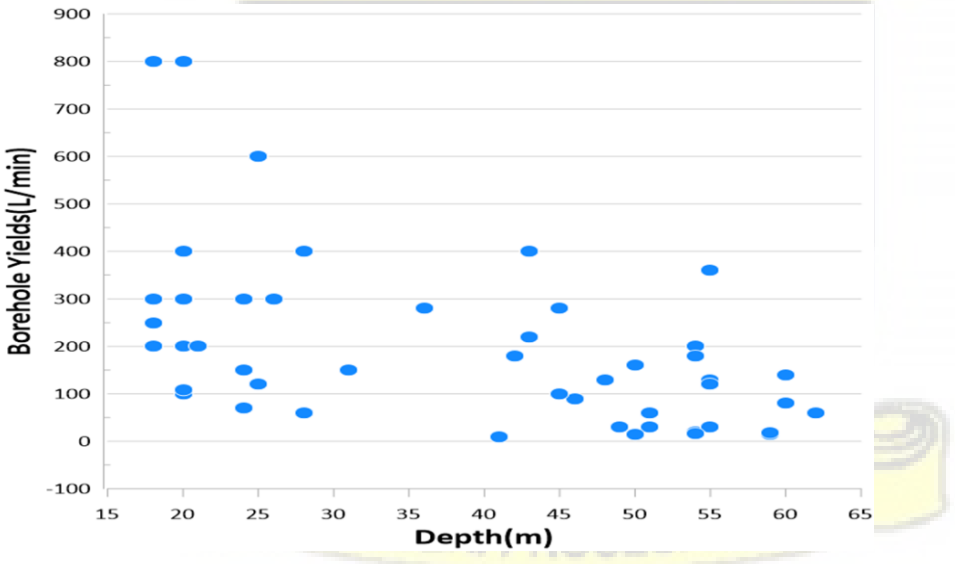

Figure 4. 3: Empirical relationship between the yield and the depth of the boreholes drilled in the aquifer of the Apollonian and the Birimian supergroup.

4.1.3 Groundwater Flow direction

The water levels vary from -0.8 a.m.s.l to 20.70 a.m.s. l, with an average of 5.17 a.m.s.l. All the water levels measured are above the average mean sea level (a.m.s.l), with the exception of a borehole developed in the aquifer of the Apollonian formation. In this borehole, the water level is below the mean sea level due to the acidity of the borehole water (pH = 5). The low pH of the borehole water aided in carbonate mineral dissolution (Hanshaw & Back, 1979) due to the existence of limestones in the rocks of the Apollonian formsation.

The groundwater flow direction as shown in Figure 4.4a and 4.4b are similar. Figure 4.4a and 4.4b shows the controlling factors affecting the groundwater flow direction of the study area. The groundwater is flowing in a downward direction from Northwest (NW), in a higher hydraulic head, towards south west (SE) closer to the sea. This indicates that the groundwater in the Lower Tano River Basin is likely flowing from topographically higher elevation to a lower elevation. Since the aquifer of the Apollonian formation is at a lower elevation, it might possibly be affected by leachates and pathogens.

A graph of hydraulic heads against the surface elevation gives an imaginary understanding of the aquifer behaviour (Figure 4.5) with a strong correlation of 0.98. Also, the slope (0.8) (Figure 4.5) and the direction of flow (Figure 4.4 a and 4.4 b) indicates that, the aquifer of the Birimian supergroup are likely a recharging zone whiles the aquifer of the Apollonian formation are likely a discharging zone.

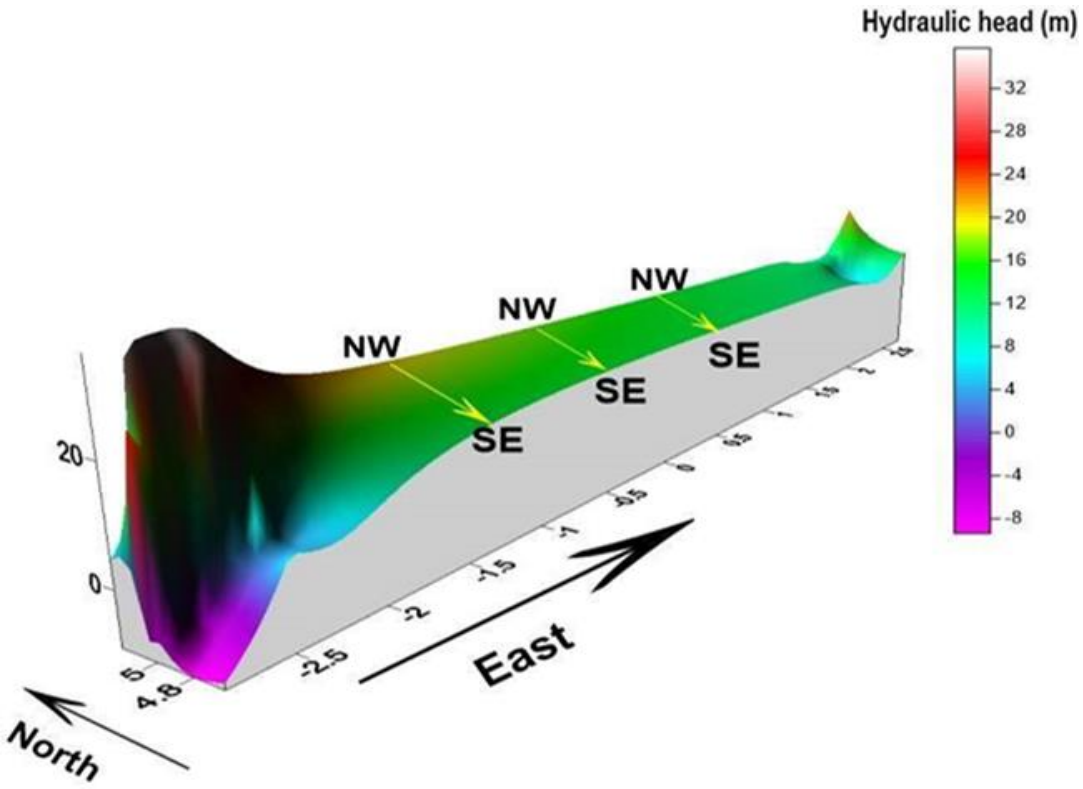

Figure 4.4a: Groundwater contour map of the study area in three dimensions.

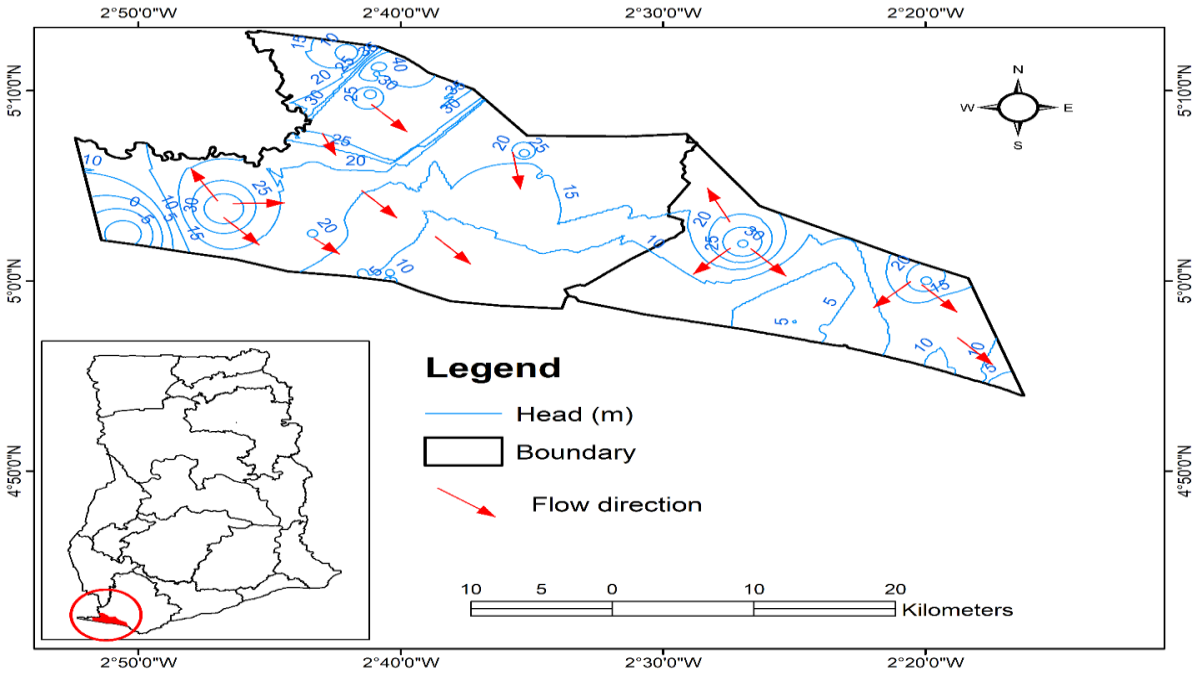

Figure 4. 4b: General groundwater flow direction of the study area

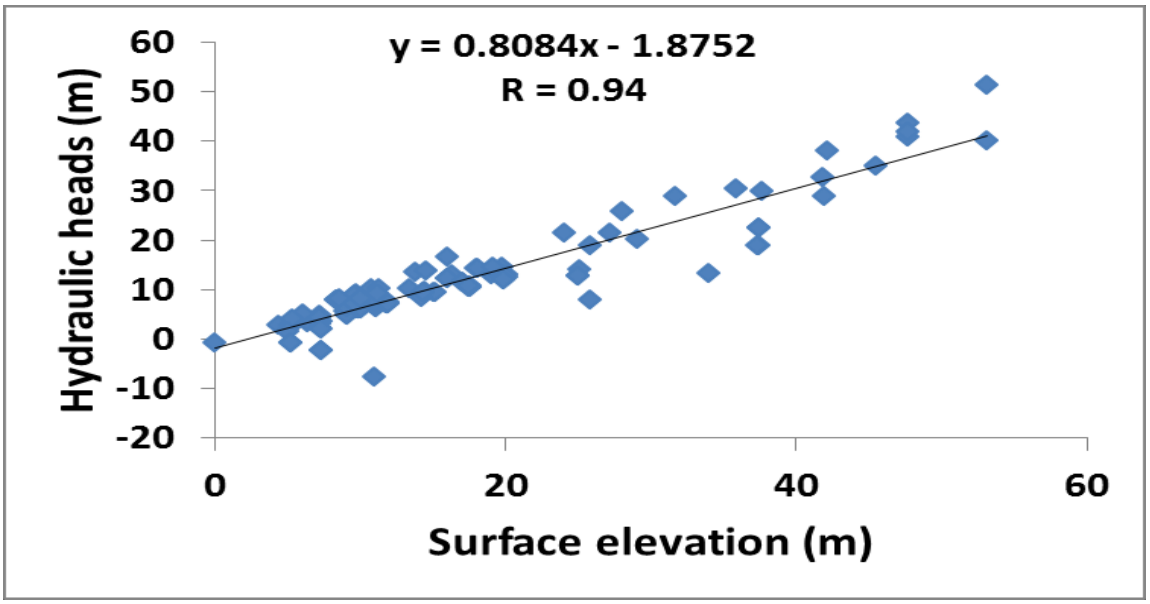

Figure 4. 5: Empirical connection between surface elevation and hydraulic heads.

4.1.4 Transmissivity

The rate of flow beneath a unit hydraulic gradient through a cross section of unit width and spreading over an entire saturated thickness of an aquifer defines aquifer transmissivity and the unit is m^2/day (Akhter & Hasan, 2016). In this study, the estimated aquifer transmissivity values range from 1.73 m^2/day to 1219.70 m^2/day with an average of 205.96 m^2/day. The average aquifer transmissivity value is high and this give an indication that the aquifer of the Apollonian formation and the Birimian supergroup within the Lower Tano River Basin are of good permeability. A borehole developed at Kwekukrom in the aquifer of the Birimian Supergroup records the minimum transmissivity (T) value of 1.73 m^2/day. The yield for the borehole was 14 l/min and the aquifer saturated thickness was 47 m. The geological formations observed during drilling contain mostly clay and schist and that might not allow the aquifer to transmit enough water due to its low porous nature.

A borehole developed at Sanzule in the aquifer of the Apollonian formation had the maximum transmissivity value of 1219.7 m^2/day. The yield for that borehole was 400 l/min and the aquifer saturated thickness was 27.5 m. The geological formation observed during drilling was weathered sandstone and clay particles. The observed geological formation indicates that the

Apollonian formation aquifer is highly porous, and its capable of yielding water and store water proficiently.

The computed transmissivity values for the newly developed boreholes are grouped per Driscoll (1989) classification. Driscoll (1989) stated that "An aquifer with transmissivity value less than 12.4 m^2 /day provides adequate amount of water for domestic use only". He likewise stated that, "An aquifer with transmissivity value of 12.4 m^2 /day or 10 times more was capable of supplying enough water for irrigation, domestic, and industrial uses". Per Driscoll (1989), classification, 20% of the groundwater sampled from the aquifer of the Apollonian formation and the Birimian super group are yielding enough water for domestic use only and the remaining 80% are yielding more water for domestic, irrigation and industrial uses.

An aquifer with least transmissivity (T<12) per Driscoll (1989), was described as an aquifer whose geological formations contain mostly clay or shale. For such an aquifer, low quantity of water is transferred from the aquifer and its only support domestic uses. Additionally, an aquifer with high transmissivity values (T>12) per Driscoll (1989), was characterized as am aquifer whose geological formation contain mostly sand. Such an aquifer produces large quantities of water, can support domestic, irrigational, and industrial uses. Even though, Driscoll (1989), classification was established for European apply countries where groundwater is in high demand, his classification can equally be used in the study area due to rise in population which might increase the growth of groundwater usage.

The spatial distribution map (Fig 4.6) for the estimated aquifer transmissivity values shows that transmissivity values ranging from 191.83 to 489.09 m^2/day, represented by shades of sea blue colour is dominant in the aquifer of the Birimian Supergroup with few representations in the aquifer of the Apollonian formation. Also, the least transmissivity values represented by shades of red are seen mostly in the aquifer of the Birimian Supergroup with few representations in the aquifer of the Apollonian formation.

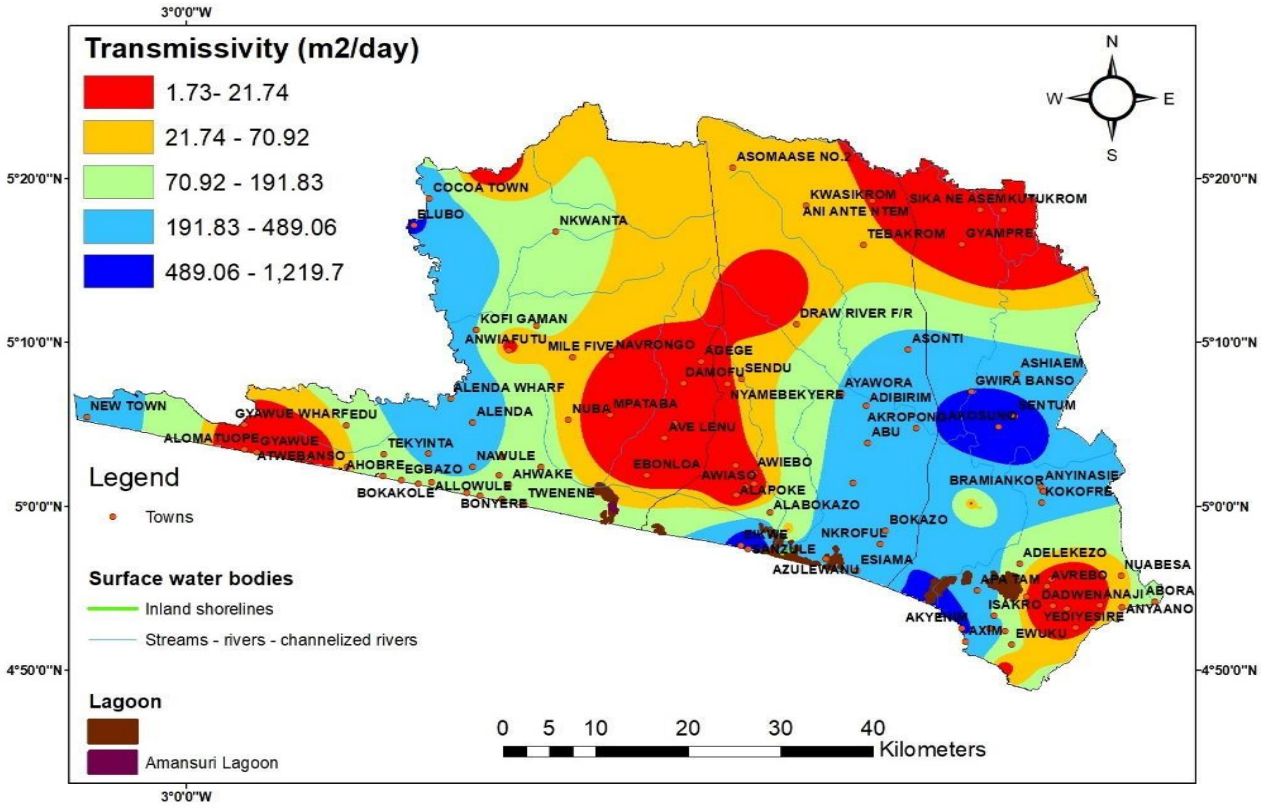

Figure 4. 6: Spatial distribution map of aquifer transmissivity values for the boreholes drilled in the major rock complexes of the study catchment.

4.1.5 Hydraulic Conductivity

Hydraulic conductivity (K) is the ability of a material to transmit water and its dependent on the porosity, pore shape and size, degree of sorting, the physical properties of the fluid as well as the usefulness of the interconnection between the pores (Akhter & Hasan, 2016). The estimated hydraulic conductivity (K) values for the drilled boreholes range from 0.04 m/day to 44.35 m/day with an average of 5.70 m/day. The borehole with the least hydraulic conductivity value is the same borehole with the lowest transmissivity value. Similarly, the borehole with the highest hydraulic conductivity content is the same borehole with the maximum transmissivity value. The K values for 96.7% of the boreholes are less than 25 m/day (Fig. 4.7). The observed geological formations during drilling give an indication that the aquifer of the Apollonian formation and the Birimian supergroup are likely to yield large quantities of water, which could support both the growing population and the industries (mining, coconut oil and gas). The maximum K values represented by shades of lemon green (Fig 4.7) covers a few portions of the aquifer of the Birimian Supergroup and the Apollonian formation.

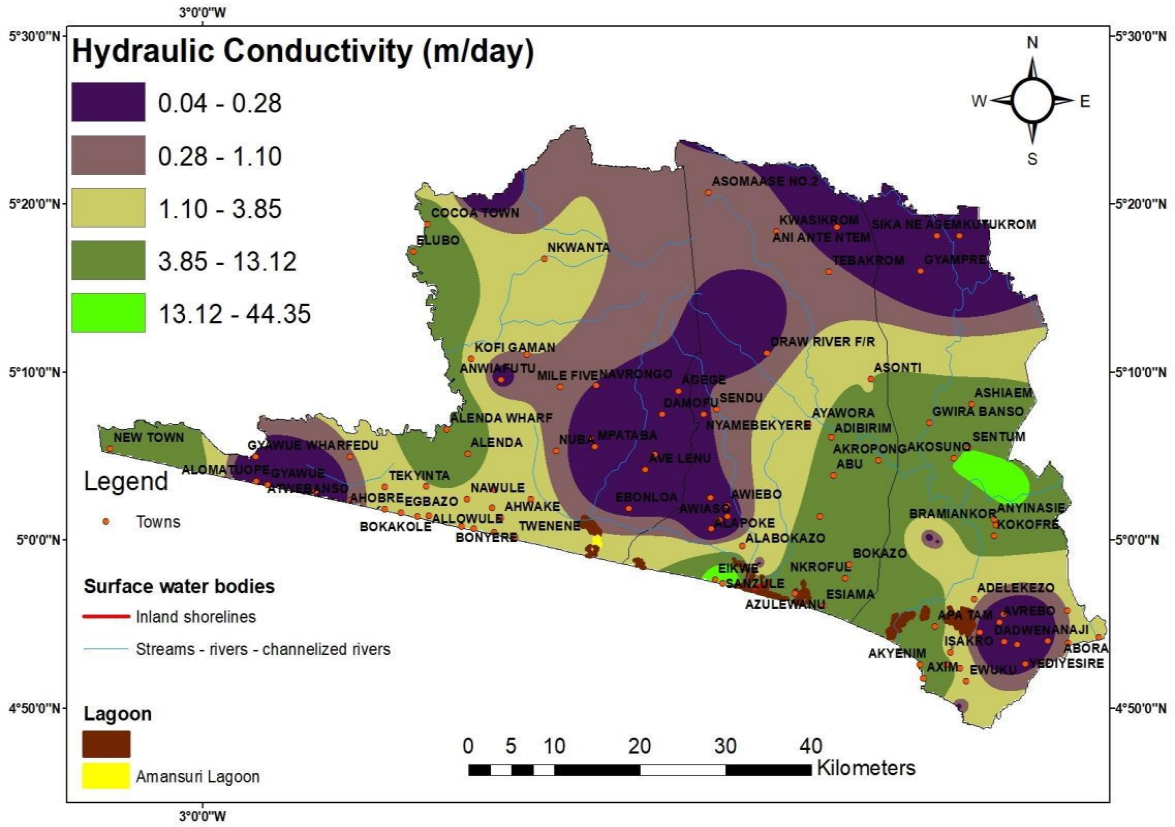

Figure 4. 7: A Spatial distribution map of the aquifer hydraulic conductivity values in the major rock complexes of the study area.

4.1.6 Specific Capacity

The specific capacity values range from 0.72 l/min/m to 122.24 l/min/m with an average of 18.80 l/min/m. The estimated specific capacity values of the boreholes, which is less than 12 l/min/m represented by shades of blue and ash colour covers mostly the aquifer of the Birimian supergroup with few representations in the aquifer of the Apollonian formation (Fig 4.8). This shows that part of the aquifers are less durable, slightly permeable, and yield enough water for domestic uses only (Johnson et al., 1966).

The specific capacity values within a range of 12 l/min/m to 17 l/min/m represented by shades of yellow colour are seen mostly in the aquifer of the Birimian Supergroup with few representations in the aquifer of the Apollonian formations (Fig 4.8). These aquifers are moderately permeable, yields limited quantity of water, and are productive and durable (Johnson et al., 1966). The specific capacity values for the boreholes greater than 17 l/min/m represented by shades of orange and red colour (Fig 4.8) are seen mostly in the aquifer of the

Apollonian formation. This aquifer is excellent, durable, highly permeable, and yields adequate amount of water for all socio-economic activities.

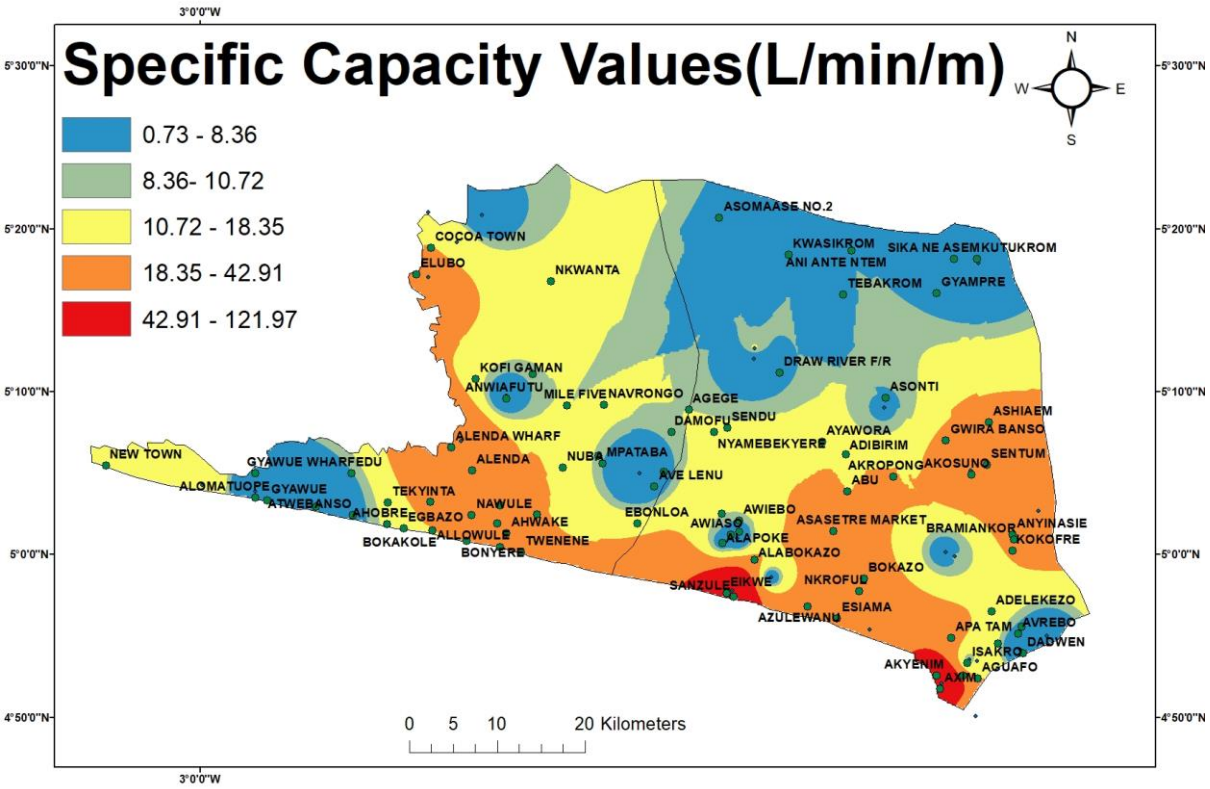

Figure 4. 8: Spatial distribution map of the aquifer specific capacity in the major rock complexes of the study area.

4.1.7. Sub-Conclusion

From the above discussed results, it is observed that the estimated aquifer hydraulic parameters are higher in the aquifer of the Apollonian formation due to high permeability and unconsolidated rocks. The attained results are like results accomplished by Water resources commission, 2012 for the Tano Basin as well as other areas outside the study location but in the same Birimian supergroup rocks (Asante-Annor & Ewusi, 2016; Ganiyu S et al., 2017; Asante-Annor, 2018).

4.2 Assessing the overall quality of surface water and groundwater together with the level of trace element contamination and groundwater suitability for domestic and agricultural purposes

Under this specific objective, the results of surface water quality, and groundwater quality and its suitability for domestic and agricultural purposes are discussed.

4.2.1 Surface water chemistry and its suitability for drinking

4.2.1.1 Results of the field data

The results of the descriptive statistical analysis of the field data for the sampled rivers and streams for each specific year are shown in Table 4.2 and Table 4.3.

Table 4.2: Descriptive statistical summary of the field data measured in the River samples (Sampling year: 2016 and 2017).

		2017						**2016**				
Parameter	TDS (mg/L)	EC µS/cm	Salinity (ppt)	pH	T(˚C)	TH (mg/L)	TDS (mg/L)	EC µS/cm	Salinity (ppt)	pH	T(˚c)	TH (mg/L)
Number of samples	14	14	14	14	14	14	9	9	9	9	9	9
Mean	650.21	972.79	1.01	6.10	27.81	124.90	74.11	110.37	0.01	6.58	25.93	48.20
Standard Error	518.61	735.54	0.65	0.21	0.76	96.02	24.72	36.90	0.01	0.17	0.32	24.43
Median	51.00	92.10	0.03	6.30	26.85	29.88	54.00	79.80	0.00	6.70	25.70	19.76
Standard Deviation	1940.46	2752.15	2.42	0.79	2.86	359.26	74.15	110.69	0.03	0.50	0.96	73.28
Sample Variance	3765384.18	7574309.70	5.85	0.63	8.16	129064.67	5498.36	12252.02	0.00	0.25	0.92	5370.37
Kurtosis	13.67	13.45	4.61	-1.52	2.48	13.89	7.54	7.57	9.00	0.13	1.18	8.06
Skewness	3.68	3.64	2.39	-0.32	1.83	3.72	2.68	2.69	3.00	0.06	1.26	2.80
Minimum	23.00	36.30	0.00	4.75	25.40	7.49	27.00	40.80	0.00	5.75	24.90	8.50
Maximum	7360.00	10460.00	7.58	7.02	34.20	1371.14	266.00	397.00	0.10	7.43	27.90	240.00
Sum	9103.00	13619.00	14.08	85.36	389.30	1748.65	667.00	993.30	0.10	59.18	233.40	433.82
Confidence Level (95.0%)	1120.39	1589.04	1.40	0.46	1.65	207.43	57.00	85.08	0.03	0.38	0.74	56.33

Table 4. 3: Descriptive statistical summary of the field data measured in the Stream samples (Sampling year: 2016 and 2017)

		2016						2017				
Parameter	TDS (mg/L)	EC µS/cm	Salinity (ppt)	pH	T(˚C)	TH (mg/L)	TDS (mg/L)	EC µS/cm	Salinity (ppt)	pH	T (˚C)	TH (mg/L)
Number of Samples	15	15	15	15	15	15	15	15	15	15	15	15
Mean	58.07	86.55	0.00	6.25	26.70	20.42	77.73	132.62	0.04	6.22	26.82	37.78
Standard Error	7.95	11.88	0.00	0.08	0.31	5.21	14.97	24.78	0.01	0.12	0.37	8.97
Median	46.00	68.20	0.00	6.30	26.80	14.84	62.00	111.30	0.03	6.30	26.30	21.87
Standard Deviation	30.79	46.00	0.00	0.31	1.20	20.17	57.96	95.97	0.05	0.45	1.41	34.73
Sample Variance	948.07	2116.17	0.00	0.10	1.43	406.97	3359.78	9209.41	0.00	0.20	2.00	1206.42
Kurtosis	2.16	2.16	0.00	-1.10	-1.22	5.80	0.20	0.13	4.36	0.30	3.24	1.37
Skewness	1.67	1.67	0.00	0.07	0.06	2.37	1.15	1.10	1.98	-0.34	1.77	1.51
Minimum	28.00	42.00	0.00	5.78	24.70	4.20	21.00	38.70	0.00	5.40	25.00	6.30
Maximum	132.00	197.30	0.00	6.75	28.50	80.93	195.00	346.00	0.20	7.10	30.60	115.13
Sum	871.00	1298.20	0.00	93.76	400.50	306.29	1166.00	1989.30	0.66	93.30	402.30	566.70
Confidence Level (95.0%)	17.05	25.47	0.00	0.17	0.66	11.17	32.10	53.14	0.03	0.25	0.78	19.23

From the above tables (Table 4.2 and 4.3), the pH of the rivers and streams sampled during the rainy season in 2016 ranges from 5.75 to 7.43 with a median value of 6.70 and a mean of 6.58, and from 5.78 to 6.75 with 6.30 as the median value and 6.25 as the mean value, respectively. Also, the pH in the 2017 (dry season) sampled rivers and streams varies from 4.75 to 7.02 with a median of 6.30 and a mean of 6.10, and from 5.40 to 7.10 with a median value of 6.30 and a mean value of 6.22, respectively.

The pH values for the rivers and streams sampled in 2016 and 2017 are acidic to neutral and are not close to the acceptable WHO (2011) pH value of 6.5 to 8.5 for drinking water. As such, they do not satisfy the standard requirement for domestic uses and aquatic life.

The total dissolved solutes (TDS) in the rivers and streams sampled in 2016 during the rainy season ranges from 27 to 266 mg/L with a mean of 74.11 mg/L and a median of 54 mg/L, and from 28 to 132 mg/L with an average of 58.07 mg/L and a median of 46 mg/L, respectively. In 2017 during the dry season, the TDS content in the sampled rivers and streams varies from 23 to 7360 mg/L with a mean of 650.21 mg/L and a median of 51 mg/L, and from 28 to 132 mg/L with a mean of 58.07 mg/L and a median of 46 mg/L, respectively. All the sampled rivers and streams for both years and seasons had TDS values below WHO (2011) permissible limit of 500 mg/L for drinking water, except the Ankobra River and Eleneano River which was sampled during the dry season.

Cañedo-Argüelles et al. (2013) stated that “Human activities such as water use, mining, industries and agricultural might increase TDS levels in water. From the above statement, agricultural practices are not rampant in the study area but gold mining especially illegal small-scale mining is rampant and most of these miners mine on most surface water or along the banks. This was evidenced during sampling especially the upstream section of the Ankobra river. Additionally, coconut oil industries (large and small) are rampant along the coast and some parts of the hinterlands especially Nkroful. Particles emanating from these

industries into the atmosphere might likely settle on surrounding surface water bodies (Eleanor River) through natural process like the harmattan winds. Since air monitoring was not carried out in this study, further investigations must be conducted to ascertain the true cause of the elevated TDS concentration in these two rivers.

The high TDS value for the Ankobra River is consistent with the TDS content measured in the Ankobra River in December 2011 by Edjah et al. (2015)

The electrical conductivity (EC) content in the rivers and streams sampled in 2016 varies from 40.80 to 397 µS/cm with a mean of 110.37 µS/cm, and a median of 79.80 µS/cm, and from 42 to 197 µS/cm with a mean of 86.55 µS/cm, and a median of 68.20 µS/cm, respectively. In 2017, the EC concentration in the sampled rivers and streams varies from 36.30 to 10460 µS/cm with a mean of 972.27 µS/cm, and a median of 92.10 µS/cm, and from 38.70 to 346 µS/cm with a mean of 132.62 µS/cm, and a median of 111.30 µS/cm, respectively. All the rivers and stream samples are below the WHO (2011) permissible limit of 1500 mg/L for drinking water, apart from Eleneano River and Ankobra River sampled from the rock of the Apollonian formation. The possible reasons accounting for the low and high TDS contents in the rivers and streams as discussed previously holds for the low and elevated EC values in the rivers and streams. There was no significant difference between the values obtained for the TDS and EC concentration in this current study and the previous study {Edjah et al. (2015)} for the rivers and streams, despite the 12 years gap between sampling and seasonal variability. The variation in pH, EC and TDS might be attributed to the seasons and time in which the samples were taken as well as human activities.

4.2.1.2 Results of the Laboratory Data and Alkalinity (as in Bicarbonate)

The results of the descriptive statistical analysis of the hydrochemical data for both sampled rivers and streams are summarized in table 4.4, 4.5, 4.6 and 4.7.

Table 4. 4: Descriptive statistical summary of the hydrochemical data for the Rivers sampled in 2016

Parameters	Ca^{2+} (mg/l)	Mg^{2+} (mg/l)	Na^{+} (mg/l)	K^{+} (mg/l)	Cl^{-} (mg/l)	HCO_3^{-} (mg/l)	SO_4^{2-} (mg/l)	NO_3^{-} (mg/l)
Number of samples	9	9	9	9	9	9	9	9
Mean	15.76	2.15	20.18	6.57	22.88	34.14	58.70	3.62
Standard Error	10.02	0.79	5.71	2.70	7.20	7.60	24.29	2.86
Median	5.02	1.41	13.20	2.01	17.99	26.82	30.00	0.71
Standard Deviation	30.07	2.37	17.14	8.10	21.61	22.81	72.87	8.59
Sample Variance	904.04	5.59	293.88	65.67	466.82	520.24	5310.20	73.78
Kurtosis	8.56	5.93	1.08	-0.19	5.43	1.83	7.83	8.96
Skewness	2.91	2.34	1.42	1.15	2.19	1.22	2.75	2.99
Minimum	2.03	0.42	4.47	0.30	6.00	9.75	17.85	0.39
Maximum	95.26	8.04	55.14	22.00	75.98	82.90	248.52	26.51
Sum	141.84	19.34	181.63	59.12	205.94	307.23	528.30	32.57
Confidence Level (95.0%)	23.11	1.82	13.18	6.23	16.61	17.53	56.01	6.60

Table 4. 5: Descriptive statistical summary of the hydrochemical data for 2016 Stream samples

Parameters	Ca^{2+} (mg/l)	Mg^{2+} (mg/l)	Na^{+} (mg/l)	K^{+} (mg/l)	Cl^{-} (mg/l)	HCO_3^{-} (mg/l)	SO_4^{2-} (mg/l)	NO_3^{-} (mg/l)
Number of samples	15	15	15	15	15	15	15	15
Mean	5.06	1.89	10.55	1.51	12.00	29.67	30.63	1.31
Standard Error	1.52	0.45	1.33	0.65	1.68	4.99	8.23	0.16
Median	2.87	1.37	9.73	0.68	10.00	24.38	34.10	1.27
Standard Deviation	5.89	1.75	5.14	2.54	6.50	19.32	31.87	0.64
Sample Variance	34.71	3.08	26.47	6.43	42.26	373.23	1015.72	0.41
Kurtosis	3.27	10.05	0.12	13.37	1.51	0.98	5.68	0.25
Skewness	2.06	2.95	0.85	3.59	1.40	1.25	1.93	0.28
Minimum	0.74	0.22	4.30	0.33	4.00	7.32	0.00	0.34
Maximum	19.63	7.75	21.29	10.47	27.99	75.59	126.56	2.56
Sum	75.95	28.32	158.23	22.67	179.94	445.00	459.50	19.59
Confidence Level (95.0%)	3.26	0.97	2.85	1.40	3.60	10.70	17.65	0.35

Table 4. 6: Descriptive statistical summary of the hydrochemical data for the Rivers sampled in 2017.

Parameters	Ca^{2+} (mg/l)	Mg^{2+} (mg/l)	Na^{+} (mg/l)	K^{+} (mg/l)	Cl^{-} (mg/l)	HCO_3^{-} (mg/l)	SO_4^{2-} (mg/l)	NO_3^{-} (mg/l)
Number of samples	14	14	14	14	14	14	14	14
Mean	8.68	25.07	46.08	10.28	272.06	51.38	30.18	0.62
Standard Error	4.06	20.90	26.34	5.90	233.75	17.04	15.57	0.05
Median	3.61	3.73	12.67	1.82	13.00	29.26	2.95	0.58
Standard Deviation	15.21	78.21	98.57	22.09	874.63	63.77	58.27	0.20
Sample Variance	231.26	6116.39	9716.55	487.95	764973.81	4067.23	3395.94	0.04
Kurtosis	12.04	13.95	12.30	10.65	13.72	9.23	2.91	0.80
Skewness	3.39	3.73	3.45	3.19	3.69	2.88	1.98	1.07
Minimum	1.19	1.10	4.99	0.19	4.00	7.32	0.00	0.40
Maximum	59.97	296.60	380.00	83.06	3298.94	256.03	181.15	1.07
Sum	121.47	350.98	645.08	143.88	3808.79	719.32	422.59	8.63
Confidence Level (95.0%)	8.78	45.16	56.91	12.75	505.00	36.82	33.65	0.11

Table 4. 7: Descriptive statistical summary of the hydrochemical data for the Streams sampled in 2017

Parameters	Ca^{2+} (mg/l)	Mg^{2+} (mg/l)	Na^{+} (mg/l)	K^{+} (mg/l)	Cl^{-} (mg/l)	HCO_3^{-} (mg/l)	SO_4^{2-} (mg/l)	NO_3^{-} (mg/l)
Count	15	15	15	15	15	15	15	15
Mean	5.28	5.97	10.28	2.26	13.33	31.70	14.68	0.50
Standard Error	1.09	1.57	1.57	0.71	2.86	7.32	6.41	0.10
Median	4.19	2.94	7.70	1.22	10.00	24.38	2.62	0.44
Standard Deviation	4.21	6.06	6.09	2.73	11.07	28.35	24.83	0.38
Sample Variance	17.70	36.75	37.03	7.47	122.59	803.51	616.74	0.15
Kurtosis	0.62	1.42	-0.28	3.90	9.56	7.76	3.15	-0.42
Skewness	1.32	1.52	0.90	2.05	2.89	2.61	1.93	0.45
Minimum	0.95	0.95	2.83	0.30	4.00	9.75	BDL	0.00
Maximum	14.56	19.25	23.23	9.88	49.98	121.92	82.30	1.26
Sum	79.27	89.55	154.26	33.93	199.94	475.48	220.16	7.55
Confidence Level(95.0%)	2.33	3.36	3.37	1.51	6.13	15.70	13.75	0.21

From the above tables (4.4, 4.5, 4.6 and 4.7), the calcium (Ca^{2+}) content in the rivers and streams sampled in 2016 varies from 2.03 to 95.26 mg/L with a mean of 15.76 mg/L, and from 0.74 mg/L to 19.63 mg/L with an average of 5.06 mg/L, respectively. In 2017 the calcium concentrations in the sampled rivers and streams varies from 1.19 to 59.97 mg/L with a mean of 8.68 mg/L, and from 0.95 mg/L to 14.56 mg/L with an average of 5.28 mg/L, respectively. All the calcium content recorded in the sampled rivers and streams for both years are all below WHO (2011) permissible limit of 75 mg/L for drinking water except the Ankobra River which was sampled from the rocks of the Apollonian during the rainy season in 2016. The high calcium content recorded for the Ankobra River indicates that the river might likely be in contact with limestones which exist in the rocks of the Apollonian formation (Fig 3.3 and 3.4).

The magnesium (Mg^{2+}) content in the rivers and streams sampled during the rainy season in 2016 varies from 0.42 to 8.08 mg/L with an average of 2.15 mg/L, and from 0.22 to 7.75 mg/L with a mean of 1.89 mg/L, respectively. During the dry season in 2017, the Mg^{2+} content in the sampled rivers and streams varies from 1.10 to 296.60 mg/L with a mean of 25.07 mg/L, and from 0.95 mg/L to 19.25 mg/L with a mean of 5.97 mg/L, respectively. All the sampled rivers and streams in both years are below WHO (2011) permissible limit of 50 mg/L for drinking water except the Ankobra River, which was sampled from the rocks of the Apollonian during the rainy season in 2016. The reasons accounting for the high calcium content for the Ankobra River as discussed previously is the same reason accounting for the high Mg^{2+} content in the Ankobra River.

The total hardness (TH) concentration in the rivers and streams sampled during the rainy season in 2016 ranges from 8.50 to 240 mg/L with an average of 48.20 mg/L, and from 4.20 mg/L to 80.93 mg/L with a mean of 20.42 mg/L, respectively. In 2017, during the dry season, the sampled rivers and streams range from 7.49 to 1371.14 mg/L with a mean of 124.90 mg/L, and from 6.30 to 115.13 mg/L with a mean of 37.78 mg/L, respectively. All the sampled rivers and streams recorded values below WHO (2011) permissible limit of 500 mg/L for drinking water except the Ankobra River, which exceeded the limit. The high TH value for the Ankobra River

sampled from the rocks of the Apollonian formation is possibly due to the elevated calcium and magnesium ion concentrations (Hunslow,1995) recorded for the river.

The Sodium (Na^+) content in the rivers and streams sampled during the rainy season in 2016 varies from 4.47 to 55.14 mg/L with a mean of 20.18 mg/L, and from 4.30 to 21.29 mg/L with a mean of 10.55 mg/L, respectively. In 2017 during the dry season, the sodium values in the rivers and streams ranges from 4.99 to 380 mg/L with an average of 46.08 mg/L, and from 2.83 to 23.23 mg/L with a mean of 10.28 mg/L respectively. The sodium content in all the sampled rivers and streams in both years are all below the WHO permissible limit of 200 mg/L for drinking water except the Ankobra river, which had sodium content above 200 mg/L.

The chloride (Cl-) concentration in the rivers and streams sampled during the rainy season in 2016 varies from 6 to 75.98 mg/L with a mean of 22.88 mg/L, and from 4 to 27.99 mg/L with an average of 12 mg/L, respectively. In 2017 during the dry season, the chloride content in the rivers and streams ranges from 4 to 3298.94 mg/L with an average of 272.06 mg/L, and from 4 to 49.98 mg/L with an average of 13.33 mg/L, respectively. All the sampled rivers and streams for both years are all below the WHO permissible limit of 250 mg/L for drinking water, except the Ankobra river which exceeded the maximum allowable limit of 600 mg/L. The obtained results are like the sodium and chloride results obtained for the Ankobra River by Edjah et al. (2015).

The source of the elevated sodium and chloride content in the Ankobra River sampled from the rocks of the Apollonian is unknown but it's likely that the elevated sodium and chloride content depends on the season and location in which the Ankobra River was sampled . The Ankobra River was sampled at the downstream section which is in Sanwoma in the rocks of the Apollonian formation. The location where the Ankobra River was sampled was 50 m away from the sea. Assuming that the sodium and chloride in the Ankobra River was coming from the sea and that no chemical fractionation ensues between the measured cations, anions, and chloride after sea salt inoculation into the atmosphere. Hence, the proportion of sea salts in the Ankobra River is determined using

the ion to chloride ratios in sea water sampled from Sanwoma. The sea water shares boundary with the downstream section of the Ankobra River at Sanwoma. The equation use is given as:

$F_i = \left\{\frac{Na^+}{Cl^-}\right\} seawater \times \left\{\frac{Na^+}{Cl^-}\right\} river$ (After Boatta et al. (2014)}.

Where all units are in milli equivalents per liter and Fi represents marine fraction, Na^+ and Cl^- represent sodium and chloride content in both seawater and the Ankobra river.

In this study the sodium content in the sampled seawater is 18500 mg/L (804.70 meq/L) and that of chloride is 29190.948 mg/L (823.44 meq/L). For the sampled Ankobra river, the sodium concentration is 380 mg/L (16.53 meq/L) and the chloride content is 3298.94 mg/L (93.06 meq/L). Putting the milli equivalent values in the above equation gives 0.17 meq/L as the marine fraction. The 0.17 meq/L represents the proportion of sea salt to the Ankobra river. Also, the Na/Cl molar ratio of the seawater is 0.98 meq/L and that of the Ankobra River is 0.18 meq/L. From the above analysis, it is likely that the elevated sodium and chloride content in the Ankobra River is not from sea water intrusion, but rather be coming from other sources such human activities or ion exchange processes. During sampling, we evidenced citizens from Sanwoma that is a town along the bank where the Ankobra river was sampled dumping their fecal waste into the Ankobra river and some citizens were washing their clothing's in the river. These human activities might possibly elevate the sodium and chloride content in the Ankobra River. In addition, the Ankobra river is in a deposition environment, as such waste water from illegal small scale miners mining at the upstream section of the river as evidenced on the field might possibly be discharging into the upstream section of the Ankobra river and that might probably flow to the downstream section where the sample was taken. Since Na and Cl was not measured at the upstream section of the Ankobra River further investigation is required.

Potassium (K^+) concentrations in the rivers and streams sampled in 2016 varies from 0.30 to 22 mg/L with an average of 6.5 mg/L, and from 0.33 to 10.47 mg/L with a mean of 1.51 mg/L,

respectively. In 2017 the potassium content in the sampled rivers and streams ranges from 0.19 to 83.06 mg/L with a mean of 10.28 mg/L, and from 0.30 to 9.88 mg/L with a mean of 2.26 mg/L, respectively. The stream and river samples for both years are all below WHO permissible limit of 12 mg/L for drinking water except Tano River, Amanzura River and Ankobra River. These rivers exceeded WHO (2011) permissible limits. The elevated potassium content in these rivers might probably be from domestic discharge (Skowron et al., 2018) which was evidenced during sampling. Another source of elevated K^+ content indicates that the rivers might be in contact with silicate minerals (feldspars, biotite, and muscovite) which exist in the underlying geology of the study area (Fig 3.3 and 3.4). Potassium concentration in the same rivers and streams as recorded by Edjah et al. (2015) ranged from 0.8 to 590 mg/L and this compares favorably with the potassium results.

The bicarbonate (HCO_3^-) concentration in the rivers and streams sampled during the rainy season in 2016 varies from 9.75 to 82.90 mg/L with an average of 34.14 mg/L, and from 7.32 to 75.59 mg/L with a mean of 29.67 mg/L, respectively. In 2017, during the dry season, the bicarbonate content in the rivers and streams varies from 7.32 to 256.03 mg/L with a mean of 51.38 mg/L, and from 9.75 to 121.92 mg/L with an average of 31.71 mg/L, respectively.

The bicarbonate content in all the sampled rivers and streams are below WHO permissible limit of 500 mg/L for drinking water.

The sulphate levels in the rivers and streams sampled during the rainy season in 2016 ranges from 17.85 to 248.52 mg/L with an average of 58.70 mg/L, and from 0.001 to 126.56 mg/L with a mean of 30.63 mg/L, respectively. In the dry season in 2017, the sampled rivers and streams, varies from 0.001 to 181.15 mg/L with a mean of 30.18 mg/L, and below detection limit {BDL (<0.001>)} to 82.30 mg/L with an average of 14.68 mg/L, respectively. The entire rivers and streams sampled in 2016 and 2017 are below WHO (2011) permissible limit of 250 mg/L for drinking water. The low sulphate concentrations indicate that sulphide minerals (Pyrites and chalcopyrite) which

exist in the underlying geology of the study area have not oxidized or mobilized completely in the surface water.

The nitrate (NO_3^-) levels recorded in the rivers and streams sampled during the rainy season in 2016 varies from 0.39 to 26.51 mg/L with a mean of 3.62 mg/L, and from 0.34 to 2.56 mg/L with an average of 1.31 mg/L, respectively. During the dry season in 2017, the nitrate concentrations in the rivers and stream ranges from 0.40 to 1.07 mg/L with an average of 0.62 mg/L, and from 0.001 to 1.26 mg/L with an average of 0.50 mg/L, respectively. The nitrate levels in all the 2016 and 2017 sampled rivers and streams are all below WHO (2011) permissible limit of 50 mg/L for drinking water.

Based on the medians (Table 4.4 to 4.7), the cation and anion concentrations in the rivers and streams is in the order:

$Na^+ > Ca^{2+} > K^+ > Mg^{2+}$ and $SO_4^{2-} > HCO3^- > Cl > NO_3^-$ (rivers sampled in 2016)

$Na^+ > Ca^{2+} > Mg^{2+} > K^+$ and $SO_4^{2-} > HCO3^- > Cl^- > NO_3^-$(streams sampled in 2016)

$Na^+ > Mg^{2+} > Ca^{2+} > K^+$ and $HCO3^- > Cl^- > SO4^{2-} > NO_3^-$ (rivers sampled in 2017)

$Na^+ > Mg^{2+} > Ca^{2+} > K^+ > HCO_3^- > Cl^- > SO_4^{2-} > NO_3^-$ (streams sampled in 2017).

During the dry season in 2017, both the rivers and streams had similar trend suggesting a hydraulic relationship between the two water bodies. Also, the dominance of sodium among the cations in the rivers and streams implies that the surface water might be in contact with silicate minerals (plagioclase, hornblende, etc.) (Mostafa et al., 2017) which exist in the underlying geology of the study area (fig 3.3 and 3.4). Another source of sodium dominance in the rivers and streams might probably be from the byproduct of rubber and coconut processes (Sultana, 2009) in the study catchment since most of the streams were sampled from the cocoa and rubber plantation zone of the study area and the rivers were sampled along the coast were production of coconut oil is rampant. Another source of Na^+ in the rivers and streams is ion exchange processes (Apello and Postma,1999).

Evaluation of the dominate sulphate content in the rivers and streams sampled in 2016 during the rainy season is computed from the iron to sulphate (Fe/SO_4^{2-}) molar ratio (Stumm & Morgan, 1981) and the result is shown in Appendix 21. The calculated Fe/SO_4^{2-} molar ratio for the surface water varies from 0.00 to 63.3. Additionally, two streams located at Nkroful and Aluku in the Birimian Super group rocks had Fe/SO_4^{2-} molar ratios to be 0.5. The value of the molar ratio is the same as the stoichiometry of pyrite (0.5) oxidation (Vaughan & Craig, 1978). This suggests that sulphate dominance in the rivers and streams sampled in 2016 during the rainy season might probably be originating from the oxidation or mobilization of pyrites which exist in the underlying geology of the study area. Iron pyrites was discovered in the Birimian Supergroup rocks by Leube et al. (1990) and Adjimah et al. (1993) and Keese,1985 discovered nodules of pyrites in the rocks of the Apollonian. Likewise, Fe/ SO_4^{2-} molar ratio for the rest of the rivers and streams sampled during the rainy season in 2016 was not close to Fe/ SO_4^{2-} for stoichiometry of pyrite (0.5) and arsenopyrite (1.0) oxidation (Vaughan & Craig, 1978). This suggests that oxidation or mobilization of sulphide minerals do not contribute more to the concentration of sulphate in the surface water sampled during the rainy season in 2016. Additionally, organic substances breakdown from soils into the rivers and streams or human influences (Craig & Andeson, 1979) could probably contribute to the sulphate dominance among the ions in the rivers and streams.

In 2017 during the dry season, bicarbonate was the dominant anion in both rivers and streams. The dominance of bicarbonate ion indicates that the surface water might be in contact with carbonate minerals (Gastmans et al., 2010) from the rocks of the Apollonian and silicate minerals (Gastmans et al., 2010) from the rocks of the Birimian supergroup of the study area. The variation in anion and cation results for the surface water sampled in 2016 and 2017 might probably be due to seasonal effects, the times in which the surface water was sampled, the lithology and human activities.

4.2.1.3 Occurrences and Distribution of Trace Elements in surface water (Assessment of surface water contamination)

In this section the descriptive statistical results of the laboratory data for the trace element in the sampled rivers and streams is presented in table 4.8,4.9,4.10, and 4.11.

Table 4. 8: Descriptive statistical summary of trace elements in the Rivers sampled in 2016.

Parameters	*Al (mg/L)*	*Cr (mg/L)*	*Mn (mg/L)*	*Fe (mg/L)*	*Co (mg/L)*	*Ni (mg/L)*	*Cu (mg/L)*	*Zn (mg/L)*	*As (mg/L)*	*Cd (mg/L)*	*Pb (mg/L)*
Number of samples	9	9	9	9	9	9	9	9	9	9	9
Mean	0.208	0.003	0.059	3.426	0.0003	0.002	0.006	0.037	0.002	0.002	2.29
Standard Error	0.074	0.001	0.028	1.276	0.0003	0.000	0.004	0.008	0.000	0.001	1.31
Median	0.127	0.003	0.028	2.119	0.0000	0.002	0.001	0.039	0.001	0.000	1.42
Mode	N/A	N/A	0.000	N/A	0.0000	N/A	0.000	N/A	0.001	0.000	0.00
Standard Deviation	0.222	0.002	0.085	3.828	0.0009	0.001	0.013	0.023	0.001	0.003	3.93
Sample Variance	0.049	0.000	0.007	14.657	0.0000	0.000	0.000	0.001	0.000	0.000	15.41
Kurtosis	1.364	-0.753	6.220	5.733	9.0000	1.367	8.643	-0.838	8.524	3.819	7.08
Skewness	1.399	0.105	2.418	2.261	3.0000	1.049	2.923	0.171	2.879	2.021	2.57
Minimum	BDL	BDL	BDL	0.016	BDL	BDL	BDL	0.004	0.001	BDL	BDL
Maximum	0.672	0.005	0.273	12.907	0.0026	0.004	0.042	0.072	0.005	0.010	12.34
Sum	1.875	0.023	0.533	30.836	0.0026	0.014	0.052	0.332	0.014	0.018	20.62
Confidence Level (95.0%)	0.171	0.001	0.065	2.943	0.0007	0.001	0.010	0.018	0.001	0.003	3.02

Table 4. 9: Descriptive statistical summary of trace elements in the Streams sampled in 2016.

Parameters	Al (mg/L)	Cr (mg/L)	Mn (mg/L)	Fe (mg/L)	Co (mg/L)	Ni (mg/L)	Cu (mg/L)	Zn (mg/L)	As (mg/L)	Cd (mg/L)	Pb (mg/L)
Number of samples	15	15	15	15	15	15	15	15	15	15	15
Mean	0.382	0.003	0.080	3.933	0.002	0.002	0.001	0.022	0.003	0.002	2.725
Standard Error	0.096	0.001	0.029	1.098	0.001	0.001	0.001	0.005	0.002	0.001	1.087
Median	0.261	0.002	0.032	2.708	0.000	0.001	0.001	0.022	0.000	0.001	0.000
Standard Deviation	0.372	0.002	0.112	4.252	0.006	0.004	0.002	0.018	0.006	0.003	4.210
Sample Variance	0.139	0.000	0.013	18.082	0.000	0.000	0.000	0.000	0.000	0.000	17.724
Kurtosis	2.479	-1.017	4.514	-0.170	10.059	7.092	1.606	5.343	9.271	-0.552	0.610
Skewness	1.492	0.623	2.052	1.022	3.142	2.563	1.503	1.820	2.942	1.048	1.426
Minimum	0.009	BDL	BDL	0.008	BDL	BDL	BDL	BDL	BDL	BDL	BDL
Maximum	1.380	0.006	0.407	12.947	0.021	0.015	0.007	0.077	0.023	0.009	12.075
Sum	5.730	0.038	1.204	58.991	0.030	0.036	0.022	0.331	0.044	0.036	40.870
Confidence Level (95.0%)	0.206	0.001	0.062	2.355	0.003	0.002	0.001	0.010	0.003	0.002	2.331

Table 4. 10: Descriptive statistical summary of trace elements in the Rivers sampled in 2017

Parameters	Al (mg/L)	Cr (mg/L)	Mn (mg/L)	Fe (mg/L)	Co (mg/L)	Ni (mg/L)	Cu (mg/L)	Zn (mg/L)	As (mg/L)	Cd (mg/L)	Pb (mg/L)
Number of samples	14	14	14	14	14	14	14	14	14	14	14
Mean	0.418	0.002129	0.026	0.459	0.0005	0.002	0.006	0.080	0.0038	0.00079	0.00679
Standard Error	0.260	0.000914	0.013	0.239	0.0002	0.001	0.003	0.040	0.0023	0.00040	0.00174
Median	0.014	0.00092	0.002	0.163	0.0001	0.002	0.002	0.025	0.0010	0.00029	0.00519
Standard Deviation	0.973	0.003418	0.047	0.894	0.0007	0.003	0.011	0.148	0.0086	0.00150	0.00652
Sample Variance	0.947	1.17E-05	0.002	0.798	0.0000	0.000	0.000	0.022	0.0001	0.00000	0.00004
Kurtosis	4.036	8.029861	2.819	11.709	1.9430	9.182	7.825	7.435	12.5008	11.18207	2.12523
Skewness	2.317	2.795799	1.860	3.336	1.7057	2.845	2.773	2.729	3.4884	3.25846	1.47690
Minimum	0.0004	0.000248	0.0003	BDL	0.0001	0.001	0.001	0.002	0.0004	0.00004	0.00004
Maximum	2.921	0.01279	0.150	3.457	0.0021	0.011	0.041	0.535	0.0329	0.00579	0.02301
Sum	5.849	0.029809	0.369	6.425	0.0067	0.034	0.088	1.125	0.0534	0.01106	0.09512
Confidence Level (95.0%)	0.562	0.001974	0.027	0.516	0.0004	0.001	0.006	0.086	0.0049	0.00087	0.00377

Table 4. 11: Descriptive statistical summary of trace elements in the Streams sampled in 2017

Parameters	Al (mg/L)	Cr (mg/L)	Mn (mg/L	Fe (mg/L)	Co (mg/L)	Ni (mg/L)	Cu (mg/L)	Zn (mg/L)	As (mg/L)	Cd (mg/L)	Pb (mg/L)
Number of samples	15	15	15	15	15	15	15	15	15	15	15
Mean	0.023	0.001	0.010	0.517	0.0002	0.002	0.002	0.022	0.002	0.0004	0.010
Standard Error	0.008	0.000	0.005	0.245	0.0001	0.000	0.000	0.006	0.000	0.0002	0.002
Median	0.009	0.001	0.001	0.219	0.0001	0.001	0.001	0.007	0.001	0.0001	0.009
Standard Deviation	0.031	0.001	0.019	0.950	0.0002	0.002	0.001	0.025	0.002	0.0009	0.007
Sample Variance	0.001	0.000	0.000	0.903	0.0000	0.000	0.000	0.001	0.000	0.0000	0.000
Kurtosis	0.989	1.571	4.453	12.438	9.6026	1.498	0.228	0.468	7.625	12.7637	0.399
Skewness	1.529	1.438	2.248	3.426	2.9947	1.477	0.957	1.315	2.706	3.5145	0.715
Minimum	0.001	0.0001	0.001	0.001	0.0001	0.001	0.001	0.003	0.0003	0.00004	0.0001
Maximum	0.093	0.002	0.063	3.825	0.0008	0.006	0.004	0.074	0.007	0.0037	0.025
Sum	0.352	0.011	0.147	7.749	0.0025	0.032	0.025	0.337	0.023	0.0061	0.150
Confidence Level (95.0%)	0.017	0.000	0.010	0.526	0.0001	0.001	0.001	0.014	0.001	0.0005	0.004

4.2.1.4 Metallic elements (Cu, Cd, Zn, Fe, and Cr)

In this study, the concentration of copper (Cu) in the rivers and streams sampled during the rainy season in 2016 vary from below detection limit (BDL (<0.001>)) to 0.042 m/L with a mean of 0.006 m/L, and from BDL (<0.001>) to 0.007 m/L with a mean of 0.001 m/L, respectively. In 2017 during the dry season, the copper content in the rivers and streams vary from 0.001 to 0.041 mg/L with a mean of 0.006 mg/L, and from 0.001 to 0.004 mg/L with an average of 0.002 mg/L, respectively. The Cu content in all the sampled rivers and streams for both 2016 and 2017 are all below WHO (2011) permissible limit of 0.05 mg/L for drinking water.

The cadmium (Cd) content in the rivers and streams sampled in 2016 during the rainy season ranges from below detection limit (BDL) (<0.001>) to 0.010 m/L with a mean of 0.002 mg/L, and from BDL (<0.001>) to 0.009 m/L with a mean of 0.002 mg/L, respectively. That of the dry season rivers and stream samples taken in 2017 ranges from 0.00 to 0.006 mg/L with a mean of 0.001 mg/L, and from 0.00 to 0.004 mg/L with an average of 0.0004 mg/L, respectively. The Cd content in all the sampled rivers and streams for both years are below WHO (2011) permissible limit of 0.003 mg/L for drinking water except Ankasa River, Ebi River, Tano River, Nobaya Stream, Franza Stream, Wowule Stream and a stream located at Ayinase. According to Water Quality Association (www.wqa.org), "Cadmium occurs naturally in zinc, lead, copper ores, coal, other fossil fuels, and shales and it is released during volcanic action. These deposits can serve as sources to surface waters and groundwater especially when in contact with low total dissolved solids (TDS) and acidic waters". In this study, the pH values for Ankasa River, Ebi River, Tano River, Nobaya Stream, Franza Stream, Wowule Stream and the stream located at Ayinase are acidic to neutral with low TDS concentration, and the geologic formation contains limestones, marl with interclasted sandy beds, cenzoic, shales (Fig 3.3 and 3.4) and sulphide minerals (Luebe et al.,1990).

Studies carried out by Gyasi (2017) shows fossils in the rocks of the Apollonian formation. From the above, it can be assumed that the source of cadmium in the above-mentioned rivers and streams is geogenic, but further investigations are required.

Another contributing factor leading to the high Cd content in the above-mentioned rivers and streams is possibly from an anthropogenic source such as effluent discharge from the activities of illegal small-scale miners (Schwartz, 2000). In the study area, illegal small-scale mining and mining industries dominate areas surrounding the Ankasa River, Tano River, Nobaya Stream, Franza Stream, and Wowule Stream. Effluents from the activities of these miners might be discharged into the surrounding surface water bodies thereby elevating the Cd contents. The Cd content in the rivers and streams compares favorably to the Cd values in the same rivers and streams obtained by Edjah, 2012.

The Zinc (Zn) content in the rivers and streams sampled during the rainy season in 2016 varies from 0.004 to 0.072 mg/L with an average of 0.037 mg/L, and from below detection limit {BDL (<0.001>)} to 0.077 mg /L with a mean of 0.022 mg/L, respectively. In 2017 during the dry season, the zinc concentration in the rivers and streams ranges from 0.002 to 0.535 mg/L with a mean of 0.08 mg/L, and from 0.003 to 0.074 mg/L with a mean of 0.022 mg/L, respectively. The zinc content in all the rivers and streams sampled in both 2016 and 2017 are below WHO (2011) permissible limits of 5 mg/L for drinking water.

The iron (Fe) content in the rivers and streams sampled during the rainy season in 2016 vary from 0.016 to 12.91 mg/L with an average of 3.43 mg/L, and from 0.008 to 12.95 mg/L with a mean of 3.93 mg/L, respectively. That of the dry season in 2017 sampled rivers and streams range from below detection limit {BDL (<0.001>)} to 3.46 mg/L with an average of 0.46 mg/L, and from 0.001 to 3.83 mg/L with a mean of 0.52 mg/L, respectively. The Fe content for 11% of the rivers (n=9) and 26 % of the streams (n= 15) sampled in 2016 during the rainy season are below WHO (2011) permissible limit of 0.3 mg/L for drinking water. Similarly, 71.4% (n = 14) of the rivers and 53.3% of the streams (n=15) sampled during the dry season in 2017 are below the WHO (2011) permissible limits of 0.3 mg/L for drinking water. The elevated Fe content for the remaining rivers and streams indicates that silicate minerals (biotite, hornblende, etc.), from the underlying geology of the study catchment (fig 3.3 and 3.4) are dissolving completely in the surface water as it flows. Another source of elevated Fe concentrations in the rivers and streams is possibly from the oxidation of iron pyrites (Luebe

et al., 1990; Adjimah et al., 1993) which exist in the rocks of the Apollonian and the Birimian supergroup of the study area. When these rocks are in contact with the surface water, the iron concentration rate is induced due to discharges from the rocks of the Birimian to the rocks of the Apollonian.

The Chromium (Cr) content in the 2016 sampled rivers and streams vary from below detection limits {BDL (<0.001>)} to 0.005 mg/L with an average of 0.003 mg/L, and from below detection limit {BDL (<0.001>} to 0.006 mg/L with a mean of 0.003 mg/L, respectively. The rivers and streams sampled in 2017 range from 0.0002 to 0.013 mg/L with an average of 0.002 mg/L, and from 0.0001 to 0.002 mg/L with a mean of 0.001 mg/L respectively. The Cr content in all the sampled rivers and streams are below WHO (2011) permissible limit of 0.05 mg/L for drinking water.

4.2.1.5 Transition metals (Ni, Co, and Mn)

The Nickel (Ni) concentration in the rivers and streams sampled during the rainy season in 2016 range from below detection limit {BDL (< 0.001>} to 0.004 mg/L with an average of 0.002 mg/L, and from BDL (<0.001>) to 0.015 mg/L with a mean of 0.002 mg/L, respectively. In 2017 during the dry season, the Ni content in the rivers and streams vary from 0.001 to 0.011 mg/L with an average of 0.002 mg/L, and from 0.001 to 0.006 mg/L with a mean of 0.002 mg/L, respectively. Nickel (Ni), concentration in the surface water sampled in both 2016 and 2017 are below WHO permissible limit of 0.006 mg/L for drinking water except Tano River and Assufofa Stream. Even though illegal small-scale mining activity was evidenced on these two water bodies, the elevated Ni content indicates that the Tano River and Assufofa stream might possibly be in contact with sulphide minerals (pyrites, chalcopyrite) from the rocks of the Birimian and the Apollonian formation. When the surface water is in contact with the sulphide minerals, the sulphide minerals oxidize or mobilize releasing Ni as a secondary mineral. Ni was one of the trace elements hosted in sulphide minerals (pyrites, arsenopyrites, chalcopyrite) discovered by Luebe et al., 1990 and Adijimah et al., 1993 in the rocks of the Birimian.

The Cobalt (Co) content in the rivers and streams sampled during the rainy season in 2016 range from BDL (<0.001>) to 0.003 mg/L with a mean of 0.0003 mg/L and from BDL (<0.001>) to 0.021 mg/L with an average of 0.002 mg/L, respectively. In 2017 during the dry season, the Co concentration in the rivers and streams range from 0.0001 mg/L to 0.002 mg/L with an average 0.0005 mg/L, and from 0.0001 to 0.0008 mg/L with a mean of 0.0002 mg/L, respectively. The Co concentration in all the sampled surface water is below WHO (2011) permissible limit of 0.05 mg/L for drinking water.

The Magnesium (Mn) content in the rivers and streams sampled during the rainy season in 2016 vary from BDL (<0.001>) to 0.27 mg/L with a mean of 0.059 mg/L, and from BDL (<0.001>) to 0.41 mg/L with an average of 0.08 mg/L, respectively. In 2017 during the dry season, the Mn content in the rivers vary from 0.0003 to 0.150 mg/L with a mean of 0.026 mg/L. That of the streams range from 0.001 to 0.063 mg/L with a mean of 0.010 mg/L. The Mn content in the surface water sampled in both 2016 and 2017 are all below the WHO permissible limit of 0.4 mg/L for drinking water.

4.2.1.6 Toxic Elements (Pb and As)

The Lead (Pb) content in the rivers and streams sampled in 2016 during the rainy season vary from BDL (<0.001>) to 12.34 mg/L with a mean of 2.29 mg/L, and from BDL (<0.001>) to 12.08 mg/L with an average of 2.73 mg/L, respectively. The concentration of lead (Pb) in 5 rivers (n=10) and 8 streams (n=15) are below the WHO (2011) permissible limit of 0.01 mg/L and the remaining 5 rivers and 7 streams are above the permissible limits for drinking water. In 2017 during the dry season, the Pb content in the rivers and streams range from 0.00004 \to 0.023 mg/L with a mean of 0.007 mg/L, and from 0.0001 to 0.025 mg/L with a mean of 0.010 mg/L, respectively. The Pb content in all the sampled surface water are below WHO (2011) permissible limit of 0.01 mg/L for drinking water except for Amanzura river, Subly stream, Kodubaku stream and Nsugene stream which exceeded the permissible limit (Fig 4.9).

Goel, 1997 stated that “lead (Pb) concentrations in natural water mainly generates from anthropogenic sources”. Looking at the activities (small- scall mining, fecal waste disposal, household waste disposal) surrounding the above-mentioned river and streams as evidenced on

the field, it can be said that the elevated lead content measured in these rivers and streams might likely be coming from an anthropogenic source. Subly, Kodubaku and Nsugene streams are close to Adamus's mining resources and there are rampant illegal small-scale mining activities at the upstream section of these streams. As such, wastewater from drains and effluent from the use of lead gasoline by these miners might possibly discharge into these streams through natural processes. like rainfall or runoffs. An extra source of elevated Pb in the river and streams might be geogenic due to the oxidation or mobilization of sulphide minerals (pyrite, chalcopyrite.) from the underlying geology to liberate Pb as a secondary mineral in the river and streams. These sulphide minerals hosted trace element like Pb which was used as a guide element for gold discovery in the rocks of Birimian {Adjimah et al. (1993)}.

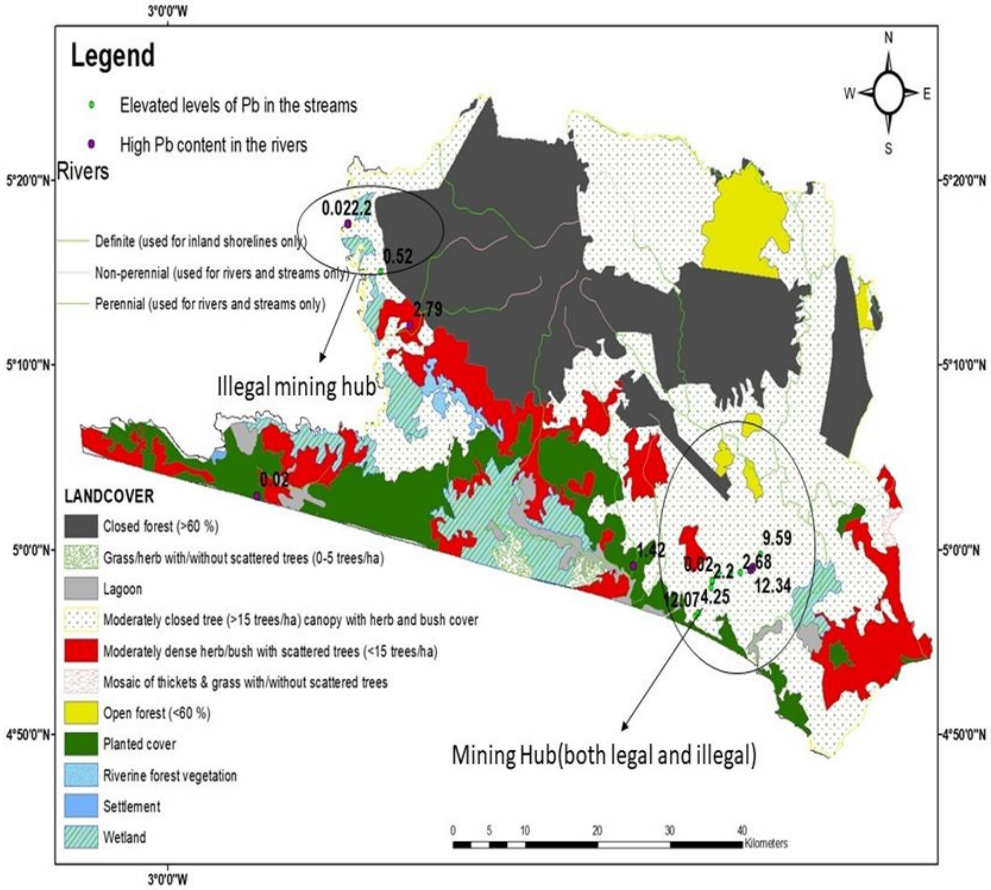

Figure 4. 9: Enhanced Pb levels in the rivers and streams sampled in both 2016 and 2017.

The Arsenic (As) content in the rivers and streams sampled during the rainy season in 2016 varies from 0.001 to 0.005 mg/L with an average of 0.002 mg/L, and from BDL (<0.001>) to 0.023 mg/L with an average of 0.003 mg/L, respectively. In 2017 during the dry season, the

sampled rivers and streams varies from 0.0004 to 0.033 mg/L with an average of 0.004 mg/L, and from 0.0003 to 0.007 mg/L with an average of 0.002 mg/L, respectively. The Arsenic concentration in the surface water sampled in 2016 and 2017 are all below the WHO (2011) permissible limit of 0.01 mg/L for drinking water apart from Ankobra River sampled from the rocks of the Apollonian formation and Franza Stream sampled from the rocks of the Birimian Supergroup. Edjah (2012) recorded enhanced levels of As in these two water bodies. The Birimian supergroup rocks of the study area contains sulphide minerals (Luebe et al., 1990). These sulphide minerals when they oxidize or mobilizes As is released.

4.2.1.7 Non-metallic elements (Al)

The Aluminum (Al) content in the rivers sampled in 2016 during the rainy season varies from BDL (<0.001>) to 0.67 mg/L with a mean of 0.208 mg/L. That of the streams sampled in 2016 during the rainy season varies from 0.009 to 1.380 mg/L with an average of 0.382 mg/L. In 2017, during the dry season, the sampled rivers, and streams ranges from 0.0004 to 2.92 mg/L with a mean of 0.42 mg/L, and from 0.001 to 0.093 mg/L with an average of 0.023 mg/L. The Aluminum (Al) content in the sampled rivers for both 2016 and 2017 are below WHO (2011) permissible limit of 0.2 mg/L for drinking water except Ebi River, Fian River and Tano River. The Al content in 8 streams (n=15) sampled in 2016 are above WHO (2011) permissible limit of 0.2 mg/L and the remaining 7 streams are lower than the permissible limit. In 2017, the Al concentration in all the sampled streams is below WHO (2011) permissible limit of 0.2 mg/L for drinking water. The source of elevated Al content in few of the rivers and streams is geogenic. Its geogenic because the underlying geology contains silicate minerals (hornblende, muscovite, biotite etc.) {(www.healthycanadians.gc.ca; (Fig 3.3 and 3.4)}and when these silicate minerals dissolves, Al is probably released due to the acidity (pH = 4.0 to 6.4) of the above-mentioned elevated rivers and streams.

Comparing the median concentrations of the measured trace elements in the rivers and streams sampled in 2016 and 2017, it is seen that iron (Fe) dominated among all the measured trace elements. This is due to the underlying geology containing silicate minerals and sulphide minerals. Most of the streams were sampled in areas underlain by the Birimian super group

rocks and most rivers were taken in areas underlain by the rocks of the Apollonian. These surface water bodies flow from the hinterlands (Birimian super group rocks) to the coast (rocks of the Apollonian formation) and the areas underlain by the rocks of the Apollonian are more in a deposition environment (fig 3.3 and 3.4) than the areas underlain by the rocks of the Birimian Super group. The dominance of Fe among the measured trace elements in the rivers and streams in both 2016 and 2017 is like the results obtained by Edjah ,2012.

4.2.1.8. Existing Relationship between the cations, anions, and trace element in the surface water

In this study, the relationship existing between the cations, anions and trace elements in the rivers and streams are investigated using Pearson correlation matrix and the results are shown in table 4.12,4.13.4.14 and 4.15. The elements that correlates are highlighted in red.

Table 4. 12: Pearson correlation of chemical and trace elements data for the Rivers sampled in 2016.

	Ca^{2+}	Mg^{2+}	Na^{+}	K^{+}	Cl^{-}	HCO_3^{-}	SO_4^{2-}	NO_3^{-}	TDS	EC	pH	TH	Al	Cr	Mn	Fe	Co	Ni	Cu	Zn	As	Cd	Pb
Ca^{2+}	1.0																						
Mg^{2+}	-0.2	1.0																					
Na^{+}	0.5	0.6	1.0																				
K^{+}	0.4	0.1	0.7	1.0																			
Cl^{-}	0.1	0.9	0.7	0.2	1.0																		
HCO_3^{-}	0.8	0.1	0.7	0.7	0.4	1.0																	
SO_4^{2-}	1.0	-0.1	0.6	0.4	0.2	0.8	1.0																
NO_3^{-}	-0.2	0.0	-0.2	-0.3	0.01	0.01	0.01	1.0															
TDS	0.1	0.9	0.9	0.4	1.0	0.4	0.2	0.01	1.0														
EC	0.1	0.9	0.9	0.4	1.0	0.4	0.2	0.01	1.0	1.0													
pH	0.6	-0.3	0.3	0.4	-0.3	0.4	0.5	-0.6	-0.2	-0.2	1.0												
TH	1.0	-0.1	0.6	0.4	0.2	0.8	1.0	-0.2	0.2	0.2	0.6	1.0											
Al	-0.4	-0.1	-0.5	-0.6	-0.3	-0.3	-0.4	0.4	-0.4	-0.4	-0.2	-0.4	1.0										
Cr	-0.6	-0.2	-0.4	0.1	-0.6	-0.5	-0.6	0.01	-0.4	-0.4	0.01	-0.7	0.2	1.0									
Mn	-0.3	0.2	-0.2	-0.4	-0.2	-0.5	-0.2	0.2	-0.2	-0.2	-0.1	-0.3	0.2	0.4	1.0								
Fe	-0.2	0.1	-0.2	-0.4	-0.2	-0.5	-0.1	0.1	-0.2	-0.2	-0.1	-0.2	0.2	0.2	1.0	1.0							
Co	-0.2	0.0	-0.2	-0.3	0.01	0.01	0.01	1.0	-0.1	-0.1	-0.6	-0.2	0.4	0.01	0.2	0.1	1.0						
Ni	0.8	-0.6	0.1	0.5	-0.3	0.6	0.7	0.1	-0.3	-0.3	0.4	0.7	-0.4	-0.2	-0.3	-0.2	0.1	1.0					
Cu	-0.2	0.0	-0.2	-0.3	0.01	0.01	-0.1	1.0	-0.1	-0.1	-0.6	-0.2	0.4	0.1	0.2	0.2	1.0	0.1	1.0				
Zn	-0.4	0.3	-0.3	-0.6	0.3	-0.4	-0.3	0.5	0.1	0.1	-0.8	-0.3	0.3	-0.3	0.3	0.4	0.5	-0.4	0.5	1.0			
As	-0.1	0.2	-0.1	-0.1	-0.2	-0.4	-0.1	-0.1	-0.1	-0.1	0.1	-0.1	-0.1	0.4	0.9	0.9	-0.1	-0.2	0.01	0.1	1.0		
Cd	-0.3	-0.3	-0.5	-0.3	-0.3	-0.1	-0.3	0.3	-0.3	-0.3	-0.2	-0.3	0.01	0.1	-0.1	-0.2	0.3	-0.1	0.3	0.1	-0.2	1.0	
Pb	-0.3	0.01	-0.2	-0.2	-0.4	-0.5	-0.2	-0.2	-0.3	-0.3	0.2	-0.3	0.01	0.6	0.9	0.8	-0.2	-0.3	-0.1	0.01	0.9	-0.1	1.0

Table 4. 13: Pearson correlation of chemical and trace elements data for the Streams sampled in 2016.

	Ca^{2+}	Mg^{2+}	Na^{+}	K^{+}	Cl^{-}	HCO_3^{-}	SO_4^{2-}	NO_3^{-}	TDS	EC	pH	TH	Al	Cr	Mn	Fe	Co	Ni	Cu	Zn	As	Cd	Pb
Ca^{2+}	1.0																						
Mg^{2+}	**0.7**	1.0																					
Na^{+}	-0.1	0.1	1.0																				
K^{+}	0.1	0.1	**0.6**	1.0																			
Cl^{-}	-0.1	0.01	0.4	0.3	1.0																		
HCO_3^{-}	0.3	**0.5**	0.1	0.3	0.4	1.0																	
SO_4^{2-}	**0.7**	**0.8**	0.01	0.01	0.1	**0.5**	1.0																
NO_3^{-}	0.2	**0.6**	0.01	0.1	-0.1	0.3	**0.6**	1.0															
TDS	0.4	**0.6**	0.2	0.1	**0.6**	**0.8**	**0.6**	0.2	1.0														
EC	0.4	**0.6**	0.2	0.1	**0.6**	**0.8**	**0.6**	0.2	**1.0**	1.0													
pH	-0.4	-0.5	-0.1	-0.3	-0.1	-0.2	-0.4	-0.4	-0.4	-0.4	1.0												
TH	**1.0**	**0.8**	0.01	0.1	-0.1	0.4	**0.8**	0.4	**0.5**	**0.5**	**-0.5**	1.0											
Al	-0.3	-0.3	-0.4	-0.2	-0.3	-0.4	-0.4	0.2	**-0.5**	-0.5	0.2	-0.4	1.0										
Cr	-0.4	-0.4	0.3	0.4	0.2	0.2	**-0.6**	-0.2	-0.1	-0.1	0.2	-0.4	0.3	1.0									
Mn	-0.4	-0.4	0.0	-0.1	-0.2	0.1	-0.3	-0.1	-0.3	-0.3	**0.6**	-0.4	0.1	0.3	1.0								
Fe	-0.4	**-0.5**	-0.3	-0.3	-0.1	0.01	-0.2	-0.1	-0.4	-0.4	**0.7**	**-0.5**	0.2	0.1	0.8	1.0							
Co	-0.1	-0.1	0.2	0.01	-0.1	-0.1	0.01	0.01	0.01	0.01	-0.1	-0.1	0.01	-0.1	0.1	0.0	1.0						
Ni	-0.2	-0.2	-0.3	-0.2	-0.3	0.01	-0.2	-0.1	-0.3	-0.3	0.4	-0.3	0.01	0.01	0.4	**0.7**	-0.1	1.0					
Cu	0.01	0.1	0.3	0.0	-0.3	0.2	-0.2	0.1	0.01	0.01	0.2	0.01	0.2	0.4	**0.5**	0.1	0.1	-0.1	1.0				
Zn	-0.2	-0.1	-0.3	-0.3	-0.1	0.2	0.01	0.2	-0.2	-0.2	0.4	-0.2	0.01	0.01	**0.5**	**0.8**	-0.3	**0.8**	0.1	1.0			
As	-0.2	-0.3	-0.3	-0.1	-0.3	-0.1	-0.4	0.1	-0.4	-0.4	-0.1	-0.3	0.4	**0.5**	0.3	0.2	0.01	0.3	0.3	0.1	1.0		
Cd	0.1	-0.3	-0.4	-0.2	0.01	0.1	**-0.5**	-0.4	0.01	0.01	0.1	-0.1	0.4	**0.5**	-0.1	0.01	-0.2	0.2	0.2	0.1	**0.5**	1.0	
Pb	-0.3	-0.2	0.3	0.01	-0.2	-0.1	**-0.6**	-0.1	-0.2	-0.2	0.4	-0.3	**0.5**	**0.6**	0.4	0.1	0.1	-0.1	**0.9**	0.01	0.3	0.3	1.0

Table 4. 14: Pearson correlation of chemical and trace elements data for the Rivers sampled in 2017.

	Ca^{2+}	Mg^{2+}	Na^{+}	K^{+}	Cl^{-}	HCO_3^{-}	SO_4^{2-}	NO_3^{-}	TDS	EC	pH	TH	Al	Cr	Mn	Fe	Co	Ni	Cu	Zn	As	Cd	pb
Ca^{2+}	1.0																						
Mg^{2+}	1.0	1.0																					
Na^{+}	1.0	1.0	1.0																				
K^{+}	1.0	1.0	1.0	1.0																			
Cl^{-}	1.0	1.0	1.0	1.0	1.0																		
HCO_3^{-}	0.2	0.1	0.3	0.4	0.1	1.0																	
SO_4^{2-}	0.8	0.7	0.7	0.7	0.8	0.01	1.0																
NO_3^{-}	-0.1	-0.2	-0.3	-0.3	-0.2	-0.1	0.3	1.0															
TDS	1.0	1.0	1.0	1.0	1.0	0.2	0.8	-0.2	1.0														
EC	1.0	1.0	1.0	1.0	1.0	0.2	0.8	-0.2	1.0	1.0													
pH	0.2	0.3	0.3	0.2	0.3	-0.2	0.1	-0.7	0.3	0.3	1.0												
TH	1.0	1.0	1.0	1.0	1.0	0.1	0.8	-0.2	1.0	1.0	0.3	1.0											
Al	0.7	0.6	0.6	0.5	0.6	0.01	0.7	0.3	0.6	0.6	-0.2	0.6	1.0										
Cr	0.01	0.01	0.01	-0.1	0.0	-0.1	-0.1	-0.1	0.01	0.01	0.1	0.01	0.3	1.0									
Mn	0.5	0.4	0.4	0.4	0.4	-0.1	0.7	0.2	0.4	0.4	0.3	0.4	0.5	0.01	1.0								
Fe	0.01	-0.1	-0.1	-0.2	-0.1	-0.1	0.1	0.6	-0.1	-0.2	-0.4	-0.1	0.7	0.4	0.2	1.0							
Co	0.8	0.7	0.7	0.6	0.7	0.01	0.7	0.1	0.7	0.7	0.1	0.7	0.9	0.4	0.7	0.5	1.0						
Ni	0.3	0.1	0.1	0.1	0.1	-0.1	0.3	0.5	0.1	0.1	-0.3	0.1	0.8	0.5	0.4	0.9	0.7	1.0					
Cu	0.01	-0.1	-0.1	-0.1	-0.1	-0.2	-0.1	0.01	-0.1	-0.1	0.1	-0.1	0.2	1.0	0.1	0.4	0.4	0.5	1.0				
Zn	0.1	0.01	-0.1	-0.1	-0.1	-0.2	0.1	0.4	-0.1	-0.1	-0.3	0.01	0.7	0.7	0.2	0.9	0.6	0.9	0.7	1.0			
As	-0.1	-0.1	-0.1	-0.1	-0.1	-0.2	-0.2	-0.1	-0.1	-0.1	0.2	-0.1	0.01	1.0	-0.1	0.1	0.2	0.3	1.0	0.5	1.0		
Cd	0.1	0.01	-0.1	-0.1	-0.1	-0.1	0.2	0.6	-0.1	-0.1	-0.4	0.01	0.7	0.3	0.5	1.0	0.6	0.9	0.3	0.8	0.1	1.0	
pb	0.01	-0.1	-0.2	-0.2	-0.1	-0.3	0.1	0.6	-0.1	-0.2	-0.3	-0.1	0.5	0.01	0.4	0.7	0.4	0.6	0.1	0.5	-0.1	0.7	1.0

Table 4. 15: Pearson correlation of chemical and trace elements data for the Streams sampled in 2017

	Ca^{2+}	Mg^{2+}	Na^{+}	K^{+}	Cl^{-}	HCO_3^{-}	SO_4^{2-}	NO_3^{-}	TDS	EC	pH	TH	Al	Cr	Mn	Fe	Co	Ni	Cu	Zn	As	Cd	Pb
Ca^{2+}	1.0																						
Mg^{2+}	0.9	1.0																					
Na^{+}	0.7	0.5	1.0																				
K^{+}	0.5	0.2	0.6	1.0																			
Cl^{-}	0.01	-0.1	-0.1	0.2	1.0																		
HCO_3^{-}	0.4	0.3	0.7	0.8	0.1	1.0																	
SO_4^{2-}	0.7	0.9	0.3	0.1	-0.1	0.2	1.0																
NO_3^{-}	0.4	0.2	0.01	0.4	0.5	0.3	0.4	1.0															
TDS	0.8	0.7	0.7	0.8	0.1	0.8	0.6	0.6	1.0														
EC	0.9	0.8	0.7	0.7	0.0	0.7	0.7	0.5	1.0	1.0													
pH	0.5	0.6	0.4	0.2	-0.3	0.3	0.4	-0.4	0.3	0.4	1.0												
TH	1.0	1.0	0.6	0.3	-0.1	0.3	0.8	0.3	0.7	0.8	0.6	1.0											
Al	-0.1	-0.2	0.2	0.3	0.4	0.5	0.1	0.3	0.3	0.2	-0.1	-0.1	1.0										
Cr	0.1	0.01	0.4	0.3	0.7	0.4	-0.1	0.5	0.4	0.2	-0.4	0.01	0.5	1.0									
Mn	-0.1	-0.3	0.01	0.3	0.8	0.3	-0.2	0.4	0.2	0.1	-0.4	-0.2	0.6	0.7	1.0								
Fe	0.01	0.01	-0.2	0.01	0.9	-0.1	0.01	0.6	0.1	0.01	-0.4	0.01	0.4	0.7	0.7	1.0							
Co	0.01	-0.1	-0.1	-0.1	0.9	0.0	0.01	0.3	0.1	0.01	-0.4	-0.1	0.3	0.7	0.9	0.9	1.0						
Ni	0.4	0.6	0.3	0.01	0.0	0.3	0.4	0.01	0.3	0.4	0.4	0.5	0.1	0.2	0.01	0.1	0.1	1.0					
Cu	0.01	-0.1	0.4	0.2	0.6	0.4	-0.1	0.3	0.2	0.1	-0.1	-0.1	0.5	0.9	0.7	0.6	0.7	0.3	1.0				
Zn	0.2	0.1	0.4	0.5	0.6	0.6	0.2	0.6	0.5	0.4	-0.2	0.1	0.6	0.9	0.8	0.5	0.7	0.3	0.8	1.0			
As	0.8	0.9	0.4	0.2	-0.1	0.2	0.9	0.4	0.7	0.8	0.3	0.9	-0.2	0.01	-0.2	0.01	0.01	0.3	-0.1	0.2	1.0		
Cd	0.1	-0.1	0.4	0.7	0.3	0.9	-0.1	0.4	0.6	0.4	0.01	-0.1	0.7	0.5	0.6	0.1	0.2	0.1	0.5	0.7	-0.1	1.0	
Pb	0.5	0.3	0.01	0.4	0.1	0.01	0.3	0.3	0.5	0.5	0.1	0.4	-0.1	-0.2	0.1	0.1	0.01	-0.3	-0.3	-0.1	0.4	0.01	1.0

The use of Pearson correlation matrix can help understand the distribution of anions, cations, and trace elements in the sampled surface water. It is also one of the essential tests that identify the relationship between two independent variables in water samples and shows how one parameter guesses the other variable (Howlader et al., 2014). The correlation coefficient (r) varies from − 1 to + 1. When r is close to − 1, the relationship is delineated as a negative slope or anti-correlated. The linkage is considered to have a positive slope or correlation when r is close to + 1. If the value of r inclines to be zero, the points are considered uncorrelated (Srivastava & Ramanathan, 2008; Howlader et al., 2014).

From Table 4.13,4.14 and 4.15, it is seen that Mg^{2+} correlated strongly with Ca^{2+} for the streams sampled during the rainy season in 2016 and the rivers and streams sampled during the dry season in 2017. The perfect relationship between Mg^{2+} and Ca^{2+} for the streams and rivers suggests that the rivers and streams are likely in contact with limestones and granitic rocks from the underlying geology (fig 3.3 and 3.4).

Also, there was a strong correlation between Na^{+} and (Ca^{2+} and Mg^{2+}) for the rivers sampled during the rainy season in 2016 (Table 4.12) and the dry season in 2017 (Table 4.14) as well as the streams sampled during the dry season in 2017 (Table 4.15). The above relationship suggests that the rivers and streams are possibly in contact with silicate minerals (feldspars, hornblende etc.) from the underlying geology (fig 33 and 3.4) of the study area. Also, the good relationship between Na^{+} and (Ca^{2+} and Mg^{2+}) reveals cation- exchange processes (Guo & Wang, 2004) among the rivers and streams.

From table 4.12 and 4.13 it is observed that K^{+} correlated strongly with Na^{+} for the rivers and streams sampled during the dry rainy season in 2016. In addition, K^{+} correlated perfectly with (Ca^{2+}, Mg^{2+} and Na^{+}) for the rivers (Table 4.14) sampled during the dry season in 2017 and K^{+} correlated strongly with (Ca^{2+}, Na^{+}) for the streams sampled during the dry season in 2017 (Table 4.15). The relationship between K^{+} and (Ca^{2+}, Mg^{2+} and Na^{+}) for the rivers and streams suggests that the rivers and streams might be in contact with silicate minerals (feldspars, hornblende, plagioclase etc.) (Drever, 1988) from the underlying geology (Fig 3.3 and 3.4).

Cl^- correlated perfectly with (Mg^{2+} and Na^+) for the rivers sampled in 2016 (Table 4.12) and Cl^- correlated strongly with (Ca^{2+}, Mg^{2+}, Na^+ and K^+) for the rivers sampled in 2017 (Table 4.14). The above relationships suggest an anthropogenic source. In the study area, peasant farming and coconut farming is common and the application of excessive fertilizer by theses farmers might possibly lead to $MgCl_2$, $CaCl_2$, NaCl, and KCl concentrations (Sriniyasamoorty et al., 2008) in the soil which requires further investigations.

HCO_3^- correlated perfectly with (Ca^{2+}, Na^+ and K^+) for the rivers sampled in 2016 (Table 4.12) and correlated strongly with Mg^{2+} for the streams sampled in 2016 (Table 4.13). In addition, there was a perfect correlation between HCO_3^- and (Na^+ and K^+) for the streams sampled in 2017 (Table 4.15). The relationship existing between HCO_3^- and (Ca^{2+} and Mg^{2+}) for the rivers and streams suggests that the alkalinity of the surface water might possibly has a direct bearing on the composition of limestones and granites from the underlying geology of the Lower Tano River basin. The good relationship between HCO_3 and (Na^+ and K+) for the rivers and streams indicate a possible occurrence of ion exchange processes. Additionally, the good connection indicates that the alkalinity of the rivers and streams probably has a direct bearing on the composition of silicate minerals from the underlying geology of the study area.

Further, there was a perfect relationship between SO_4^{2-} and (Ca^{2+}, Na^+ and HCO_3^-) for the rivers sampled in 2016 (Table 4.12) and (Ca^{2+}, Mg^{2+} and HCO_3^-) for the streams sampled in 2016 (Table 4.13). For 2017 samples, SO_4^{2-} correlated perfectly with (Ca^{2+}, Mg^{2+}, Na^+, K^+ and Cl^-) for the rivers (Table 4.14) and (Ca^{2+} and Mg^{2+}) for the streams (Table 4.15). The good relationship between SO_4^{2-} and (Ca^{2+} and Mg^{2+}) for the surface water suggests the possible occurrence of ion exchange processes (Mariotti, 1994). The good relationship between SO_4^{2-} and (Na^+ and K^+) for the rivers and streams suggest a possible anthropogenic source {Sophocleous et al. (2002)} and the probable source could be linked to untreated sewage disposal which was evidenced during sampling. Also, the good relationship between SO_4^{2-} and Mg^{2+} for the rivers and streams suggests a possible occurrence of ion exchange processes or the existence of magnesium calcareous materials in the study catchment which needs further

investigations. Additionally, the relationship between SO_4^{2-} and HCO_3^- for the rivers and streams suggests that anthropogenic or geogenic sources probable affects the alkalinity of the rivers and streams or a possible occurrence of reverse ion- exchange processes.

NO_3^- correlated strongly with (Mg^{2+} and SO_4^{2-}) for the streams sampled in 2016 (Table 4.13) and correlated perfectly with Cl^- for the streams sampled in 2017 (Table 4.15). The relationship between NO_3^- and Cl^- for the streams is probably linked to reverse ion exchange processes or anthropogenic sources. Also, human activities such as fertilizer application and sewage disposal could be the possible reason accounting for the good relationship between NO_3^- and (Mg^{2+} and SO_4^{2-}) for the streams. The streams were mostly located in the forested zone of the study area where cocoa farming and rubber plantation is practiced.

In 2016, TDS and EC correlated perfectly with (Mg^{2+}, Na^+, and Cl^-) for the rivers (Table 4.12) and (Mg^{2+}, Cl^-, HCO_3^- and SO_4^{2-}) for the streams (Table 4.13). Also in 2017, TDS and EC correlated perfectly with (Ca^{2+}, Mg^{2+}, Na^+, K^+, Cl^- and SO_4^{2-}) for the rivers (Table 4.14) and correlated strongly with (Ca^{2+}, Mg^{2+}, Na^+, K^+, SO_4^{2-} , NO_3^- and HCO_3^-) for the streams (Table 4.15). The existing relationship between TDS /EC and the above-mentioned ions in both rivers and streams suggest the likelihood of the ions being involved in physiochemical reactions and one such reactions is ion exchange processes and oxidation – reduction processes (Subba Rao, 2002).

For the rivers sampled in 2016, pH correlated strongly with (Ca^{2+} and SO_4^{2-}) and negatively with NO_3^- (Table 4.12). Also, pH correlated negatively with Mg^{2+} for the streams sampled in 2016 (Table 4.13). In 2017, pH correlated negatively with NO_3^- for the rivers (Table 4.14) and strongly with (Ca^{2+} and Mg^{2+}) for the streams (Table 4.15). The good relationship between pH and Ca^{2+} for the rivers and Ca^{2+} and Mg^{2+} for the streams indicates carbonate mineral dissolution and weathering of silicate minerals from the underlying geology of the study area.

The relationship between pH and SO_4^{2-} for the rivers specifies the oxidation of sulphide minerals (pyrites, chalcopyrite) (Hunslow, 1995) from the underlying geology. The negative

relationship between pH and NO_3^- for the rivers suggests the likely absence of fertilizer application in the study area. In addition, the negative relationship between pH and Mg^{2+} for the streams suggests the acidity of the streams does not influence the weathering of ferromagnesium mineral (Biotite) from the underlying geology.

In 2016, TH in the sampled rivers correlated perfectly with (Ca^{2+}, Na^+, HCO_3^-, SO_4^{2-} and pH) (Table 4.12). Also, TH correlated strongly with (Ca^{2+}, Mg^{2+}, SO_4^{2-}, EC, TDS) and negatively correlated with pH for the streams sampled in 2016 (Table 4.13). In 2017, there was a perfect correlation between TH and (Ca^{2+}, Mg^{2+}, Na^+, K^+, Cl^-, SO_4^{2-}, EC and TDS) for the rivers (Table 4.14) and TH correlated strongly with (Ca^{2+}, Mg^{2+}, Na^+, SO_4^{2-}, EC, TDS, and pH) for the streams (Table 4.15). The relationship between TH and (Ca^{2+} and Mg^{2+}) for the rivers and streams reveals calcium and magnesium ion concentration in the rivers and streams. Also, the relationship between TH and (EC and TDS) for the rivers and streams suggests a possible modification of surface water chemistry and the amount of dissolved calcium and magnesium probably contributes to the components of EC and TDS in the surface water of the study area. The relationship between TH and HCO_3^- for the rivers suggest the possibility of carbonate hardness (Drever, 1988) due to dissolution of limestones from the underlying geology. The connection between TH and (Na^+, K^+) for the rivers and TH and K^+ for the streams indicates the presence of silicate hardness or the possibility of cation-exchange (Drever, 1988). The link between TH and SO_4^{2-} for the rivers and streams suggests sulphide hardness.The good relationship between TH and pH for the rivers and streams sampled in 2016 and 2017, respectively suggests a probable geochemical reaction.

In 2016, the Al content for the rivers and streams correlated negatively with (Na^+ and K^+) and (TDS and EC), respectively (Table 4.12 and 4.13). In addition, the Al concentration for the rivers and streams sampled in 2017 (Table 4.14 and 4.15) correlated strongly with (Ca^{2+}, Mg^{2+}, Na^+, K^+, Cl^-, SO_4^{2-}, TDS, EC, and TH) and HCO_3^-, respectively. The negative relationship between Al and (Na^+ and K^+) indicates that the presence of sodium and potassium in the rivers and streams does not influence the Al concentrations. Also, the negative linkage between Al

and (TDS and EC) suggests that Al is probably not involved in the physiochemical reactions of the streams. The good relationship between Al and (Ca^{2+}, Mg^{2+}, Na^{+}, and K^{+}) for the rivers sampled in 2017 suggests the weathering of silicate minerals (feldspar, hornblende, plagioclase etc.) from the underlying geology and granitic rocks (Fig 3.3 and 3.4). The good linkage between Al and TH is from a geogenic source. Additionally, the good connection between Al and Cl^{-} for the rivers sampled in 2017 is likely from an anthropogenic source, but studies have shown that biotite which is present in the underlying geology (Fig 3.3 and Fig 3.4) releases chloride {Henry & Diagle. (2018)}.

The good relationship between Al and SO_4^{2-} for the rivers is possibly geogenic due to the oxidation or mobilization of sulphide minerals (pyrites, chalcopyrite etc.) (Luebe et al., 1990) and weathering of silicate minerals (plagioclase, feldspar, hornblende etc.) from the underlying geology of the study area. The good relationship between Al and (TDS and EC) suggests the Al being one of the major constituents of EC and TDS in the rivers sampled in 2017. Further, the good relationship between Al and HCO_3^{-} suggest the weathering of silicate minerals (feldspar, hornblende, plagioclase etc.) and granitic rock from the underlying geology (Fig 3.3 and 3.4).

For the rivers sampled in 2016, Cr correlated negatively with (Ca^{2+}, HCO_3^{-}, SO_4^{2-},TH). In 2017, Cr in the streams correlated strongly with (Cl^{-}, NO_3^{-} and Al). The good relationship between Cr and Cl^{-} indicates that the streams might be in contact with ultra-mafic rocks from the underlying geology. These rocks when it weathers, it releases Cr which might interacts with Cl^{-} in the rivers and streams which have been rain fed. Dampare et al. (2008) recorded high concentration of Cr in ultra-mafic rock of the Birimian Supergroup rocks of south western Ghana and the Lower Tano River Basin records high rainfall amount (WRC,2012). The good relationship between Cr and NO_3^{-} is from an anthropogenic source or possibly the occurrence of rock- water interaction which requires further investigations. The good relationship between Cr and Al suggests a possible weathering of ultra-mafic rocks and silicate minerals from the underlying geology.

Further in 2016, Mn negatively correlated with HCO_3^- for the rivers (Table 4.12). This suggests the possible non- weathering of ferromagnesian minerals like biotite from the underlying geology. Also in 2016, Mn correlated strongly with pH for the streams (Table 4.13) and this suggest a possible weathering of banded manganese or ferromagnesian minerals from the underlying geology of the study area. In 2017, Mn correlated strongly with (Ca^{2+} and Al) for the rivers (Table 4.14) suggesting a possible weathering of monzonite rocks or silicate minerals (hornblende, plagioclase etc.) from the underlying geology. Also, there was a strong relationship between Mn and SO_4^{2-} for the rivers (Table 4.14). Since low values of Mn and SO_4^{2-} in the rivers was recorded in the chemical and trace element analysis, the good correlation could be coming from an anthropogenic source which requires further investigation. Also, in 2017 Mn correlated strongly with (Cl^-, Al, Cr) for the streams (Table 4.15). The good relationship between Mn and Al suggests a possible weathering of Monzonite rocks from the underlying geology. Additionally, the good relationship between Mn and Cl^- might possibly be from anthropogenic sources or rock-water interaction but further investigation is required. In addition, the good linkage between Mn and Cr is from the weathering of ferromagnesium minerals and ultra-mafic rocks of the underlying geology of the study area.

A highly negative correlation exists between Fe and HCO_3^- for the rivers sampled in 2016 (Table 4.12). This indicates the absence of Fe geochemical processes in the rivers. The perfect relationship between Fe and Mn for the rivers and streams sampled in 2016 (table 4.12 and 4.13) suggests that weathering of Monzonite rocks or ferromagnesium mineral like biotite from the underlying geology (Fig 3.3 and Fig 3.4).

A good relationship between Fe and pH for the streams sampled in 2016 (Table 4.13) suggests a possible geochemical processes or weathering of silicate minerals and sulphide minerals {pyrite (FeS2) and chalco- pyrite (CuFeS2)} oxidation from the underlying geology

The strong correlation between Fe and TH for the streams sampled in 2016 (Table 4.13) suggest Fe hardness.

In 2017, Fe correlated strongly with (NO_3^- and Al) for the rivers (Table 4.14) and (Cl^-, NO_3^-, Cr and Mn) for the streams (Table 4.15). When sulphide mineral oxidizes, the oxidation possibly induces an increase in the rates of sulphates and this also persuades other trace elements (Mariotti, 1994). This probably constitutes the good conditions for the flow of oxidant elements especially nitrates. According to Mariotti, 1994, pyrite intervenes as an electron exchanger in a de-nitrification reaction given by the equation:

$$FeS_2 + 14NO_3^- + 4H^+ \rightarrow 7N_2(g) + 10SO_4^{2-} + 5Fe^{2+} + 2H_2O \ldots. \text{Eq } 4.1$$

In the oxidizing part, the ferrous iron is unstable in solution and precipitates in the form of hydroxide or oxide. In the mist of elevated nitrate contents, the above equation can be reduced depending on the overall reaction {Strebel et al. (1990)}:

$$5Fe^{2+} + NO_3^- + 7H_2O \rightarrow 5FeOOH + \tfrac{1}{2} N_2(g) + 9H^+ \ldots \text{Eq } 4.2$$

The decrease of nitrates is formed by electron exchange with powerful reducers like pyrite (FeS_2) organic carbon. Its therefore assumed that the above deductions might possibly be the reason why Fe correlated strongly with NO_3^- in the rivers and streams but further investigations are required.

Also, the good relationship between Fe and Al for the rivers suggests the weathering of granites, monzonites, and silicate minerals (hornblende, biotite, etc.) from the underlying geology of the study area. Additionally, the good connection between Fe and Cl^- for the streams suggests a possible rock-water interaction which requires further investigation. The good relationship between Fe and Cr suggests rock weathering.

For the rivers sampled in 2016 (Table 4.12), Co correlates perfectly with NO_3^- and its possibly from an anthropogenic source. Also, Co negatively correlated with pH for the rivers (Table 4.12). Also, for the rivers sampled in 2017 (Table 4.14), Co correlated strongly with (Ca^{2+}, Mg^{2+}, Na^+, K^+, Cl^-, SO_4^{2-}, TDS, EC, TH, Al, Mn, and Fe) and for the streams (Table 4.15), Co correlated perfectly with (Cl^-, Cr, Mn, and Fe). The relationship between Co and (Ca^{2+} and Mg^{2+}) for the rivers suggest a possible dissolution of carbonate minerals or shales from the

underlying geology to release Co as a secondary mineral (Hitzman et al., 2017). The good relationship between Co and TH suggests that Co possibly contributes to the TH of the rivers. Uren, 2013 stated that "In sedimentary rocks Co and Mn are very variable, but as a rule of thumb, they are lowest in coarse - grained sediments e.g., sandstones and highest in fine-grained sediments e.g., shales". In the study area even though rock outcrops were not sampled and analyzed for mineral composition, the underlying geology is made up of sedimentary rocks with sand stones and shales and the concentration of Co and Mn in the rivers and streams were minimal hence the statement made by Uren, 2013 possibly holds for the strong correlation existing between Co and Mn in the rivers and streams.

The good linkage between Co and (Na^+, K^+, and Al) might possibly be from a geogenic source and the probable source must be investigated in future works. The good relationship between Co and Fe in the rivers and streams suggest sulphide mineral oxidation or mobilization to release Co as a secondary mineral. The good relationship between Co and (SO_4^{2-}) for the rivers and streams also suggests the oxidation or mobilization of sulphide minerals to release Co as a secondary mineral. The good relationship between Co and Cl reveals rock-water interactions which requires further investigations. The good relationship between Co and (TDS and EC) indicates that Co possibly contributes to the river water mineralization of the study area.

In 2016, Ni correlated strongly with (Ca^{2+}, K^+, HCO_3^-, SO_4^{2-}, and TH) for the rivers (Table 4.12) and Fe for the streams (Table 4.13). The good relationship between Ni and (Ca^{2+}, K^+) suggests a possible rock-water interaction. The good linkage between Ni and (TH, HCO_3^-) indicates the probability of sulphide mineral hardness and same geochemical processes respectively.

The good correlation between Ni and (Fe, SO_4^{2-}) for the streams and rivers, respectively, specifies sulphide mineral oxidation or mobilization to release Ni as a secondary mineral. Studies carried out by Adjimah et al (1993) reveals that the sulphide minerals in the rocks of the Birimian hosted Ni as one of the pathfinder elements for the exploration of gold . Likewise, Ni highly correlated negatively with Mn for the rivers sampled in 2016. In 2017, Ni correlated

strongly with (NO_3^-, Al, Cr, Fe, Co) for the rivers and correlated strongly with TH for the streams. The good relationship between Ni and NO_3^- for the rivers suggests a possible rock-water interaction which requires further investigation. In addition, the good relationship between Ni and Al for the rivers suggests rock weathering. But this requires further investigations since studies have shown nickel incorporation into silicate minerals (Manceau & Calas, 1985; Decarreau et al., 1987; Hseu, 2006). The good linkage between Ni and Cr for the rivers suggest rock weathering. Studies carried out by Hseu (2006), and Oze et al. (2004) shows that Ni and Cr are present in elevated concentration in soils produced from ultramafic rocks. The good relationship between Ni and Co shows sulphide mineral oxidation or mobilization to release Ni and Co as secondary minerals.

Cu correlated perfectly with NO_3^- for the rivers sampled in 2016. This suggest a likely rock-water interaction but further investigations are required. The perfect relationship between Cu and Co for the rivers suggest a possible sulphide mineral (chalcopyrite) mobilization to release Co as a secondary mineral. The exceedingly negative correlation between Cu and pH for rivers indicates that the pH of the rivers possibly has no significant influence on the mobilization of sulphide minerals. In 2016, Cu correlated strongly with Mn for the streams. This indicates a geogenic origin and its possibly linked to the existence of sulphide mineral (chalcopyrite etc.) mobilization to release Mn as a secondary mineral. In 2017, there was a perfect correlation between Cu and Cr and a strong correlation between Cu and Ni for the rivers. For the streams, there was a strong correlation between Cu and (Cl^-, Al, Cr, Mn, Fe, Co). The good relationship between Cu and (Fe, Co, and Ni) suggest the probability sulphide minerals (chalcopyrite, pyrites) mobilization to release Co, and Ni as a secondary mineral. Fe, Cu, Co, and Ni have been discovered as path finder trace elements used in the exploration of gold in the Birimian supergroup rocks (Leube et al., 1990; Adjimah et al., 1993). In addition, the good linkage between Cu and Cr suggests a possible geogenic source. The good relationship between Cu and Cl is probably from rock-water interaction which requires further investigations.

Zn correlated negatively with (K^+ , pH) but correlated strongly with NO_3^- for the rivers sampled in 2016 (Table 4.12). The relationship between Zn and NO_3^- suggest a possible rock- water interaction which requires further investigations. Also, in 2016, Zn correlated strongly with (Ni and Fe) for the streams (Table 4.13) suggesting that the streams are possible in contact with sulphide mineral (pyrites and chalcopyrite) where Zn, Ni and Fe are released into the rivers. Adjimah et al., 1993 discovered sulphide minerals hosting trace elements like Zn, Ni etc. which were used as pathfinder elements for the exploration of gold in the Birimian super group rocks. In addition, Zn correlated strongly with Mn for the sampled streams suggesting the likelihood of a high stream discharge (Khan et al., 1998) from the upstream environment (Birimian supergroup rocks) to the downstream environment (Apollonian formation), since the study area is in a deposition environment. In 2017, Zn correlated strongly with (Fe, Co, Ni and Cu) for the sampled rivers (Table 4.14) suggesting that the rivers are in contact with sulphide minerals from the underlying geology. Also, the good relationship between Zn and Al (Table 4.14) for the rivers is possibly from geogenic sources which requires further investigations. The strong relationship between Zn and Cr for the rivers (Table 4.14) is from a geogenic source. Additionally, for the streams sampled in 2017 (Table 4.15), Zn correlated strongly with (K^+, Cl^- and NO_3^-) suggesting the possible presence of anthropogenic sources or rock-water interaction, but further investigations are required. Also, there was a good relationship between Zn and HCO_3^- for the streams (Table 4.15) suggesting a probable geochemical processes. The good relationship between Zn and TDS for the streams suggests that Zn is contributing to the mineralization of the stream. The good relationship between Zn and (Al, Cr, Mn, Fe, Co, and Cu) for the streams might likely be derived from geogenic sources.

In 2016, As in the sampled rivers correlated perfectly with Fe and Mn (Table 4.12) suggesting that the rivers might likely be in contact with ferromagnesium minerals or sulphide minerals (Pyrites, Chalcopyrite etc.) where trace elements such as As, **Mn**, **Fe**, Cu, Ag etc. are hosted as pathfinder elements for the discovery of gold (Luebe et al., 1990) in the rocks of the Birimian.

Also, in 2016 and 2017, As correlated strongly with Cr for the streams and rivers, respectively suggesting a geogenic source. Also, there was a perfect and a strong correlation between As and (Cu and Zn) for the rivers sampled in 2017 indicating a geogenic source like sulphide mineral mobilization. Additionally, in 2017, As correlated perfectly with (Ca^{2+}, Mg^{2+}, HCO_3^-) for the streams (Table 4.15) indicating that the streams might possibly be in contact with sulphide minerals, silicate minerals (hornblende etc.) and monzonite rocks of the study area. Works carried out by Alam et al. (2014) suggests that "the weathering of silicate minerals is an essential Arsenic releasing mechanism and that elevated pH and low redox potential promotes the weathering of silicate minerals and release As concentration. The good relationship between As and TH suggest a likely arsenic hardness in the rivers and streams. In addition, the perfect relationship between As and SO_4^{2-} for the streams (Table 4.15) suggests a probable oxidation of sulphide minerals. The perfect correlation between As and (EC and TDS) for the streams indicates that As is one of the major elements that contribute to the mineralization of the streams.

In 2016, the Cd in the sampled rivers (Table 4.12) correlated negatively with Na^+. Also, for the streams, Cd negatively correlated with SO_4^{2-} (Table 4.13) suggesting that SO_4^{2-} liberated from anthropogenic or geogenic sources is possibly not contributing to Cd content in the streams. In addition, Cd in the streams correlated strongly with (Cr and As) suggesting a probable geogenic source. In 2017, Cd correlated strongly with NO_3^- for the rivers (Table 4.14) indicating a possible anthropogenic source. Also, Cd correlated strongly and perfectly with (Al, Cr, Mn, Fe, Co, Ni, Zn and Cu) suggesting a possible geogenic source. Also, Cd correlated strongly with K^+ for the streams (Table 4.15) suggesting a possible anthropogenic source. In addition, Cd correlated perfectly with HCO_3^- for the streams indicating a possible geochemical process but further investigations are required. Likewise, Cd correlated strongly with TDS for the streams suggesting that Cd in the streams might possibly be involved in physiochemical reactions of the streams.

Pb in the rivers sampled in 2016 (Table 4.12) negatively correlated with HCO_3^- indicating the absence of Pb geochemical processes. In addition, there was a perfect correlation between Pb

and (Fe, Mn, Co and As) suggesting rock weathering {sulphide minerals (pyrites, arsenopyrites, chalcopyrite) oxidation}. Additionally, Pb correlated perfectly with Cr suggesting a possible rock-water interaction which requires further investigations. For the stream sampled in 2016 (Table 4.13), Pb correlated negatively with SO_4^{2-} but correlated strongly with (Al, Cr, and Cu). The negative relationship between Pb and SO_4^{2-} indicates that SO_4^{2-}might possible not influence the presence of Pb in the rivers and streams. The good relationship between Pb and (Al and Cr) for the streams sampled in 2016 suggests a possible geogenic or anthropogenic source. Additionally, the perfect relationship between Pb and Cu for the streams suggests the mobilization of sulphide minerals (Chalcopyrite's) to release Pb as a secondary mineral. In 2017, the Pb content in the rivers (Table 4.14) correlated strongly with NO_3^- suggesting a possible anthropogenic source. Also, a good relationship was observed between Pb and Al in the stream suggesting a possible geogenic source. Also, the good relationship between Pb and (Fe, Ni and Zn) is from a geogenic source (sulphide mineral oxidation or mobilization) The good linkage between Pb and Cd suggests a probable anthropogenic source, which requires further investigation. For the streams sampled in 2017 (Table 4.15), Pb correlated strongly with Ca^{2+}. This possibly indicate rock-water interaction which requires further investigation. Also, Pb correlated strongly with (EC and TDS) signifying that Pb contributes to the stream mineralization.

The above correlated parameters being negative or positive, shows that the measured ions and trace elements in the rivers and streams are coming from the same geochemical processes and have a strong to moderate influence on each other. Also from the above correlation, it can be said that the chemistry of surface water in the Lower Tano River Basin is possibly controlled by rock weathering with few being controlled by anthropogenic sources. In addition, it can be concluded that the Nickel (Ni) content (Table 4.12) in the rivers sampled in 2016, the Total hardness (TH) concentration in the stream sampled in 2016 (Table 4.13), the Cobalt (Co) content in the rivers sampled in 2017 and the Zinc (Zn) content in the streams sampled in 2017 are important drinking water parameters that exists in the rivers and streams of the Lower Tano River Basin. This is because Ni, TH, Co and Zn, significantly correlated with 6, 6, 12, and 11 parameters, respectively out of the 23 measured variables. Additionally, the measured

parameters showing moderate to weak correlation indicates that multiple sources and flow are likely responsible for the surface water (rivers and streams) quality in the Lower Tano River Basin.

4.2.2 Groundwater chemistry and its suitability for drinking

4.2.2.1 Results of the field data

The results of the descriptive statistical analysis of the field data for the hand dug wells and boreholes sampled in each specific year are shown in table 4.16, 4.17, 4.18,4.19,4.20 and 4.21, respectively.

Table 4. 16: Descriptive statistics of field parameters for the Boreholes drilled in 2013

Field Parameters	*T°c*	*pH*	*EC (µS/cm)*	*TDS (mg/L)*
Number of samples	30	30	30	30
Mean	24.73	6.94	219.22	114.42
Standard Error	0.08	0.02	7.85	5.21
Median	24.90	6.98	218.00	108.30
Mode	24.90	6.99	219.00	108.00
Standard Deviation	0.44	0.10	43.02	28.55
Sample Variance	0.19	0.01	1850.86	815.15
Kurtosis	-0.59	1.43	2.18	1.90
Skewness	-0.59	-1.21	-0.66	0.49
Minimum	24.00	6.67	103.00	52.00
Maximum	25.50	7.11	301.00	194.00
Sum	742.00	208.22	6576.70	3432.70
Confidence Level (95.0%)	0.16	0.04	16.06	10.66

Table 4. 17: Descriptive statistics of the field parameters for the Boreholes drilled in 2014 to 2015

Field Parameters	*EC(µS/cm)*	*Salinity*	*TDS (mg/L)*	*pH*
Number of Samples	18	18	18	18
Mean	268.22	0.09	113.58	6.27
Standard Error	57.48	0.02	27.56	0.15
Median	168.50	0.08	70.90	6.20
Mode	N/A	0.08	70.90	6.00
Standard Deviation	243.86	0.09	116.93	0.65
Sample Variance	59469.01	0.01	13673.20	0.42
Kurtosis	10.84	16.28	11.62	-0.04
Skewness	3.08	3.95	3.22	0.23
Minimum	101.00	0.04	34.20	5.20
Maximum	1150.00	0.43	542.20	7.70
Sum	4828.00	1.61	2044.40	112.80
Confidence Level (95.0%)	121.27	0.04	58.15	0.32

Table 4. 18: Descriptive statistics of field parameters for the Hand dug wells sampled in 2016.

Field Parameters	*T°C*	*Salinity*	*pH*	*TDS (mg/L)*	*EC (µS/cm)*
Number of samples	36	36	36	36	36
Mean	27.48	0.17	6.42	298.78	454.05
Standard Error	0.23	0.04	0.07	34.27	50.40
Median	27.35	0.10	6.41	224.00	345.50
Mode	27.70	0.00	6.20	215.00	321.00
Standard Deviation	1.35	0.22	0.44	205.64	302.38
Sample Variance	1.82	0.05	0.20	42286.15	91432.69
Kurtosis	-0.25	4.68	1.42	-0.97	-0.94
Skewness	-0.21	1.86	0.79	0.68	0.68
Minimum	24.00	0.00	5.63	30.00	44.20
Maximum	29.90	1.00	7.80	709.00	1063.00
Sum	989.20	6.00	230.94	10756.25	16345.90
Confidence Level (95.0%)	0.46	0.07	0.15	69.58	102.31

Table 4. 19: Descriptive statistics of field parameters for the Boreholes sampled in 2016

Parameters	*TDS mg/L*	*EC µS/cm*	*Salinity*	*T°C*	*pH*
Number of Samples	44	44	44	44	44
Mean	164.34	261.47	0.05	27.75	6.33
Standard Error	16.15	25.27	0.01	0.15	0.09
Median	145.00	245.50	0.00	27.65	6.27
Mode	85.00	127.60	0.00	27.50	6.80
Standard Deviation	107.10	167.62	0.09	1.00	0.61
Sample Variance	11469.39	28095.86	0.01	1.00	0.37
Kurtosis	0.74	-0.06	6.22	0.63	2.37
Skewness	1.03	0.75	2.36	-0.16	0.88
Minimum	27.00	39.70	0.00	25.30	5.26
Maximum	484.00	721.00	0.40	30.00	8.51
Sum	7231.00	11504.80	2.10	1220.90	278.50
Confidence Level (95.0%)	32.56	50.96	0.03	0.30	0.19

Table 4. 20: Descriptive statistics of field parameters for the Hand dug wells sampled in 2017

Parameters	*T° C*	*pH*	*TDS mg/L*	*EC µS/cm*	*Salinity*
Number of samples	30	30	30	30	30
Mean	28.31	5.98	220.07	396.41	0.17
Standard Error	0.35	0.16	27.16	48.22	0.03
Median	28.20	5.97	181.00	328.50	0.11
Mode	28.40	5.60	375.00	682.00	0.00
Standard Deviation	1.83	0.89	148.79	264.12	0.16
Sample Variance	3.35	0.80	22137.10	69759.48	0.03
Kurtosis	7.67	-0.22	-0.70	-0.62	0.60
Skewness	-1.75	-0.46	0.70	0.71	1.03
Minimum	21.40	4.10	24.00	43.20	0.00
Maximum	31.70	7.40	546.00	994.00	0.63
Sum	764.50	179.27	6602.00	11892.30	5.24
Confidence Level (95.0%)	0.72	0.33	55.56	98.62	0.06

Table 4. 21: Descriptive statistics of field parameters for the Boreholes sampled in 2017

Parameters	*TDS mg/L*	*EC µS/cm*	*T˚C*	*PH*	*Salinity*
Number of samples	53	53	53	53	53
Mean	150.06	252.82	28.46	6.02	0.06
Standard Error	13.65	21.48	0.22	0.11	0.01
Median	113.00	206.00	28.00	6.05	0.03
Mode	85.00	127.60	27.50	6.20	0.00
Standard Deviation	99.38	156.35	1.57	0.78	0.08
Sample Variance	9875.75	24444.14	2.48	0.61	0.01
Kurtosis	1.46	0.22	-0.32	1.40	5.43
Skewness	1.28	0.93	0.80	0.03	2.08
Minimum	39.00	70.00	26.00	4.10	0.00
Maximum	484.00	721.00	32.02	8.51	0.40
Sum	7953.20	13399.50	1508.42	319.13	3.10
Confidence Level (95.0%)	27.39	43.09	0.43	0.22	0.02

From table 4.16, the temperature for the boreholes drilled in 2013 vary from 24° C to 25.50° C with a mean of 24.73° C. The temperature for the boreholes drilled from 2014 to 2015 was not measured due to faulty meters. In 2016 during the rainy season, the temperature of the hand dug well and boreholes sampled from the aquifer of the Apollonian formation and the Birimian Supergroup (Table 4.18 and 4.19) range from 24° C to 29.90° C with a mean of 27.48° C and from 25.30° C to 30° C with a mean of 27.75° C, respectively. For the hand dug wells and boreholes sampled in 2017 during the dry season, the temperature varies from 21.40° C to 31.70° C with an average of 28.31° C and from 26° C to 32.02° C with a mean of 28.46° C (Table 4.20 and 4.21), respectively.

From table 4.16, the pH of the boreholes drilled in 2013 vary from 6.67 to 7.11 with a mean of 6.94. The least pH value is recorded for a borehole drilled at Kamgbunli in the aquifer of the Apollonian formation and the maximum pH value is recorded for a borehole drilled at Bobrama also in the aquifer of the Apollonian formation. The pH of the entire borehole water is slightly acidic to neutral but falls within WHO (2011) permissible limit of 6.5 to 8.5 for drinking water.

For the boreholes drilled from 2014 to 2015 (Table 4.17), the pH varies from 5.2 to 7.7 with a mean of 6.27. The minimum and maximum pH is recorded for a borehole drilled at Kengen and Newtown, respectively and both boreholes are in the aquifer of the Apollonian formation.

The pH of the borehole water is acidic to neutral with 80 % (n=18) below WHO (2011) permissible limit of 6.5 to 8.5 for drinking water.

For the hand dug wells sampled in 2016 (Table 4.18), the minimum pH value (pH = 5.63) is recorded for a hand dug well sampled at Nkroful in the aquifer of the Birimian Supergroup and the maximum pH (pH = 7.80) is recorded for a hand dug well sampled at Ankobra in the aquifer of the Apollonian formation. 67% (n = 36) of the sampled hand dug wells are below WHO (2011) permissible limit of 6.5 to 8.5 for drinking water and the remaining 33% are within the acceptable limits. Out of the 26 acidic hand dug well (n=36) water, 19 hand dug wells were sampled from the aquifer of the Apollonian formation and the remaining 7 were sampled from the aquifer of the Birimian Supergroup rocks. The minimum pH (pH = 5.26) of the borehole water sampled in 2016 (Table 4.19) is recorded for a borehole sampled at Salman in the aquifer of the Birimian Supergroup and the maximum pH (pH = 8.51) is measured for a borehole sampled at Ankobra in the aquifer of the Apollonian formation. 68.18% of the sampled boreholes (n=44) are below WHO (2011) permissible limit of 6.5 to 8.5 for drinking water. Out of the 27 (n=44) acidic borehole water, 18 boreholes were sampled from the aquifer of the Apollonian formation and the remaining 9 were taken from the aquifer of the Birimian Super group.

For the hand dug wells sampled in 2017 (Table 4.20), the minimum and maximum pH is recorded (pH = 4.10 and 7.40) for hand dug wells sampled at Elubo in the aquifer of the Apollonian formation (fig 3.54). 66.7% of the hand dug wells (n=30) all sampled from the aquifer of the Birimian supergroup are below WHO (2011) permissible limit of 6.5 – 8.5 for drinking water. Also, for the 2017 borehole samples, the minimum and maximum pH (pH = 4.0 and 8.51) values is recorded for boreholes sampled at Atwinbaso and Ampaim, respectively. These boreholes are all located in the aquifer of the Apollonian formation. 81.48% of the boreholes (n=54) are below WHO (2011) permissible limit of 6.5 – 8.5 for drinking water and out of the 44 acidic borehole water, 28 boreholes were taken from the aquifer

of the Apollonian formation and the remaining 16 are taken from the aquifer of the Birimian Supergroup.

The acidity of most groundwater samples is attributed to clay minerals like silica and kaolin which exist in the rocks of the Apollonian and the Birimian supergroup. These clay minerals act as H^+ buffers (Sjostrom, 1993).

Another source of low pH in the groundwater is attributed to the oxidation and hydrolysis of sulphide minerals {Preda and Cox (2000, 2001)}. In the study area, Luebe et .al (1990) discovered sulphide minerals like pyrites in the rocks of the Birimian and Keese,1985 also discovered nodules of pyrites in the rocks of the Apollonian. When these pyrites interact with the groundwater, H^+ concentration in the groundwater increases lowering the pH of the groundwater.

Infiltration of rainwater also lowered the pH of the groundwater. The study area records high amount of rainfall and Edjah et al. (2015) observed that the source of groundwater recharge in the study area was of meteoric origin. Also, the pH of the sampled rainwater for this study ranges from 5.2 to 6.5 and the TDS varies from 8.9 to 20 mg/L

In the study area, there are lots of trees and during cellular respiration by the trees, CO_2 gas is released and that dissolves in the groundwater resulting in the formation of H_2CO_3. When H_2CO_3 dissociates it leads to an increase in HCO_3^- and H^+(Isa et al., 2012). Once H^+ increases, the pH of the groundwater is lowered.

Also, parts of the Lower Tano River Basin are composed of granites, phyllites and schists (Fig 3.3 and 3.4) and according to Wright et al.1985, these types of rocks produce acidic water.

From figure 4.10, it is seen that the aquifer of the Apollonian formation produces most acidic groundwater. The results of the pH values for the groundwater sampled from 2013 to 2017 are like the results obtained by Edjah et al. (2015) who worked in parts of the Lower Tano

river basin. In addition, WRC (2012) recorded low pH values (< 7) for some groundwater across the Tano Basin.

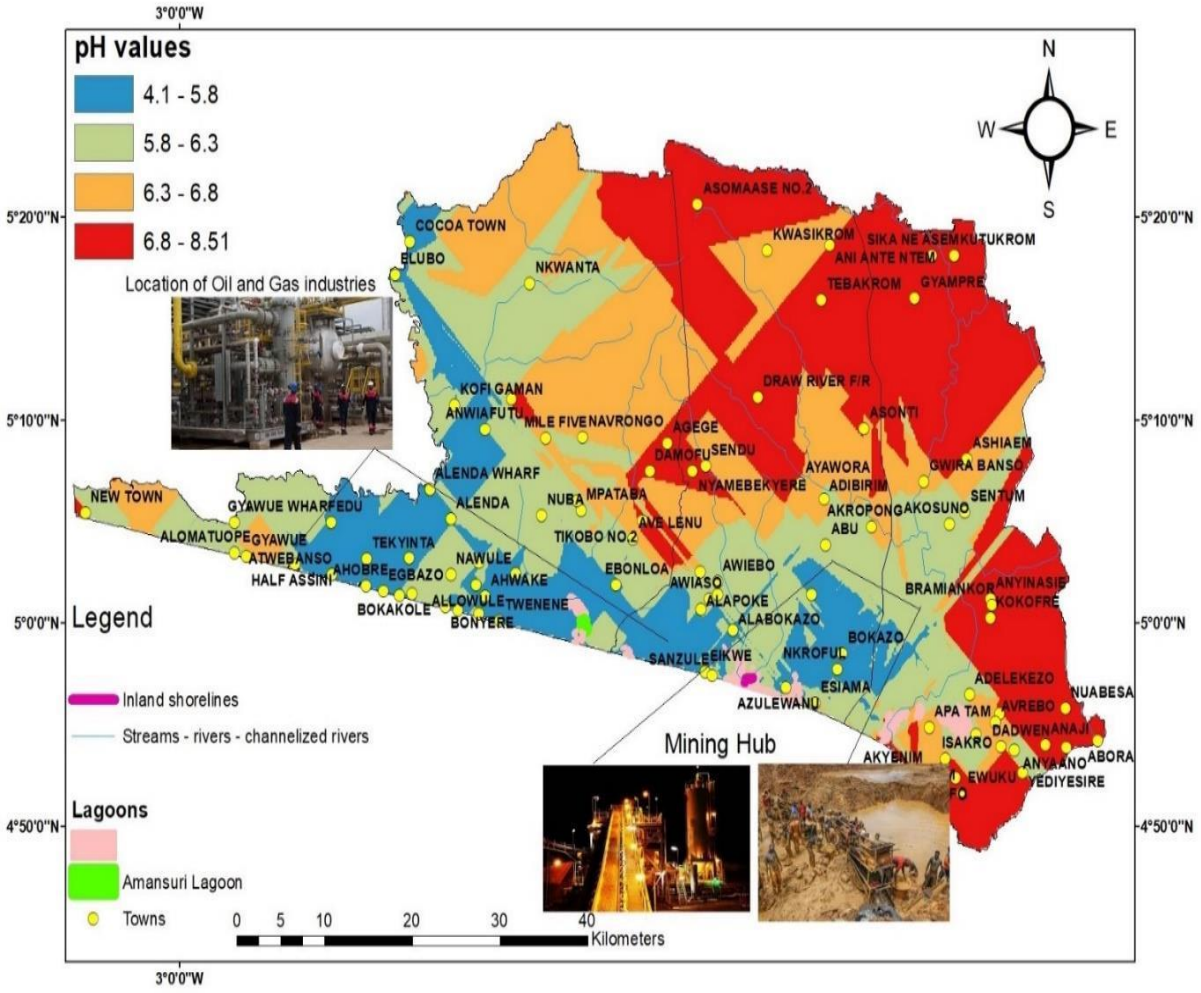

Figure 4. 10: Spatial distribution map of pH in groundwater of the Lower Tano River Basin.

TDS is an important parameter that can influence the major compositions in groundwater quality (Paznand & Javanshir, 2014). From table 4.16, the minimum TDS concentration (TDS = 52 mg/L) for the boreholes drilled in 2013 is recorded at Kegyina in the aquifer of the Birimian Supergroup and the maximum TDS concentration (TDS= 194 mg/L) is measured at Mpeasem in the aquifer of the Apollonian formation.

Also, from table 4.17, the minimum TDS concentration (TDS= 34. 2 mg/L) for the boreholes drilled from 2014 to 2015 is measured in a borehole developed at Alumatuope in the aquifer

of the Apollonian formation and the maximum TDS concentration (TDS=542.2 mg/L) occurs in a borehole drilled at Newtown, also in the aquifer of the Apollonian formation.

In 2016, the minimum TDS concentration (TDS = 30 mg/L) is recorded for a hand dug well sampled at Gyegyekrom in the aquifer of the Birimian Supergroup and the maximum TDS (TDS= 709 m/L) content is recorded for a hand dug well sampled at Esiama in the aquifer of the Apollonian formation. Also in 2016, the minimum and maximum TDS concentrations (TDS= 27 mg/L and 484 mg/L) are recorded for boreholes sampled at New Nzulezu and Asanda, respectively. Both boreholes were taken from the aquifer of the Apollonian formation.

In 2017, the minimum and maximum TDS (TDS = 24 m/L and 546 m/L, respectively) content is recorded for hand dug wells sampled (Table 4.20) at Gyegyekrom in the aquifer of the Birimian Supergroup and Esiama in the aquifer of the Apollonian formation, respectively. For the borehole samples, the minimum and maximum TDS concentrations (TDS= 39 mg/L and 484 mg/L) is measured in boreholes sampled at Tiekobo no 1 and Esiama respectively. Both boreholes are in the aquifer of the Apollonian formation.

The degree of groundwater quality can be classified as fresh if the TDS is < 1000 mg/L; brackish if the TDS is between 1000 to 10,000 mg/L; saline if the TDS is ranged from 10,000 to 1,000,000 mg/L (Todd, 1980). Accordingly, the entire quality of the sampled groundwater (n=211) is fresh.

The spatial distribution map of TDS (Fig 4.11) indicates that all the sampled groundwater are below WHO (2011) desirable limit of 500 mg/L and maximum permissible limit of 1500 mg/L. The low TDS content in the groundwater reveals a that the groundwater has short residence time which will be explained further in the 5th specific objective.

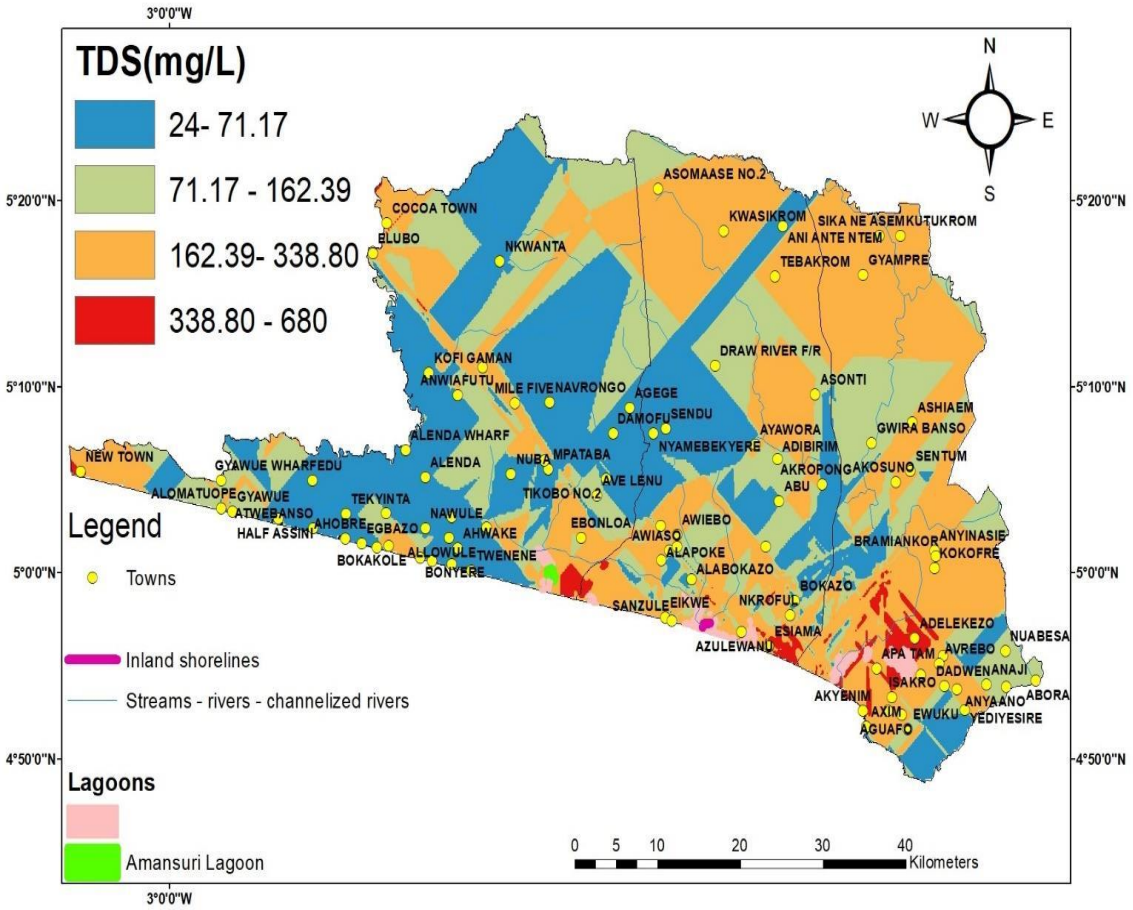

Figure 4. 11: Spatial distribution map of TDS values in groundwater in the Lower Tano River Basin.

For the boreholes, the electrical conductivity (EC) values in 2013 samples (Table 4.16) had the maximum value (EC = 301 µS/cm) recorded for a borehole drilled at Mpeasem in the aquifer of the Apollonian formation and the minimum value (EC = 103 µS/cm) recorded for a borehole drilled at Kegyina in the aquifer of the Birimian Supergroup.

From 2014 to 2015 (Table 4.17), the minimum and maximum EC concentration (EC = 101 µS/cm and 1150 µS/cm) is recorded in boreholes drilled at Alumatupe and Newtown respectively. Both towns are in the aquifer of the Apollonian formation.

The EC content in the hand dug wells sampled in 2016 (Table 4.18) had the minimum value (EC = 44.20 µS/cm) recorded for a hand dug well sampled at Gyegyekrom in the aquifer of the Birimian Supergroup and the maximum value (EC = 1063 µS/cm) recorded for a hand dug well sampled at Esiama in the aquifer of the Apollonian formation. In 2016, the minimum and

maximum EC (EC = 39.70 µS/cm and 721 µS/cm) (Table 4.19) content are recorded in boreholes sampled at New Nzulezu and Asanta, respectively. Both boreholes are in the aquifer of the Apollonian formation.

The EC content in the hand dug wells sampled in 2017 (Table 4.20) had the minimum EC value (EC = 43.20 µS/cm) recorded for a hand dug well sampled at Gyegyekrom in the aquifer of the Birimian Supergroup and the maximum value (EC = 994 µS/cm) recorded for a hand dug well sampled at Esiama in the aquifer of the Apollonian formation. Also in the same year, the minimum EC value (EC = 70 µS/cm) is measured in a borehole sampled at Tiekobo no 1 and the maximum EC (EC = 721 µS/cm) value is recorded in a borehole sampled at Esiama. Both boreholes are in the aquifer of the Apollonian Formation.

Per WHO (2011), the most desirable limit of EC in drinking water is 1500 µS/cm. EC in groundwater can be classified as type I, if the enrichments of salts are low (EC<1500 µS/cm); type II, if the enrichment of salts are medium (EC: 1,500 and 3000 µS/cm); and type III, if the enrichments of salts are high (EC > 3000 µS/cm) (Sarath Prasanth et al, 2012). According to the above classification of EC, 100% of the total groundwater samples (n=211) fall under type I (low enrichment of salts). The low EC values (EC< 1500 µS/cm) recorded for the groundwater is an indication of short residence time (Hunslow, 1995) which will be explained in the 5th specific objective. Also, from Fig (4.12), the minimum EC values in the groundwater represented by shades of green colour is concentrated mostly in the aquifer of the Birimian supergroup with few representations in the aquifer of the Apollonian formation.

The results obtained for TDS and EC for the groundwater samples is like the results obtained by Edjah et al. (2015) and WRC (2012).

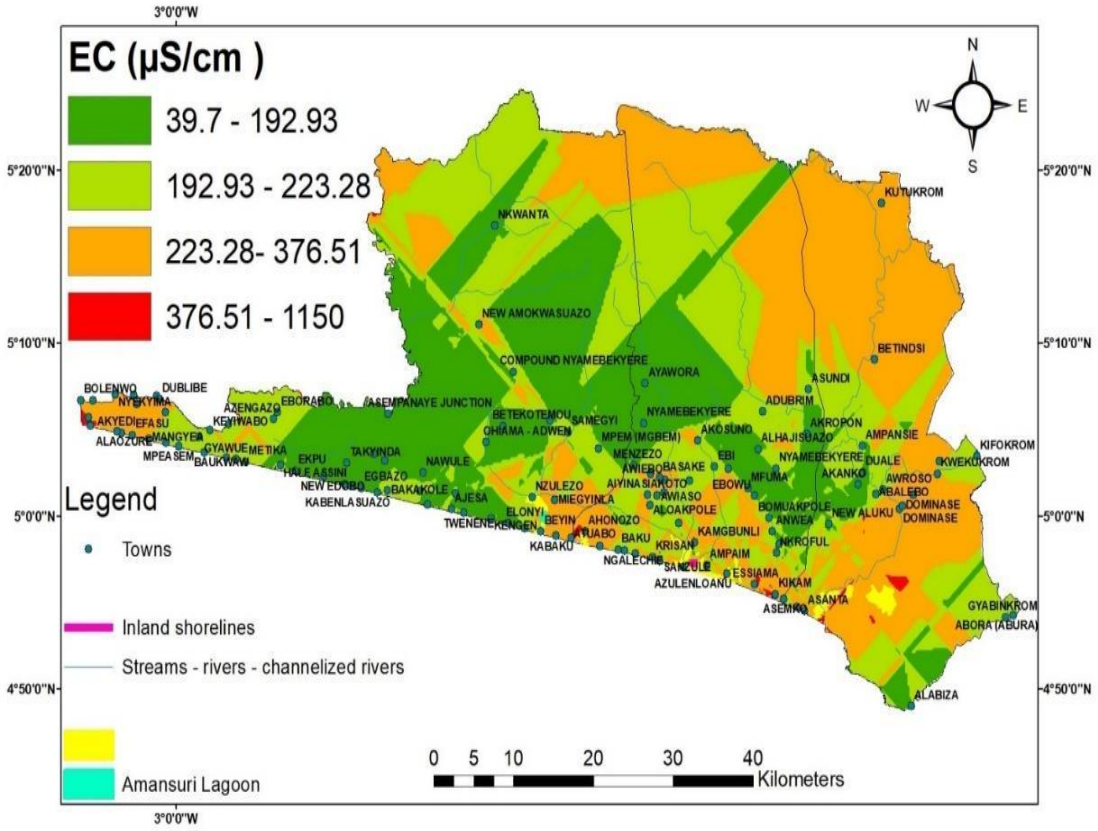

Figure 4. 12: Spatial distribution map of EC (µS/cm) concentrations in groundwater in the Lower Tano River Basin.

4.2.2.2 Results of the Laboratory analysis (Hydrochemical data) and Alkalinity (as in Bicarbonate) in groundwater

The results of the descriptive statistical summaries of the hydrochemical data are shown in table 4.22,4.23 and 4.24,4.25, and 4.26.

Table 4. 22: Descriptive statistics of the hydrochemical data for the Boreholes drilled in 2013

Parameters (mg/L)	Ca^{2+}	Mg^{2+}	TH	Cl^{-}	SO_4^{2-}	NO_3^{-}
Number of samples	30	30	30	30	30	30
Mean	70.70	42.30	110.77	39.21	6.77	1.20
Standard Error	4.16	3.77	7.19	5.50	0.43	0.08
Median	67.50	41.50	104.00	31.50	6.86	1.09
Mode	53.00	23.00	111.00	12.00	10.00	1.09
Standard Deviation	22.81	20.63	39.39	30.12	2.37	0.42
Sample Variance	520.22	425.60	1551.63	907.46	5.61	0.18
Kurtosis	2.08	-1.33	-0.39	-0.79	1.13	1.74
Skewness	1.05	0.18	0.63	0.52	-0.32	1.37
Minimum	35.00	12.00	58.00	0.04	0.01	0.54
Maximum	143.00	79.00	205.00	96.00	11.00	2.31
Sum	2121.00	1269.00	3323.00	1176.38	202.96	34.83
Confidence Level (95.0%)	8.52	7.70	14.71	11.25	0.88	0.16

Table 4. 23: Descriptive statistics of the hydrochemical data for the Boreholes drilled in 2014 to 2015

Parameters (mg/L)	Ca^{2+}	Mg^{2+}	Na^{+}	K^{+}	TH	HCO_3^{-}	Cl^{-}	SO_4^{2-}
Number of samples	18	18	18	18	18	18	18	18
Mean	22.83	4.84	22.49	3.08	76.00	55.83	32.42	8.82
Standard Error	4.93	1.51	8.37	0.91	15.37	14.41	11.50	1.95
Median	15	2.65	14	1.8	45	26	24.1	8
Mode	15	2.6	N/A	1.1	37	162	5.5	2
Standard Deviation	20.91	6.39	35.51	3.85	65.22	61.15	48.79	8.05
Sample Variance	437.21	40.84	1261.15	14.86	4253.41	3739.09	2380.02	64.78
Kurtosis	1.27	5.49	16.38	4.65	-0.38	-0.21	16.35	4.24
Skewness	1.47	2.57	3.97	2.24	1.14	1.25	3.96	1.78
Minimum	4	0.7	3.4	0.2	19	5	5.5	1
Maximum	71	22.6	162	14.6	196	171	224	33
Sum	411	87.1	404.8	55.4	1368	1005	583.6	150
Count	18	18	18	18	18	18	18	17
Confidence Level(95.0%)	10.40	3.18	17.66	1.92	32.43	30.41	24.26	4.14

Table 4. 24: Descriptive statistics of the hydrochemical data for the Hand dug wells sampled in 2016

Parameters (mg/L)	Ca^{2+}	Mg^{2+}	TH	Na^{+}	K^{+}	Cl^{-}	HCO_3^{-}	SO_4^{2-}	NO_3^{-}
Number of samples	36	36	36	36	36	36	36	36	36
Mean	19.56	3.86	64.73	44.97	13.50	47.76	38.72	54.64	2.13
Standard Error	2.48	0.90	7.85	5.13	2.94	6.82	5.81	6.54	0.47
Median	17.44	2.18	56.49	32.36	7.46	30.99	26.82	46.53	1.27
Mode	N/A	N/A	N/A	N/A	0.63	19.99	12.19	N/A	0.36
Standard Deviation	14.89	5.41	47.09	30.79	17.63	40.90	34.84	39.26	2.83
Sample Variance	221.57	29.31	2217.48	947.78	310.75	1672.97	1213.72	1541.10	8.03
Kurtosis	2.07	19.36	0.86	0.19	5.99	2.62	5.14	1.46	5.10
Skewness	1.20	4.01	1.11	1.02	2.28	1.67	1.97	1.37	2.43
Minimum	1.47	0.41	7.13	5.20	0.32	6.00	4.88	6.23	0.27
Maximum	69.21	31.31	191.73	125.10	81.61	171.95	170.69	149.51	11.06
Sum	704.12	138.94	2330.34	1619.09	485.99	1719.47	1393.74	1967.19	76.58
Confidence Level(95.0%)	5.04	1.83	15.93	10.42	5.96	13.84	11.79	13.28	0.96

Table 4. 25: Descriptive statistics of the hydrochemical data for the Boreholes sampled in 2016

Parameters (mg/L)	Ca^{2+}	Mg^{2+}	TH	Na^{+}	K^{+}	Cl^{-}	HCO_3^{-}	SO_4^{2-}	NO_3^{-}
Number of samples	44	44	44	44	44	44	44	44	44
Mean	13.01	3.91	48.60	25.97	3.57	26.54	37.05	34.85	1.04
Standard Error	1.75	0.52	4.94	2.51	0.65	2.81	6.22	5.14	0.13
Median	9.74	2.57	40.38	24.61	1.61	22.99	24.38	25.47	0.87
Mode	N/A	N/A	N/A	N/A	2	6.00	26.82	N/A	0.29
Standard Deviation	11.64	3.42	32.78	16.67	4.34	18.67	41.27	34.07	0.87
Sample Variance	135.40	11.70	1074.23	277.76	18.80	348.50	1703.34	1161.01	0.76
Kurtosis	4.09	3.37	0.95	3.08	2.84	0.88	5.49	4.35	5.16
Skewness	1.73	1.67	0.95	1.41	1.86	1.03	2.26	1.98	1.90
Minimum	0.52	0.17	7.77	3.78	0.23	4.00	2.44	0.23	0.29
Maximum	58.10	16.46	154.98	86.30	17.07	83.97	182.88	148.16	4.60
Sum	572.32	172.19	2138.19	1142.80	156.90	1167.64	1630.39	1533.37	45.92
Confidence Level(95.0%)	3.54	1.04	9.96	5.07	1.32	5.68	12.55	10.36	0.27

Table 4. 26: Descriptive statistics of the hydrochemical data for the Hand dug well sampled in 2017

Parameters (mg/L)	Ca^{2+}	Mg^{2+}	TH	Na^{+}	K^{+}	Cl^{-}	HCO_3^{-}	SO_4^{2-}	NO_3^{-}
Number of Samples	30	30	30	30	30	30	30	30	30
Mean	23.26	5.95	82.57	40.37	11.18	44.19	94.07	27.53	1.11
Standard Error	3.63	0.74	11.21	5.32	1.89	6.88	16.58	5.17	0.16
Median	16.45	5.28	67.00	31.35	7.82	26.99	60.96	16.20	0.76
Mode	22.47	4.67	75.34	26.58	6.94	23.99	60.96	0.00	3.16
Standard Deviation	19.88	4.06	61.41	29.14	10.35	37.69	90.79	28.33	0.89
Sample Variance	395.14	16.52	3771.18	849.25	107.13	1420.73	8242.28	802.87	0.80
Kurtosis	0.18	-0.21	0.38	0.09	1.35	0.74	1.33	0.39	1.92
Skewness	1.10	0.72	1.13	1.04	1.42	1.24	1.34	1.09	1.59
Minimum	1.39	0.65	9.95	5.94	0.66	4.00	2.44	0.00	0.28
Maximum	72.21	15.02	232.69	110.20	39.72	133.96	353.56	97.76	3.60
Sum	697.73	178.44	2477.04	1211.15	335.44	1325.59	2822.20	826.04	33.21
Confidence Level(95.0%)	7.42	1.52	22.93	10.88	3.86	14.07	33.90	10.58	0.33

Table 4. 27: Descriptive statistics of the hydrochemical data for the Boreholes sampled in 2017

Parameters(mg/L)	Ca^{2+}	Mg^{2+}	TH	Na^{+}	K^{+}	Cl^{-}	HCO_3^{-}	SO_4^{2-}	NO_3^{-}
Number of Samples	53	53	53	53	53	53	53	53	53
Mean	9.50	7.38	46.91	24.40	3.32	20.48	55.50	31.34	0.89
Standard Error	1.34	0.98	4.89	2.24	0.72	2.24	6.43	5.57	0.11
Median	6.44	5.22	38.68	17.96	1.79	17.99	43.89	12.62	0.76
Mode	20.09	N/A	12.00	34.59	3.28	19.99	26.82	0.00	0.38
Standard Deviation	9.78	7.11	35.63	16.32	5.27	16.28	46.80	40.53	0.78
Sample Variance	95.65	50.62	1269.20	266.49	27.73	265.06	2190.30	1643.07	0.61
Kurtosis	4.71	4.50	3.65	2.50	31.43	5.59	2.69	3.57	5.92
Skewness	2.02	1.93	1.59	1.41	5.13	1.95	1.57	1.85	2.03
Minimum	0.78	0.20	4.63	3.58	0.19	2.00	2.44	0.00	0.05
Maximum	48.03	36.07	186.07	85.67	36.59	89.97	219.45	165.76	4.06
Sum	503.53	391.06	2486.17	1293.23	175.70	1085.69	2941.73	1660.97	44.58
Confidence Level (95.0%)	2.70	1.96	9.82	4.50	1.45	4.49	12.90	11.17	0.22

In 2013 (Table 4.22), the minimum calcium (Ca =35 mg/L) content in the borehole water is recorded for a borehole drilled at Nyamebekyere in the aquifer of the Birimian Supergroup and the maximum (Ca = 143 mg/L) value is recorded for a borehole drilled at Dadwen (Table 4.22) also in the aquifer of the Birimian Supergroup.

In 2014 and 2015 (Table 4.23), the minimum calcium concentration (Ca = 4 mg/L) is recorded for a borehole drilled at Elloyin and the maximum calcium value (Ca = 71 mg/L) is recorded for a borehole drilled at Ehoaka, all in the aquifer of the Apollonian formation.

In 2016, the lowest and highest calcium values (Ca= 1.47 mg/L and 69.21 mg/L) in the hand dug well water (Table 4.24) is recorded for hand dug wells sampled at Bobrama and Esiama, respectively. Both hand dug wells are in the aquifer of the Apollonian formation. For

the boreholes samples (Table 4.25), the minimum and maximum calcium concentration (Ca = 0.52 mg/L and 58.10 mg/L) is measured in boreholes sampled at Atwibanso and Ankobra new site. Both towns are in the aquifer of the Apollonian formation.

In 2017 (Table 4.26), the minimum calcium content (Ca = 1.39 mg/L) is measured in a hand dug well sampled at Gyegyekrom in the aquifer of the Birimian Supergroup and the maximum calcium (Ca = 72.21 mg/L) content is measured in a hand dug well sampled at Esiama in the aquifer of the Apollonian formation. For the borehole samples (Table 4.27), the minimum calcium concentration (Ca = 0.78 mg/L) is measured in a borehole sampled at Nglekazo in the aquifer of the Apollonian formation and the maximum value (Ca =48.03 mg/L) is recorded for a borehole sampled at Salman in the aquifer of the Birimian Supergroup.

Figure 4.13 shows the spatial distribution map of Ca^{2+} in the groundwater of the study area. From the map, high calcium content represented by shades of red is seen in groundwater sampled from the aquifer of the Birimian Supergroup (NE and SE) of the study catchment.

The source of the elevated calcium in the groundwater is attributed to carbonate mineral dissolution and the chemical breakdown of feldspars and plagioclase. In the study area, carbonate minerals like limestones exist in the rocks of the Apollonian and silicate minerals (feldspars and plagioclase) exist in the rocks of the Birimian Supergroup (Fig 3.3 and 3.4).

The low calcium content for the groundwater might probably be derived from the occurrence of slow chemical weathering of silicate minerals (hornblende, etc.), granitic rocks and the dissolution of carbonate minerals {Goldich, 1938; Appello and Postma (1999); Fig 3.3 and 3.4} from the underlying geology. This might be due some of the groundwater having high pH (pH = 6.3 to 8.5) values.

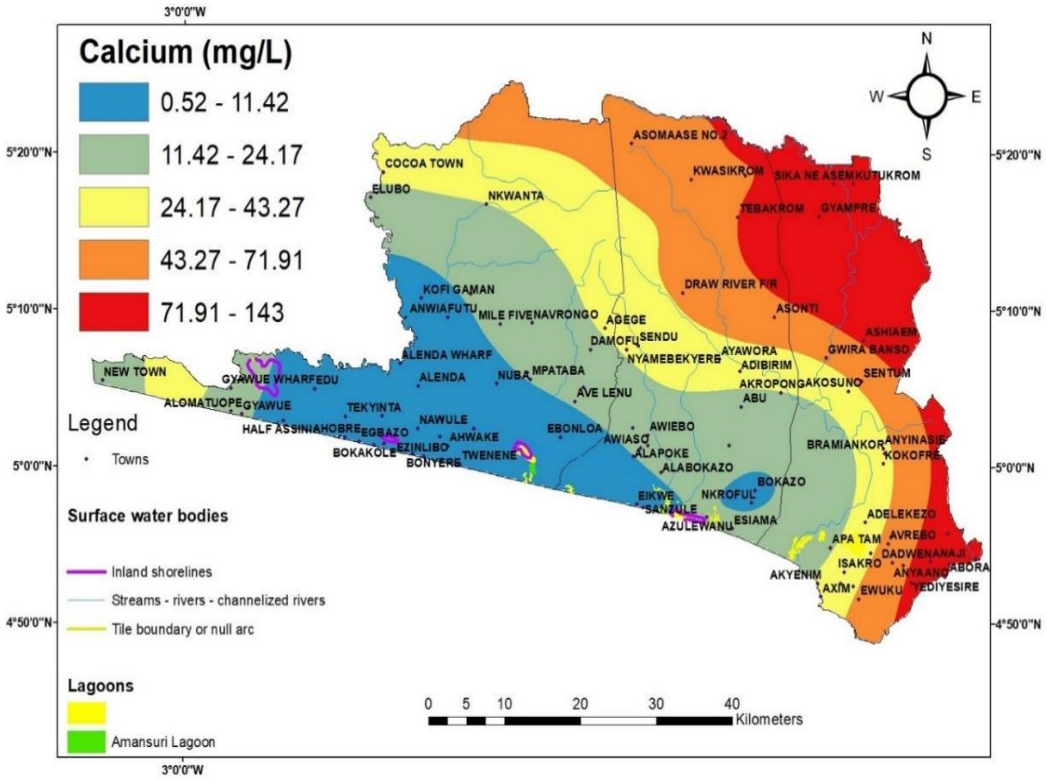

Figure 4.13: Spatial distribution map of calcium concentrations in groundwater in the Lower Tano River Basin

In 2013, the minimum (Mg^{2+} = 12 mg/L) magnesium concentration is recorded for boreholes drilled at Ankyernin in the aquifer of the Birimian Supergroup, and Akpendue in the aquifer of the Apollonian formation. The maximum Mg^{2+} value (Mg^{2+} = 79 mg/L) is measured in a borehole drilled at Kutukrom, in the aquifer of the Birimian Supergroup.

From 2014 to 2015 (Table 4.23), the minimum and maximum Mg^{2+} concentration (Mg^{2+} = 0.7 mg/L and 22.6 mg/L) is measured for boreholes drilled at Effasu and Newtown, respectively. Both boreholes are in the aquifer of the Apollonian formation.

In 2016, the minimum magnesium (Mg^{2+}) concentration (Mg^{2+} = 0.41 mg/L) is measured in a hand dug well (Table 4.24) sampled at Half Assini in the aquifer of the Apollonian formation and the maximum (Mg^{2+}= 31.31 mg/L) is recorded in a hand dug well sampled at Ankobra also in the same aquifer. In that same year, the minimum and maximum Mg^{2+} concentration (Mg^{2+}= 0.17 mg/L and 16.46 mg/L) (Table 4.25) is measured in boreholes

sampled at Tiekobo 1 and Azelenuano, respectively. Both boreholes are in the aquifer of the Apollonian formation.

In 2017 (Table 4.26), the minimum Mg^{2+} content (Mg^{2+}= 0.65 mg/L) is recorded in a hand dug well sampled at Elubo in the aquifer of the Birimian formation and the maximum concentration (Mg^{2+}=15.02 mg/L) is measured in a hand dug well sampled at Nkroful also in the aquifer of the Birimian formation. Also, in 2017, the minimum Mg^{2+} concentration (Mg^{2+}= 0.20 mg/L) (Table 4.27) is recorded in a borehole sampled at Ngelekyi in the aquifer of the Apollonian formation and the maximum (Mg^{2+}= 0.41 mg/L) is measured in a borehole sampled at Kamgbunli also in the aquifer of the Apollonian formation.

The spatial distribution map of magnesium (Fig 4.14) reveals that groundwater located in the aquifer of the Birimian Supergroup (SE and NE zone) represented by shades of red colour is above WHO (2011) permissible limit of 50 mg/ L for drinking water. The high Magnesium content in groundwater from the aquifer of the Birimian Supergroup (SE and NE zone) might be derived from the high weatherability of hornblende (CaMgSi2O22(OH)2), biotite [K (Mg, Fe)3(AlSi3) O (O10 H, F)2] etc., which exist in the Birimian Supergroup rocks of the study area (See, fig 3.3 and 3.4). The rest of the groundwater mostly situated in the aquifer of the Apollonian formations with few in the aquifer of the Birimian supergroup of the study catchment (Fig 4.14) are below WHO permissible limit of 50 mg/L for drinking water. The reasons accounting to the low Mg^{2+} values recorded for the groundwater is the same reasons for the low calcium values in the aquifer of the Apollonian formation and the Birimian supergroup as discussed in previous chapters.

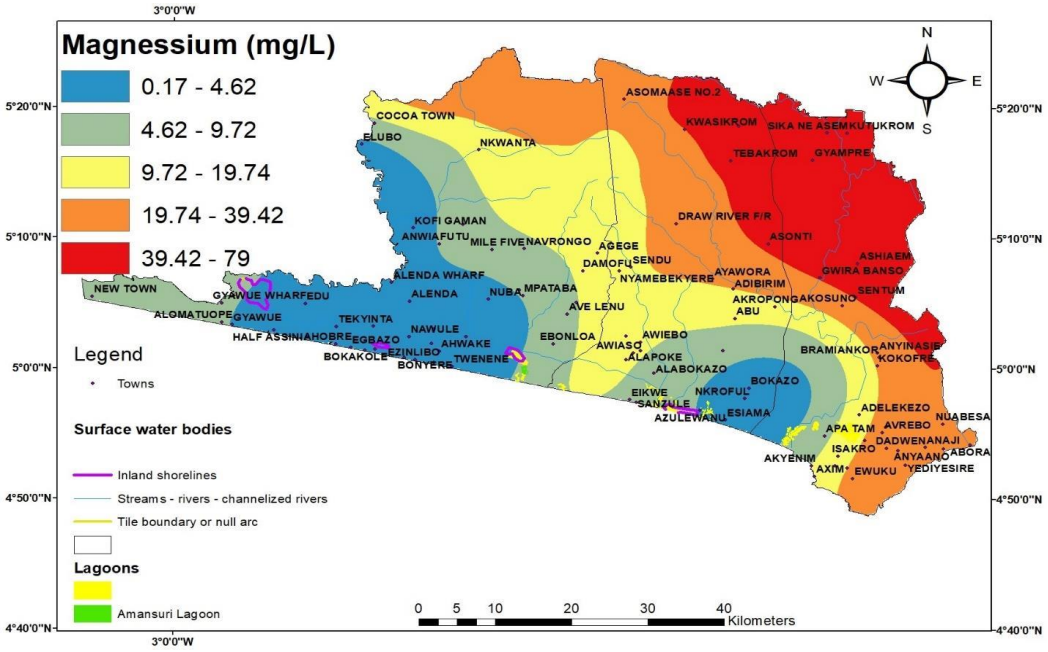

Figure 4. 14: Spatial distribution map of magnesium concentrations in groundwater in the Lower Tano River Basin.

For the total hardness, the maximum allowable limit for drinking purpose is 500 mg/L and the most desirable limit is 100 mg/L per the WHO (2011) permissible limit. Groundwater exceeding the limit of 300 mg/L is considered very hard. The sampled groundwater is classified based on McCarly and Sawyer (1967). The classification is shown in Table 4.28 to 4.30.

Table 4. 28: Classification of Total hardness concentration in the Boreholes drilled in 2013 and 2014 to 2015{After McCarly and Sawyer (1967)}

Concentration as $CaCO_3$(mg/L)	Water Type	2013 (n=30)	2014 -2015 (n=18)
0 - 75	Soft	5	13
75 - 150	Moderately Hard	20	1
150-300	Hard	5	4
>300	Very Hard		

Table 4. 29: Classification of Total hardness concentration in the groundwater sampled in 2016 {After McCarly and Sawyer. (1967)}

Concentration as $CaCO_3$ (mg/L)	Water Type	Hand dug wells (n=36)	Boreholes (n=44)
0 - 75	Soft	25	33
75 - 150	Moderately Hard	10	10
150-300	Hard	1	1
>300	Very Hard		

Table 4. 30: Classification of Total hardness concentration in the groundwater sampled in 2017 {After McCarly and Sawyer. (1967)}

Concentration as $CaCO_3$ (mg/L)	Water Type	Hand dug wells (n=30)	Boreholes (n=53)
0 - 75	Soft	16	44
75 - 150	Moderately Hard	9	8
150-300	Hard	5	1
>300	Very Hard		

Out of 30 boreholes drilled in 2013 and 18 boreholes drilled from 2014 to 2015, 5 and 13 boreholes are soft water (Table 4.28), respectively, 20 and 1 borehole are moderately hard water, respectively and 5 and 4 boreholes produce hard water, respectively.

In 2016, 25 hand dug wells and 33 boreholes produce soft water (Table 4.29). Also 10 hand dug wells and 10 boreholes produce moderately hardwater and one hand dug well and a borehole produces hard water (Table 4.29).

In 2017, 16 hand dug wells and 44 boreholes gives soft water. 9 hand dug wells and 8 boreholes produces moderately hardwater and the water for 5 hand dug wells and a borehole gives hard water (Table 4.30)

The moderately hard to hard water produced by fewer hand dug wells and boreholes might be coming from the dissolution of carbonate minerals and weathering of silicate minerals from the aquifer of the Apollonian formation and Birimian supergroup.

From Table 4.23, the minimum and maximum sodium (Na^+) concentrations (Na^+ = 3.40 mg/L and 162 mg/L) in the boreholes drilled from 2014 to 2015 is measured at Ehoaka and Newtown respectively. Both boreholes are in the aquifer of the Apollonian formation.

Also, in 2016, the minimum Na^+ content (Na^+ = 5.20 mg/L) is measured in a hand dug well sampled at Ampaim in the aquifer of the Apollonian formation and the maximum (Na^+ = 125.10 mg/L) is measured in a hand dug well sampled at Nkroful in the aquifer of the Birimian Supergroup. For the 2016 borehole samples, the least sodium concentration (Na^+ = 3.78 mg/L) (Table 4.25) is measured for a borehole sampled at New Nzulezo, in the aquifer of the Apollonian formation and the highest is recorded (Na^+ = 86.30 mg/L) for a borehole sampled at Aluku in the aquifer of the Birimian supergroup.

In 2017 (Table 4.26), the minimum Na^+ concentration (Na^+ = 5.94 mg/L) is measured in a hand dug well sampled at Gyegyekrom in the aquifer of the Birimian Supergroup and the maximum (Na^+ = 110.20 mg/L) is recorded in a hand dug well sampled at Nkroful also in the aquifer of the Apollonian formation. In that same year, the minimum and maximum sodium concentration (Na^+ = 3.58 mg/L and 85.67 mg/L) (Table 4.27) is recorded in boreholes sampled at Tiekobo 1 and Esiama, respectively. Both boreholes are in the aquifer of the Apollonian formations.

Looking at the spatial distribution map (Fig 4.15), it is seen that high sodium content represented by shades of red colour are mostly seen in the aquifer of the Apollonian formation with few representations in the aquifer of the Birimian Supergroup.

The sources of elevated sodium are attributed to the weathering of silicate minerals like plagioclase and hornblende {Freeze and Cherry (1979)}, which exist in the underlying geology of the study area.

Additionally, ion exchange processes {Apello and Postma, 1999; Zereg et al., (2018)} is another factor behind the elevated Na^+ in the groundwater but will be explained further in the third specific objective. In general, the sodium content in the entire groundwater samples is below WHO (2011) permissible limit of 200 mg/L for drinking water.

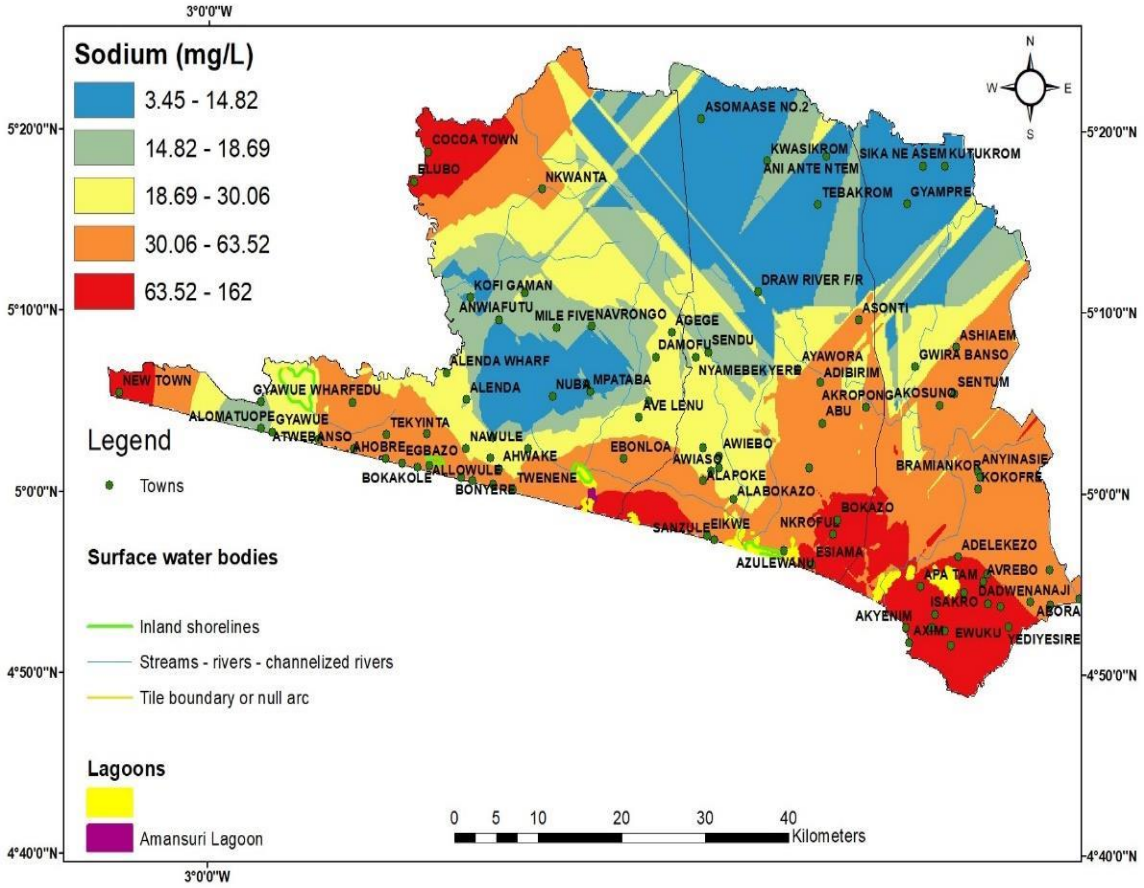

Figure 4. 15: Spatial distribution map of sodium concentration in groundwater in the Lower Tano River Basin

The potassium (K^+) content, in the boreholes drilled from 2014 to 2015 (Table 4.23), recorded the minimum and maximum K^+ concentrations (K^+= 0.2 mg/L and 14.60 mg/L) in boreholes drilled at Allengenzule and Newtown, respectively. Both boreholes are in the aquifer of Apollonian formation.

In 2016, the minimum and maximum potassium (Table 4.24), concentrations (K^+= 0.32 mg/L and 81.61 mg/L) are recorded in hand dug wells sampled at Gyegyekrom and Elubo, respectively. Both hand dug wells are in the aquifer of the Birimian Supergroup. Likewise, in 2016 the minimum K^+ concentration (K+= 0.23 mg/L) is measured (Table 4.25) in a borehole sampled at Salman in the aquifer of the Birimian Supergroup and the maximum potassium content (K^+ = 17.07 mg/L) is measured in a borehole sampled at Nyanzinli in the aquifer of the Apollonian formation.

In 2017, the minimum and maximum potassium content (0.66 mg/L and 39.72 mg/L) (Table 4.26) is measured in hand dug wells sampled at Nkroful in the aquifer of the Birimian Supergroup. Also, in that same year, the minimum potassium concentration (K^+= 0.19 mg/L) is measured in a borehole (Table 4.27) sampled at Salman in the aquifer of the Birimian Supergroup and the maximum potassium concentrations (K^+= 36.5 9 mg/L) is measured in a borehole sampled at Esiama in the aquifer of the Apollonian formation.

The spatial distribution map of potassium (Fig 4.16) reveals high potassium (> 12 mg/L) values in groundwater sampled from the aquifer of the Apollonian formation (Southern and southwestern) with few sampled from the aquifer of the Birimian (Northwestern zone of the study catchment) Supergroup. The elevated potassium content is represented by shades of red and orange colour.

Potassium is known to be very low in groundwater (Apello & Postma, 2005) but the high recorded potassium concentrations might probably be derived from the weathering of silicate minerals (biotite, muscovite, hornblende etc.) from the underlying geology. Another source of elevated potassium in the groundwater is linked to anthropogenic sources and one such source is the application of KCl (Potassium chloride) fertilizer by coconut farmers in the study area. Another anthropogenic source might be from domestic wastewater and sewage water disposal (Skowron et al., 2018) which was evidenced during sampling. Also, most houses had no proper drainage systems and toilet facilities. Additional contributing factor for the elevated potassium content is cation-exchange processes (Drever, 1988). Clay minerals and limestones exist in the underlying geology of the study area (Fig 3.3 and 3.4) and these minerals are appropriate cation-exchange sites (Appelo & Postma, 2005).

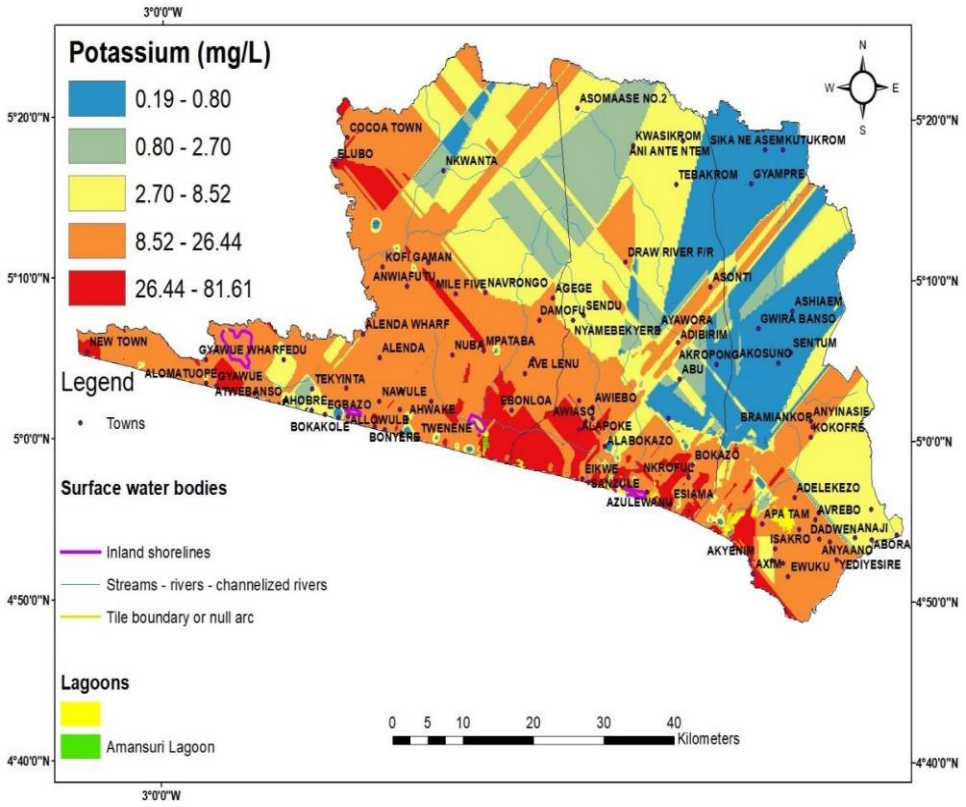

Figure 4.16: Spatial distribution map of K^+ concentration in groundwater in the Lower Tano River Basin.

In 2013 borehole samples (Table 4.22), the minimum and maximum chloride value (Cl = 0.04 mg/L and 96 mg/L) is recorded in boreholes drilled at Nyamebekyere and Kutukrom, all in the aquifer of the Birimian Supergroup, respectively.

In 2014 and 2015, the minimum and maximum concentrations of chloride (Cl = 5.5 mg/L and 224 mg/L) (Table 4.23) is recorded in two separate boreholes drilled at Ehoaka and Newtown, respectively. Both boreholes are in the aquifer of the Apollonian formation.

In 2016, the minimum chloride concentration (Cl= 6 mg/L) is recorded for a hand dug well sampled at Gyegyekrom in the aquifer of the Birimian Supergroup and the maximum (Cl = 171.95 mg/L) (Table 4.24) is recorded for a hand dug well sampled at Ankobra in the aquifer of the Apollonian formation.

In 2016, the minimum chloride content (Cl= 4 mg/L) (Table 4.25) is measured in a borehole sampled at Tiekobo no1 in the aquifer of the Apollonian formation and Salman, in the aquifer

of the Birimian Supergroup. The maximum Cl concentration (Cl= 83.97 mg/L) is recorded in a borehole sampled at New Nzulezo in the aquifer of the Apollonian formation.

In 2017, the minimum chloride content (Cl = 4 mg/L) is measured in hand dug wells sampled at Asemda, Ampaim, Atuabo and Gyegyekrom (Table 4.26). These towns are in the aquifer of the Apollonian formation, except for Gyegyekrom, which is in the aquifer of the Birimian Supergroup. Likewise, the maximum chloride concentration (Cl = 133.96 mg/L) is measured in a hand dug well sampled at Elubo in the aquifer of the Birimian Supergroup. For the borehole samples, the minimum Cl^- concentration (Cl = 2.00 mg/L) is measured in a borehole sampled at New Nzulezu and the maximum (Cl = 89.97 mg/L) is recorded in a borehole sampled at Esiama. Both boreholes are in the aquifer of the Apollonian formation.

The spatial distribution map of chloride is illustrated in Figure 4.17. From the map, the highest chloride values represented by shades of red colour are seen mostly in groundwater sampled from the aquifer of the Apollonian formation (some parts of the coastal area) with few groundwater sampled from the aquifer of the Birimian Supergroup (some parts of the NE and NW). All the sampled groundwater within the basin is below WHO (2011) permissible limit of 250 mg/L for drinking water. Normally, chloride is not a significant component in the underlying rock formation of the study area (Fig 3.3 and 3.4). Therefore, chloride will only be present in minimal quantity in the groundwater through possible organic matter decomposition in the soil, ion exchange processes, and atmospheric sources (Freeze & Cherry, 1979).

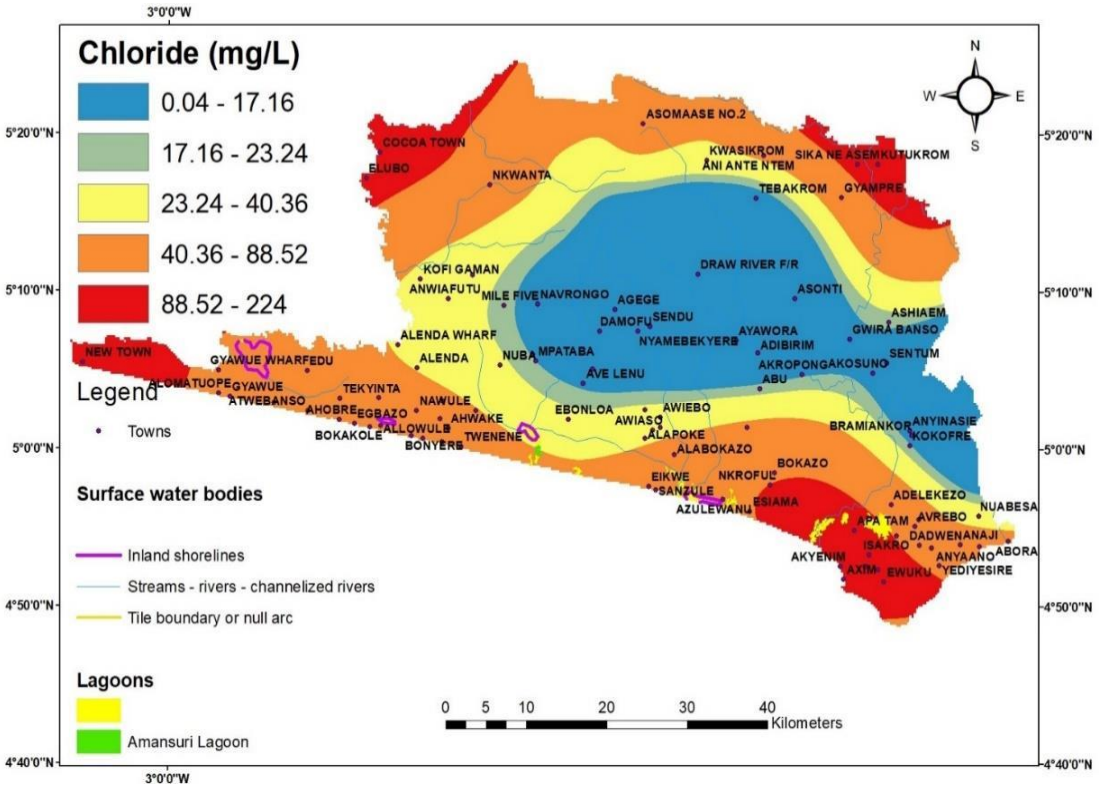

Figure 4. 17: Spatial distribution map of Chloride concentrations in groundwater in the Lower Tano River basin.

For the boreholes drilled from 2014 to 2015, the minimum (HCO_3^- = 5 mg/L) and maximum (HCO_3^- = 171 mg/L) bicarbonates levels (Table 4.23) is recorded for boreholes drilled at Elloyin and Kamgbunli, respectively. Both boreholes are drilled in the aquifer of the Apollonian formation.

In 2016, the minimum and maximum bicarbonate concentration (HCO_3^- = 4.88 mg/L and 170.69 mg/L) is measured (Table 4.24) in hand dug wells sampled from Ampaim and Asanta, respectively. Both towns are underlain by the Apollonian formation. Also, for the borehole samples the minimum (HCO_3^- = 2.44 mg/L) and maximum (HCO_3^- = 182.88 mg/L) bicarbonates content (Table 4.25) is measured in boreholes sampled from Salman in the aquifer of the Birimian Supergroup.

In the same way, the minimum bicarbonate concentration ($HCO3^-$= 2.44 mg/L) for 2017 hand dug well samples is measured in a hand dug well sampled at Elubo in the aquifer of the Birimian Supergroup and the maximum (HCO_3^- = 353.56 mg/L) is recorded for a hand dug well sampled

at Esiama in the aquifer of the Apollonian formation. Also, for the 2017 boreholes samples, the minimum bicarbonate concentration ($HCO3^-$= 2.44 mg/L) is recorded for a borehole sampled at Atwinbanso in the aquifer of the Apollonian formation and the maximum concentration (HCO_3^- = 219.45 mg/L) (Table 4.27) is recorded for a borehole sampled at Salman in the aquifer of the Birimian Supergroup.

The spatial distribution map of bicarbonate concentrations in groundwater within the study area (Fig 4.18) shows high bicarbonate content in groundwater sampled from the aquifer of the Birimian Supergroup (Southeastern Zone). The high bicarbonate content is represented by shades of red colour. There is fewer representation of elevated bicarbonate concentration in groundwater sampled from the aquifer of the Apollonian formation (coastal).

The groundwater with elevated bicarbonate concentration in the aquifer of the Birimian Supergroup and the Apollonian formation is attributed to the dissolution of carbonate minerals and weathering of silicate minerals (Stumm and Morgan 1996) from the underlying geology of the study area.

In general, the bicarbonate content in the groundwater is all below WHO (2011) permissible limit of 500 mg/L for drinking water.

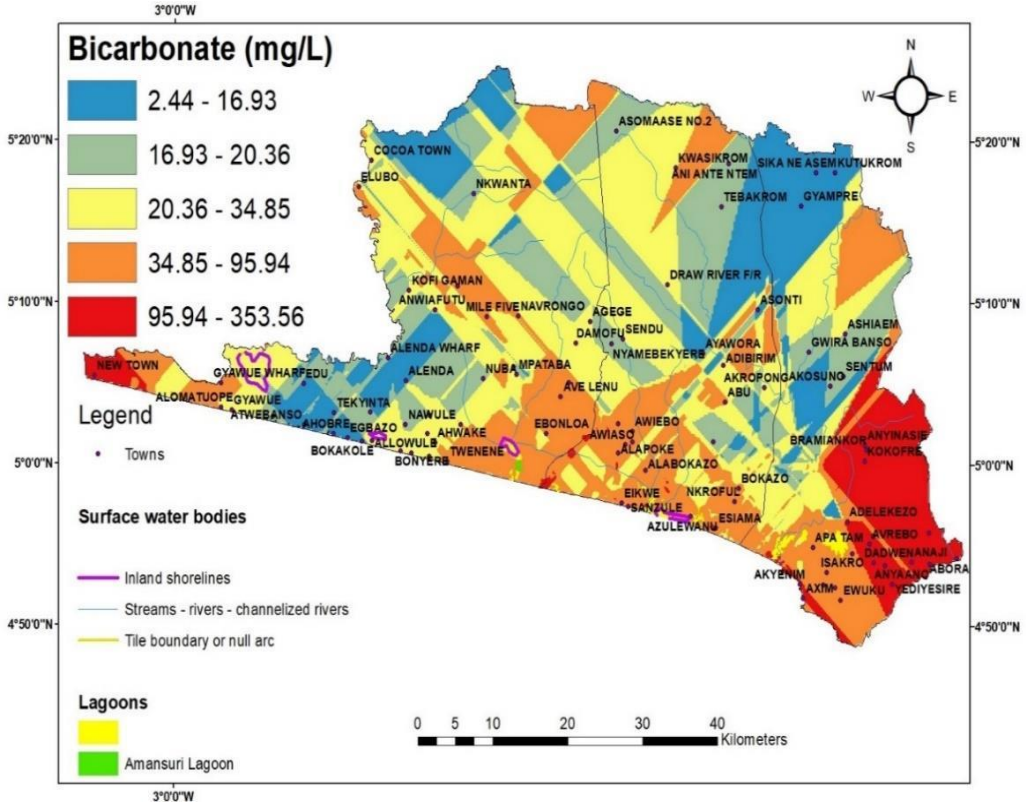

Figure 4. 18: Spatial distribution map of bicarbonate content in groundwater in the Lower Tano River Basin.

The sulphate levels in the groundwater sampled from 2013 to 2017 are all below WHO (2011) permissible limit of 250 mg/L for drinking water. The spatial distribution map (Fig 4.19) of sulphate in the sampled groundwater shows slightly high sulphate (>80 mg/L) values represented by shades of red colour taken from the aquifer of the Apollonian formation with fewer representations sampled from the aquifer of the Birimian Supergroup.

According to Berner and Berner (1987), sulphate ion concentration in natural water must generally be in the range of 2 mg/L to 80 mg/L. However, in the study area, some groundwater in the aquifer of the Apollonian formation (Fig 4.19) and the Birimian Supergroup were greater than 80 mg/L. The high sulphate values measured in the groundwater may possibly be attributed to anthropogenic and geogenic sources. To confirm the possible sources being geogenic, Fe/SO_4^{2-} molar ratio for groundwater is calculated. The results from the calculations (Appendix 21 to 26) show that a hand dug well sampled from Nkroful in the aquifer of the Birimian Supergroup fall under the stoichiometry of pyrite oxidation. The rest of the groundwater samples did not satisfy the Fe/SO_4^{2-} molar ratios of 0.5 and 1.0 for the

stoichiometry of pyrite oxidation, respectively. This reveals that pyrite oxidation is probably not responsible for the mass production of sulphate (Stumm & Morgan, 1981) in the groundwater sampled from the aquifer of the Apollonian formation and the Birimian supergroup. of the study area.

In the study area, farming is not done on a large scale, hence, ammonium sulphate fertilizer might not be applied ruling out ammonium sulphate fertilizers as a possibly anthropogenic contributor to the elevated sulphate content measured in the groundwater.

In the study catchment legal and illegal small-scale mining are rampant. Hence, in the processes of gold, these miners use sulphuric acid. The use of sulphuric acid will possibly lead to acid-mine drainage. The acid-mine drainage may not eliminate the sulphate ion leading to elevated sulphate ion content in some of the groundwater. This must be investigated further using isotopes of sulphide-34 and oxygen-18.

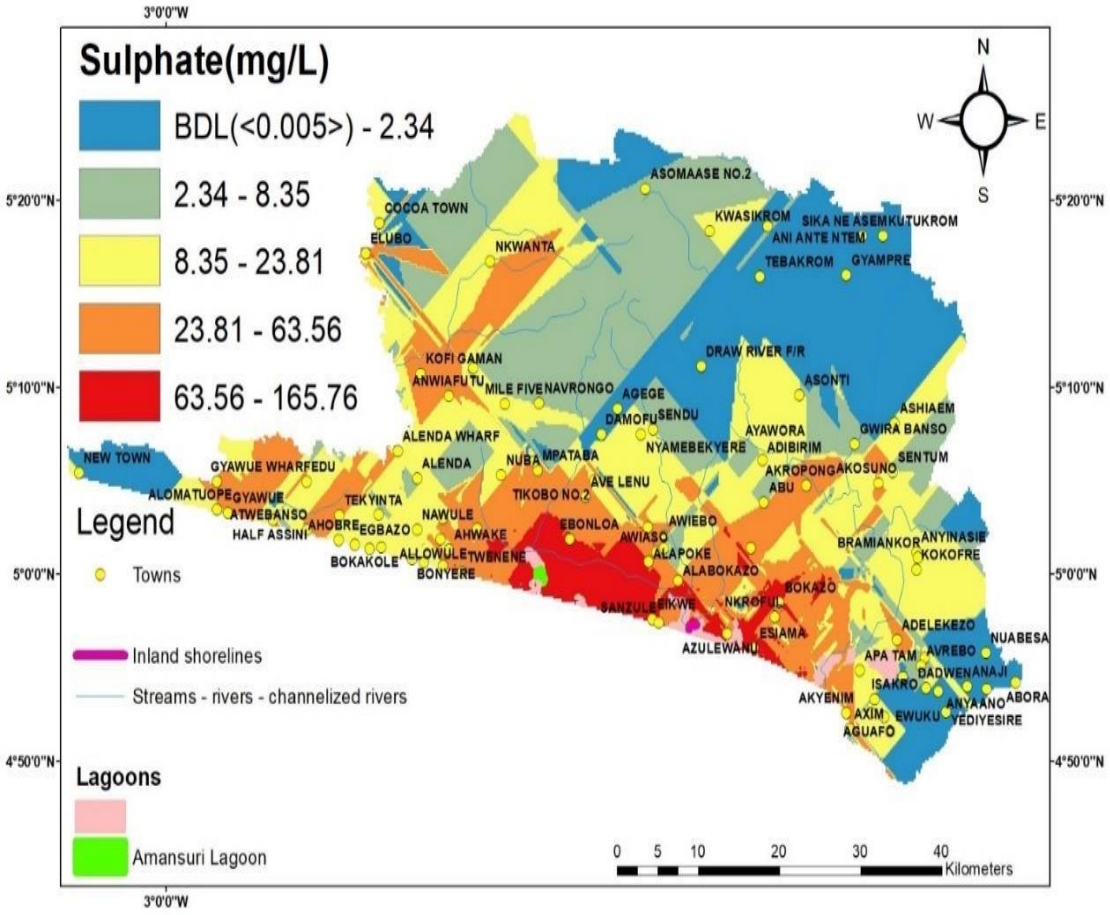

Figure 4. 19: Spatial distribution map of sulphate concentration in groundwater in the Lower Tano River Basin.

For the boreholes drilled in 2013 (Table 4.21), the minimum and maximum nitrate concentration (NO_3^- = 0.54 mg/L and 2.31 mg/L) is measured in a borehole drilled at Asanta and Ellonye, respectively. Both boreholes are in the aquifer of the Apollonian formation.

In 2016, the minimum nitrate concentration (NO_3^- = 0.27 mg/L) is measured in a hand dug well sampled in Aniwa and the maximum value (NO_3^- = 11.06 mg/L) is measured in a hand dug well sampled at Elubo. Both hand dug wells are in the aquifer of the Birimian Supergroup. Also in that same year, the minimum nitrate concentrations (NO_3^- = 0.29 mg/L) are measured in boreholes sampled at Kamgbunli, Sawoman, Aluku and Nyanzinli and the maximum nitrate content is recorded in a borehole (NO_3^- = 4.60 mg/L) sampled at New Nzulezu. All these boreholes are in the aquifer of the Apollonian formation except a borehole sampled at Aluku which is in the aquifer of the Birimian Supergroup.

Equally, in 2017, the minimum concentration of nitrate (NO_3^- = 0.28 mg/L) is measured in a hand dug well sampled at Esiama in the aquifer of the Apollonian formation and the maximum ($NO3^-$ = 3.60 mg/L) is recorded in a hand dug well sampled at Elubo in the aquifer of the Birimian Supergroup. For the borehole samples, the minimum and maximum nitrate concentration (NO_3^- = 0 .05 mg/L and 4.06 mg/L) is measured in boreholes sampled at Ampaim and Ngelekyi, respectively. Both boreholes are in the aquifer of the Apollonian formation.

From the spatial distribution map of nitrate (Fig 4.20), it is observed that all the groundwater sampled in the study area are below the WHO (2011) permissible limit of 50 mg/L. The low nitrate content in the groundwater is possibly attributed to less vigorous anthropogenic activities.

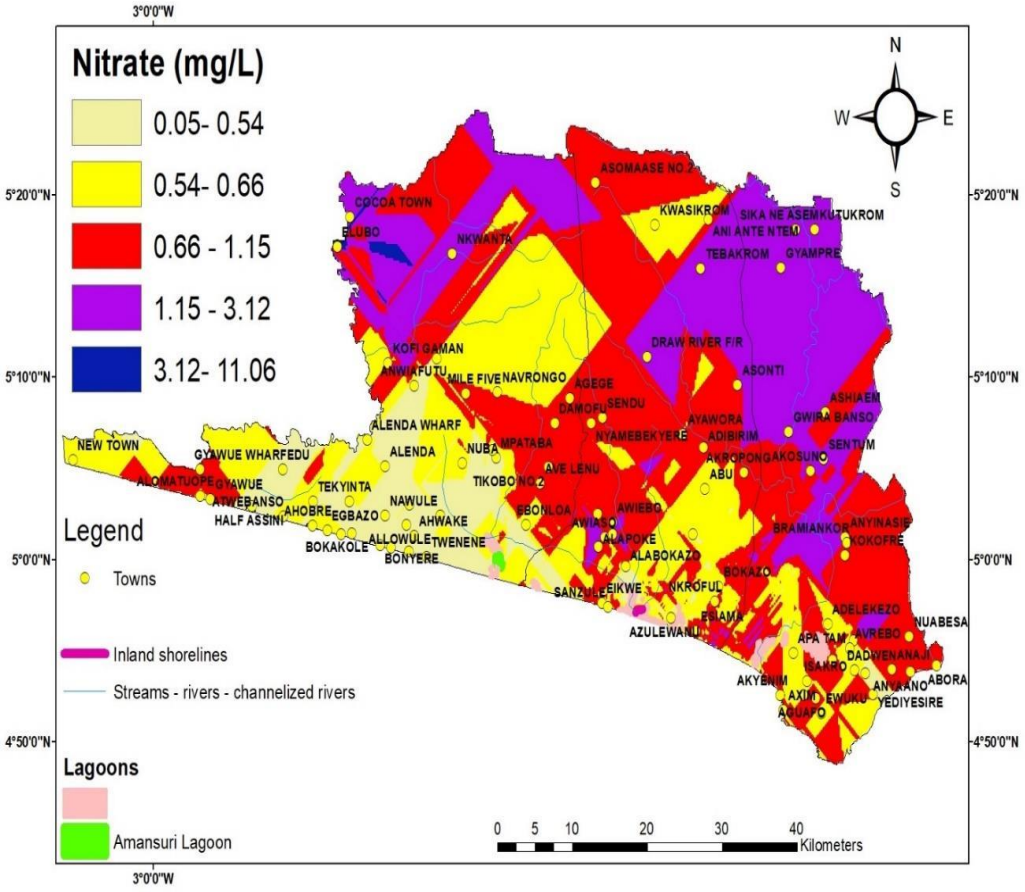

Figure 4. 20: Spatial distribution map of nitrate content in groundwater in the Lower Tano River Basin.

Based on the medians (Table 4.21 to 4.27), the cation and anion concentrations in the groundwater is in the order:

$Ca^{2+} > Mg^{2+}$ and $Cl^{-} > SO_4^{2-} > NO_3^{-}$ (Boreholes drilled in 2013).

$Ca^{2+} > Mg^{2+} > Na^{+} > K^{+}$ and $Cl^{-} > SO_4^{2-} > HCO_3^{-} > NO_3^{-}$ (Boreholes drilled in 2014 to 2015).

$Na^{+} > Ca^{2+} > K^{+} > Mg^{2+}$ and $SO_4^{2-} > Cl^{-} > HCO_3^{-} > NO_3^{-}$(Hand dug well sampled in 2016)

$Na^{+} > Ca^{2+} > Mg^{2+} > K^{+}$ and $SO4^{2-} > HCO3^{-} > Cl^{-} > NO3^{-}$ (Boreholes sampled in 2016).

$Na^{+} > Ca^{2+} > Mg^{2+} > K^{+}$ and $HCO_3^{-} >. Cl^{-} > SO_4^{2-} > NO_3^{-}$ (Hand dug wells sampled in 2017).

$Na^{+} > Ca^{2+} > Mg^{2+} > K^{+}$ and $HCO_3^{-} > Cl^{-} > SO4^{2-} > NO3^{-}$ (Boreholes sampled in 2017).

The rivers and streams sampled in 2016 had Na^+ as the dominant cation and SO_4^{2-} as the dominant anion. In the same way, the hand dug wells and the boreholes sampled in 2016 had Na^+ as the dominant cation and SO_4^{2-} as the dominant anion. These samples were taken during the wet seasons. The rivers, streams, hand dug wells and boreholes sampled in 2017 had Na^+ as the dominant cation and HCO_3^- as the dominant anion. These samples were taken during the dry seasons.

Also, a hydraulic relationship existed between the streams sampled in 2016 and the boreholes sampled in 2016 and this is due to their similar trends which will be explained further in the fourth specific objective. Also, a relationship existed between the hand dug wells and the boreholes sampled in 2017.

The variation of cations and anions in the sampled groundwater is attributed to the seasons in which the samples were taken, the time, lithology, and human activities.

4.2.2.3 Occurrences and Distribution of Trace Elements in Groundwater of the Lower Tano River Basin (Assessment of groundwater contamination)

Under this section, the results for the measured trace elements in the groundwater is discussed. Statistical comparison for trace elements including minimum, maximum, median, mean, standard deviation etc. in the groundwater samples are presented in Table 4.31,4.32,4.33,4.34,4.35 and 4.36.

Table 4. 31: Descriptive statistical summary of trace elements in the Boreholes drilled in 2013

Parameters	*Cu (mg/L)*	*Mn(mg/L)*	*Fe(mg/L)*	*Cr(mg/L)*	*Pb(mg/L)*	*As(mg/L)*	*Al(mg/L)*	*Zn(mg/L)*
Number of samples	30	30	30	30	30	30	30	30
Mean	0.002	0.028	0.108	0.008	0.000	0.000	0.004	0.004
Standard Error	0.001	0.008	0.030	0.008	0.000	0.000	0.002	0.002
Median	0.000	0.000	0.000	0.000	0.000	0.000	0.000	0.000
Mode	0.000	0.000	0.000	0.000	0.000	0.000	0.000	0.000
Standard Deviation	0.006	0.045	0.166	0.042	0.000	0.000	0.011	0.009
Sample Variance	0.000	0.002	0.028	0.002	0.000	0.000	0.000	0.000
Kurtosis	14.922	0.684	0.209	30.000			22.217	4.822
Skewness	3.913	1.460	1.276	5.477			4.514	2.375
Minimum	0.000	0.000	0.000	0.000	0.000	0.000	0.000	0.000
Maximum	0.030	0.140	0.520	0.230	0.000	0.000	0.060	0.030
Sum	0.050	0.830	3.240	0.230	0.000	0.000	0.110	0.110
Count	30.000	30.000	30.000	30.000	30.000	29.000	29.000	29.000
Confidence Level (95.0%)	0.002	0.017	0.062	0.016	0.000	0.000	0.004	0.003

Table 4. 32: Descriptive statistical summary of trace elements in the Boreholes drilled from 2014 to 2015

Parameters	*Co(mg/L)*	*Cu(mg/L)*	*Pb(mg/L)*	*Cd(mg/L)*	*Cr (mg/L)*	*Mn(mg/L)*	*Ni(mg/L)*	*Zn(mg/L)*	*Al(mg/L)*	*Fe(mg/L)*	*As(mg/L)*
Number of samples	18	18	18	18	18	18	18	18	18	18	18
Mean	**0.002**	**0.019**	**0.068**	0.000	**0.004**	**0.057**	0.**006**	**0.069**	**0.358**	**0.578**	**0.008**
Standard Error	0.001	0.014	0.011	0.000	0.001	0.017	0.003	0.003	0.171	0.277	0.005
Median	0.001	0.001	0.054	0.000	0.002	0.028	0.003	0.066	0.130	0.250	0.001
Mode	0.000	0.000	0.049	0.000	0.002	0.028	0.002	0.059	0.110	0.300	0.001
Standard Deviation	0.004	0.060	0.045	0.000	0.005	0.072	0.011	0.013	0.725	1.174	0.021
Sample Variance	0.000	0.004	0.002	0.000	0.000	0.005	0.000	0.000	0.525	1.377	0.000
Kurtosis	2.119	14.436	-0.915	-0.736	8.824	4.361	8.576	-0.901	16.230	13.413	12.731
Skewness	1.825	3.736	0.672	1.121	2.792	2.150	2.910	-0.001	3.957	3.572	3.504
Minimum	0.000	0.000	0.010	0.000	0.000	0.005	0.000	0.044	0.050	0.000	0.000
Maximum	0.013	0.250	0.150	0.001	0.020	0.270	0.045	0.090	3.200	5.000	0.087
Sum	0.044	0.350	1.221	0.004	0.067	1.029	0.115	1.235	6.450	10.400	0.149
Confidence Level (95.0%)	0.002	0.030	0.022	0.000	0.002	0.036	0.006	0.007	0.360	0.584	0.011

Table 4. 33: Descriptive statistical summary of trace elements for Hand dug wells sampled in 2016.

Parameters	*Al (mg/L)*	*Cr (mg/L)*	*Mn (mg/L))*	*Fe (mg/L)*	*Co (mg/L)*	*Ni (mg/L)*	*Cu (mg/L)*	*Zn (mg/L)*	*As (mg/L)*	*Cd (mg/L)*	*Pb (mg/L)*
Number of samples	35.00	35.000	35.00	35.00	35.00	35.00	35.00	35.00	35.00	35.00	36.00
Mean	0.065	0.030	0.048	0.642	0.000	0.002	0.005	0.812	0.007	0.007	**0.96**
Standard Error	0.017	0.026	0.021	0.252	0.000	0.000	0.003	0.779	0.006	0.003	0.53
Median	**0.032**	**0.002**	**0.010**	**0.273**	**0.000**	**0.001**	**0.000**	**0.019**	**0.000**	**0.000**	**0.00**
Mode	N/A	N/A	0.000	N/A	0.000	0.000	0.000	N/A	0.000	0.000	0.00
Standard Deviation	0.102	0.155	0.124	1.488	0.001	0.002	0.016	4.672	0.035	0.020	3.19
Sample Variance	0.010	0.024	0.015	2.215	0.000	0.000	0.000	21.832	0.001	0.000	10.17
Kurtosis	14.424	34.471	13.931	27.682	32.878	7.348	17.863	35.996	35.682	17.140	17.48
Skewness	3.484	5.854	3.726	5.094	5.639	2.452	4.229	5.999	5.962	4.061	4.14
Minimum	0.004	0.0004	BDL	0.013	BDL	BDL	BDL	0.0002	BDL	BDL	BDL
Maximum	0.545	0.917	0.594	8.743	0.006	0.011	0.080	28.067	0.213	0.105	16.30
Sum	2.281	1.060	1.677	22.455	0.009	0.057	0.171	29.229	0.247	0.253	34.67
Confidence Level (95.0%)	0.035	0.053	0.042	0.511	0.000	0.001	0.005	1.581	0.012	0.007	1.08

Table 4. 34: Descriptive statistical summary of trace elements for Boreholes sampled in 2016.

Parameters	*Al (mg/L)*	*Cr (mg/L)*	*Mn (mg/L)*	*Fe (mg/L)*	*Co (mg/L)*	*Ni (mg/L)*	*Cu (mg/L)*	*Zn (mg/L)*	*As (mg/L)*	*Cd (mg/L)*	*Pb (mg/L)*
Number of samples	44	44	44	44	44	44	44	44	45	44	44
Mean	0.08	0.00	0.78	**2.94**	0.00	0.02	0.05	0.41	0.00	0.001	0.46
Standard Error	0.02	0.00	0.69	1.42	0.00	0.01	0.03	0.33	0.00	0.000	0.16
Median	**0.01**	**0.00**	**0.04**	**0.17**	**0.00**	**0.00**	**0.00**	**0.04**	0.00	0.000	**0.00**
Mode	N/A	0.00	0.00	0.00	0.00	0.00	0.00	N/A	0.00	0.000	0.00
Standard Deviation	0.15	0.00	4.60	9.42	0.01	0.08	0.19	2.22	0.00	0.002	1.05
Sample Variance	0.02	0.00	21.14	88.76	0.00	0.01	0.04	4.93	0.00	0.000	1.10
Kurtosis	9.45	-0.07	43.90	17.95	34.89	43.04	36.85	43.74	7.96	11.840	6.30
Skewness	2.94	0.98	6.62	4.29	5.71	6.53	5.91	6.60	2.91	3.339	2.63
Minimum	BDL	BDL	BDL	BDL	BDL	BDL	BDL	BDL	BDL	BDL	BDL
Maximum	0.76	0.01	30.57	47.42	0.08	0.53	1.23	14.78	0.01	0.012	4.25
Sum	3.39	0.06	34.52	129.49	0.14	0.76	2.07	18.20	0.03	0.038	20.15
Confidence Level (95.0%)	0.05	0.00	1.40	2.86	0.00	0.02	0.06	0.67	0.00	0.001	0.32

Table 4. 35: Descriptive statistical summary of trace elements for Hand dug wells sampled in 2017.

Parameters	*Al (mg/L)*	*Cr (mg/L)*	*Mn (mg/L)*	*Fe (mg/L)*	*Co (mg/L)*	*Ni (mg/L)*	*Cu (mg/L)*	*Zn (mg/L)*	*As (mg/L)*	*Cd (mg/L)*	*Pb (mg/L)*
Number of samples	30	30	30	30	30	30	30	30	30	30	30
Mean	0.128	0.001	0.009	0.158	0.000	0.001	0.002	0.018	0.001	0.0005	0.035
Standard Error	0.089	0.000	0.004	0.033	0.000	0.000	0.000	0.004	0.000	0.000	0.006
Median	**0.005**	**0.001**	**0.001**	**0.101**	0.000	**0.001**	**0.002**	**0.008**	**0.001**	**0.000**	**0.026**
Mode	N/A	N/A	0.000	0.000	N/A	N/A	N/A	N/A	N/A	N/A	N/A
Standard Deviation	0.485	0.001	0.020	0.155	0.000	0.001	0.001	0.024	0.001	0.001	0.032
Sample Variance	0.235	0.000	0.000	0.024	0.000	0.000	0.000	0.001	0.000	0.000	0.001
Kurtosis	20.848	0.646	11.147	1.696	7.077	0.317	0.543	9.235	5.544	9.328	0.462
Skewness	4.483	1.015	3.186	1.250	2.702	0.943	0.858	2.801	1.921	3.050	1.173
Range	2.484	0.004	0.092	0.605	0.002	0.003	0.006	0.118	0.004	0.004	0.114
Minimum	BDL	BDL	BDL	BDL	BDL	BDL	BDL	BDL	BDL	BDL	BDL
Maximum	2.484	0.004	0.09	0.605	0.002	0.003	0.006	0.118	0.004	0.004	0.114
Sum	3.838	0.042	0.261	3.480	0.009	0.038	0.070	0.550	0.035	0.015	1.055
Confidence Level(95.0%)	0.181	0.000	0.007	0.069	0.000	0.000	0.001	0.009	0.000	0.000	0.012

BDL = Below detection limit (<0.001>)

Table 4. 36: Descriptive statistical summary of trace elements for Boreholes sampled in 2017.

Parameters	*Al (mg/L)*	*Cr (mg/L)*	*Mn (mg/L)*	*Fe (mg/L)*	*Co (mg/L)*	*Ni (mg/L)*	*Cu (mg/L)*	*Zn (mg/L)*	*As (mg/L)*	*Cd (mg/L)*	*Pb (mg/L)*
Number of samples	55	55	55	55	55	55	55	55	55	55	55
Mean	0.053	0.001	0.069	0.087	0.001	0.004	0.027	0.052	0.002	0.002	0.003
Standard Error	0.018	0.000	0.016	0.012	0.000	0.001	0.015	0.015	0.001	0.001	0.001
Median	**0.003**	**0.001**	**0.013**	**0.067**	0.000	**0.002**	**0.002**	**0.021**	**0.001**	**0.000**	**0.000**
Mode	0.001	0.001	0.471	0.038	0.006	0.011	0.004	0.013	0.003	0.000	0.000
Standard Deviation	0.133	0.001	0.117	0.069	0.002	0.008	0.110	0.113	0.005	0.009	0.005
Sample Variance	0.018	0.000	0.014	0.005	0.000	0.000	0.012	0.013	0.000	0.000	0.000
Kurtosis	13.573	4.559	4.451	0.265	5.891	16.048	40.775	20.882	24.307	50.209	10.462
Skewness	3.560	1.901	2.233	0.809	2.532	3.757	6.149	4.331	4.891	6.970	2.909
Minimum	0.0002	0.0001	0.0003	0.004	0.00003	0.0004	0.001	0.002	0.0004	0.00002	0.00003
Maximum	0.715	0.005	0.471	0.277	0.008	0.046	0.772	0.690	0.031	0.069	0.026
Sum	2.919	0.064	3.791	3.028	0.056	0.242	1.504	2.834	0.135	0.108	0.147
Confidence Level (95.0%)	0.036	0.000	0.032	0.024	0.001	0.002	0.030	0.030	0.001	0.003	0.001

4.2.2.4 Metallic elements (Cu, Cd, Zn, Fe, and Cr)

The measured Copper (Cu) content in the boreholes drilled in 2013 (Table 4.31) varies from 0.00001 mg/L to 0.03 mg/L with a mean of 0.002 mg/L. For the boreholes drilled from 2014 to 2015 (Table 4.32), the Cu content ranges from 0.00001 mg/L to 0.25 mg/L with an average of 0.019 mg/L. In 2016, the Cu content in the hand dug wells and boreholes varies from below detection limit (BDL) to 0.08 mg/L with a mean of 0.05 mg/L, and from below detection limit (BDL) to 1.23 mg/L with an average of 0.005 mg/L, respectively (Table 4.33 and 4.34). In 2017, the Cu content for both hand dug wells and boreholes ranges from BDL to 0.01 mg/L with a mean of 0.02 mg/L and from 0.001 mg/L to 0.77 mg/L with a mean of 0.027 mg/L, respectively (Table 4.35 and 4.36). The spatial distribution map of copper for the sampled groundwater shows that few of the groundwater represented by shades of red and orange colour (Fig 4.21) are above WHO (2011) permissible limit of 0.05 mg/L for drinking water. This groundwater was mostly sampled from the aquifer of the Birimian Supergroup with few samples taken from the aquifer of the Apollonian formation. The sources of the elevated copper content are linked to the oxidation of sulphide minerals {chalcopyrite ($CuFeS_2$)} from the underlying geology of the study area (Luebe et al., 1990; Adjimah et al., 1993). Another possible factor responsible for the high Cu content in groundwater sampled from the aquifer of the Apollonian formation and the Birimian supergroup might possibly be from anthropogenic sources. Examples of such sources are mining activities, application of sewage sludge, fungicides, fertilizers in agricultural application and waste emission (Flemming & Trevors, 1989). In the study catchment, illegal and legal small-scale mining activities is rampant and studies carried out by Kabata-Pendias, 2001, indicated that catchments with extensive mining activities have Cu content in soils to be as high as 2000 mg/kg. Cocoa farming are rampant in the upper parts of the study area and it is likely that the cocoa farmers use Cu containing fungicides to control mildew on their farms but further studies must be carried out. Also, studies carried out by Addo-Fordjour et al. (2013) indicates that cocoa farmers in Ghana uses copper-based fungicide on their farms. Hence, the

application of Cu fungicides might probably lead to Cu accumulation in soils and through natural processes like rainfall and runoffs, Cu might leach into the aquifers leading to elevated Cu content in groundwater. Since Cu in soils was not measured in this study, the impact of Cu fungicides applications on groundwater in the Lower Tano River Basin must be investigated in future.

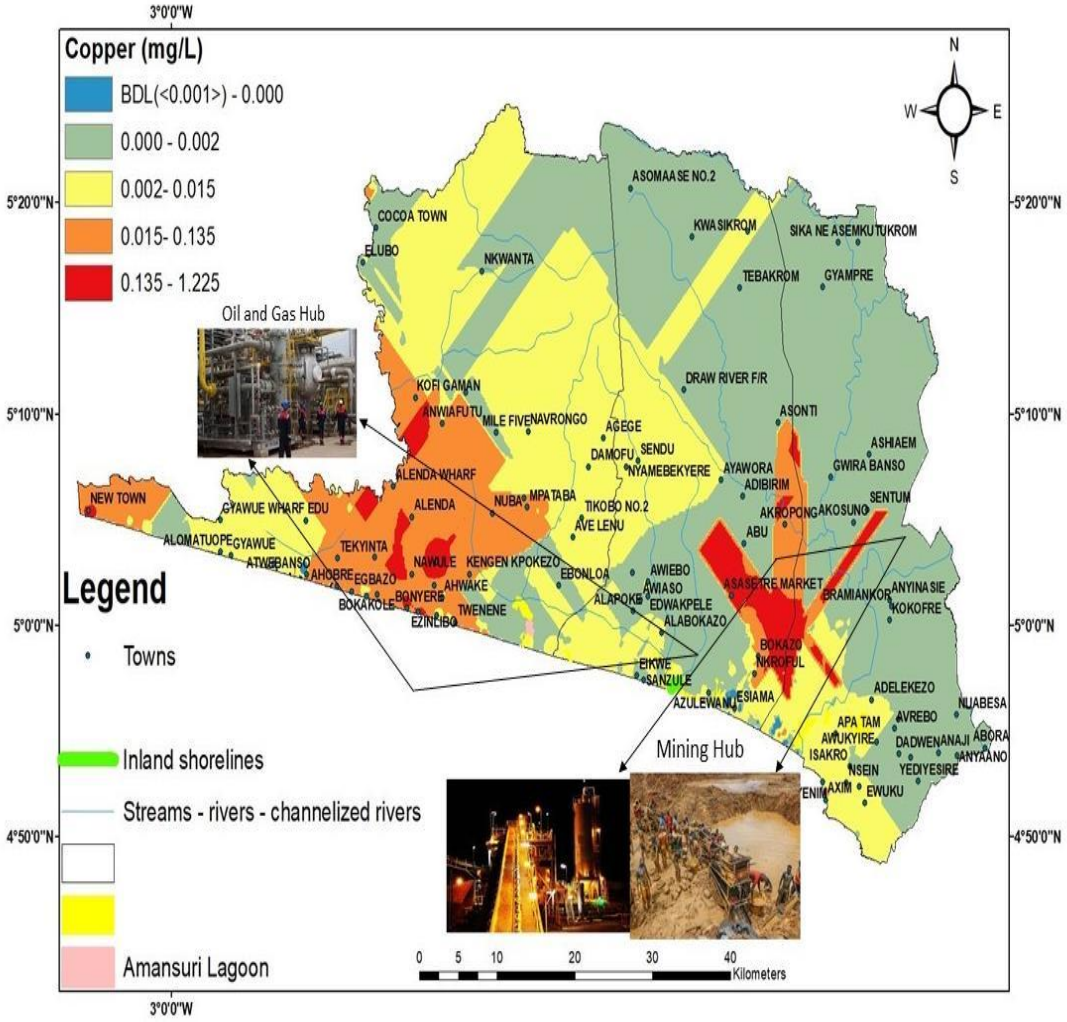

Figure 4. 21: Spatial distribution map of copper (Cu) content in groundwater in the study catchment.

The Cadmium (Cd) content in boreholes drilled from 2014 to 2015 varies from 0 to 0.001 mg/L with an average of 0.0002 mg/L. All the newly drilled boreholes are below WHO (2011) permissible limit of 0.003 mg/L for drinking water.

For the hand dug wells sampled in 2016, the Cd content ranges from below detection limit (BDL <0.001>) to 0.11 mg/L with a mean of 0.007 mg/L. 21.6% of the hand dug wells (n= 35) are lower than WHO (2011) permissible limit of 0.003 mg/L and the remaining 78.4% are above the permissible limit. For the boreholes sampled in 2016, the Cd content varies from below detection limit (BDL<0.001) to 0.01 mg/L with an average of 0.001 mg/L. 11.1% of the boreholes (n= 44) exceeded WHO (2011) permissible limits for drinking water.

In 2017, the Cd concentrations in the sampled hand dug wells varies from below detection limit (BDL<0.001) to 0.004 mg/L with a mean of 0.0005 mg/L. All the hand dug wells are below WHO (2011) permissible limit of 0.003 mg/L except a hand dug well sampled at Elubo in the aquifer of the Birimian super group. In addition, the Cd content in the boreholes sampled in 2017 ranges from 0.00002 to 0.07 mg/L with a mean of 0.002 mg/L. Cd content in boreholes sampled at Tiekobo number 1, Bonyere and Atwinbanso all in the aquifer of the Apollonian formation exceeded the WHO (2011) permissible limit of 0.003 mg/L.

Spatial distribution map of Cd (Fig 4.22) shows that groundwater samples with elevated Cd content represented by shades of red colour are dominant in the aquifer of the Birimian supergroup with few representations in the aquifer of the Apollonian formation. These elevated Cd values might possibly be derived from anthropogenic factors probably from effluent discharge from mining activities finding their way into the aquifers through natural processes like rainfall. Common sources of cadmium involve the disposal of cadmium containing wastes, plating operation, corrosion of galvanized pipes, discharge from metal refineries, erosion of natural deposits and runoff from paints and waste batteries (Smith et al., 1995). In the study catchment, the above factors are rare except "erosion of natural deposits, discharge from metal refineries like the mining industries and corrosion of galvanized fitting used in the construction of boreholes". These three might be the probable sources through which cadmium could be released in significant quantities into the groundwater, especially the hand dug wells since it is exposed. Nevertheless, since there are no previous cadmium data on rocks, soil, surface

water, and groundwater and this study did not measure Cd in soils and rocks, further studies must be carried out to define the actual sources of high Cd groundwater within the Lower Tano River Basin. Also, the elevated Cd content in the groundwater might possibly be geogenic. Liu et al. (2017), stated that "marine primary production of shale might increase the Cd content in groundwater. Looking at the underlying geology of the zones represented by shades of red (Fig. 3.3 and 3.4), the aquifer of the Apollonian formation contains shale and that might probably dissolve in the groundwater releasing Cd but further investigations is required. According to ATSDR, 2012 and UNEP, 2010, "anthropogenic sources of cadmium are fossil fuel combustion, phosphate fertilizer manufacturing, iron production, **cement production**, steel production, road dust, **municipal and sewage sludge incineration**, and emissions from non-ferrous metal production. From the above given factors, it is likely that the Cd content in groundwater sampled from the aquifer of the Apollonian formation is possibly from the production of cement since there is a cement production company at Nawulley and Half Assini. In addition, there is a municipal sewage sludge incineration at Old Kablazuazo and the town is underlain by the rocks of the Apollonian formation.

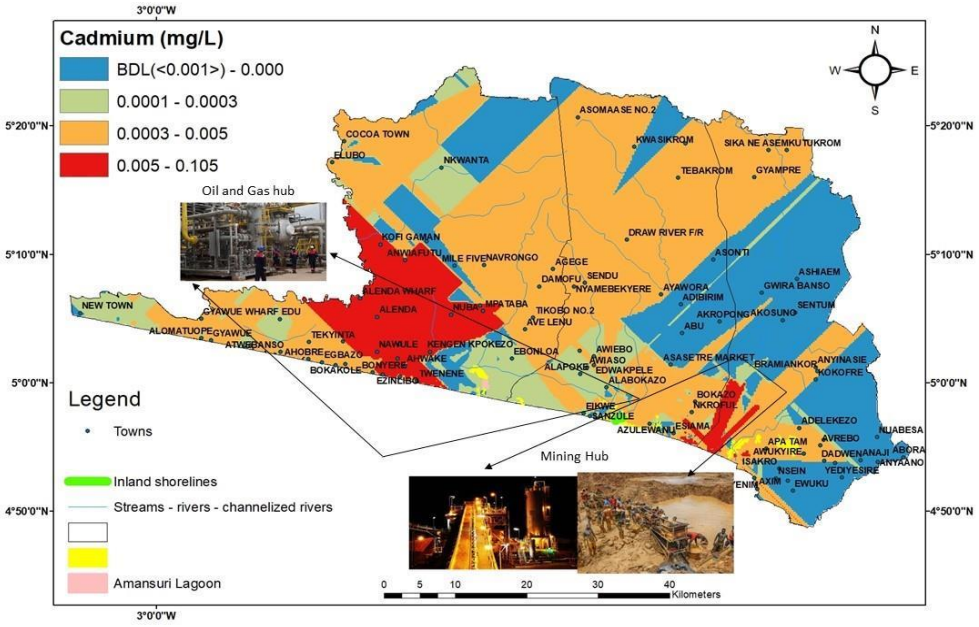

Figure 4. 22: Spatial distribution map of Cd concentrations in groundwater drawn in the Lower Tano River Basin.

The concentration of Zinc (Zn) in the boreholes drilled in 2013 varies from 0.00001 m/L to 0.03 m/L with a mean of 0.004 mg/L. That of the boreholes drilled from 2014 to 2015 had a Zn content varying from 0.04 mg/L to 0.09 mg/L with a mean of 0.069 mg/L. In 2016, the Zn content in the hand dug wells and the boreholes varies from 0.0002 mg/L to 28.07 mg/L with a mean of 0.81 mg/L, and from below detection limit (BDL <0.001) to 14.78 mg/L with an average of 0.41 mg/L, respectively. In 2017, the Zn content in the hand dug wells varies from BDL to 0.12 mg/L with a mean of 0.02 mg/L. That of the boreholes varies from 0.002 mg/L to 0.69 mg/L with an average of 0.05 mg/L.

All the hand dug wells sampled in both 2016 and 2017 are below WHO (2011) permissible limit of 5 mg/L, except for a hand dug well sampled at Elubo in the aquifer of the Birimian Supergroup. For the boreholes, all the samples are below the WHO (2011) permissible limits of 5 mg/L, except for a borehole sampled at Salman also in the aquifer of the Birimian supergroup. At Salman, virtually all the gold mining industries as well as illegal small-scale mining activities are concentrated in and around the town. In areas underlain by the Birimian supergroup rocks, Luebe et al. (1990) and Adjimah et al. (1993) discovered sulphide minerals (pyrites, chalcopyrite's) hosting trace elements like Cu, Pb, As, **Zn**, Ni etc. as pathfinder element for the exploration of gold. It is therefore possible that the oxidation of these sulphide minerals from the aquifer of the Birimian supergroup might release Zn as a secondary mineral into the groundwater elevating the Zn content. The spatial distribution map of Zinc in groundwater within the basin is presented in figure 4.23.

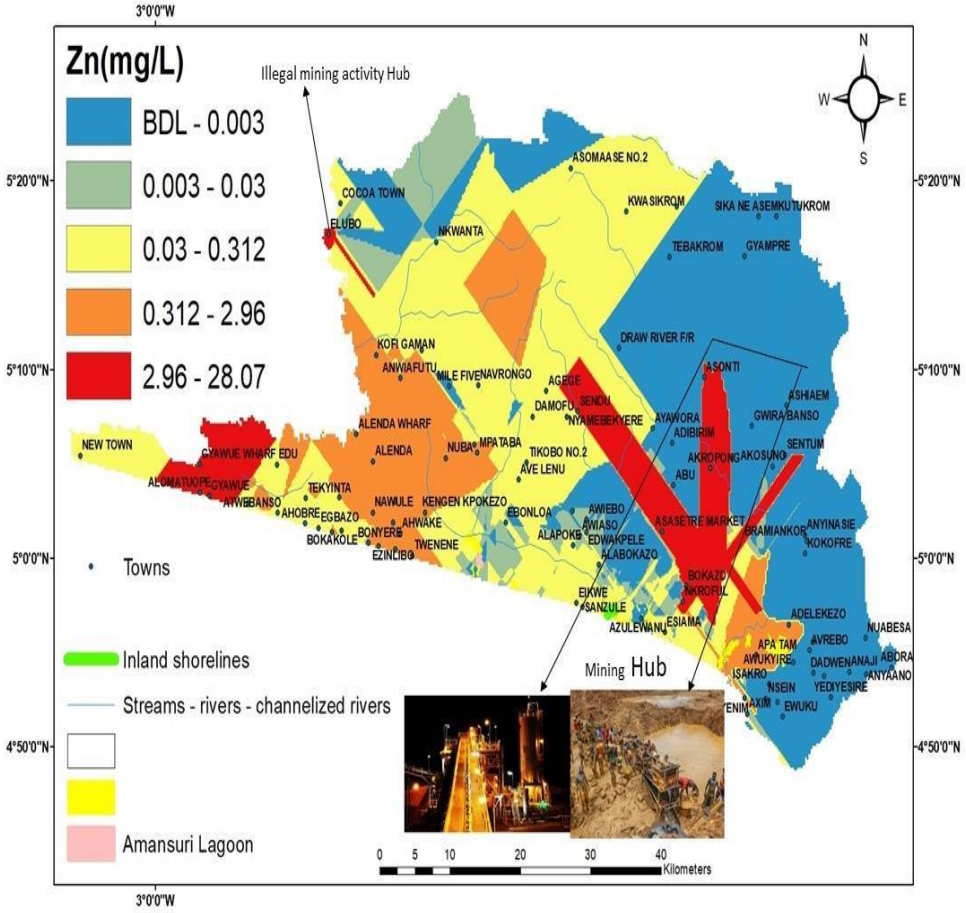

Figure 4. 23: Spatial distribution map of Zn content in groundwater in the Lower Tano River Basin.

The chromium (Cr) concentration for the boreholes drilled in 2013 varies from 0.00001 to 0.23 m/L with a mean of 0.008 m/L. That of the boreholes drilled from 2014 to 2015 ranges from 0.00001 to 0.02 m/L with an average of 0.004 mg/L. In 2016, the Cr in the sampled hand dug wells varies from 0.0004 mg/L to 0.92 mg/L with an average of 0.03 mg/L. That of Cr in the sampled boreholes varies from BDL to 0.01 mg/L with a mean of 0.001 mg/L. In 2017, Cr in the sampled hand dug wells and boreholes varied from BDL to 0.004 mg/L with a mean of 0.001 mg/L and from 0.0001 m/L to 0.005 mg/L with an average of 0.001 mg/L, respectively.

The Cr content in two hand dug wells (n=36) sampled in 2016 are above the WHO (2011) permissible limit of 0.05 mg/L and the remaining 34 hand dug wells and all the hand dug wells sampled in 2017 are below the WHO permissible limit for drinking water. Likewise, the Cr

content in the boreholes sampled in 2013, 2014 to 2015, 2016, and 2017 are all lower than the WHO permissible limit of 0.05 mg/L except for a borehole sampled at Ayisakro in the aquifer of the Birimian Supergroup.

From the results, the high Cr content in groundwater sampled at Nkroful, Bomuakpole and Ayisakro, in the aquifer of the Birimian Supergroup is linked to the weathering of ultra-mafic rocks from the underlying geology. Dampare et al. (2008) discovered high Cr content in ultra-mafic rocks of the Birimian superroup. Also, the high Cr values is attributed to anthropogenic sources. This is because the above-mentioned three towns fall within the mining zone and during combustion process at the mining sites, particles emanating from the sites might be distributed into the atmosphere and on the soil. This particle might settle at the bottom of a cell floatation and that could directly be discharged unto the onsite wetlands, thus possibly leaching into the aquifer resulting in an elevated Cr concentration in the groundwater. Since there are no data on the Cr content in soils and rocks of the study area and these two were not sampled in this study, proper geochemical studies just like works undertaken by Izbicki et al. (2008a) should be conducted in future.

The concentration of iron (Fe) in the boreholes drilled in 2013 varies from 0.00001 mg/L to 0.52 mg/L with an average of 0.11 mg/L. For the boreholes drilled from 2014 to 2015, the Fe content ranges from 0.00001 mg/L to 5 mg/L with a mean of 0.58 mg/L. For the hand dug wells sampled in 2016, the Fe content varies from 0.01 mg/L to 8.74 mg/L with a mean of 0.64 mg/L. For the boreholes sampled in 2016, the Fe content varies from below detection limit (BDL<0.001) to 47.4 mg/L with a mean of 2.94 mg/L. In 2017 the Fe concentration in the sampled hand dug wells and boreholes varied from BDL to 0.61 mg/L with an average of 0.16 mg/L, and from 0.004 mg/L to 0.28 mg/L with an average of 0.087 mg/L, respectively.

The sampled groundwater shows that 40.5% (n=35) of the hand dug wells sampled in 2016 had Fe content lower than the WHO (2011) permissible limit of 0.3 mg/L and the remaining

59.5% are higher than the permissible limits. In 2017, 96.7% of the hand dug wells (n=30) are lower than the WHO permissible limit of 0.3 mg/L and the remaining 3.33% are higher than the permissible limit. For the boreholes, 13.3% (n=30) had Fe values greater than WHO (2011) permissible limit in 2013 and the remaining 86.7% of the boreholes are lower than the permissible limits. 16.7% of the boreholes sampled from 2014 to 2015 are greater than the WHO (2011) permissible limits and the remaining 83.3% are lower than the permissible limits. In 2016 and 2017, the Fe content in 65.9% and all the boreholes (n=55) in both respective years are lower than the WHO (2011) permissible limits and the remaining 34.1% of the boreholes sampled in 2016 are higher than the WHO permissible limit of 0.3 mg/L for drinking water. The high Fe content in most groundwater is attributed to the oxidation or mobilization of sulphide minerals (pyrite, chalco- pyrite etc.) from the underlying geology of the study area (Luebe et al., 1990). Oxidation of sulphide minerals by oxygen through proton production is also a significant sulphate and iron source in groundwater (Kortatsi, 2004) of the study area. The reaction equation for oxidation of sulphide minerals by oxygen through proton production is given by:

$FeS_2 + O_2 + H2O \rightarrow SO_4^{2-} + Fe^{2+} + H^+$ ……. Eq 4.3

In the presence of ferrous iron, Pyrite is oxidized as:

$FeS_2 + 7/2O_2 + H2O = Fe^{2+} + 2\ SO_4^{2-} + 2H^+$…… Eq 4.4

Equation 4.3 is the primary rate determining the step of acid drainage formation (Stumm & Morgan, 1981). The development of equations 4.3 and 4.4 depends on the pH of the groundwater. If the pH is higher than 3.0, (as in the case of the study area where the groundwater pH is between 4.5 to 6.8 pH unit), then there is precipitation of ferric hydroxide [Fe (OH)3] and this is given by the equation, $Fe^{3+} + 3H2O = Fe(OH)3 + 3H^+$... Eq 4.5.

This equation (eq 4.5) gives an idea of possible acid- mine drainage reactions in groundwater (hand dug wells and boreholes) of the study area. This produces iron (III) hydroxide {Fe $(OH)_3$} which is possibly a secondary source of Fe for the basin groundwater. Conversely, if pH of the groundwater is less than 3.0 and Fe^{3+} is in contact with unoxidized pyrite, then Fe^{3+} consumed by the oxidation of pyrite due to the strong oxidant of Fe^{3+}. This is presented by the equation,

$FeS_2 + 14Fe^{3+} + 8H_2O = 15Fe^{2+} + 2SO4^{2-} + 16H^{+}$…. Eq 4.6

The above equations suggests that oxygen is necessary to start the oxidation of pyrite and to recycle Fe^{2+} to Fe^{3+} {Stumm & Morgan. (1981)}

However, if an accumulation of mine waste products contains high amount of dissolved Fe^{3+} from the previous oxidation period, then the oxidation of pyrite will continue for a long time even in the absence of oxygen supply. When both precipitation of ferric hydroxide and oxidation of ferrous iron take place, the coupled reaction is described as

$Fe^{2+} + ¼\ O_2 + 5/2\ H_2O = Fe\ (OH)3 + 2H^{+}$…Eq 4.7

Ideally, the above reactions produce high sulphate concentrations, low pH and Fe / SO_4^{2-} molar ratios of 1.0 (for arsenopyrite oxidation) and 0.5 (for pyrite oxidation) (Kortatsi, 2004) Generally, the low sulphate content in the groundwater coupled with the fact that no groundwater satisfied the Fe /SO_4^{2-} molar of 1.0 and 0.5 for the stoichiometry of arsenopyrite and pyrite respectively (Appendix 21 to 26) suggests the possibility of arsenopyrite and pyrite oxidation processes in groundwater being partially responsible for the concentration of iron in the groundwater of the study area.

Another source of elevated Fe in the groundwater is attributed to ferromagnesium mineral like biotite which exist in the underlying geology of the study area.

Additional reason accounting for the high Fe concentration in the groundwater might be from the removal of dissolved oxygen by organic matter, leading to reduced conditions. Under reducing conditions, the solubility of Fe-bearing minerals (hornblende, biotite, mica etc.) which exist in the underlying geology increases, leading to enrichment of dissolved iron in the groundwater.

Further, the presence of elevated Fe content in the groundwater could possibly be associated with chemical weathering of silicate minerals (hornblende, and plagioclase) which possibly dissolve or percolate through the fractures to enrich the aquifers, (Darko, 2006).

Though organic matter content in the soil zone of the groundwater was not measured in this study, the brown colorization of groundwater evidenced during sampling is an indication of a possible presence of organic matter in the soil zone of the study area. Hence, at a comparatively lower pH, higher Fe concentrations in the groundwater might have resulted from organic matter, interaction of oxidized Fe minerals and subsequent dissolution of Fe_2CO_3. This type of water was clear when first drawn from the hand dug wells and boreholes, but soon became cloudy and changed to brownish by the precipitation of Fe $(OH)_3$. This was a common problem evidenced in most parts of the study region during the sampling campaign. Figure 4.24 presents the spatial distribution map of iron concentration in groundwater within the study area. From the map (Fig 4.24), higher concentrations of iron were seen in the aquifer of the Birimian super group.

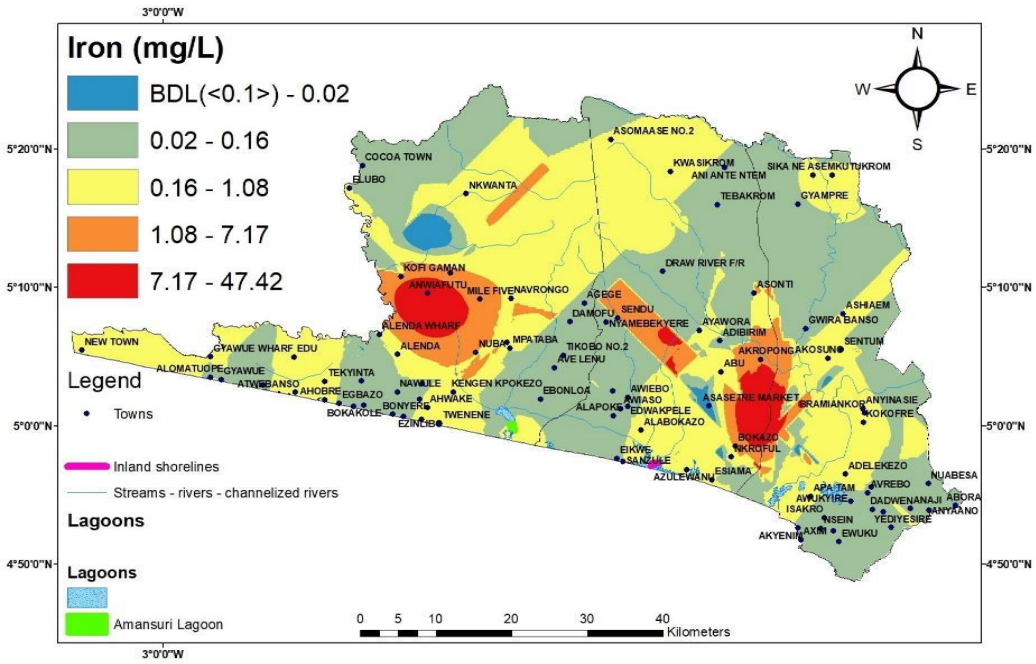

Figure 4. 24: Spatial distribution map of iron content in groundwater in the study catchment.

4.2.2.5 Transition Metals (Ni, Mn, and Co)

For the boreholes drilled from 2014 to 2015, nickel (Ni) content in the boreholes ranges from 0.0001 to 0.05 mg/L with a mean of 0.006 mg/L. In 2016, the Ni content in the sampled hand dug wells and boreholes varies from BDL to 0.01 mg/L with a mean of 0.002 mg/L, and from BDL to 0.53 mg/L with an average of 0.02 mg/L, respectively. In 2017, the Ni concentration in the hand dug wells and the boreholes ranges from BDL to 0.003 mg/L with a mean of 0.001 mg/L, and from 0.0004 to 0.046 mg/L with an average of 0.004 mg/L, respectively.

Figure 4.25 shows the spatial distribution map of nickel content in the groundwater of the Lower Tano River Basin. From the map, groundwater represented by shades of red and orange colour, mostly seen in the aquifer of the Birimian Supergroup with few observed in the aquifer of the Apollonian formation are above WHO (2011) permissible limit of 0.006 mg/L for drinking water. The rest of the groundwater represented by shades of different colours are below the acceptable range. Even though legal and illegal small-scale mining activities is rampant in the study area, the elevated Ni content might possibly be from the oxidation of

sulphide minerals to release Ni as a secondary mineral. In the study area, Luebe et al., 1990 Adjimah et al., 1993 discovered Ni as one of the trace elements hosted in sulphide minerals in the underlying geology of the study area.

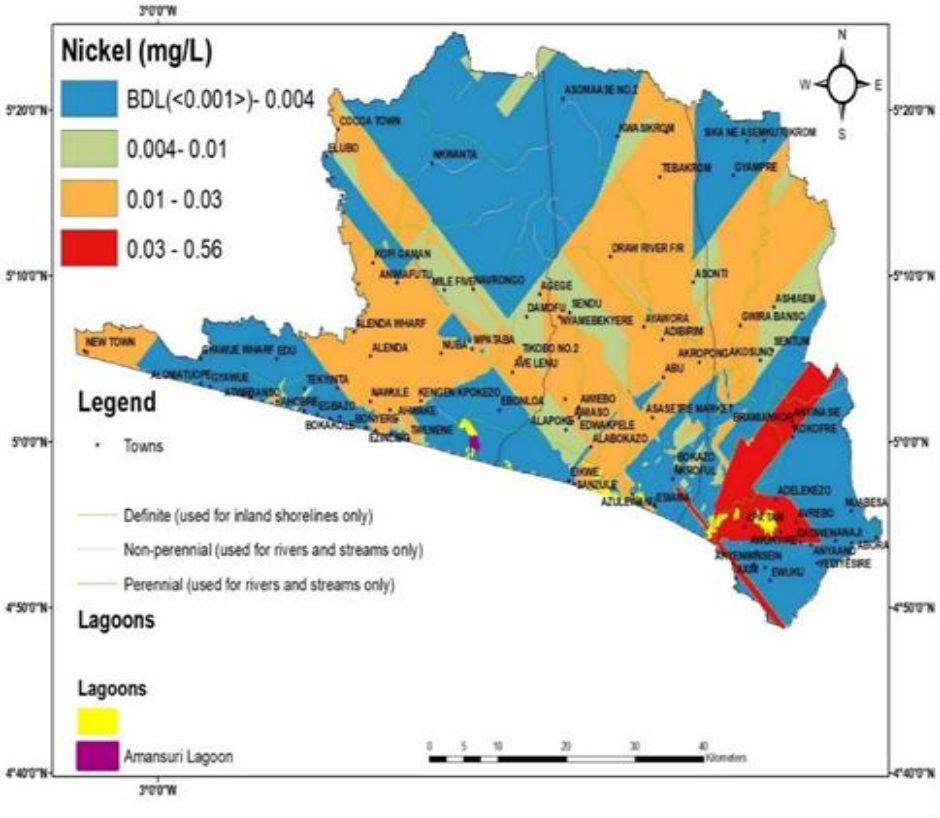

Figure 4. 25: Spatial distribution map of Ni concentrations in groundwater in the study area.

The manganese (Mn) content in the boreholes drilled in 2013 varies from 0 to 0.14 mg/L with a mean of 0.03 mg/L. That of the boreholes drilled from 2014 to 2015 varied from 0.01 to 0.27 mg/L with a mean of 0.06 mg/L. In 2016, the Mn concentration in the hand dug wells and the boreholes ranges from BDL to 0.59 mg/L with an average of 0.05 mg/L, and from BDL to 30.57 mg/L with a mean of 0.78 mg/L, respectively. Also in 2017, the Mn content in the hand dug wells and the boreholes ranges from BDL to 0.09 mg/L with a mean of 0.009 mg/L and from 0.0003 to 0.47 mg/L with an average of 0.069 mg/L, respectively.

The spatial distribution map of manganese in the groundwater is presented in Fig 4.26. From the map, the Mn content represented by shades of blue and grey are below the WHO (2011) permissible limit of 0.4 mg/L. The rest of the groundwater, represented by shades of orange

and red are above the WHO (2011) permissible limit of 0.4 mg/L. Also, from the map the elevated Mn content dominated the aquifer of the Birimian Supergroup with fewer representations in the aquifer of the Apollonian formation.

In the Birimian Supergroup rocks, studies conducted by Junner et al. (1942) and Kesse (1985) identified occurrences of manganiferrous oxide. In addition, Melcer (1995), Nsuta deposit, service (1943), Kleinscrot el al. (1994), Dzibodi-Adjimah and Sorbor (1993), Mucke et al. (1999), Nyame and Beukes (2006), Dzibodi-Adjimah (2003) etc. identified various sources of Mn in the Birimian Supergroup rocks. The natural sources of Mn mention by the above authors could possibly be one of the contributing factors leading to the high recorded Mn content in the groundwater. Also, the Birimian supergroup rocks contains banded manganese and monzonite rocks (Fig 3.3 and 3.4) which when weathers might release Mn content into the groundwater.

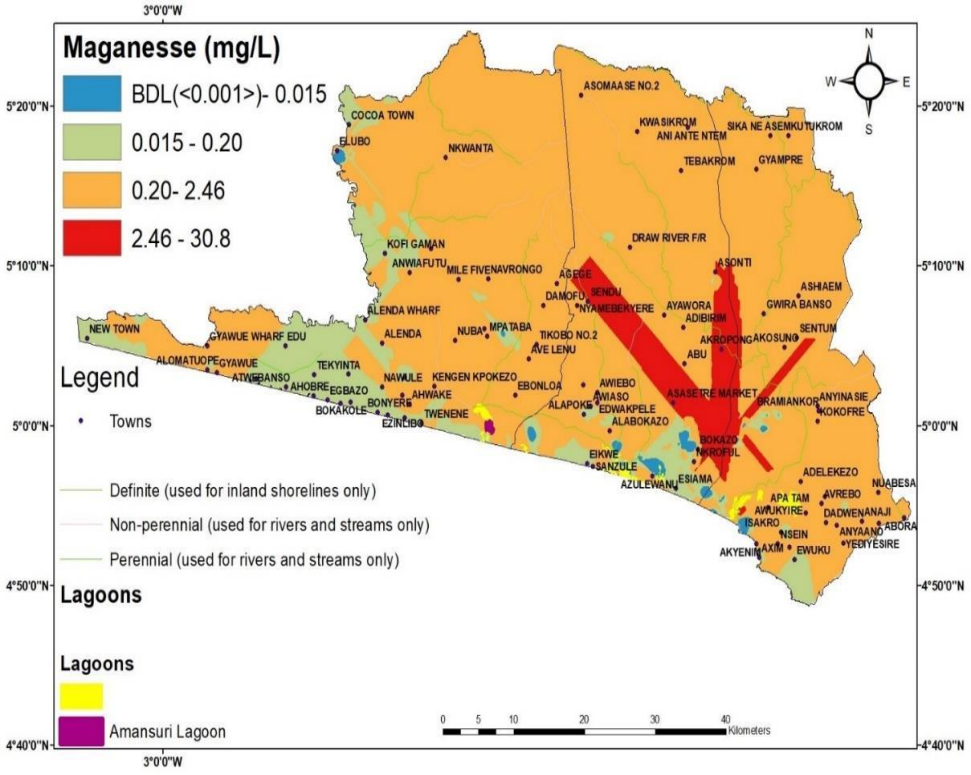

Figure 4. 26: Spatial distribution map of Mn in the groundwater in the study area.

The Cobalt (Co) content in the boreholes drilled from 2014 to 2015 varies from 0.00001 to 0.01 mg/L with an average of 0.002 mg/L. In 2016, the Co concentration in the sampled hand dug wells and the boreholes ranges from BDL to 0.006 mg/L with an average of 0.0003 mg/L, and from BDL to 0.08 mg/L with a mean of 0.003 mg/L, respectively. For

2017 samples, the Co content in the sampled hand dug wells and the boreholes ranges from BDL to 0.002 mg/L with a mean of 0.0003 mg/L, and from 0.00001 to 0.3 mg/L with a mean of 0.001 mg/L, respectively. The Co content in all the groundwater is lower than WHO permissible limit of 0.05 mg/L except for a borehole sampled at Old Kablazuaso in the aquifer of the Apollonian formation. The source of the Co content in the borehole might be geogenic or anthropogenic but further investigations are required.

4.2.2.6 Toxic Elements (Pb and As)

The lead (Pb) content in the boreholes drilled in 2013 are very minimal. That of the boreholes drilled from 2014 to 2015 ranges from 0.01 to 0.15 mg/L with an average of 0.07 mg/L. In 2016, the Pb content in the hand dug wells and the boreholes varies from BDL to 16. 30 mg/L with a mean of 0.96 mg/L, and from BDL to 4.25 mg/L with an average of 0.46 mg/L, respectively. In 2017, the Pb concentration in the hand dug wells and the boreholes ranges from BDL to 0.11 mg/L with an average of 0.04 mg/L, and from 0.00003 to 0.03 mg/L with a mean of 0.003 mg/L, respectively.

Figure 4.27 shows the spatial distribution map of lead content in groundwater of the study area. From the map, it is seen that groundwater represented by shades of blue, seen mostly in the aquifer of the Birimian Supergroup is below WHO (2011) permissible limit of 0.01 mg/L. The rest are higher than the permissible limit of 0.01 mg/L. The sources of elevated lead in the groundwater might be anthropogenic or geogenic. The anthropogenic source of Pb could possibly be linked to plumbing fixtures (Lee et al., 1989) used for the borehole construction and effluent discharge from rampant illegal small-scale mining. The use of lead as a smelter metal for the purification of gold by these miners produce by products. When these byproducts settle on top of soils or drains, they will be discharged into surrounding surface water bodies through natural process like rainfall or runoff. These surface water bodies could probably recharge the groundwater leading to elevated Pb content in the groundwater.

Another source of elevated Pb concentration in the groundwater is anthropogenic activities. In this research, during sampling, we evidenced the citizens unsanitary disposing off their sewage into the rivers especially the Tano River and the Ankobra River. Also, most houses in the study area built after 1970 uses pit latrine, and these houses are still in existence without any modern toilet facilities. An extra source of anthropogenic lead content in the groundwater might probably be from past oil seepages seen by early explorers in 1896 (Ghana geological survey, bulletin number 40). These seepages might probably be existing in the rock matrixes of the study catchment. The geogenic sources of Pb in the study area include the oxidation of sulphide minerals (arsenopyrite (FeAsS), chalco- pyrite ($CuFeS_2$) and pyrite (FeS_2)) to release Pb as a secondary mineral. Luebe et al. (1990) and Adjimah et al. (1993) discovered trace element like As, **Pb**, Cu, Zn, Ni etc. as host elements in sulphide minerals (pyrites, arsenopyrites, chalcopyrite) in the Birimian Super group rocks.

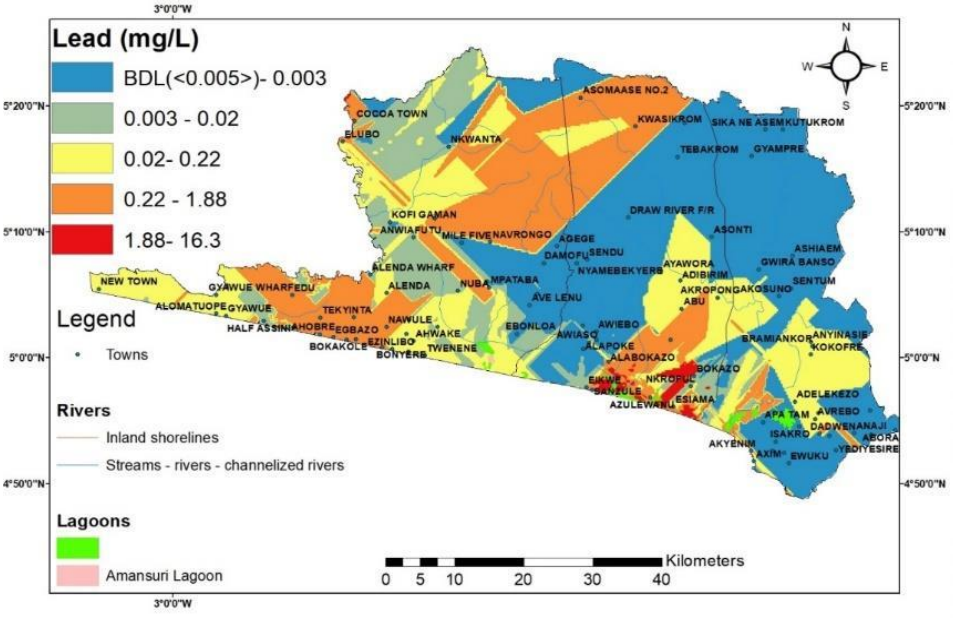

Figure 4. 27: Spatial distribution Map of lead content in the groundwater in the study catchment.

The arsenic (As) content in boreholes drilled in 2013 are very minimal but that of the boreholes drilled from 2014 to 2015 ranges from 0.00001 to 0.09 mg/L with an average of 0.008 mg/L. In 2016, the As content in the hand dug wells varies from BDL to 0.21 mg/L with a mean of 0.007 mg/L. For the boreholes sampled in 2016, the As concentration varies from BDL to 0.01

mg/L with a mean 0.001 mg/L. In 2017, the As concentration in both the hand dug wells and the boreholes varies from BDL to 0.004 mg/L with an average of 0.001 mg/L, and from 0.0004 to 0.031 mg/L with a mean of 0.002 mg/L, respectively.

Hand dug wells sampled in 2016 and 2017 had arsenic content below the WHO permissible limit of 0.01 mg/L, except a hand dug well located at Asanta in the aquifer of the Apollonian formation. For the boreholes drilled in 2013, the arsenic content is below the WHO permissible limit of 0.01 mg/L. From 2014 to 2015, 16 boreholes (n= 18) are below the WHO (2011) permissible limits and the remaining 2 boreholes situated at Asanta and Newton in the aquifer of the Apollonian formation are above the permissible limits. In 2016 and 2017, the arsenic levels in all the boreholes are below the WHO (2011) permissible limit of 0.01 mg/L with the exclusion of a borehole situated at Salman, in the aquifer of the Birimian Supergroup. The main source of Arsenic in an environment is attributed to chemical manufacturing, application of pesticides, metal smelting, and coal combusting (Diaz-Barringa et.al., 1993). However, in the study area, apart from metal smelting and the application of pesticides, the rest of the above-mentioned sources are not common. Another source of elevated As in the groundwater is related to the oxidation of sulphide minerals from the underlying geology. When these sulphide minerals oxidize As is mobilized as a primary mineral in the groundwater. Smedley et al. (2007) and Kortatsi et al. (2008b) revealed mineralized volcano- sedimentary Birimian supergroup rocks as common sources of Arsenic.

4.2.2.7 Non-Metallic Elements (Al)

Aluminum (Al) concentrations in the boreholes drilled in 2013 varies from 0.00001 to 0.06 mg/L with a mean of 0.004 mg/L. From 2014 to 2015, the Al content in the drilled boreholes ranges from 0.05 to 3.2 mg/L with an average of 0.36 mg/L. In 2016, the Al content in the sampled hand dug wells and boreholes varies from 0.004 mg/L to 0.55 mg/L with an average of 0.07 mg/L, and from BDL to 0.76 mg/L with an average of 0.08 mg/L, respectively. In 2017, the Al content in the sampled hand dug wells and the boreholes ranges from BDL to 2.48 mg/L

with an average of 0.13 mg/L, and from 0.0002 to 0.72 mg/L with a mean of 0.05 mg/L, respectively.

The Al content in the hand dug well sampled in 2016 and 2017 are all below WHO permissible limit of 0.2 mg/L, except four hand dug wells sampled at Esiama, Elubo and Azelenuano all in the aquifer of the Apollonian formation. The Al content in this hand dug wells are above the WHO (2011) permissible limit of 0.2 mg/L for drinking water. The boreholes sampled from 2013 to 2017 had Al content in most of the boreholes below the permissible limit of 0.2 mg/L. Correspondingly, fewer boreholes sampled at Effasu, Mangyea, Alumatupe, Jawey, Twenen, Kengen, Esiama, Azulenuano, all in the aquifer of the Apollonian formation and Aluku Alabokazo, Aniwafuto (chips), and Elubo all in the aquifer of the Birimian Supergroup had Al content above the WHO (2011) permissible limit of 0.2 mg/L. The source of high Al content in the groundwater is linked to the chemical weathering of silicate minerals (Hornblende, Biotite etc.) and granitic rocks which exist in the underlying geology of the study area.

The variation in trace elements in the groundwater is linked to the seasons in which the samples were taken, the time, the lithology, and human activities. Among the measured trace elements Fe had the highest occurrences. This is due to Fe being among the most abundant trace elements in the earth's crust and Fe being released through inter blended processes such as water–rock interaction (Melegy et al., 2013). The increased Fe concentration in the groundwater is linked to natural sources such as biological processes and chemical processes in the rocks. The trace element results obtained for the groundwater in the aquifer of the Birimian supergroup and the Apollonian formation is like that of the surface water discussed in previous chapters as well as studies carried out by Edjah 2012 and Doyi et al. (2018) in the Lower Tano River Basin.

4.2.3. Pearson Correlation Matrix

Under this section, Pearson correlation matrix is used to establish the relationship between the cations, anions, and trace elements in the groundwater. The obtained results are shown in Table 4.37,4.38,4.39,4.40,4.41 and 4.42, respectively. The ions that correlated are highlighted in red.

Table 4. 37: Pearson correlation matrix of hydrochemical data and trace element data for the Boreholes drilled in 2013.

	Ca^{2+}	Mg^{2+}	TH	No_3^-	SO_4^{2-}	Cl^-	pH	EC	TDS	As	Al	Zn	CU	Mn	Fe	Cr	Pb
Ca^{2+}	1.0																
Mg^{2+}	0.7	1.0															
TH	0.9	0.9	1.0														
NO_3^-	0.2	0.3	0.3	1.0													
SO_4^{2-}	0.3	0.2	0.3	-0.2	1.0												
Cl^-	0.4	0.5	0.6	0.0	0.2	1.0											
pH	0.0	0.0	0.0	0.3	-0.2	-0.3	1.0										
EC	0.4	0.5	0.5	0.1	0.4	0.4	-0.4	1.0									
TDS	0.5	0.5	0.5	0.1	0.3	0.5	-0.4	0.9	1.0								
As										1.0							
Al	0.2	0.1	0.2	0.01	0.1	0.01	0.2	0.01	0.01		1.0						
Zn	-0.2	-0.3	-0.3	-0.2	-0.5	-0.1	0.1	-0.2	-0.2		0.1	1.0					
CU	-0.1	-0.3	-0.2	0.0	-0.5	-0.1	0.3	-0.2	-0.2		0.1	0.4	1.0				
Mn	0.1	0.2	0.1	-0.1	0.1	0.3	-0.8	0.4	0.5		-0.1	-0.1	-0.1	1.0			
Fe	0.1	0.1	0.1	-0.2	0.3	0.4	-0.8	0.5	0.5		-0.2	-0.2	-0.1	0.9	1.0		
Cr	-0.2	-0.1	-0.1	0.4	0.01	0.01	0.2	-0.1	-0.1		0.1	-0.1	0.0	-0.1	-0.1	1.0	
Pb																	1

Table 4. 38: Pearson correlation matrix of hydrochemical data and trace element data for the Boreholes drilled from 2014 to 2015.

	Ca^{2+}	Mg^{2+}	TH	Na^{+}	K^{+}	HCO_3^{-}	SO_4^{2-}	Cl^{-}	pH	EC	TDS	Al	Zn	Cu	Mn	Fe	Cr	Pb	Co	Cd	Ni	As
Ca^{2+}	1																					
Mg^{2+}	0.3	1.0																				
TH	0.9	0.7	1.0																			
Na^{+}	0.1	0.8	0.4	1.0																		
K	0.1	0.6	0.3	0.8	1.0																	
HCO_3^{-}	0.9	0.6	1.0	0.4	0.3	1.0																
SO_4^{2-}	0.4	0.3	0.4	0.3	0.5	0.3	1.0															
Cl^{-}	0.1	0.7	0.4	1.0	0.8	0.4	0.3	1.0														
pH	0.7	0.5	0.8	0.5	0.6	0.8	0.3	0.5	1.0													
EC	0.5	0.8	0.8	0.9	0.7	0.7	0.4	0.9	0.7	1.0												
TDS	0.5	0.8	0.7	0.9	0.7	0.7	0.4	0.9	0.7	1.0	1.0											
Al	-0.3	-0.1	-0.3	0.01	-0.1	-0.2	0.01	0.01	-0.3	-0.2	-0.1	1.0										
Zn	0.2	0.2	0.2	-0.1	0.1	0.2	0.3	-0.1	0.01	0.01	0.01	0.3	1.0									
Cu	0.1	0.7	0.4	1.0	0.9	0.4	0.3	0.9	0.6	0.9	0.9	-0.1	0.01	1.0								
Mn	0.5	0.5	0.6	0.01	0.01	0.6	0.1	0.01	0.3	0.3	0.2	-0.2	0.3	-0.1	1.0							
Fe	-0.2	-0.1	-0.2	-0.1	-0.1	-0.1	0.1	0.01	-0.3	-0.1	-0.1	0.3	0.3	-0.1	-0.2	1.0						
Cr	-0.3	0.2	-0.1	0.4	0.2	-0.1	0.1	0.4	-0.1	0.2	0.2	0.9	0.3	0.3	-0.2	0.4	1.0					
Pb	-0.1	0.0	-0.1	-0.1	0.1	-0.2	-0.2	-0.1	0.1	-0.1	-0.1	-0.3	-0.1	0.01	0.2	-0.5	-0.4	1.0				
Co	0.3	0.7	0.5	0.6	0.8	0.5	0.2	0.5	0.6	0.7	0.6	-0.2	0.3	0.7	0.4	-0.2	0.0	0.2	1.0			
Cd	-0.3	-0.2	-0.3	-0.2	-0.2	-0.3	-0.2	-0.2	-0.2	-0.3	-0.3	-0.2	-0.3	-0.2	-0.1	0.3	-0.1	0.3	-0.2	1.0		
Ni	0.5	0.9	0.7	0.9	0.7	0.7	0.3	0.8	0.7	1.0	1.0	-0.2	0.1	0.8	0.4	-0.1	0.2	-0.1	0.7	-0.2	1.0	
As	0.01	0.2	0.1	0.4	0.8	0.01	0.1	0.3	0.4	0.3	0.3	-0.1	0.3	0.6	-0.1	-0.1	0.0	0.2	0.8	-0.2	0.3	1.0

Table 4. 39: Pearson correlation matrix of hydrochemical data and trace element data for the Hand dug wells sampled in 2016.

	Ca^{2+}	*Mg^{2+}*	*TH*	*Na^{+}*	*K^{+}*	*HCO_3^{-}*	*SO*	*Cl*	*NO*	*PH*	*EC*	*TDS*	*Al*	*Zn*	*Cu*	*Mn*	*Fe*	*Cr*	*Pb*	*Co*	*Cd*	*Ni*	*As*
Ca^{2+}	1																						
Mg^{2+}	0.2	1.0																					
TH	0.9	0.6	1.0																				
Na^{+}	0.4	0.4	0.5	1.0																			
K^{+}	0.3	-0.1	0.2	0.7	1.0																		
HCO_3^{-}	0.3	0.1	0.3	0.5	0.2	1.0																	
SO_4^{2-}	0.5	0.01	0.4	0.5	0.7	0.0	1.0																
Cl^{-}	0.5	0.6	0.7	0.8	0.5	0.3	0.3	1.0															
NO_3^{-}	0.4	0.01	0.3	0.5	0.6	0.3	0.3	0.5	1.0														
PH	0.1	0.1	0.1	0.2	0.0	0.1	-0.2	0.3	0.2	1.0													
EC	0.6	0.1	0.5	0.8	0.7	0.4	0.6	0.7	0.6	0.2	1.0												
TDS	0.5	0.1	0.5	0.8	0.7	0.3	0.5	0.7	0.6	0.1	1.0	1.0											
Al	-0.1	-0.2	-0.1	-0.1	0.01	-0.1	-0.1	-0.1	0.01	-0.1	-0.2	-0.2	1.0										
Zn	-0.2	0.01	-0.1	-0.1	-0.1	-0.1	-0.1	-0.1	-0.1	-0.2	-0.1	-0.1	0.01	1.0									
Cu	-0.1	-0.1	-0.1	-0.2	-0.1	-0.1	-0.2	-0.1	-0.1	0.01	-0.2	-0.2	0.3	0.01	1.0								
Mn	-0.1	0.5	0.2	0.2	-0.1	-0.1	-0.1	0.3	-0.1	0.01	0.01	0.01	-0.1	0.8	-0.1	1.0							
Fe	-0.1	-0.1	-0.2	0.4	0.4	0.01	0.4	0.1	0.01	-0.2	0.2	0.2	0.1	0.01	-0.1	0.1	1.0						
Cr	-0.1	-0.1	-0.1	-0.1	-0.1	-0.2	-0.1	-0.1	-0.1	-0.2	-0.1	-0.1	0.1	0.01	0.01	0.01	-0.1	1.0					
Pb	0.01	-0.1	-0.1	0.5	0.5	0.01	0.4	0.2	0.2	0.01	0.4	0.4	0.01	-0.1	0.01	0.01	0.8	-0.1	1.0				
Co	-0.2	-0.1	-0.2	0.4	0.4	0.01	0.3	0.1	-0.1	-0.2	0.2	0.2	0.01	0.01	0.01	0.1	0.9	0.01	0.8	1.0			
Cd	0.3	0.1	0.3	0.3	0.1	0.2	0.01	0.5	0.5	0.6	0.4	0.4	-0.1	-0.1	-0.1	0.01	-0.1	0.01	0.2	-0.1	1.0		
Ni	0.01	-0.3	-0.1	-0.2	0.01	-0.1	-0.2	-0.1	0.01	0.01	-0.2	-0.1	0.7	-0.1	0.4	-0.2	-0.1	0.01	0.2	0.1	0.1	1.0	
As	0.01	-0.1	-0.1	-0.1	-0.1	-0.1	0.1	0.01	-0.1	-0.2	0.1	0.1	-0.1	0.01	-0.1	-0.1	0.01	0.01	0.01	0.01	-0.1	-0.1	1.0

Table 4. 40: Pearson correlation matrix of hydrochemical data and trace element data for the boreholes sampled in 2016

	Ca^{2+}	Mg^{2+}	TH	Na^{+}	K^{+}	HCO_3^{-}	SO_4^{2-}	Cl^{-}	NO_3^{-}	pH	EC	TDS	Al	Zn	Cu	Mn	Fe	Cr	Pb	Co	Cd	Ni	As
$Ca^{2\sim}$	1																						
Mg^{2+}	0.01	1.0																					
TH	0.9	0.5	1.0																				
Na^{+}	0.1	-0.1	0.1	1.0																			
K^{+}	0.01	0.01	0.01	0.6	1.0																		
HCO_3^{-}	0.5	-0.1	0.4	0.1	0.01	1.0																	
SO_4^{2-}	0.3	0.2	0.3	0.6	0.4	-0.3	1.0																
Cl^{-}	0.3	0.2	0.3	0.4	0.2	-0.1	0.1	1.0															
NO_3	0.01	0.2	0.01	-0.1	-0.1	-0.1	-0.1	0.2	1.0														
PH	0.2	0.01	0.1	0.01	0.01	0.4	-0.2	0.01	-0.1	1.0													
EC	0.4	0.3	0.5	0.2	0.1	0.3	0.2	0.4	-0.2	0.3	1.0												
TDS	0.4	0.3	0.5	0.3	0.2	0.3	0.2	0.5	-0.2	0.3	0.9	1.0											
Al	-0.1	-0.2	-0.2	0.4	0.3	-0.1	0.2	0.2	0.01	-0.2	0.1	0.01	1.0										
Zn	-0.1	-0.1	-0.1	-0.2	-0.1	-0.1	-0.1	-0.2	0.01	-0.1	-0.2	-0.2	-0.1	1.0									
Cu	-0.2	-0.2	-0.2	-0.1	-0.1	-0.1	-0.1	-0.2	0.01	-0.1	-0.2	-0.2	0.01	1.0	1.0								
Mn	-0.1	-0.1	-0.1	-0.2	-0.1	-0.1	0.01	-0.2	0.01	-0.1	-0.2	-0.2	-0.1	1.0	1.0	1.0							
Fe	0.01	0.01	0.01	-0.3	-0.1	-0.1	-0.1	-0.2	0.2	-0.2	-0.2	-0.2	0.01	0.7	0.7	0.7	1.0						
Cr	0.2	-0.2	0.1	-0.1	0.01	0.1	0.0	-0.1	-0.2	-0.3	-0.1	0.01	0.01	-0.1	-0.1	-0.1	-0.1	1.0					
Pb	0.1	0.3	0.2	0.1	0.2	0.1	0.1	0.01	-0.3	-0.1	0.1	0.2	-0.1	-0.1	-0.1	-0.1	-0.1	0.4	1.0				
Co	-0.2	0.01	-0.2	0.01	-0.1	-0.1	0.01	0.01	-0.2	0.01	-0.2	-0.1	-0.1	0.01	-0.1	0.01	-0.1	-0.1	0.3	1.0			
Cd	0.4	0.1	0.4	-0.1	-0.1	0.01	0.01	0.3	-0.3	0.1	0.2	0.2	-0.1	0.01	0.01	0.01	-0.1	0.3	0.2	0.01	1.0		
Ni	0.6	0.01	0.5	0.1	0.01	0.2	0.01	0.4	-0.2	0.01	0.2	0.2	-0.1	0.01	0.01	0.01	0.01	0.1	0.01	0.01	0.7	1.0	
As	0.1	0.5	0.3	0.01	-0.1	0.2	0.01	0.01	-0.2	0.2	0.2	0.2	-0.1	-0.1	-0.1	-0.1	-0.1	0.01	0.3	0.1	0.1	0.01	1.0

Table 4. 41: Pearson correlation matrix of hydrochemical data and trace element data for the Hand dug wells sampled in 2017

	Ca^{2+}	Mg^{2+}	TH	Na^{+}	K^{+}	HCO_3^{-}	SO_4^{2-}	Cl^{-}	NO_3^{-}	PH	EC	TDS	Al	Zn	Cu	Mn	Fe	Cr	Pb	Co	Cd	NI	As
Ca^{2+}	1																						
Mg^{2+}	0.6	1.0																					
TH	1.0	0.8	1.0																				
Na^{+}	0.5	0.6	0.6	1.0																			
K^{+}	0.5	0.6	0.6	0.8	1.0																		
HCO_3^{-}	0.7	0.6	0.7	0.5	0.5	1.0																	
SO_4^{2-}	0.4	0.5	0.5	0.6	0.5	0.4	1.0																
Cl^{-}	0.4	0.3	0.4	0.6	0.5	0.01	0.01	1.0															
NO_3^{-}	0.01	-0.1	0.01	0.3	0.2	-0.2	0.2	0.3	1.0														
PH	0.6	0.4	0.6	0.1	0.3	0.6	0.3	-0.1	-0.2	1.0													
EC	0.8	0.7	0.9	0.8	0.8	0.7	0.5	0.6	0.2	0.3	1.0												
TDS	0.8	0.7	0.9	0.8	0.8	0.7	0.5	0.6	0.2	0.3	1.0	1.0											
Al	-0.2	0.01	-0.1	0.2	0.2	-0.2	-0.2	0.4	0.4	-0.5	0.2	0.1	1.0										
Zn	-0.2	-0.1	-0.1	0.01	0.01	-0.2	0.1	0.01	0.3	-0.2	-0.2	-0.2	0.2	1.0									
Cu	0.3	0.4	0.4	0.4	0.4	0.2	0.5	0.2	0.2	0.4	0.3	0.3	0.1	0.6	1.0								
Mn	-0.2	-0.1	-0.2	0.01	0.1	-0.3	-0.2	0.2	0.3	-0.5	0.01	0.01	0.8	0.3	0.01	1.0							
Fe	0.8	0.7	0.8	0.4	0.3	0.5	0.4	0.2	-0.1	0.6	0.6	0.6	-0.1	-0.1	0.3	-0.1	1.0						
Cr	0.4	0.5	0.5	0.5	0.5	0.5	0.4	0.01	0.1	0.4	0.5	0.5	0.1	0.2	0.5	0.01	0.3	1.0					
Pb	0.8	0.5	0.8	0.3	0.4	0.5	0.2	0.3	0.01	0.6	0.6	0.7	0.01	-0.1	0.4	-0.1	0.7	0.3	1.0				
Co	-0.2	0.01	-0.1	0.1	0.1	-0.2	-0.2	0.2	0.3	-0.4	0.01	0.01	0.7	0.2	0.01	1.0	-0.1	0.1	0.01	1.0			
Cd	-0.1	0.2	0.01	0.4	0.3	-0.1	0.01	0.4	0.4	-0.4	0.2	0.1	0.7	0.7	0.5	0.6	-0.2	0.3	-0.1	0.5	1.0		
Ni	0.1	0.2	0.1	0.2	0.2	-0.1	0.3	0.1	0.3	-0.1	0.1	0.1	0.5	0.7	0.6	0.6	0.2	0.3	0.2	0.6	0.7	1.0	
As	0.6	0.6	0.6	0.2	0.3	0.4	0.2	0.1	-0.1	0.5	0.4	0.4	-0.1	0.01	0.4	-0.2	0.6	0.5	0.5	-0.1	0.01	0.2	1.0

Table 4. 42: Pearson correlation matrix of hydrochemical data and trace element data for the boreholes sampled in 2017

	Ca^{2+}	Mg^{2+}	TH	Na^{+}	K^{+}	HCO_3^{-}	SO_4^{2-}	Cl^{-}	NO_3^{-}	PH	EC	TDS	Al	Zn	Cu	Mn	Fe	Cr	Pb	Co	Cd	Ni	As
Ca^{2+}	1																						
Mg^{2+}	0.5	1.0																					
TH	0.8	0.6	1.0																				
Na^{+}	0.3	0.1	0.3	1.0																			
K^{+}	0.3	0.0	0.3	0.7	1.0																		
HCO_3^{-}	0.8	0.6	0.7	0.2	0.0	1.0																	
SO_4^{2-}	0.3	0.4	0.3	0.6	0.5	0.01	1.0																
Cl^{-}	0.2	0.1	0.2	0.7	0.6	0.01	0.2	1.0															
NO_3^{-}	0.01	0.01	0.1	0.2	0.2	0.01	0.01	0.2	1.0														
PH	0.2	0.1	0.3	0.01	0.2	0.2	-0.1	0.01	0.1	1.0													
EC	0.4	0.4	0.4	0.2	0.1	0.6	0.01	0.1	0.3	0.1	1.0												
TDS	0.5	0.4	0.5	0.2	0.1	0.6	0.01	0.2	0.3	0.2	0.9	1.0											
Al	0.3	0.3	0.1	0.2	0.1	0.3	0.01	0.3	-0.1	-0.1	0.3	0.4	1.0										
Zn	-0.1	-0.2	-0.2	-0.1	-0.1	-0.1	-0.1	-0.1	-0.1	0.0	-0.1	-0.1	0.1	1.0									
Cu	-0.1	-0.1	-0.1	-0.1	0.01	-0.1	-0.1	-0.1	0.01	0.1	0.01	0.01	0.01	0.9	1.0								
Mn	0.3	0.2	0.3	-0.1	-0.1	0.3	0.1	-0.2	0.01	0.1	0.1	0.1	0.01	-0.1	-0.1	1.0							
Fe	-0.2	-0.3	-0.2	0.4	0.2	-0.2	0.3	0.01	-0.1	-0.3	-0.2	-0.2	-0.2	0.1	0.1	-0.3	1.0						
Cr	0.3	0.01	0.2	0.3	0.3	0.1	0.3	0.2	0.1	-0.1	0.1	0.1	0.2	0.01	0.01	0.01	0.3	1.0					
Pb	0.01	-0.1	0.01	0.01	0.01	0.01	-0.2	0.1	0.01	0.01	0.1	0.2	0.6	0.1	0.1	-0.1	-0.3	-0.1	1.0				
Co	0.3	0.2	0.2	-0.1	-0.1	0.2	0.01	0.1	0.01	0.01	0.1	0.1	0.3	0.01	0.01	0.7	-0.3	0.01	0.3	1.0			
Cd	-0.1	-0.1	-0.2	-0.1	0.0	-0.1	-0.1	-0.1	0.01	0.01	-0.1	-0.1	0.01	0.9	1.0	0.01	0.1	-0.1	0.01	0.01	1.0		
Ni	0.1	0.01	0.01	-0.3	-0.1	0.01	-0.2	0.01	-0.1	0.01	-0.1	-0.1	0.01	0.3	0.4	0.3	-0.3	-0.1	0.1	0.6	0.4	1.0	
As	0.01	0.01	0.1	-0.1	-0.1	0.1	-0.1	-0.2	-0.2	-0.1	0.1	0.2	-0.1	-0.1	-0.1	0.3	0.2	0.01	-0.1	0.01	-0.1	0.01	1.0

From, the above tables (table 4.37 to 4.42), the cations, anions and trace elements that correlated are highlighted in red. Mg^{2+} correlated strongly with Ca^{2+} for the boreholes drilled in 2013, and hand dug wells and boreholes sampled in 2017. The study area records high amount of rainfall (Fig 1.3 to 1.6), as such, carbon dioxide (CO_2) released from the atmosphere and decaying organic matter might likely dissolve in the rainwater to form a weak carbonic acid i.e., $CO_2 + H_2O \rightarrow H_2CO_3 \rightarrow H^+ + (HCO_3^-)$ (Apello & Postma, 1999). The acid possibly attacks the limestone which exist in the underlying geology, dissolving $CaCO_3$ or $MgCO_3$ to yield an aqueous solution of HCO_3^- , **Ca and Mg^{2+}** in the groundwater.

TH corelated strongly with Ca^{2+} and Mg^{2+} for the boreholes drilled in 2013, boreholes drilled from 2014 to 2015, hand dug wells and boreholes sampled in 2016 and boreholes sampled in 2017. The good relationship is linked to the dissolution of limestones and weathering of silicate minerals (hornblende, plagioclase, biotite etc.) from the underlying geology of the study area.

For the boreholes drilled from 2014 to 2015 (Table 4.35) Na^+ correlated strongly with Mg^{2+}. In 2016, Na^+ correlated strongly with TH for the hand dug wells (Table 4.36) and Na^+ correlated strongly with (Ca^{2+}, Mg^{2+} and TH) for the hand dug wells sampled in 2017. The good relationship between Na^+ and (Ca^{2+} and Mg^{2+}) suggest the possibility of cation-exchange processes at the soil-water interface (Guo & Wang. 2004) which will be explained further in the 3rd specific objective. Also, the good relationship between Na^+ and (Ca^{2+} and Mg^{2+}) indicates the possible weathering of silicate minerals (hornblende, plagioclase, feldspar, etc.) from the underlying geology (Fig 3.3 and 3.4). Bowser and Jones (2002) argued that territories subjugated by silicate minerals is the primary source of **Na^+, Ca^{2+} and Mg^{2+}.**in groundwater. The good relationship between Na^+ and TH indicates that the presence of sodium hardness in the groundwater

The boreholes drilled from 2014 to 2015 had K^+ correlating strongly with (Mg^{2+} and Na^+). In addition, K^+ correlated strongly with Na^+ for the hand dug wells and boreholes sampled in

2016. For the hand dug wells sampled in 2017, K^+ correlated strongly with (Ca^{2+}, Mg^{2+}, TH and Na^+). Also, for the boreholes sampled in 2017, K^+ correlated strongly with Na^+. The good relationship between K^+ and Na^+ is linked to the chemical weathering of silicate minerals (biotite, feldspars) from the underlying geology of the study area (Fig 3.3 and 3.4). In addition, the good relationship between K^+ and Mg^{2+} is linked to the weathering of granitic rocks which exist in the study area. Also, the relationship between K^+ and Mg^{2+} suggest a possible cation - exchange processes (Drever, 1988). The good relationship between K^+ and TH suggest potassium hardness in the groundwater.

HCO_3^- correlated strongly with (Ca^{2+}, Mg^{2+}, and TH) for the boreholes drilled from 2014 to 2015. Also, HCO_3^- correlated strongly with Na^+ for the hand dug wells sampled in 2016. For the boreholes sampled in 2016, HCO_3^- correlated strongly with Ca^{2+}. In 2017, HCO_3^- in the sampled hand dug wells and boreholes correlated strongly with (Ca^{2+}, Mg^{2+}, TH, K^+, Na^+), and (Ca^{2+}, Mg^{2+} and TH), respectively. Groundwater containing bicarbonate, calcium and magnesium could be altered to one containing bicarbonate, sodium, and potassium (Kister & Hardt, 1966). Hence, the good relationship between HCO_3^- and the above-mentioned elements is linked to Base- Exchange reactions. In addition, the good relationship between HCO_3^- and (Ca^{2+} and Mg^{2+}) represents the dissolution of carbonate minerals (limestones etc.) and chemical weathering of granitic rocks. The good relationship between HCO_3^- and TH indicates the presence of carbonate hardness (Drever, 1988) in the sampled groundwater due to the groundwater interacting with carbonate minerals and silicate minerals from the underlying geology.

Also, the good relationship between HCO_3^- and (Na^+ and K^+) suggests a possible cation exchange processes were Na^+ and K^+ from silicate mineral (feldspars, plagioclase etc) weathering from the underlying geology are specially desorbed into the groundwater. In addition, the relationship between HCO_3^- and Ca^{2+} probably indicate a recharging aquifer which will be explained in the 3rd and 4th specific objective and dissolution of carbonate

minerals (Khashogji and El Maghraby, 2013) and weathering of silicate mineral (plagioclase, hornblende, etc) (Gastmans et al. 2010) from the underlying geology of the study area.

SO_4^{2-} correlated strongly with K^+ for the boreholes drilled from 2014 to 2015. For the hand dug wells and boreholes sampled in 2016, SO_4^{2-} correlated strongly with (Ca^{2+}, Na^+ , K^+) and SO_4^{2-} correlated strongly with Na^+, respectively. In 2017, SO_4^{2-} correlated strongly with (Mg^{2+}, TH, Na^+ , K^+) for the hand dug wells and SO_4^{2-} correlated strongly with (Na^+ , K^+). The good relationship between SO_4^{2-} and (Ca^{2+}, Mg^{2+}) is ascribed to ion-exchange processes. The good relationship between SO_4^{2-} and (Na^+ and K^+) is accredited to anthropogenic sources (Sophocleous et al., 2002). Also, the good relationship between SO_4^{2-} and Mg^{2+}indicate that sulphide mineral dissolution from the underlying geology is the basis for sulphate loading in the groundwater (Liu et al., 2019).

In 2013, Cl^- correlated strongly with Mg^{2+} and TH for the drilled boreholes. For the boreholes drilled from 2014 to 2015, Cl^- correlated strongly with Mg^{2+}, Na^+ and K^+. For the hand dug wells sampled in 2016, Cl^- correlated strongly with Ca^{2+}, Mg^{2+}, TH, Na^+ and K^+. In 2017, Cl^- correlated strongly with Na^+ and K^+ for the hand dug wells and boreholes sampled in 2017. The relationship between Cl^- and (Na^+, K^+) in the groundwater is linked to ion exchange processes and imitates the contribution of rainfall recharge, which will be explained further in the 4th specific objective. The good relationship between Cl^- and ($Ca^{2+,}$ Mg^{2+}) is linked to rock-water interactions. The good linkage between Cl^- and TH indicates chloride hardness in the groundwater.

Additionally, NO_3^- correlated strongly with Na^+, K^+ and Cl^- in the hand dug wells sampled in 2016. The good relationship between NO_3^- and (Na^+ and K^+) indicates a possible ion exchange process. That of NO_3^- and Cl^- is due to anthropogenic sources such as prolonged minimal application of fertilizers by peasant farmers, cocoa farmers, and coconut farmers in the study

area. Another source is attributed to effluents discharge from the surrounding industries such as coconut oil industries, but further investigations is required.

pH correlated strongly with Ca^{2+}, Mg^{2+}, TH, Na^{+}, K^{+}, HCO_3^{-} and Cl^{-} for the boreholes drilled from 2014 to 2015. For the hand dug wells sampled in 2017, pH correlated strongly with Ca^{2+}, TH and HCO_3^{-}. The good relationship between pH and (Ca^{2+}, Mg^{2+}, $^{-}$) indicate carbonate mineral dissolution and silicate mineral (plagioclase, biotite, feldspar etc.) weathering from the underlying geology. The good relationship between pH and TH suggests the dissolution of carbonate minerals from the rocks of the Apollonian and chemical weathering of silicate minerals from the rocks of the Birimian supergroup. Additionally, the good connection between pH and (Na^{+}, K^{+}) suggest weathering of silicate minerals (plagioclase, hornblende feldspars, etc.) from the underlying geology. The good relationship between pH and Cl^{-} is attributed to a contaminated source which requires further investigations. The good relationship between pH and HCO_3^{-} indicates same geochemical processes.

EC correlated strongly with (Mg^{2+} and TH) for the boreholes drilled in 2013. For the boreholes drilled from 2014 to 2015, EC correlated strongly with Ca^{2+}, Mg^{2+}, TH, Na^{+}, K^{+}, HCO_3^{-} , pH and Cl^{-}. For the hand dug wells and boreholes sampled in 2016, EC correlated strongly with Ca^{2+}, TH, Na^{+}, K^{+}, SO_4^{2-}, Cl^{-} and NO_3^{-} , and TH, respectively. For the hand dug wells and boreholes sampled in 2017, EC correlated strongly with Ca^{2+}, $Mg^{2+,}$ TH, Na^{+}, K^{+}, HCO_3^{-} , SO_4^{2-}, and Cl^{-}, and HCO_3^{-}, respectively. The good relationship between EC and the above-mentioned elements indicates that the above analyzed ions possibly contributed to the groundwater mineralization of the study area. The good relationship between EC and (SO_4^{2-}, NO_3^{-}) indicates that anthropogenic sources or geogenic sources possibly aids in the mineralization of groundwater in the study area. Also, the good relationship between EC and (Ca^{2+}, Mg^{2+}, TH, Na^{+}, K^{+}, SO_4^{2-}, Cl^{-} and HCO_3^{-}, NO_3^{-}) indicates that most of the above-mentioned ions are probably involved in physiochemical reactions such as oxidation-reduction and ion-exchange (Subba Rao, 2002).

There was a good relationship between TDS and EC for the boreholes drilled in 2013, the boreholes drilled from 2014 to 2015, the hand dug wells and boreholes sampled in 2016, and the hand dug wells and boreholes sampled in 2017. TDS reveals the behavior of EC in groundwater (Patil et al., 2010). Also, TDS correlated strongly with Mg^{2+}, TH and Cl for the boreholes drilled in 2013. For the boreholes drilled from 2014 to 2015, TDS correlated strongly with (Ca^{2+}, Mg^{2+}, TH, Na^{+}, K^{+}, HCO_3^{-}, Cl^{-} and pH). For the hand dug wells sampled in 2016 there was a strong correlation between TDS and (Ca^{2+}, TH, Na^{+}, $K^{+,}$ SO_4^{2-}, Cl^{-}, and NO_3^{-}) and for the boreholes sampled in 2016, TDS correlated strongly with (TH and Cl^{-}). For the hand dug wells sampled in 2017, TDS correlated strongly with Ca^{2+}, Mg^{2+}, TH, Na^{+}, K^{+}, HCO_3^{-}, SO_4^{2-}, and Cl^{-}). For the boreholes sampled in 2017, TDS correlated strongly with Ca^{2+}, TH and HCO_3). The relationship between the TDS and the above mention ions in the groundwater shows that the above - mentioned elements is involved in a long-term physiochemical reaction such as ion exchange and oxidation – reduction (Subba Rao, 2002).

Al negatively correlated with pH for the hand dug wells sampled in 2017. The pH of natural water generally varies from 4 to 10 (Apello & Postma, 1999). Comparatively small changes of pH can have a critical effect on the adsorption of ions onto, and from the surface of sediments. The relatively low mean pH (5.98) recorded during the dry season for the hand dug wells could possibly not influence the weathering of silicate mineral (Hornblende, granite, biotite etc.) from the underlying geology to release Al as a primary ion in the groundwater.

Zn correlated negatively with SO_4^{2-} for the boreholes drilled in 2013. This shows that SO_4^{2-} is not influenced during sulphide mineral (pyrites, arsenopyrites, cha;copyrites) oxidation to release Zn as a secondary mineral in the groundwater. (Luebe et al.,1990) discovered Zn as one of the trace elements hosted in the sulphide minerals of the study area.

Cu correlated strongly with SO_4^{2-} for the boreholes drilled in 2013. For the boreholes drilled from 2014 to 2015, Cu correlated strongly with Mg^{2+}, Na^{+}, K^{+}, Cl^{-}, pH, EC, and TDS. For the

boreholes sampled in 2016, Cu correlated perfectly with Zn. Additionally, Cu correlated strongly with (SO_4^{2-} and Zn) and perfectly with Zn for the hand dug wells and boreholes sampled in 2016, respectively. The good relationship between Cu and (SO_4^{2-}, Zn) is possibly from the oxidation of sulphide bearing minerals {arsenopyrite (FeAsS), **chalco- pyrite ($CuFeS_2$)** and pyrite (FeS_2)} (Luebe et al., 1990; Adjimah et al., 1993) to liberate SO_4^{2-} and Zn, as secondary mineral in the groundwater. In addition, the good relationship between Cu and (Mg^{2+}, Na^+, K^+) suggests the likelihood of rock weathering. When rainfall containing Cl interacts with chalco-pyrite from the underlying geology, transportation of mobilized Cu in the groundwater occurs thus leading to the good relationship between Cu and Cl^-. Additionally, the sulphide minerals are present in the underlying geology of the study area, hence drainage of sulfuric acid may significantly contribute to the acidity (Hunslow, 1995) of the groundwater thus leading to a good relationship exists between Cu and pH for the boreholes drilled from 2014 to 2015. The good relationship between Cu and (EC and TDS) indicates that the mobilization of sulphide minerals {chalcopyrite ($CuFeS_2$)} from the underlying geology influences the mineralization of the groundwater.

Mn correlated negatively with pH for the boreholes drilled in 2013. This indicates that the pH of the sampled groundwater does not influence the weathering of ferromagnesium (Biotite) minerals or banded manganese formation. In addition to the boreholes drilled in 2013, Mn correlated strongly with TDS. This suggests that the weathering of ferromagnesium (Biotite) minerals or banded manganese formation minerals adds to the mineralization of the groundwater. For the boreholes drilled from 2014 to 2015, Mn correlated strongly with (Ca^{2+}, Mg^{2+}). This indicates a possible weathering of silicate minerals (biotite, hornblende, feldspar, muscovite, quartz, staurolite, etc.) (fig 3.3 and 3.4) from the underlying geology. The good relationship between Mn and HCO_3^- has explained the weathering of ferromagnesium (Biotite) minerals or banded manganese formation of the study area. The good connection between Mn and TH indicates manganese hardness in the groundwater. For the hand dug wells and

boreholes sampled in 2016, Mn correlated strongly with (Mg^{2+} and Zn), and perfectly with Zn respectively. Geochemically, Mn behaves like **Mg^{2+}**, Ni, Fe and Co and tends to partition into minerals that form in the early stages of magmatic crystallization (Post, 1999). Hence, the good relationship between Mn and Mg^{2+} is likely to be seen. Additionally, Mn and Zn are found as trace elements in groundwater that ensue as crystal structure of minerals seen in rocks and the occurrence of Mn and Zn in groundwater is dependent on the mobility and the weathering condition (Handa, 1986). Hence, the good relationship between Mn and Zn is likely to be observed. For the hand dug wells sampled in 2017, Mn correlated negatively with pH. This indicates the absence of same geochemical processes.

In addition, Mn correlated strongly with Al and the possible reason might be from the weathering of silicate minerals (hornblende, biotite etc.) from the underlying geology.

For the boreholes drilled in 2013, Fe negatively correlated with pH and Fe correlated strongly with pH for the hand dug wells sampled in 2017. In the study area, the underlying geology is rich in pyrites, and the pH of the boreholes sampled in 2013 were neutral to basic (6.7 – 7.7). Hence there is a non-occurrence of geochemical processes (Hunslow, 1995). For the boreholes sampled in 2017, the pH was acidic to basic, hence the is a possible geochemical process or or oxidation of sulphide minerals or weathering of silicate minerals or granitic rocks from the underlying geology. Fe correlated strongly with TDS for the boreholes drilled in 2013 and the hand dug wells sampled in 2017. The good relationship indicates that Fe controls the groundwater mineralization in the 2013 sampled boreholes and 2017 sampled hand dug wells. For the hand dug wells sampled in 2017, Fe correlated strongly with (Ca^{2+}, Mg^{2+}, TH, and HCO_3^-). This is attributed to the weathering of granitic rocks, and silicate minerals (hornblende, etc.) from the underlying geology. Additionally, for the hand dug wells sampled in 2017, Fe correlated strongly with EC and this indicates that Fe controls the mineralization of the hand dug wells sampled in 2017. The good relationship between Fe and (Cu and Zn) for the boreholes sampled in 2016 suggest sulphide minerals {chalco- pyrite ($CuFeS_2$), pyrites }

oxidation. Luebe et al., 1990; Adjimah et al., 1993 discovered trace elements like As, Pb, Cu, **Zn,** Ni etc. hosted in the sulphide minerals. These trace elements were used as pathfinder elements for the discovery of gold in the study area. Similarly for the boreholes drilled in 2013 and the boreholes sampled in 2016, Fe correlated strongly with Mn. Looking at the geological map of the study area (fig 3.3 and 3.4), it is seen that the rocks of the Apollonian is in a coastal alluvial plain. Alluvial plain is naturally not rich in trace elements but are porous, coarse, and permeable (Kesse, 1985) enough to facilitate the contamination of groundwater with trace elements such as Fe and Mn. Such plains usually have elevated organic- matter which might enhance microbial activities that in turn produce a reducing environment protruding the dissolution of Fe and Mn (Postawa et al., 2013; Weng et al., 2007). Studies have shown that coastal aquifers are vulnerable to salinization and previous investigations elsewhere have found that elevated salinity is responsible for the dissolution of Fe and Mn (Zang et al., 2020; Liu et al., 2019; Pezzetta et al., 2011) in groundwater. Also, the coastal zone of the study area is the hub for oil and gas industries and a target for urbanization and studies have proven and confirmed that urbanization correlates with high Fe and Mn content in groundwater (Onodera, 2008; Fadly et al., 2017). In the study area, even though the rock matrixes contain Fe and Mn bearing minerals like hornblende, biotite etc., the hydrogeological information with respect to natural conditions are limited. Hence, the good relationship between Fe and Mn suggests a possible-non-homogeneous geochemical processes such as different ion concentrations in the aquifer system and different mineral dissolution rate, but further investigations is required. Fe is normally present at elevated concentration than Mn (Postawa et al., 2013; Giblin, 2009). However, in this study, the analyzed Fe values is higher than Mn for all the sampled groundwater and this possibly confirm the heterogeneous geochemical nature of the aquifer of the Birimian supergroup and the Apollonian formation, where Fe and Mn were irregularly dispersed.

For the boreholes drilled from 2014 to 2015, Cr correlated perfectly with Al. Cr also correlated strongly with (Mg^{2+}, TH, Na^{+}, K^{+}, HCO_3^{-}, EC, TDS, Cu) for the hand dug wells sampled in 2017. Chromite is an oxide mineral that contains Fe, **Mg^{2+}**, **Al**, **Ca^{2+}** and **Cr** in variable proportions depending on their deposits (Murthy et al., 2011; Sanchez-Segado et al., 2015). Chromite transpires exclusively in mafic and ultramafic igneous rocks {Papp & Lipin. (2006)}. In the study area, ultramafic rocks and minor mafic igneous rocks which are undifferentiated are found in the underlying geology (Fig 3.3 and 3.4; Dampare et al. (2008)}and it can be inferred that the possible occurrence of mafic and ultramafic weathering from the underlying geology of the study area led to the good relationship between Fe and (Cr, Al, Mg^{2+}) in the groundwater of the study area.

The good relationship between Cr and (Cu, $Na^{+}$and K^{+}) indicates a possible rock weathering with rock-water interactions but further investigations are required.

Also, the good relationship between Cr and HCO_3^{-} indicates a possible rock-water interaction (McClain & Maher, 2016). The good relationship between Cr and (EC and TDS) is attributed to similar geochemical processes such as ion exchange processes and Cr possibly added to the groundwater mineralization of the study area.

For the boreholes drilled from 2014 to 2015, Pb correlated negatively with Fe, suggesting that Pb might possibly not influence Fe in the aquifer system. For the hand dug wells sampled in 2016 and 2017, Pb correlated strongly with (Na^{+}, K^{+} and Fe), and (Ca^{2+}, Mg^{2+}, TH, HCO_3^{-}, pH EC, TDS, and Fe), respectively. For the boreholes sampled in 2017, Pb correlated strongly with Al. The good relationship between Pb and (Na^{+}, K^{+} , Ca^{2+}, Mg^{2+}, Fe, Al) suggests a possible rock -water interaction. Pb released as a secondary mineral from the oxidation of pyrites {arsenopyrite (FeAsS), chalco- pyrite ($CuFeS_2$) and pyrite (FeS_2)} (Luebe et al., 1990) might possibly dissolve into surrounding surface waterbodies and through natural processes like rainfall or run off might be carried to the water table and leached into the aquifer to interact

with Na^+, K^+, Ca^{2+}, Mg^{2+},Fe , Al released from the weathering of silicate minerals (Biotite, Muscovite, hornblende,, sericite, feldspars, etc.),granitic rocks, monzonite rocks and carbonates mineral (limestones, clay minerals etc.) dissolution from the underlying geology. The strong positive correlation shown between Pb and TH suggest Pb hardness in the groundwater. Also, the good linkage between Pb and HCO_3^- suggests a possible rock-water interactions.

For the boreholes drilled from 2014 to 2015, Co correlated strongly with Mg^{2+}, TH, Na^+, K^+, HCO_3^-, Cl^-, pH, EC, TDS, and Cu. For the hand dug wells sampled in 2016, Co strongly correlated with Fe and Pb and for the hand dug wells sampled in 2017, Co correlated perfectly with Mn and strongly with Al. For the boreholes sampled in 2017, Co correlated strongly with Mn. A relationship exists between Cobalt (Co) and Manganese (Mn) in rocks or soils due to their similar characteristics or properties and are frequently in **ferromagnesian minerals** where their respective divalent radii permit them to replace readily for Fe (II) and Mg (II) (Goldschmidt, 1958). In sedimentary rocks the concentrations of Mn and Co are highly variable, but as a rule they are uppermost in fine-grained sediments e.g., **shales** (Goldschmidt, 1958). The above, has explained the good relationship between Co and (Mn, Mg^{2+}, Na^+, K^+, Al, Fe) that existed in the groundwater. The relationship between Co and (Fe, Pb and Cu) reveals the oxidation of sulphide minerals (pyrites, arsenopyrites, chalcopyrite etc.) from the underlying geology to release Co and Pb as secondary minerals in the groundwater of the study area. The relationship between Co and Cl^- is probably related to rock-water interaction. That is when the sulphide minerals from the underlying geology of the study area oxidizes, Co is liberated as a secondary mineral in the groundwater and when rainfall containing Cl interacts with the host rocks Co will probably be transported into the aquifers. The good relationship between Co and (EC and TDS) indicates similar geochemical processes where Co controls the mineralization of groundwater. The good linkage between Co and pH suggests same geochemical source.

Also, Cd correlated strongly with Cl^-, NO_3^-, and pH for the hand dug wells sampled in 2016. In addition, Cd correlated strongly with Al, Zn, Cu, Mn, and Co for the hand dug wells sampled in 2017. For the boreholes sampled in 2017, Cd correlated strongly with Zn and Cu. The good relationship between Cd and (Zn, Cu, Co) are attributed to rock-water interaction. The good relationship between Cd and (Al, Mn) is possibly from the dissolution of clay mineral and carbonate minerals from the underlying geology of the study area. This is possible because works carried out by Appel and Ma. (2002), Buerge-Weirich et al. (2002) and He et al. (2005) shows that high Cd concentration in sediments and soils are normally linked to the abundance of **carbonates, clay minerals,** organic matter, and hydrous oxides, as well as other physicochemical settings, such as high pH, and/or anoxic conditions. But further investigations are required. The good relationship between Cd and pH implies same geochemical processes. The good relationship between Cd and (Cl^- and NO_3^-) indicates a probable anthropogenic source.

For the boreholes drilled from 2014 to 2015, Ni correlated strongly with (Ca^{2+}, Mg^{2+}, TH, Na^+, K^+, HCO_3^-, Cl^-, pH, EC, TDS, Cu, Co). For the hand dug wells and boreholes sampled in 2016, Ni correlated strongly with Al and (Ca^{2+}, TH and Cd), respectively. In 2017, Ni correlated strongly with (Al, Cu, Zn, Mn, Co, and Cd) for the hand dug wells and (Co) for the boreholes. In the underlying geology of the study area, the omnipresence of pyrites, chalcopyrite and arsenopyrites which host trace elements like **Ni**, Zn, Co etc. {Luebe et al. (1990)} possibly influences the groundwater mineralization leading to the good relationship between Ni and (EC, TDS) in the groundwater. The good relationship between Ni and (Zn, Co, Cu). suggests the oxidation of sulphide minerals (chalcopyrite's etc.) from the underlying geology to release Cu as a primary mineral and Ni, Zn and Co as secondary minerals in the groundwater. The good connection between Ni and Cl suggests rock -water interaction. That is Ni released as a secondary mineral from the oxidation of sulphide minerals from the underlying geology probably interacts with Cl^- in rainwater from the unsaturated zone to the saturated zone.

The rocks of the Apollonian and the Birimian formation of the study area are rich in pyrites, hence drainage of sulfuric acid may significantly contribute to the acidity (Hunslow, 1995) of the aquifer thereby leading to the strong correlation between Ni and pH. Also, the good correlation between Ni and (Na^+, K^+) indicates rock weathering. The good relationship between Ni and pH specifies sulphide mineral oxidation to release Ni as a secondary mineral in the groundwater. The good connection between Ni and HCO_3^- suggests same geochemical sources in the groundwater.

For the boreholes drilled from 2014 to 2015, As correlated strongly with K^+, Cu and Co. For the borehole sampled in 2016, As correlated strongly with Mg^{2+} and for the hand dug wells sampled in 2017, As correlated strongly with (Ca^{2+}, Mg^{2+}, TH, pH, Fe, Cr, and Pb). The good relationship between As and (Fe, Pb, Cu, and Co) suggest sulphide mineral oxidation or mobilization to release Pb and Cu as secondary minerals and As, Fe and Cu as primary minerals in the groundwater. In addition, the good relationship existing between As and (Ca^{2+}, Mg^{2+}, and K^+) suggest a possible geogenic sources and the good connection between As and pH indicates sulphide mineral oxidation to release As as a primary mineral in the groundwater. The good relationship between As and TH reveals arsenic hardness in the groundwater. As correlated strongly with Cr, and this suggest a possible rock-water interaction.

4.2.4 Calculation of Water Quality Index (WQI)

WQI is a significant parameter aimed at categorizing groundwater suitability for drinking (Magesh et al., 2012) purposes. It also provides the composite influence of individual water quality parameters on the overall water quality (Mitrs and ASABE Member, 1998). To calculate the water quality index for the Lower Tano River Basin, each chemical and trace element parameters are assigned a weight. The weights in each parameter are grounded on its respective WHO (2011) standards. The assigned weight illustrates the importance of the parameters and its impact on the water quality index. A usual water quality index procedure follows three steps which involve Parameter selection, assessment of quality function for each

selected parameter and accumulation through mathematical equation (Tyagi s et al., 2013). WQI offers a sole number that signifies the overall water quality at a certain site and time based on some water quality parameters. WQI allows comparison between different sampling locations. It also simplifies a complex dataset into easily reasonable and practical information. Additionally, water quality classification system used in the water quality index denotes the suitability of water for drinking. Table 4.43 and 4.44 shows the assigned weight and its relative weights for the cations, anions, and trace element parameters, respectively for this study.

Table 4. 43: Relative weight of hydrochemical parameters.

Chemical Parameters	WHO standards (2011)	Weight (wi)	Relative weight (Wi, 2013)	Relative weight (Wi, 2014 - 2015)	Relative weight (Wi, 2016 and 2017)
pH (on scale)	6.5 - 8.5	4	0.25	0.18	0.17
EC (µS/cm)	500	4	0.25	0.18	0.17
TDS (mg/L)	500	4	0.25	0.18	0.17
Ca^{2+} (mg/L)	75	2	0.13	0.09	0.09
Mg^{2+}(mg/L)	50	2	0.06	0.05	0.04
TH (mg/L)	500	2	0.13	0.09	0.09
$HCO3^-$(mg/L)	500	3		0.14	0.13
$SO4^{2-}$(mg/L)	250	4	0.25	0.18	0.17
NO_3^- (m/L)	50	5	0.31		0.22
Cl^-(mg/L)	250	3	0.19	0.14	0.13
Na^+ (mg/L)	200	2		0.09	0.09
K^+ (mg/L)	12	2		0.09	0.09

Table 4. 44: Relative weight of trace element parameters

Trace elements	WHO (2011) Standards	Weight (wi)	Relative weight (Wi, 2013)	Relative weight (Wi, 2014 - 2015)	Relative weight (Wi, 2016 and 2017)
Cr	0.05	5	0.31	0.23	0.22
Mn	0.4	4	0.25	0.18	0.17
Fe	0.3	4	0.25	0.18	0.17
Co	0.05	1		0.05	0.04
Ni	0.006	1		0.05	0.04
Cu	0.05	2	0.13	0.09	0.09
Zn	5	1	0.06	0.05	0.04
As	0.01	5	0.31	0.23	0.22
Cd	0.003	5		0.23	0.22
Pb	0.01	5	0.31	0.23	0.22
Al	0.2	2		0.09	0.09
		∑ wi= 72	∑Wi = 3.44	∑Wi = 3.02	∑Wi = 3.08

The relative weight is computed from the equation:

$$Wi = \frac{wi}{\sum_{i=1}^{n} wi} \qquad \text{Eq 4.8}$$

The relative weight = Wi

The weight of each parameter = w_i

The number of parameters = n

The quality ranking scale for each parameter is calculated by dividing its content in each groundwater sample by its respective WHO (2011) drinking water standard. After, the result is multiplied by 100. The above is given by the equation:

$$qi = \left(\frac{ci}{si}\right) \times 100 \qquad \text{Eq 4.9}$$

Where qi is the quality rating

Ci is the concentration of each parameter in each groundwater sample in mg/L.

Si is the WHO standard for each chemical parameter in mg/L according to the WHO (2011) guidelines. In calculating the final stage of WQI, the Si is determined for each parameter. The sum of Si values gives the WQI for each groundwater sample.

$$Sli = Wi \times qi \qquad \text{Eq 4.10}$$

$$WQI = \sum Sli \qquad \text{Eq 4.11}$$

Where Sli is the sub –index of the ith parameter.

Qi is the rating based on the concentration of the ith parameter.

n is the number of parameters.

The statistical summary of WQI results for groundwater sampled from 2013 to 2017 is presented in appendix 27 to 29. A spatial distribution map showing WQI values with the water quality classification for the various groundwater in the sampled years (2013 to 2017) is presented in Figure 4.28 a, b, c. The ground water quality classification with respect to WQI is tabulated below.

Table 4. 45: Water quality classification and water types based on WQI

Range	Type of water
<50	Excellent water
50-100	Good water
100-200	Poor water
200-300	Very poor water

In this study, 212 samples were analyzed for WQI. Among these samples, groundwater sampled from 2013 to 2015 had 20.83% of the samples(n=48) showing excellent water, 47.92% falling under good water, 12.5% were poor in quality and the remaining 8.33% and 10.42% fall under very poor and unsuitable water, respectively. Comparing Figure 4.2 to Figure 4.28 a, it is seen that the Apollonian formation aquifer which yielded more water are excellent to unsuitable for drinking (31.39 to 389.45), while the aquifer of the Birimian supergroup which yielded less water are excellent to good for drinking (31.39 – 389.45).

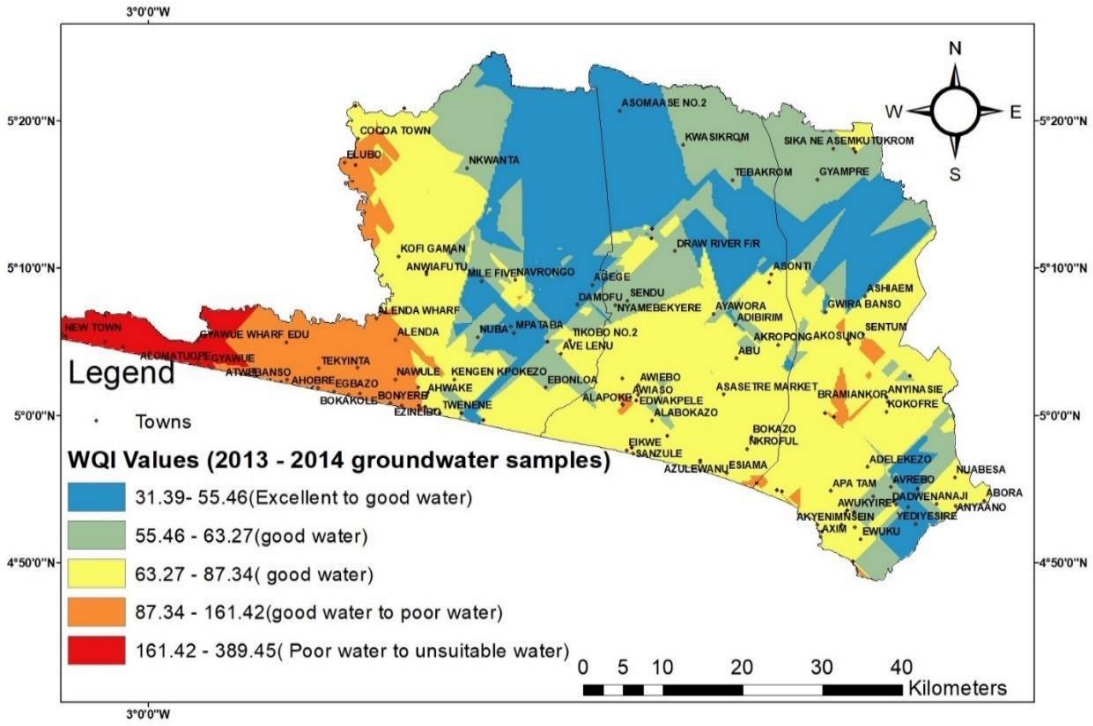

Figure 4. 28a Spatial distribution map of water quality index WQI) for groundwater sampled from 2013 to 2015.

The groundwater sampled in 2016 had 8% of the samples (n=80) falling under excellent for drinking, 13.6% shows good water, 8.8% falls under poor water and the remaining 6.4% and 41.25% of the groundwater were very poor and unsuitable for drinking, respectively. The

spatial distribution map for WQI in groundwater sampled in 2016 (Fig 4.28 b) shows that the aquifer of the Apollonian formation and the Birimian supergroup both yielded excellent to unsuitable water for drinking.

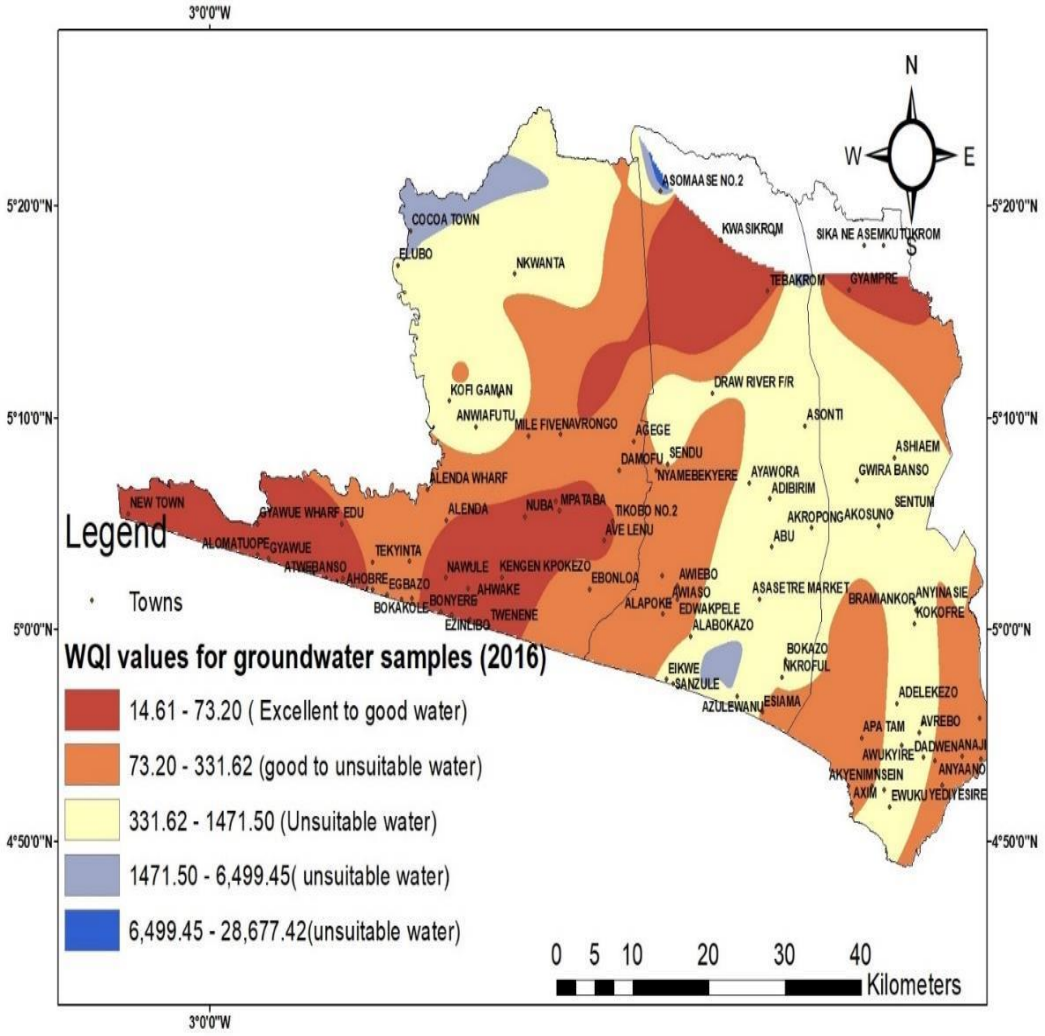

Figure 4.28b: Spatial distribution map of water quality index (WQI) for groundwater sampled in 2016.

In 2017, 50% of the sampled groundwater falls under excellent water quality, 8.33% are good water, 16.7% are poor water, and the remaining 2.38% and 13.10% are very poor and unsuitable for drinking respectively. A spatial distribution map of WQI for 2017 groundwater samples is shown in Figure 4.28 c. Figure 4.28 c indicates that the aquifer of the Apollonian formation mostly yielded excellent water (represented by shades of blue colour) for drinking.

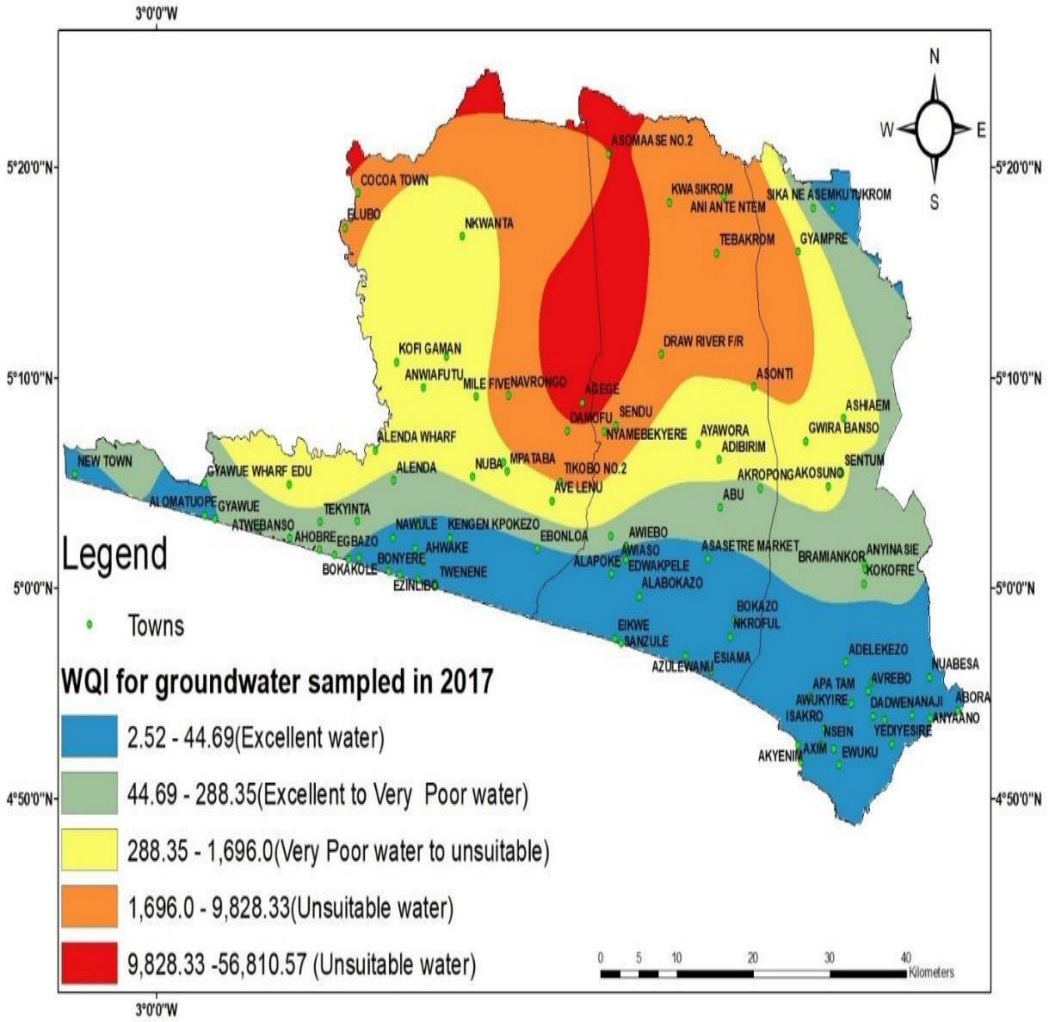

Figure 4.28c: Spatial distribution map of water quality index (WQI) for groundwater sampled in 2017.

Comparing the quality of the newly boreholes (Fig 4.28 a) drilled in the aquifer of the Apollonian formation and the Birimian supergroup to that of the existing groundwater (Fig 4.28 b and 4.28 c) sampled from both aquifers in 2016 and 2017, it is seen that the existing groundwater is off better quality than the newly developed groundwater. This reveals that the topographic position of the sampling points, the mineral composition, the depth, the seasons in which the samples were taken, the lithology and human activities possibly affected the quality of groundwater in the study area.

4.2.5 Groundwater quality for irrigation

Groundwater quality for irrigation depends on the quality of water, soil type, plus salt tolerance characteristics of the plants etc. On similar terms, the suitability of groundwater for

irrigation is characterized based on the chemistry, which varies both temporally and spatially. The temporal variability in a particular area is often assigned to anthropogenic reasons (Adhikary et al., 2012) whiles spatial variations is due to its natural hydrogeological setting. In this section, the quality of groundwater for irrigation in the Lower Tano River Basin using chemical indices is assessed. A statistical summary of the calculated chemical indices is tabulated and shown in appendix 27, 28 and 29.

4.2.5.1 Sodium Hazard – Sodium Adsorption ratio

The determination of Alkali hazard and sodium in groundwater (hand dug wells and boreholes) is determined by the relative absolute cation concentrations. This is expressed in terms of SAR (Shahid and Mahmoudi, 2014), i.e.

$$SAR = \frac{Na^{+}}{\sqrt{\frac{Ca^{2+} + Mg^{2+}}{2}}} \quad \text{..... Eq 4.12}$$

Where the concentrations of Ca^{2+}, Mg^{2+} and Na^{+} is expressed as meq/L.

In addition, there is a substantial relationship between the extent to which sodium is adsorbed by the soils and SAR values of irrigation water (Singh et. al., 2008). If irrigation water is low in calcium and high in sodium, cation-exchange reaction might become saturated with sodium. This can destroy the structure of the soil due to scattering of clay particles. In this study, the results obtained from the calculation of SAR are interpolated using inverse distance weighting (IDW) interpolation model in ArcGIS 10.5 software and the SAR classification for irrigation is shown in Table 4.46 and 4.47.

Table 4. 46: Sodium Hazard (SAR) and Salinity Hazard for irrigation water (adapted from USSL 1954)

Sodium Hazard	Salinity Hazard	Range	Scale/Class	Water Class
S1	C1	<10	Low	Excellent
S2	C2	10-18	Medium	Good
S3	C3	18 - 26	High	Doubtful
S4	C4	>26	Very High	Unsuitable

Table 4. 47: Suitability of groundwater (hand dug well) for irrigation based on Sodium Hazard (USSL, 1954).

Sodium Hazard/SAR	Range	Class	2016 (n=36)	2017 (n=30)
S1	<10	Excellent	34	30
S2	10 - 18	Good	2	
S3	18 -26	Doubtful		
S4	>26	Unsuitable		

SAR values in the hand dug wells sampled in 2016 and 2017 range from 0.51 to 15.12 and 0.65 to 5.12, respectively. The SAR values in the hand dug wells is classified into various classes. From Table 4.46 and 4.47, majority of the hand dug wells sampled in both 2016 and 2017 fell under excellent category for irrigation and 2 hand dug wells sampled in 2016 fell under good water for irrigation.

Table 4.48: Suitability of groundwater (boreholes) for irrigation based on Sodium Hazard (USSL, 1954).

Sodium Hazard/SAR	Range	Class	2014-2015(n=18)	2016 (n=44)	2017 (n=
S1	<10	Excellent	18	44	50
S2	10 - 18	Good			
S3	18 -26	Doubtful			
S4	>26	Unsuitable			

The calculated SAR values for the boreholes drilled from 2014 to 2015 range from 0.11 to 5.14, that for the boreholes sampled in 2016 and 2017 range from 0.28 to 6.01 and 0.29 to 5.02, respectively. Based on the calculated SAR values (Fig 4.28), it can be said that the groundwater in the aquifer of the Apollonian formation and the Birimian supergroup yields excellent water for irrigation.

The USSL diagram (Fig 4.29) indicates that majority of the groundwater samples are within C1-S1 category representing very low salinity medium sodium water, which can be used, for irrigation. But one borehole in the aquifer of the Birimian supergroup falls within C3-S3 category. This shows that the borehole cannot be used for irrigation (Kumar et al., 2007). Figure 4.30 shows the spatial distribution map of SAR in groundwater in the aquifer of the Birimian super group and the Apollonian formation and from the map, it is seen that the groundwater in both aquifers is excellent for irrigation.

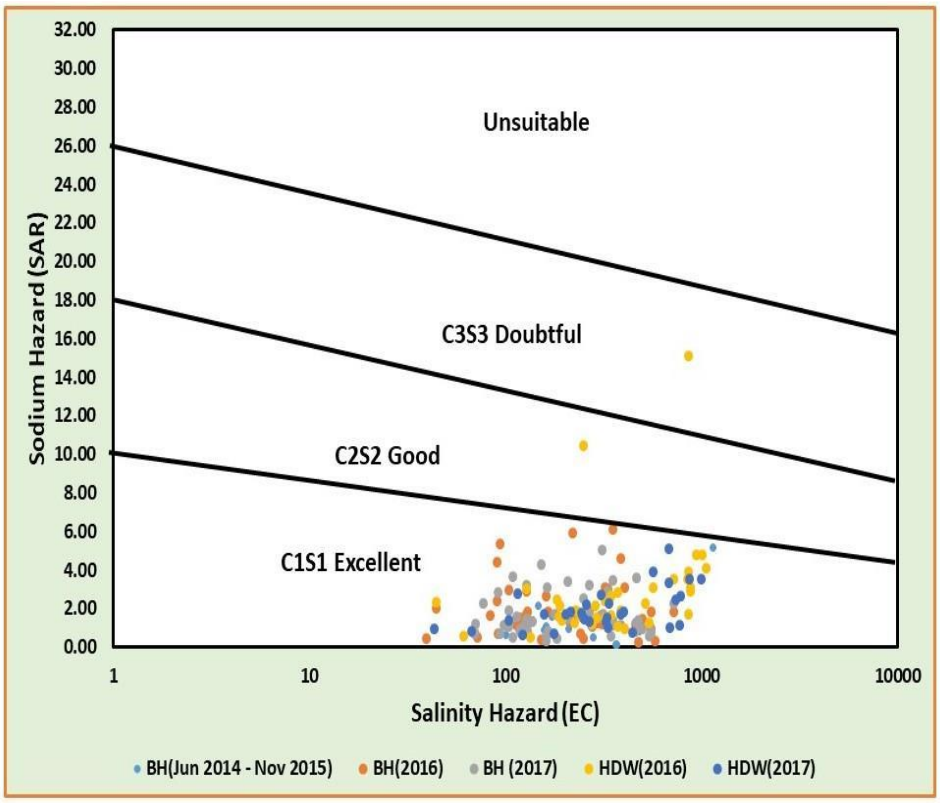

Figure 4. 29: The quality of water for irrigation in relation to Salinity Hazard and Sodium Hazard based on USSL (1954).

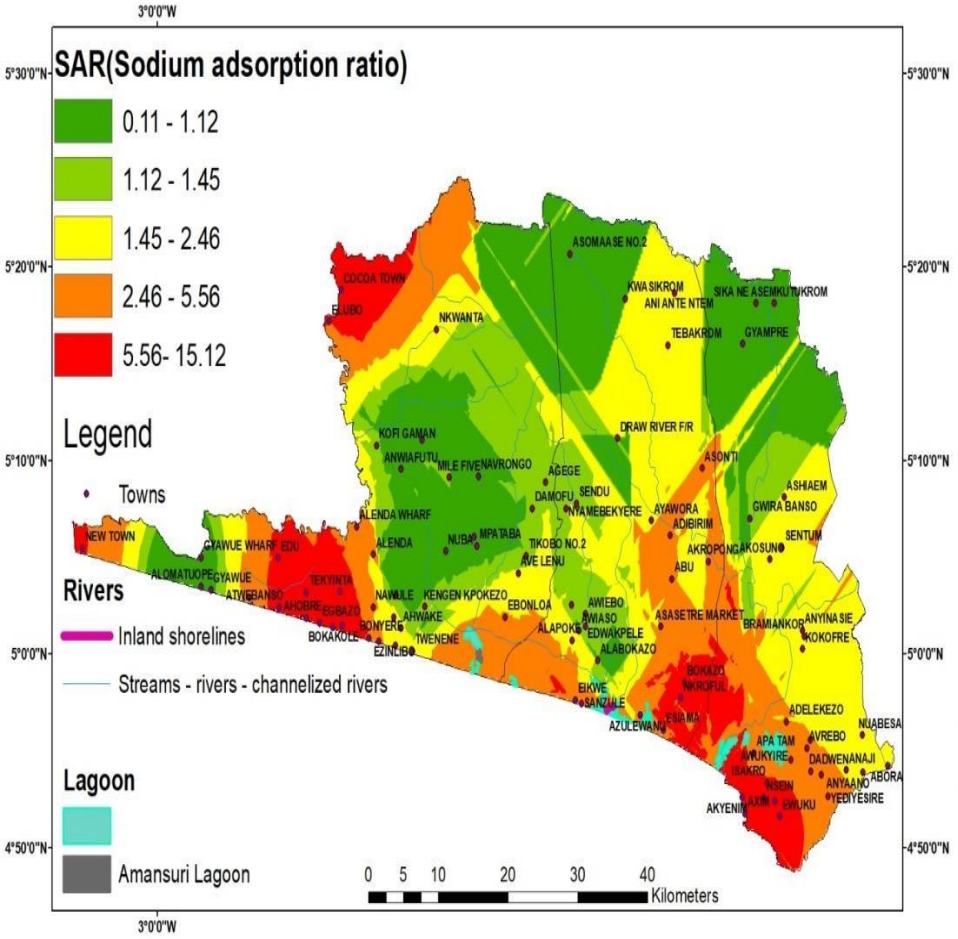

Figure 4. 30: Spatial distribution map of groundwater suitability for irrigation based on SAR.

4.2.5.2 Sodium Percentage (Na %)

The Na% (Wilcox, 1995; Richards, 1954) is estimated using the formula:

$$Na\% = \frac{Na^{+} + K^{+}}{Ca^{2+} + Mg^{2+} + Na^{+} + K^{+}} \ldots\ldots\ldots\ldots\ldots \text{Eq 4.13}$$

All concentrations are in meq/L.

Na% is calculated for the groundwater in the study catchment (Table 4.46) and the obtained result is interpolated using IDW (Fig 4.31). Table 4.46 shows the classification of groundwater suitability for irrigation based on Na%.

Table 4. 49: Sodium percent classification of groundwater within the lower Tano River Basin (After Wilcox, 1955).

Na%	Water class	HDW (2016) n=36	HDW (2017) n=30	BH (2014-2015) n= 18	BH (2016) n=44	BH (2017) n=53
<20	Excellent			2	2	3
20 - 40	Good	3	5	5	7	9
40 - 60	permissible	11	13	9	17	20
60 - 80	doubtful	16	11	2	13	18
>80	unsuitable	6	1	0	5	3

The calculated Na% in the hand dug wells sampled in 2016 ranges from 29.82% to 96.38% and that of 2017 varies from 29.27% to 80.82%. For the boreholes sampled from 2014 to 2015, the Na% varies from 4.47% to 71.57% and in 2016 and 2017 groundwater samples, the Na% varies from 15.26% to 90.63% and 16.21% to 89.15%, respectively.

The spatial distribution map of Na% (Fig 4.31) shows that groundwater located in some parts of the coastal aquifer (Apollonian formation), some parts of NE and southern aquifer (Birimian supergroup) represented by shades of red gave out doubtful to unsuitable water for irrigation.

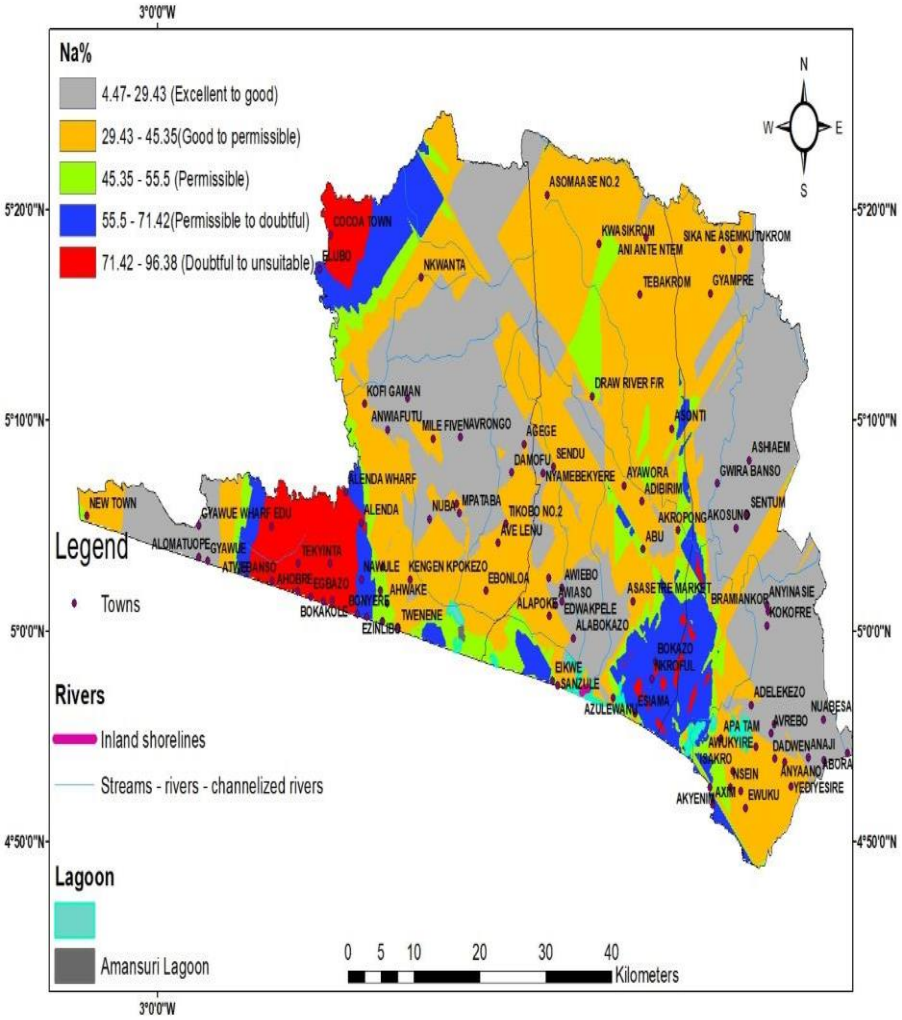

Figure 4. 31: Spatial distribution map of groundwater suitability for irrigation based on Na%.

Wilcox (1955) used EC and Na% to estimate the quality of groundwater for irrigation purposes. The computed results from the Wilcox diagram (Fig 4.32) shows that majority of the sampled groundwater falls under very good to good water for irrigation. Also from the diagram, fewer groundwater samples fall within good to permissible water for irrigation while few groundwater samples fall under permissible to doubtful water for irrigation, and one sample fall under doubtful to unsuitable water for irrigation. The samples that fall under permissible to doubtful water for irrigation indicate the presence of excess sodium in the groundwater. This possibly restricts the movement of water and circulation of air through the soils (Collins & Jenkins, 1996; Saleh et al., 1999).

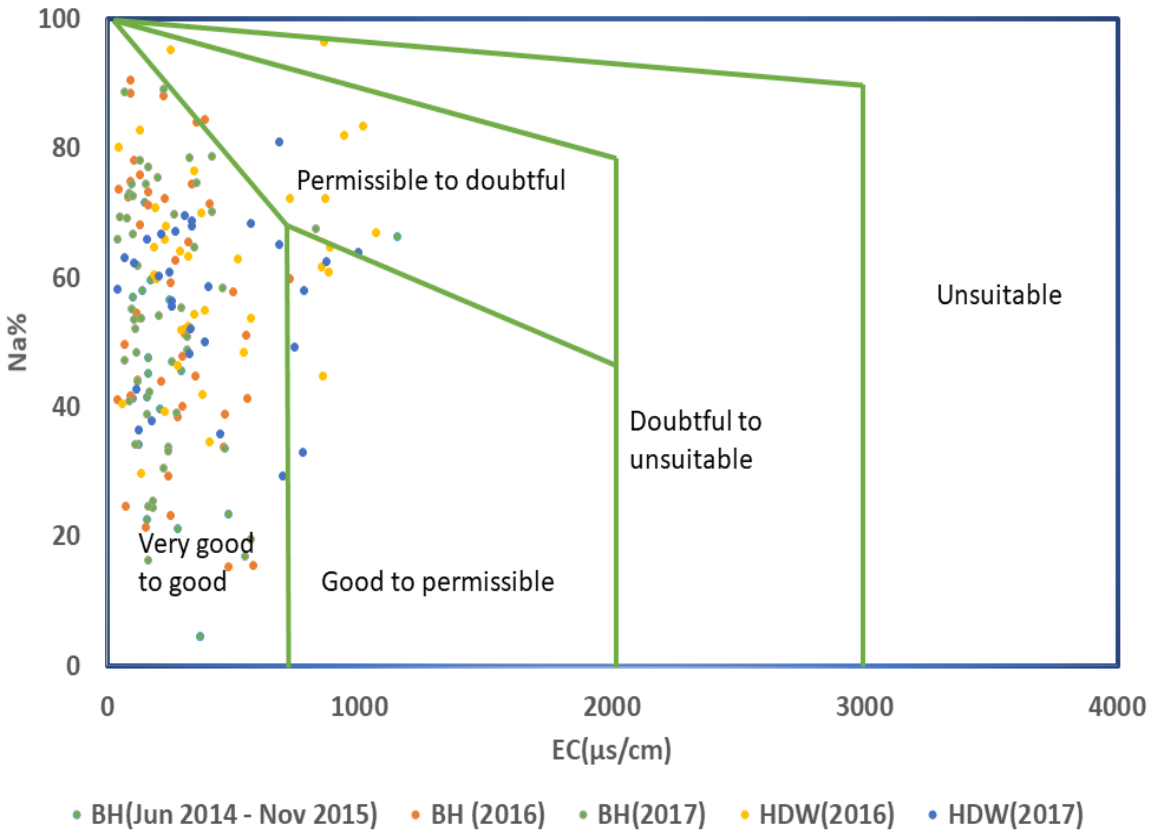

Figure 4. 32: Wilcox diagram for classifying the suitability of groundwater for irrigation.

4.2.5.3. Residual sodium carbonate (RSC)

The amount of carbonate and bicarbonate in excess of alkaline earths (Ca+ Mg) affects the suitability of groundwater for irrigation. When the sum of bicarbonate and carbonate is in excess of calcium and magnesium, there may be a likelihood of complete precipitation of Mg^{2+} and Ca^{2+} (Raghunath, 1987). To compute the effects of bicarbonate and carbonate, (Eaton, 1950) residual sodium carbonate (RSC) the equation below is used

$$(HCO_3^- + CO_3^{2-}) - (Mg^{2+} + Ca^{2+}) \quad \text{..... Eq 4.14}$$

In accordance with Eaton (1950), an elevated RSC value (>5 meq/L) in water leads to an increase in the adsorption of sodium in the soil. This can be harmful to the soil when the water is used for irrigation. This is due to the increase in soil sodium adsorption, which finally leads to soil blockage. In this study, calculation of the above RSC equation reveals that RSC in the boreholes drilled from 2014 to 2015 ranges from -0.90 to -0.05 meq/L. In 2016, the RSC content in the sampled hand dug wells and boreholes varies from -3.51 to 1.33 meq/L and -1.93 to 1.30 meq/L, respectively. In 2017, the RSC in the sampled hand dug wells and the

boreholes range from 2.57 to 1.92 meq/L and 1.88 meq/L to 1.05 meq/L, respectively. The RSC concentration for the groundwater in the study area is classified and presented in Table 4.50. In this study, all the groundwater sampled from 2014 to 2017 in both the aquifer of the Apollonian formation and the Birimian supergroup is suitable and safe for irrigation.

Table 4.50: Groundwater suitability for irrigation based on RSC (After Eaton, 1950)

RSC	Water Class	HDW (2016) (n=36	HDW (2017) (n=30)	BH (2014 to 2015) (n=18)	BH (2016) (n=44	BH (2017) (n = 54)
<2.5	Suitable	36	30	18	44	54
2.5 - 5	Unsuitable					
>5	Harmful					

4.2.5.4. Magnesium Hazard (MH)

Darab and Szaboles (1964) proposed magnesium hazard (MH) concentration for groundwater suitability for irrigation. Calculation of MH in groundwater is given by the equation:

$$MH = \left(\frac{Mg^{2+}}{Ca^{2+} + Mg^{2+}}\right) \times 100 \ldots\ldots\ldots\ldots \text{Eq 4.15}$$

Where all equations are expressed I meq/L.

Table 4. 51: Suitability of groundwater for irrigation based on MH%

MH %	Water Classification	BH (2013) (n=30)	BH (2014-2015) (n=18)	HDW (2016) (n= 36)	BH (2016) (n= 44)	HDW (2017) (n= 30)	BH (2017) (n= 54)
<50	Suitable	30	18	32	32	25	12
>50	Unsuitable			4	12	5	38

Computation of the above equation reveals that the MH for the boreholes drilled in 2013 and from 2014 to 2015 range from 18.46% to 47.45%, and 5.77% to 49.51%, respectively. In 2016, the MH for the hand dug wells and the boreholes vary from 2.48% to 72.41% and 4.37% to 90.03%, respectively. For the hand dug wells and the boreholes sampled in 2017, the MH content range from 2.95% to 81.44% and 2.75% to 92.15%, respectively.

Table 4.51 gives the classification of groundwater suitability for irrigation based on MH in the groundwater of the study area. From the Table, it is seen that majority of the groundwater in all the above- mention years are suitable for irrigation and few are unsuitable.

Generally, the spatial distribution map of MH for the groundwater (Fig 4.33) reveals that groundwater mostly in parts of the aquifer of the Apollonian formation with few in the aquifer of the Birimian supergroup represented by shades of red colour are unbefitting for irrigation. Likewise, the most suitable groundwater (hand dug wells and boreholes) quality for irrigation represented by shades of green concentrates in the aquifer of the Birimian supergroup with fewer representations in the aquifer of the Apollonian formation of the study area.

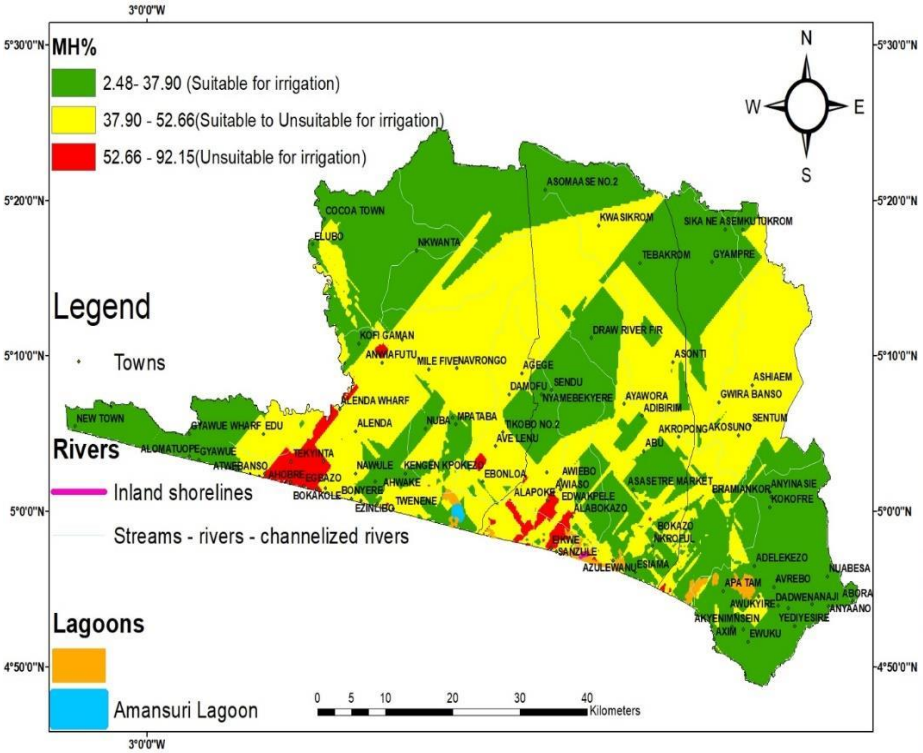

Figure 4. 33: Spatial distribution map of groundwater suitability for irrigation in the study area based on MH%.

4.2.5.5 Permeability Index (PI)

Sodium, bicarbonate, calcium, and magnesium are factors that affect the permeability of soils when there is a long-term irrigational practice. Doneen (1962), classified the suitability of water for irrigation based on the equation:

$$PI = \left(\frac{Na^{+} + \sqrt{HCO3^{-}}}{Ca^{2+} + Mg^{2+} + Na^{+}}\right) \times 100 \qquad \text{Eq 4.16}$$

All ions are expressed in meq/L.

Table 4. 52: Groundwater suitability for irrigation based on the Permeability Index (PI)

PI Class	PI%	Water Class	BH (2014 – 2015) (n=18)	HDW, 2016 (n= 36)	BH, 2016 (n=44)	HDW,2017,(n=30)	BH,2017 (n=54
Class I	≥ 75	Suitable	13	27	30	24	44
Class II	25-75	Suitable	5	9	14	6	10
Class III	< 25	Unsuitable					

Assessment of the above equation indicates that the PI value for the boreholes drilled from 2014 to 2015, ranges from 49.26% to 105.53%. That of the hand dug wells and boreholes sampled in 2016 ranges from 47.55% to 137.56%, and 39.92% to 157.92%, respectively. In addition, the PI for the hand dug wells and the boreholes sampled in 2017 varies from 49.98% to 194.85%, and 47.68% to 223.74%, respectively. From table 4.52 and Fig 4.34, it is observed that the groundwater in the aquifer of the Apollonian formation and the Birimian supergroup of the Lower Tano River Basin is suitable for irrigation based on Doneen permeability index (PI).

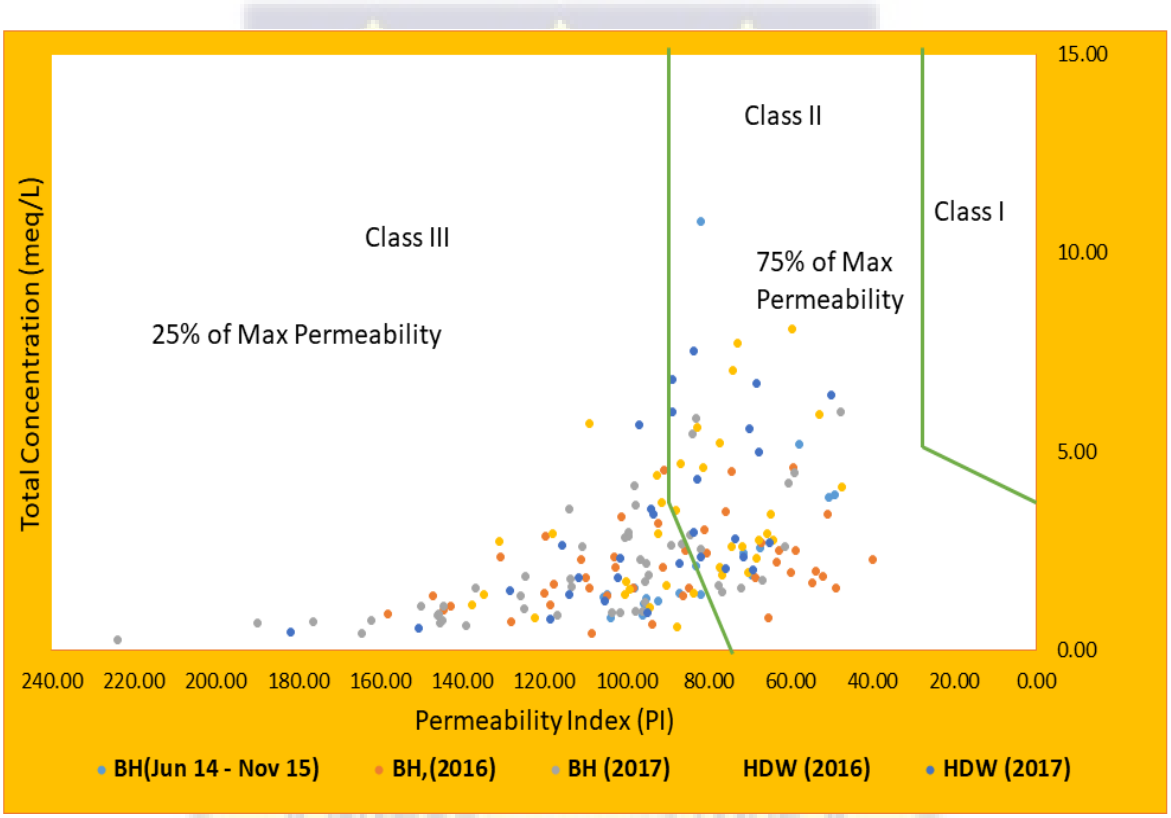

Figure 4. 34: Groundwater suitability for irrigation based on Doneen permeability Index (PI) (Doneen 1964) (HDW =hand dug wells, BH =Boreholes)

4.2.5.6 Chlorinity Index

In this study, the concentration of chloride and its suitability for agriculture is described. The description or classification is done based on Ramesh et al. (2012) classification. The authors pointed out that "irrigation water, which is saline, is poisonous to plants". Figure 4.35 reveals that the chlorinity index for groundwater sampled from 2013 to 2017 in the aquifer of the Birimian supergroup and the Apollonian formation is suitable for all crops.

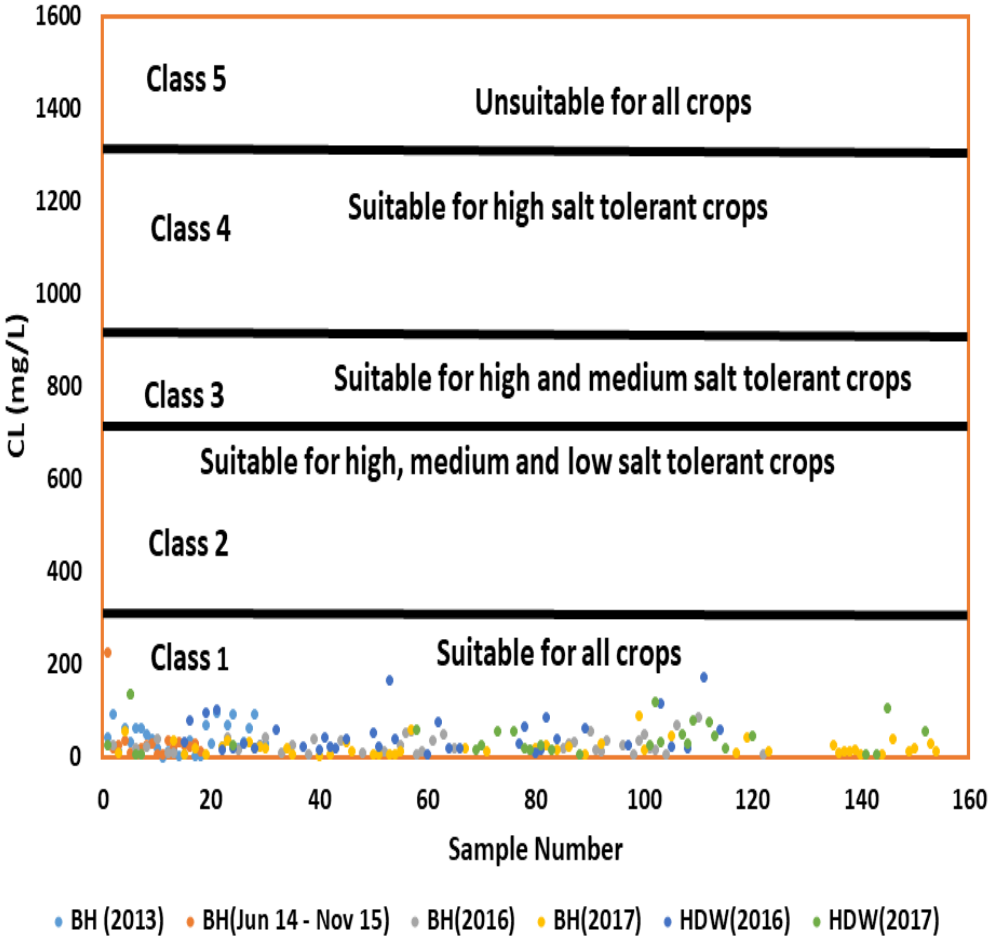

Figure 4. 35: Groundwater suitability for crop production in the study area based on Chlorinity index (Ramesh et al. (2012)) (HDW = hand dug wells, BH = Boreholes)

In general, assessment of the above-described chemical indices for groundwater suitability for irrigation reveals that most groundwater in the aquifer of the Birimian super group and the Apollonian formation in the Lower Tano River Basin is suitable for irrigation and a few are unsuitable. The obtained results are like works carried out by Edjah et al. (2015). The variation in WQI results is linked to the lithology of the study area and human activities The

statistical summary results for the above-mentioned chemical indices are shown in Appendix 27,28, and 29.

4.2.6. Sub -Conclusion

From the results of the second specific objective, it is observed that the surface water and groundwater sampled from the rocks of the Apollonian and the Birimian supergroup are acidic to neutral. Also, most of the surface water had low TDS/EC concentrations whiles the groundwater had short residence time due to low TDS concentration with low salt enrichment due to the EC values being less than 1500 µS/cm. The weathering of minerals from the rocks of the Apollonian formation and the Birimian supergroup are the main processes controlling the surface water and groundwater chemistry of the study area. Greater percentage of groundwater per the calculated WQI results were chemically suitable for drinking. Salinity was not a major concern when considering groundwater for irrigation in the Lower Tano River Basin.

4.3 Determination of the Hydrogeochemical Processes that produces the Chemical Characteristics or Compositions of the Aquifers.

Under this section, the results of the third specific objective are discussed. The outcome of the results will provide a detailed hydrogeochemical description of the Birimian super group aquifer and the Apollonian formation aquifer within the Lower Tano River Basin. The results of the groundwater sampled in 2013 were not included due to lack of adequate field and hydrochemical data.

Results of groundwater sampled from 2014 to 2017 is analyzed using models such as Durov (1948) diagram, Ficklin diagram (Ficklin et al., 1992), Piper (1944) diagram, (Gibbs, 1970) diagram, compositional diagrams, and hydrogeochemical modelling. The above-mentioned models are done with the aid of software's like AquaChem 2015, Grapher and Microsoft excel 2016. The analyzed results are combined with the lithological formation of the aquifer to

provide an insight into the evolution and chemical compositions of groundwater. Hydrogeochemical molar ratio is employed to help direct the evolution of groundwater and ion exchange processes (Aastri, 1994). For this, Chloro – Alkaline indices and different molar ratios as indicated by Schoeller (Schoeller, 1977) is employed. The analysis of the results is backed by hydrogeochemical modelling, where calculation of Saturation Index (SI) of the minerals in the rocks of the Apollonian and the Birimian supergroup of the study area are calculated using PHREEQC hydrogeochemical modelling software (Parkhurst et al., 2013).

4.3.1 Geochemical processes controlling the chemistry of groundwater

4.3.1.1. Ficklin diagram

The Ficklin plot (Ficklin et al., 1992) is a scatter diagram in which the pH is plotted against the sum of the trace metals. This is a very effective and easy way of classifying water samples based on the differences in the sum of the base metal concentrations (Manjo et al., 2012). Differences in the sum of trace element concentrations of different groundwater samples help in differentiating various geological controls and this is usually based on their resultant chemistry. From the study, the Ficklin plot (Fig 4.36) exhibits two water types. Out of these water types, 70% of the groundwater are near – neutral low-metal water, due to their pH values which lies within six to nine. This suggests that the pH of most groundwater is not influence by the geochemistry of the aquifers. Further to the diagram (Fig 3.6), the remaining 30% of the groundwater lie in the acid –low- metal water. This type of water gives an indication that minority of the groundwater samples from both aquifers have low pH and this influenced the aquifer geochemistry. The Ficklin diagram has explained why positive and negative strong correlation exist between the pH and fewer trace element in the groundwater as previously discussed.

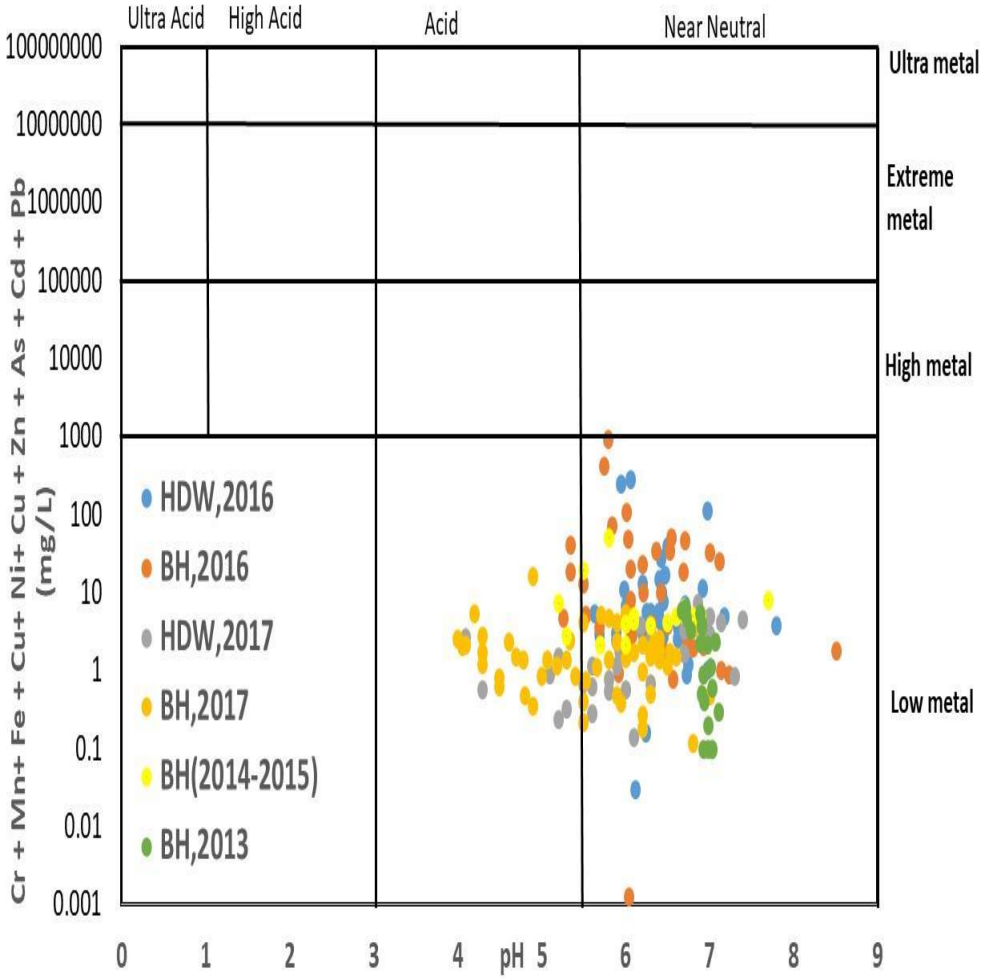

Figure 4. 36: Ficklin diagram (Ficklin et al., 1992) showing variations in trace element concentrations as a function of pH for the groundwater in the study area.

4.3.1.2. Durov diagram

(Durov, 1948) is a composite plot consisting of two ternary diagrams where the anions of interest are plotted against the cations of interest. The main purpose of the Durov diagram is to cluster the hydrochemical and physicochemical data points in order to identify groundwater samples with similar chemical compositions as well as reveal useful properties and relationships for the groundwater samples. This method is used to evaluate the various water types and present the absolute or total concentrations of cation or anions, pH, and TDS. In this study, the Durov diagram for the sampled groundwater within the study area is presented in Figure 4.37 a to 4.37 e.

The Durov diagram (Durov 1948) for the boreholes drilled from 2014 to 2015 (Fig 4.37 a) reveals six geochemical processes. From the six geochemical processes (Fig 4.37 a), three boreholes (n=18) drilled in the aquifer of the Apollonian formation laid in field two, that is water rich in Ca – HCO_3^- or Mg -HCO_3^- thus representing recharge water or water from a limestone aquifer (Belkhiri et al., 2012) and this will be explained further using Gibbs diagram in subsequent chapters and stable isotopes in the 4th specific objective.

In addition, two boreholes drilled in the aquifer of the Birimian supergroup plots in field 3 that is water rich in Na-HCO_3^-. This represents water undergoing reverse ion exchange (Belkhiri et al., 2012). Additionally, one borehole (n=18) drilled in the aquifer of the Apollonian formation and two boreholes drilled in the aquifer of the Birimian supergroup laid in field 4, that is water rich in Ca- $SO4^{2-}$. This signifies water that is in contact with a contaminated source (Belkhiri et al., 2012) or sulphide minerals from the underlying geology. Five boreholes and three boreholes drilled in the aquifer of the Apollonian formation and the aquifer of the Birimian supergroup, respectively are plotting in field 5. This characterize water with no dominant cation or anion that is groundwater undergoing a possible simple dissolution or mixing (Belkhiri et al., 2012). Also, one borehole drilled in the aquifer of the Apollonian formation are seen in field six that is water rich in Na^+- SO_4^{2-} thus groundwater possibly receiving influences from anthropogenic sources (Belkhiri etal., 2012). Additionally, one borehole in the aquifer of the Apollonian formation is seen in field seven that is water rich in Na-Cl, suggesting ion exchange (Belkhiri et al., 2012) which will be explained further in subsequent chapters.

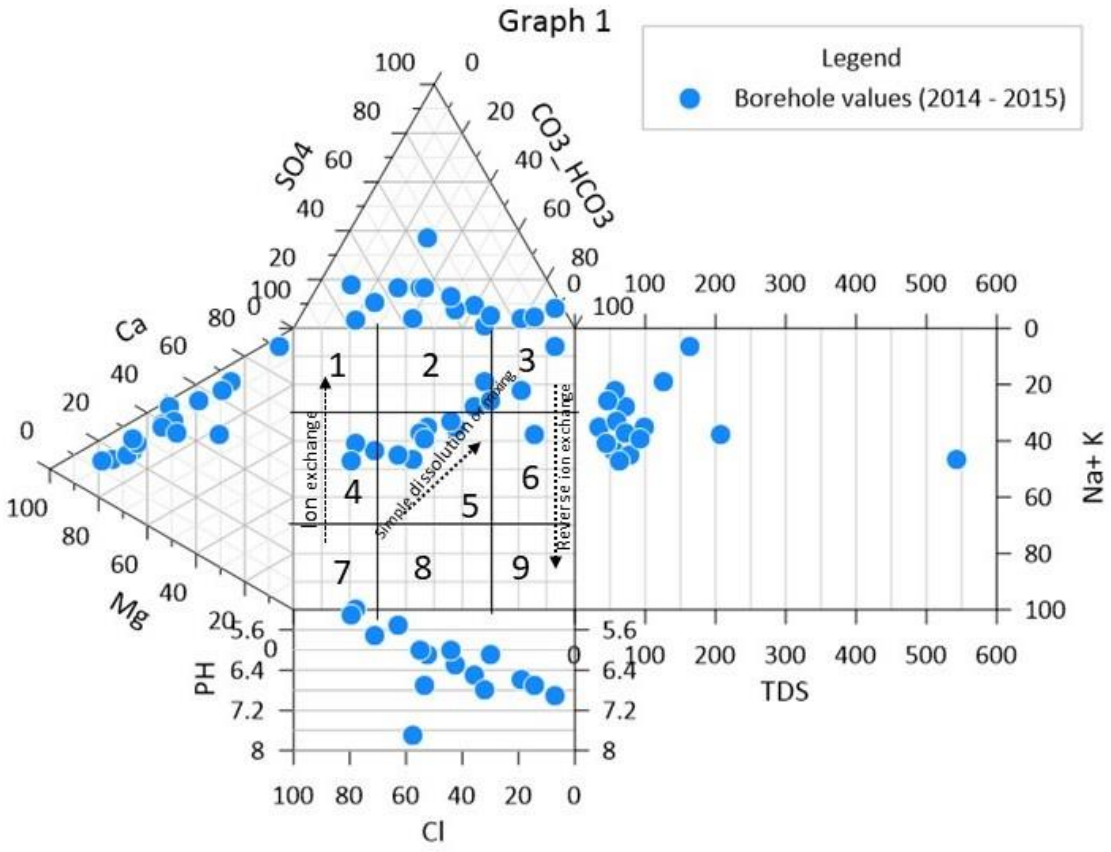

Figure 4. 37a: Durov diagram (1948) of boreholes drilled from 2014 to 2015 in the Lower Tano River Basin.

For the hand dug wells and boreholes sampled in 2016 (Fig 4.37 b and Fig 4.37 c), six geochemical processes are seen. Out of the six, four hand dug wells sampled from the aquifer of the Apollonian formation are plotting in field one, that is water rich in Ca^{2+} - HCO_3^- or Mg^{2+}-HCO_3^- representing recharging water. Also, fourteen hand dug wells (8 sampled from the aquifer of the Apollonian formation and 6 sampled from the aquifer of the Birimian supergroup) and three boreholes (two sampled from the aquifer of the Apollonian formation and one sampled from the aquifer of the Birimian supergroup) are seen in field two, that is water rich in Ca^{2+} - Mg^{2+} and HCO_3^- - CO_3^{2-}. This signifies recharging groundwater or groundwater from a limestone aquifer (Lloyd, 1965). One borehole sampled from the aquifer of the Birimian supergroup is seen in field three, that is water rich in Na^+ - HCO_3^-, representing water undergoing reverse ion exchange (Belkhiri et al., 2012). Additionally, four hand dug wells sampled from the aquifer of the Apollonian formation

and seven boreholes (five in the aquifer of the Apollonian formation and two in the aquifer of the Birimian supergroup) are plotting in field four that is water rich in Ca^{2+} -SO_4^{2-}. This discloses groundwater in contact with a contaminated source or sulphide minerals from the underlying geology. Thirteen hand dug wells (8 sampled from the Aquifer of the Apollonian formation and 5 taken from the aquifer of the Birimian supergroup) and thirty borehole samples (16 taken from the aquifer of the Apollonian formation and 14 sampled from the aquifer of the Birimian supergroup) are seen in field five that is water undergoing simple dissolution or mixing. Also, one hand dug well and three borehole samples all taken from the aquifer of the Birimian supergroup are plotting in field 6 that is water rich in Na^{+} - SO_4^{2-} indicating water affected by anthropogenic sources (Zaporozec, 1972; Lloyd & Heathcote, 1985).

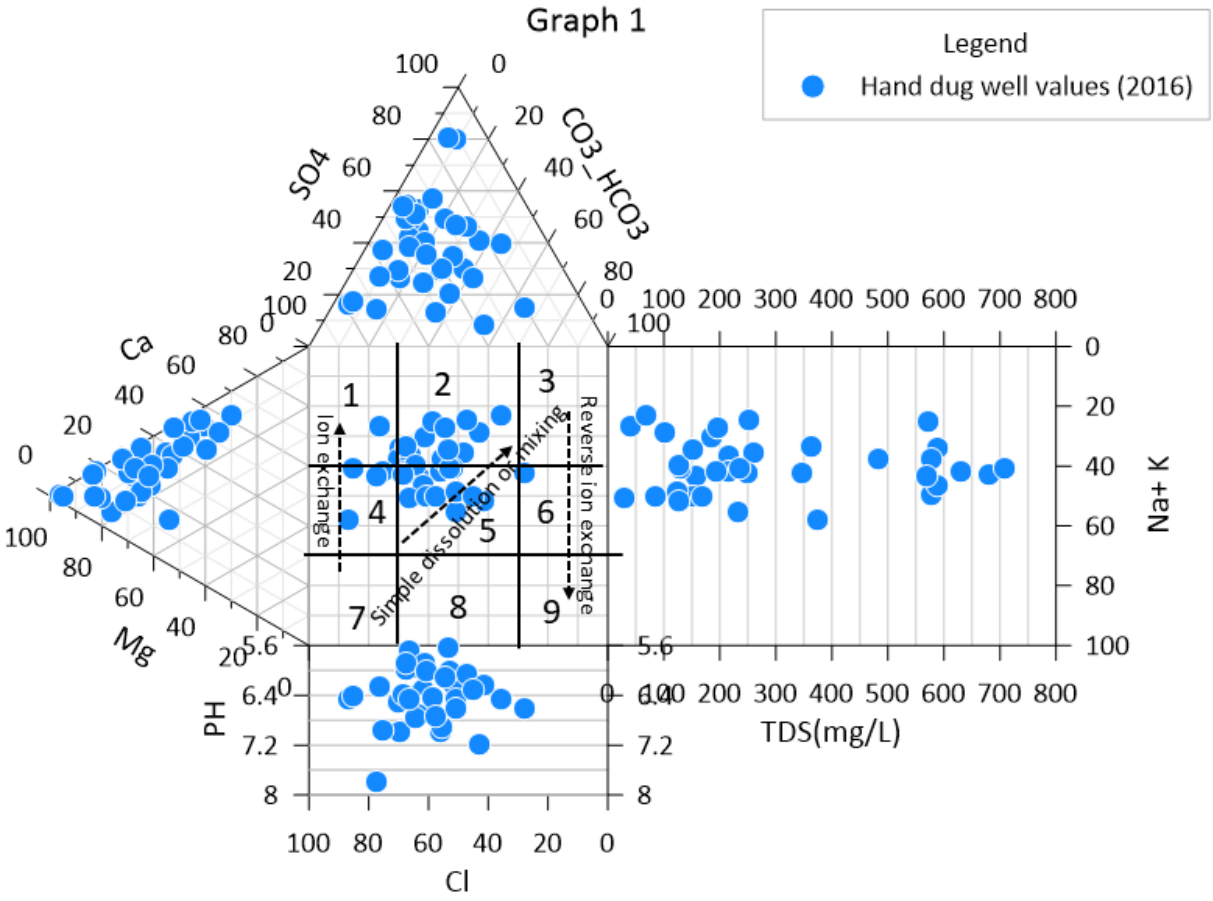

Figure 4.37b: Durov diagram (1948) of hand dug wells sampled in 2016 within the Lower Tano River Basin.

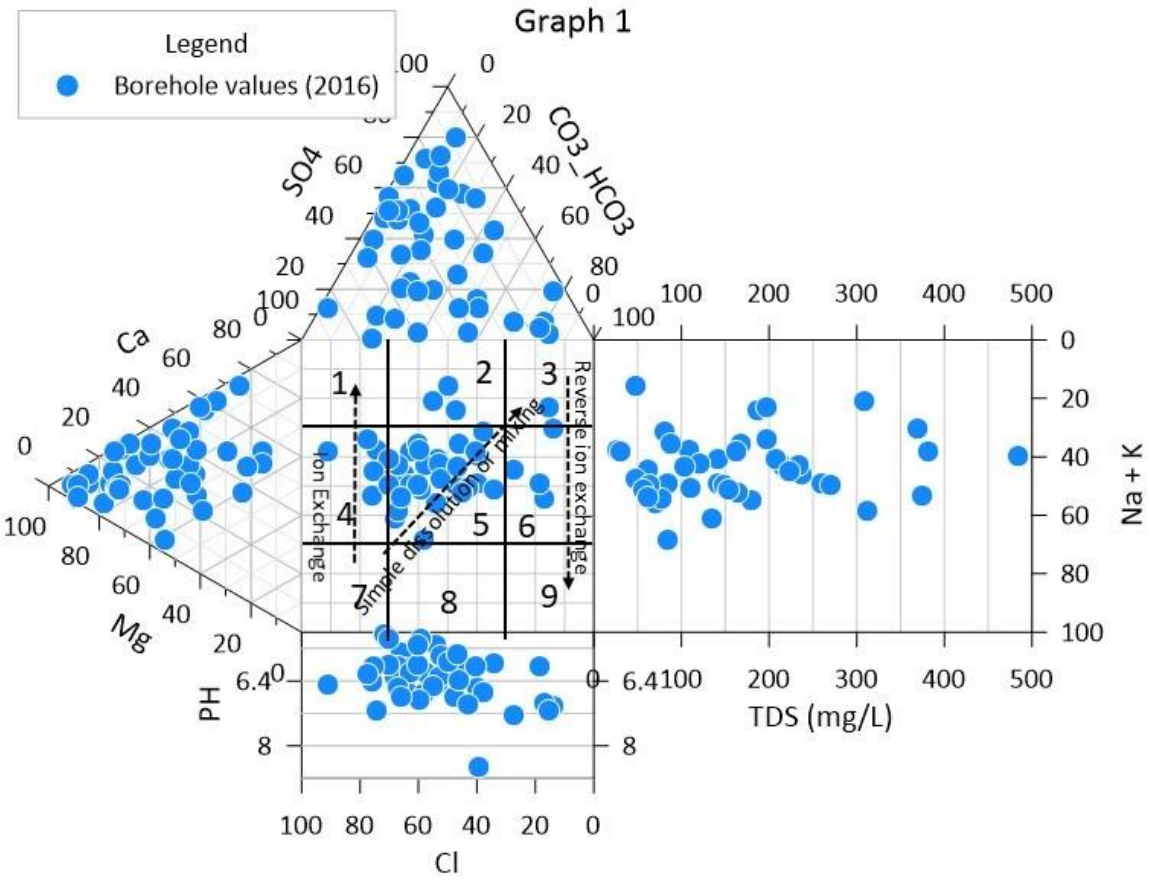

Figure 4.37c: Durov diagram (1948) of boreholes sampled in 2016 within the Lower Tano River Basin.

For the hand dug wells and boreholes sampled in 2017 six and seven geochemical processes are observed, respectively. Out of the six and seven, three hand dug wells (two sampled from the aquifer of the Apollonian formation and one taken from the aquifer of the Birimian supergroup) and six boreholes (four sampled from the aquifer of the Apollonian formation and two sampled from the aquifer of the Birimian supergroup) are seen in field two, that is water rich in Ca^{2+} - Mg^{2+} and HCO_3^- - CO_3^{2-} suggesting water from a limestone aquifer or recharge areas. One hand dug well sampled from the aquifer of the Birimian supergroup is seen in field three that is water rich in Na^+ -HCO_3^-, hence water undergoing reverse ion exchange (Belkhiri et al., 2012). Also, six hand dug wells (two taken from the aquifer of the Apollonian formation and four sampled from the aquifer of the Birimian supergroup) and three boreholes (one taken from the aquifer of the Apollonian formation and two sampled from the aquifer of the Birimian supergroup) are showing in field four, that is water rich in Ca^{2+} - SO_4^{2-}. Additionally, fifteen hand dug well (eight

sampled from the aquifer of the Apollonian formation and six taken from the aquifer of the Birimian supergroup) and thirty-two boreholes (twenty sampled from the aquifer of the Apollonian formation and twelve sampled from the aquifer of the Birimian supergroup) are seen in field five indicating water undergoing mixing or simple dissolution. Also, five hand dug well (three taken from the aquifer of the Apollonian formation and two sampled from the aquifer of the Birimian supergroup) and eleven boreholes (eight sampled from the aquifer of the Apollonian formation and three taken from the aquifer of the Birimian supergroup) are seen in field six that is water rich in Na^{+}- SO_4^{2-} thus water influenced by anthropogenic sources (Zaporozec, 1972; Lloyd & Heathcote, 1985). In addition, three boreholes sampled from the aquifer of the Apollonian formation are seen in field eight that is water rich in chloride and have non – dominant cation which may imitate inverse ion exchange of sodium and chloride water (Zaporozec, 1972; Lloyd & Heathcote, 1985).

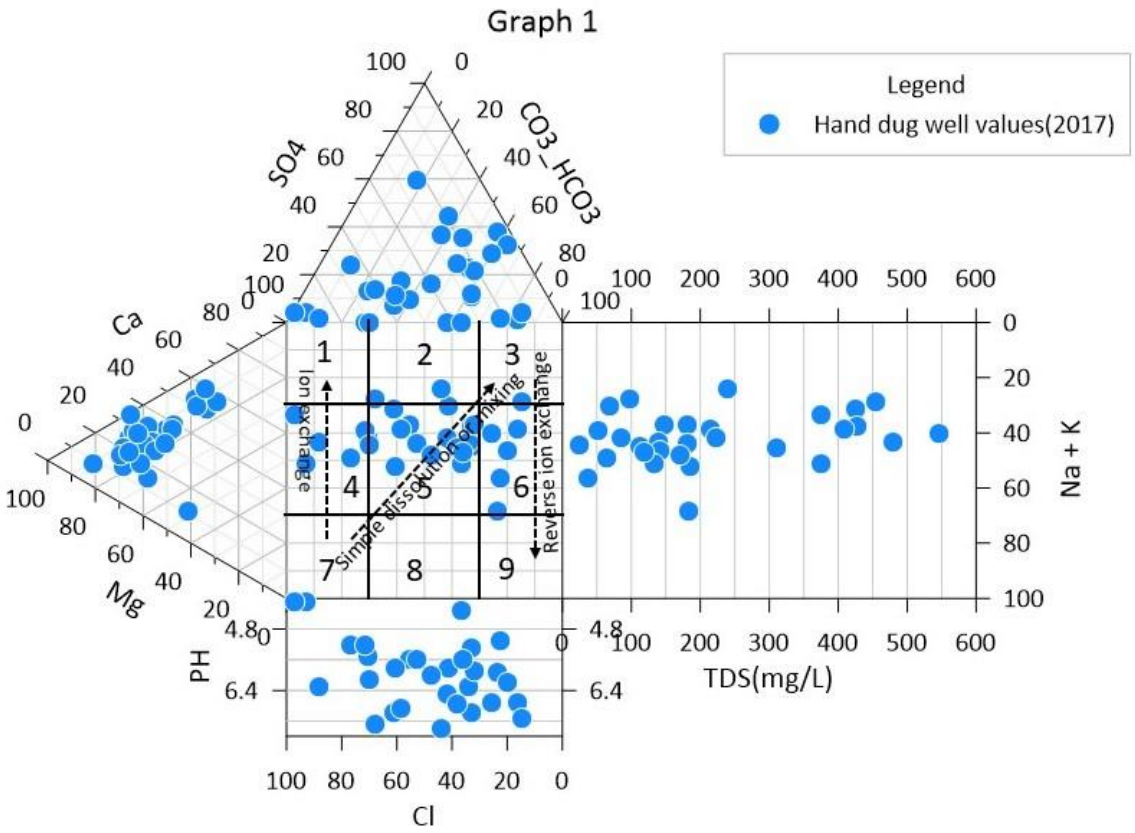

Figure 4.37d: Durov diagram (1948) of hand dug wells sampled in 2017.

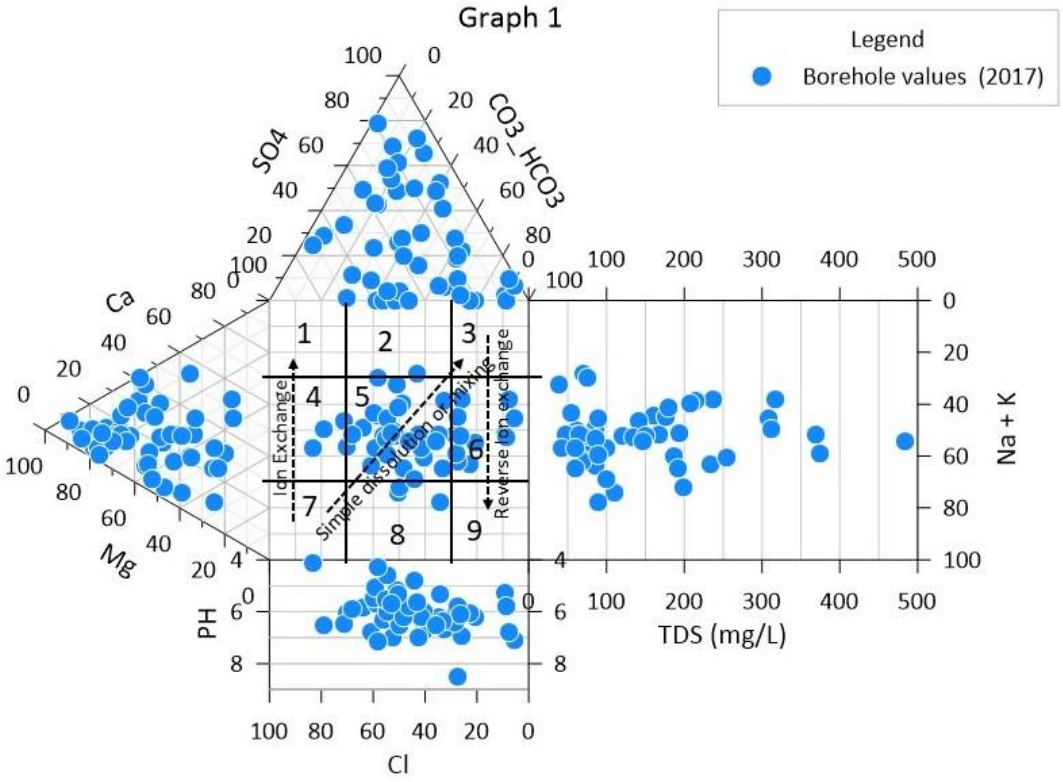

Figure 4.37 e: Durov diagram (1948) of boreholes sampled in 2017.

4.3.2. Hydrogeochemical facies and Evolution

With groundwater flowing from the aquifer of the Birimian super group to the Apollonian formation (Fig 4.4a,b), a series of water–rock interactions might occur, which probably will increase the ion concentrations in the groundwater. In regulating the factors affecting the groundwater chemistry within the basin, it is vital to investigate the hydrogeochemical transition of groundwater along a flow path or direction. This will give a better understanding of rock – water interactions in the aquifer. Chebotarev (1955), through many studies, have identified that the major anions in a regional groundwater system follow the sequence:

$HCO3^- \rightarrow HCO3^- + SO4^{2-} \rightarrow SO4^{2-} + HCO3^- \rightarrow SO4^{2-} + Cl \rightarrow Cl^- + SO4^{2-} \rightarrow Cl^-$

along a flow path (Li et al., 2011).

Variation of cations and anions along groundwater flow direction and hydrogeochemical facies are explained using Stiff and Piper diagram (Stiff (1951; Piper, 1944, Fig 4.38 a, b, c).

The Piper diagram is used to identify the relationship that exist between the cations and anions in the groundwater. Those with similar quality plots together as a group. Also, the stiff diagram is used to explain the factors that controls the groundwater evolution.

From Fig 4.38 a and 4.38 c, it is seen that the Piper diagram and the Stiff diagram gave similar groundwater water types and the groundwater evolution for 2014 to 2015 and 2017 samples are also similar. In figure 4.38a and figure 4.38c, three groundwater types are observed. These groundwater types are **mixed (Ca-Mg-Cl) water**, **Na-Cl water** and **Ca-Mg-HCO_3^- water**. The mixed groundwater type indicates that the ions are equally dominant in the groundwater sampled from the aquifer of the Apollonian formation and the Birimian supergroup. The Na-Cl water suggests ion exchange processes which proposes that the 2014-2015 and 2017 groundwater samples was flowing from a recharge zone to a discharge zone. but this will be explained further in subsequent chapters. The Ca-Mg-HCO_3^- groundwater implies that the aquifer of the Birimian supergroup and the Apollonian formation were recharged extensively by rainwater, but it will be explained further using stable isotopes of $\delta^{18}O$ and $\delta^{2}H$ in the 4th specific objective.

For the groundwater evolution for 2014 – 2015 and 2017 samples (figure 4.38 a and 4.38 c), it is observed that the groundwater is evolving from Ca-HCO_3^- water type (recharging water or fresh water) to a Na-Cl water type (recharge - discharge).

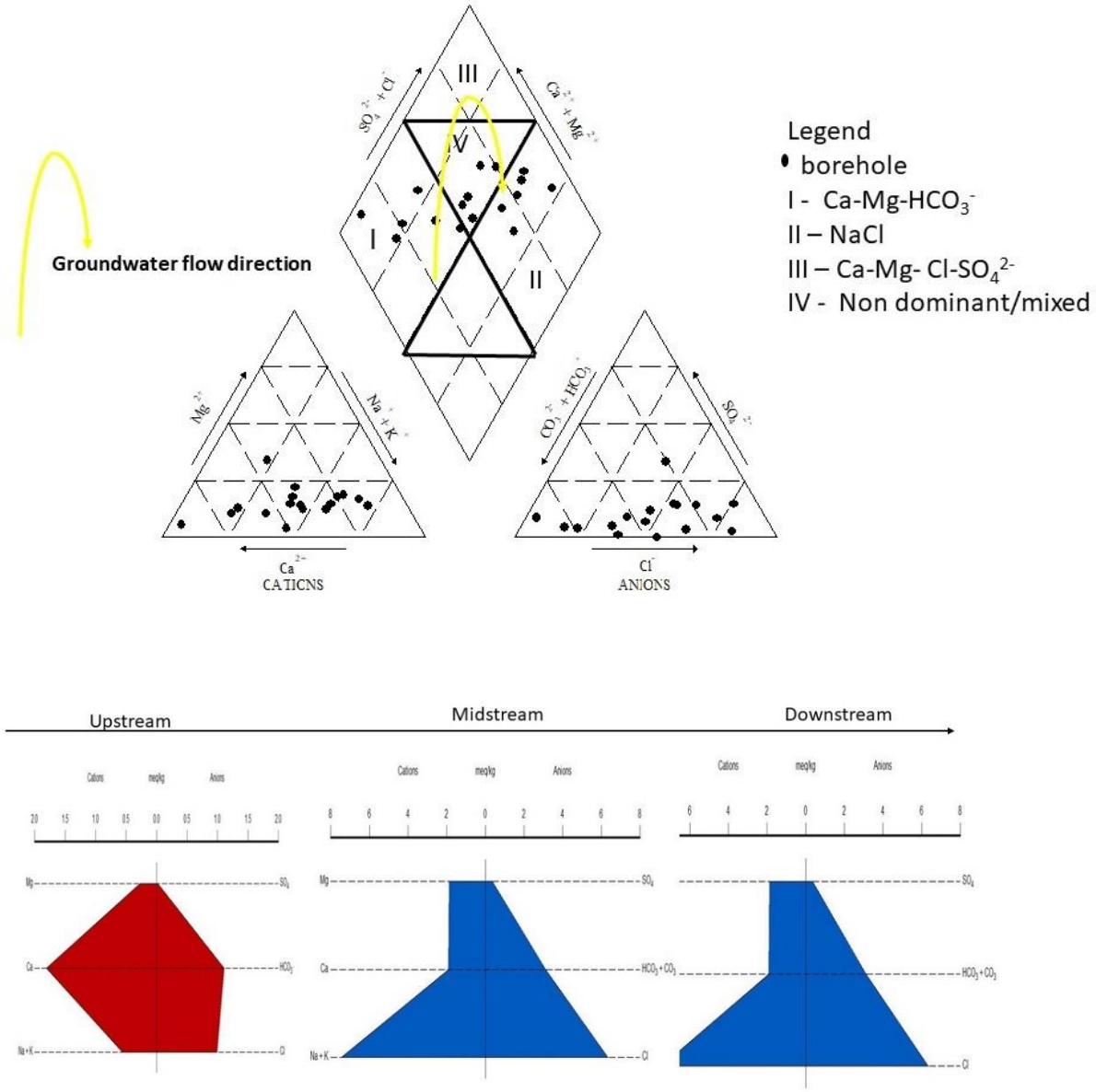

Figure 4. 36a: Piper (1944) and Stiff (1951) diagram showing the transition of groundwater chemistry along a flow direction (2014 – 2015)

For the groundwater sampled in 2016, four groundwater types are seen (Fig 4.38 b) and these water types are **Na-Cl water type**, **mixed water type (Ca-Mg-Cl and Na-Ca- HCO_3^-), Ca-Mg-Cl-SO_4^{2-} water type,** and **Ca-Mg-HCO_3^- water type**. The Na-Cl, Ca-Mg-HCO_3^- and mixed groundwater types have been discussed previously, but the Ca-Mg-Cl-SO_4^{2-} groundwater type infers that the groundwater has been in contact with a contaminated source or sulphide minerals from the underlying geology. Also, the groundwater evolves from Ca-

HCO_3^- (recharge water or fresh water) to Na-Cl water type (recharge to discharge) per the Stiff diagram shown in figure 4.38c.

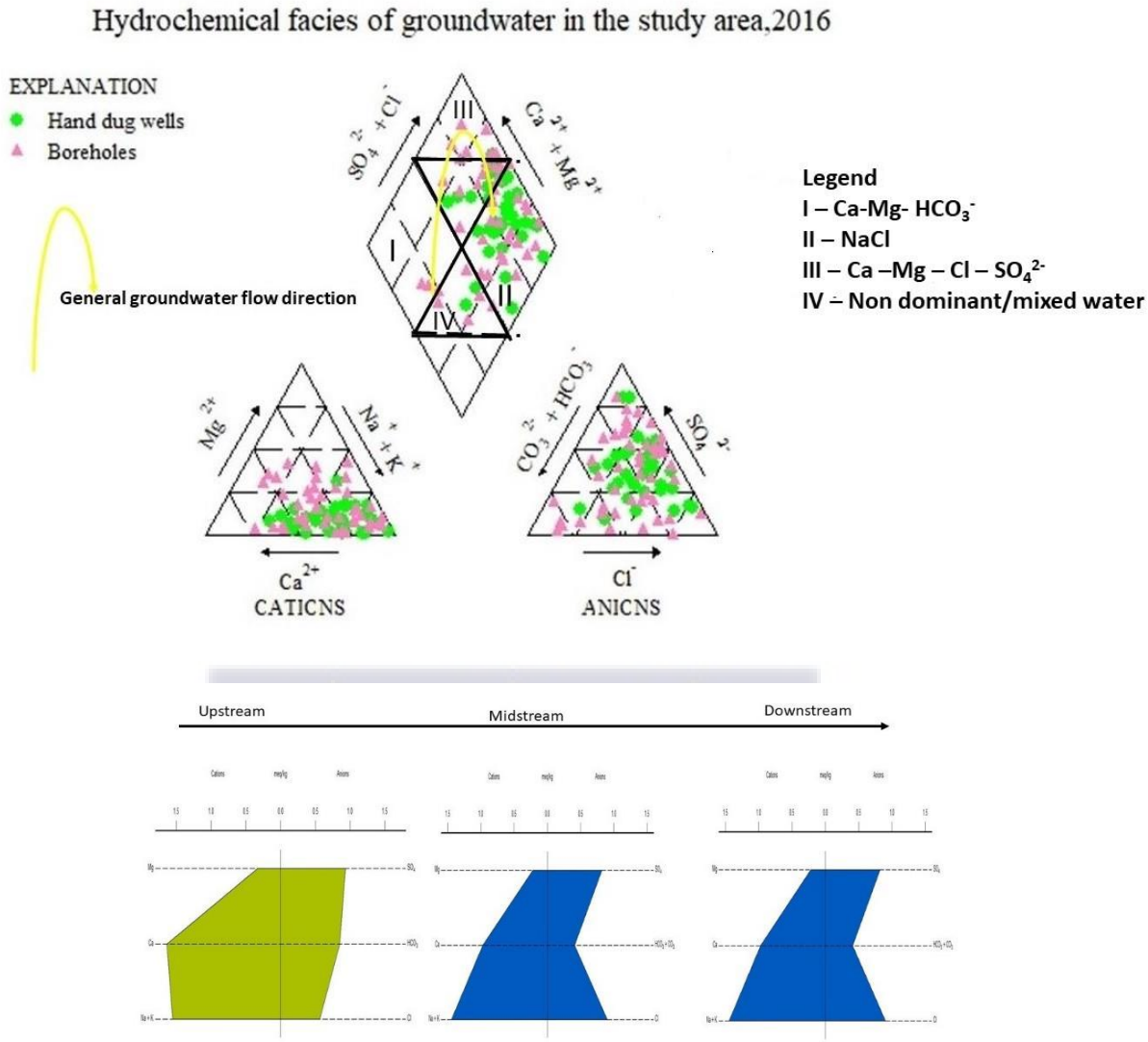

Figure 4.38 b: Piper (1944) and Stiff (1951) diagram showing the transition of groundwater chemistry along a flow direction (2016).

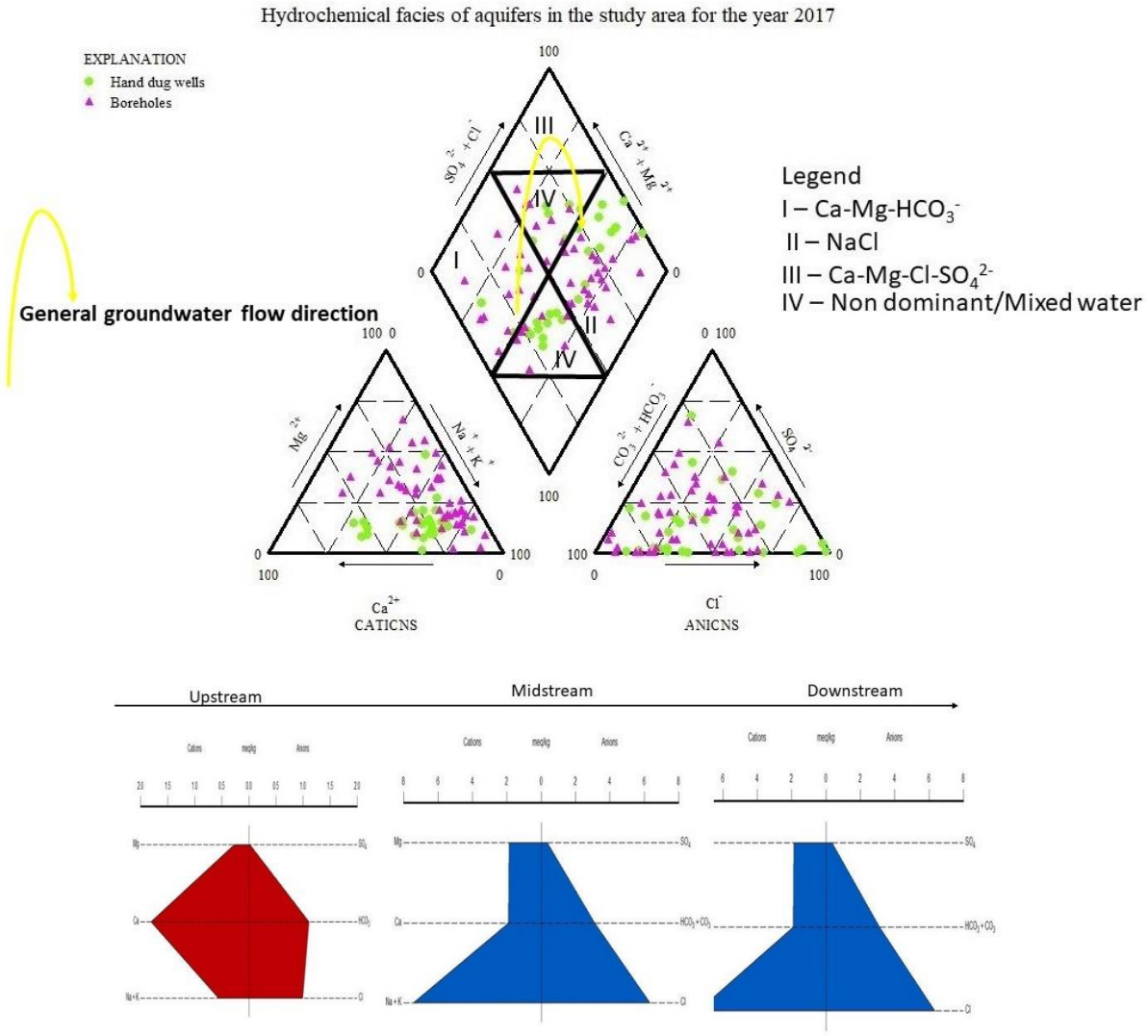

Figure 4.38 c: Piper (1944) and Stiff (1951) diagram showing the transition of groundwater chemistry along a flow direction (2017).

Table 4. 53: Characterization of groundwater types based on Piper (1944) Trilinear diagram and Stiff (1951) diagram.

Type of water	2014 – 2015 (n=18)	2016 (n=80)	2017 (n=84)
Na - Cl	7	28	30
Ca- Cl	6	6	2
Ca – HCO_3^-	5	1	3
Na – SO_4^{2-}		24	19
Na -HCO_3		8	15
Mg – SO_4^{2-}		2	6
Ca -SO_4^{2-}		11	3
Mg-Cl			3
Mg-HCO_3^-			3

The variation in groundwater evolution is attributed to rock- water interactions and ion exchange processes which will be explained further in subsequent chapters.

The Piper diagram, the Stiff diagram, and Table 4.53 revealed Na-Cl type of water as the dominant groundwater type in the aquifer of the Apollonian formation and the Birimian supergroup. To account for the possible reasons behind the dominate Na-Cl groundwater type, Na/Cl molar ratio (Meybeck, 1987) are calculated for the sampled groundwater in the study area and the calculated results is shown in Table 4.54 to 4.56.

Table 4. 54: Relationship of dissolved Na^+ and Cl^- in groundwater sampled from 2014 to 2015

Sample Id	Location	Rock Formation	Na^+ (meq/l)	Cl^- (meq/l)	Na/CL
BH 1	Newtown	Apollonian formation	6.79	6.32	1.1
BH 2	Effasu	Apollonian formation	0.58	0.56	1.0
BH 3	Mangyea	Apollonian formation	0.60	0.74	0.8
BH 4	Mpeasem	Apollonian formation	0.49	0.99	0.5
BH 5	Alumatuape	Apollonian formation	0.32	0.28	1.1
BH 6	Jawey	Apollonian formation	0.24	0.24	1.0
BH 7	Annor Adjaye SHS	Apollonian formation	0.52	0.50	1.1
BH 8	Allengenzule	Apollonian formation	0.71	0.71	1.0
BH 9	Agyeza	Apollonian formation	0.99	0.85	1.2
BH 10	Ehoaka	Apollonian formation	0.13	0.16	0.8
BH 11	Ehoaka	Apollonian formation	0.13	0.16	0.9
BH 12	Twenen	Apollonian formation	0.75	1.02	0.7
BH 13	Kengen	Apollonian formation	0.43	0.64	0.7
BH 14	Elloyin	Apollonian formation	0.82	0.88	0.9
BH 15	Kangbunli	Apollonian formation	0.94	0.72	1.3
BH 16	Azuleleounu	Apollonian formation	0.63	0.65	1.0
BH 17	Asanda	Apollonian formation	0.85	0.76	1.1
BH 18	Asanda	Apollonian formation	0.33	0.30	1.1

BH = Boreholes

Table 4. 55: Relationship of dissolved Na^+ and Cl^- in groundwater sampled in 2016.

Sample number	Community	Rock Formation	Na (meq/l)	Cl(meq/l)	Na/Cl	Sample number	Community	Rock Formation	Na (meq/l)	Cl (meq/l)	Na/Cl
HDW1	Esiama	Apollonian formation	1.43	0.90	1.6	BH1	Salman	Birimian Supergroup	1.68	0.17	9.9
HDW2	Nkroful	Birimian supergroup rocks	5.44	2.20	2.5	BH2	Kamgbuli	Apollonian formation	0.94	0.23	4.1
HDW3	Kikam	Apollonian formation	3.12	2.65	1.2	BH3	Kamgbuli	Apollonian formation	0.30	1.18	0.2
HDW4	Kikam	Apollonian formation	3.76	2.88	1.3	BH4	Asemko	Apollonian formation	1.63	0.68	2.4
HDW5	Aniwa	Birimian supergroup rocks	1.02	0.56	1.8	BH5	Ampaim	Apollonian formation	1.22	1.02	1.2
HDW6	Kikam	Apollonian formation	1.14	0.85	1.3	BH6	Aniwa	Birimian Supergroup	1.22	0.34	3.6
HDW7	Ampain	Apollonian formation	0.23	0.51	0.4	BH7	Nkroful	Birimian Supergroup	1.98	0.73	2.7
HDW8	Asanta	Apollonian formation	1.87	0.62	3.0	BH8	Sanwoma	Apollonian formation	1.47	1.47	1.0
HDW9	Nkroful	Birimian supergroup	0.78	0.45	1.7	BH9	Aluku	Birimian Supergroup	3.75	1.52	2.5
HDW10	Kikam	Apollonian formation	1.78	1.18	1.5	BH10	Awiebo	Apollonian formation	0.59	0.17	3.5
HDW11	Bomuakpole	Birimian Supergroup	1.33	0.62	2.1	BH11	Esiama	Apollonian formation	0.69	0.34	2.0
HDW12	Kikam	Apollonian formation	1.94	1.47	1.3	BH12	Ampain	Apollonian formation	2.81	0.96	2.9
HDW13	Ankobra	Apollonian formation	4.25	4.85	0.9	BH13	Salman	Birimian Supergroup	0.34	0.45	0.8
HDW14	Asanta	Apollonian formation	0.85	0.79	1.1	BH14	Nkroful	Birimian Superroup	1.52	0.56	2.7
HDW15	Gyegyekrom	Apollonian formation	0.31	0.17	1.8	BH15	Bobrama	Apollonian formation	1.29	0.79	1.6
HDW16	Kikam	Apollonian formation	1.38	2.09	0.7	BH16	Bomuakpole	Apollonian formation	0.81	0.90	0.9

HDW17	Asanta	Apollonian formation	0.92	1.13	0.8	BH17	Sanwoma	Apollonian formation	0.62	1.52	0.4
HDW18	Esiama	Apollonian formation	2.96	1.86	1.6	BH18	Alabokazo	Apollonian formation	0.23	0.39	0.6
HDW19	Aniwa	Birimian supergroup	1.26	0.23	5.6	BH19	Aluku	Birimian supergroup	1.01	0.34	3.0
HDW20	Esiama	Apollonian formation	0.85	0.45	1.9	BH20	Alabokazo	Apollonian formation	0.86	1.02	0.8
HDW21	Elubo	Birimian supergroup	3.57	2.37	1.5	BH21	Asanta	Apollonian formation	1.31	0.73	1.8
HDW22	Asanta	Apollonian formation	2.98	1.64	1.8	BH22	Salaman	Birimian Supergroup	0.31	0.11	2.8
HDW23	Ankobra	Apollonian formation	2.78	1.75	1.6	BH23	Telekobokaso	Birimian supergroup	1.27	1.02	1.3
HDW24	Esiama	Apollonian formation	4.88	3.27	1.5	BH24	Aluku	Birimian supergroup	1.79	1.41	1.3
HDW25	Esiama	Apollonian formation	0.93	0.62	1.5	BH25	Esiama	Apollonian formation	0.65	0.45	1.4
HDW26	Nkroful	Birimian Supergroup	1.47	0.51	2.9	BH26	Ankobra newsite	Apollonian formation	1.49	1.97	0.8
HDW27	Esiama	Apollonian formation	2.32	1.64	1.4	BH27	Sanwoma	Apollonian formation	1.24	0.51	2.4
HDW28	Gyegyekrom	Apollonian formation	0.66	0.39	1.7	BH28	Old Kablasuazo	Apollonian formation	1.49	0.68	2.2
HDW29	Elubo	Birimian Supergroup	0.99	0.62	1.6	BH29	Azulenloa	Apollonian formation	0.81	0.62	1.3
HDW30	Azulenloanu	Apollonian formation	0.99	0.56	1.7	BH30	Azuleno	Apollonian formation	1.29	1.13	1.1
HDW31	Half Assini	Apollonian formation	1.25	0.68	1.8	BH31	Fante new site	Apollonian formation	0.37	0.23	1.6
HDW32	Bobrama	Apollonian formation	0.95	0.56	1.7	BH32	Elubo	Birimian supergroup	2.11	1.18	1.8
HDW33	Asanta	Apollonian formation	2.09	1.07	1.9	BH33	Bomuakpole	Apollonian formation	1.17	0.39	3.0
HDW34	Sanwoma	Apollonian formation	0.98	0.56	1.7	BH34	NyanZinli	Apollonian formation	1.10	0.68	1.6

HDW35	Bobrama	Apollonian formation	2.78	1.13	2.5	BH35	Atwibanso	Apollonian formation	0.52	0.28	1.8
HDW36	Ankobra	Apollonian formation	4.20	4.68	0.9	BH36	New Nzulezu	Apollonian formation	0.16	0.17	1.0
						BH37	NEW Ankasa	Apollonian formation	0.40	0.28	1.4
						BH38	Bonyere	Apollonian formation	2.49	1.41	1.8
						BH39	Atwibaso	Apollonian formation	1.25	0.56	2.2
						BH40	Awiafoto	Apollonian formation	0.35	0.56	0.6
						BH41	Aniwafuto(chips)	Apollonian formation	0.70	0.17	4.1
						BH42	New Nzulezu(2)	Apollonian formation	0.63	2.37	0.3
						BH43	Tiekobo 1	Apollonian formation	0.80	0.11	7.1
						BH44	Bobrama	Apollonian formation	1.05	1.13	0.9

HDW = Hand dug wells and BH = Boreholes

Table 4. 56: Relationship of dissolved Na^+ and Cl^- in groundwater sampled in 2017

Sample Number	Community	Rock Formation	Na^+ (meq/l)	Cl^- (meq/l)	Na/Cl	Sample Number	Community	Rock Formation	Na^+ (meq/l)	Cl^+ (meq/l)	Na/Cl
HDW 1	Nkroful	Birimian Supergroup	0.80	0.68	1.2	BH1	Sanzule	Apollonian formation	0.82	0.23	3.6
HDW 2	Aluku	Birimian supergroup	1.96	1.64	1.2	BH2	Nyaniba	Apollonian formation	2.01	1.07	1.9
HDW 3	Kikam	Apollonian formation	1.61	0.56	2.9	BH3	Ampaim	Apollonian formation	0.92	0.85	1.1
HDW 4	Nkroful	Birimian Supergroup	0.53	0.51	1.0	BH4	Atwinbanso	Apollonian formation	0.64	0.56	1.1
HDW 5	Esiama	Apollonian formation	1.76	3.38	0.5	BH5	Elubo	Apollonian formation	1.96	1.58	1.2
HDW 6	Elubo	Birimian Supergroup	3.69	3.78	1.0	BH6	Awiefoto	Apollonian formation	0.42	0.17	2.5
HDW 7	Kikam	Apollonian formation	1.61	1.30	1.2	BH7	Esiama	Apollonian formation	3.73	2.54	1.5
HDW 8	Half Assini	Birimian Supergroup	0.47	0.73	0.6	BH8	Old Kablazuaso	Apollonian formation	0.48	0.56	0.9
HDW 9	Bomuakpole	Apollonian formation	1.16	1.52	0.8	BH9	Fante New Town	Apollonian formation	0.85	0.23	3.8
HDW 10	Nkroful	Birimian supergroup	1.15	0.45	2.6	BH10	Half Assini SHS	Apollonian formation	1.60	0.90	1.8
HDW 11	Kikam	Apollonian formation	3.14	2.14	1.5	BH11	Salman	Birimian supergroup	0.33	0.17	1.9
HDW 12	Kikam	Apollonian formation	1.03	2.26	0.5	BH12	Salman	Birimian supergroup	0.73	0.17	4.3
HDW 13	Elubo	Birimian Supergroup	3.18	3.78	0.8	BH13	Esiama	Apollonian formation	2.39	1.30	1.8
HDW 14	Nkroful	Birimian Supergroup	4.79	1.58	3.0	BH14	Azuleno	Apollonian formation	1.50	0.39	3.8

HDW 15	Aniwa	Birimian Supergroup	1.16	0.73	1.6	BH15	Bomuakpoley	Birimian supergroup	0.58	0.34	1.7
HDW 16	Asemda	Apollonian formation	0.80	0.11	7.1	BH16	Salman	Apollonian formation	0.35	0.11	3.1
HDW 17	Gyegyekrom	Apollonian formation	0.37	0.17	2.2	BH17	Nkroful	Birimian Supergroup	0.63	0.56	1.1
HDW 18	Esiama	Apollonian formation	1.48	0.90	1.6	BH19	Esiama	Apollonian formation	0.60	0.45	1.3
HDW 19	Ampaim	Apollonian formation	0.36	0.56	0.6	BH20	Ankobra newsite	Apollonian formation	0.78	0.34	2.3
HDW 20	Eikwe	Apollonian formation	3.78	1.52	2.5	BH21	Ampiam	Apollonian formation	0.52	0.11	4.6
HDW 21	Atuabo	Apollonian formation	2.12	0.11	18.8	BH22	Nkroful	Birimian supergroup	1.22	0.68	1.8
HDW 22	Benyin	Apollonian formation	3.50	2.99	1.2	BH23	New Nzulazu	Apollonian formation	0.28	0.17	1.7
HDW 23	Esiama	Apollonian formation	4.47	0.73	6.1	BH24	Tiekobo 1	Apollonian formation	0.16	0.11	1.4
HDW 24	Gyegyekrom	Apollonian formation	0.26	0.11	2.3	BH25	Bobrama	Apollonian formation	1.34	1.18	1.1
HDW 25	Bobrama	Apollonian formation	1.58	1.30	1.2	BH26	New Nzulazu	Apollonian formation	0.70	0.06	12.5
HDW 26	Elubo	Birimian Supergroup	0.83	0.68	1.2	BH27	Bonyere	Apollonian formation	1.15	0.51	2.3
HDW 27	Kikam	Apollonian formation	1.25	0.79	1.6	BH28	Kamgbunli	Apollonian formation	1.13	0.90	1.3
HDW 28	Kikam	Apollonian formation	1.77	1.41	1.3	BH29	Aluku	Birimian Supergroup	1.97	1.64	1.2
HDW 29	Azulenuano	Apollonian formation	1.07	0.56	1.9	BH30	Atwinbanso	Apollonian formation	0.75	0.62	1.2
HDW 30	Aniwa	Apollonian formation	1.03	0.39	2.6	BH31	Asemko	Apollonian formation	0.72	0.23	3.2

						BH32	Salman	Birimian Supergroup	0.74	0.11	6.6
						BH33	Azeneluno	Apollonian formation	1.50	0.39	3.8
						BH34	Aluku	Birimian Supergroup	0.52	0.34	1.5
						BH35	Alabokazo	Apollonian formation	0.23	0.96	0.2
						BH36	Kamgbunli	Apollonian formation	0.36	0.34	1.1
						BH37	Ankasa	Apollonian formation	0.51	0.96	0.5
						BH38	Telekobokaso	Birimian Supergroup	1.42	0.56	2.5
						BH39	Alabokazo	Apollonian formation	0.96	0.62	1.5

HDW =Hand dug wells and BH = Boreholes

The computation of the Na/Cl molar ratio (Table 4.54 – 4.56) for 2014 to 2015 borehole samples reveals that, 40% of the boreholes (n=18) is greater than one, 38% is less than one and 22% o is equal to one.

In 2016, the calculated Na/Cl molar ratio results for the sampled groundwater indicates that 78.8% of the groundwater (n= 80) is greater than one, 19.25% is less than one and 2% is equal to one.

In 2017, the calculated Na/Cl molar ratio results show that 67.9% of the groundwater (n=84) is greater than one, 30.14% is less than one and 2% is equal to one.

Assessment of the above Na/Cl molar ratio reveals that most groundwater in the Lower Tano River Basin have Na^+ /Cl^- molar ratio to be greater than one. This implies that ion exchange processes (Garrels & Mackenzie, 1967) are the dominant factor controlling sodium and chloride ion content in the aquifer of the Apollonian formation and the Birimian supergroup rocks. Additionally, few groundwater samples had Na/Cl molar ratio greater than one and this represents Na^+ released from silicate mineral (feldspar, hornblende, plagioclase, granite etc.) weathering (Garrels & Mackenzie, 1967). Lesser groundwater samples had Na^+ /Cl^- molar ratio to be equal to one. indicating the presence of halite dissolution (Meybeck, 1987) in the aquifer of the Apollonian formation and the Birimian supergroup rocks. In the study area, halite is absent in the general geology (Fig 3.3 and 3.4) but if halite is present then it might be through evaporation, which concentrates in the soil zone, before moving into the aquifer by direct rainfall infiltration. Little groundwater samples had Na^+ / Cl^- lesser than one. This suggests minimal seawater intrusion (Meybeck, 1987).

4.3.4 Groundwater mineralization Processes

A clear understanding of the main factors affecting the chemical quality of groundwater mineralization is important for groundwater resource development and protection. To do this, Gibbs (1970) diagram is employed. Gibbs (1970) proposed a diagram, which includes two sub-

diagrams. One of the sub-diagrams represent the relationship between TDS and the weight ratio of Cl^- versus (Cl^- + $HCO3^-$) and the other denotes the relationship between TDS and the weight ratio of Na^+ versus (Na^+ + Ca^{2+}). The geochemistry behind the basis of the Gibbs (1970) diagram is the geological formations and the composition of groundwater. In the diagram, three distinct fields are established. These fields are rock dominance, evaporation dominance, and precipitation dominance (Li et al., 2013 a; Gibbs, 1970).

The Gibbs (1970) diagram (Fig 4.39 a, b) plotted for 2014 to 2015, 2016 and 2017 hydrochemical data suggests that rock weathering and rainfall is the chemical quality controlling the groundwater mineralization of the aquifer of the Birimian supergroup and the Apollonian formation. The groundwater lying in the rock dominance zone (Fig 4.39 a, b) has explained the results obtained for the Person correlation matrix, the dominance of sodium, and calcium in the groundwater of the study area as well as the results of the Fickling diagram discussed in subsequent chapters. Also, the groundwater lying in the rainfall dominance zone has explained the Ca-HCO_3^- groundwater type obtained from the Durov and Piper diagram as well as the low recorded TDS content for the groundwater. But it will be explained further using stable isotopes of oxygen-18 and deuterium in the 4th specific objective.

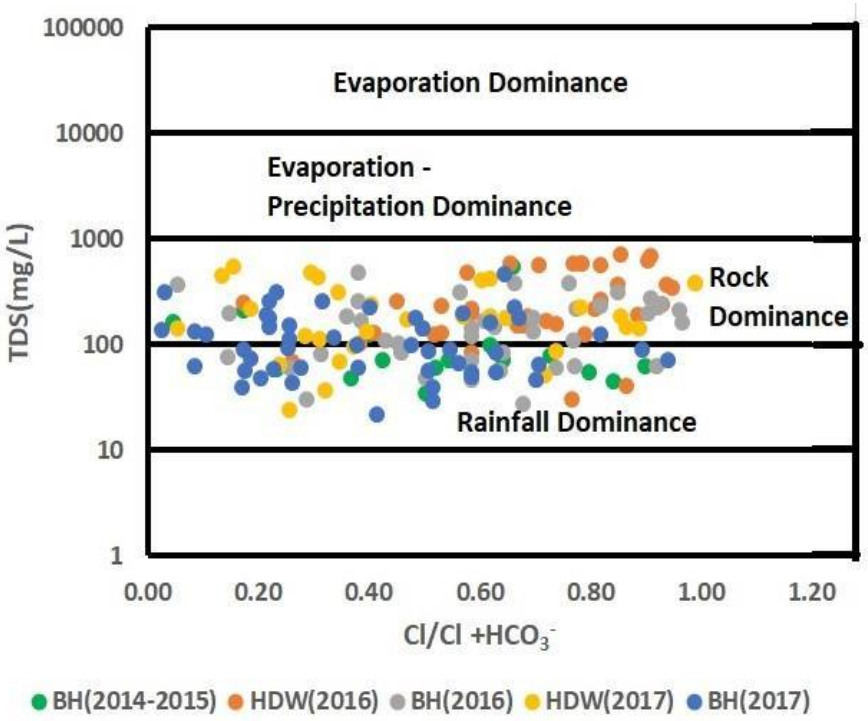

Figure 4. 37a: Gibbs (1970) diagram indicating the general mechanisms of groundwater evolution

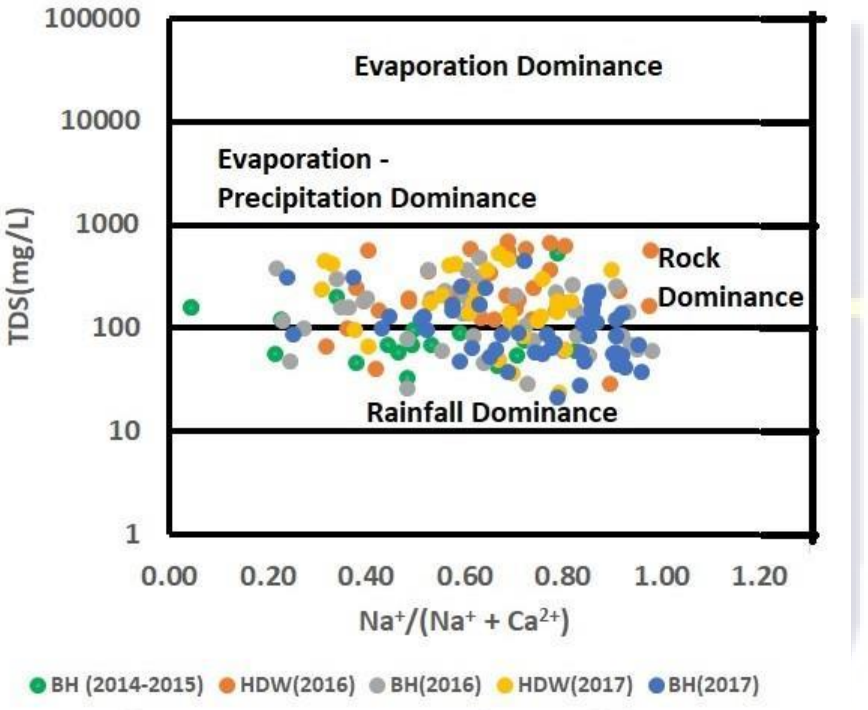

Figure 4.39 b: Gibbs (1970) diagram indicating the general mechanisms of groundwater evolution

4.3.4.1 Rock weathering

Since rock weathering is one of the major sources of chemical quality controlling the groundwater mineralization of the Apollonian formation aquifer and the aquifer of the Birimian supergroup, compositional diagrams are used to interpretate and confirm the accession. This is done by plotting Na^+ against Cl^- (Fig 4.40) and Na^+ against HCO_3^- (Fig 4.41)

For Na^+ vs Cl^- plot (Fig 4.40) and Na^+ vs HCO_3^- plot (Fig 4.41), a strong positive correlation is observed. Also, most of the groundwater samples are plotting above the 1:1 equiline. This suggests ion exchange (Hounslow, 1995) process. Fig 4.40 and 4.41 has explained the Piper diagram and the Stiff diagram where most samples were Na-Cl groundwater type and evolving from Ca-HCO_3^- to Na-Cl and Ca-SO_4^{2-} to Na-Cl. The effects of ion-exchange processes in the groundwater implies a change in aquifer chemistry along a flow direction.

Also, looking at the diagrams (Fig 4.40 and 4.41), it is seen that few groundwater samples are plotting on or near the 1:1 equiline. This shows that the hydrochemical evolution of groundwater sampled from the aquifer of the Birimian super group and the Apollonian formation might be controlled by the effect of limited dissolve carbonate equilibria and limited mixing with rainfall (Hounslow, 1995). This explains the Gibbs diagram where 50% of the groundwater was lying in the rock dominance zone and 50% was lying in the rainfall dominance zone.

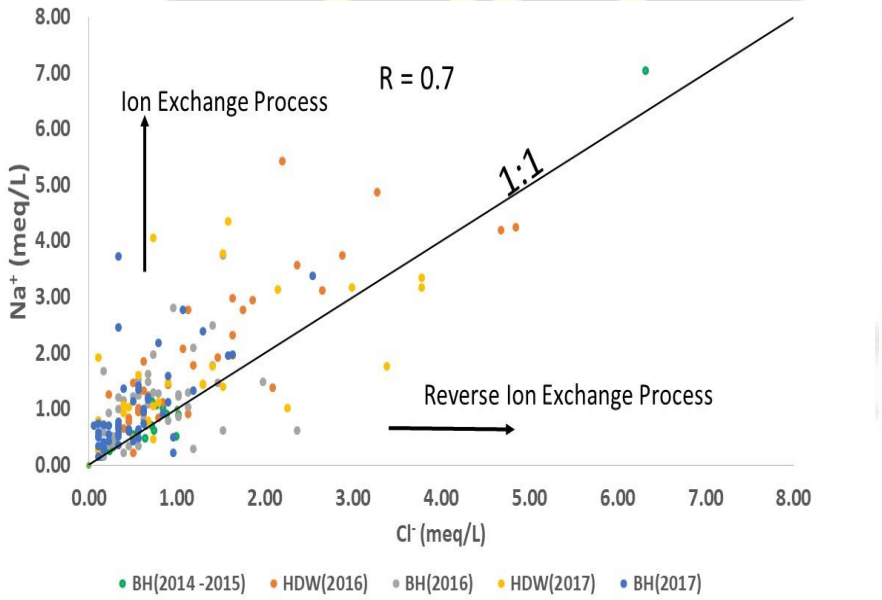

Figure 4. 38: Relationship between Cl^- and Na^+ drawn for the sampled groundwater in the study area.

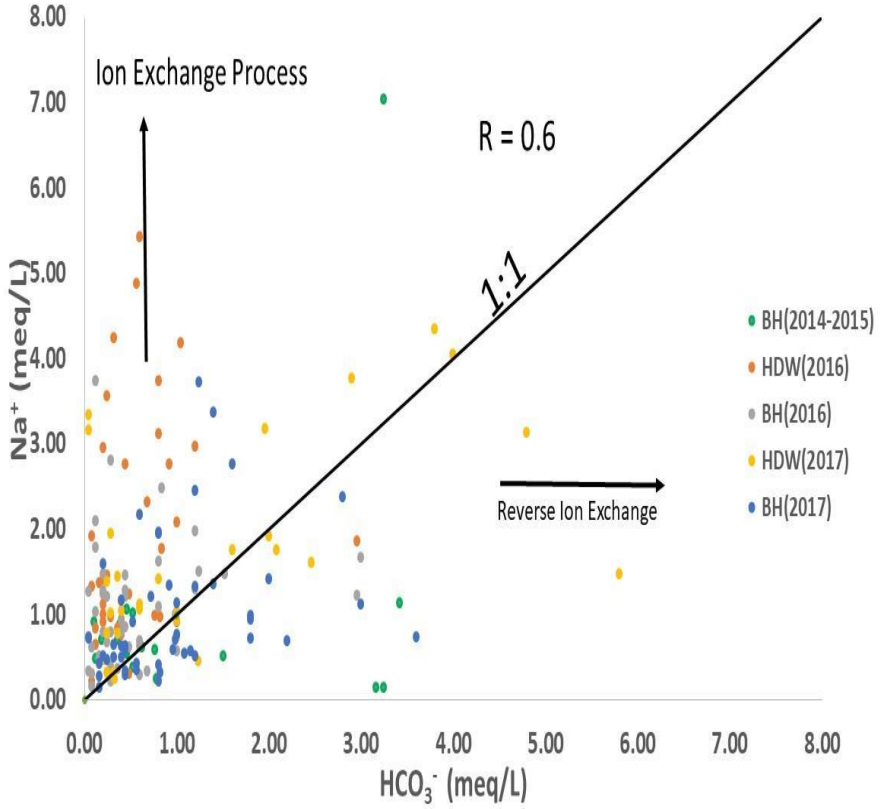

Figure 4. 39: Relationship between Na^+ and $HCO3^-$ drawn for the sampled groundwater in the study area.

The hydrochemical data of groundwater sampled from the aquifer of the Apollonian formation and the Birimian supergroup is plotted on $Ca^{2+} + Mg^{2+}$ vs. $SO_4^{2-} + HCO_3^-$ diagram (Fisher & Mulican, 1997). From the diagram (Fig 4.42), 5% of the sampled groundwater is clustered around the 1:1 equiline. This reveals dissolution of carbonate minerals from the underlying geology. Also, 55% of the sampled groundwater are lying below the 1:1 equiline representing excess $SO_4^{2-} + HCO_3^-$. This suggests weathering of silicate minerals from the underlying geology. Figure 4.42 has confirmed the Gibbs diagram where 50% of the groundwater were lying in the rock dominance zone. Additionally, the remaining 40% of the groundwater samples are plotting above the 1:1 equiline revealing excess magnesium and calcium (reverse ion - exchange) ion concentration (Fisher & Mulican, 1997). The strong positive correlation

between $Ca^{2+} + Mg^{2+}$ and $SO_4^{2-} + HCO_3^-$ reveals the occurrence of rock weathering (Hounslow, 1995) as a major factor controlling the groundwater chemistry of the study area.

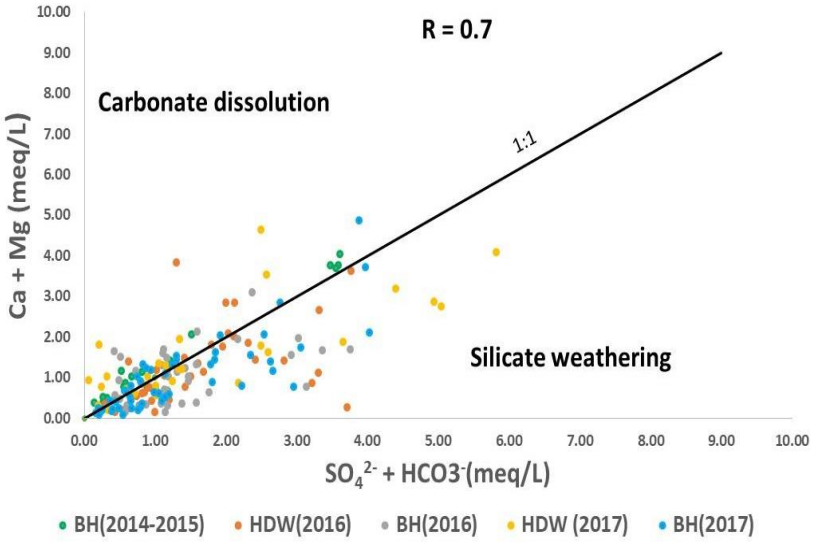

Figure 4. 40: Relationship between (Ca + Mg) vs ($SO_4^{2-} + HCO_3^-$) in the sampled groundwater within the study area.

Groundwater undergoing ion exchange would typically plot along a line whose slope is -1, whiles groundwater plotting close to the zero value on the x-axis is not influenced by ion exchange (Jankowski et al., 1998). In this study, the most likely additional sources of Mg^{2+} and Ca^{2+} contribution to the groundwater chemistry apart from cation- exchange is the dissolution of carbonate minerals and the weathering of silicate minerals as explained previously. To explain further, $Ca^{2+} + Mg^{2+} - HCO_3^- - SO_4^{2-}$ vs $Na^+ - Cl^-$ (McClean & Jankowski, 2000) plot in meq/L is used (Fig 4.43). The diagram (Fig 4.43) shows that groundwater sampled from 2014 to 2015 plots along a line with slope (-0.04) (close to the zero value of the x-axis). This indicates that cation exchange processes (McClean & Jankowski, 2000) are not influencing the chemistry of the aquifers. Also, groundwater sampled in 2016 and 2017 plots along a line with slope -0.9 and -0.8 (away from the zero value of the x-axis), respectively (Fig 4.43). This suggests that in the rainy season, the chemistry of the aquifers is influenced by cation-exchange processes (McClean & Jankowski, 2000).

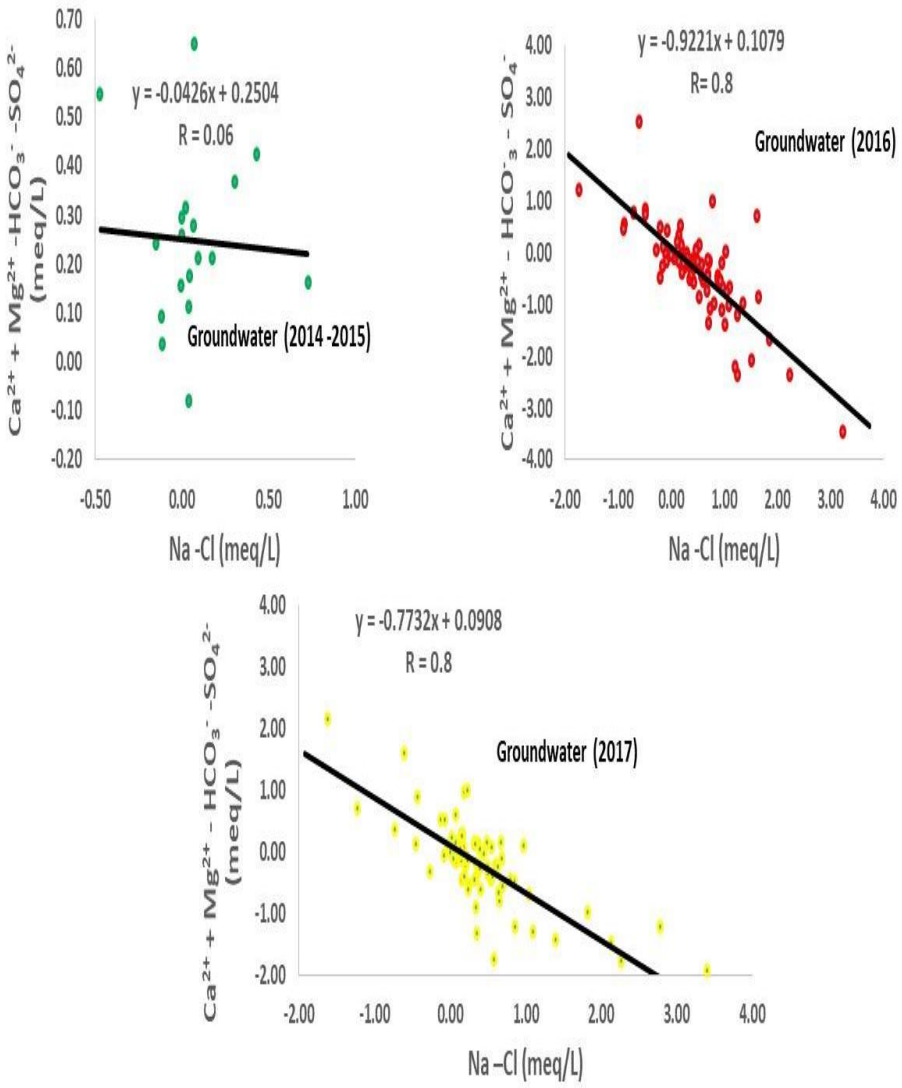

Figure 4. 41: Relationship between Ca^{2+} + Mg^{2+} – HCO_3^- - SO_4^{2-} and Na-Cl for the sampled groundwater within the study area (2014 – 2017).

\A plot of Na^+ + K^+ vs TC (Total cations) for groundwater sampled from 2014 to 2017 is also drawn. From the plot (Fig 4.44), it is seen that all the groundwater sampled from the aquifer of the Apollonian formation and the Birimian supergroup are clustering along the equiline in a linear spread. This reveals an increasing contribution of alkalis with increasing dissolved solids (Singh et al., 2013) in both aquifers.

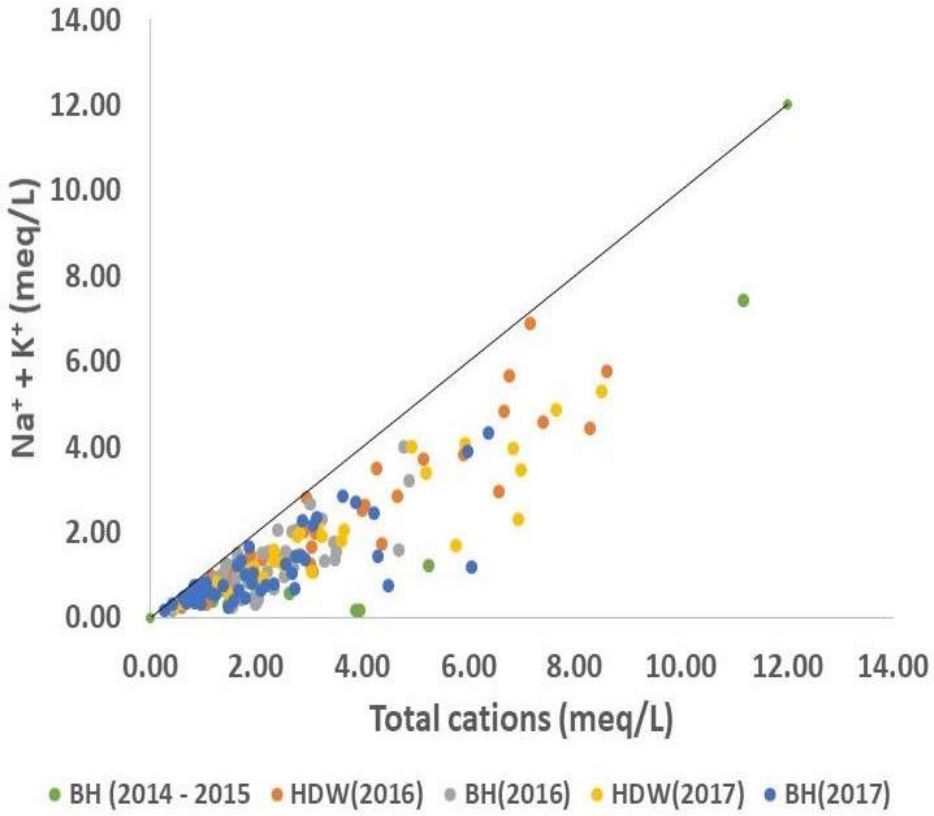

Figure 4. 42: Relationship between Na^+ +K^+ and Total cations in the sampled groundwater in the study area.

4.3.4.1.1 Cation Exchange

Cation exchange is an important natural process that can have significant impact on the evolution of the aquifer chemistry (Li et al., 2013 a). In further studying the occurrence of cation exchange reactions in the groundwater taken from the aquifer of the Apollonian formation and the Birimian supergroup, two Chloro Alkaline Indices (CAI - 1 and CAI -2) proposed by Schoeller (1965) are used. These indices are expressed as:

$$CAI - 1 = Cl - \frac{(Na+K)}{Cl} \quad \text{Eq 4.17}$$

$$CAI - 2 = Cl - \frac{(Na+K)}{SO_4} + HCO_3 + CO_3 + NO_3 \quad \text{Eq 4.18}$$

Where all values are expressed in meq/L.

Results from the computation of the above equations is shown from Appendix 30 to 34. If negative values for the two indices are achieved from the results, reverse reaction expressed as $Ca^{2+} + 2NaX = 2Na^+ + CaX_2$ is probably taking place. Likewise, if positive values for the

two indices are obtained, cation exchange expressed as $2Na^{+} + CAX_2 = Ca^{2+} + 2NaX$ is occurring. Results obtained from the calculation of the two-chloro alkaline indices are plotted and shown in Fig 4.45 a and 4.45 b.

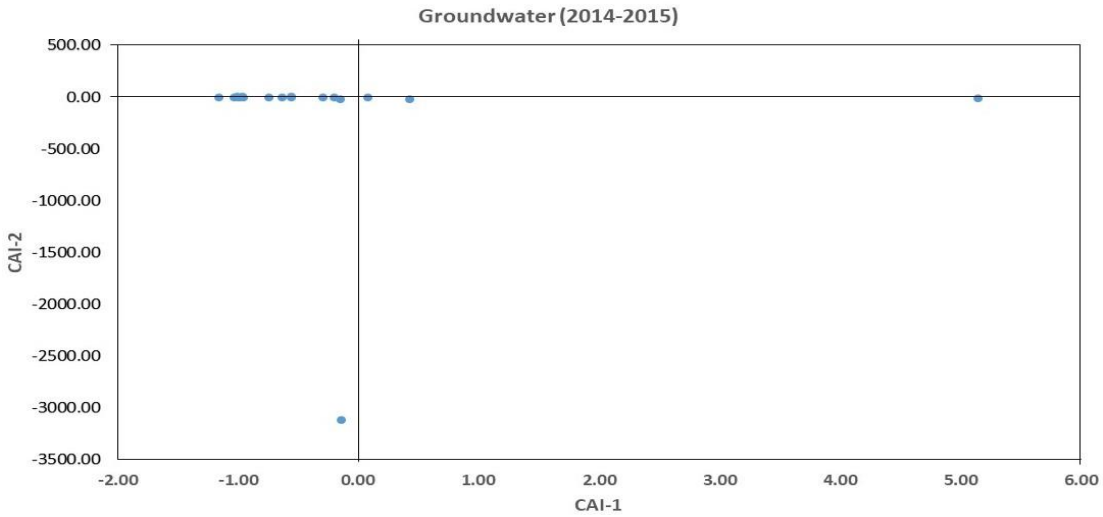

Figure 4. 43a: Bivariate plot for studying cation exchange in the sampled groundwater (2014 – 2015) within the Lower Tano River Basin

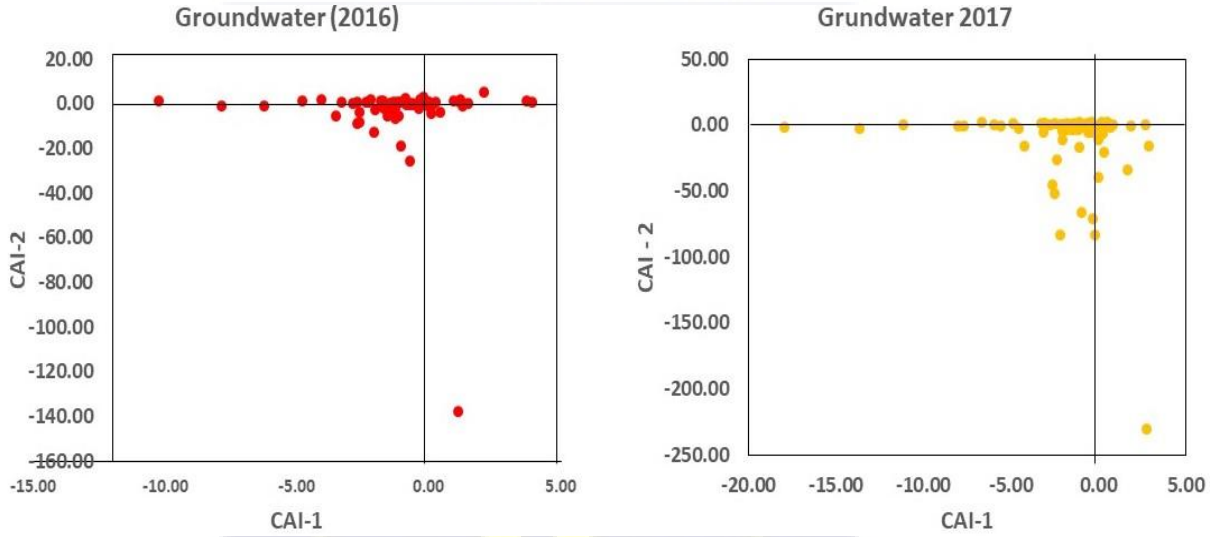

Fig 4.45b: Bivariate plot for studying cation exchange in groundwater (2016 and 2017) within the Lower Tano River Basin

From the above diagrams (Fig 4.45 a and Fig 4.45 b), it is observed that most of the groundwater are plotting in the negative zone. This indicate that majority of the groundwater sampled in the aquifer of the Apollonian formation and the Birimian super group have undergone reverse cation- exchange processes. However, few of the groundwater samples taken from the aquifer of the Apollonian formation and the Birimian supergroup have also undergone cation- exchange and are seen in the positive zone. The cation- exchange processes

decrease the calcium content whiles increasing the sodium concentration in the groundwater. Likewise, the reverse cation - exchange processes increase the calcium content whiles decreasing the sodium content in the groundwater (Marghade et al., 2011).

To further investigate the effects cation- exchange (including reverse cation exchange) has on the salinity of groundwater in the aquifer of the Apollonian formation and the Birimian supergroup, a bivariate plot of $(Ca^{2+} + Mg^{2+}) - (HCO_3^- + SO_4^{2-})$ and $(Na^+ + K^+ - Cl^-)$ is drawn and $(Ca^{2+} + Mg^{2+}) - (HCO_3^- + SO_4^{2-})$ suggests the increment or decrement of $(Ca^{2+} + Mg^{2+})$ caused by processes excluding precipitation/dissolution of limestones (dolomite, calcite).

$Na^+ + K^+ - Cl^-$ represents the increment of Na^+ induced by processes excluding halite dissolution, (Li et al., 2014 b). If cation- exchange is the main process affecting groundwater salinity, the relationship between the above- mentioned ions will be linear and the slopes will be close to -1. Figure 4.46, indicates that the relationship between $(Ca^{2+} + Mg^{2+}) - (HCO_3^- + SO_4^{2-})$ and $(Na^+ + K^+ - Cl^-)$ for the groundwater sampled from 2014 to 2017 conforms to the following linear equations, thus:

y= -0.023x +0.2506, R = 0.04, in 2014 to 2015

y=-0.3587x - 0.1371, R =0.39 in 2016 and

y=-0.6648x + 0.143, R = 0.75 in 2017.

From the above equations, it is mathematically observed that the fitted slopes are not closer to the theoretical value of -1 for groundwater sampled from 2014-2015 and 2016. This shows that cation - exchange between calcium, magnesium and sodium is not the main possible hydrochemical process affecting the salinity of fewer boreholes developed in 2014 to 2015 and groundwater sampled during the rainy season. Similarly, the groundwater sampled in 2017 had a fitted slope approximately equal to -1. This suggests that cation - exchange between calcium, magnesium and sodium is the main hydrochemical processing controlling the salinity of groundwater during the dry season. The differences between the slopes and the theoretical value of -1 for the groundwater sampled from the aquifer of the Apollonian formation and the Birimian supergroup indicates that groundwater salinity is not affected by cation- exchange

processes, but other factors such rainfall as observed in the Piper and Gibbs diagrams and this will be further explained using stable isotopes of $\delta^{18}O$ and $\delta^{2}H$.

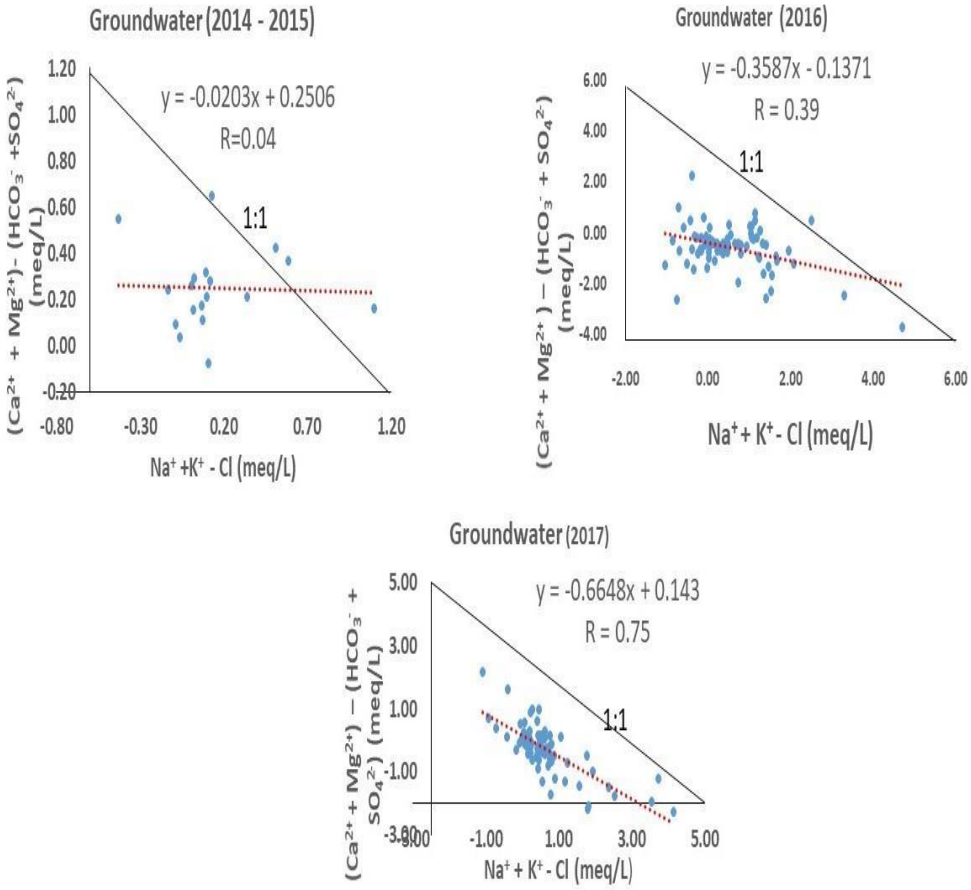

Figure 4. 44: Bivariate diagram for cation exchange reaction in groundwater sampled from the aquifer of the Apollonian formation and the Birimian supergroup.

4.3.4.2 Precipitation (Rainfall)

Further to the Gibbs diagram, another dominant factor controlling groundwater mineralization in the aquifer of the Birimian supergroup and the Apollonian formation is rainfall. The high rainfall amount (Fig 1.3 to 1.6) recorded and observations made by Edjah et al. 2015 indicates that rainfall influence the groundwater mineralization and that can increase Na^+ and Cl^- levels in the groundwater of the two aquifers (Hounslow, 1995).

Generally, evaporation causes an increase in the concentrations of chemical ions in groundwater and if it is dominant and no ions are precipitated, the Na^+/Cl^- ratio is unchanged

(Jankowski & Acworth, 1997). A plot of Na/Cl vs EC would also give a horizontal line, which suggests concentration by transpiration and evaporation.

In this study, the plot (Fig 4.47) illustrates a drop in Na/Cl ratio and decrease in EC in the groundwater sampled from 2014 – 2017. This is potentially from the loss of TDS and HCO_3^- due to rainfall recharge with short residence time. This explains why low TDS content was measured in all the groundwater samples taken from the aquifer of the Apollonian formation and the Birimian supergroup rocks.

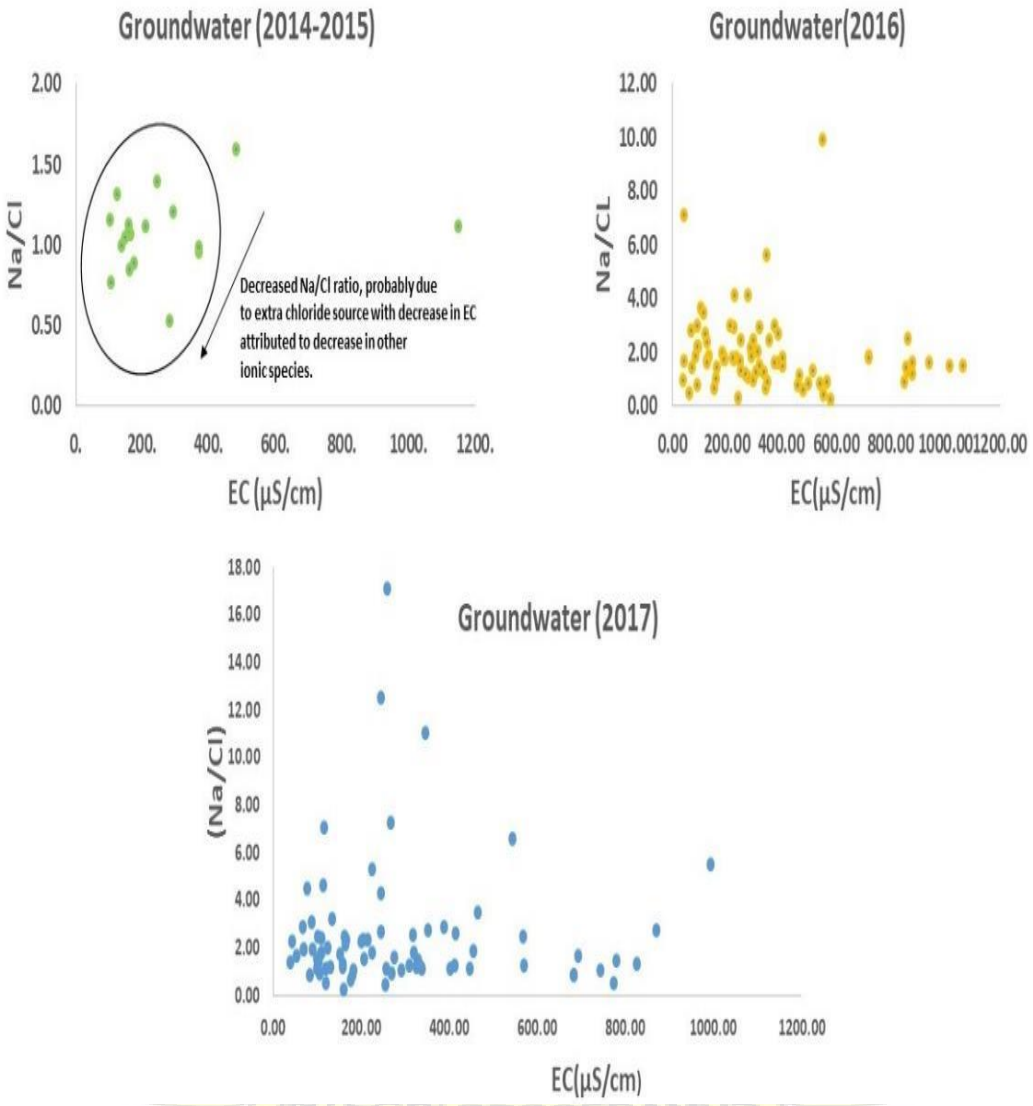

Figure 4. 45: Relationship between Na/Cl and EC in the sampled groundwater within the Lower Tano River Basin.

4.3.5. Hydrogeochemical modelling

In this study, the controls on natural chemistry of groundwater in the aquifer of the Apollonian formation and the aquifer of the Birimian supergroup is discussed using hydrochemical model (PHREEQC). Also, the chemical reactions in the various aquifer systems (Garrels & Mackenzie, 1971) are defined. One speciation in PHREEQC used in this study is the saturation indices (SI). The saturation indices (SI) are quantitative deviation of groundwater from equilibrium with respect to its dissolved minerals and its defined (Garrels & Mackenzie, 1971; Stumm & Morgan, 1981) as:

$$SI - Log\ \frac{IAP}{K_{sp}} \qquad Eq\ 4.19$$

Where Ksp is the thermodynamic equilibrium constant for the mineral at the measured temperature and *IAP* is the Ion Activity Product of the mineral-water reaction. A positive SI indicates that the solution is supersaturated with the occurrence of precipitation. A negative SI indicates that the solution is under- saturated with dissolution occurrences. An SI of ± 0.5 indicates equilibrium conditions. Considering the general geology (Fig 3.3 and 3.4) of the Lower Tano River Basin, Aragonite, Albite, Quartz, Amorphous Silica, Ca-Montmorillonite, Gibbsite, K-feldspar, K-mica, Kaolinite, Calcite, Dolomite, and Chalcedony are considered as possible mineral phases existing in the aquifer of the Apollonian formation and the Birimian supergroup.

To perform the hydrogeochemical modelling on the groundwater in both aquifers, cation-exchange between calcium and sodium are taken into consideration due to the essential processes of calcium and magnesium.

From the groundwater geochemical modelling, it is observed that the saturation index (SI) for carbonate minerals in almost all the groundwater samples are under-saturated with aragonite, dolomite, and calcite (Fig 4.48) except for three groundwater samples. The under saturation with respect to the above-mentioned minerals suggests that carbonates and silicate

minerals from the underlying geology have dissolved and weathered respectively without reaching equilibrium. This is due to short residence time, and a fast-flowing velocity (Halim et al., 2010). Also, the remaining three groundwater samples all taken from the aquifer of the Birimian supergroup rocks are saturated with aragonite. This indicates that calcium ion from silicate minerals (Hornblende, etc.) in the underlying geology have reached equilibrium. This is due to long residence time and a slow flowing velocity (Halim et al., 2010) due to highly fractured rocks of the Birimian.

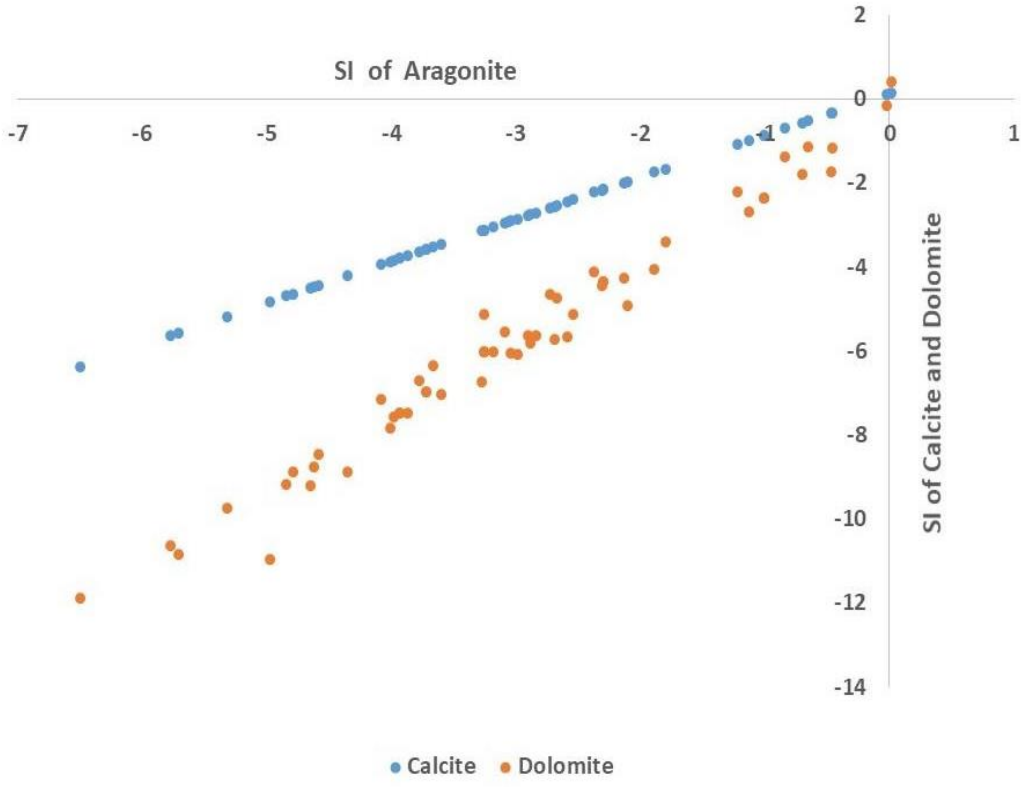

Figure 4. 46: Saturation index of carbonate minerals in the groundwater within the Lower Tano River Basin.

In fig 4.49, the saturation index of silicate minerals for most groundwater sampled in the aquifer of the Apollonian and the Birimian supergroup are undersaturated with chalcedony, quartz, and amorphous silica. This means that silica in the underlying geology exist in other forms and have not reached equilibrium due to short residence time and rainwater recharge (Halim et al., 2010). Additionally, four groundwater samples are supersaturated with chalcedony (Fig 4.49). The super saturation could be linked to input from excess silica from the underlying geology.

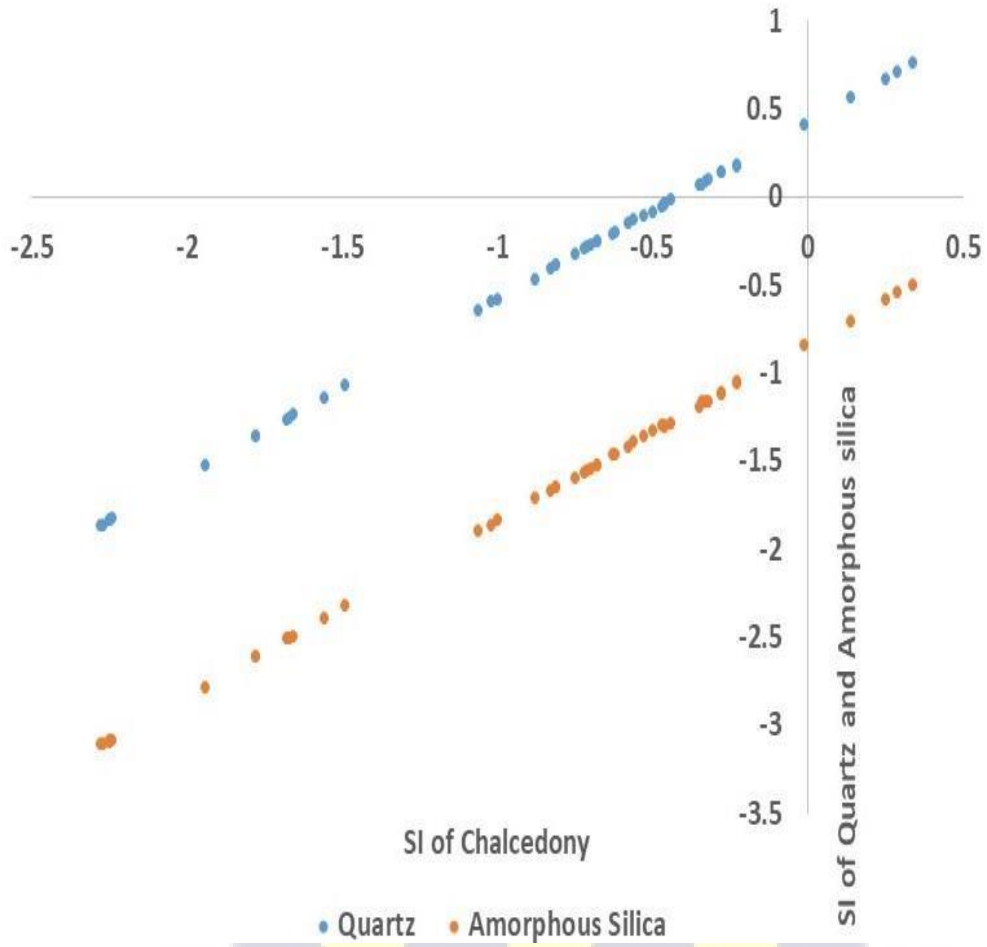

Figure 4. 47: Saturation index of silicate minerals in groundwater within the Lower Tano River Basin.

The saturation index (SI) for alumino- silicate minerals (Fig 4.50) in the groundwater is in the order of K– mica > kaolinite> gibbsite > Ca-montmorillonite > K feldspar. More variation is also noted in SI for all the alumino-silicate minerals in groundwater taken from the aquifer of the Apollonian formation and the Birimian supergroup. This suggests a possible differential intensities of rock weathering.

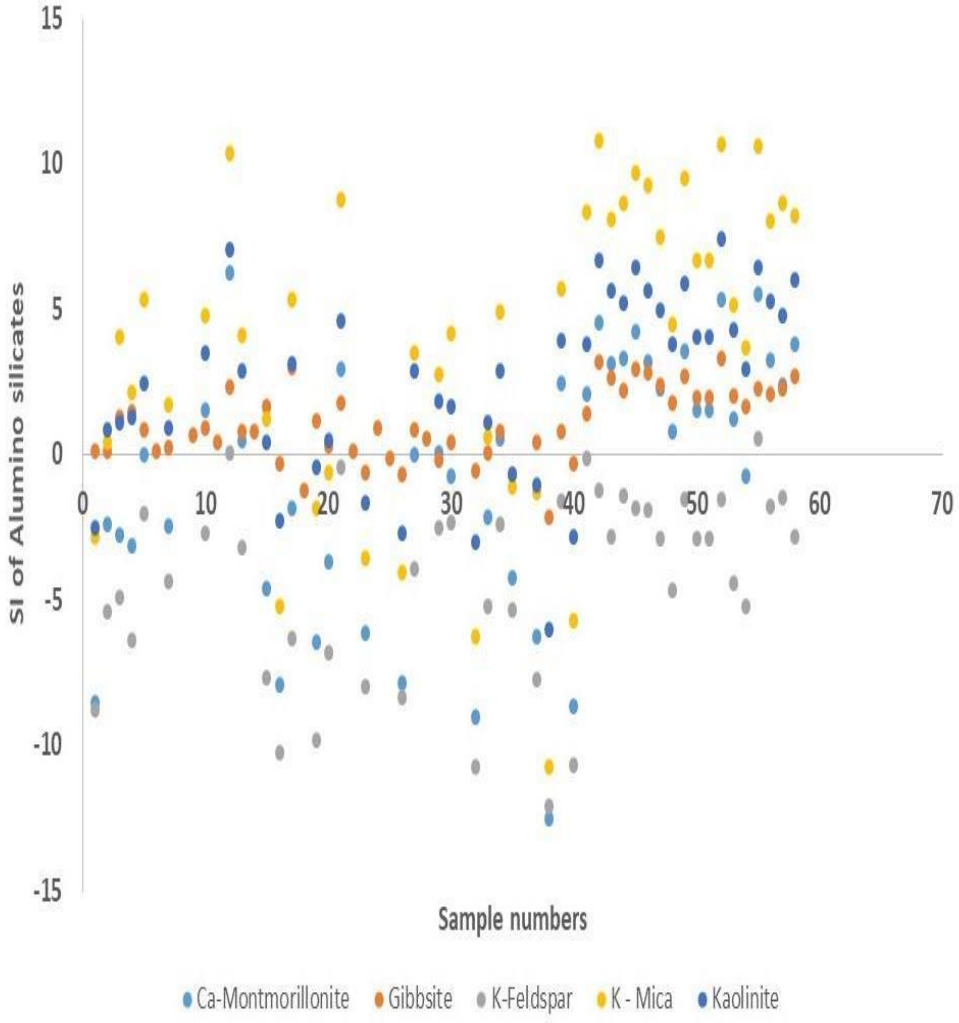

Figure 4. 48: Saturation index of alumino silicates in groundwater within the Lower Tano River Basin.

The activity ratio of the major ions in the groundwater sampled from both aquifer of the Apollonian formation and the Birimian supergroup are also plotted on mineral stability diagrams of

$CaAl_2Si_2O_8 + 2H^+ + 3H_2O \leftrightarrow Al_2Si_2O_5(OH)_4 + Ca^{2+} + H_4SiO_2$

$2NaAlSi_3O_8 + 2H^+ + 9H_2O \leftrightarrow Al_2Si_2O_5(OH)_4 + 2Na^+ + 4H_4SiO_2(aq)$ (Belkhiri et al., 2010). The stability diagrams (Fig 4.51a to 4.51d) will help understand the controls of natural chemistry of groundwater. From Figure 4.5a, calcium in 42 groundwater samples (n=58) with 22 taken from the aquifer of the Birimian supergroup and 20 taken from the aquifer of the

Apollonian formation lie in the kaolinite stability field. This suggests dilution of calcium ion. The calcium content in the remaining 16 groundwater samples all taken from the aquifer of the Apollonian formation plots in the gibbsite stability fields. This suggests that as Kaolinite is being formed, the pH of the groundwater is decreased (Belkhiri et al., 2010). This is another reason why some of the groundwater sampled from the aquifer of the Apollonian formation were acidic. Also, the flow of groundwater is unrestricted due to unconsolidated rocks of the Apollonian.

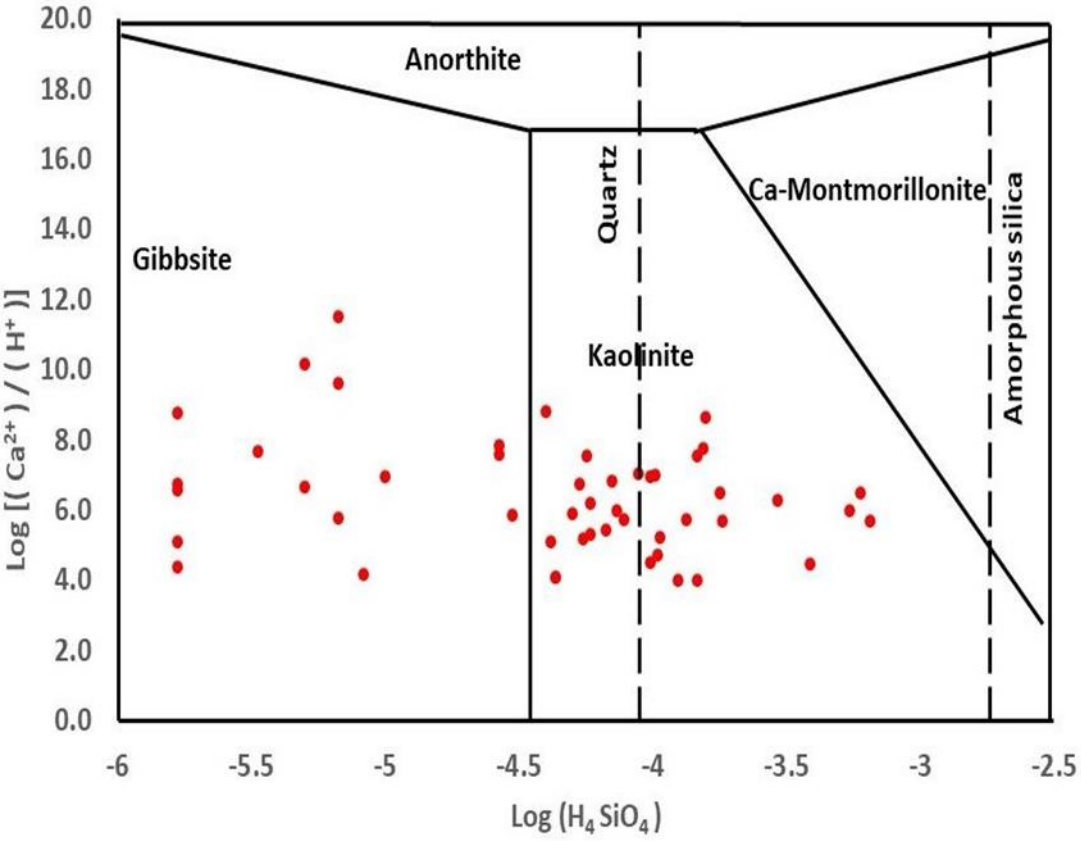

Figure 4.49a Calcium stability diagram for groundwater samples within the Lower Tano River Basin

Figure 4.51 b shows that magnesium in 20 groundwater samples taken from the aquifer of the Apollonian formation plots in the gibbsite stability field. This indicates that as Kaolinite is being formed the pH of the groundwater is reduced and the flow of groundwater is unrestricted due to unconsolidated rocks of the Apollonian. Also, the magnesium ion in 6 groundwater sampled from the aquifer of the Birimian supergroup plots in the Mg- montmorillonite stability

fields. This is due to the weathering of granites, hornblende etc. from the underlying geology. Also, the flow of groundwater is restricted due to highly fractured rocks of the Birimian. Additionally, magnesium in 32 groundwater samples from the aquifer of the Apollonian formation and the Birimian supergroup plots in the Kaolinite stability fields. This suggests dilution of Mg^{2+} ion.

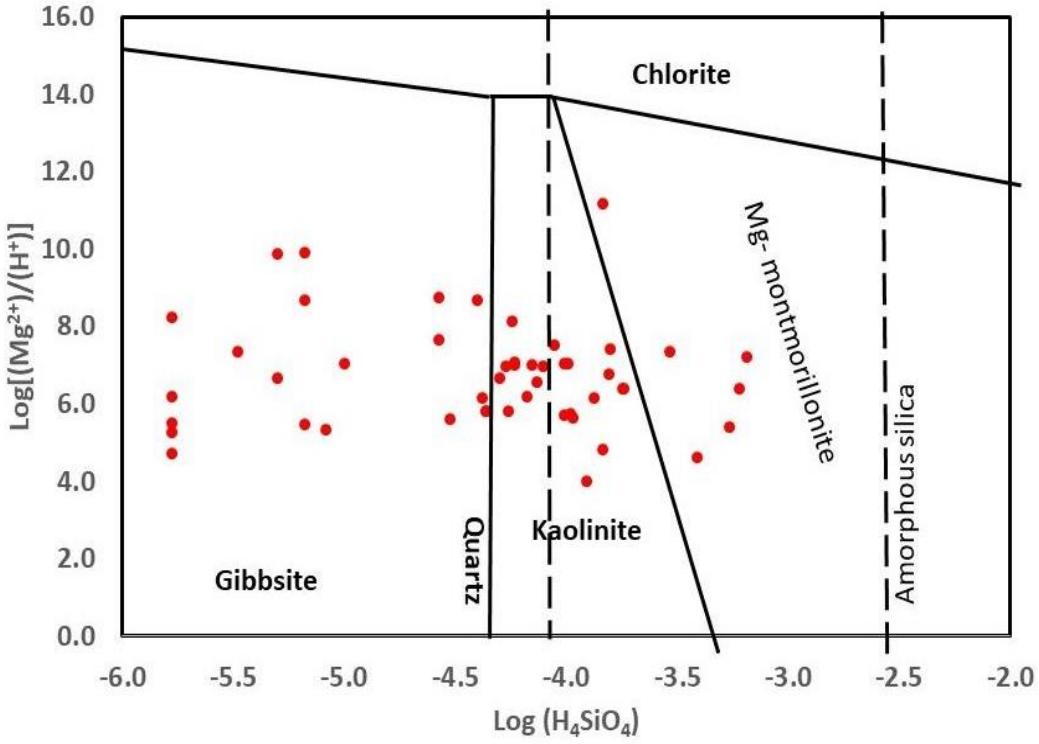

Figure 4.51b: Magnesium stability diagram for groundwater samples within the Lower Tano River Basin.

Fig 4.51c shows that potassium in 13 groundwater samples all taken from the aquifer of the Birimian supergroup rocks plots in the K-feldspar stability field. This suggests a possible dissolution of amorphous silica producing kaolinite. In addition, potassium in 40 groundwater samples both taken from the aquifer of the Apollonian formation and the Birimian supergroup plots in the muscovite stability field. This suggests dissolution of kaolinite and the formation of muscovite and K – feldspar. Potassium in 5 groundwater samples all taken from the aquifer of the Apollonian formation plots in the gibbsite stability fields indicating that the flow of water in the aquifer are unrestricted (thus initial stage of weathering) and have a short residence time resulting in very low mineralization thus possibly producing fresh groundwater.

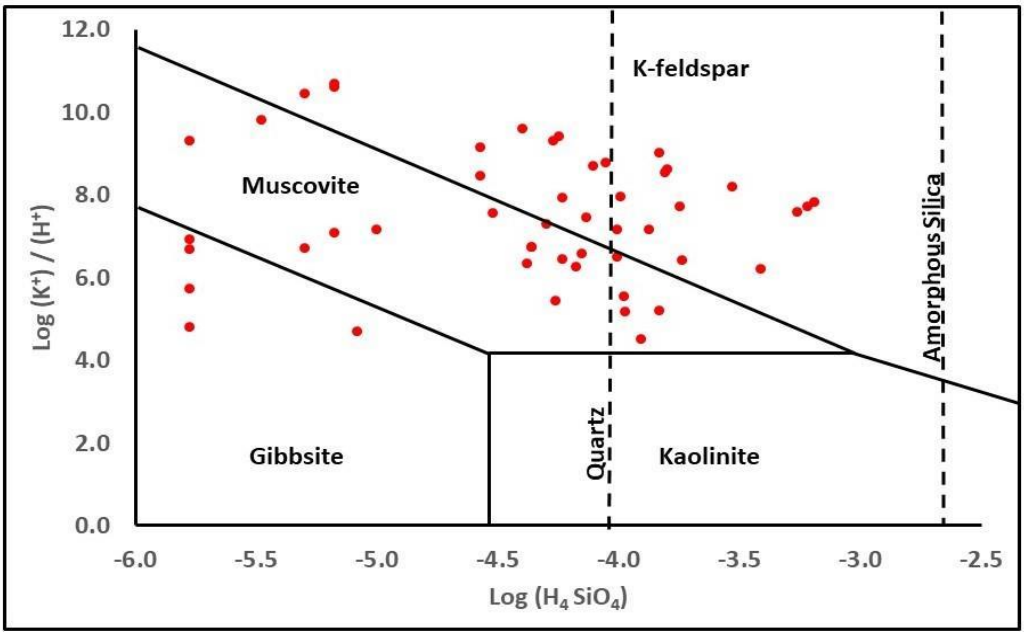

Fig 4.51c: Potassium stability diagram for groundwater samples within the study area.

Fig 4.51d also reveals that sodium in 13 groundwater samples all taken from the aquifer of the Apollonian formation plots in the gibbsite stability field suggesting the formation of Kaolinite with decreasing pH of the groundwater (Belkhiri et al., 2010) and the flow of groundwater is unrestricted. Also, sodium in 10 groundwater samples all taken in the aquifer of the Birimian supergroup rocks plots in the Na-Montmorillonite stability field. This suggests silicate minerals (hornblende, plagioclase, feldspar etc.) weathering. Also, the groundwater in the Na-montmorillonite fields indicate that the flow of groundwater is restricted due to highly fractured rocks of the Birimian and decreased interconnection between the fractures that control the movement of groundwater in the aquifer of the Birimian super group. Both Mg – montmorillonite and Na- montmorillonite in the aquifer of the Apollonian formation and the Birimian super group reveals longer residence time with high degree of rock-water interactions. In addition, sodium in 35 groundwater samples plots in the Kaolinite stability fields. This indicates a probable dilution of sodium ion concentration and a decrease in pH in the groundwater.

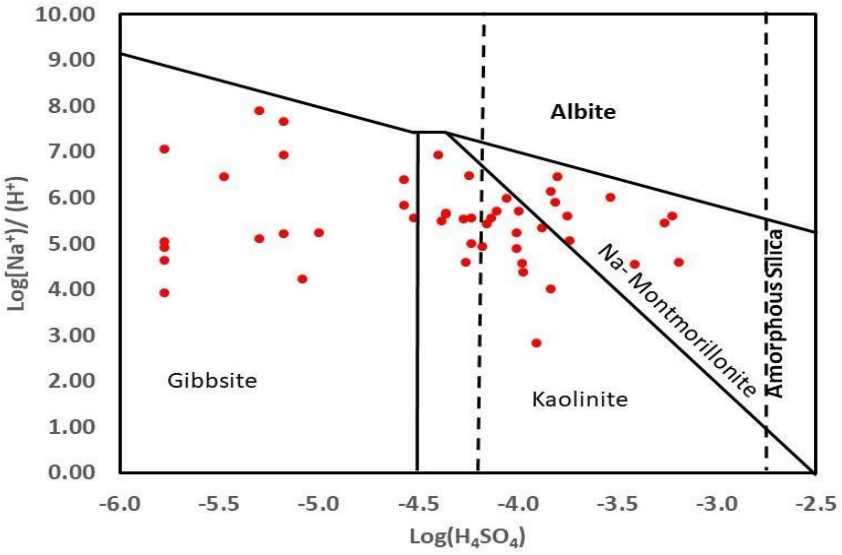

Fig 4.51d: Sodium stability diagram for groundwater samples in the study area.

The diagram (Fig 4.51a to Fig 4.51d) reveals kaolinite stability field as the most dominant followed by gibbsite and montmorillonite. The dominance of Kaolinite in the sampled groundwater indicates that infiltrating water enhanced by soil CO_2 might possibly reacts with limestone and clay minerals from the aquifer of the Apollonian formation and silicate minerals particularly plagioclase feldspar, biotite etc. from the aquifer of the Birimian super group. The infiltrating water releases Ca^{2+}, Mg^{2+}, Na^{+} and HCO_3^{-}, resulting in a more silica-rich clay mineral imitative of the clay minerals and silicate minerals contained in the aquifer of the Apollonian formation and the Birimian super group, respectively. This infers that incongruent dissolution controls the natural chemistry of groundwater in the aquifer of the Apollonian formation and the Birimian supergroup of the Lower Tano River Basin.

This is explained further using HCO_3^{-} and SiO_2 ratio (Hounslow, 1995). In this ratio, silicate weathering releases a considerable amount of silica into groundwater, since carbonate dissolution will not release silica into the groundwater. Hence, groundwater with HCO_3^{-} / $SiO_2 > 10$ suggests carbonate mineral weathering as the dominant factor controlling the natural chemistry of the groundwater, whiles groundwater with HCO_3^{-} / $SiO_2 < 10$ shows silicate weathering as the dominant factor controlling the natural groundwater chemistry. The computed values are shown in table 4.57.

Table 4. 57: Values and HCO_3^- / SiO_2 values showing the dominant weathering activity of groundwater within the Lower Tano River Basin.

Sample number	HCO_3^-	SiO_2	Na^+	K^+	Cl^-	HCO_3^-/SIO_2	$SIO_2/Na^+ + K^+ - Cl^-$	SIy = SIg-SI k
1	48.77	-3.08	32.94	18.66	45.99	-15.83	-0.55	2.66
2	12.19	-1.36	11.94	0.56	12.00	-53.79	-2.71	-0.75
3	60.96	-2.39	17.32	13.19	23.99	-25.51	-0.37	0.18
4	58.52	-2.49	13.73	1.58	4.00	-23.50	-0.22	0.18
5	21.95	-1.29	33.63	17.35	45.99	-17.02	-0.26	-1.61
6	121.92	BDL	32.70	1.14	19.99	0.00	0.00	0.13
7	60.96	-1.46	21.46	8.34	14.00	-41.75	-0.09	-0.66
8	85.34	-3.10	77.82	36.59	89.97	-27.53	-0.13	0
9	60.00	BDL	16.55	0.82	8.00	0.00	0.00	0.69
10	19.51	-0.84	7.67	0.74	6.00	-23.22	-0.35	-2.59
11	75.00	BDL	10.80	3.57	25.99	0.00	0.00	0.44
12	39.01	-0.50	37.10	0.70	41.99	-78.02	0.12	-4.71
13	24.38	-1.06	11.73	1.14	33.99	-23.00	0.05	-2.04
14	14.63	BDL	7.55	1.53	4.00	0.00	0.00	0.83
15	219.45	-3.09	17.03	0.82	4.00	-71.02	-0.22	1.2
16	14.63	-2.50	11.13	0.33	19.99	-5.85	0.29	1.97
17	26.82	-3.10	13.79	2.12	16.00	-8.65	36.45	-0.14
18	24.38	BDL	14.69	1.43	19.99	0.00	0.00	-1.24
19	20.00	-3.08	5.94	0.74	4.00	-6.49	-1.15	1.61
20	36.58	-1.71	24.57	2.99	14.00	-21.39	-0.13	-0.2
21	353.56	-1.16	34.05	8.06	31.99	-304.79	-0.11	-2.8
22	121.92	BDL	32.70	1.14	19.99	0.00	0.00	0.13
23	12.19	-1.89	11.08	0.66	17.99	-6.45	0.30	1.05
24	231.64	BDL	100.10	37.45	55.98	0.00	0.00	0.94
25	48.77	BDL	44.98	7.45	55.98	0.00	0.00	-0.12
26	17.07	-2.32	45.02	7.61	57.98	-7.36	0.43	1.99
27	110.00	-1.11	22.06	3.56	21.99	-99.10	-0.31	-2.01
28	14.63	BDL	32.18	6.94	53.98	0.00	0.00	0.54
29	34.14	-0.58	10.04	0.78	17.99	-58.86	0.08	-2.01
30	75.00	-1.29	10.80	3.57	25.99	-58.14	0.11	-1.2
31	70.00	-1.12	13.34	0.76	12.00	-62.50	-0.53	0
32	9.75	-2.61	6.47	0.75	6.00	-3.74	-2.13	2.45
33	2.44	-1.16	73.00	8.30	133.96	-2.10	0.02	-1.05
34	24.38	-1.05	24.15	6.53	25.99	-23.22	-0.22	-2.05

35	17.07	-1.32	45.02	7.61	57.98	-12.93	0.25	0
36	34.14	-1.83	8.33	0.80	12.00	-18.66	0.64	0
37	14.63	-2.61	32.18	6.94	53.98	-5.61	0.18	1.48
38	2.44	-2.50	17.24	1.79	21.99	-0.98	0.84	3.85
39	24.38	-0.54	11.73	1.14	33.99	-45.15	0.03	-3.09
40	50.00	-2.78	7.56	0.19	6.00	-17.99	-1.59	2.52
41	197.64	-1.19	156.00	13.70	224.00	-166.08	0.02	-2.39
42	46.36	-1.52	13.30	2.60	19.80	-30.50	0.39	-3.5
43	37.82	-1.52	13.90	1.00	26.20	-24.88	0.13	-2.99
44	91.50	-1.30	11.30	1.50	35.10	-70.38	0.06	-2.99
45	17.08	-1.42	7.30	0.80	10.00	-12.03	0.75	-3.47
46	47.58	-1.67	5.60	2.60	8.40	-28.49	8.35	-2.82
47	28.06	-1.59	12.00	1.70	17.60	-17.65	0.41	-2.57
48	10.98	-1.56	16.40	0.20	25.30	-7.04	0.18	-2.01
49	31.72	-1.46	22.80	6.00	30.00	-21.73	1.22	-3.15
50	197.64	-1.65	3.00	0.90	5.50	-119.78	1.03	-2.04
51	192.76	-1.65	3.10	0.90	5.50	-116.82	1.10	-2.04
52	23.18	-1.28	17.30	1.70	36.00	-18.11	0.08	-4.1
53	7.32	-1.54	9.90	0.50	22.70	-4.75	0.13	-2.29
54	6.10	-1.86	18.80	1.30	31.30	-3.28	0.17	-1.3
55	208.62	-0.70	21.60	2.80	25.50	-298.03	0.64	-4.2
56	21.96	-1.16	14.50	2.00	22.90	-18.93	0.18	-3.16
57	28.06	-1.55	19.60	8.90	27.10	-18.10	-1.11	-2.52
58	31.72	-1.39	7.70	0.20	10.70	-22.82	0.50	-3.28

From table 4.57, it is seen that silica in the sampled groundwater ranges from BDL (below detection limit) to 38.83 mg/L. All the groundwater samples had HCO_3^-/ SiO_2 less than 10. The computed HCO_3^-/ SiO_2 reveals rock weathering as the main geochemical process contributing to the formation of kaolinite in the aquifer of the Apollonian formation and the Birimian supergroup and it's in line with the Gibbs (1970) diagram illustrated in previous chapters. Also computed SiO_2 / (Na^+ + K^+ - Cl^-) ratio indicates that 98% of the sampled groundwater (n=58) are less than 1, suggesting cation-exchange reaction as the significant processes through which Na^+ enters the groundwater in both aquifers.

To identify the intensity of weathering, the difference in saturation index of gibbsite to that of the saturation index of K-feldspar (SIy = SIg – SIk) is calculated (Table 4.57). This was done to identify the zones of recharge (initial stage of weathering) and the zones of discharge (intensive weathering) (Chidambaram et al., 2012). Based on the SIy values, the groundwater is classified into initial, transitional, and final stages of weathering. Positive SIy values suggest initial stage of weathering, negative SIy values suggests final stage of weathering and SIy values near zero suggest transitional stage of weathering. In Figure 4.52, it is seen that groundwater mostly located in the aquifer of the Birimian supergroup with few in the aquifer of the Apollonian formation represented by shades of red and orange colour are regions of possible recharge or initial stages of weathering. Discharge zones or final stages of weathering are seen in groundwater situated mostly in the aquifer of the Apollonian formation with few in the aquifer of the Birimian super group. This groundwater is represented by different shade of colours except red and orange. The differences between the rock – water interactions in the groundwater are attributed to different lithological conditions of the aquifer of the Apollonian and the Birimian supergroup rocks and rainfall.

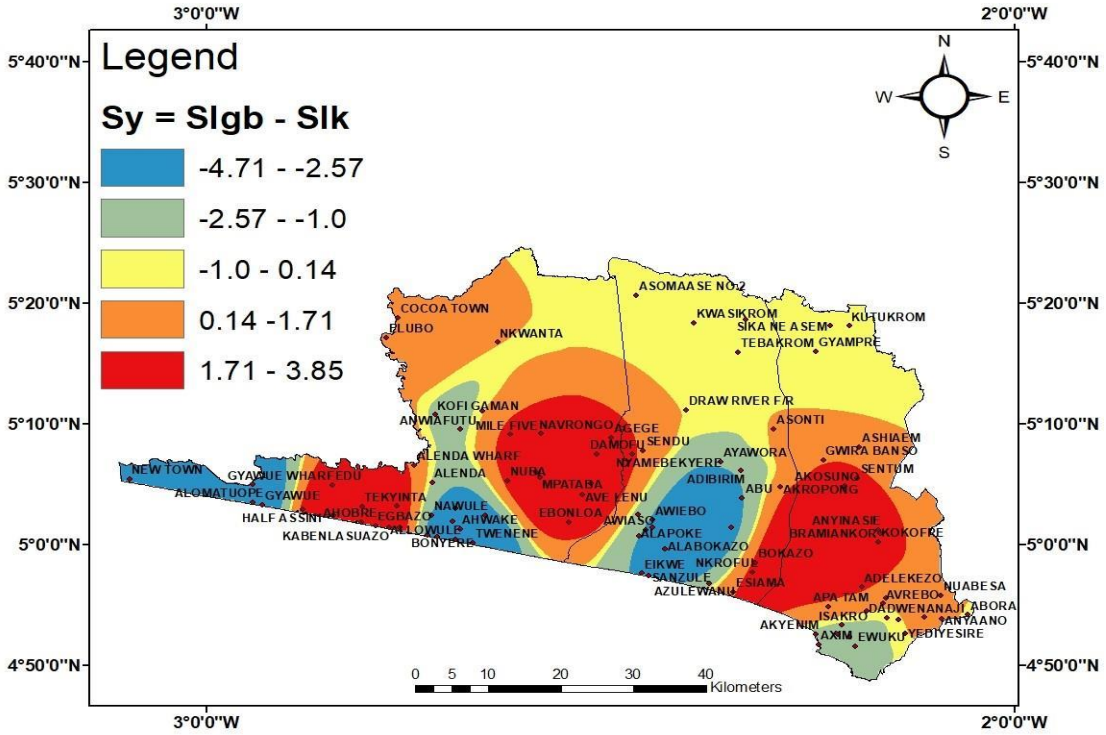

Figure 4. 50: Spatial distribution map of SI (Gibbsite – K-feldspar) in the sampled groundwater within the Lower Tano River Basin.

4.3.5 Sub -Conclusions

From the above results, it is observed that Na-Cl type of groundwater was predominant in the aquifer of the Apollonian formation and the Birimian supergroup. In addition, rock-water interactions, rainfall, ion exchange processes, and incongruent dissolution are the predominant processes that took place in both aquifers. The mineral stability diagrams indicates that Kaolinite was the most stable mineral in the aquifer of the Apollonian formation and the Birimian supergroup. This therefore enhanced ion exchange processes in the groundwater of the study area due to kaolinite having a low cation-exchange capacity of 1-15 meq/100 g (Appelo & Postma, 2005).

4.4. Sources of Recharge to the aquifer system

The role of $\delta^{18}O$ and $\delta^{2}H$ as an effective tracer can efficiently define the interrelationships between surface water and groundwater (Yurtsever & Gat, 1981). It can also assist in identifying the sources of groundwater recharge. Hence in these studies, the sources of recharge and recharge mechanism is identified using $\delta^{18}O$ and $\delta^{2}H$ compositions in rainwater,

rivers, streams, hand dug wells and boreholes sampled in 2016 and 2017. The isotopic composition data for groundwater sampled in 2013 and from 2014 to 2015 was not measured due to technical issues beyond control.

4.4.1 Isotopic composition ($\delta^{18}O$ and $\delta^{2}H$) in Rainwater

The statistical summary of the isotopic compositions ($\delta^{18}O$ and $\delta^{2}H$) and deuterium excess (d-excess) in rain water sampled in January, February, March, August, and December 2016(rainy season) and 2017 (dry seasons) is shown in Table 4.58. That of April, May, June, July, September, October, and November 2016 and 2017 is shown in Table 4.59.

Table 4. 58: Statistical summary of stable isotope composition in rainfall sampled in January, February, March, August,and December (2016 and 2017) within the Lower Tano River Basin.

Parameters	$\delta^{18}O$	$\delta^{2}H$	*d -excess*
Number of samples	24	24	24
Mean	-0.51	7.74	11.84
Standard Error	0.19	1.65	0.70
Median	-0.39	8.40	12.10
Mode	-0.33	11.72	14.32
Standard Deviation	0.95	8.07	3.44
Sample Variance	0.90	65.17	11.81
Kurtosis	-0.18	-0.21	-0.07
Skewness	-0.69	-0.32	0.08
Minimum	-2.64	-9.53	6.35
Maximum	0.80	22.00	20.00
Sum	-12.29	185.84	284.16
Confidence Level (95.0%)	0.40	3.41	1.45

Table 4. 59: Statistical summary of stable isotope composition in rainfall sampled in April, May, June, July, September, October, and November (2016 and 2017) within the Lower Tano River Basin.

Parameters	$\delta^{18}O$	$\delta^{2}H$	*d- excess*
Number of samples	38	38	38
Mean	-1.75	-2.67	11.30
Standard Error	0.16	1.34	0.39
Median	-1.85	-4.22	11.17
Mode	-1.02	-0.62	8.73
Standard Deviation	0.99	8.25	2.39
Sample Variance	0.97	67.98	5.73
Kurtosis	0.81	1.51	-0.40
Skewness	0.46	0.63	0.19
Minimum	-3.91	-23.11	6.33
Maximum	0.51	18.00	16.00
Sum	-66.35	-101.30	429.52
Confidence Level (95.0%)	0.32	2.71	0.79

From Table 4.58, the isotopic composition in rain water sampled in January, February, March, August, and December 2016 and 2017 during the dry seasons ranges from -2.64 to 0.80 for $\delta^{18}O$‰ V-SMOW with a mean of -0.51 V-SMOW. That of $\delta^{2}H$ ‰ V-SMOW values range between -9.53 and 22.0 with a mean of 7.74. From table 4.59, the isotopic compositions in rainwater sampled in April, May, June, July, September, October, and November 2016 and 2017 during the wet season ranges from -3.91 to 0.59 ‰ V- SMOW for δ^{18} O with a mean of -1.75 ‰ V-SMOW. That of δ^{2} H varies from -23.11 to 18‰ V-SMOW with a mean of -2.67 ‰. The linear relationship between δ^{2} H and δ^{18} O with a correlation coefficient of 0.9 for the rains sampled in January, February, March, August, and December is given by

δ^{2} H = 7.69 δ^{18} O + 11.68 (Fig 4.53a)

And that of April, May, June, July, September, October, and November is given by

δ^{2} H = 8δ^{18}O + 11.31. (Fig 4.53b)

The slopes for January, February, March, August, and December, and April, May, June, July, September, October, and November are virtually identical to the global meteoric water line (GMWL of Craig, 1961) of 8 and the local meteoric water line (LMWL of Akiti, 1986) of 7.86. Nevertheless, the intercepts are above the GMWL of 10 and below the LMWL of 13.61. The intercepts for January, February, March, August, and December, and April, May, June, July, September, October, and November (2016 and 2017) are different from the GMWL and the LMWL (Akiti, 1986). This is due to the differences in climatic conditions.

The deuterium excess in rainwater sampled in April, May, June, July, September, October, and November ranges from 6.33‰ to 16‰ V-SMOW with a mean of 11.30‰ and that of January, February, March, August, and December varied from 6.35‰ to 20.0‰ V-SMOW with a mean of 11.84‰.

More depleted isotopic composition ($\delta^{18}O$ and $\delta^{2}H$) in rainwater sampled in April, May, June, July, September, October, November was greater than rainwater sampled in January, February,

March, August, and December. The effects of low rainfall amount over January, February, March, August, and December might have caused the enrichment of oxygen and hydrogen isotope signatures in the sampled rainwater. Similarly, the effects of high rainfall amount over April, May, June, July, September, October and, November might cause the significant depletion of oxygen and hydrogen isotopes in the sampled rainwater.

Since the study area is known for high rainfall amount, it is likely that the sources of surface water and groundwater might be derived from the local rains with depleted isotopic compositions (Yurtsever & Gat, 1981). To prove this the rainfall regression lines obtained in this study together with the local meteoric water line (LMWL) of Ghana (Akiti, 1986) and the global meteoric water line (GMWL) (Craig, 1961) is used as reference lines in investigating the sources of surface water and groundwater recharge within the Lower Tano River Basin.

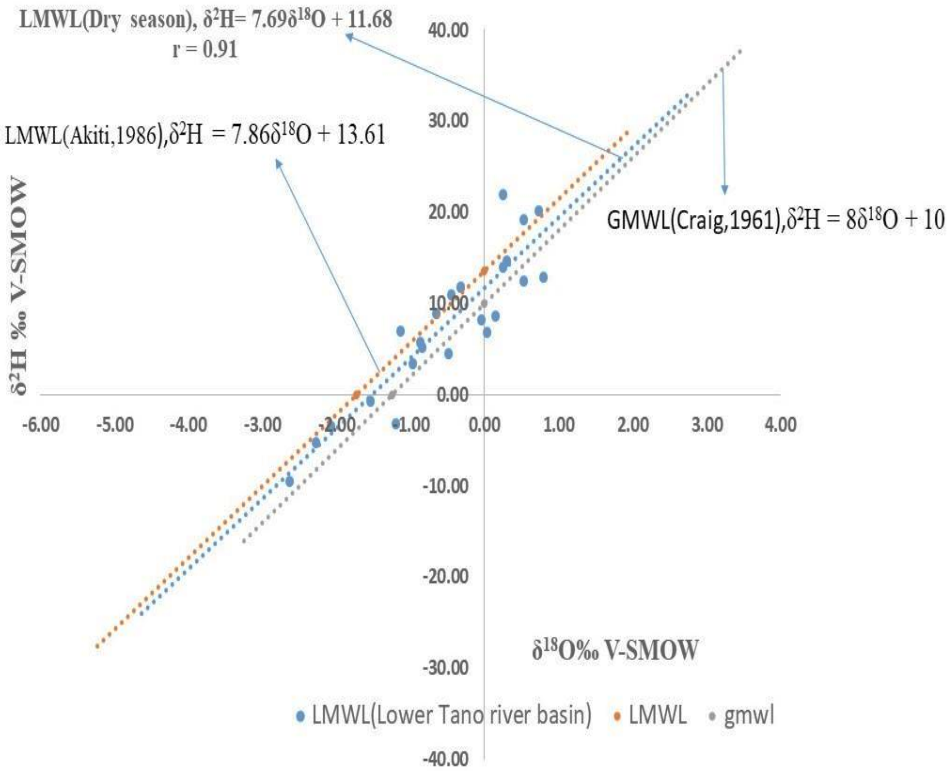

Figure 4. 51a Schematic plot of δ^2H versus $\delta^{18}O$ for rainfall sampled in January, February, March, Aug, September, and December, 2016 and 2017.

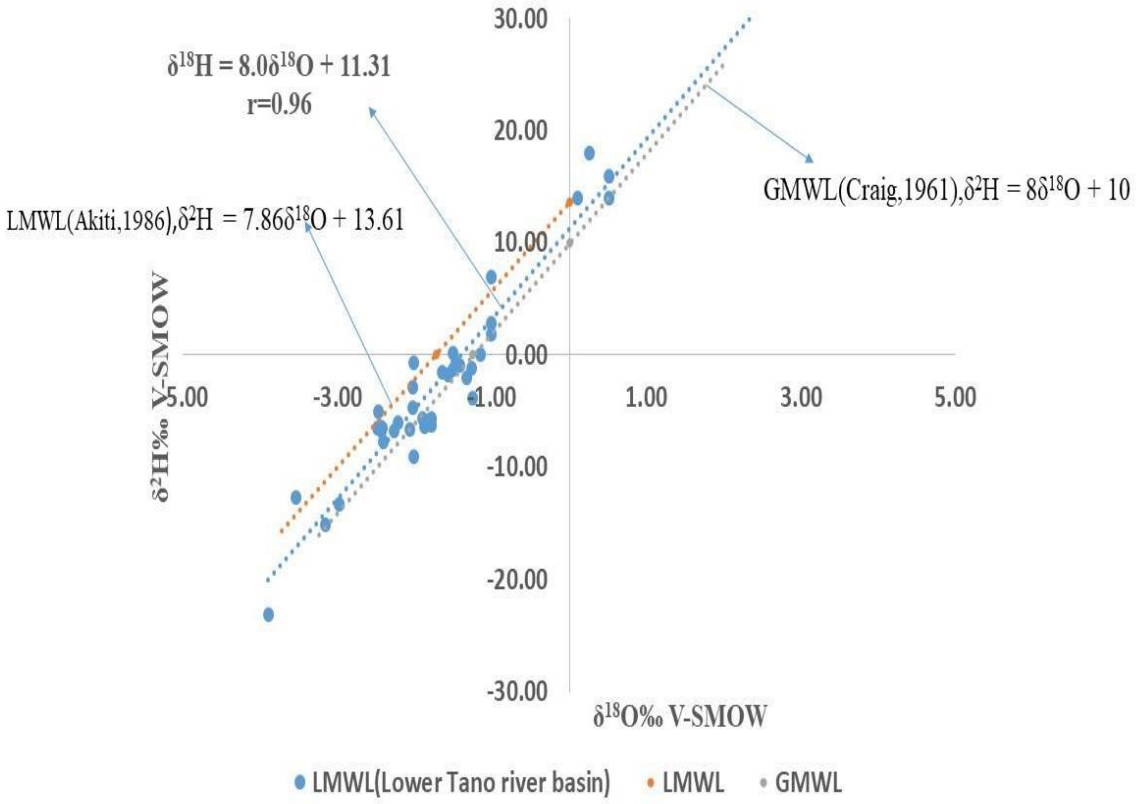

Figure 4.53b: Schematic plot of δ^2H versus $\delta^{18}O$ for rainfall sampled in April, May, June, July, October, November 2016 and 2017

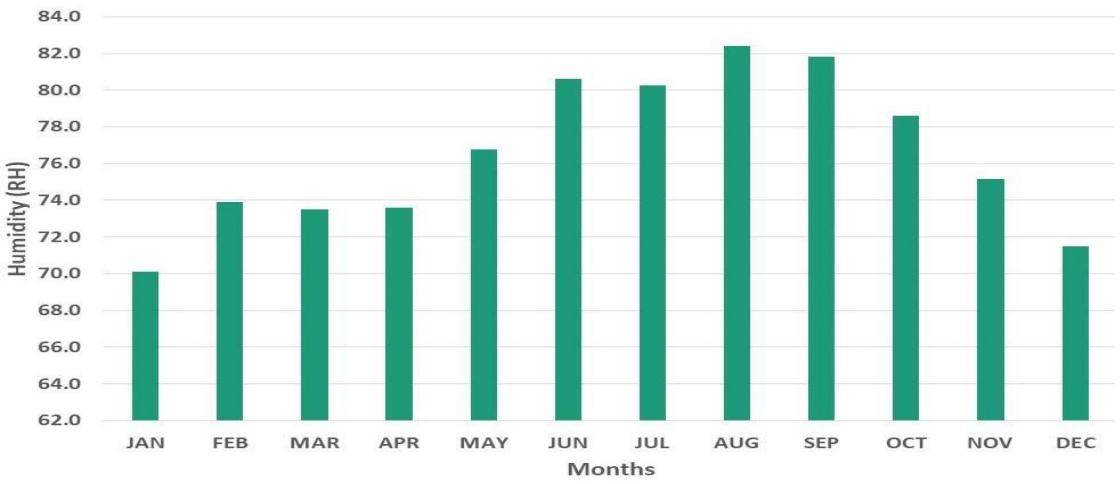

Figure 4. 52: Average monthly humidity in the study area from 2006 to 2017 (Data from Ghana Meteorological Authority)

4.4.2. Isotopic Composition ($\delta^{18}O$ and $\delta^{2}H$) in Rivers

Table 4. 60: Statistical summary of stable isotope composition in Rivers sampled in 2016 and 2017 within the Lower Tano River Basin.

	2016			*2017*		
Parameters	$\delta^{18}O$	$\delta^{2}H$	d- excess	$\delta^{18}O$	$\delta^{2}H$	d- excess
Number of samples	9	9	9	14	14	14
Mean	-2.11	-5.93	10.96	-0.67	1.35	6.74
Standard Error	0.17	0.97	0.76	0.42	1.47	2.08
Median	-2.19	-6.20	11.27	-1.29	0.43	9.10
Mode	N/A	N/A	N/A	N/A	N/A	N/A
Standard Deviation	0.50	2.92	2.27	1.57	5.48	7.79
Sample Variance	0.25	8.54	5.13	2.46	30.08	60.67
Kurtosis	4.12	-0.71	1.53	3.08	0.21	3.55
Skewness	1.70	0.33	-1.16	1.73	0.80	-1.97
Minimum	-2.72	-10.01	6.17	-2.17	-5.20	-14.32
Maximum	-0.94	-1.35	13.36	3.51	13.76	12.57
Sum	-19.00	-53.35	98.66	-9.43	18.93	94.37
Confidence Level (95.0%)	0.39	2.25	1.74	0.91	3.17	4.50

The $\delta^{18}O$ of the sampled rivers in 2016 and 2017 ranges from -2.72 ‰ to −0. 94 ‰ with a mean of -2.11‰ and from -2.17 ‰ to 3.51 ‰ V-SMOW with a mean of -0.67 ‰, respectively (Table 4.60). The $\delta^{2}H$ of the rivers sampled in both 2016 and 2017 varies between -10.01 ‰ and - 1.35 ‰V-SMOW with a mean of -2.11 and from -5.20 ‰ to 13.76 ‰ V-SMOW with a mean of 1.35 respectively. Also, the deuterium excess for the rivers in both 2016 and 2017 ranges from 6.17‰ to 13.36‰ with a mean of 10.96‰ and from -14.32‰ to 12.57‰ with a mean of 6.74, respectively. The equation of the local evaporation line of the rivers (Fig 4.55) is

$\delta^{2}H = 3.75\delta^{18}O + 3.14.$

In addition, the regression line for the rivers sampled in both 2016 and 2017 is

$\delta^{2}H = 4.8\ \delta^{18}O + 4.3$ (2016).

$\delta^{2}H = 3.2\ \delta^{18}O + 3.5$ (2017).

The slopes of the regression lines in both 2016 and 2017 are below the slopes of the GMWL and the LMWL and the regression line for January, February, March, August, and December (dry

seasons) and April, May, June, July, September, October, and November (wet season). Since the slope of the regression line for the rivers sampled in 2016 and 2017 are below the slopes of the GMWL and the LMWL's, it can be said that the isotopic composition of the rivers is affected by evaporation.

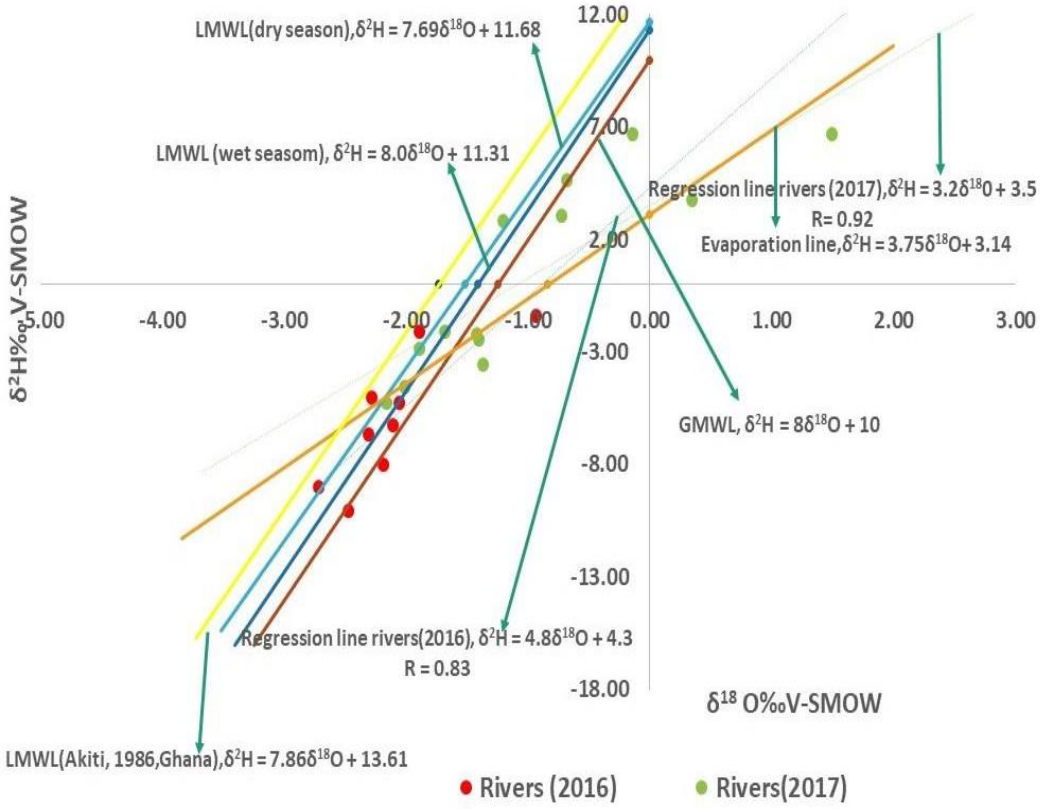

Figure 4. 53: Isotopic compositions in the rivers sampled in 2016 and 2017 within the Lower Tano River Basin.

4.4.3. Isotopic Composition ($\delta^{18}O$ and $\delta^{2}H$) in Streams

Table 4. 61: A statistical summary of the isotopic compositions of the streams sampled in 2016 and 2017.

	2016			*2017*		
Parameters	$\delta^{18}O$	$\delta^{2}H$	d-excess	$\delta^{18}O$	$\delta^{2}H$	d-excess
Number of samples	15	15	15	15	15	15
Mean	-2.36	-6.70	12.24	-1.23	-0.24	9.57
Standard Error	0.32	1.28	1.40	0.18	0.98	0.81
Median	-2.03	-5.67	10.39	-1.53	0.06	10.77
Mode	N/A	N/A	N/A	N/A	N/A	N/A
Standard Deviation	1.25	4.96	5.43	0.71	3.81	3.12
Sample Variance	1.57	24.56	29.51	0.50	14.51	9.75
Kurtosis	2.64	0.86	3.09	2.91	3.73	0.41
Skewness	-1.82	-1.32	1.96	1.68	1.44	-0.94
Minimum	-5.31	-17.20	7.37	-1.88	-5.74	2.95
Maximum	-1.07	-1.22	25.68	0.70	10.43	14.54
Sum	-35.37	-100.50	183.62	-18.40	-3.60	143.59
Confidence Level (95.0%)	0.69	2.74	3.01	0.39	2.11	1.73

For the isotopic compositions, $\delta^{18}O‰$ V-SMOW in the streams sampled in 2016 vary from -5.31 to -1.07 with a mean of -2.3 and that of 2017 ranges from -1.88 to 0.70 with a mean of -1.23 (Table 4.61). Likewise, $\delta^{2}H$ ‰ V-SMOW in the streams sampled in both 2016 and 2017, ranges from - 17.20 to -1.22 with a mean of -6.70 and -5.74 to 10.43 with a mean of -0.24 respectively. The deuterium excess in the streams varies from 7.37‰ to 25.68‰ V-SMOW with a mean of 12.24 V-SMOW in 2016 and from 2.95‰ to 14.54‰ V-SMOW with a mean of 9.57 V- SMOW in 2017.

The equation of the local evaporation line for the streams as shown in Fig (4.56) is

$\delta^{2}H = 4.42\delta^{18}O + 4.46.$

In addition, the regression line for the streams sampled in both 2016 and 2017 is

$\delta^{2}H = 3.81\ \delta^{18}O + 2.28$ (2016) and $\delta^{2}H = 4.59\ \delta^{18}O + 5.39$ (2017), respectively.

The slope for the regression lines in both 2016 and 2017 was less than the slope for the GMWL, the LMWL (Akiti, 1986) and the rainfall regression lines for both dry and wet season of the study area. Significant differences are seen in the oxygen and hydrogen isotope signatures in the stream, rivers, and rainwater. The forested canopies around the streams prevented a possible evaporation and this caused the isotopic compositions of the streams to be more depleted than the rivers. The mean and median of oxygen and hydrogen isotope compositions in the streams and rivers are also slightly similar. This has explained why a hydraulic relationship existed between the streams and the rivers sampled in 2017.

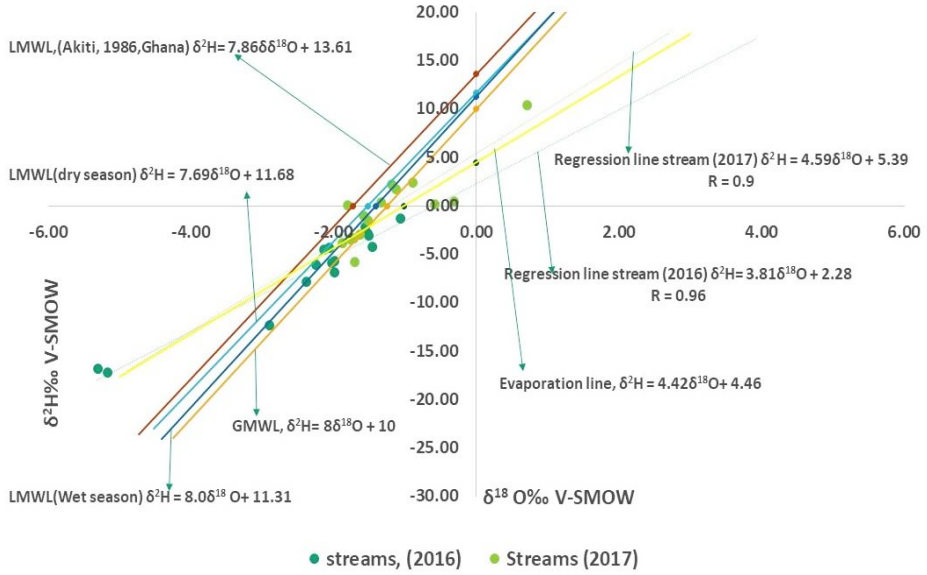

Figure 4. 54: Isotopic compositions in the streams sampled in 2016 and 2017.

4.4.4. Isotopic Composition ($\delta^{18}O$ and $\delta^{2}H$) in Lagoons.

Table 4. 62: A statistical summary of the isotopic compositions of the Lagoons sampled in 2016 and 2017.

	2016			*2017*		
Parameters	$\delta^{18}O$	$\delta^{2}H$	d - excess	$\delta^{18}O$	$\delta^{2}H$	d - excess
Number of samples	3	3	3	3	3	3
Mean	-1.17	-2.27	7.12	-1.00	0.98	8.95
Standard Error	0.37	1.46	1.52	0.15	0.99	0.36
Median	-1.43	-2.77	8.61	-1.06	0.06	8.64
Mode	N/A	N/A	N/A	N/A	N/A	N/A
Standard Deviation	0.63	2.53	2.63	0.26	1.72	0.63
Sample Variance	0.40	6.39	6.90	0.07	2.95	0.40
Kurtosis	0.00	0.00	0.00	0.00	0.00	0.00
Skewness	1.52	0.86	-1.73	1.03	1.72	1.68
Minimum	-1.64	-4.51	4.09	-1.22	-0.08	8.54
Maximum	-0.45	0.47	8.66	-0.71	2.96	9.68
Sum	-3.52	-6.81	21.36	-2.99	2.94	26.86
Confidence Level (95.0%)	1.57	6.28	6.52	0.65	4.26	1.57

The $\delta^{18}O$‰ V-SMOW compositions in the Lagoon sampled in both 2016 and 2017 varies from -1.64 to -0.45 with a mean of 1.17 and from -1.22 to -0.71 with a mean of -1 respectively. That of $\delta^{2}H$ ‰ V-SMOW in the Lagoon ranges from -4.51 to 0.47 with a mean of -2.27 in 2016 and from -0.08 to 2.96 with a mean of 0.98 in 2017. Figure 4.57 shows the relationship between $\delta^{2}H$ and $\delta^{18}O$ for the sampled Lagoons.

Similarly, the deuterium excess for the lagoon sampled in both 2016 and 2017 varies from 4.09‰ to 8.66‰ with a mean of 7.12 and from 8.54 ‰ to 9.68 ‰ with a mean of 8.95

respectively. The equation of the local evaporation line for the lagoons as shown in Figure 4.57 is

$\delta^2H = 4.94\,\delta^{18}O + 4.72$.

The slope of the local evaporation line for the lagoons was lower than the slopes of the LMWL, the rainfall regression lines of the study area and the GMWL. This suggests that the sampled Lagoons are affected by evaporation.

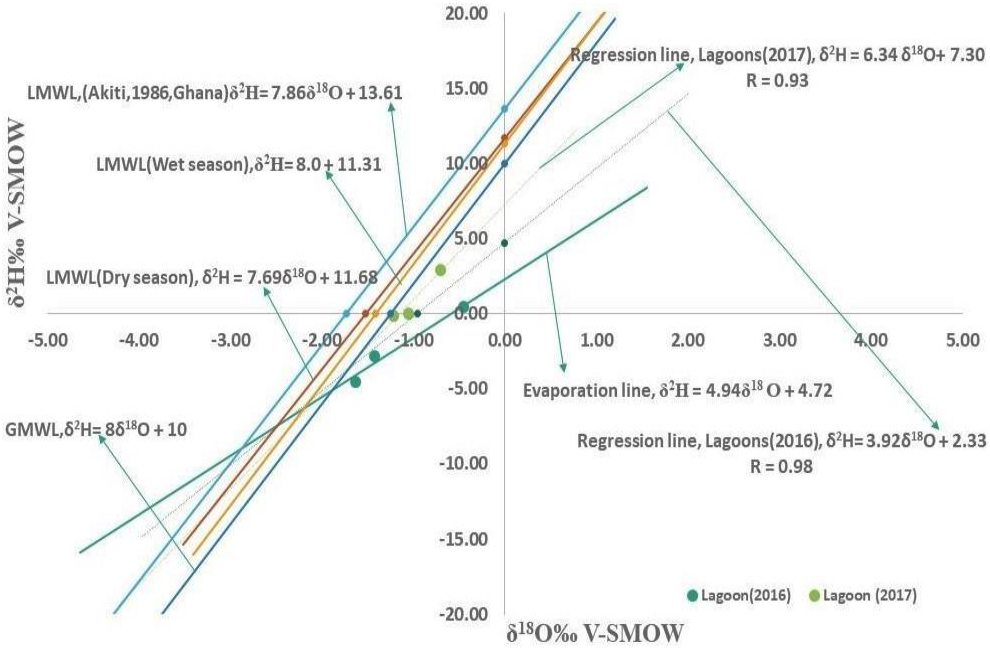

Figure 4. 55: Isotopic compositions in the Lagoon sampled in 2016 and 2017.

4.4.5. Isotopic Composition ($\delta^{18}O$ and δ^2H) in Seawater

Table 4. 63: A statistical summary of the isotopic compositions of the Lagoons sampled in 2016 and 2017.

	2016			*2017*		
Parameters	$\delta^{18}O$	δ^2H	d- excess	$\delta^{18}O$	δ^2H	d-excess
Number of samples	3	3	3	9	9	9
Mean	-0.97	-2.62	5.13	0.85	5.90	-0.88
Standard Error	0.63	3.64	1.95	0.45	1.92	1.73
Median	-1.39	-2.87	5.52	1.01	6.67	-1.63
Mode	N/A	N/A	N/A	N/A	6.34	N/A
Standard Deviation	1.10	6.30	3.37	1.36	5.76	5.20
Sample Variance	1.20	39.72	11.36	1.84	33.23	27.09
Kurtosis	0.00	0.00	0.00	5.38	6.43	4.05
Skewness	1.48	0.17	-0.51	-1.86	-2.28	1.23
Minimum	-1.79	-8.80	1.58	-2.43	-8.55	-9.01
Maximum	0.28	3.80	8.29	2.66	12.27	10.89
Sum	-2.91	-7.87	15.39	7.63	53.08	-7.96
Confidence Level (95.0%)	2.73	15.66	8.37	1.04	4.43	4.00

The $\delta^{18}O‰$ V-SMOW compositions in seawater sampled in both 2016 and 2017 ranges from -1.79 to 0.28 with a mean of 0.97 and from -2.43 to – 2.66 with a mean of 0.85, respectively. $\delta^{2}H$ ‰ V-SMOW in the seawater ranges from -8.80 to 3.80 with a mean of -2.62 in 2016 and from -8.55 to 12.27 with a mean of 5.90 in 2017. The relationship between $\delta^{2}H$ and $\delta^{18}O$ for the seawater is shown in Figure 4.58. In 2016, the deuterium excess for the seawater samples varies from 1.58‰ to 8.29 ‰ with a mean of 5.13 ‰ and in 2017, the deuterium excess ranges from -9.01‰ to 10.89‰ with a mean of -0.88‰. The equation of the local evaporation line for the seawater as shown in Fig 4.58 is given as $\delta^{2}H = 4.48\ \delta^{18}O + 2.01$. The slope of the regression line is lower than the GMWL, LMWL (Akiti, 1986) and the rainfall regression lines of the study area.

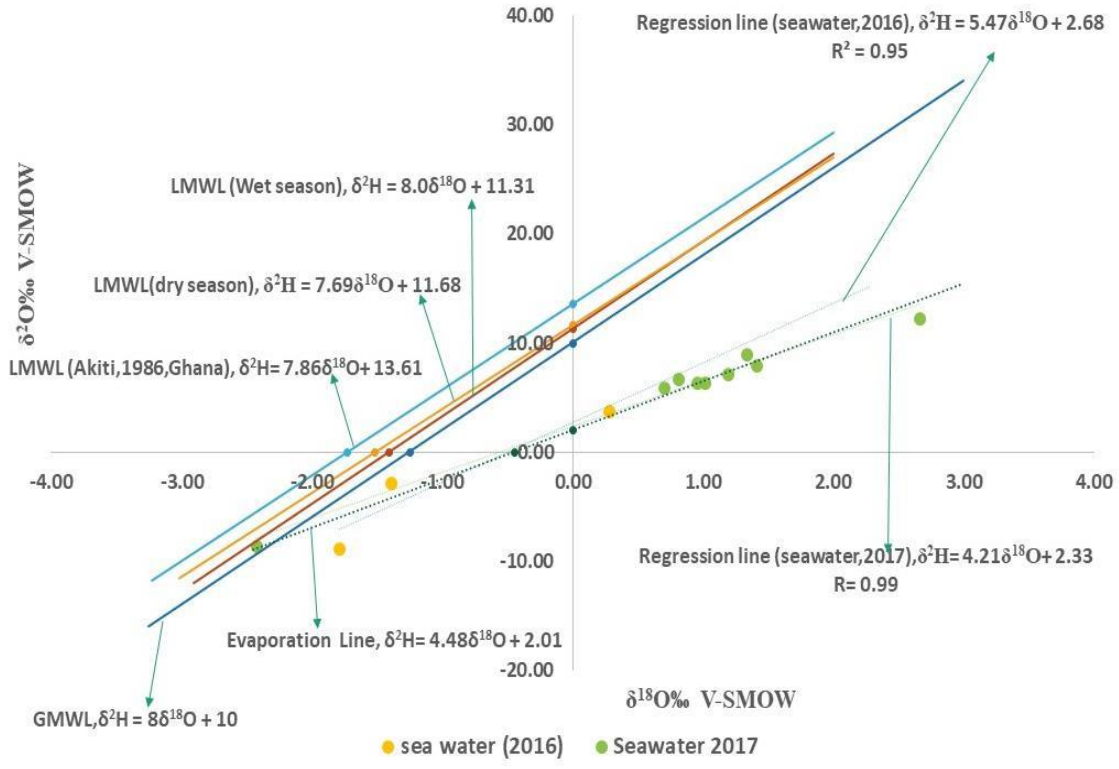

Figure 4. 56: Isotopic compositions in seawater sampled in 2016 and 2017.

The global meteoric water line, the local meteoric water line and the rainfall regression lines determined for this study is inserted in Figure 4.55 to Figure 4.58. The lines are inserted to serve as reference lines in discussing the sources of recharge for the surface water. Further to

the plots (Fig 4.55 to 4.58), the following observations were made for the isotopic ratios (δ^2 H and δ^{18} O) in the surface water (River, Stream, Lagoon and Seawater) and that is:

- No surface water (River, Stream, Lagoon and Seawater) plots on the local meteoric water line proposed by Akiti (1986).
- 10 sampled Rivers and 7 sampled Streams plots on the local rainfall regression lines determine for the study area.
- 2 sampled Rivers, 8 sampled streams and 1 sampled Seawater plots on the GMWL
- 3 sampled Streams plots above and beneath the meteoric water lines.
- 10 sampled rivers, 12 sampled streams, 6 sampled lagoons, and 11 seawater samples plots below the meteoric water lines.

From figure 4.55 to 4.58, it is seen that the surface water is mainly of meteoric origin with few from other sources and the recharge mechanism is direct infiltration. Also, the surface water plotting above and beneath the meteoric water lines are highly depleted and the depletion might be as a result of the forested canopy in which the samples were taken. These forested canopies serve as a shade, which induces high humidity, thus reducing the rate of evaporation but further investigations are required using carbon-14 isotope. The surface water plotting below the meteoric water lines indicates that the surface water is evaporated and the source of recharge is from other sources apart from rainwater. Also, the recharge mechanism is not direct infiltration. These surface water (10 Rivers, 12 Streams and 6 Lagoons) were not shaded along their banks and the absence of shade induces low humidity thus increasing the rate of evaporation.

4.4.6 Isotopic Composition ($\delta^{18}O$ and $\delta^{2}H$) in Groundwater

Table 4. 64: A statistical summary of the isotopic compositions of the hand dug wells sampled in 2016 and 2017.

	2016			2017		
Parameters	$\delta^{18}O$	$\delta^{2}H$	d - excess	$\delta^{18}O$	$\delta^{18}H$	d - excess
Number of samples	36	36	36	30	30	30
Mean	-2.77	-8.61	13.85	-1.49	-2.44	9.47
Standard Error	0.22	0.81	0.99	0.12	0.70	0.71
Median	-2.24	-6.81	11.04	-1.66	-3.31	9.86
Mode	N/A	N/A	N/A	-1.74	-4.53	N/A
Standard Deviation	1.32	4.88	5.92	0.66	3.81	3.89
Sample Variance	1.74	23.77	35.09	0.44	14.53	15.15
Kurtosis	0.02	0.37	-0.24	0.96	4.18	4.76
Skewness	-1.21	-1.16	1.12	1.23	1.96	-1.98
Range	4.65	17.995	19.77	2.67	17.03	17.36
Minimum	-5.97	-20.83	7.26	-2.5	-6.94	-2.65
Maximum	-1.32	-2.84	27.03	0.17	10.09	14.71
Sum	-99.59	-310.14	498.57	-44.66	-73.15	284.13
Confidence Level(95.0%)	0.45	1.65	2.00	0.25	1.42	1.45

Table 4. 65: A statistical summary of the isotopic compositions of the boreholes sampled in 2016 and 2017.

	2016			2017		
Parameters	$\delta^{18}O$	$\delta^{2}H$	d -excess	$\delta^{18}O$	$\delta^{2}H$	d - excess
Number of samples	45	45	45	55	55	55
Mean	-2.61	-8.51	12.43	-2.01	-7.22	9.60
Standard Error	0.14	0.59	0.59	0.10	0.30	0.63
Median	-2.36	-7.91	12.04	-2.20	-7.24	9.60
Mode	N/A	N/A	N/A	-2.29	N/A	N/A
Standard Deviation	0.94	3.95	3.97	0.75	2.26	4.64
Sample Variance	0.88	15.58	15.75	0.56	5.10	21.52
Kurtosis	6.35	5.16	6.75	20.35	-0.72	5.98
Skewness	-2.58	-2.24	2.41	3.67	0.16	0.34
Range	4.50	18.66	20.75	5.62	9.08	34.34
Minimum	-5.96	-22.55	7.19	-3.29	-11.72	-6.92
Maximum	-1.46	-3.89	27.94	2.33	-2.64	27.42
Sum	-117.51	-382.80	559.26	-110.59	-397.29	527.91
Confidence Level (95.0%)	0.28	1.19	1.19	0.20	0.61	1.25

In the study area, the stable isotopic composition in the hand dug wells sampled in 2016 and 2017 range between – 5.97, and -1.32 ‰ V-SMOW with a mean of -2.77 ‰ V- SMOW and -2.5 to 0.17 ‰ V-SMOW with a mean of -1.49‰ V-SMOW, respectively (Table 4.64). The mean value of -2.77‰ for $\delta^{18}O$ in the hand dug wells sampled in 2016 is like the mean value of -2.8‰ obtained by Akiti (1980) for groundwater sampled from the Accra plains of Ghana.

The δ^2H values in the hand dug well sampled in 2016 and 2017 range between -20.83 and -2.84 ‰ V-SMOW with a mean of -8.61 ‰ V-SMOW and -6.94 to 10.09‰ V-SMOW with a mean of -2.44‰ V-SMOW, respectively. The evaporation line for the hand dug wells is given as

$\delta^2H = 4.22\delta^{18}O + 3.59$, ($R^2$= 0.87) and the regression line for the hand dug wells for both years is given as $\delta^2H = 3.57\ \delta^{18}O + 1.27$, (2016) and $\delta^2H = 6.34\ \delta^{18}O + 7.67$, (2017). The regression lines suggest that the composition of oxygen and hydrogen isotopes in the hand dug wells sampled in 2016 are more affected by evaporation than those sampled in 2017. This means that either the hand dug wells are recharged by rainfall enriched in heavy isotopes or that the enrichment took place in the unsaturated zone. The relationship between δ^2H and $\delta^{18}O$ for the hand dug wells in both 2016 and 2017 is shown in figure 4.59.

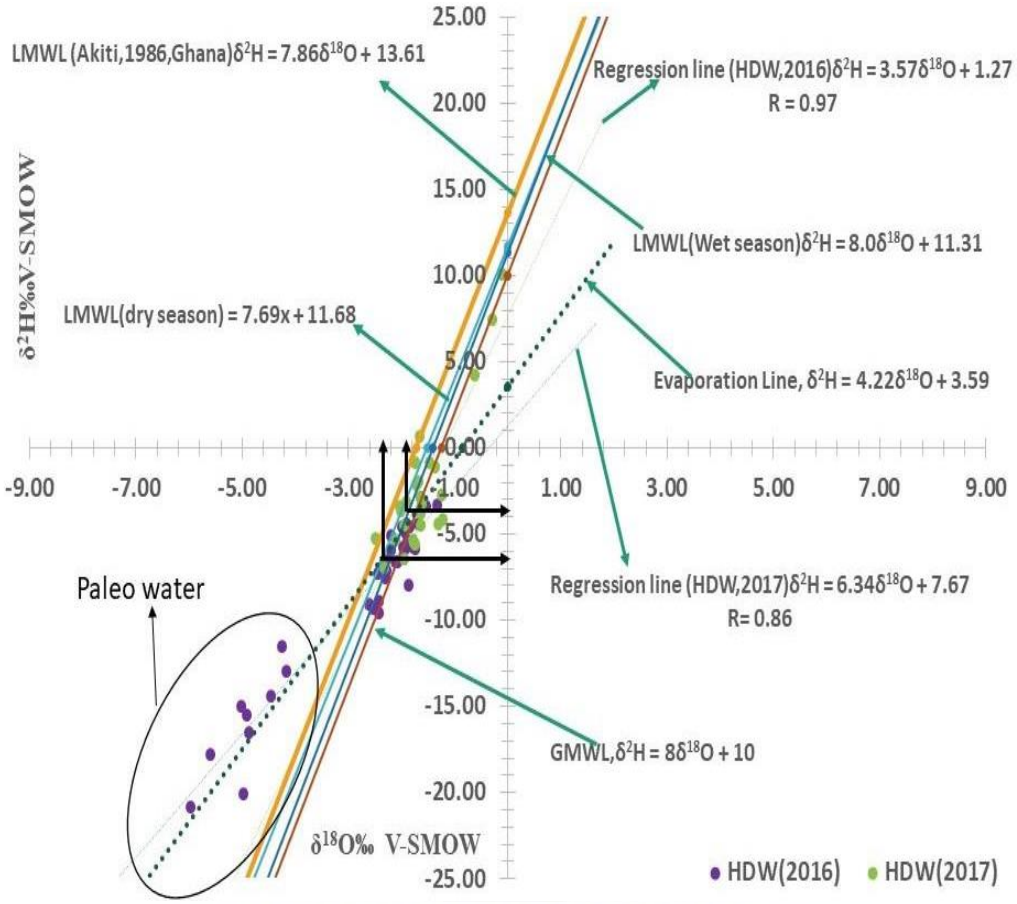

Figure 4. 57: Isotopic compositions in the hand dug wells sampled in 2016 and 2017.

The $\delta^{18}O$‰ V-SMOW in the boreholes sampled in 2016 and 2017 vary from -5.96 to -1.46 with a mean of -2.61 and -3.29 to 2.33 with a mean of -2.01 (Table 4.65), respectively. Similarly, the $\delta^{2}H$‰ V-SMOW for the boreholes sampled in 2016 and 2017, ranges from -22.55 to -3.89 with a mean of -8.51 and -11.72 to -2.64 with a mean of -7.22 respectively. The mean $\delta^{18}O$ value for the boreholes sampled in 2016 and 2017 is slightly like the mean value of -2.8‰ obtained by Akiti (1980). The evaporation line for the boreholes is given as $\delta^{2}H = 3.71\ \delta^{18}O + 0.9$ ($r^2 = 1$) and the regression lines for the boreholes sampled in both 2016 and 2017 are given as $\delta^{2}H = 3.98\delta^{18}O + 1.88$ (2016) and $\delta^{2}H = 3.63\ \delta^{18}O + 0.5$(2017), respectively (Fig 4.60). Both regression lines show that the boreholes are subjected to evaporation but the boreholes sampled in 2017 are more evaporated than those sampled in 2016.

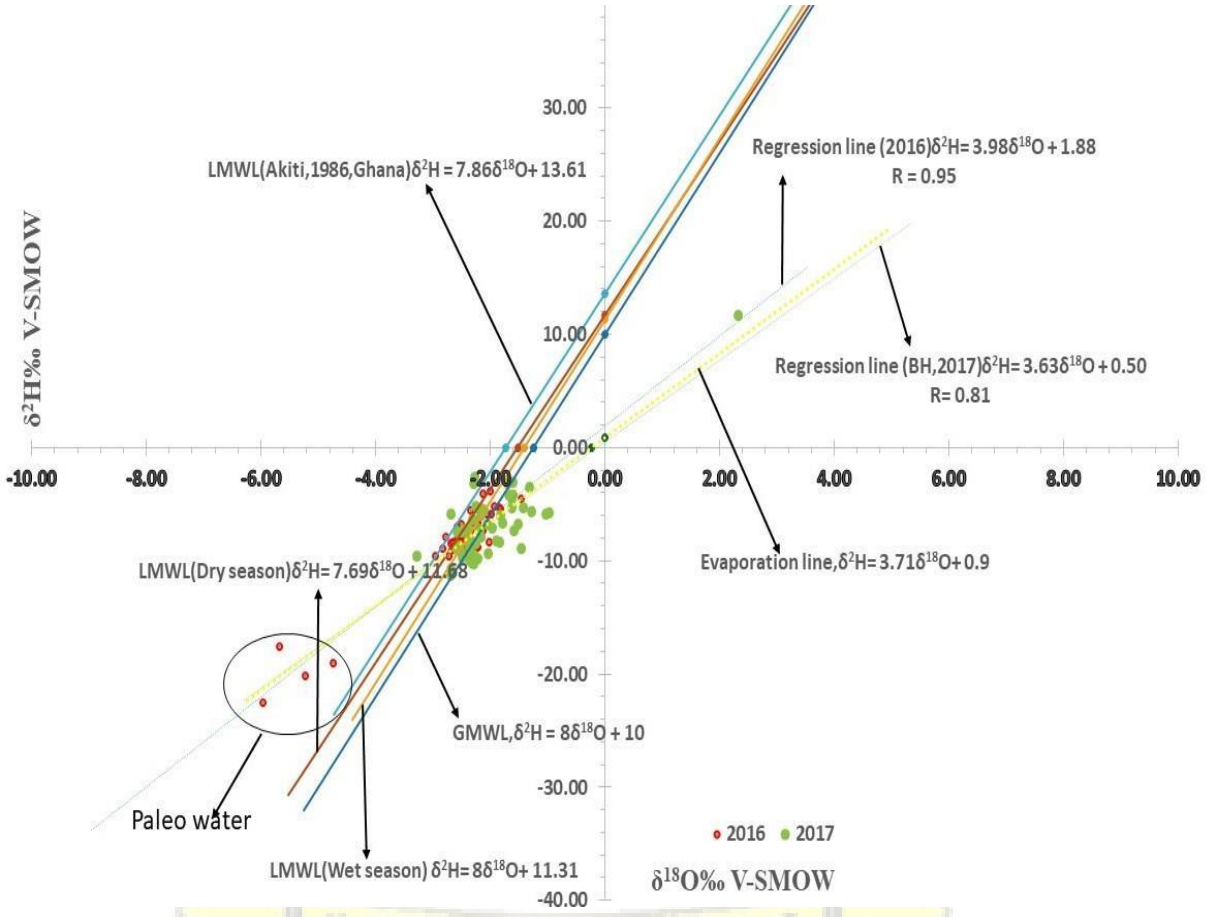

Figure 4. 58: Isotopic compositions in the boreholes sampled in 2016 and 2017.

The global meteoric water line, the local meteoric water line and the rainfall regression lines determined for this study is inserted in Figure 4.59 and Fig 4.60. These lines serve as reference lines in discussing the sources of groundwater recharge.

From figure 4.59 and 4.60, the following observations are made for the isotopic composition of oxygen and hydrogen isotope in the hand dug wells sampled in 2016 (n= 37) and 2017 (n= 30). The observations are

- 11 hand dug wells sampled in 2016 and 13 hand dug wells sampled in 2017 plots on the rainfall regression lines of the study area.
- 2 hand dug wells sampled in 2017 plots on the LMWL proposed by Akiti ,1986.
- 8 hand dug wells sampled in 2016 and 5 hand dug wells sampled in 2017 cluster around the GMWL.
- 9 hand dug wells sampled in 2016 and 10 hand dug wells sampled in 2017 plots below the meteoric water lines.
- 9 hand dug wells sampled in 2016 plots above and beneath the meteoric water lines.

For the boreholes sampled in 2016 (n= 45) and 2017(n= 56), the following observations are made, that is

- 27 samples taken in 2016 and 26 samples taken in 2017 cluster around the rainfall regression lines of the study area.
- 5 boreholes sampled in 2016 cluster around the local meteoric water line (Akiti, 1986).
- 4 boreholes sampled in both 2016 and 2017 plots above and beneath the meteoric water lines
- 4 boreholes sampled in 2016 and 8 boreholes sampled in 2017 cluster around the GMWL.
- The remaining 5 boreholes sampled in 2016 and 22 boreholes sampled in 2017 plots below the meteoric water lines.

From figure 4.59 to 4.60, it is observed that the source of groundwater recharge in the Lower Tano River basin is mainly meteoric with no significant evaporation. Also, recharge mechanism is rapid without any significant evaporation and gaseous exchange. This agrees favorably to the results obtained by Edjah et al., 2015 and 2019. This explains why rainwater was one of the chemical qualities controlling the mineralization of 50% of the groundwater in the study area (Fig 4.39a).

Additionally, it is seen that fewer groundwater (9 hand dug wells and 5 boreholes) samples were evaporated. This reveals that the groundwater might be undergoing evaporation due to limited degree of kinetic evaporation before or during infiltration process. In addition, most of the hand dug wells were opened without covers and there might be an occurrence of direct evaporation. Also, the recharge mechanism is not rapid and the source of recharge might be from the surface water, which will be explained further in subsequent chapters.

The groundwater lying above and beneath the meteoric water lines (GMWL and LMWL's) are highly depleted and the depletion might be as a result of the forested canopy where samples were taken. These forested canopies serve as a shade, which induces high humidity, thus reducing the rate of evaporation but further investigations are required using carbon-14 isotope.

Comparing the isotopic regression lines of the sampled groundwater and the sampled surface water, it is observed that the regression line for the hand dug wells sampled in 2017 is like that of the lagoon sampled in 2017. This indicates that the sampled lagoon might possibly be influencing the hand dug well recharge of the study area. The oxygen and hydrogen compositions in the boreholes sampled in 2016 are slightly like the hand dug wells sampled in 2016. These indicate that the source of the borehole water sampled in 2016 might probably be related to the 2016 hand dug wells instead of rainwater recharge. This explains why a hydraulic relationship existed between the hand dug wells and the boreholes sampled in 2016 as discussed in the 2nd specific objective.

Also, from fig 4.59 to 4.60 and fig 4.61, it is observed that most of the groundwater samples were clustering around the rainfall regression lines (wet and dry seasons) of the study area.

This indicates that, local modern rainwater is a significant source of groundwater recharge in the aquifer of the Apollonian formation and the Birimian supergroup. The intercept and slopes for the groundwater (hand dug wells and boreholes) regression lines for both 2016 and 2017 are less than the LMWL's (Akiti, 1986) and less than the rainfall regression lines of the study area. This explains the important effect of evaporative enrichment on the groundwater within the basin (Wassenaar et al., 2011).

Also from Figure 4.61, the groundwater appears to be grouped in a narrow range signifying a well-mixed system with relatively constant isotopic compositions. This suggest that rainwater recharging the aquifer of the Apollonian formation and the Birimian supergroup is relatively homogeneous with evaporation playing an insignificant role on the infiltration processes.

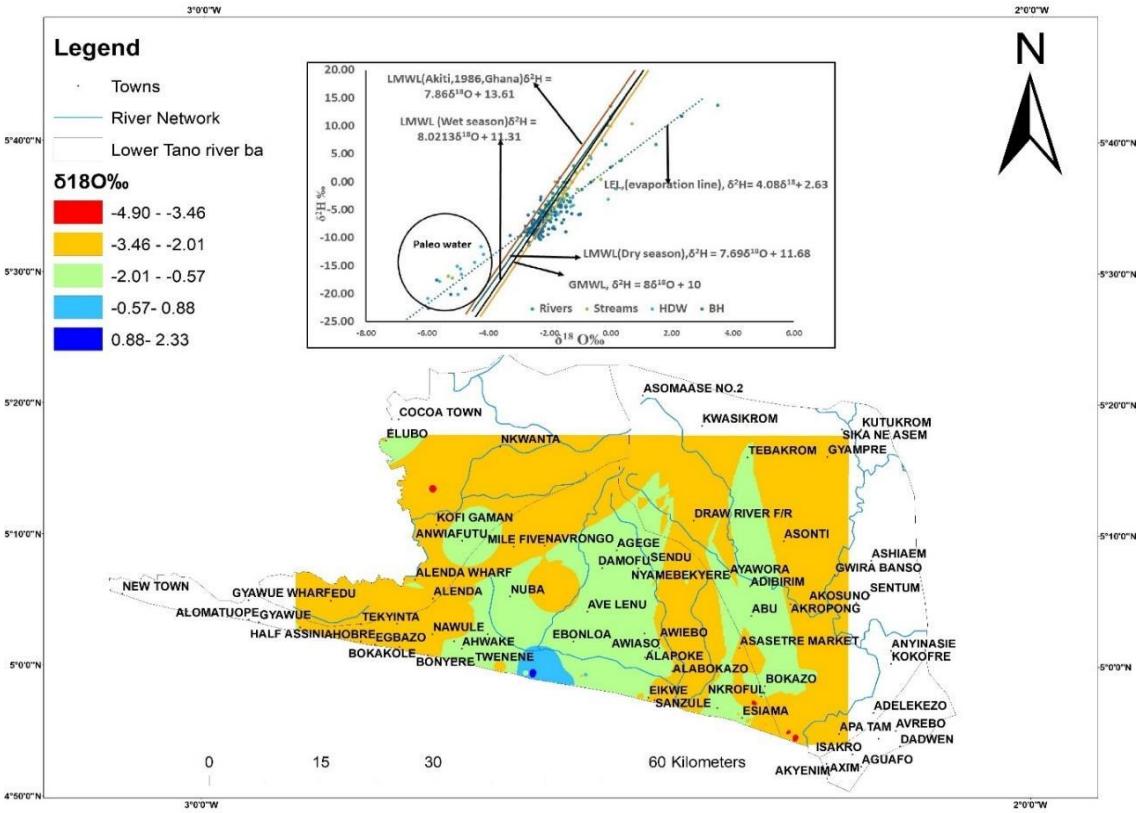

Figure 4. 59: Spatial distribution map of $\delta^{18}O‰$ values in the sampled groundwater of the study area.

4.4.7 Deuterium excess in groundwater of the study area

The deuterium excess for the hand dug wells sampled in 2016 and 2017 ranges between 7.26 and 27.03 ‰ V-SMOW with a mean of 13.85 ‰ V-SMOW and -2.65 to 14.71‰ V-SMOW

with a mean of 9.47 ‰ V-SMOW, respectively (Table 4.66). For the boreholes sampled in 2016, the deuterium excess varies from 7.19‰ to 27.94‰ with a mean of 12.43‰ and in 2017 the deuterium excess ranges from -6.92‰ to 27.42‰ with a mean of 9.60‰ (Table 4.67). The deuterium excess depends on conditions prevalent during primary evaporation, consisting of sea surface temperature, variation in humidity and wind speed, which gives information on the sources of water vapour {Gat, 1983; Clark & Fritz. (1997)}. Non-equilibrium evaporation causes a reduction in the deuterium excess, which suggests an increment in vapor phases. However, equilibrium processes will not change the deuterium excess for any of the phases.

In this study, majority of the groundwater (hand dug wells and boreholes) have deuterium excess values close to that of rainfall and a few are close to evaporation. The plot (Fig 4.62) specifies a strong and a positive correlation (Hand dug wells (2016), r = 0.94, hand dug wells (2017), r = 0.7, boreholes (2016), r = 0.95, boreholes (2017), r = 0.76) existing between oxygen -18 and deuterium excess for the groundwater sampled from the aquifer of the Apollonian formation and the aquifer of the Birimian supergroup. The positive d-excess values (>10‰) for most of the groundwater samples is consistent with the origin, which is derived from rainfall. The positive d-excess values provided additional evidence to groundwater recharge from surface water, which will be explained further in subsequent chapters. Also, few of the groundwater has lower d-excess values, which suggest an evaporative enrichment of groundwater during the recharge process. This is due to slow recharge rates which requires further investigations in future works.

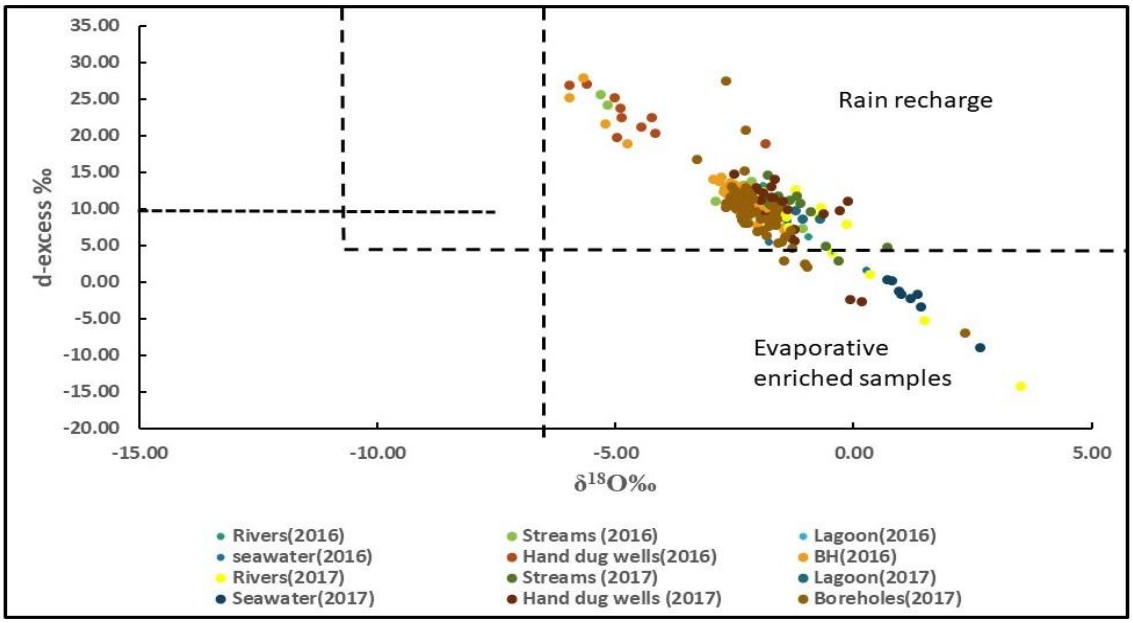

Figure 4. 60: A cross plot of d-excess‰ against δ18O‰ in surface water and groundwater of the study area.

4.4.8 Quantification of River water contribution to Groundwater recharge of the study area.

A two-component mixing equation is used in this study to estimate the proportion of the sampled rivers (Pr) and the sampled streams (Pstream) in the groundwater sampled from the aquifer of the Apollonian formation and the Birimian supergroup. The equation used is defined as:

$$P_r = \frac{\delta^{18}O_{gw} - \delta^{18}O_{precipitation}}{\delta^{18}O_{rivers} - \delta^{18}O_{precipitation}} \times 100 \qquad \text{eq 4.20}$$

Where $\delta^{18}O_{gw}$ is the value of groundwater, $\delta^{18}O_{precipitation}$ is the average value of precipitation (rainfall), $\delta^{18}O_{river}$ is the average value of the rivers, and P_r is the contribution of the river to the recharge of the groundwater (Rai et al., 2009; Clark & Fritz, 1997; Table 4.66).

Table 4. 66: Proportion of Rivers and Streams to recharge of groundwater samples taken in 2016

Sample ID	Sample location	$\delta^{18}O_{gw}$	mean $\delta^{18}O_{rainwater}$	mean $\delta^{18}O_{streams}$	mean $\delta^{18}O_{Rivers}$	$\delta^{18}O_{gw}$ - mean $\delta^{18}O_{rainwater}$	mean $\delta^{18}O_{River}$ - mean $\delta^{18}O_{rainwater}$	Pr	mean $\delta^{18}O_{stream}$ - mean $\delta^{18}O_{rainwater}$	P_{stream}	P_r %	P_{stream} %
HDW 1	Esiama	-2.11	-0.1	-2.36	-2.11	-2.0	-2.04	1.0	-2.29	0.89	100.05	89.27
HDW 2	Nkroful	-1.89	-0.1	-2.36	-2.11	-1.8	-2.04	0.9	-2.29	0.79	88.96	79.37
HDW 3	Kikam	-1.96	-0.1	-2.36	-2.11	-1.9	-2.04	0.9	-2.29	0.83	92.51	82.55
HDW 4	Kikam	-1.84	-0.1	-2.36	-2.11	-1.8	-2.04	0.9	-2.29	0.77	86.85	77.49
HDW 5	Aniwa	-1.74	-0.1	-2.36	-2.11	-1.7	-2.04	0.8	-2.29	0.73	81.84	73.03
HDW 6	Kikam	-2.21	-0.1	-2.36	-2.11	-2.1	-2.04	1.0	-2.29	0.94	104.83	93.53
HDW 7	Ampain	-2.20	-0.1	-2.36	-2.11	-2.1	-2.04	1.0	-2.29	0.93	104.16	92.94
HDW 8	Asanta	-1.86	-0.1	-2.36	-2.11	-1.8	-2.04	0.9	-2.29	0.78	87.71	78.26
HDW 9	Nkroful	-1.95	-0.1	-2.36	-2.11	-1.9	-2.04	0.9	-2.29	0.82	92.11	82.19
HDW 10	Kikam	-1.94	-0.1	-2.36	-2.11	-1.9	-2.04	0.9	-2.29	0.82	91.62	81.75
HDW 11	Bomuakpole	-2.14	-0.1	-2.36	-2.11	-2.1	-2.04	1.0	-2.29	0.90	101.40	90.48
HDW 12	Kikam	-1.53	-0.1	-2.36	-2.11	-1.5	-2.04	0.7	-2.29	0.64	71.57	63.86
HDW 13	Ankobra	-1.86	-0.1	-2.36	-2.11	-1.8	-2.04	0.9	-2.29	0.78	87.71	78.26
HDW 14	Asanta	-2.40	-0.1	-2.36	-2.11	-2.3	-2.04	1.1	-2.29	1.02	114.12	101.83
HDW 15	gyegyEKROM	-2.39	-0.1	-2.36	-2.11	-2.3	-2.04	1.1	-2.29	1.01	113.63	101.39
HDW 16	Kikam	-2.12	-0.1	-2.36	-2.11	-2.1	-2.04	1.0	-2.29	0.90	100.43	89.61
HDW 17	Asanta	-1.75	-0.1	-2.36	-2.11	-1.7	-2.04	0.8	-2.29	0.73	82.33	73.46
HDW 18	Esiama	-1.98	-0.1	-2.36	-2.11	-1.9	-2.04	0.9	-2.29	0.84	93.65	83.56
HDW 19	Aniwa	-1.99	-0.1	-2.36	-2.11	-1.9	-2.04	0.9	-2.29	0.84	94.27	84.12
HDW 20	Esiama	-2.24	-0.1	-2.36	-2.11	-2.2	-2.04	1.1	-2.29	0.95	106.29	94.84
HDW 21	Elubo	-1.53	-0.1	-2.36	-2.11	-1.5	-2.04	0.7	-2.29	0.64	71.68	63.96
HDW 22	Asanta	-1.86	-0.1	-2.36	-2.11	-1.8	-2.04	0.9	-2.29	0.78	87.71	78.26
HDW 23	Ankobra	-1.51	-0.1	-2.36	-2.11	-1.4	-2.04	0.7	-2.29	0.63	70.59	62.99
HDW 24	Esiama	-1.90	-0.1	-2.36	-2.11	-1.8	-2.04	0.9	-2.29	0.80	89.87	80.19
HDW 25	Esiama	-1.69	-0.1	-2.36	-2.11	-1.6	-2.04	0.8	-2.29	0.71	79.40	70.85
HDW 26	Nkroful	-1.63	-0.1	-2.36	-2.11	-1.6	-2.04	0.8	-2.29	0.68	76.70	68.44
HDW 27	Esiama	-1.78	-0.1	-2.36	-2.11	-1.7	-2.04	0.8	-2.29	0.75	83.98	74.93
HDW 28	Esiama	-1.83	-0.1	-2.36	-2.11	-1.8	-2.04	0.9	-2.29	0.77	86.24	76.95
HDW 29	Gyegyekrom	-2.08	-0.1	-2.36	-2.11	-2.0	-2.04	1.0	-2.29	0.88	98.47	87.86
HDW 30	Elubo	-1.63	-0.1	-2.36	-2.11	-1.6	-2.04	0.8	-2.29	0.68	76.46	68.23
HDW 31	Azulenloanu	-1.32	-0.1	-2.36	-2.11	-1.3	-2.04	0.6	-2.29	0.55	61.30	54.70
HDW 32	Half Assin(1)	-2.29	-0.1	-2.36	-2.11	-2.2	-2.04	1.1	-2.29	0.97	108.49	96.81
HDW 33	Bobrama	-2.08	-0.1	-2.36	-2.11	-2.0	-2.04	1.0	-2.29	0.88	98.47	87.86
HDW 34	Asanta	-1.75	-0.1	-2.36	-2.11	-1.7	-2.04	0.8	-2.29	0.73	82.33	73.46
HDW 35	Sanwoma	-1.92	-0.1	-2.36	-2.11	-1.9	-2.04	0.9	-2.29	0.81	90.67	80.90
HDW 36	Bobrama	-2.08	-0.1	-2.36	-2.11	-2.0	-2.04	1.0	-2.29	0.88	98.47	87.86
BH 1	Salman(3)	-2.06	-0.1	-2.36	-2.11	-2.0	-2.04	1.0	-2.29	0.87	97.49	86.99
BH 2	Kamgbuli	-1.81	-0.1	-2.36	-2.11	-1.7	-2.04	0.9	-2.29	0.76	85.27	76.08
BH 3	Kamgbuli	-2.26	-0.1	-2.36	-2.11	-2.2	-2.04	1.1	-2.29	0.96	107.31	95.75
BH 4	Asemko	-2.25	-0.1	-2.36	-2.11	-2.2	-2.04	1.1	-2.29	0.95	106.72	95.22

BH 5	Ampaim	-1.46	-0.1	-2.36	-2.11	-1.4	-2.04	0.7	-2.29	0.61	68.15	60.81
BH 6	Aniwa	-2.52	-0.1	-2.36	-2.11	-2.5	-2.04	1.2	-2.29	1.07	119.99	107.06
BH 7	Nkroful	-2.06	-0.1	-2.36	-2.11	-2.0	-2.04	1.0	-2.29	0.87	97.49	86.99
BH 8	Sanwoma	-2.02	-0.1	-2.36	-2.11	-2.0	-2.04	1.0	-2.29	0.85	95.54	85.24
BH 9	Aluku	-1.93	-0.1	-2.36	-2.11	-1.9	-2.04	0.9	-2.29	0.81	91.24	81.41
BH 10	Awiebo	-2.32	-0.1	-2.36	-2.11	-2.3	-2.04	1.1	-2.29	0.98	110.19	98.32
BH 11	Esiama	-2.41	-0.1	-2.36	-2.11	-2.3	-2.04	1.1	-2.29	1.02	114.57	102.23
BH 12	Ampain	-1.46	-0.1	-2.36	-2.11	-1.4	-2.04	0.7	-2.29	0.61	68.15	60.81
BH 13	Salman	-2.33	-0.1	-2.36	-2.11	-2.3	-2.04	1.1	-2.29	0.99	110.94	98.99
BH 14	Nkroful	-2.53	-0.1	-2.36	-2.11	-2.5	-2.04	1.2	-2.29	1.07	120.23	107.28
BH 15	Bobrama	-2.66	-0.1	-2.36	-2.11	-2.6	-2.04	1.3	-2.29	1.13	126.85	113.19
BH 16	Bomuakpole	-2.35	-0.1	-2.36	-2.11	-2.3	-2.04	1.1	-2.29	1.00	111.62	99.60
BH 17	Sanwoma	-2.36	-0.1	-2.36	-2.11	-2.3	-2.04	1.1	-2.29	1.00	112.32	100.22
BH 18	Alabokazo	-2.78	-0.1	-2.36	-2.11	-2.7	-2.04	1.3	-2.29	1.19	132.90	118.58
BH 19	Aluku (1)	-1.99	-0.1	-2.36	-2.11	-1.9	-2.04	0.9	-2.29	0.84	94.04	83.91
BH 20	Alabokazo(2)	-2.58	-0.1	-2.36	-2.11	-2.5	-2.04	1.2	-2.29	1.10	122.77	109.55
BH 21	Asanta(6)	-2.46	-0.1	-2.36	-2.11	-2.4	-2.04	1.2	-2.29	1.04	116.99	104.38
BH 22	Salaman(1)	-2.49	-0.1	-2.36	-2.11	-2.4	-2.04	1.2	-2.29	1.06	118.63	105.85
BH 23	Telekobokaso	-2.12	-0.1	-2.36	-2.11	-2.1	-2.04	1.0	-2.29	0.90	100.56	89.73
BH 24	Aluku	-1.81	-0.1	-2.36	-2.11	-1.7	-2.04	0.9	-2.29	0.76	85.49	76.28
BH 25	Esiama	-2.54	-0.1	-2.36	-2.11	-2.5	-2.04	1.2	-2.29	1.08	120.97	107.93
BH 26	Ankobra newsite	-2.37	-0.1	-2.36	-2.11	-2.3	-2.04	1.1	-2.29	1.01	112.77	100.62
BH 27	Sanwoma	-2.06	-0.1	-2.36	-2.11	-2.0	-2.04	1.0	-2.29	0.87	97.64	87.12
BH 28	Old Kablasuazo	-2.56	-0.1	-2.36	-2.11	-2.5	-2.04	1.2	-2.29	1.09	122.18	109.02
BH 29	Azulenloa	-2.69	-0.1	-2.36	-2.11	-2.6	-2.04	1.3	-2.29	1.14	128.20	114.39
BH 30	Azuleno	-2.18	-0.1	-2.36	-2.11	-2.1	-2.04	1.0	-2.29	0.92	103.54	92.38
BH 31	Fante new site	-2.58	-0.1	-2.36	-2.11	-2.5	-2.04	1.2	-2.29	1.10	123.10	109.84
BH 32	Elubo	-2.00	-0.1	-2.36	-2.11	-1.9	-2.04	0.9	-2.29	0.84	94.51	84.33
BH 33	Bomuakpole(1)	-2.18	-0.1	-2.36	-2.11	-2.1	-2.04	1.0	-2.29	0.92	103.36	92.23
BH 34	NyanZinli(1)	-2.22	-0.1	-2.36	-2.11	-2.1	-2.04	1.1	-2.29	0.94	105.14	93.81
BH 35	Atwibanso(1)	-2.34	-0.1	-2.36	-2.11	-2.3	-2.04	1.1	-2.29	0.99	111.18	99.21
BH 36	New Nzulezu(1)	-2.51	-0.1	-2.36	-2.11	-2.4	-2.04	1.2	-2.29	1.06	119.29	106.44
BH 37	NEW Ankasa	-1.84	-0.1	-2.36	-2.11	-1.8	-2.04	0.9	-2.29	0.77	86.73	77.39
BH 38	Bonyere	-2.35	-0.1	-2.36	-2.11	-2.3	-2.04	1.1	-2.29	1.00	111.67	99.64
BH 39	Atwibaso(2)	-2.73	-0.1	-2.36	-2.11	-2.7	-2.04	1.3	-2.29	1.16	130.26	116.23
BH 40	Awiafoto	-2.65	-0.1	-2.36	-2.11	-2.6	-2.04	1.3	-2.29	1.13	126.50	112.87
BH 41	Aniwafuto(chips)	-2.13	-0.1	-2.36	-2.11	-2.1	-2.04	1.0	-2.29	0.90	100.83	89.97
BH 42	New Nzulezu(2)	-2.27	-0.1	-2.36	-2.11	-2.2	-2.04	1.1	-2.29	0.96	107.63	96.03
BH 43	Tiekobo 1	-2.45	-0.1	-2.36	-2.11	-2.4	-2.04	1.2	-2.29	1.04	116.70	104.13
BH 44	Bobrama	-1.83	-0.1	-2.36	-2.11	-1.8	-2.04	0.9	-2.29	0.77	86.24	76.95
BH 45	Ankobra (3)	-1.41	-0.1	-2.36	-2.11	-1.3	-2.04	0.7	-2.29	0.59	65.70	58.63

Table 4. 67: Proportion of Rivers and Streams to recharge of groundwater samples taken in 2017

Sample ID	Sample Location	$\delta^{18}O_{gw}$	mean $\delta^{18}O_{rainwater}$	mean $\delta^{18}O_{streams}$	mean $\delta^{18}O_{Rivers}$	$\delta^{18}O_{gw}$ - mean $\delta^{18}O_{rainwater}$	mean $\delta^{18}O_{River}$ - mean $\delta^{18}O_{rainwater}$	Pr	mean $\delta^{18}O_{stream}$ - mean $\delta^{18}O_{rainwater}$	P_{stream}	P_r %	P_{stream} %
HDW1	Nkroful	-1.74	-1.8	-1.23	-0.67	0.036	1.10	0.033	0.55	0.066	3.3	6.6
HDW2	Aluku	-1.78	-1.8	-1.23	-0.67	-0.004	1.10	-0.003	0.55	-0.007	-0.3	-0.7
HDW3	Kikam	-1.74	-1.8	-1.23	-0.67	0.036	1.10	0.033	0.55	0.066	3.3	6.6
HDW4	Nkroful	-1.95	-1.8	-1.23	-0.67	-0.174	1.10	-0.158	0.55	-0.316	-15.8	-31.6
HDW5	Esiama	-1.65	-1.8	-1.23	-0.67	0.126	1.10	0.114	0.55	0.230	11.4	23.0
HDW6	Elubo	-1.31	-1.8	-1.23	-0.67	0.466	1.10	0.423	0.55	0.848	42.3	84.8
HDW7	Kikam	-1.63	-1.8	-1.23	-0.67	0.146	1.10	0.133	0.55	0.266	13.3	26.6
HDW8	Half Assini	-1.66	-1.8	-1.23	-0.67	0.116	1.10	0.105	0.55	0.211	10.5	21.1
HDW9	Bomuakpole	-1.96	-1.8	-1.23	-0.67	-0.184	1.10	-0.167	0.55	-0.334	-16.7	-33.4
HDW10	Nkroful	-1.91	-1.8	-1.23	-0.67	-0.134	1.10	-0.121	0.55	-0.243	-12.1	-24.3
HDW11	Kikam	-1.68	-1.8	-1.23	-0.67	0.096	1.10	0.087	0.55	0.175	8.7	17.5
HDW12	Kikam	-2.11	-1.8	-1.23	-0.67	-0.334	1.10	-0.303	0.55	-0.607	-30.3	-60.7
HDW13	Elubo	-1.65	-1.8	-1.23	-0.67	0.126	1.10	0.114	0.55	0.230	11.4	23.0
HDW14	Nkroful	-1.48	-1.8	-1.23	-0.67	0.296	1.10	0.269	0.55	0.539	26.9	53.9
HDW15	Aniwa	-1.38	-1.8	-1.23	-0.67	0.396	1.10	0.359	0.55	0.721	35.9	72.1
HDW16	Asemda	-1.6	-1.8	-1.23	-0.67	0.176	1.10	0.160	0.55	0.321	16.0	32.1
HDW17	Gyegyekrom	-2.33	-1.8	-1.23	-0.67	-0.554	1.10	-0.502	0.55	-1.008	-50.2	-100.8
HDW18	esiama	-1.63	-1.8	-1.23	-0.67	0.146	1.10	0.133	0.55	0.266	13.3	26.6
HDW19	Ampaim	-1.76	-1.8	-1.23	-0.67	0.016	1.10	0.015	0.55	0.030	1.5	3.0
HDW20	Eikwe	-2.5	-1.8	-1.23	-0.67	-0.724	1.10	-0.656	0.55	-1.317	-65.6	-131.7
HDW21	Atuabo	-1.8	-1.8	-1.23	-0.67	-0.024	1.10	-0.022	0.55	-0.043	-2.2	-4.3
HDW22	Benyin	-1.6	-1.8	-1.23	-0.67	0.176	1.10	0.160	0.55	0.321	16.0	32.1
HDW23	Esiama	-1.24	-1.8	-1.23	-0.67	0.536	1.10	0.486	0.55	0.976	48.6	97.6
HDW24	Gyegyekrom	-1.23	-1.8	-1.23	-0.67	0.546	1.10	0.495	0.55	0.994	49.5	99.4
HDW25	bobrama	-2.02	-1.8	-1.23	-0.67	-0.244	1.10	-0.221	0.55	-0.444	-22.1	-44.4
HDW26	Elubo	-1.9	-1.8	-1.23	-0.67	-0.124	1.10	-0.112	0.55	-0.225	-11.2	-22.5
HDW27	Kikam	-1.72	-1.8	-1.23	-0.67	0.056	1.10	0.051	0.55	0.102	5.1	10.2
HDW28	Kikam	-2.04	-1.8	-1.23	-0.67	-0.264	1.10	-0.239	0.55	-0.480	-23.9	-48.0
HDW29	Azuleno	-1.63	-1.8	-1.23	-0.67	0.146	1.10	0.133	0.55	0.266	13.3	26.6
HDW30	Aniwa	-1.62	-1.8	-1.23	-0.67	0.156	1.1	0.142	0.5	0.284	14.2	28.4
BH1	Sanzule	-2.25	-1.8	-1.23	-0.67	-0.474	1.1	-0.430	0.5	-0.862	-43.0	-86.2
BH2	Nyaniba	-2.29	-1.8	-1.23	-0.67	-0.514	1.1	-0.466	0.5	-0.935	-46.6	-93.5
BH3	Ampaim	-2.37	-1.8	-1.23	-0.67	-0.594	1.1	-0.539	0.5	-1.080	-53.9	-108.0
BH4	Atwinbanso	-2.27	-1.8	-1.23	-0.67	-0.494	1.1	-0.448	0.5	-0.898	-44.8	-89.8
BH5	Elubo	-1.61	-1.8	-1.23	-0.67	0.166	1.1	0.151	0.5	0.302	15.1	30.2
BH6	Awiefoto	-1.69	-1.8	-1.23	-0.67	0.086	1.1	0.078	0.5	0.157	7.8	15.7
BH7	Esiama	-1.32	-1.8	-1.23	-0.67	0.456	1.1	0.414	0.5	0.830	41.4	83.0
BH8	Old Kablazuaso	-2.17	-1.8	-1.23	-0.67	-0.394	1.1	-0.357	0.5	-0.716	-35.7	-71.6
BH9	Fante New Town	-1.79	-1.8	-1.23	-0.67	-0.014	1.1	-0.013	0.5	-0.025	-1.3	-2.5
BH10	half Assin SHS	-2.16	-1.8	-1.23	-0.67	-0.384	1.1	-0.348	0.5	-0.698	-34.8	-69.8
BH11	Salman	-2.34	-1.8	-1.23	-0.67	-0.564	1.1	-0.511	0.5	-1.026	-51.1	-102.6
BH12	Salman	-2.49	-1.8	-1.23	-0.67	-0.714	1.1	-0.647	0.5	-1.299	-64.7	-129.9

BH13	Esiama	-1.9	-1.8	-1.23	-0.67	-0.124	1.1	-0.112	0.5	-0.225	-11.2	-22.5
BH14	Azuleno	-1.63	-1.8	-1.23	-0.67	0.146	1.1	0.133	0.5	0.266	13.3	26.6
BH15	Bomuakpolley	-2.48	-1.8	-1.23	-0.67	-0.704	1.1	-0.638	0.5	-1.281	-63.8	-128.1
BH16	Salman	-2.36	-1.8	-1.23	-0.67	-0.584	1.1	-0.529	0.5	-1.062	-52.9	-106.2
BH17	Nkroful	-2.05	-1.8	-1.23	-0.67	-0.274	1.1	-0.248	0.5	-0.498	-24.8	-49.8
BH18	Esiama	-2.68	-1.8	-1.23	-0.67	-0.904	1.1	-0.820	0.5	-1.644	-82.0	-164.4
BH19	Ankobra newsite	-2.2	-1.8	-1.23	-0.67	-0.424	1.1	-0.384	0.5	-0.771	-38.4	-77.1
BH20	Ampin	-2.11	-1.8	-1.23	-0.67	-0.334	1.1	-0.303	0.5	-0.607	-30.3	-60.7
BH21	Nkroful	-2.58	-1.8	-1.23	-0.67	-0.804	1.1	-0.729	0.5	-1.462	-72.9	-146.2
BH22	New Nzulazu	-2.14	-1.8	-1.23	-0.67	-0.364	1.1	-0.330	0.5	-0.662	-33.0	-66.2
BH23	Tiekobo	-2.45	-1.8	-1.23	-0.67	-0.674	1.1	-0.611	0.5	-1.226	-61.1	-122.6
BH24	Bobrama	-2.51	-1.8	-1.23	-0.67	-0.734	1.1	-0.665	0.5	-1.335	-66.5	-133.5
BH25	New Nzulazu	-2.68	-1.8	-1.23	-0.67	-0.904	1.1	-0.820	0.5	-1.644	-82.0	-164.4
BH26	Bonyere	-2.31	-1.8	-1.23	-0.67	-0.534	1.1	-0.484	0.5	-0.971	-48.4	-97.1
BH27	Kamgbunli	-2.28	-1.8	-1.23	-0.67	-0.504	1.1	-0.457	0.5	-0.917	-45.7	-91.7
BH28	Aluku	-1.68	-1.8	-1.23	-0.67	0.096	1.1	0.087	0.5	0.175	8.7	17.5
BH29	Atwinbanso	-2.37	-1.8	-1.23	-0.67	-0.594	1.1	-0.539	0.5	-1.080	-53.9	-108.0
BH30	Asemko	-2.19	-1.8	-1.23	-0.67	-0.414	1.1	-0.375	0.5	-0.753	-37.5	-75.3
BH31	Salman	-2.54	-1.8	-1.23	-0.67	-0.764	1.1	-0.693	0.5	-1.390	-69.3	-139.0
BH32	Azeneluno	-2.03	-1.8	-1.23	-0.67	-0.254	1.1	-0.230	0.5	-0.462	-23.0	-46.2
BH33	Aluku	-2.57	-1.8	-1.23	-0.67	-0.794	1.1	-0.720	0.5	-1.444	-72.0	-144.4
BH34	Alabokazo	-2.38	-1.8	-1.23	-0.67	-0.604	1.1	-0.548	0.5	-1.099	-54.8	-109.9
BH35	Kamgbunli	-2.53	-1.8	-1.23	-0.67	-0.754	1.1	-0.684	0.5	-1.372	-68.4	-137.2
BH36	Ankasa	-2.31	-1.8	-1.23	-0.67	-0.534	1.1	-0.484	0.5	-0.971	-48.4	-97.1
BH37	Telekobokaso	-1.82	-1.8	-1.23	-0.67	-0.044	1.1	-0.040	0.5	-0.080	-4.0	-8.0
BH38	Alabokazo	-1.52	-1.8	-1.23	-0.67	0.256	1.1	0.232	0.5	0.466	23.2	46.6
BH39	Awiafotu junction	-1.63	-1.8	-1.23	-0.67	0.146	1.1	0.133	0.5	0.266	13.3	26.6
BH40	Azulenenuo	-2.22	-1.8	-1.23	-0.67	-0.444	1.1	-0.402	0.5	-0.807	-40.2	-80.7
BH41	Salman	-2.33	-1.8	-1.23	-0.67	-0.554	1.1	-0.502	0.5	-1.008	-50.2	-100.8
BH42	Sanzule	-1.59	-1.8	-1.23	-0.67	0.186	1.1	0.169	0.5	0.339	16.9	33.9
BH43	Ngelekazo(kerrela hotel)	-2.33	-1.8	-1.23	-0.67	-0.554	1.1	-0.502	0.5	-1.008	-50.2	-100.8
BH44	Eikwe	-1.8	-1.8	-1.23	-0.67	-0.024	1.1	-0.022	0.5	-0.043	-2.2	-4.3
BH45	Ngelekazo	-1.43	-1.8	-1.23	-0.67	0.346	1.1	0.314	0.5	0.630	31.4	63.0
BH46	sanzule	-3.29	-1.8	-1.23	-0.67	-1.509	1.1	-1.368	0.5	-2.745	-136.8	-274.5
BH47	Krisan	-1.6	-1.8	-1.23	-0.67	0.176	1.1	0.160	0.5	0.321	16.0	32.1
BH48	ngelekpolley	-1.83	-1.8	-1.23	-0.67	-0.054	1.1	-0.049	0.5	-0.098	-4.9	-9.8
BH49	Baku	-1.28	-1.8	-1.23	-0.67	0.496	1.1	0.450	0.5	0.903	45.0	90.3
BH50	Keegan	-2.29	-1.8	-1.23	-0.67	-0.514	1.1	-0.466	0.5	-0.935	-46.6	-93.5
BH51	Asemda	-2.69	-1.8	-1.23	-0.67	-0.914	1.1	-0.829	0.5	-1.663	-82.9	-166.3
BH52	Ngelekyi	-1.46	-1.8	-1.23	-0.67	0.316	1.1	0.287	0.5	0.575	28.7	57.5
BH53	Twenen	-1.5	-1.8	-1.23	-0.67	0.276	1.1	0.251	0.5	0.503	25.1	50.3
BH54	Half Assin(shs)	-2.26	-1.8	-1.23	-0.67	-0.484	1.1	-0.439	0.5	-0.880	-43.9	-88.0
BH55	Atwinbanso	-1.96	-1.8	-1.23	-0.67	-0.184	1.1	-0.167	0.5	-0.334	-16.7	-33.4

The average value of δ^{18} O in rainwater sampled in both 2016 and 2017 is -0.1‰ and -1.8‰, respectively (Table 4.66 and 4.67). The average value of δ^{18} O in the rivers sampled in 2016 and 2017 is -2.11‰ and -0.67‰, respectively. Substituting δ^{18} O values in each sampled groundwater, the average value of δ^{18} O in rain water and rivers into Eq 4.20, gives a result, which shows that the proportion of river water to groundwater recharge for 2016 and 2017 samples varies from 61.30% to 132.90% and -136.83% to 49.54% respectively (Table 4.66 and 4.67).

Comparing the spatial distribution map of Figure 4.63 a and Figure 4.63 b, it is observed that groundwater sampled in 2016 are recharged more by the rivers than the groundwater sampled in 2017. This is due to seasonal effects.

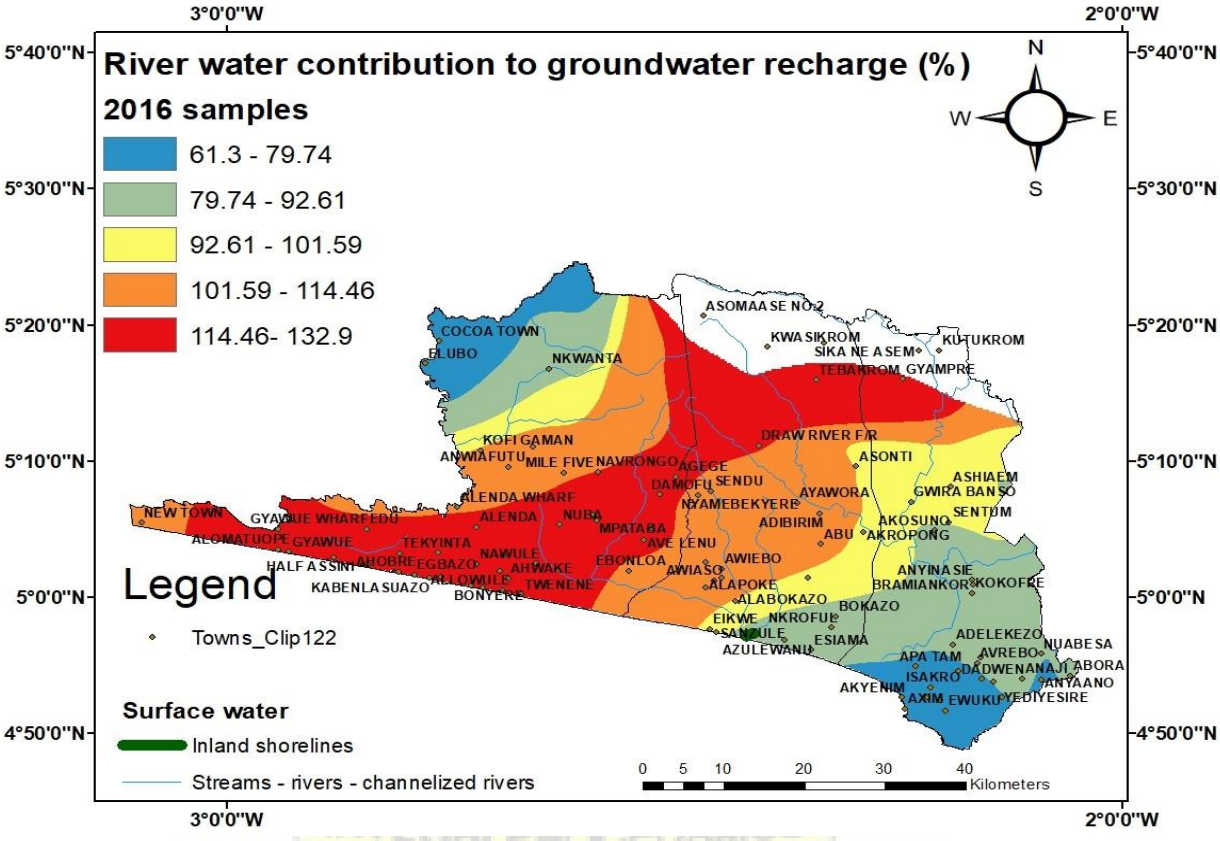

Figure 4. 61a: Spatial variation of River contribution to 2016 groundwater recharge in the study area.

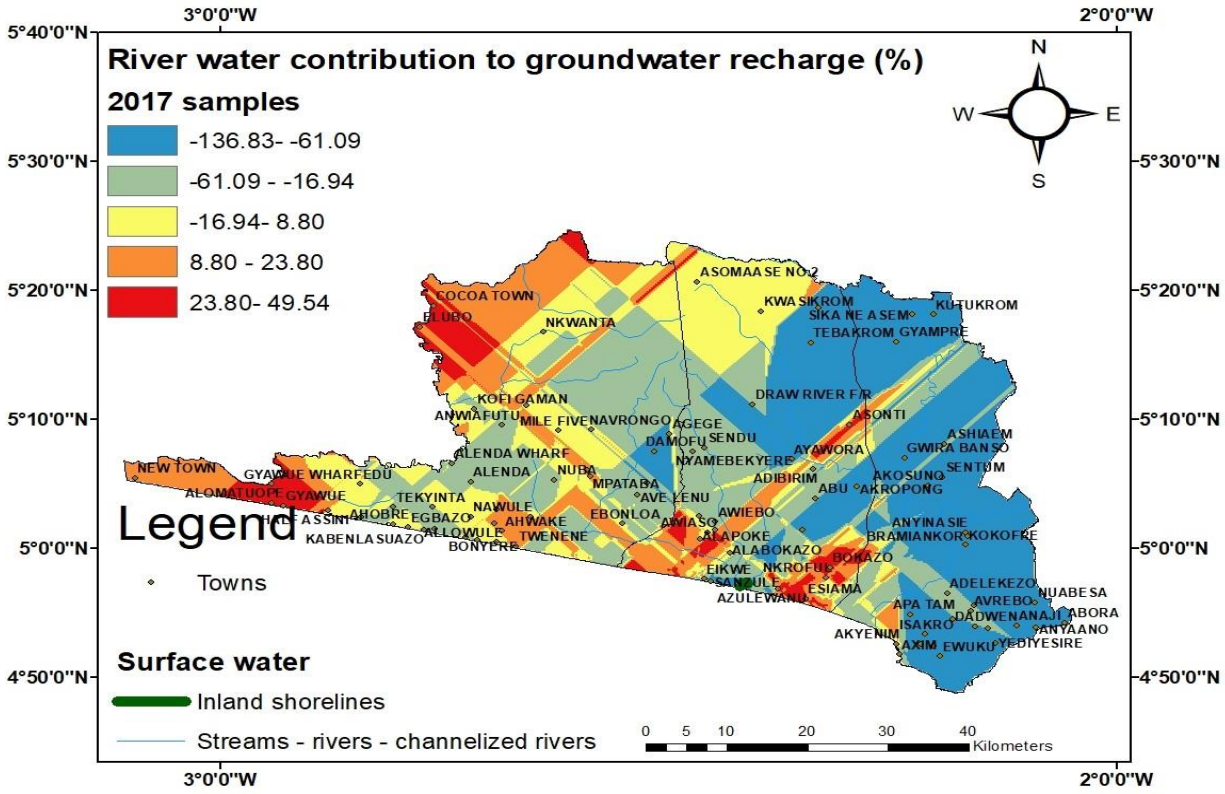

Fig 4.63 b: Spatial variation of River water contribution to 2017 Groundwater recharge in the study area.

4.4.9 Quantification of sampled stream water contribution to sampled groundwater recharge in the study area

In order to measure the contribution of the stream flow to the recharge of the groundwater, the binary mixing equation or the two-component separation method is applied:

$$P_S = \frac{(\delta^{18}O_{gw} - \delta^{18}O_{precipitation})}{(\delta^{18}O_{streams} - \delta^{18}O_{Precipitation})} \times 100 \qquad \text{Eq 4.21}$$

Where δ^{18}Ogw, δ^{18}Op, and δ^{18}Ostreams are the respective isotopic composition of the sampled groundwater, the sampled rainwater, and the sampled streams. P_S is the contribution of the sampled streams to the recharge of the sampled groundwater. The δ^{18} O value of the stream water in 2016 and 2017 is -2.36‰ and -1.23‰ respectively (Table 4.66 and 4.67). These two are the average value of δ^{18}O in the streams sampled in 2016 and 2017. The average δ^{18} O values of the rainwater sampled in 2016 and 2017 is also stated in Table 4.66 and 4.67. δ^{18}O value for each sampled groundwater, the average δ^{18}O value in the

sampled rainwater and the sampled streams is substituted into equation 4.21. The obtained results (Table 4.66 and 4.67) shows that the proportion of the sampled stream to that of the 2016 and 2017 sampled ground recharge varies from 54.70% to 118.58% and -274.52% to 99.38 %, respectively. Comparing Figure 4.64a and Figure 4.64b, it is seen that the groundwater sampled in 2016 are recharged more by the streams than the groundwater sampled in 2017. This explains why a hydraulic connection existed between the streams and the boreholes sampled in 2016 as discussed previously in the 2nd specific objective.

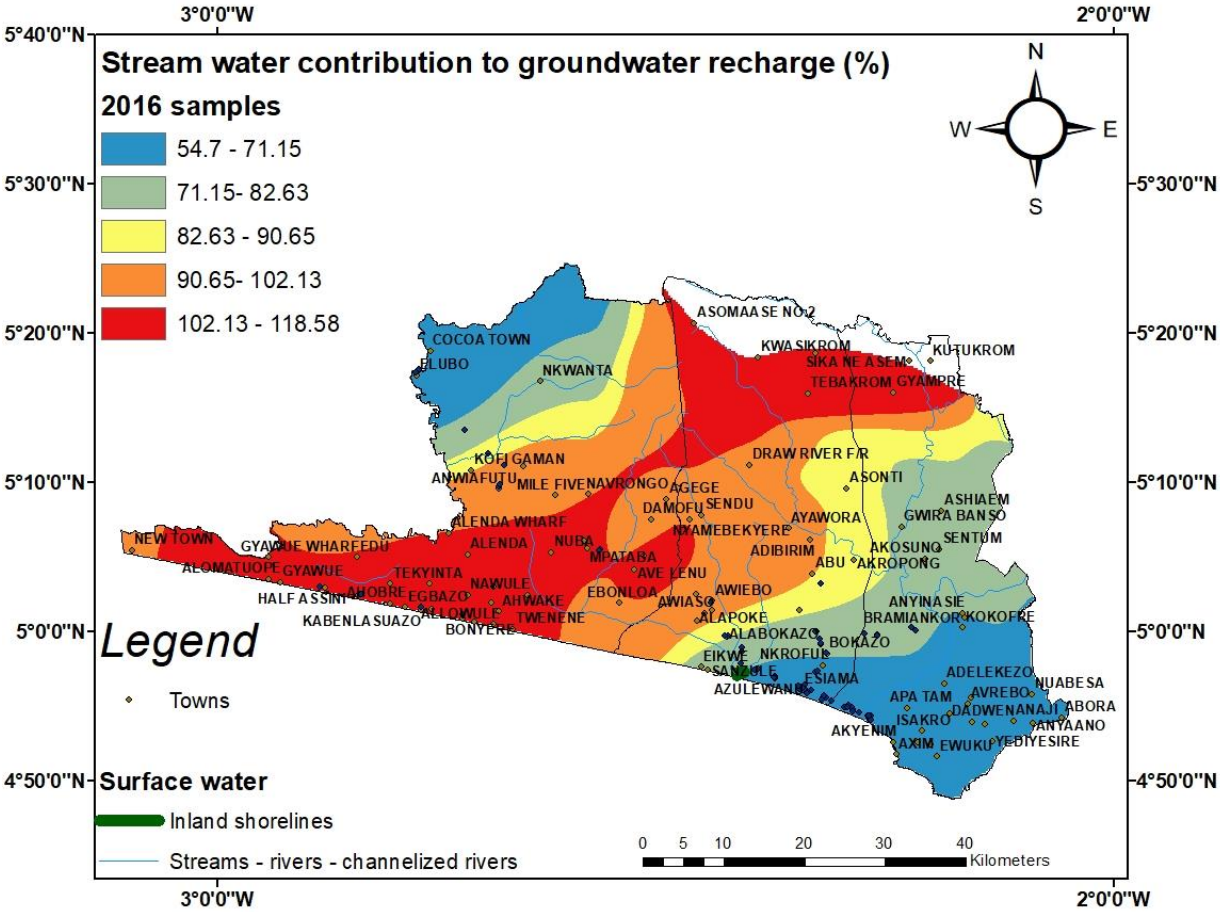

Figure 4. 62a: A Spatial variation map of stream water contribution to 2016 groundwater recharge in the study area.

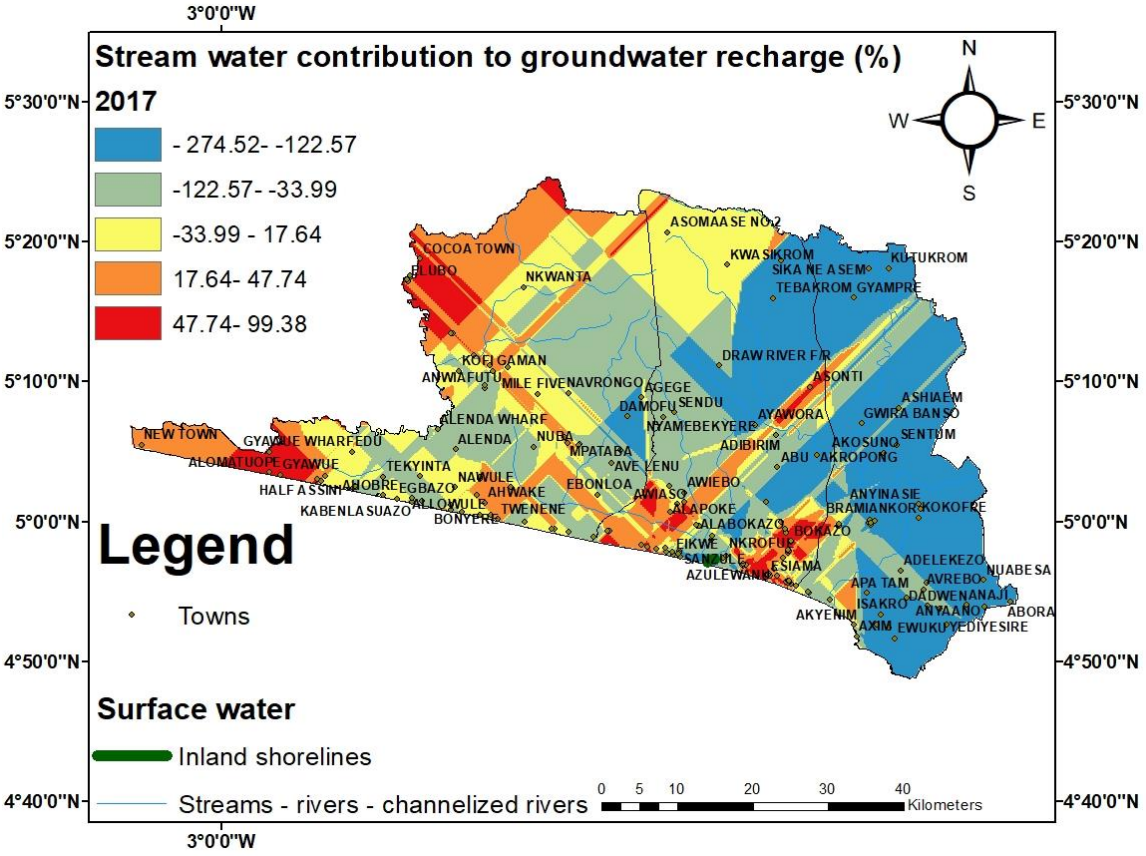

Figure 4.64b: A Spatial variation map of stream water contribution to 2017 groundwater recharge in the study area.

4.4.10. Sub-Conclusion

The results of the 4th specific objective shows that the source of surface water and groundwater recharge is mainly meteoric with few from other sources such as the rivers and streams. The recharge mechanism was rapid for majority of the groundwater while few of the groundwater lost some water through evaporation.

4.5. Groundwater age determination (Residence time)

Tritium is regularly used as an indicator for sources of groundwater and as an age tracer in aquifer systems (Bouchaou et al., 2008). In Accordance with Lu et al. (2008), "aquifers having tritium concentrations greater than 1.0 TU are deduced as aquifers mixed with modern water or recharged after 1952 when tritium was released into the air because of atmospheric nuclear weapon testing. In this study, the tritium content in surface water (rain and rivers) and groundwater (hand dug wells and boreholes) are measured. The results obtained for the rain samples are compared with other results in Ghana and beyond. In addition, the results obtained

for tritium in groundwater are used to determine the ages in which the the groundwater was recharged.

4.5.1. Tritium concentration results in the sampled Surface water

In this study, tritium was measured in 35 rainfall samples and 3 rivers. The average tritium concentration of rainwater and rivers is 3.32 TU and 2.64 TU, respectively and the tritium results is presented in table 4.68.

Table 4. 68: Results of tritium content in rainfall and Rivers sampled within the Lower Tano River Basin. All units are in tritium units (TU).

Sample Number	Type of Sample	TU
1	Rainfall	10.11
2	Rainfall	6.77
3	Rainfall	5.5
4	Rainfall	3.47
5	Rainfall	2.84
6	Rainfall	5.97
7	Rainfall	4.2
8	Rainfall	3.36
9	Rainfall	3.09
10	Rainfall	2.91
11	Rainfall	1.94
12	Rainfall	6.09
13	Rainfall	2.15
14	Rainfall	3.73
15	Rainfall	2.03
16	Rainfall	1.27
17	Rainfall	2.1
18	Rainfall	2.42
19	Rainfall	2.72
20	Rainfall	3.52
21	Rainfall	2.72
22	Rainfall	2.96
23	Rainfall	1.34
24	Rainfall	1.8
25	Rainfall	1.67
26	Rainfall	1.11
27	Rainfall	2.84
28	Rainfall	3.09
29	Rainfall	2.63
30	Rainfall	2.25
31	Rainfall	4.73
32	Rainfall	3.05
33	Rainfall	4.27
34	Rainfall	3.07
35	Rainfall	2.32
36	River	2.8
37	River	2.04
38	River	3.08

The obtained tritium results in the rainwater (Table 4.68) shows a decline in tritium concentration as compared to IAEA, (1980). This is deduced by the fact that during the dry and the wet seasons in the northern hemisphere where Ghana lies, the border layer between the troposphere and the stratosphere is possibly lowered. This decline might probably be accompanied by the release of tritium produced in the upper levels of the atmosphere into the troposphere, thereby increasing the flux of tritiated water to the ground by rainfall.

The levels of tritium content in the rainwater of the study area were lower than the tritium values obtained by Akiti (1980) for rainwater in some regions of southern Ghana. Acheampong and Hess (2000) measured tritium content in precipitation in 1994, and their values fall within the range of values obtained for the tritium concentration in the rainwater for the study area. The only difference is that the mean tritium content in their rainfall data was less than the average tritium concentration obtained for the rainwater in this study. In addition, the obtained tritium results for the rainwater in this study is in accordance with other published literature such as Lopez et.al. (1994), Blagojevich, (2003), Eriksson (1983), and Villa and Manjon (2004). The obtained tritium values in the rainwater of the study area can be explained by the fact that the study area is close to the Gulf of Guinea and the effect of the ocean water with very low tritium content is to decrease the tritium concentrations in rainwater. Similar works conducted by Hayashi et al. (1999) in Japan, which is also affected by the Pacific Ocean, reported slightly similar results.

It can therefore be reasoned that the tritium values for the sampled rain are in full accord with the recorded tritium contents of other investigators in similar oceanic terrain. Importantly, information obtained from this study combined with tritium measurements in the three sampled rivers may prove valuable for future hydrological investigations in the study catchment.

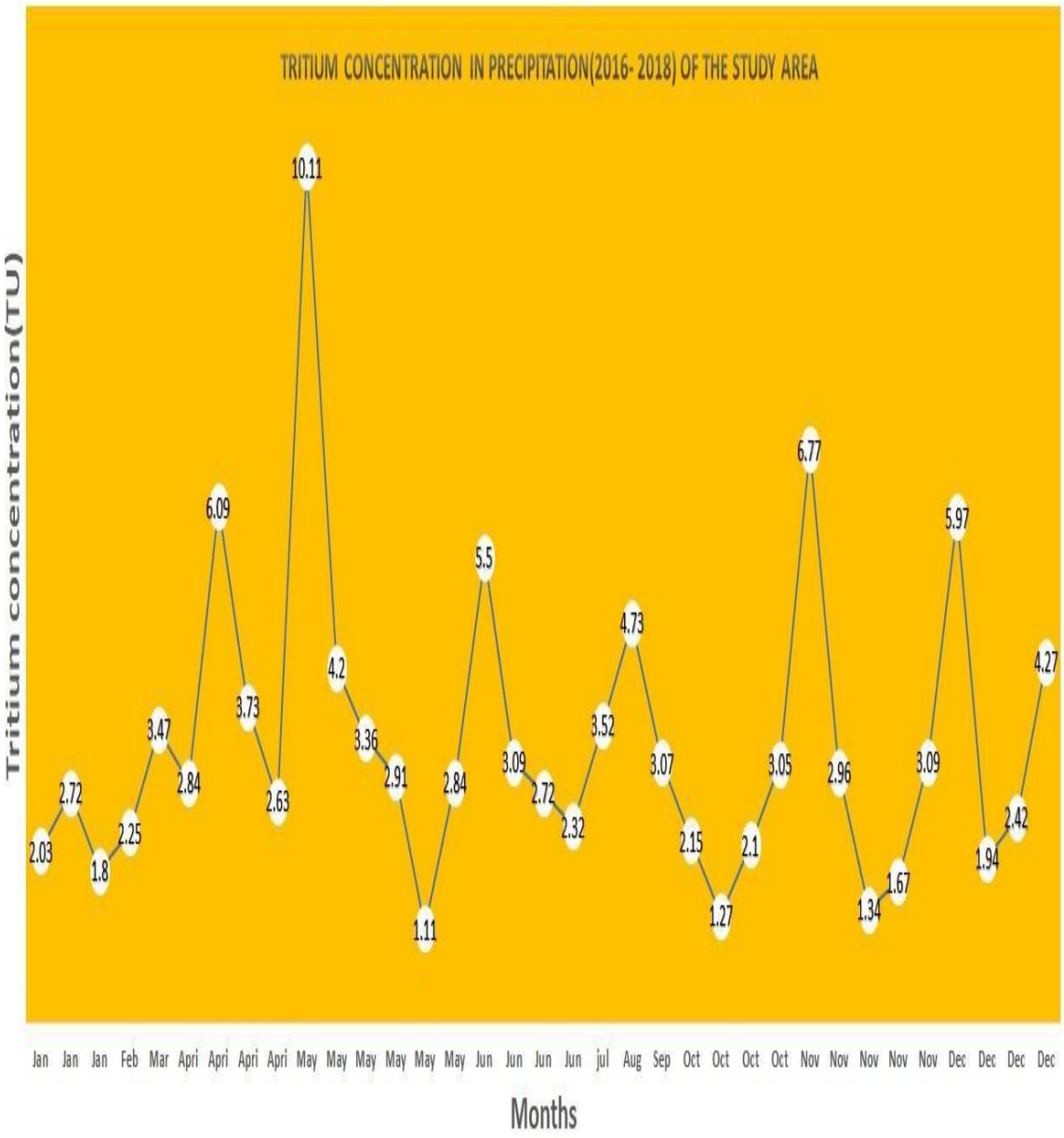

Figure 4. 63: Tritium concentration in the sampled rainwater of the Lower Tano River Basin

4.5.2. Results of Tritium concentration in the sampled Groundwater

Due to limited funds, tritium was measured in eighteen borehole samples located around the three sampled rivers. The results obtained is tabulated below:

Table 4.69: Tritium results for the sampled groundwater in te aquifer of the Apollonian formation and the Birimian supergroup. All units are in tritium units (TU).

Type of water	Town	Latitude	Longitude	Tritium
HDW	Esiama	4.93708	-2.34753	6.76
HDW	Half Assin	5.05041	-2.88695	4.03
HDW	Bobrama	4.91499	-2.29979	1.68
HDW	Elubo	5.29211	-2.77604	4.31
HDW	Esiama	4.94086	-2.34531	3.89
HDW	Kikam	4.92601	-2.32429	2.16
HDW	Aniwa	4.9233	-2.32594	2.65
BH	Kamgbunli	4.98212	-2.41549	5.91
BH	Elubo	5.29322	-2.77609	4.16
BH	Azeleno	4.94827	-2.38005	1.74
BH	Bomuakpolley	4.99989	-2.33273	1.94
Bh	Aluku	4.99479	-2.2645	2.3
BH	New Nzulezu	5.09191	-2.57354	3.03
BH	Telekobokazo	4.98707	-2.32713	0.99
BH	Tiekobo 1	5.05328	-2.32713	3.29
BH	Bobrama	4.91497	-2.29765	1.26
BH	Awiefoto	5.16214	-2.68664	4.36
BH	Salman	5.00452	-2.22655	1.8
BH	Ankobra New Site	4.90565	-2.27132	1.77

HDW – Hand dug well and BH – Borehole.

The tritium values in the groundwater ranges from 0.99 TU to 6.76 TU with a mean of 3.05 TU. The mean tritium value of the sampled groundwater was slightly like the mean tritium value of the rainwater. Tritium values in groundwater less than one are an indicative of old water and it implies that the groundwater was recharged before the thermonuclear bomb testing in 1952 (IAEA,1981). In this study, 17 (n=18) of the analyzed groundwater samples recorded tritium values greater than one, suggesting a probable recent or modern recharge (i.e., direct infiltration of recent rainfall in the study area). This means that 17 of the sampled groundwater were possibly recharged after the thermonuclear bomb test in 1952, making them newer in age and indicates that most of the groundwater in the aquifer of the Apollonian formation and the Birimian supergroup are of modern recharge. The tritium values in the sampled groundwater were also less than the tritium values (6.5 TU to 20 TU) obtained by Akiti (1980). This indicate that tritium values in groundwater located at the southeastern portion of Ghana would have decayed simultaneously by 2020 due to the half-life of tritium, which is

12.32 years. Similarly, the tritium values in the groundwater were in the range obtained by Adomako et al. (2010) and Ganyaglo (2015).

The tritium values obtained for most of the groundwater samples were also like modern day meteoric water values except one borehole located at Telekobokaso, in the aquifer of the Birimian Supergroup. That borehole had low tritium value (0.99 TU) which might possibly be due to tritium gradually decaying to its natural background levels after the cessation of a thermonuclear bomb tests in 1963 (www.iaea.com). Since $\delta^{18}O$ and $\delta^{2}H$ isotopic compositions in the borehole at Telekobokaso are not highly depleted than the rest of the groundwater samples, the low Tritium value recorded must be investigated further.

The spatial distribution map of tritium in groundwater in the aquifer of the Apollonian formation and the Birimian supergroup (Fig 4.66) did not show a definite flow pattern indicating intermittent aquifers in the study area.

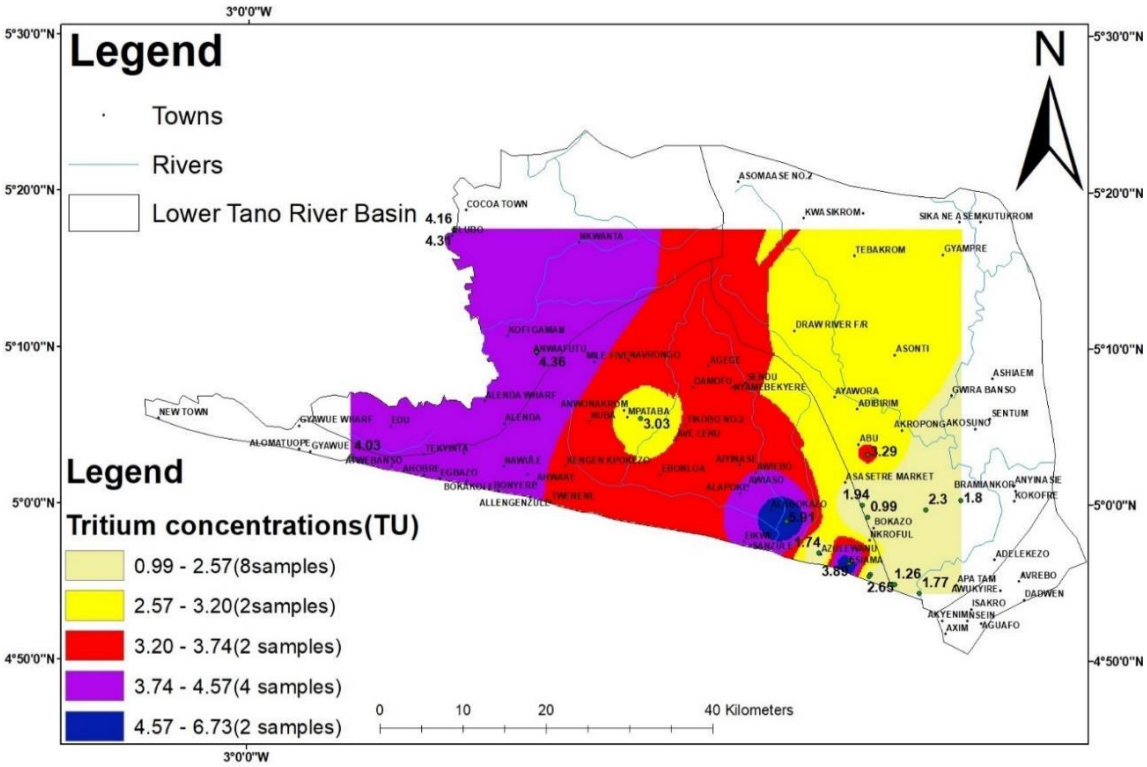

Figure 4.64: Spatial distribution map of tritium concentrations (TU) in ground water of the study area.

In the absence of long-term monitoring of tritium in rainfall in Ghana, approximation of the input signal since the bomb pulse in the early 1960s is done using the most proximate station (Aranyossy and Gaye 1992), which for Ghana is Bamako (Mali). This long-term tritium activity records in rainwater compiled by the I.A.E.A GNIP, from April 1963 to October 1998 are plotted in figure 4.67 together with the tritium values of rainwater, rivers, and groundwater sampled from the study area. From figure 4.67, two types of groundwater are observed that is groundwater recharged between 1960 - 1965, and 1965 – 1970. From the period in which the groundwater was recharged, it can be said that the aquifer of the Apollonian formation and the Birimian supergroup is of modern recharge with short residence time. This provides a general reason for low TDS content recorded for groundwater sampled from the aquifer of the Apollonian formation and the Birimian supergroup of the study area.

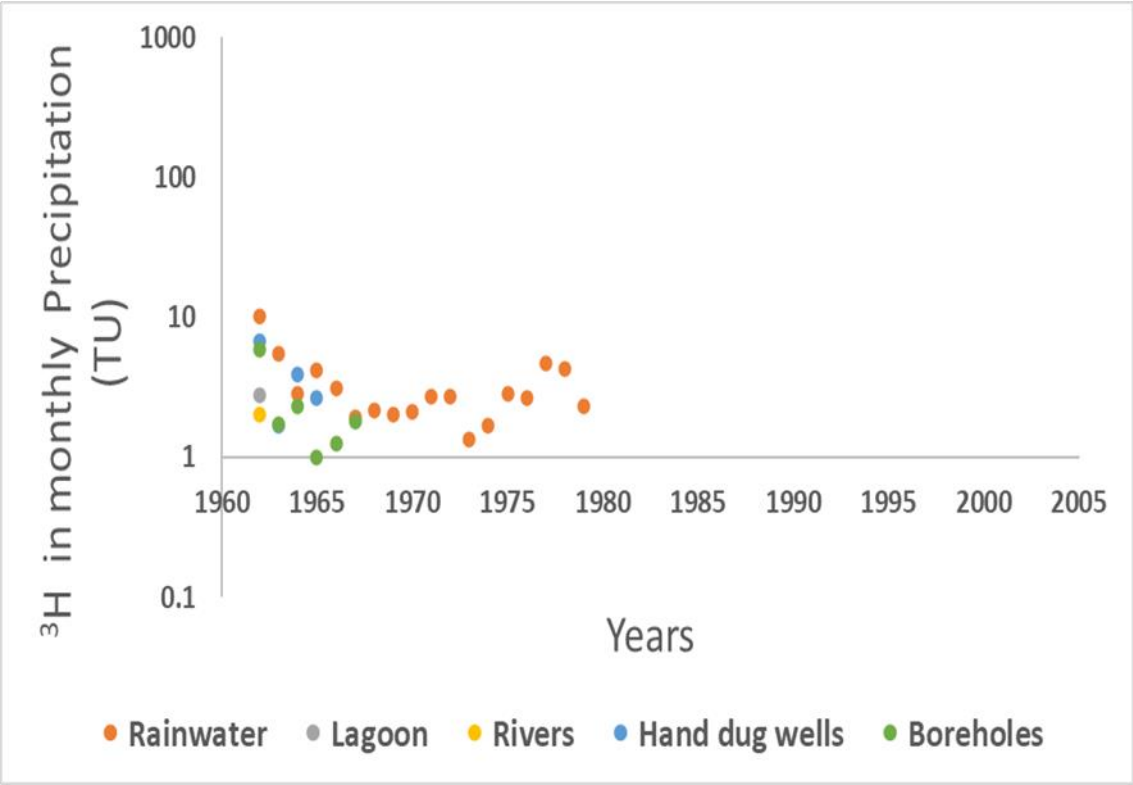

Figure 4.67: Tritium activity in monthly precipitation at the IAEA monitoring station in Bamako, Mali, from 1963 to 1999 (IAEA GNIP); with surface water and groundwater samples.

CHAPTER FIVE

CONCLUSIONS AND RECOMMENDATION

5.1 General Conclusions

Under this section the conclusion remarks under each specific objective is discussed. This will help understand the hydrogeology of the Lower Tano River Basin and that will help assist in the optimal decision-making regarding groundwater resources management to ensure sustainability.

5.1.1 Estimation of aquifer hydraulic parameters

The present study reports on the estimation of aquifer hydraulic parameters in the Lower Tano River Basin of Ghana. Based on the computed results, the depths of the boreholes range from 18 to 62 m, the yield of the boreholes range from 10 to 800 l/min, the groundwater levels range from -0.8 to 20.70 a.m.s.l, the transmissivity values range from 1.73 to 1219.70 m^3/day, the hydraulic conductivity values vary from 0.04 to 44.35 m/day, and the specific capacity values range from 0.72 to 122.24 L/min/m. With respect to the obtained aquifer hydraulic parameter results, the subsurface formation at the drilling sites was seen to be composed mainly of limestones, claystones along with conglomerates, sandstones, granites etc. Also, with respect to the computed aquifer hydraulic parameters, two types of aquifers were observed. That is the unconfined aquifer of the Apollonian formation and semi-confined aquifer of the Birimian supergroup. The computed water levels implies that groundwater in the Lower Tano River basin flows from the aquifer of the Birimian supergroup to the aquifer of the Apollonian formation and that was related to the deposition environment of the basin. Also, the estimated aquifer hydraulic parameters of the aquifer of the Apollonian formation and the Birimian supergroup had the potential to yield adequate amount of water for the growing population.

5.1.2 Assessing the overall quality of groundwater including the level of trace elements contamination and its suitability for domestic and agricultural purposes

This study provides an improved understanding of the hydrochemical factors that determines the suitability of groundwater for domestic and agricultural purposes. Combined use of cations, anions and trace elements was successfully employed to help assess the overall quality of groundwater and trace the sources of contamination.

The pH for the surface water and groundwater was acidic to neutral. The pH values of groundwater sampled from the aquifer of the Apollonian formation ranged from 4.1 to 6.8 with most samples below WHO (2011) permissible limit of 6.5 to 8.5. The pH of groundwater sampled from the aquifer of the Birimian supergroup ranged from 4.1 to 8.5 with most samples below WHO (2011) permissible limit of 6.5 to 8.5.

The TDS content for the surface water and groundwater revealed the occurrence of low mineralization with fresh groundwater (TDS < 1000 mg/L).

The electrical conductivity values for most of the surface water and all the groundwater were below WHO (2011) permissible limit of 1500 µS/cm for drinking water. In addition, the EC content in the groundwater sampled from the aquifer of the Apollonian formation and the Birimian supergroup had low enrichment of salts (EC<1500 µS/cm) making the groundwater drinkable.

The ions Ca^{2+}, Mg^{2+}, Na^{+}, K^{+}, Cl^{-}, SO_4^{2-}, NO_3^{-}, and HCO_3^{-} concentrations in the sampled surface water and the groundwater were minimal with Na^{+}, HCO_3^{-} and SO_4^{2-} dominating. Na^{+}, HCO_3^{-} and SO_4^{2-} ions were more than 93% of the total TDS concentrations in the surface water and the groundwater.

Based on a comparison with the WHO (2011) standards, problems with 40% of the surface water and groundwater quality for drinking were mostly related to high amount of Cu, Cd, Zn, Cr, Fe, Ni, Mn, Co, Pb, As, whereas the anions and cations did not influence the quality.

Results of the water quality index (WQI) indicated that groundwater quality status for majority of the groundwater were good for drinking with few unsuitable groundwater due to high concentration of Cu, Cd, Zn, Cr, Fe, Ni, Mn, Co, Pb, As. The increasing concentration of the trace elements in the groundwater sampled from the aquifer of the Apollonian formation and the Birimian supergroup was mainly geogenic with few anthropogenic sources. Groundwater suitability for drinking was low in the aquifer of the Apollonian formation. Even though the quality of groundwater was deteriorating for drinking purposes, most were suitable for irrigation based on SAR, PI, and chlorinity index. However, Na%, RSC, and MH % indices gave different results.

The calculated groundwater indices within the basin suggest that 40% of the groundwater in the aquifer of the Apollonian formation and the aquifer of the Birimian supergroup were unsuitable for irrigation, whiles the remaining 60% was suitable for irrigation.

5.1.3 Determination of the Hydrogeochemical processes that produces the chemical characteristics or compositions of the aquifer system

The Ficklin diagram used in this study demonstrated that most groundwater with high pH values and low trace elements were near – neutral low-metal water (pH = 6-9). Few groundwater with low pH content and high trace metals were acid-low metal water (pH = 4-6). The groundwater classification using the Ficklin diagram provided a useful information, which could be used to develop an appropriate water pollution and remediation strategies in the Lower Tano river basin.

The Durov diagram illustrated that all the groundwater in the aquifer of the Apollonian formation and the Birimian supergroup were young with TDS content being less than 1000 mg/L. In accordance to the Durov diagram, the groundwater sampled from the aquifer of the Apollonian formation and the Birimian supergroup was mainly classified as Na-Cl water type.

There were also representations of Ca-HCO_3, Na-HCO_3 and Na-SO_4^{2-} in groundwater sampled from the aquifer of the Apollonian formation and the Birimain supergroup.

Piper (1944) and Stiff (1951) diagrams used in the hydrochemical classification of the water types from 2014 to 2015 and 2017 groundwater samples showed a transition from Ca-Mg-HCO_3^- water type to Na-Cl water type along the flow direction. For the groundwater sampled in 2016, the Piper diagram and Stiff diagram evolve from Ca-Mg-Cl-SO4 to NaCl water type. The above water types were under the influence of natural processes and climatic conditions.

Gibbs (1970) diagram illustrated rock weathering and rainfall as the two major cause of variation in the groundwater hydrochemistry.

Different ionic ratios (Na^+/Cl^-, Na^+/HCO_3^-, $Ca^{2+} + Mg^{2+}$ Vs $SO_4^{2-} + HCO_3^-$, $Ca^{2+} + Mg^{2+} - HCO_3^- - SO_4^{2-}$ Vs $Na^+ - Cl^-$, $Na^+ + K^+$ Vs TC etc) were used to decipher different geochemical processes influencing the chemistry of groundwater in the aquifer of the Birimian supergroup and the Apollonian formation. All the results under ionic ratio suggested rock weathering, precipitation and ion exchange processes as the main processes governing the hyrochemical evolution of groundwater in the aquifer of the Apollonian formation and the Birimian supergroup.

The results of saturation index calculation indicated that carbonate minerals in most groundwater samples were undersaturated with respect to dolomite, aragonite, and calcite. Also, silicate minerals in most of the groundwater samples were under saturated with chalcedony, quartz, and amorphous silica. The saturation index (SI) for alumino silicate minerals in the groundwater samples was in the order of K– mica > kaolinite> gibbsite > Ca-montmorillonite > K feldspar. Stability diagram for calcium, magnesium sodium and potassium identified kaolinite and montmorillonite as the stable weathered products from weathering of primary minerals namely limestones, clay minerals, feldspars, plagioclase, hornblende etc.

The above result has not only helped in the understanding of the hydrogeochemical characteristics of the aquifer of the Apollonian formation and the Birimian supergroup but it has aided in providing a comprehensive understanding of the mineralization processes that supports the hydrochemical evolution and the hydrodynamic functioning of the aquifer of the Apollonian formation and the Birimian supergroup of the Lower Tano River Basin. This has therefore provided an important aquifer information for researchers and decision makers to formulate scientifically reasonable groundwater resource management strategies for the Lower Tano river basin of Ghana.

5.1.4 Investigating the sources of recharge to the aquifer system and age determination to understand the recharge sources

This study is the first systematic attempt to identify the sources of recharge in the Lower Tano river basin using isotopes ($\delta^{18}O$, $\delta^{2}H$). The Lower Tano river basin was characterized by properties such as geology and elevation that influence groundwater recharge. The isotopic results reveal that the sources of recharge for the groundwater within the basin was meteoric especially from the local rains. The isotopic binary mixing equation revealed that, rain fed rivers and streams also contributed to the groundwater recharge in the study area. These sources of recharge varied spatially according to their importance. Significantly, the influence of the rivers and the streams to the groundwater recharge was active in almost all the samples taken across the study area except for fewer samples. The spatial variability in the concentration of the isotopes ($\delta^{18}O$, $\delta^{2}H$) in the groundwater reflects the limited lateral connectivity of the aquifers due to the heterogeneity of their minerals. The tritium(^{3}H) results indicates that the groundwater was of modern recharge with short residence time. This is due to the groundwater being recharged between 1960 to 1965 and 1965 to 1970.

The isotopic composition results in the surface water and the groundwater will help in designing sustainable groundwater management strategies which will aid in the identification of active recharge zones in the Lower Tano River Basin.

5.2 Recommendations

Based on the present study, the following recommendations are made for better protection and management of groundwater resources within the Lower Tano River Basin.

- Groundwater quality monitoring must be conducted annually.
- Due to high concentrations of Cu, Cd, Zn, Cr, Fe, Ni, Mn, Co, Pb, and As in few hand dug wells and boreholes, the health impacts, especially on children have to be assessed across the Lower Tano River Basin.
- Environmentally friendly, cost effective and easy to adopt iron removal technology must be developed or contaminated groundwater must be restored using a cost-effective method such as managed aquifer recharge, thus using rainwater to dilute the concentration of trace element in the groundwater and this must be done when considering groundwater development in the study area.
- Special indication mark in the form of colour painting must be carried out to identify the hand dug wells and the borehole water contaminated with Cu, Cd, Zn, Cr, Fe, Ni, Mn, Co, Pb and As.
- Areas showing groundwater unsuitability for irrigation must be investigated further and appropriate soil amendments should be applied when considering large-scale farming in the Lower Tano River Basin.
- For an effective management of groundwater systems in the study area, a yearly estimation of the amount of water per domestic or industrial usage using the safe yield approach introduced by Todd, 1959, Theis, 1940, Lee, 1915, Alley et al. (1999), Sophocleous, 2000a, and Alley and Leake. (2004) must be considered.

REFERENCES

Aastri, J. C. V. (1994). Groundwater chemical quality in river basins, hydrogeochemical facies and hydrogeochemical modeling," Bharathidasan University, Thiruchirapalli, Tamil Nadu, India.

Abdelshafy, M., Saber, M., Abdelhaleem, A., Abdelrazek, S.M., & Seleem, E.M. (2019). Hydrogeochemical processes and evaluation of groundwater aquifer at Sohag city, *Egypt. Sci. Afr., 6*, e00196.

Abdul-Ganiyu, S., Hirohiko, I., Apusiga Adongo, T., & Kranjac-Berisavljevic, G. (2017). Evaluating Borehole Performance in Tolon and Wa West Districts of Northern Ghana. *African Journal of Applied Research (AJAR), [S.l.], 3*(2), 73-84, oct. 2017. ISSN 2408-7920.

Abollino, O., & Aceto, M., & Buoso, S., Gasparon, M., Green, W., Malandrino, M., & MentastI, E. (2004). Distribution of major, minor and trace metals in lake environments of Antarctica. *Antarctic Science - ANTARCT SCI. 16.* 277-291. 10.1017/S0954102004002111.

Abraitis, P.K., & Patrick, R., & Vaughan, D.J. (2004). Variations in the Compositional, Textural and Electrical Properties of Natural Pyrite: A Review. *International Journal of Mineral Processing, 74*, 41-59. *International Journal of Mineral Processing. 74.* 41-59. 10.1016/j.minpro.2003.09.002.

Acheampong, S. Y. (1996). *Geochemical evolution of shallow groundwater system in the Southern Voltaian Sedimentary Basin of Ghana*. PhD Thesis, University of Nevada Reno.

Acheampong, S., & Hess, J.W. (2000). *Origin of the shallow groundwater system in the southern Voltaian Sedimentary Basin of Ghana: An isotopic approach. Journal of Hydrology. 233*, 37-53. 10.1016/S0022-1694(00)00221-3.

Ackah, M., Agyemang, O., Anim, A., Osei, J., Bentil, N., Kpattah, L., Gyamfi, E., & Hanson, J. (2011). Assessment of groundwater quality for drinking and irrigation: The case study of Teiman-Oyarifa Community, Ga East Municipality, Ghana. Proc Int Acad Ecol Environ Sci. 1.

Addo-Fordjour, P., Gyamfi, H., Fei-Baffoe, B., & Akrofi, A. Y. (2013). Impact of copper-based fungicide application on copper contamination of cocoa plants and soils in the Ahafo Ano North District, Ashanti region, Ghana. *Ecology, Environment and Conservation, 19*, 303-310.

Adewoyin, O. O., Kayode, O. T., Omeje O., & Odetunmibi O. A. (2019). Risk assessment of heavy metal and trace elements contamination in groundwater in some parts of Ogun state, *Cogent Engineering, 6*(1), 1632555, DOI: 10.1080/23311916.2019.1632555

Adhikary, S., & Elahi, M., & Hossain, A.M. (2012). Assessment of Shallow Groundwater Quality from Six Wards of Khulna City Corporation, Bangladesh. *International Journal of Applied Sciences and Engineering Research. 1*. 488-498. 10.6088/ijaser.0020101050.

Adomako, D, Maloszewski, P., Stumpp, C., Osae, S., & Akiti, T. T. (2010) Estimating groundwater recharge from water isotope (δ2H, δ18O) depth profiles in the Densu River basin, Ghana, Hydrological Sciences Journal, 55:8, 1405-1416, DOI: 10.1080/02626667.2010.527847

Adomako, D., Osae, S., & Akiti, T., Faye, S., & Maloszewski, P. (2010). Geochemical and isotopic studies of groundwater conditions in the Densu River Basin of Ghana. *Environmental earth sciences. 62*. 1071-1084. 10.1007/s12665-010-0595-2.

Adomako, D., Osae, S., & Akiti, T.T. et al. (2011). Geochemical and isotopic studies of groundwater conditions in the Densu River Basin of Ghana. Environ Earth Sci 62, 1071–1084 (2011). https://doi.org/10.1007/s12665-010-0595-2.

Affum, A.O., Osae, S.D., Nyarko, B.J.B., Afful, S. Fianko, R.J., Akiti, T.T., Adomako, D., Acquaah, S.O., Dorluku, M., Antoh, E., Barnes, F., &Affum E.A. (2015). Total coliforms, arsenic, and cadmium exposure through drinking water in the Western Region of Ghana: application of multivariate statistical technique to ground water quality. *Environ. Monti. Assess., 1*, 2-23

Aghazadeh, N., & Moghaddam, A. A. (2010). Assessment of Groundwater Quality and its Suitability for Drinking and Agricultural Uses in the Oshnavieh Area, Northwest of Iran. *Journal of Environmental Protection, 1*, 30-40. 10.4236/jep.2010.11005.

Aghazadeh, N., Chitsazan, M., & Golestan, Y. (2016). Hydrochemistry and quality assessment of groundwater in the Ardabil area, Iran. *Applied Water Science. 7*. 10.1007/s13201-016-0498-9.

Agyemang, V.O. (2019). Hydrochemical Assessment of Groundwater Quality for Drinking, Domestic and Irrigation Purposes in Afigya Kwabre District, Ghana. *J Hydrogeol Hydrol Eng., 8*, 3.

Ahn, P.M. (1961). Soils of the lower Tano basin, south-western Ghana. Ministry of Food and Agriculture, Scientific Services Division, Soil and Land-use Survey Branch, Kumasi, p 266, Available online at http://library.wur.nl/ isric/index2.html?url=http://library. wur.nl/WebQuery/isric/ 2533.

Akaha & Promise, A. (2008). Critical overview of transboundary aquifers shared by South Africa. *Hydrogeology Journal 16*(6), 1207-1214.

Akhter, G., & Hasan, M. (2016). Determination of aquifer parameters using geoelectrical sounding and pumping test data in Khanewal District, Pakistan. *Open Geosciences, 8,* 630–638.

Akiti T. T. (1980). *Etudé géochimique et isotopique de quelqués aquifers du Ghana.* (Thesis.) Univeristé Paris-Sud. 232 pp.

Akiti T. T. (1987). Environmental isotope study of groundwater in crystalline rocks of the Accra Plains, Ghana. Proceedings of the 4th Working Meeting, Isotopes in Nature, Leipzig, September 1986.

Akiti, T.T. (1980). *Geochemical and isotopic studies of groundwater in Upper West Region of Ghana*. Unpublished PhD Thesis, Universitie´de Paris Sud.

Akiti, T.T. (1986). Environmental Isotope Study of Groundwater in Crystalline Rocks of the Accra Plains. In: 4th Working Meeting on Isotopes in Nature, Proceedings of an Advisory Group Meeting, IAEA, Vienna.

Akoachere, R., & Yaya, O., & Egbe, S., & Thomson, A.E., & Nji, B., & Besem, T. D. (2019). GIS-Hydrogeochemical Model of the Yaoundé Fractured Rock Aquifer, Cameroon: Aquifer Setting, Seasonal Variations in Groundwater-Rock Interaction and Water Quality. Journal of Geoscience and Environment Protection. 07. 232-263. 10.4236/gep.2019.75018.

Akoto-Bamford, S., & Osae, E., & Aboh, K., & Biney, C., & Antwi, L. (1990). Environmental Impact of the Gold Mining Industry in Ghana. *Biological trace element research,* 26-27. 279-85. 10.1007/BF02992682.

Alam, M.d S., & Wu, Y., & Cheng, T. (2014). Silicate Minerals as a Source of Arsenic Contamination in Groundwater. *Water Air and Soil Pollution. 225*. 10.1007/s11270-014-2201-9.

Alley et al. (1999) Alley, William & Reilly, T.E. & Franke, O.L. (1999). Sustainability of Ground-Water Resources. U.S. Geological Survey Circular 1186. 1186.

Alley, W.M., & Leake, S.A. (2004). The Journey from Safe Yield to Sustainability. *Ground Water, 42,* 12-16. http://dx.doi.org/10.1111/j.1745-6584.2004.tb02446.x

Allison G.B., & Hughes M.W. (1977). The history of tritium fallout in southern Australia as inferred from rainfall and wine samples. *Earth Planet. Sci. Lett. 36,* 334–340.

Amasa, S. K. (1975). "Arsenic Pollution at Obuasi Goldmine, Town and Surrounding Countryside" *Environmental Health Perspectives, 12*, 131.

Amoo, M. (2014). Palynostratigraphical and Paleo environmental Studies of Bonyere-1 Well; Onshore Tano Basin, Western Ghana: A Report Submitted to The Department of Earth Science University of Ghana in Partial Fulfillment for The Award of a Bachelor of Science Degree in Earth Science.

Amu-Mensah, F., Amu-Mensah, M., Akrong O.M., Addico, G., & Darko, H. (2019) Hydrology of the major water sources of Lake Bosumtwe in Ghana. *West Afr J Appl Ecol.* https://doi.org/10.13140/RG.2.2.27485.97761

Anim- Gyampo, M., & Anornu, G.K., & Appiah-Adjei, E., & Agodzo, S. (2019). Quality and health risk assessment of groundwater in the shallow aquifers within the Atankwidi basin of Ghana. Groundwater for sustainable Development.9.100217.10.1016/ j.gsd.2019.100217.

Anim-Gyampo, M., & Zango, M., & Ampadu, B. (2014). Assessment of Drinking Water Quality of Groundwaters in Bunpkurugu-Yunyo District of Ghana. *Environment and Pollution. 3.* 10.5539/ep.v3n3p1.

Annor, A., Acquah, J., & Ansah, E. (2018) Hydrogeological and Hydrochemical Assessment of Basin Granitoids in Assin and Breman Districts of Ghana. *Journal of Geoscience and Environment Protection, 6,* 31-57. doi: 10.4236/gep.2018.69004.

Annor, A., Acquah, J., & Ansah, E. (2018). Hydrogeological and Hydrochemical Assessment of Basin Granitoids in Assin and Breman Districts of Ghana. *Journal of Geoscience and Environment Protection, 6,* 31-57. doi: 10.4236/gep.2018.69004.

Antwi-Agyei, P., Horgah J. N., & Foli, G. (2009). Trace element contamination of soils around gold mines tailing dams at Obuasi, Ghana. *Afri. J. Envir. Sci. Technol. 13*(11), 353–359.

APHA, (2012). *Standard methods for the examination of water and wastewater, 22nd edition* edited by E. W. Rice, R. B. Baird, A. D. Eaton and L. S. Clesceri. American Public Health Association (APHA), American Water Works Association (AWWA) and Water Environment Federation (WEF), Washington, D.C., USA.

Apodaca, L. E., Jeffrey, B. B., & Michelle, C. S. (2002). Water quality in shallow alluvial aquifers, Upper Colorado River Basin, Colorodo. *Journal of the American Water Resources Association, 38,* 133–143.doi:10.1111/j.1752-1688.2002.tb01541.x

Appel, C., & Ma, L.Q. (2002). Concentration, pH and surface charge effects on cadmium and lead sorption in three tropical soils. *Journal of Environmental Quality, 31,* 581-589.

Appelo, C., & Postma, D. (2005). *Geochemistry, Groundwater and Pollution. 2nd Edition,* Balkema, Rotterdam. http://dx.doi.org/10.1201/9781439833544.

Appelo, C.A.J., & Postma, D. (1996). Geochemistry, Groundwater & Pollution. Balkema, Rotterdam.

Appelo, C.A.J., & Postma, D. (1999). Chemical Analysis of Groundwater, Geochemistry, Groundwater & Pollution. Balkema, Rotterdam.

Araguas-Araguas, L., Danesi, P., Froehlich, K., & Rozanski, K.: Global monitoring of the isotopic composition of precipitation, *J. Radioanal. Nucl. Ch., 205*, 189–200, https://doi.org/10.1007/BF02039404, 1996.

Armah, F.A., Obiri, S., Yawson, D.O., Afrifa, E.K.A., Yengoh, G.T., Alkan Olsson, J., & Odoi, J.O. (2011). Assessment of legal framework for corporate environmental behaviour and perceptions of residents in mining communities in Ghana. Journal of Environmental Planning and Management 54(2):193-209.

Armah, T. (2002). *Hydrochemical and geophysical studies of groundwater salinity, Central Region, Ghana*. Thesis (PhD). University of Ghana

Asante, K., Agusa, T., Annamalai, S., Ansa-Asare, O., Biney, C., & Tanabe, S. (2007). Contamination status of arsenic and other trace elements in drinking water and residents from Tarkwa, a historic mining township in Ghana. *Chemosphere. 66.* 1513-22. 10.1016/j.chemosphere.2006.08.022.

Asante-Annor, A., & Ewusi, A. (2016). Hydrogeological Properties of the Rocks in Adansi Mining Area, Ghana. *Ghana Mining Journal, 16*, 31. 10.4314/gmj.v16i1.4.

Asare-Donkor, N., & Boadu, T., & Adimado, A. (2016). Evaluation of groundwater and surface water quality and human risk assessment for trace metals in human settlements around the Bosomtwe Crater Lake in Ghana. *SpringerPlus. 5*, 10.1186/s40064-016-3462-0.

Ato, A.F., Oscar, Y.D., Akoto, B., Samuel, O., & Moi, P.A.N. (2010). Mining and heavy metal pollution: assessment of aquatic environments in Tarkwa (Ghana) using multivariate statistical analysis. *J. Environ. Statistics, 1*(4), 1-13 http://www.jenstat.org

ATSDR. (2012). "Public Sector Digital Communication Management Best Practices, Health Risk Communication Primer." Centers for Disease Control and Prevention, Agency for Toxic Substances and Disease Registry. http://www.atsdr.cdc.gov/risk/riskprimer.

Atta-Darkwa, T. (2016). Assessment of groundwater quality for irrigation in the Oda river basin, Ejisu-Besease, Ghana. *International journal of current research, 8*, 30994-31001.

Atta-Darkwa, T., Akolgo, G., & Kyei-Baffour, R. N., Agyare, W., & Abagale, F. (2016). Hydrological classification of the Besease inland valley bottom in Ghana for crop production using the water table fluctuation method:. *International Journal of Water Resources and Environmental Engineering, 8*, 81-91. 10.5897/IJWREE2015.0599.

Atta-Peters, D., & Garrey, P. (2014). Source Rock Evaluation and Hydrocarbon Potential in the Tano Basin, South Western Ghana, West Africa. *International Journal of Oil, Gas and Coal Engineering. 2*(5), 66-77. doi: 10.11648/j.ogce.20140205.11.

Atta-Peters, D., Agama1, C. I., Asiedu, D. K., & Apesegah, E. (2013). Palynology, palynofacies and palaeo environments of sedimentary organic matter from Bonyere – 1 Well, Tano basin, western Ghana: *International Letters of Natural Sciences, 5,* 27-45.

Attwa, M., Akca, I., Basokur, A.T., & Günther, T. (2014). Structure-based geoelectrical models derived from genetic algorithms: a case study for hydrogeological investigations along Elbe River coastal area, Germany. *J Appl Geophys*. doi:10.1016/ j.jappgeo.2014.01.006

Attwa, M., Henaish, A., & Zamzam, S. (2019). Detection and Prediction of Geo-environmental Hazards in Urban Areas and Desert Lands Using an Integrated Structural and Geophysical Approach: Cases from Egypt. 10.1007/978-3-030-18350-9_4.

Banoeng-Yakubo, B., Yidana, Sandow, E., Nti Akabzaa, T., & Asiedu, D. (2009). Analysis of groundwater quality using water quality index and conventional graphical methods: The Volta region, Ghana. *Environmental earth sciences. 59. 8*67-879. 10.1007/s12665-009-00829.

Banoeng-Yakubu B, Yidana SM, Ajayi JO, Loh Y, & Aseidu D (2011) Hydrogeology and groundwater resources of Ghana: a review of the hydrogeology and hydrochemistry of Ghana. In: McMann JM (ed) Potable water and sanitation, vol 142. Nova Science New York, NY.

Barzegar, R., Moghaddam, A.A., Najib, M., Kazemian, N., & Adamowski, J. (2016). Characterization of hydrogeologic properties of the Tabriz plain multilayer aquifer system, *NW Iran. Arab J Geosci 9*, 147.

Batte, A.G., Barifaijo, E., Kiberu, J.M., Kawule, W., Muwanga, A., Owor, M., & Kisekulo, J. (2010). Correlation of geoelectric data with aquifer parameters to delineate the groundwater potential of hard rock terrain in Central Uganda. *Pure Appl. Geophys., 167*, 1549-1559, 10.1007/s00024-010-0109-x.

Belkhiri, L., Abderrahmane, B., Mouni, L., & Baouz, T. (2010). Multivariate Statistical Characterization of Groundwater Quality in Ain Azel Plain, Algeria. *African Journal of Environmental Science and Technology, 4*, 526-534. 10.4314/ajest.v4i8.71307.

Bempa, (2014). *Arsenic Contamination of groundwater in south western part of Ashanti Region of Ghana,* A thesis approved by the Faculty of Environmental Sciences and Processing Engineering at the Brandenburg University of Technology in Cottbus-

Senftenberg in partial fulfilment of the requirement for the award of the academic degree of Doctor of Philosophy(Ph.D.) in Environmental Sciences.

Berner, E.K., & Berner, R.A. (1987). *The global water cycle geochemistry and the environment: Englewood* Cliffs, N.J., Prentice-Hall, 397 p.

Bethke, C. M., & Johnson, T. M. (2008). Groundwater age and age dating, *Annu. Rev. Earth Pl. Sc., 36,* 121–152.

Beyer, M., Morgenstern, U., & Jackson, B. (2014). Review of dating techniques for young groundwater (< 100 years) in New Zealand, *J. Hydrol., 53,* 93–111, 2014

Blagojevich R.R. (2003). Use of Tritium in Assessing Aquifer Vulnerability, http://www.epa.state.il.us/water/tritium.html

Boateng, T. K., Opoku, F., Osafo Acquaah, S., & Akoto, O. (2015). Pollution evaluation, sources and risk assessment of heavy metals in hand-dug wells from Ejisu- Juaben Municipality, Ghana. *Environmental Systems Research, 4,* 18 DOI: 10.1186/s40068-015-0045-y.

Boateng, T.K., Opoku, F., Acquaah, S.O., & Akoto, O. (2015) Pollution evaluation, sources and risk assessment of heavy metals in hand-dug wells from Ejisu-Juaben Municipality, Ghana. Environmental Systems Research, 4, 18. https://doi.org/10.1186/s40068-015-0045-y.

Boatta, F., Calabrese, S., D'Alessandro, W., & Parello, F. (2014). Chemical Composition of Atmospheric Bulk Deposition at the Industrial Area of Gela (Sicily, Italy).

Boghici, R. (2003). *User Manual 51: A Field Manual for Groundwater Sampling.* Texas Water Development Board, Austin, TX

Bouchaou, L., Michelot, J.L., Vengosh, A., Hsissou, Y., Mohamed, Q., Gaye, C.B., Bullen, T.D., & Zuppi, G.M.. (2008). Application of multiple isotopic and geochemical tracers for investigation of recharge, salinization, and residence time of water in the Souss-Massa aquifer, southwest of Morocco. *Journal of Hydrology. 352,* 267-287. 10.1016/j.jhydrol.2008.01.022.

Boulton, N. (1954). Unsteady radial flow to a pumped well allowing for delayed yield from storage. *International Association of Scientific Hydrology. 37.* 472-77.

Boulton, N.S. (1963) Analysis of Data from Non-Equilibrium Pumping Tests Allowing for Delayed Yield from Storage. *Proceedings of the Institute of Civil Engineers, 26,* 469-482. http://dx.doi.org/10.1680/iicep.1963.10409

Bowser, C.J., & Jones, B.F. (2002). Mineralogical controls on the composition of natural waters dominated by silicate hydrolysis. *Am. J. Sci., 302,* 582-662.

Brammer, H. (1962). Soils. In J. B. Wills (Ed.), *Agriculture and land use in Ghana, Ministry of Agriculture,* Accra, Ghana (pp. 84-114). London: Oxford University Press.

Bürge, D., Hari, R., Xue, H., Behra, P., & Sigg, L. (2002). Adsorption of Cu, Cd, and Ni on Goethite in the Presence of Natural Groundwater Ligands. *Environmental science & technology*, *36*, 328-36. 10.1021/es010892i.

Burns, D. A., Plummer, L. N., McDonnell, J. J., Busenberg, E.,Casile, G. C., Kendall, C., Hooper. R. P., Freer. J. E., Peters, N. E., Beven, K., & Schlosser, P. (2003). The geochemical evolution of riparian ground water in a forested piedmont catchment, *Ground Water, 41,* 913–925, 2003.

Burton, W. C., Plummer, L. N., Busenberg, E., Lindsey, B. D., & Gburek, W. J. (2002). Influence of fracture anisotropy on ground water ages and chemistry, Valley and Ridge Province, Pennsylvania, *Ground Water, 40,* 242–257, 2002.

Cañedo-Argüelles, M., Kefford, B.J., Piscart, C., Prat, N., Schäfer, R.B., & Schulz, C.J. (2013). Salinisation of rivers: an urgent ecological issue. *Environ Pollut., 173*, 157-67. doi: 10.1016/j.envpol.2012.10.011. Epub 2012 Nov 29. PMID: 23202646.

Cao, Y., Tang, C., Song, X., Liu, C., & Zhang, Y. (2016) Identifying the hydro chemical characteristics of rivers and groundwater by multivariate statistical analysis in the Sanjiang Plain, China. *Appl Water Sci., 6,* 169–178

Cartwright, I., & Morgenstern, U. (2012). Constraining groundwater recharge and the rate of geochemical processes using environ-mental isotopes and major ion geochemistry: Ovens Catchment, *Southeast Australia, J. Hydrol., 475,* 137–149.

Chandrasekar, N., & Prince, J. (2012). Delineation of groundwater potential zones in Theni district, Tamil Nadu, using remote sensing, GIS and MIF techniques. *Geoscience Frontiers, 3,* 189-196. 10.1016/j.gsf.2011.10.007.

Chebotarev, I. (1955). Metamorphism of Natural Waters in the Crust of Weathering. *Geochimica et Cosmochimica Acta, 8,* 22-32. https://doi.org/10.1016/0016-7037(55)90015-6

Chegbeleh LP, Akurugu BA, Yidana SM (2020) Assessment of groundwater quality in the Talensi District, Northern Ghana. Sci World J. https://doi.org/10.1155/2020/8450860.

Chemistry. Willey, New York. 780 pp.

Chen, J., Hubbard, S., & Rubin Y. (2001). Estimating Hydraulic Conductivity at the South Oyster Site from Geophysical Tomographic Data using Bayesian Techniques based on the Normal Linear Regression Model, *Wat. Resour. Res., 37(*6), 1603–1613, 2001.

Chen, X.H., & Ayers, J.F. (1998). Aquifer properties determined from two analytical solutions. *Ground Water 36*(5), 783–791.

Clark, I., & Fritz, P.F. (1998). *Environmental Isotopes in Hydrology.* Lewis Publishers. 328pp

Clark, I.D., & Fritz, P. (1997). Environmental Isotopes in Hydrogeology CRC Press.

Cobbina, S., Duwiejuah, A., Quansah, R., Obiri, S., & Bakobie, N. (2015). Comparative Assessment of Heavy Metals in Drinking Water Sources in Two Small-Scale Mining Communities in Northern Ghana. *Int. J. Environ. Res. Public Health. 12*. 10620-10634. 10.3390/ijerph120910620.

Collins, R., & Jenkins, A. (1996). The Impact of Agricultural Land Use on Stream Chemistry in the Middle Hills of the Himalayas, Nepal. Journal of Hydrology, 185, 71-86. http://dx.doi.org/10.1016/0022-1694(95)03008-5

Cooper, H.H., & Jacob, C.E. (1946). A generalized graphical method for evaluating formation constants and summarizing well field history, Am. Geophys. *Union Trans., 27*, 526-534.

Cox, L. R. (1952). Cretaceous and Eocene fossils from the Gold Coast: Gold Coast Geol. Survey. *Bull., 17,* 68.

Craig E, & Anderson, M.P. (1979). The effects of urbanization of ground water quality. A case study of ground water ecosystems. *Environ Conserv., 30*(2), 104–130.

Craig, E., & Anderson, M. P. (1979). The effect of urbanization of groundwater quality—A case study. *Groundwater, 17,* 456–482

Craig, H. (1961). Isotopic Variations in Meteoric Waters. *Science, 133,* 1702-1703. http://dx.doi.org/10.1126/science.133.3465.1702

CWSA, (2013). Unpublished reports from Community water and sanitation agency (CWSA), 2013): CWSA (2013). Reports on Western region borehole logs, Unpublished reports retrieved from CWSA, Tarkoradi, Western Region, Ghana

Dampare, S., Shibata, T., Asiedu, D., Osae, S., & Banoeng-Yakubo, B. (2008). Geochemistry of Paleoproterozoic metavolcanic rocks from the southern Ashanti volcanic belt, Ghana: Petrogenetic and tectonic setting implications. *Precambrian Research - PRECAMBRIAN RES., 162,* 403-423. 10.1016/j.precamres.2007.10.001.

Dansgaard, W. (1964). Stable isotopes in precipitation. *Tellus, 16,* 436–468.

Darko, H., Ansa-Asare, O., & Paintsil, A. (2013). A number Description of Ghanaian Water Quality – A Case Study of the Southwestern and Coastal Rivers Systems of Ghana. *Journal of Environmental Protection. 04*.1318-1327.10.4236/jep.2013.411153.

Darko, P.K., Duah, A.A., & Dapaah-Siakwan, S. (2003). Groundwater Assessment: An Element of Integrated Water Resources Management – The Case of Densu River Basin. CSIR-Water Research Institute, WRI/CAR No. 54.

Daughney, C. J., Morgenstern, U., van der Raaij, R., & Reeves, R. R. (2010). Discriminant analysis for estimation of groundwater age from hydrochemistry and well construction: Application to New Zealand aquifers, *Hydrogeol. J., 18,* 417–428, 2010.

Decarreau, A., Colin, F., Herbillon, A., Manceau, A., Nahon, D., Paquet, H., Trauthbadaud, D., & Trescases, J. J. (1987). Domain segregation in Ni-Fe-Mg-smectites. *Clays and Clay Minerals, 35*, 1-10.

Devadas, Dr. D., & Rao, N., & Rao, B., & Rao, K., & Subrahmanyam, A. (2007). Hydrogeochemistry of the Sarada river basin, Visakhapatnam district, Andhra Pradesh, India. *Environmental Geology, 52,* 1331-1342. 10.1007/s00254-006-0577-6

Dike, E.F.C., & Dan-Hassan, M.A. (1990). The Geology and Aquifer Properties of the Tertiary Kern-Kerr Formation, Bauchi State. Proc. Nig. Assoc. Hydrogeologists 3rd National Conf. Zaranda Hotel Bauchi. pp117-133.

Doneen, L.D. (1962). The Influence of Crop and Soil on Percolating Water. Proceedings of the 1961 Biennial Conference on Groundwater Recharge, 156-163.

Dorleku, M., Nukpezah, D., & Carboo, D. (2018). Effects of small-scale gold mining on heavy metal levels in groundwater in the Lower Pra Basin of Ghana. *Applied Water Science, 8.* 126. 10.1007/s13201-018-0773-z.

Doyi, I., Essumang, D., Gbeddy, G., Dampare, S., Kumassah, E., & Saka, D. (2018). Spatial distribution, accumulation and human health risk assessment of heavy metals in soil and groundwater of the Tano Basin, Ghana. *Ecotoxicology and Environmental Safety, 165*. 10.1016/j.ecoenv.2018.09.015.

Drever, J.I. (1988). *The Geochemistry of Natural Waters. 2nd Edition*, Prentice-Hall, Englewood Cliffs, 437 p.

Driscoll, F.G., (1989). Groundwater and Wells. Second edition. Johnson Filtration System.

Durov, S.A. (1948). Classification of natural waters and graphic presentation of their composition. *Dokl Akad Nauk SSSR, 59*(1), 87–90.

Dzigbodi-Adjimah, K. & Asamoah, N. D. (2009). "The Geology of the Gold Deposits of Prestea Gold Belt of Ghana", *Ghana Mining Journal, 11,* 7 - 18.

Eaton, F.M. (1950) Significance of Carbonates in Irrigation Waters. *Soil Science, 69,* 123-134. https://doi.org/10.1097/00010694-195002000-00004

Edjah, (2012). Hydrogeochemistry and hydrogeological studies of Ellembelle and Jomoro districts of the Western Region of Ghana, Thesis work submitted to the University of Ghana in partial fulfilment of the requirement for the degree of master of Philosophy in Nuclear Earth Science,2012.

Edjah, A.K.M., Akiti, T.T., Osae, S., et al. (2017). Hydrogeochemistry and isotope hydrology of surface water and groundwater systems in the Ellembelle district, Ghana, West Africa. *Appl Water Sci 7*, 609–623. https://doi.org/10.1007/s13201-015-0273-3.

Edmunds W. M., Hinsby K., Marlin C., Melo T., Manzano M., Vaikmäe R., & Travi Y. (2001) in Palaeowaters in Coastal Europe: evolution of groundwater since the late Pleistocene, Evolution of groundwater systems at the European coastline, Geological Society, London, Special Publications, eds Edmunds W. M., Milne C. J. 189, pp 289–311.

Egbi, C.D., Anornu, G., Appiah-Adjei, E.K., et al (2018). Evaluation of water quality using hydrochemistry, stable isotopes, and water quality indices in the Lower Volta River Basin of Ghana.

Ehya, F., & Marbouti, Z. (2016). Hydrochemistry and contamination of groundwater resources in the Behbahan plain, SW Iran. *Environmental Earth Sciences. 75*. 10.1007/s12665-016-5320-3.

Eisenlohr, B.N., & Hirdes, W. (1992). The structural development of the early Proterozoic Birimian and Tarkwaian rocks of southwest Ghana, West Africa. *J. Afr. Earth Sci., 14*, 313-325

El Baghdadi, M., Zantar, I., Jouider, A., & Nadem, S., & Medah, R. (2019). Evaluation of hydrogeochemical quality parameters of groundwater under urban activities. Case of Beni Mellal city (Morocco). *Euro-Mediterranean Journal for Environmental Integration. 4*. 10.1007/s41207-018-0087-4.

Elango, L., Kannan, R., & Kumar, S. (2003). Major ion chemistry and identification of hydrogeochemical processes of groundwater in a part of Kancheepuram district, Tamil Nadu, India. *J. Environ Geosci.*, *10*(4), 157–166. https://doi.org/10.1306/eg100403011.

Elangovan, K. (1997). Hydrogeochemistry of groundwater formingheavy scales in water supply system of Salem district, Tamil Nadu (334 pp.). Unpublished Ph.D. Thesis, Mysore Univer-sity, Mysore Tamata, 1990.

Eriksson E. (1983). Stable isotopes and tritium in precipitation. In Guidebook on nuclear techniques in hydrology, *Technical Reports Series I.A.E.A. 91*, 19–27.

Eriksson, E. (1983) Stable isotopes and tritium in precipitation. Guidebook on Nuclear Techniques in Hydrology, pp.19–33. IAEA, Vienna.

Esdaile, L.J., & Chalker, J.M. (2018). The Mercury Problem in Artisanal and Small-Scale Gold Mining. Chemistry – *A Eur. J., 24*, 6905-6916.

Ewusi, A., Apeani, B.Y., Ahenkorah, I., Nartey, R.S. (2017). Mining and metal pollution: assessment of water quality in the Tarkwa mining area. *Ghana Min.J., 17* (2) (2017), pp. 17-31.

Fadly, M., Prayogi, T.E., Mohamad, F., et al (2017). Groundwater Quality Assessment in Jakarta Capital Region for the Safe Drinking Water. IOP Conference Series: *Materials Sci and Engine 180*(1), 012063. https://doi.org/10.1088/1757-899X/180/1/012063

Felmy A. R., Girvln., C., & Jenne, E. A. (1984). Minteq--a computer program for calculating aqueous geochemical equilibria. EPA-600/3-84-032, N.T.I.S. PB84-157148.

Fianko, J. R. (2009). The hydrochemistry of groundwater in rural communities within the Tema District, Ghana. Environmental monitoring and assessment. 168. 441-9. 10.1007/s10661-009-1125-0.

Ficklin, W.H., Plumlee, G.S., Smith, K.S., & McHugh, J.B. (1992). Geochemicalclassification of mine drainages and natural drainages in mineralizedareas. Proceedings of the 7th International Symposium on Water-Rock Interaction, Balkema, Rotterdam, pp 381–384.

Fijani, F., Moghaddam, A.A., Tsai, F.T.C., & Tayfur, G. (2016). Analysis and Assessment of Hydrochemical Characteristics of Maragheh-Bonab Plain Aquifer. Water Resour Manage, Northwest of Iran. doi:10.1007/s11269-016-1390-y.

Fisher, S. (2002). *Groundwater quality Kentucky. Information circular 6 series XII*, ISSN. 0095-5583, Health Canada Environment and Work Place Health.

Fisher, S.R., & Mullican, W.F. (1997). Hydrogeochemical evaluation of sodium-sulphate and sodium-chloride groundwater beneath the northern Chihuahua desert, Trans-Pecos, Texas, USA. *Hydrogeology Journal, 5*(2), 4-16.

Flemming, C.A., & Trevors, J.T. (1989). Copper Toxicity and Chemistry in the Environment: A Review. *Water, Air, Soil & Pollution, 44*, 143-158. http://dx.doi.org/10.1007/BF00228784.

Freeze, R.A., & Cherry, J.A. (1979). *Groundwater*. Prentice-Hall Inc., Englewood Cliffs, *7632*, 604.

Fritz, P., & Fontes, J.Ch. (1980). *Handbook of Environmental Isotope Geochemistry*. (Vol. I), The Terrestrial Environment, A. Amsterdam, the Netherlands: Elsevier, 545pp

Ganyaglo, S. Y. (2015). *Hydrogeochemical and Isotopic Studies of Groundwater in Coastal Aquifers of Ghana: Case Study in the Central Region* [PhD] [Doctoral dissertation, University of Ghana, Legon], http://197.255.68.203/handle/123456789/21211.

Ganyaglo, S. Y., Osae, S., Akiti, T., Armah, T., Gourcy, L., Vitvar, T., Ito, M., & Appiah Otoo, I. (2017). Groundwater residence time in basement aquifers of the Ochi-Narkwa Basin in the Central Region of Ghana. *Journal of African Earth Sciences, 134*. 10.1016/j.jafrearsci.2017.07.028.

García-López, S., & Escarcena, F.J., Benavente, J., & Cruz-Sanjulián, J.J. (1994). Natural and anthropogenic sources of tritium in carbonate aquifers to the south of Sierra Nevada (Spain). *Journal of Environmental Hydrology, 2*(2), 2-31.

Garrels R. M., & MacKenzie F.T. (1971). *Evolution of Sedimentary Rocks.* Norton, New York.

Garrels, R.M., & Mackenzie, F.T. (1967). Origin of the Chemical Composition of Some Springs and Lakes. In: Stumm, W., Ed., *Equilibrium Concepts in Natural Water Systems, Chap. 10,* American Chemical Society, Washington DC, 222-242. http://dx.doi.org/10.1021/ba-1967-0067.ch010

Gaskin, C.J., & Happell, B. (2014). On exploratory factor analysis: A review of recent evidence, an assessment of current practice, and recommendations for future use. *Int. J. Nurs. Stud., 51*, 511-521

Gastmans, D., Chang, H., & Hutcheon, I. (2010). Groundwater geochemical evolution in the northern portion of the Guarani Aquifer System (Brazil) and its relationship to diagenetic features. *Applied Geochemistry - APPL GEOCHEM. 25*. 16-33. 10.1016/j.apgeochem.2009.09.024.

Gat, J.R. (1980) The isotopes of hydrogen and oxygen in precipitation. In *Handbook of Environmental Isotope Geochemistry*, eds. P. Fritz and J.-C. Fontes, *1, 21–47*. Elsevier, Amsterdam.

Gat, J.R. (1983). Palaeoclimates and Palaeowaters: A Collection of Environmental Isotope Studies: Proceedings of an Advisory Group Meeting on the Variations of the Isotopic Composition of Precipitation and of Groundwater During the Quaternary as a Consequence of Climatic Changes, IAEA.

Geological map of Ghana, Geological Survey Dept, GSD.

Ghana Geological Survey (GSS) (2009). Geological Map of Ghana—1:1000000. Geological Survey Department, Accra, Ghana.

Ghana Statistical service (GSS) (2012). Population and Housing Census. Retrieved from https://statsghana.gov.gh

Ghana survey department (GSD) (2009). Geological map of Kumasi Metropolis.

Gibbs, R.J. (1970). Mechanisms controlling world water chemistry. Science 170:795–840.

Giblin, A.E. (2009). Iron and manganese. Chief. Elsevier Press, *Encyclopedia of Inland Waters*, pp 35–44.

Glynn, P. D., & Plummer, L. N. (2005). Geochemistry and the understanding of ground-water systems, *Hydrogeol. J., 13*, 263–287.

Goel, P.K. (1997). Water pollution causes, effects and control, 1st ed.; Published by Poplai: H.S. for New Age International (P) Limited, New Delhi, 1997, 97-115.

Goldberg, E.D., Hodge, V., Koide, M., Griffin, J.J. (1976). Metal Pollution in Tokyo as recorded in sediments of the Palace most. *Geochem, J., 10,* 165-174.

Goldich, S. S. (1938). A study in rock-weathering. *The Journal of Geology, 46(*1), 17–58. doi:10.1086/624619

Goldschmidt, V. M. (1958). *Geochemistry*, Oxford University Press, Oxford.

Goode, D. J. (1996). Direct simulation of groundwater age. *Wat. Resour. Res., 32*, 289–296.

Gorsuch, R. (1983). *Factor analysis (2nd ed.).* Hillsdale, NJ: Lawrence Erlbaum Associates.

Grimestad, G. (2002) A reassessment of ground water flow conditions and specific yield at Borden and Cape Cod. *GroundWater, 40*(1), 14–24

Guo, H., & Wang, Y. (2004). Hydrogeochemical Processes in Shallow Quaternary Aquifers from the Northern Part of the Datong Basin, China. *Applied Geochemistry. 19,* 19-27. 10.1016/S0883-2927(03)00128-8.

Gyasi, S. (2017). Palynology, Palynofacies and Hydrocarbon Potential of Cretaceous Sediments in the Offshore Tano Basin http://ugspace.ug.edu.gh/handle/123456789/29075.

Hadzi, G.Y., Essumang, D.K., & Adjei, J.K. (2015). Distribution and risk assessment of heavy metals in surface water from pristine environments and major mining areas in Ghana. *J. Health Pollut., 5* (9), 86-99, 10.5696/2156-9614-5-9.86.

Halim, M., Majumder, R., Nessa, S., Oda, K., Hiroshiro, Y., & Jinno, K. (2010). Arsenic in shallow aquifer in the eastern region of Bangladesh: Insights from principal component analysis of groundwater compositions. Environmental Monitoring and Assessment. 161. 453-472. 10.1007/s10661-009-0760-9.

Halima, M.A., Majumder, R.K., Nessa, S.A., Hiroshiro, Y., Sasaki, K., Saha, B.B., & Jinno, K. Evaluation of processes controlling the geochemical constituents in deep groundwater in Bangladesh: spatial variability on arsenic and boron enrichment J. Hazardous Mater., 180 (2010), pp. 50-62

Hamidu, H. S.W., Muhammad, A. B., & Garga, M. A. (2016). Kana Groundwater Potentials Estimation of a Basement Terrain Using Pumping Test Data for Parts of Sanga Local Government Area, Kaduna State, Northwestern Nigeria. *Open Journal of Modern Hydrology, 6,* 222-229.

Handa, B. K. (1986). 'Trace Elements Content of Groundwater in the Basaltic Rocks in Some Parts of Indian Peninsula', in K. B. Power and S. S. Thigale (eds), *Hydrogeology of Volcanic Terranes*, University of Poona, Pune, 83–104.

Hanshaw, B. B., & William B. (1979). Major geochemical processes in the evolution of carbonate—Aquifer systems, *Journal of Hydrology, 43*(1–4), 287-312,ISSN 0022-1694, https://doi.org/10.1016/0022-1694(79)90177-X.

Hasan, M., Shang, Y., Akhter, G., & Jin, W. (2018b), Evaluation of groundwater potential in Kabirwala area, Pakistan: a case study by using geophysical, geochemical and pump data. *Geophysical Prospecting, 66,* 1737–1750. https://doi.org/10.1111/1365-2478.12679.

Hasan, M., Shang, Y., Jin, W.J., Akhter, G. (2020). Estimation of hydraulic parameters in a hard rock aquifer using integrated surface geoelectrical method and pumping test data in southeast Guangdong, China. *Geosciences Journal, 25.* 10.1007/s12303-020-0018-7.

Hatcher, L. (1994). A Step-by-Step Approach to Using the SAS System for Factor Analysis and Structural Equation Modeling. SAS Institute, Inc., Cary.

Hayashi, Y., Momoshima, N., Kakiuchi, H., & Madea, Y. (1999). Relation between tritium concentration and chemical composition in rain in Fukuoka. *Journal of Radioanalytical Nuclear Chemistry 239,* 517.

He, Z., Yang, X., & Stoffella, P. (2005). Trace Eelements in Agroecosystems and Impacts on the Environment. *Journal of trace elements in medicine and biology: organ of the Society for Minerals and Trace Elements (GMS) 19*, 125-40. 10.1016/j.jtemb.2005.02.010.

Heidari, M., & Moench, A.F. (1997) Evaluation of unconfined-aquifer parameters from pumping test data by nonlinear least squares. *J. Hydrol, 192*(1), 300–313

Helgeson, H. C., Brown, T. H., Nigrini, A., & Jones, T. A. (1970). Calculation of mass transfer in geochemical processes involving aqueous solutions. *Geochimica et Cosmochimica Acta, 34*, 569–592.

Helstrup, T., Jørgensen, N., & Banoeng-Yakubo, B. (2007). Investigation of hydrochemical characteristics of groundwater from Cretaceous—Eocene limestone aquifer in southern Ghana and Togo using hierarchical cluster analysis. *Hydrogeology Journal, 15*, 977-989. 10.1007/s10040-007-0165-1.

Hem, J.D. (1985). *Study and Interpretation of the Chemical Characteristics of Natural Water. 3rd Edition,* US Geological Survey Water-Supply Paper 2254, University of Virginia, Charlottesville, 263 p.

Hem, J.D. (1986). Study and interpretation of the chemical characteristics of natural waters. United States Geological Survey, Water Supply Paper 1473. USGS, Washington, D.C.

Hem, J.D. (1991). Study and Interpretation of the Chemical Characteristics of Natural Water. Geological Survey Water-Supply Paper 1973, U.S. Government Printing Office, Washington DC, 363 p.

Hem, J.D. (2002). Study and interpretation of the chemical characteristics of natural water. US Geochemical Survey Water Supply, Paper 2254

Henry, D., & Daigle, N. (2018). Chlorine incorporation into amphibole and biotite in high-grade iron-formations: Interplay between crystallography and metamorphic fluids. *American Mineralogist, 103*, 55-68. 10.2138/am-2018-6143.

Hirdes, W., & Leube, A. (1989). On gold mineralisation of the Proterozoic Birimian Supergroup in Ghana. BGR Rep. No. 104 248, 179 pp.

Hirdes, W., Davis, D.W., & Eisenlohr, B.N. (1992). Reassessment of Proterozoic granitoid ages in Ghana on the basis of U/Pb zircon and monazite dating. *Precambr. Res., 56*, 89-96.

Hitzman, M., Bookstrom, A., Slack, J., & Zientek, M. (2017). Cobalt—Styles of Deposits and the Search for Primary Deposits. 10.3133/ofr20171155.

Hoeing, M., Baeten, H., Vanhentenrijk, S., Vassileva, E., & Quevauviller, P.H. (1998). Critical discussion on the need for an effective mineralization procedure for the analysis of plant material by atomic spectrometric methods. *Analytica Chimica Acta., 358*, 85-94.

Hounslow, A.W. (1995). *Water Quality Data: Analysis and Interpretation*. CRC Press LLC, Lewis Publishers, Boca Raton.

Howlader, M.F., Deb, P.K., Mazumder, A.T.M.S.H., & Ahmed, M. (2014). Evaluation of water resources around Barapukuria coal mine industrial area, Dinajpur, Bangladesh. *Appl Water Sci., 4*, 203–222. https://doi.org/10.1007/s13201-014-0207-5

Hseu, Z. Y. (2006). Concentration and distribution of chromium and nickel fractions along a serpentinitic toposequence. *Soil Science, 171*, 341-353

Hunt, B. (2006). Characteristics of unsteady flow to wells in unconfined and semi-confined aquifers. *J. Hydrol, 325*(1– 4), 154–163.

Hussain, I., Abu-Rizaizab, O. S., Habibb, M.A.A., & Ashfaqc, M. (2008). Revitalizing a traditional dryland water supply system: the karezes in Afghanistan, Iran, Pakistan and the Kingdom of Saudi Arabia. *Water International, 33*(3), 333-349.

IAEA www.iaea.org/water.

IAEA (1981). International Atomic Energy Agency, 1981, Statistical treatment of environmental isotope data in precipitation: Vienna, Austria, International Atomic Energy Agency Technical Series Report no. 206, 255 p., http://www-naweb.iaea.

org/napc/ih/documents/IAEA%20Monographs/TRS%20206%20Statistical%20treatment%20GNIP%20data%20 1981.pdf.

IAEA (1992). Statistical treatment of data on environmental isotopes in precipitation. IAEA, Vienna. Tech. Rep. No. 331.

IAEA (2009). https://www.iaea.org/publications/reports/annual-report-2009

IAEA (International Atomic Energy Agency) (1980) Arid zone hydrology: investigations with isotope techniques. In: Proceedings of an advisory group meeting. Vienna: IAEA

INTERNATIONAL ATOMIC ENERGY AGENCY, Isotope Hydrology (1983) (Vienna, 12-16 Sept. 1983), Proceedings Series - International Atomic Energy Agency, IAEA, Vienna (1984).

Ishaku, J.M., Kwada, I.A., Adekeye, J.I.D. (2009). Hydrogeological Characterization And Water Supply Potential Of Basement Aquifers In Taraba State, N.E. Nigeria. *Nature and Science, 7*(3), ISSN 1545-0740.

ISO Guide 34. www.inorganicventures.com

ISO/IEC 17025 ISO - ISO/IEC 17025 — Testing and calibration laboratories

Izbicki et al. (2008a). Chromium Concentrations, Chromium Isotopes, and Nitrate in the Unsaturated Zone at the Water–table Interface, El Mirage, California (2008) Written comm. to the Lahontan Regional Water Quality Control Board, December24,2008http://www.swrcb.ca.gov/lahontan/publications_forms/available_documents/molycorp_elmirage1208.pdf.

Jacintha, T.G.A., Rawat, K.S., Mishra, A., & Singh, S.K. (2016). Hydrogeochemical characterization of groundwater of Penninsular Indian region using multivariate statistical techniques. *Applied Water Science, 7(*6), 3001–3013. doi:10.1007/s13201-016-0400-9.

Jankowski, J., & Acworth, R. (1997). Impact of Debris Flow Deposits on Hydrogeo- Chemical Process and the Development of Dry Land Salinity in the Yass River Catchment, New South Wales, Australia. *Hydrogeology Journal, 5,* 71-88. http://dx.doi.org/10.1007/s100400050119.

Jankowski, J., Acworth, R.I., & Shekarforoush, S. (1998). Reverse ion-exchange in deeply weathered porphyritic dacite fractured aquifer system, Yass, New South Wales, Australia. In: Arehart GB, Hulston JR (eds) proceedings of 9th international symposium water–rock interaction. Taupo, New Zealand, 30th March–April 1998, Balkema, Rotterdam, pp 243–346.

Jenne, E. A. (1981). Geochemical Modeling; A Review. PNL-3574, Pacific Northwest Laboratory, Richland, Washington.

Johnson, C.R., Greenkorn, R.A., & Woods, E.G. (1966). Pulse-testing: a new method for describing reservoir flow properties between wells. *J Pet Technol., 18*(12), 1–599.

Jørgensen, N., & Banoeng-Yakubo, Bruce. (2001). Environmental isotopes (18O, 2H, and 87Sr/86Sr) as a tool in groundwater investigations in the Keta Basin, Ghana. Hydrogeology Journal. 9. 190-201. 10.1007/s100400000122.

Junner, N.R. (1940). Geology of the Gold Coast and Western Togoland (with Revised Geological Map). Gold Coast Geological Survey Bulletin No. 11, 75 p.

Junner, N. R., Hirst, T. and Service, H., (1942), "The Tarkwa Goldfield". Gold Coast Geological Survey, Memoir, No. 6, pp. 48-55.

Kabata-Pendias, A., & Pendias, H. (2001). *Trace Elements in Soils and Plants. 3rd Edition*, CRC Press, Boca Raton, 403 p.

Kaka, E.A., Akiti, T.T., & Nartey, V.K. (2011). Stable isotopes of water as indicator of Groundwater – Volta Lake interactions in the southwestern margin of the Volta- Lake, *Elixir Agriculture, 39*, 4888-4894.

Karanth, K.R. (1987). *Ground Water Assessment Development and Management.* McGraw Hill Publishing Company Ltd., New Delhi.

Karmakar, H.N., & Das, K. P. (2012) Impact of Mining on Ground & Surface water. International Mine Water Association. www. IMWA.info.

Katz, B.G., Chelette, A.R., & Pratt, T.R. (2004) Use of chemical and isotopic tracers to assess nitrate contamination and ground water age, Woodville Karst Plain, USA. *J Hydrol 289*, 36–61,

Kauffman, S., & Libby, W.F. (1954). The natural distribution of tritium. *Physics Review 93*, 1337–1344.

Kavurmac, M., & Ustun, A.K. (2016). Assessment of groundwater quality using DEA and AHP: a case study in the Sereflikochisar region in Turkey. *Environ Monit Assess 188*, 258.

Kendall, C., & McDonnell, J. J. (1998). *Isotope tracers in catchment hydrology*. Elsevier, Amsterdam.

Kesse, G. O. (1985). The Mineral and Rock Resources of Ghana. Geological Survey Department 642 A.A., Rotterdam: Balkema.

Khan Y.S.A., Hossain, M.S., Hossain, S.M.G.A., & Halimuzzaman, A.H.M. (1998). An environmental assessment of trace metals in the Ganges-Brahamputra-Meghna estuary. *Journal of Remote Sensing and Environment, 2*, 103–17.

Khan, M.S. (1970). Cretaceous and Tertiary rocks of Ghana with a historical account of oil exploration. *Ghana Geological Survey Bulletin 40*, 43.

Khashogji, M.S., & El Maghraby, M.M.S. (2013). Evaluation of groundwater resources for drinking and agricultural purposes, Abar Al Mashi area, south Al Madinah Al Munawarah City, Saudi Arabia. *Arab J. Geosci.*, *6*(10), 3929–3942. https://doi.org/10.1007/s12517-012-0649-8.

Kim, C-K., Rho, B-H., & Lee, K. (1998). Environmental Tritium in the Areas Adjacent to Wolsong Nuclear Power Plant. *Journal Of Environmental Radioactivity - J Environ Radioact. 41*. 217-231. 10.1016/S0265-931X(97)00093-3.

Kister L. R., & Hardt W. F. (1966). Salinity of the ground water in western Pinal County, Arizona. United States Department of the Interior, Geological Survey.

Kitson, A.E. (1928) Provisional Geological Map of the Gold Coast and Western Togoland, with Brief Descriptive Notes Thereon. Sir Ranford Slater, Governor of the Gold Coast, London.

Knutsson, G. (1994). Acidification Effects on Groundwater—Prognosis of the Risks for Future. IAHS Publication No. 222.

Kollet, S.J., & Zlotnik, V.A. (2005). Influence of aquifer heterogeneity and return flow on pumping test data interpretation. *J. Hydrol 300*, 267–285

Kord, M., Moghaddam, A.A. (2014). Spatial analysis of Ardabil plain aquifer potable groundwater using fuzzy logic, *Journal of King Saud University – Science, 26(*2), Pages 129-140, ISSN 1018-3647, https://doi.org/10.1016/j.jksus.2013.09.004(https://www.sciencedirect.com/science/article/pii/S1018364713000682)

Kortatsi, B. (2006). Hydrochemical characterization of groundwater in the Accra plains of Ghana. *Environmental Geology, 50*, 299-311. 10.1007/s00254-006-0206-4.

Kortatsi, B. K., & Sekpey, N. K. (1993). Chemical and isotope evidence for the origin of groundwater in the crystalline basement complex of the upper regions of Ghana. Regional Trends in African Geology. Proceedings of the 9th International Geological Conference (Accra, 2nd to 7th November, 1992) Geological Survey of Africa

Kortatsi, B.K. (2004). *Hydrochemistry of Groundwater in the Mining Area of Tarkwa-Prestea, Ghana.* PhD Thesis Report, University of Ghana, Accra, 132 p.

Kortatsi, B.K. (2006). Concentration of trace metals in boreholes in the Ankobra Basin, Ghana. *West Afr. J. Appl. Ecol., 10,* 73-87 (15 pages)

Kumar, A., Singh, C.K., Bostick, B., Nghiem, A., Mailloux, B., & van Geen, A. (2020). Regulation of groundwater arsenic concentrations in the Ravi, Beas, and Sutlej floodplains of Punjab, India Geochem. *Cosmochim. Acta, 276*, 384-403

Kumar, M., Ramanathan, A.L., Someshwar Rao, M., & Kumar, B. (2006). Identification and evaluation of hydrogeochemical processes in the groundwater environment of Delhi, India. *Environmental Geology, 50,* 1025-1039. 10.1007/s00254-006-0275-4.

Kurland, L.T., Faro, S.W., & Siedler, H. (1960). Minamata disease: the outbreak of a neurological disorder in Minamata, Japan, and its relation to ingestion of sea food containing mercury compounds. *World Neurol., 1,* 370–95

Lawrence, F., & Upchurch, S. (1982). Identification of Recharge Areas Using Geochemical Factor Analysis. *Ground Water, 20,* 680 - 687. 10.1111/j.1745-6584.1982.tb01387.x.

Lee, C.H. (1915). The determination of safe yield of underground reservoirs of the closed-basin type. *Trans Am Soc Civ Eng., 78,* 148–151

Leube, A., et al. (1990). The early Proterozoic Birimian Supergroup of Ghana and some aspects of its associated gold mineralization Precambrian Research.

Leube, A., Hirdes, W., Mauer, R., & Kesse, G. O. (1990). The early Proterozoic Birimian Super group of Ghana and some aspects of its associated gold mineralization. *Precambrian Research, 46(*1-2), 139-165. doi:10.1016/0301-9268(90)90070-7.

Leung, C.M., & Jiao, J.J. (2006). Heavy Metal and Trace Element Distributions in Groundwater in Natural Slopes and Highly Urbanized Spaces in Mid-Levels Area, Hong Kong. *Water Research, 40,* 753-767. http://dx.doi.org/10.1016/j.watres.2005.12.016

Li, P., Qian, H., Wu, J., Zhang, Y., & Zhang, H. (2013a) Major ion chemistry of shallow groundwater in the Dongsheng Coalfield, Ordos Basin, China. *Mine Water Environ 32*(3), 195–206. doi:10.1007/s10230-013-0234-8.

Li, P., Wu, J., & Qian, H. (2014b). Hydrogeochemistry and quality assessment of shallow groundwater in the southern part of the Yellow River Alluvial Plain (Zhongwei Section), *China. EartSci Res J., 18*(1), 27–38. doi:10.15446/esrj.v18n1.34048.

Li, P.Y., Qian, H., & Wu, J.H. (2011). Hydrochemical Characteristics and Evolution Laws of Drinking Groundwater in Pengyang County, Ningxia. Northwest China. *E-Journal of Chemistry, 8*(2), 565–575.

Liu, J.T., et al. (2019) Hydrochemical Characteristics and Quality Assessment of Groundwater for Drinking and Irrigation Purposes in the Futuan River Basin, China. *Arabian Journal of Geosciences, 12,* 560. https://doi.org/10.1007/s12517-019-4732-2.

Liu, J.T., et al. (2019). Hydrochemical Characteristics and Quality Assessment of Groundwater for Drinking and Irrigation Purposes in the Futuan River Basin, China. *Arabian Journal of Geosciences, 12,* 560. https://doi.org/10.1007/s12517-019-4732-2

Liu, Y., Xiao, T., Perkins, R.B., Zhu, J., Zhu, Z., Xiong, Y., & Ning, Z. (2017). Geogenic cadmium pollution and potential health risks, with emphasis on black shale. *J. Geochem. Explor., 176*, 42-49, 10.1016/j.gexplo.2016.04.004

Lloyd, J.W. (1965). The hydrochemistry of the aquifers of north-eastern Jordan. *J. Hydrol., 3*, 319-330.

Lloyd, W.J., & Heathcote, A.J. (1985). *Natural Inorganic Chemistry in Relation to Groundwater*. Claredon Press, Oxford, 250 p.

Lu, Y., Tang, C., Chen, J., Song, X., Li, F., & Sakura, Y. (2008). Spatial characteristics of water quality, stable isotopes and tritium associated with groundwater flow in the Hutuo River alluvial fan plain of the North China Plain. *Hydrogeology Journal, 16.* 1003-1015. 10.1007/s10040-008-0292-3.

MacDonald, A.M., & Calow, R.C. (2009). Developing groundwater for secure rural water supplies in Africa. *Desalination, 248*, 546–556.

Macdonald, R. W., McLaughlin, F. A., & Carmack, E. C. (2002). Fresh water and its sources during the SHEBA drift in the Canada Basin of the Arctic Ocean. *Deep-Sea Res. 49*, 1769 –1785.

Mahato, Dr. M., Singh, P., & Tiwari, A. (2016). Hydrogeochemical Evaluation of Groundwater Quality and Seasonal Variation in East Bokaro Coalfield Region, Jharkhand. *Journal of the Geological Society of India, 88,* 173-184. 10.1007/s12594-016-0476-8.

Mahmood, K., et al. (2015). Assessment of the intrinsic vulnerability to groundwater contamination in Lahore, Pakistan." *Pakistan Journal of Scientific and Industrial Research Series A: Physical Sciences, 58*(1), 8+. GaleAcademicOneFile, link.gale.com/apps/doc/A406710277/AONE?u=anon~cd1171b9&sid=googleScholar&xid=ba9d3d50

Majumdar, R.K., & Das, D. (2011). Hydrological Characterization and Estimation of Aquifer Properties from Electrical Sounding Data in Sagar Island Region, South 24 Parganas, West Bengal, India. *Asian Journal of Earth Sciences, 4*, 60-74. 10.3923/ajes.2011.60.74.

Manceau, A., & Calas, G. (1985). Heterogeneous distribution of nickel in hydrous silicates from 794 New Caledonia ore-deposits. *American Mineralogist, 70*, 549-558.

Manjo, K., Kumar, B., & Padhy, P.K. (2012). Characterisation of metals in water and sediments of Subarnarekha River along the projects' sites in lower basin, India. *Univ J Environ Res Technol, 2(*5), 402–410.

Marghade, D., Malpe, D.B., & Zade, A. (2011). Major ion chemistry of shallow groundwater of a fast growing city of Central India. *Environmental monitoring and assessment, 184*, 2405-18. 10.1007/s10661-011-2126-3.

Mariotti, A. (1994). De´nitrification in situ dans les eaux souterraines, processus naturels ou provoque´s: une revue. *Hydrogeology, 3*, 43 – 68.

Masarik J., & Reedy, R.C. (1995) Terrestrial cosmogenic-nuclide production systematics calculated from numerical simulations. *Earth Planet. Sci. Lett. 136*(3/4), 381–395.

Masoud, A.A. (2014). Groundwater quality assessment of the shallow aquifers west of the Nile Delta (Egypt) using multivariate statistical and geostatistical techniques. *Journal of African Earth Sciences, 95*, 123-137 DOI 10.1016/j.jafrearsci.2014.03.006

McClain, C., & Maher, K. (2016). Chromium fluxes and speciation in ultramafic catchments and global rivers. *Chemical Geology. 426.* 10.1016/j.chemgeo.2016.01.021.

McGuire, K. J., DeWalle, D. R., & Gburek, W. J.: Evaluation ofmean residence time in subsurface waters using oxygen-18 fluctuations during drought conditions in the mid-Appalachians, *J. Hydrol., 261*, 132–149, 2002

McGuire, K., & McDonnell, J. (2006). A Review and Evaluation of Catchment Transit Time Modeling. *Journal of Hydrology. 330.* 10.1016/j.jhydrol.2006.04.020.

McLean, W., & Jankowski, J. (2000). Groundwater quality and sustainability in an alluvial aquifer, Australia. In: Sililo et al (eds) Proceedings of XXX IAH congress on groundwater: past achievements and future challenges. Cape Town South Africa 26th November-1st December 2000. AA Balkema, Rotterdam, Brookfield

Meybeck, M. (1987). Global Chemical Weathering of Surficial Rocks Estimated from River Dissolved. *American Journal of Science, 287,* 401-428. https://doi.org/10.2475/ajs.287.5.401

Mitra, B.K., & ASABE Member (1998). Spatial and temporal variation of ground water quality in sand dune area of Aomori Prefecture in Japan.

Moench, A.F. (1995). Combining the Neuman and Boulton models for flow to a well in an unconfined aquifer. *Groundwater, 33*, 378–384

Möller, P., Rosenthal, E., S. Geyer, J. Guttman, P. Dulski, M. Rybakov, M. Zilberbrand, C. Jahnke, A. (2007). Flexer Hydrochemical processes in the lower Jordan valley and in the Dead Sea area. *Chem. Geol., 239*, 27-49.

Molson, J. W., & Frind, E. O. (2005). How old is the water? Simulating groundwater age at the watershed scale, *IAHS Publ., 297,* 482–488, 2005.

Moore, K. B., Ekwurkel, B., Esser, B. K., Hudson, G. B., & Moran, J. E. (2006). Sources of groundwater nitrate revealed using res-idence time and isotope methods, *Appl. Geochem., 21*, 1016–1029.

Morgenstern, U., & Daughney, C. J. (2012). Groundwater age for identification of baseline groundwater quality and impacts of land-use intensification – The National Groundwater Monitoring Pro-gramme of New Zealand, *J. Hydrol.*, 456–457, 79–93.

Morgenstern, U., Stewart, M. K., & Stenger, R. (2010). Dating of stream water using tritium in a post nuclear bomb pulse world: continuous variation of mean transit time with streamflow, Hydrol. *Earth Syst. Sci., 14*, 2289–2301, doi: 10.5194/hess-14-2289-2010, 2010.

Morgenstern, U., van der Raaij, R., & Baalousha, H. (2012). Ground-water flow pattern in the Ruataniwha Plains as derived from the isotope and chemistry signature of the water, GNS Science Report 2012/23, GNS Science, Lower Hutt, New Zealand, 50pp., available at: http://www.gns.cri.nz/static/pubs/2012/SR_2012-023. pdf (last access: 5 February 2015), 2012.

Morris, B., Stuart, M. E., Darling, W. G., & Gooddy, D. C. (2005). Use of groundwater age indicators in risk assessment to aid water supply operational planning, *J. Chart. Inst. Water Environ. Man., 19*, 41–48, 2005.

Mostafa, M.G., Uddin, S.M.H., & Haque, A.B.M.H. (2017). Assessment of hydro-geochemistry and groundwater quality of Rajshahi City in Bangladesh. *Appl Water Sci.* https://doi.org/10.1007/s13201-017-0629-y

Mostafa, M.G., Uddin, S.M.H., & Haque, A.B.M.H. (2017). Assessment of hydrogeochemistry and groundwater quality of Rajshahi City in Bangladesh. *Appl Water Sci.* https://doi.org/10.1007/s13201-017-0629-y

Murthy, Y.R., Tripathy, S.K., & Kumar, C.R. (2011). Chrome ore beneficiation challenges & opportunities – a review. Miner. *Eng. 24* (5), 375–380.

Narany, S., Ramli, M.F., Aris, A.Z., Nor, W., Sulaiman, A., Juahir, H., & Fakharian, K. (2014). Identification of the hydrogeochemical processes in groundwater using classic integrated geochemical methods and geostatistical techniques Amol-Babol Plain, Iran. *Sci. World J.*, 1–15

Neuman, S.P. (1972). Theory of flow in unconfined aquifers considering delayed gravity response of the water table, Water Resources Research, vol. 8, no. 4, pp. 1031-1045.

Neuman, S.P. (1974). Effect of partial penetration on flow in unconfined aquifers considering delayed gravity response, *Water Resources Research*, *10*(2), 303-312.

Neuman, S.P. (1975). Analysis of pumping test data from anisotropic unconfined aquifers considering delayed gravity response, *Water Resources Research, 11*(2), 329-342.

New Zealand Ministry of Health (2008). Drinking-water standards for New Zealand 2005 (revised 2008), Ministry of Health, Wellington, New Zealand.

Nordstrom, D. K., Plummer, L. N., Wigley, T. M. L., Wolery, T. J.,Ball, J. W., Jenne, E. A., et al. (1979). A comparison of computerized chemical models for equilibrium calgllations inaqueous systems. In E. A. Jenne (Ed.), Washington, DC: AmericanChemical Society, Symposium Series 93.

Nwankwor, G.I., Gillham, R.W., van der Kamp, G., & Akindunni, F.F. (1992). Unsaturated and saturated flow in response to pumping of an unconfined aquifer: field evidence of delayed drainage. *Groundwater, 30,* 690–700

Nyarko, E., Lamptey, A.M., & Amaning, D.A. (2015). Application of water quality index for assessment of the nearshore coastal waters of Accra, Ghana. *Journal of Pollution Research.*

O'Brien, K. (1979) Secular variations in the production of cosmogenic isotopes in the Earth's atmosphere. *J. Geophys. Res., 84,* 423–431.

Oberthür, T., Vetter, U., Schmidt Mumm, A., Weiser, T., Amanor, J.A., Gyapong, W.A., Kumi, R., & Blenkinsop, T.G. (1994). The Ashanti gold mine at Obuasi, Ghana: Mineralogical, geochemical, stable isotope and fluid inclusion studies on the metallogenesis of the deposit. In: Oberthür, T. (Ed.), *Metallogenesis of selected gold deposits in Africa,* Geologisch Jshrbook. Jb., D100, 31-129.

Obiri-Danso, K., Adjei, B., Stanley, K., & Jones, K. (2009). Microbiological quality and metal levels in wells and boreholes water in some peri-urban communities in Kumasi, Ghana. *African Journal of Science and Technology, 31*.

Official Method 4500-P E (Ascorbic acid method) in the Association of Official Analytical Chemists (AOAC International, 2007).

Official Method 4500-SO42- E (Turbidimetric method) was used for the determination of sulphate (AOAC International, 2007).

Okogbue, C.O., Omonona, O.V., & Aghamelu, O.P. (2012). Qualitative assessment of ground water from Egbe-Mopa basement complex area, North-Central Nigeria. Environ Earth Sci 67:1069–1083.

Okon, I.A., Akaerue, E.I., & Felix, I.P. (2018). Determination of Aquifer Hydraulic Parameters Using Single Well Pumping Test Borehole Data within Boki Local Government Area, Cross River State, South Eastern Nigeria. *Journal of Environment and Earth Science, 8*(3).

Olago, D.O. (2018). Constraints and Solutions for Groundwater Development, Supply and Governance in Urban Areas in Kenya.

Onodera, S.I., Saito, M., Sawano, M., et al. (2008). Effects of intensive urbanization on the intrusion of shallow groundwater into deep groundwater: Examples from Bangkok and Jakarta. *Sci Total Environ 404*(2–3), 401–410. https://doi.org/10.1016/j.scitotenv. 2008.08.003.

Oze, C., Fendorf, S., Bird, D.K., & Coleman, R.G. (2004). Chromium geochemistry in serpentinized ultramafic rocks and serpentine soils from the Franciscan Complex of California. Am. J. Sci. 304, 67-101

Papp, J.F., & Lipin, B.R. (2006). Chromite in Kogel, J.E., Trivedi, N.C., Barker, J.M., and Drukowski, S.T., Industrial Minerals and Rocks-Commodities, Markets, and Uses, 7th Edition, AIME, Society for Mining, Metallurgy, and Exploration, Inc., Littleton, CO, p. 309-333.

Parkhurst, D. (1995). User guide to PHREEQC - A computer program for speciation, reactionpath, advective-transport, and inverse geochemical calculations. US Geological Survey Water Resources Investigation Report 95-4227.

Parkhurst, D.L., & Appelo, C.A.J. (2013). Description of Input and Examples for PHREEQC Version 3—A Computer Program for Speciation, Batch-Reaction, One-Dimensional Transport, and Inverse Geochemical Calculations. US Geological Survey Techniques and Methods, Book 6, Chapter A43, 497 p. http://pubs.usgs.gov/tm/06/a43.

Pazand, K., & Javanshir, A. (2013). Rare earth element geochemistry of spring water, north western Bam, NE Iran. *Applied Water Science, 4,* 58-. 10.1007/s13201-013-0125-y.

Paznand, K., & Javanshir, AR (2014). Rare earth element geochemistry of spring water, north western Bam, NE Iran. *Appl Water Sci., 4,* 1–9

Pelig-Ba, K. B. (1998). Trace elements in groundwater from some crystalline rocks in the Upper Regions of Ghana. *Water, Air & Soil Poll., 103,* 71-89

Pelig-Ba, K. B., Kortatsi, B. K., & Edmunds, W. M. (1990). Application of isotope techniques in Groundwater studies in the Upper Regions of Ghana. Paper presented at the Regional Seminar on Isotope in Hydrology for Developing Countries in Africa from 15th to 19th October 1990 in Vienna, Austria.

Pelig-Ba, K.B., Biney, C.A., & Antwi, L.A. (1991). *Water Air Soil Poll., 59,* 333–345.

PerkinElmer® Optima™ 7000 DV ICP-OES instrument, Inc. Shelton, CT, USA www.perkinelmer.com

Pezzetta, E., Lutman, A., Martinuzzi, I., Viola, C., Bernardis, G., & Fuccaro, V. (2011). Iron concentrations in selected groundwater samples from the lower Friulian Plain, northeast

Italy: Importance of salinity. *Environmental Earth Sciences. 62*. 377-391. 10.1007/s12665-010-0533-3.

Piper, A.M. (1944). A graphic procedure in the geochemical interpretation of water-analyses. *Trans Am Geophys Union, 25*(6), 914–928. doi:10.1029/TR025i006p00914.

Plummer, L. N., Busby, J. F., Lee, R. W., & Hanshaw, B. B. (1990). Geochemical modeling of the madison aquifer in parts of Montana, Wyoming and South Dakota. *Water Resources Research, 26,* 1981–2014.

Plummer, L. N., Jones, B. F., & Truesdell, A. H. (1976). WAT-EQF — A fortran IV version of water, a computer program for calculating chemical equilibrium of natural waters *US GeolSurvey water resources investigations report 76,* 1361.

Plummer, L. N., Parkhurst, D. L., & Thorstenson, D. C. (1983). Development of reaction models for groundwater systems. *Geochimica et Cosmochimica Acta, 47,* 665–685.

Post, J. E. (1999). Manganese oxide minerals: crystal structures and economic and environmental significance. Proceedings of the National Academy of Sciences of the United States of America, 96(7), 3447-54.

Postawa, A., Hayes, C., Bower, M., Croll, B., Ferrante, M., Górski, J., … Szuster-Janiaczyk, Agnieszka. (2013). Best Practice Guide on the Control of Iron and Manganese in Water Supply.

Postawa, A., Hayes, C., Criscuoli, A., Macedonio, F., Angelakis, A.N., Rose, J.B., Maier, A., & McAvoy, D.C. (2013*). Best practice guide on the control of iron and manganese in water supply*. IWA publishing, London, UK

Prickett, T.A. (1965). Type-curve solution to aquifer tests under water-table conditions, *Ground Water, 3*(3), 5-14.

Purvance, D.T., & Andricevic, R. (2000). On the electrical-hydraulic conductivity correlation in aquifers Water Resour. Res., 36 (2000), pp. 2905-2913.

Patil, S. N., Rokade, V. M., Patil, Sandeep P., Patil Sachin., andJagadale Shantaram (2010) Hydrogeochemical Investigation ofGroundwater from Faizpur area of Jalgaon District, Maharashtra,Journal of Applied Geochemistry 12 (2): 217-223

Qing, X., Zong, Y., & Shenggao, L. (2015). Assessment of heavy metal pollution and human health risk in urban soils of steel industrial city (Anshan), Liaoning, Northeast China. Ecotoxicology and environmental safety. 120. 377-385. 10.1016/j.ecoenv.2015.06.019.

Ragunath, H.M. (1987). *Groundwater*. Wiley Eastern Ltd, New Delhi, pp 563.

Ramesh, K., Bhuvana, J.P., & Li, T. (2012). Hydrochemical characteristics of groundwater for domestic and irrigation purposes in Periyakulam Taluk of Theni District, Tamil Nadu. *I Res J Environ Sci., 1,* 19–27.

Ramessur, R. T. (2000). Determination of some dissolved trace metals from groundwater in Mauritius using inductively-coupled plasma-mass spectrometry. Science and Technology-Research Journal, Vol. 5. University of Mauritius, Réduit, Mauritius, 14.

Rao, G. V., et al. (2015). "Estimation of Aquifer Properties Using Pumping Tests: Case Study of Pydibhimavaram Industrial Area, Srikakulam, India." World Academy of Science, Engineering and Technology, *International Journal of Environmental, Chemical, Ecological, Geological and Geophysical Engineering, 9,* 1170-1174.

Richards, L.A. (1954). Diagnosis and Improvement of Saline Alkali Soils, Agriculture, 160, Handbook 60. US Department of Agriculture, Washington DC.

Roether, W. (1967). Estimating the tritium input to groundwater from wine samples: groundwater and direct run-off contribution to central European surface waters. Isotopes in Hydrology, pp. 73–91. IAEA, Vienna.

Runnels, D. D. (1978). American research in the geochemical modelling of groundwater. *Journal of the Geological Societyof India, 29,* 135–144

Rural Water Supply Network (RWSN)-IRC Wash. (2010). Retrieved from https://www.ircwash.org

Sahib, L.Y., Marandi, A., & Schüth, C. (2016). Strontium isotopes as an indicator for groundwater salinity sources in the Kirkuk region, Iraq. *Sci. Total Environ. 562,* 935–945. https://doi.org/10.1016/j.scitotenv .2016.03.185

Saka, D., Akiti, T., Osae, S., Appenteng, M., & Gibrilla, A. (2013). Hydrogeochemistry and isotope studies of groundwater in the Ga West Municipal Area, Ghana. *Applied Water Science, 3,* 10.1007/s13201-013-0104-3.

Saleh, A., Al-Ruwaih, F., & Shehata, M. (1999). Hydrogeochemical processes operating within the main aquifers of Kuwait.*J Arid Environ., 42,* 195–209.

Salifu, M., Aidoo, F., Hayford, M.S., Adomako, D., & Asare, E. (2017). Evaluating the suitability of groundwater for irrigational purposes in some selected districts of the Upper West region of Ghana. *Appl. Water Sci., 7,* 653-662, 10.1007/s13201-015-0277-z

Sanchez-Segado, S., & Jha, A. (2013). Physical Chemistry of Roasting and Leaching Reactions for Chromium Chemical Manufacturing and Its Impact on Environment - A Review. 10.1002/9781118662199.ch25.

Sarath Prasanth, S.V., & Jitheshlal, K., Chandrasekar, N., & Gangadhar, K. (2012). Evaluation of groundwater quality and its suitability for drinking and agricultural use in the coastal stretch of Alappuzha District, Kerala, India. Applied Water Science - Springer. 10.1007/s13201-012-0042-5.

Sarikhani, R., Dehnavi, A., Ahmadnezhad, Z., & Kalantari, N. (2015). Hydrochemical characteristics and groundwater quality assessment in Bushehr Province, SW Iran. *Environmental Earth Sciences, 74*, 10.1007/s12665-015-4651-9.

Sattar, G.S., Keramat, M., & Shahid, S. (2016). Deciphering transmissivity and hydraulic conductivity of the aquifer by vertical electrical sounding (VES) experiments in Northwest Bangladesh. *Applied Water Science. 6*(1), 35–45. doi:10.1007/s13201-014-0203-

Schmoll, O., Howard, G., Chilton, P.J., & Chorus, I. (eds). (2006). Protecting groundwater for health: managing the quality of drinking water sources. WHO/IWA, London.

Schoeller, H. (1977). Geochemistry of Groundwater. In: Groundwater Studies—An International Guide for Research and Practice. UNESCO, Paris, Ch. 15, 1-18.

Schwartz, M.O. (2000): Cadmium in Zinc Deposits: Economic Geology of a Polluting Element, *International Geology Review, 42*(5), 445-469

Sethy, S.N., Syed, T.H., Kumar, A., & Sinha, D. (2016) Hydrogeochemical characterization and quality assessment of groundwater in part of Southern Gangetic Plain. *Environ Earth Sci., 75*, 232.

Shahab, A., Shihua, Q., Rashid, A., Hasan, F.U., & Sohail, M.T. (2016). Evaluation of Water Quality for Drinking and Agricultural Suitability in the Lower Indus Plain in Sindh Province, Pakistan. *Pol. J. Environ. Stud., 25.* doi: 10.15244/pjoes/63777.

Shahid, S.A., & Mahmoudi, H. (2014). National strategy to improve plant and animal production in theUnited Arab Emirates. Soil and water resources Annexes.

Shannon, D. W., Morray, J. R., & Smith, P. R. (1977). Use of achemical equilibrium model computer code to analyze scale formation and corrosion in geothermal brines Proceedings inSymposium on Oil Field and Geothermal Chemistry Con-ference 770609, pp. 21–36.

Sidle, W.C. (1998). Selected isotope methods for source water flow, flow component and residence time estimates in watershed investigations. USEPA, Cincinnati, OH, USA. Technical Report NRMRL/WSWRD/WQMB/98-12-01.

Sigma-Aldrich, USA https://www.sigmaaldrich.com

Signes-Pastor, A., Burló, F., Mitra K., & Carbonell-Barrachina, A.A. (2007). Arsenic biogeochemistry as affected by phosphorus fertilizer addition, redox potential and pH in a West Bengal (India) soil. *Geoderma, 137,* 504–510.

Sikandar, P., & Christen, E. (2012). Geoelectrical Sounding for the Estimation of Hydraulic Conductivity of Alluvial Aquifers. *Water Resources Management. 26*. 10.1007/s11269-011-9954-3.

Sikdar, P. K., Sarkar S.S., & Palchoudhury, S. (2001). Geochemical evolution of groundwater in the quater-nary aquifer of Calcutta and Howrah, India. *Journal of Asian Earth Sciences, 19,* 579–594. doi:10.1016/S1367-9120(00)00056-0.

Singh, S.K., Srivastava, P.K., Pandey, A.C., & Gautam, S.K. (2013). Integrated assessment of groundwater infuenced by a confuence river system: concurrence with remote sensing and geochemical modelling. *Water Resour Manag., 27*(12), 4291–4313. https://doi. org/10.1007/s11269-013-0408-y.

Sinha, R., Israil, M., & Singhal, D.C. (2009). A hydrogeophysical model of the relationship be-tween geoelectric and hydraulic parameters of anisotropic aquifers. *Hydrogeol. J. 17,* 495 –503

Sjöström, J. (1993). Combined studies of soil and groundwater chemistry, southwest Sweden, focusing on Al and SO4. *Appl Geochem Suppl.* (2), 281–283.

Skowron, K., Hulisz, K., Gryń, G., Olszewska, H., Kapischke, N.W., & Paluszak, Z. (2018). Comparison of selected disinfectants efficiency against Listeria monocytogenes biofilm formed on various surfaces. *International Microbiology, 21,* 10.1007/s10123-018-0002-5.

Skowron, P., Skowronska, M., Bronowicka-Mielniczuk, U., Filipek, T., Igras, J., Kowalczyk-Juśko, A., & Krzepiłko, A. (2018). Anthropogenic sources of potassium in surface water: The case study of the Bystrzyca river catchment, Poland. *Agriculture Ecosystems & Environment, 265,* 454-460. 10.1016/j.agee.2018.07.006.

Smedley, P. L., Edmunds, W. M., West, J. M., Gardner, S. J., & Pelig-BA, K. B. (1995). Vulnerability of Shallow Groundwater Quality due to Natural Geochemical Environment. Health problems related to groundwater in the Obuasi and Bolgatanga areas, Ghana. Report prepared for ODA under the ODA/BGS Technology Development and Research Programme. Project 92/5

Smith, L.A., Means, J.L., & Chen, A. (1995). Remedial Options for MetalsContaminated Sites, Lewis Publishers, Boca Raton, Fla, USA.

Solomon D. K., & Cook, P. G. (2000). 3H and 3He. In Environmental Tracers in Subsurface Hydrology (eds.P. Cook and A. L. Herczeg). Kluwer Academic, Dordrecht, pp. 397–424.

Sophocleous, M. (2000). From Safe Yield to Sustainable Development of Water Resources—The Kansas Experience. *Journal of Hydrology, 235,* 27-43. http://dx.doi.org/10.1016/S0022-1694(00)00263-8

Sophocleous, M. (2002). Interactions Between Groundwater and Surface Water: The State of the Science. *Hydrogeology Journal, 10,* 52-67. 10.1007/s10040-001-0170-8.

Soupios, P.M., Kouli, M., Vallianatos, F., Vafidis, A., Stavroulakis, G. (2007). Estimation of aquifer hydraulic parameters from surficial geophysical methods: a case study of Keritis Basin in Chania (Crete–Greece). *Journal of Hydrology, 338*(1), 122–131. doi:10.1016/j.jhydrol.2007.02.028

Spostigo, G., & Mattigod, S. V. (1979). *GEOCHEM: a computer program for the calculation of chemical equilibria in soil solution and other natural water systems*. Riverside: Department of Soil and Environmental Sciences, University of California.

Sri, N., & Muhammed, C. (2012). Equation estimation of porosity and hydraulic conductivity of Ruhrtal aquifer in Germany using near surface geophysics, *Journal of Applied Geophysics, 84,* 77-85, ISSN 0926-9851, https://doi.org/10.1016/j.jappgeo.2012.06.001.(https://www.sciencedirect.com/science/article/pii/S0926985112000985)

Srinivasamoorthy, K., Chidambaram, S., Prasanna, M.V. et al. (2008). Identification of major sources controlling groundwater chemistry from a hard rock terrain — A case study from Mettur taluk, Salem district, Tamil Nadu, India. *J Earth Syst Sci 117*, 49. https://doi.org/10.1007/s12040-008-0012-3.

Srivastava, K.S., & Ramanathan, L.A. (2008) Geochemical Assessment of Groundwater Quality in Vicinity of Bhalswa Landfill. Delhi; India by Using Graphical and Multivariable Statistical Methods. Environmental. Geology, 53, 1509-1528. http://dx.doi.org/10.1007/s00254-007-0762-2

Stewart, M. K., Morgenstern, U., & Mc Donnell, J. J. (2010). Trunca-tion of stream residence time: how the use of stable isotopes hasskewed our concept of stream water age and origin, *Hydrol. Pro-cess., 24,* 1646–1659, 2010

Stiff, H.A. Jr. (1951) The interpretation of chemical water analysis by means of patterns. *J Petrol Technol, 3*(10), 15–17. Doi: 10.2118/ 951376-G.

Strebel, O., Boettcher, J., & Fritz, P. (1990). Use of isotope fractionation of sulfate-sulfur and sulfate-oxygen to assess bacterial desulfurication in a sandy aquifer. *Journal of Hydrology 121*, 155–172.

Stumm, W., & Morgan, J.J. (1981). *Aquatic Chemistry: An Introduction Emphasizing Chemical Equilibria in Natural Waters. 2nd Edition*, John Wiley & Sons Ltd., New York.

Stumm, W., & Morgan, J.J. (1996). *Aquatic chemistry*. Wiley, New York, p 1022.

Subba Rao, N. (2002). Geochemistry of groundwater in parts of Guntur district Andhra Pradesh, India, *Environmental Geology*, *41*, 552-562

Sultana, S. (2009). Hydrogeochemistry of the Lower Dupi Tila Aquifer in Dhaka City, Bangladesh. TRITA-LWR degree project 09-35, 1–42

Suprapti, A., & Pongmanda, S. (2020). Estimation of aquifer parameters using pumping tests: case study of hotel Makassar paradise. IOP Conference Series: Earth and Environmental Science. 419. 012118. 10.1088/1755-1315/419/1/012118.

Szabolcs, I., & Darab, C. (1964). The Influence of Irrigation Water of High Sodium Carbonate Content of Soils. Proceedings of 8th International Congress of ISSS, *Trans II*, 803-812.

Tartakovsky, G.D., & Neuman, S.P. (2007). Three-dimensional saturated-unsaturated flow with axial symmetry to a partially penetrating well in a compressible unconfined aquifer, Water Resources Research, W01410, doi:1029/2006WR005153.

Tatou, R.D., Kabeyene, V.K., & Mboudou, G.E. (2017). Multivariate Statistical Analysis for the Assessment of Hydrogeochemistry of Groundwater in Upper Kambo Watershed (Douala Cameroon). *Journal of Geoscience and Environment Protection*, *5*, 252-264. https://doi.org/10.4236/gep.2017.53018.

Tay C., & Momade, F.W.Y. (2006). Trace Metal Contamination in Water from Abandoned Mining and Non-Mining areas in the Northern Parts of the Ashanti Gold Belt, Ghana. *West African Journal of Applied and Ecology*, *10*, 189-207.

Tay, C. (2019). Hydrogeochemical Processes Influencing Groundwater Quality within the Lower Pra Basin, Ghana. 10.13140/RG.2.2.25616.56320.

Tay, C., & Hayford E. (2016). Levels, Source determination and Health implications of trace metals in groundwater within the Lower Pra Basin, Ghana. *Environmental Earth Sciences*, *75*(18), 1-19.

Tay, C., & Momade, F. (2006) Trace Metal Contamination in Water from Abandoned Mining and Non-Mining areas of the Northern Parts of the Ashanti Gold Belt. *West African Journal of Applied Ecology*, 10, 187–207.

Tay, C., Dorleku, M., & Doamekpor, L. (2019). Human Exposure Risks Assessment of Heavy Metals in Groundwater within the Amansie and Adansi Districts in Ghana using Pollution Evaluation Indices, *27*, 23 41.

Tay, C.K., Hayford, E.K., & Hodgson, I.O.A. (2017). Application of multivariate statistical technique for hydrogeochemical assessment of groundwater within the Lower Pra Basin, Ghana. *Appl. Water Sci., 7,* 1131–1150 https://doi.org/10.1007/s13201-017-0540-6

Taylor, C.B., & Roether, W. (1982). A uniform scale for reporting low-level tritium measurements in water. *International Journal of Applied Radiation and Isotopes, 33,* 377–82.

Taylor, P.N., Moorbath, S., Leube, A., & Hirdes, W. (1992). Early Proterozoic crustal evolution in the Birimian of Ghana: Constraints from geochronology and isotope geology. *Precambr. Res., 56,* 97-111.

Tesoriero, A.J., Spruill, T.B., & Eimers L. (2004). Geochemistry of shallow groundwater in coastal plain environments in the south-eastern United States: implication for aquifer susceptibility. *Appl Geochem, 19,* 1471–1482.

Theis C.V. (1934). Progress report on the ground water supply of Lea County, New Mexico: New Mexico state Engineer, 11th Biennial Report,1932 – 1934, 121 – 134.

Theis, C. V. (1940). The source of water derived from wells: Essential factors controlling the response of an aquifer to development, *Civil Eng., 10*, 277–280,

Tiimub, B.M., Frimpong, S., Kuffour, R.A., Dwumfour, A.B., Monney, I., & Obiri- Danso, K. (2012). Groundwater quality at Achiase and Wabiri in the Ejisu Juaben municipality of the Ashanti region in Ghana, *International Journal of Development and Sustainability, 1*(3), 939-956.

Todd D. K. (1980). *Groundwater hydrology.* Wiley, New York. US NRC. (2000). Copper in drinking water. Washington, DC, National Research Council, National Academy Press.

Todd, D.K. (1959). *Groundwater hydrology.* John Wily & Sons, Inc., New York.

Todd, D.K. (1980). *Groundwater Hydrology. 2nd Edition,* John Wiley & Sons, New York.

Tyagi, S., & Sharma, B., & Singh, P. (2013). Water Quality Assessment in Terms of Water Quality Index. *American Journal of Water Resources. 1,* 34-38. 10.12691/ajwr-1-3-3.

U.S. Salinity Laboratory (1954). Diagnosis and Improvement of Saline and Alkaline soils. U.S. Dept. of Agriculture. *Hand Book, No.* 60, 160.

Uddameri, V., & Honnungar, V., & Uddameri, E. (2013). Assessment of groundwater water quality in central and southern Gulf Coast aquifer, TX using principal component analysis. *Environmental Earth Sciences, 71*. 2653-2671. 10.1007/s12665-013-2896-8.

Ugada, U et al (2013b). Hydrogeophysical evaluation of aquifer hydraulic characteristics using surface geophysical data; a case study of Umuahia and environs, *Southeastern Nigeria Arab journal of geosciences.*

UNEP, (2010). *Final Review of Scientific Information on Cadmium*. United Nations Environment Programme, pp. 201.

Unterweger, M.P., Coursey, B.M., Shima, F.J., & Mann, W.B. (1980). Preparation and calibration of the 1978 National Bureau of Standards tritiated water standards Int. J. Appl. Radiat. Isotopes, 31 (1980), pp. 611-614.

Uren, N. (2013). *Cobalt and Manganese*. 10.1007/978-94-007-4470-7_12.

Vander Velpen, B.P.A. (1988). *Resist's User guide- ITC, Department of Earth resources survey,* Kansal the Netherlands.

Vaughan, D.J., & Craig, J.R. (1978). *Mineral Chemistry of Metal Sul-phides*. Cambridge Univ. Press, Cambridge, UK. 493.

Villa, M., & Manjon, G. (2004). Low-level measurements of tritium in water. *Applied radiation and Isotopes, 61*, 319-323

Wassenaar, L., Athanasopoulos, P., & Hendry, M. (2011). Isotope hydrology of precipitation, surface and ground waters in the Okanagan Valley, British Columbia, *Canada J. Hydrol., 411* (1), 37-48.

Water Quality Association (www.wqa.org)

Water Research Commission (WRC) Ghana (2012). Tano River basin – Integrated Water Resources Management Plan. Retrieved from http://doc.wrc-gh.org.

Water Resources Commission (2012). Tano Basin-Integrated Water Resource Management Plan October-2012 doc.wrc.gh.org/pdf/Tano%Basin%20IWRM%20Plan.Pdf.

Weaver M.C.J., Cave, L., & Talma, A.S. (2007). Groundwater Sampling: A Comprehensive guide for sampling method, WRC Report No TT 303/07, pp 168.

Weiss, W., & Roether, W. (1980). The rates of tritium input to the world oceans. *Earth Planet. Sci. Lett. 49*(2), 435–446.

Weiss, W., Bullacher, J., & Roether, W. (1979). Evidence of pulsed discharges of tritium from nuclear energy installations in central European precipitation. In Behaviour of Tritium in the Environment, pp. 17-30, IAEA-SM-232/18, IAEA, Vienna, 1979.

Weng, H-X., Qin, Y-C., & Chen, X-H. (2007). Elevated iron and manganese concentrations in groundwater derived from the Holocene transgression in the Hang-Jia-Hu Plain, China. *Hydrogeology Journal, 15,* 715-726. 10.1007/s10040-006-0119-z.

WHO (2011). *Guidelines or Drinking-Water Quality. 4th Edition*, World Health Organization, Geneva.

Wilcox, L.V. (1955). Classification and use of irrigation water. US Geological Department Agri. *Circ. 969,* 19.

Wilcox, L.V. (1995). Classification and Use of Irrigation Waters. US Department of Agriculture, Washington DC, *Circ. 969*, 19

Wolery, T. J. (1979). Calculation of chemical equilibrium between aqueous solutions and minerals: The EQ3/EQ6 software package (41 pp.). Livermore, University of California, Lawrence Livermore Laboratory (UCRL 52658).

Wolery, T. J. (1983). EQ3NR: A computer program for geo-chemical aqueous specification — Solubility calculations (191pp.). Livermore, California: Users Guide and documentation, Lawrence Livermore National Lab UCRL-53414.

Wu, C.M., Yeh, .J.T.C., Zhu, J., Lee, T.H., Hsu, N.S., Chen, C.H., & Sancho, A.F. (2005). Traditional analysis of aquifer tests: Comparing apples to oranges? *Water Resour Res 41*, W09402. doi:10.1029/2004 WR003717.

www.britanica.com.

www.healthycanadians.gc.ca

Yadav, I., & Singh, S., & Devi, N. (2014). Assessment of groundwater quality with special reference to arsenic in Nawalparasi district, Nepal using multivariate statistical techniques. *Environmental Geology. 72*. 10.1007/s12665-013-2952-4.

Yang, Y., Deng, Y., & Wang, Y. (2016). Major geogenic factors controlling geographical clustering of urolithiasis in China. *Sci. Total Environ, 571*, 1164-1171, 10.1016/j.scitotenv.2016.07.117

Yidana, S. M., Fynn, O. F., Chegbeleh, L. P., Nude, P. M., & Asiedu, D. K. (2013). Hydrogeological conditions of a crystalline aquifer: simulation of optimal abstraction rates under scenarios of reduced recharge. *The Scientific World Journal*, 606375. https://doi.org/10.1155/2013/606375

Yidana, S., Banoeng-Yakubo, B., Abdul, S., & Aliou, A.T. (2012). Groundwater quality in some Voltaian and Birimian aquifers in northern Ghana—application of multivariate statistical methods and geographic information systems. *Hydrological Sciences Journal-journal Des Sciences Hydrologiques - HYDROLOG SCI J. 57*. 1-16. 10.1080/02626667.2012.693612.

Yidana, S.M., Ophori, D., & Banoeng-Yakubo, B. (2008). Hydrogeological and hydrochemical characterization of the voltaian basin: the Afram plains area. *Ghana Environ Geol., 55*, 1213–1223.

Yurtsever, Y., & Gat, J. (1981) Atmospheric waters. Stable Isotope Hydrology: Deuterium and Oxygen-18 in the Water Cycle. (J.R. Gat, R. Gonfiantini, Eds) *Technical Reports Series 210*, IAEA, Vienna, 103-142.

Zaharin, A. A., Abdullah, M. H., Kim, K. M. W., & Praveena, S. M. (2008). Compositional change of groundwater chemistry in the shallow aquifer of small Tropical Island due to seawater intrusion. 20th Salt water intrusion meeting June 23-27, 2008. Naples, Florida, USA.

Zaporozec, A. (1972). Graphical interpretation of water

Zereg, S, & Boudoukha, A., & Lahcen, B. (2018). Impacts of natural conditions and anthropogenic activities on groundwater quality in Tebessa plain, Algeria. *Sustainable Environment Research. 28*. 10.1016/j.serj.2018.05.003.

Zhan, H., & Zlotnik, V.A. (2002). Ground water flow to horizontal or slanted wells in unconfined aquifer. *Water Resour Res.*, *38*(7), 1108.

Zhang et al. (2020). Enhanced adsorption of tetracycline by an iron and manganese oxides loaded biochar: kinetics, mechanism and column adsorption Bioresour. *Technol.*

APPENDICES

Appendix 1: Available data for the Rivers sampled in 2016

Sample ID	Name of river	Location	Date Sample
RIV 1	Ankobra	Ankobra	09/05/2016
RIV 2	Fia	Awiebo	09/06/2016
RIV 3	Anuyayo	Ayinasi – Half Assini Road	09/06/2016
RIV 4	Ellonyi	Ellonyi	09/06/2016
RIV 5	Bile	Nkroful	09/06/2016
RIV 6	Amanzura	Esiama to Elubo road	09/06/2016
RIV 7	EBI	Esiama to Elubo road	09/07/2016
RIV 8	Tano	Elubo	09/07/2016
RIV 9	Ankasa	Ankasa	09/07/2016

Appendix 2: Available data for the Streams sampled in 2016

Sample ID	Name of stream	Location	Date Sample
Stre 1	Subile	Nkroful	09/05/2016
Stre 2	Abobre	Nkroful	09/05/2016
Stre 3	Nobaya(Left)	Nkroful	09/05/2016
Stre 4	Franza	Nkroful	09/05/2016
Stre 5	Nobaya(right)	Nkroful	09/05/2016
Stre 6	Nsuengene	Teleku-bokazo to Aluku	09/06/2016
Stre 7	Edwele	Teleku-bokazo to Aluku	09/06/2016
Stre 8	Kodubaku	Teleku-bokazo to Aluku	09/06/2016
Stre 9	Ngontubile	Teleku-bokazo to Aluku	09/06/2016
Stre 10	Broma	Teleku-bokazo to Aluku	09/06/2016
Stre 11	Wowule	Teleku-bokazo to Aluku	09/06/2016
Stre 12	Unknown name	Elubo	09/06/2016
Stre 13	Unknown name	Elubo	09/06/2016
Stre 14	Assufofoa	Atuabo	09/07/2016
Stre 15	Unknown Name	Ayinasi	09/07/2016

Appendix 3: Available data for the Lagoon sampled in 2016

Sample ID	Name of Lagoon	Location	Date Sample
Lag1	Amanzura	Ampaim	09/06/2016
Lag2	Dominee	Old Kablazuazo	09/07/2016
Lag3	Amanzura	Axim - Elubo road	09/07/2016

Appendix 4: Available data for the Seawater sampled in 2017

Sample ID	Location	Date Sample
SEA 1	Ankobra	09/03/2016
SEA 2	Asanta	09/04/2016
SEA 3	Kikam	09/04/2016

Appendix 5: Available data for Rivers sampled in 2017

Sample ID	Name of River	Location	Date Sample
RIV 1	Fia	Awiebo	17/03/2017
RIV 2	Ebi	Esiama to Elubo road	17/03/2017
RIV 3	Amanzura	Esiama to Elubo road	16/04/2017
RIV 4	Eleneano	Esiama to Elubo road	16/04/2017
RIV 5	Ankobra	Ankobra	31/12/2017
RIV 6	Bile	Nkroful	28/12/2017
RIV 7	Anuyayo	Ayinasi - Half Assin Road	30/12/2017
RIV 8	Ebi	Esiama to Elubo road	28/12/2017
RIV 9	Amanzura	Esiama to Elubo road	28/12/2017
RIV 10	Ellonyi	Ellonyi	30/12/2017
RIV 11	Ankasa	Ankasa	28/12/2017
RIV 12	Unknown river	Salman	30/12/2017
RIV 13	Tano	Elubo	28/12/2017
RIV 14	Fia	Awiebo	28/12/2017

Appendix 6: Available data for Streams sampled in 2017

Sample number	Name of Stream	Location	Date Sample
Stre 1	Unknown name	Ayinasi	28/12/2017
Stre 2	Unknown name	Esiama to Elubo	28/12/2017
Stre 3	Assufo(2)	Atuabo	28/12/2017
Stre 4	Unknown name	Nkroful	30/12/2017
Stre 5	Subile	Nkroful	30/12/2017
Stre 6	Kodubaku	Teleku-bokazo to Aluku	30/12/2017
Stre 7	Nsugene	Teleku-bokazo to Aluku	30/12/2017
Stre 8	Bonuma	Teleku-bokazo to Aluku	30/12/2017
Stre 9	Edweleza	Teleku-bokazo to Aluku	30/12/2017
Stre 10	ngontubile	Teleku-bokazo to Aluku	30/12/2017
Stre 11	Wowule	Teleku-bokazo to Aluku	30/12/2017
Stre 12	Abobre	Nkroful	30/12/2017
Stre 13	Nobaya	Nkroful	31/12/2017
Stre 14	Franza	Nkroful	31/12/2017

Appendix 7: Available data for Lagoons sampled in 2017

Sample Number	Name of Laoon	Location	Date Sample
Lag1	Dominee	Old Kablasuazo	28/12/2017
Lag2	Amanzura	Axim - Elubo road	31/12/2017
Lag3	Amanzura	Ampaim	31/12/2017

Appendix 8: Available data for Seawater sampled in 2017

Sample ID	Location	Date Sample
SEA 1	Asanta	14/02/2017
SEA 2	Ankobra	14/02/2017
SEA 3	Krisen(2)	15/02/2017
SEA 4	Ebonyi	16/02/2017
SEA 5	Atuabo	16/02/2017
SEA 6	Old Kablasuazo	28/12/2017
SEA 7	Asanta	31/12/2017
SEA 8	Kikam (6)	31/12/2017
SEA 9	Ankobra	31/12/2017

Appendix 9: Available data for the boreholes drilled in 2013

Sample ID	Location	Date of sample	Sample ID	Location	Date of sample
NB1	Alumatoape	05/08/2013	NB16	Nyamebekyere	20/08/2013
NB2	Mpeasem	06/08/2013	NB17	Samenye	21/08/2013
NB3	Kamgbunli	07/08/2013	NB18	Domiabra	22/08/2013
NB4	Elubo	08/08/2013	NB19	Sowudazem	23/08/2013
NB5	Bobrama	09/08/2013	NB20	Alapoke	24/08/2013
NB6	Akanko	10/08/2013	NB21	Aniwafutu	25/08/2013
NB7	Gwira ampansie	11/08/2013	NB22	Ankyernin	26/08/2013
NB8	Ndatiem	12/08/2013	NB23	Fawoman	27/08/2013
NB9	Ayisakro	13/08/2013	NB24	Dadwen	28/08/2013
NB10	Kegyina	14/08/2013	NB25	Akpendue	29/08/2013
NB11	Nyamebekyere	15/08/2013	NB26	Obengkrom	30/08/2013
NB12	Akonu	16/08/2013	NB27	Cocoatown	31/08/2013
NB13	Ellanda Wharf	17/08/2013	NB28	Kutukrom	01/09/2013
NB14	Gwira Aiyinase	18/08/2013	NB29	Ghana Nungua	02/09/2013
NB15	Sanzule	19/08/2013	NB30	Ankajeri	03/09/2013

Appendix 10: Available data for the boreholes drilled in 2014 to 2015.

Sample ID	Location	Date of Sample
TBH 01	Newtown	28/10/2014
TBH 02	Effasu	29/10/2014
TBH 03	Mangyea	30/10/2014
TBH 04	Mpeasem	31/10/2014
TBH 05	Alumatuape	30/11/2014
TBH 06	Jawey	01/12/2014
TBH 07	Annor Adjaye SHS	02/12/2014
TBH 08	Allengenzule	03/12/2014
TBH 09	Agyeza	04/12/2014
TBH 10	Ehoaka	11/01/2015
TBH 11	Duplicate of Ehoaka	12/01/2015
TBH 12	Twenen	13/01/2015
TBH 13	Kengen	14/01/2015
TBH 14	Elloyin	15/01/2015
TBH 15	Kangbunli	16/01/2015
TBH 16	Azuleleounu	17/01/2015
TBH 17	Asanda(1)	24/06/2015
TBH 18	Asanda (2)	25/06/2015

Appendix 11: Available data for the hand dug wells sampled in 2016.

Sample ID	Location	Date Sample	Sample ID	Location	Date Sample
ESI 1	Esiama	09/03/2016	BOB 3	Bobrama	09/04/2016
KIK 5	Kikam	09/03/2016	ANI 1	Aniwa	09/05/2016
ANKO 2	Ankobra	09/03/2016	NKRO 1	Nkroful	09/05/2016
ANKO 1	Ankobra	09/03/2016	ESI 7	Esiama	09/05/2016
ANKO 3	Ankobra	09/03/2016	ESI 4	Esiama	09/05/2016
KIK 3	Kikam	09/04/2016	ESI 6	Esiama	09/05/2016
KIK 1	Kikam	09/04/2016	ESI 8	Esiama	09/05/2016
ASAN 2	Asanta	09/04/2016	ANI 2	Aniwa	09/05/2016
KIK 2	Kikam	09/04/2016	NKR 4	Nkroful	09/05/2016
KIK 4	Kikam	09/04/2016	NKRO 5	Nkroful	09/06/2016
ASAN 4	Asanta	09/04/2016	GYEGYE 2	Gyegyekrom	09/06/2016
ASAN 5	Asanta	09/04/2016	BOMUA 2	Bomuakpole	09/06/2016
KIK 7	Kikam	09/04/2016	ELU 1	Elubo	09/06/2016
ESI 2	Esiama	09/04/2016	AZULE 1	Azulenloanu	09/06/2016
ASAN 6	Asanta	09/04/2016	GYEGYE 1	Gyegyekrom	09/07/2016
BOB 2	Bobrama	09/04/2016	AMP 1	Ampain	09/07/2016
ASAN 7	Asanta	09/04/2016	HAAS 1	Half Assini	09/07/2016
SAN 3	Sanwoma	09/04/2016	ELU 2	Elubo	09/07/2016

Appendix 12: Available boreholes sampled in 2016

Sample ID	Location	Date Sample	Sample ID	Location	Date Sample
ASAN 6	Asanta	09/03/2016	ALUK 3	Aluku	09/06/2016
SAN 4	Sanwoma	09/03/2016	AZULEN 2	Azulenloa	09/06/2016
SAN 1	Sanwoma	09/03/2016	AZULEN 3	Azuleno	09/06/2016
SAN 2	Sanwoma	09/04/2016	ELU 3	Elubo	09/06/2016
BOB 1	Bobrama	09/04/2016	BOKPO 1	Bomuakpole	09/06/2016
Ankonew 1	Ankobra newsite	09/04/2016	NEWN 1	New Nzulezu	09/06/2016
BOB 4	Bobrama	09/04/2016	ATWI 2	Atwibaso	09/06/2016
ASEM 1	Asemko	09/05/2016	AWIA 1	Awiafoto	09/06/2016
NKR 2	Nkroful	09/05/2016	ANIWA 1	Aniwafuto(chips)	09/06/2016
ESI 3	Esiama	09/05/2016	NEWN 2	New Nzulezu	09/06/2016
NKR 3	Nkroful	09/05/2016	AWIE 1	Awiebo	09/07/2016
ESI 5	Esiama	09/05/2016	AMP 5	Ampain	09/07/2016
SAL 3	Salman	09/06/2016	AlAB 1	Alabokazo	09/07/2016
KAMG 2	Kamgbuli	09/06/2016	ALAB 2	Alabokazo	09/07/2016
KAMG 1	Kamgbuli	09/06/2016	Teleko 1	Telekobokaso	09/07/2016
Amp 2	Ampaim	09/06/2016	OLD KABLA 1	Old Kablasuazo	09/07/2016
Ani sch	Aniwa	09/06/2016	FAN 2	Fante new site	09/07/2016
ALUK 2	Aluku	09/06/2016	NYAN 1	Nyanzinli	09/07/2016
SAL 2	Salman	09/06/2016	ATWI 1	Atwibanso	09/07/2016
BOMUA 3	Bomuakpole	09/06/2016	NEWAN 1	New Ankasa	09/07/2016
ALUK 1	Aluku	09/06/2016	BONY 1	Bonyere	09/07/2016
SAL 1	Salaman	09/06/2016	TIEKO 1	Tiekobo 1	09/07/2016

Appendix 13: Available data for the hand dug well sampled in 2017.

Sample number	Location	Date Sample	Sample number	Location	Date Sample
Asem 1	Asemda	14/02/2017	NKR 1	Nkroful	30/12/2017
EIK 1	Eikwe	15/02/2017	ANI 2	Aniwa	30/12/2017
ATUA 1	Atuabo	16/02/2017	ANI 1	Aniwa	30/12/2017
BEN 1	Benyin	16/02/2017	KIK 1	Kikam	31/12/2017
ELU 5	Elubo	28/12/2017	ESI 8	Esiama	31/12/2017
ELU 2	Elubo	28/12/2017	KIK 2	Kikam	31/12/2017
ELU 1	Elubo	28/12/2017	KIK 3	Kikam	31/12/2017
GYEGYE 1	Gyegyekrom	28/12/2017	KIK 7	Kikam	31/12/2017
GYEGYE 2	Gyegyekrom	28/12/2017	ESI 4	Esiama	31/12/2017
HASS 1	Half Assini	29/12/2017	AMP 1	Ampaim	31/12/2017
NKR 5	Nkroful	30/12/2017	ESI 7	Esiama	31/12/2017
ALUK1	Aluku 3	30/12/2017	BOB 2	Bobrama	31/12/2017
NKR4	Nkroful	30/12/2017	KIK 4	Kikam	31/12/2017
BOMUA 1	Bomuakpole	30/12/2017	KIK 5	Kikam	31/12/2017
NKR 3	Nkroful	30/12/2017	AZULE 1	Azuleno	31/12/2017

Appendix 14: Available data for the boreholes sampled in 2017

Sample number	Location	Date Sample	Sample number	Location	Date Sample
Sanzu1	Sanzule(1)	15/02/2017	AWIA 1	Awiafotu junction	28/12/2017
SAN 2	Sanzule(2)	15/02/2017	NEWN 1	New Nzulazu	29/12/2017
EIK 2	Eikwe(2)	15/02/2017	NEWN 2	New Nzulazu(2)	29/12/2017
SAN 3	sanzule (3)	15/02/2017	BONY 1	Bonyere	29/12/2017
KRIS 1	Krisan(1)	15/02/2017	KAMG 1	Kamgbunli	29/12/2017
NGELEK 2	ngelekpolley(2)	15/02/2017	KAMG 2	Kamgbunli 2	29/12/2017
BA 1	Baku	15/02/2017	SAL 3	Salman 3	29/12/2017
NGE 1	Ngelekyi	15/02/2017	SAL 2	Salman 2	30/12/2017
NGELEK 1	Ngelekazo	16/02/2017	SAL1	Salman 1	30/12/2017
NGELEK 2	Ngelekazo(2)	16/02/2017	SAL 3	Salman(3)	30/12/2017
KEEG 1	Keegan(1)	16/02/2017	NKR4	Nkroful(4)	30/12/2017
ASEM2	Asemda	16/02/2017	BOKPO 1	Bomuakpolley	30/12/2017
TWEN 2	Twenen(2)	16/02/2017	NKR 6	Nkroful (6)	30/12/2017
NKR	Nkroful	17/02/2017	ALUK 2	Aluku 2	30/12/2017
ATWI 1	Atwinbanso(1)	28/12/2017	AZULEN 3	Azeneluno 3	30/12/2017
ELU 2	Elubo (2)	28/12/2017	ALUK1	Aluku 1	30/12/2017
AWIA 1	Awiefoto	28/12/2017	Teleko 2	Telekobokaso(2)	30/12/2017
OLD KABLA 1	Old Kablazuaso	28/12/2017	Amp 5	Ampaim(5)	31/12/2017
FAN 2	Fante New SITE	28/12/2017	ESI 6	Esiama (6)	31/12/2017
HAAS 1	Half Assini	28/12/2017	ESI1	Esiama (1)	31/12/2017
TIEKO 1	Tiekobo (1)	28/12/2017	AZULEN 2	Azuleno (2)	31/12/2017
ATWI 2	Atwinbanso (2)	28/12/2017	ESI 5	Esiama(5)	31/12/2017
SAL 5	Salman 5	28/12/2017	ANKONEW 1	Ankobra newsite	31/12/2017
ALAB 2	Alabokazo 2	28/12/2017	AMP 2	Ampiam	31/12/2017
NEWAN2	New Ankasa 2	28/12/2017	BOB 4	Bobrama(4)	31/12/2017
ALAB 1	Alabokazo 1	28/12/2017	ASEM1	Asemko(1)	31/12/2017
			AZULEN2	Azulenenuo 2	31/12/2017

Appendix 15: Available cations and anion data with their ionic balances for boreholes drilled in 2014 to 2015

Sample Id	Location	Ca^{2+} (meq/l)	Mg^{2+} (meq/l)	Na^{+}(meq/l)	K^{+}(meq/l)	Cl^{-} (meq/l)	HCO^{-}_{3}(meq/l)	SO^{2-}_{4}(meq/l)	NO_3^- (meq/l)	(A/B)*100(Ionic Balance
NB1	Newtown	1.90	1.86	6.79	0.35	6.32	2.65	0.35	0.00	7.73
NB2	Effasu	0.75	0.06	0.58	0.07	0.56	0.62	0.12	0.00	5.26
NB3	Mangyea	0.55	0.16	0.60	0.03	0.74	0.51	0.00	0.00	3.73
NB4	Mpeasem	1.80	0.27	0.49	0.04	0.99	1.23	0.02	0.00	7.39
NB5	Alumatuape	0.35	0.15	0.32	0.02	0.28	0.33	0.04	0.00	12.37
NB6	Jawey	0.90	0.18	0.24	0.07	0.24	0.82	0.04	0.00	11.71
NB7	Annor Adjaye SHS	0.60	0.21	0.52	0.04	0.50	0.59	0.12	0.00	6.14
NB8	Allengenzule	0.30	0.22	0.71	0.01	0.71	0.25	0.08	0.00	8.64
NB9	Agyeza	1.05	0.37	0.99	0.15	0.85	0.43	0.69	0.00	13.35
NB10	Ehoaka	3.44	0.21	0.13	0.02	0.16	2.65	0.31	0.00	9.93
NB11	Ehoaka	3.44	0.21	0.13	0.02	0.16	2.59	0.31	0.00	11.03
NB12	Twenen	0.30	0.28	0.75	0.04	1.02	0.31	0.23	0.00	-6.17
NB13	Kengen	0.25	0.12	0.43	0.01	0.64	0.10	0.02	0.00	3.61
NB14	Elloyin	0.15	0.18	0.82	0.03	0.88	0.08	0.17	0.00	2.17
NB15	Kangbunli	2.20	1.72	0.94	0.07	0.72	2.80	0.19	0.00	14.10
NB16	Azuleleounu	0.75	0.43	0.63	0.05	0.65	0.59	0.17	0.00	13.97
NB17	Asanda	0.70	0.26	0.85	0.23	0.76	0.54	0.21	0.00	14.87
NB18	Asanda	0.65	0.12	0.33	0.01	0.30	0.49	0.04	0.00	13.86

Appendix 16: Available cations and anion data with their ionic balances for hand dug wells sampled in 2016

Sample ID	Name of Town	Ca^{2+} (meq/l)	Mg^{2+} (meq/l)	Na^{+} (meq/l)	K^{+} (meq/l)	Cl^{-} (meq/l)	HCO_3^{-} (meq/l)	SO_4^{2-} (meq/l)	NO_3^{-} (meq/l)	(A/B)*100
ESI 1	Esiama	0.97	0.22	1.43	0.01	0.90	1.00	0.82	0.01	-1.95
NKR 5	Nkroful	0.14	0.12	5.44	1.46	2.20	0.60	3.11	0.02	9.36
KIK 5	Kikam	1.99	0.10	3.12	0.70	2.65	0.80	1.23	0.17	9.88
KIK 3	Kikam	1.76	0.10	3.76	1.06	2.88	0.80	1.52	0.03	12.22
ANI 1	Aniwa	0.43	0.17	1.02	0.27	0.56	0.20	0.61	0.02	14.90
KIK 1	Kikam	0.93	0.25	1.14	0.17	0.85	0.20	0.98	0.09	7.96
AMP 1	Ampain	0.31	0.04	0.23	0.02	0.51	0.08	0.22	0.01	-15.21
ASAN 2	Asanta	0.66	0.21	1.87	0.16	0.62	1.97	0.45	0.02	-2.67
NKR 1	Nkroful	0.46	0.17	0.78	0.15	0.45	0.40	0.46	0.02	8.17
KIK 2	Kikam	0.83	0.31	1.78	0.19	1.18	0.84	0.84	0.02	3.79
BOMUA 2	Bomuakpole	0.55	0.20	1.33	0.02	0.62	0.08	0.85	0.02	14.87
KIK 4	Kikam	1.04	0.44	1.94	0.58	1.47	0.40	1.34	0.04	10.45
ANKO 1	Ankobra	1.25	2.58	4.25	0.20	4.85	0.32	0.99	0.03	14.46
ASAN 4	Asanta	0.90	0.14	0.85	0.06	0.79	0.36	0.77	0.02	0.12
GYEGYE 2	Gyegyekrom	0.67	0.09	0.31	0.01	0.17	0.48	0.42	0.02	-0.99
KIK 7	Kikam	0.97	0.41	1.38	0.27	2.09	0.16	0.47	0.01	5.49
ASAN 5	Asanta	0.84	0.19	0.92	0.04	1.13	0.20	1.30	0.02	-14.22
ESI 6	Esiama	0.73	0.04	2.96	0.55	1.86	0.20	1.22	0.04	12.53

Appendix 16: Available cations and anion data with their ionic balances for hand dug wells sampled in 2016(Continuation)

Sample ID	Name of Town	Ca^{2+} (meq/l)	Mg^{2+} (meq/l)	Na^{+} (meq/l)	K^{+} (meq/l)	Cl^{-} (meq/l)	HCO_3^{-} (meq/l)	SO_4^{2-} (meq/l)	NO_3^{-} (meq/l)	(A/B)*100
ANI 2	Aniwa	0.12	0.32	1.26	0.20	0.23	0.20	1.68	0.00	-5.05
ESI 2	Esiama	0.44	0.14	0.85	0.04	0.45	0.12	0.59	0.02	10.68
ELU 2	Elubo	1.06	0.06	3.57	2.09	2.37	0.24	3.07	0.18	7.30
ASAN 6	Asanta	1.34	0.09	2.98	0.73	1.64	1.20	1.22	0.03	11.37
ANKO 2	Ankobra	1.06	0.76	2.78	0.06	1.75	0.92	0.88	0.01	13.34
ESI 7	Esiama	2.22	0.62	4.88	0.88	3.27	2.80	1.57	0.16	4.93
ESI 4	Esiama	1.65	0.35	0.93	0.13	0.62	1.00	1.11	0.02	5.44
NKR 4	Nkroful	2.01	0.64	1.47	0.25	0.51	0.24	3.08	0.01	6.59
ESI 8	Esiama	3.45	0.17	2.32	0.62	1.64	0.68	3.08	0.02	9.49
GYEGYE 1	Gyegyekrom	0.08	0.09	0.66	0.01	0.39	0.12	0.32	0.01	-0.63
ELU 1	Elubo	1.64	0.12	0.99	0.27	0.62	0.76	1.19	0.01	7.88
AZULE 1	Azulenloanu	0.27	0.27	0.99	0.06	0.56	0.28	0.46	0.01	9.65
HAAS 1	Half Assini	1.32	0.03	1.25	0.22	0.68	0.48	1.12	0.01	10.59
BOB 2	Bobrama	0.10	0.10	0.95	0.02	0.56	0.40	0.15	0.02	1.48
ASAN 7	Asanta	0.76	0.67	2.09	0.52	1.07	1.00	1.82	0.01	1.78
SAN 3	Sanwoma	0.18	0.24	0.98	0.05	0.56	0.82	0.13	0.01	-2.46
BOB 3	Bobrama	0.07	0.07	2.78	0.02	1.13	1.47	0.94	0.04	-9.87
ANKO 3	Ankobra	1.91	0.93	4.20	0.37	4.68	1.04	0.96	0.08	4.57

Appendix 17: Available cations and anion data with their ionic balances for boreholes sampled in 2016.

Sample Id	Sample Location	Ca^{2+} (meq/l)	Mg^{2+} (meq/l)	Na^{+} (meq/l)	K^{+} (meq/l)	Cl^{-} (meq/l)	HCO_3^{-} (meq/l)	SO_4^{2-} (meq/l)	NO_3^{-} (meq/l)	(A/B)*100
SAL 3	Salman	1.53	0.16	1.68	0.08	0.17	3.00	0.76	0.01	-6.47
KAMG 2	Kamgbuli	1.44	0.12	0.94	0.04	0.23	0.40	2.53	0.03	-11.44
KAMG 1	Kamgbuli	1.08	0.61	0.30	0.01	1.18	0.60	0.53	0.00	-7.30
ASEM 1	Asemko	0.34	0.30	1.63	0.40	0.68	0.80	0.96	0.02	4.12
Amp 2	Ampaim	0.31	0.54	1.22	0.21	1.02	0.44	0.37	0.01	10.95
Ani sch	Aniwa	0.08	0.26	1.22	0.02	0.34	0.24	0.63	0.03	12.31
NKR 2	Nkroful	0.21	0.17	1.98	0.05	0.73	1.20	0.38	0.02	1.75
SAN 2	Sanwoma	0.56	0.04	1.47	0.04	1.47	0.44	0.20	0.03	-0.34
ALUK 2	Aluku	0.56	0.20	3.75	0.25	1.52	0.12	3.02	0.01	1.10
AWIE 1	Awiebo	0.21	0.31	0.59	0.04	0.17	1.00	0.09	0.01	-4.56
ESI 3	Esiama	0.47	0.21	0.69	0.05	0.34	0.24	0.94	0.02	-4.00
AMP 5	Ampain	1.20	0.48	2.81	0.40	0.96	0.28	3.08	0.01	6.00
SAL 2	Salman	0.28	0.21	0.34	0.01	0.45	0.04	0.46	0.03	-8.11
NKR 3	Nkroful	1.63	0.33	1.52	0.03	0.56	1.24	0.93	0.03	11.97
BOB 1	Bobrama	0.11	1.03	1.29	0.04	0.79	0.44	0.88	0.04	6.89
BOMUA 3	Bomuakpole	0.64	0.38	0.81	0.02	0.90	0.20	0.99	0.01	-6.50
SAN 4	Sanwoma	0.41	0.52	0.62	0.03	1.52	0.48	0.00	0.00	-11.76
AlAB 1	Alabokazo	0.78	0.55	0.23	0.01	0.39	0.28	1.31	0.01	-11.99
ALUK 1	Aluku	0.25	0.10	1.01	0.03	0.34	0.98	0.10	0.00	-1.29
ALAB 2	Alabokazo	0.16	0.53	0.86	0.08	1.02	0.44	0.13	0.02	0.65
ASAN 6	Asanta	0.78	0.25	1.31	0.22	0.73	1.20	0.27	0.03	6.88

Appendix 17: Available cations and anion data with their ionic balances for boreholes sampled in 2016 (Continuation).

Sample Id	Sample Location	Ca^{2+} (meq/l)	Mg^{2+} (meq/l)	Na^{+} (meq/l)	K^{+} (meq/l)	Cl^{-} (meq/l)	HCO_3- (meq/l)	SO_4^{2-} (meq/l)	NO_3^{-} (meq/l)	(A/B)*100
SAL 1	Salaman	0.18	0.14	0.31	0.01	0.11	0.08	0.52	0.02	-6.31
Teleko 1	Telekobokaso	0.85	0.39	1.27	0.02	1.02	0.04	1.38	0.01	1.56
ALUK 3	Aluku	0.49	0.21	1.79	0.26	1.41	0.12	1.01	0.02	3.53
ESI 5	Esiama	0.12	0.13	0.65	0.04	0.45	0.60	0.03	0.01	-7.58
Ankonew 1	Ankobra newsite	2.90	0.20	1.49	0.10	1.97	1.52	0.85	0.00	3.72
SAN 1	Sanwoma	1.87	0.10	1.24	0.08	0.51	2.95	0.08	0.02	-3.98
OLD KABLA 1	Old Kablasuazo	0.08	0.08	1.49	0.01	0.68	0.20	0.95	0.01	-5.00
AZULEN 2	Azulenloa	0.48	0.09	0.81	0.02	0.62	0.40	0.03	0.01	13.73
AZULEN 3	Azuleno	0.78	1.35	1.29	0.07	1.13	0.20	1.40	0.01	12.24
FAN 2	Fante new site	0.70	0.79	0.37	0.08	0.23	0.36	0.80	0.02	15.59
ELU 3	Elubo	0.47	0.45	2.11	0.20	1.18	0.12	1.36	0.01	9.70
BOKPO 1	Bomuakpole	0.79	0.73	1.17	0.02	0.39	1.97	0.12	0.02	4.18
NYAN 1	NyanZinli	0.68	0.03	1.10	0.44	0.68	0.80	0.21	0.00	14.21
ATWI 1	Atwibanso	0.09	0.11	0.52	0.01	0.28	0.16	0.24	0.02	1.62
NEWN 1	New Nzulezu	0.18	0.07	0.16	0.01	0.17	0.08	0.21	0.01	-5.20
NEWAN 1	NEW Ankasa	1.24	0.06	0.40	0.02	0.28	0.28	0.82	0.01	10.98
BONY 1	Bonyere	0.18	0.17	2.49	0.17	1.41	0.84	0.54	0.04	3.34
ATWI 2	Atwibaso	0.03	0.14	1.25	0.02	0.56	0.20	0.38	0.01	10.62
AWIA 1	Awiafoto	0.94	0.67	0.35	0.09	0.56	0.68	0.43	0.04	8.77
ANIWA 1	Aniwafuto(chips)	0.15	0.17	0.70	0.14	0.17	0.60	0.58	0.03	-8.53
NEWN 2	New Nzulezu	1.11	0.54	0.63	0.06	2.37	0.08	0.34	0.07	-10.20
TIEKO 1	Tiekobo 1	0.31	0.01	0.80	0.09	0.11	0.28	0.50	0.01	15.17
BOB 4	Bobrama	0.93	0.23	1.05	0.01	1.13	0.12	0.60	0.01	8.77

Appendix 18: Available cations and anion data with their ionic balances for hand dug wells sampled in 2017.

Sample Id	Sample Location	Ca^{2+} (meq/l)	Mg^{2+} (meq/l)	Na^{+} (meq/l)	K^{+} (meq/l)	Cl^{-} (meq/l)	HCO_3^{-} (meq/l)	SO_4^{2-} (meq/l)	NO_3^{-} (meq/l)	(B/A)*100
NKR 5	Nkroful	0.31	0.11	0.80	0.03	0.68	0.24	0.14	0.01	8.28
ALU 3	Aluku	0.53	0.49	1.96	0.19	1.64	0.28	0.61	0.01	11.08
KIK 1	Kikam	1.30	0.49	1.61	0.19	0.56	3.00	0.04	0.01	-0.08
NKR 4	Nkroful	0.24	0.06	0.53	0.02	0.51	0.20	0.00	0.01	8.55
ESI 8	Esiama	3.60	1.05	1.76	0.53	3.38	2.08	0.42	0.00	8.30
Elu 5	Elubo	0.46	0.57	3.69	0.68	3.78	0.20	0.17	0.05	12.59
Kik2	Kikam	1.06	0.48	1.61	0.47	1.30	1.80	0.00	0.01	7.67
Half Ass 1	Half Assini	0.79	0.13	0.47	0.09	0.73	0.30	0.17	0.01	10.12
Bomua 1	Bomuakpole	1.12	0.38	1.16	0.18	1.52	1.20	0.28	0.02	-3.07
NKR 3	Nkroful	0.56	0.33	1.15	0.15	0.45	1.00	0.17	0.03	14.06
KIK 3	Kikam	2.30	0.58	3.14	0.82	2.14	4.80	0.96	0.02	-7.38
KIK7	Kikam	0.66	0.36	1.03	0.30	2.26	0.28	0.04	0.02	-4.99
ELU2	Elubo	1.76	0.05	3.18	0.21	3.78	0.04	0.17	0.05	12.54
NKR1	Nkroful	2.47	1.24	4.79	1.02	1.58	3.80	1.61	0.02	15.19
ANI 2	Aniwa	1.12	0.38	1.16	0.18	0.73	2.00	0.75	0.01	-10.31

Appendix 18: Available cations and anion data with their ionic balances for hand dug wells sampled in 2017 (Continuation).

Sample Id	Sample Location	Ca^{2+} (meq/l)	Mg^{2+} (meq/l)	Na^{+} (meq/l)	K^{+} (meq/l)	Cl^{-} (meq/l)	HCO_3^{-} (meq/l)	SO_4^{2-} (meq/l)	NO_3^{-} (meq/l)	(B/A)*100
ASEM 1	Asemda	0.24	1.07	0.80	0.13	0.11	1.47	0.97	0.02	-7.18
GYEGYE 2	Gyegyekrom	0.52	0.12	0.37	0.02	0.17	0.32	0.39	0.02	6.65
ESI 4	Esiama	3.25	0.83	1.48	0.21	0.90	5.79	0.28	0.01	-9.57
AMP 1	Ampaim	0.18	0.10	0.36	0.04	0.56	0.24	0.00	0.01	-8.64
EIK 1	Eikwe	1.22	0.66	3.78	0.28	1.52	2.89	1.43	0.04	0.54
ATU 1	Atuabo	1.05	0.79	2.12	0.12	0.11	2.00	1.01	0.02	12.92
BENY 1	Benyin	2.98	1.16	3.50	0.28	2.99	1.96	1.03	0.00	13.88
ESI 7	Esiama	2.47	0.78	4.47	0.87	0.73	4.00	1.93	0.02	12.57
GYEGYE 1	Gyegyekrom	0.07	0.13	0.26	0.02	0.11	0.40	0.01	0.00	-5.14
BOB 2	Bobrama	0.41	0.56	1.58	0.51	1.30	0.80	0.27	0.01	12.41
ELU 1	Elubo	2.06	0.24	0.83	0.36	0.68	1.00	0.98	0.06	12.52
KIK 4	Kikam	0.85	0.51	1.25	0.18	0.79	0.60	2.04	0.02	-10.38
KIK 5	Kikam	0.48	0.37	1.77	0.21	1.41	1.60	0.58	0.01	-12.03
Azule 1	Azuleno	0.35	0.39	1.07	0.08	0.56	0.98	0.00	0.01	9.43
ANI 1	Aniwa	0.39	0.27	1.03	0.23	0.39	1.00	0.76	0.01	-6.33

Appendix 19: Available cations and anion data with their ionic balances for the boreholes sampled in 2017.

Sample ID	Sample Location	Ca^{2+} (meq/l)	Mg^{2+} (meq/l)	Na^{+} (meq/l)	K^{+} (meq/l)	Cl^{-} (meq/l)	HCO_3^{-} (meq/l)	SO_4^{2-} (meq/l)	NO_3^{-} (meq/l)	(A/B)*100
Sanzu 1	Sanzule	0.08	0.08	0.82	0.06	0.23	0.16	0.83	0.01	-8.10
NKR 2	Nkroful	0.42	0.36	2.01	0.04	1.07	0.32	1.36	0.00	1.21
AMP 2	Ampaim	0.15	0.65	0.92	0.07	0.85	0.52	0.14	0.00	8.85
ATWI 1	Atwinbanso	0.06	0.17	0.64	0.04	0.56	0.40	0.00	0.00	-3.23
ELU 2	Elubo	0.32	0.59	1.96	0.19	1.58	0.80	0.00	0.02	12.13
AWI 1	Awiefoto	0.14	0.14	0.42	0.13	0.17	0.80	0.00	0.03	-9.63
ESI 6	Esiama	1.59	0.78	3.73	0.94	2.54	1.40	2.96	0.03	0.77
OLD KABLA 1	Old Kablazuaso	0.05	0.14	0.48	0.01	0.56	0.24	0.01	0.01	-9.30
FAN 2	Fante New Town	0.57	0.16	0.85	0.15	0.23	0.96	0.34	0.02	6.06
HAAS 1	Half Assini	0.16	0.04	1.60	0.07	0.90	0.20	0.56	0.00	5.67
SAL 1	Salman	0.15	0.22	0.33	0.00	0.17	0.66	0.00	0.00	-7.84
SAL 2	Salman	0.68	0.77	0.73	0.01	0.17	1.80	0.04	0.00	4.24
ESI 1	Esiama	1.35	0.40	2.39	0.07	1.30	2.80	0.26	0.02	-1.95
AZULEN 2	Azuleno	1.00	1.90	1.50	0.08	0.39	1.40	3.45	0.01	-7.87
BOKPO 1	Bomuakpolley	0.11	0.41	0.58	0.02	0.34	1.15	0.00	0.00	-14.19
SAL 3	Salman	0.24	0.28	0.35	0.01	0.11	0.44	0.21	0.02	5.92
NKR 4	Nkroful	0.18	0.22	0.63	0.03	0.56	0.44	0.00	0.01	2.61

Appendix 19: Available cations and anion data with their ionic balances for the boreholes sampled in 2017 (Continuation).

Sample ID	Sampling Location	Ca^{2+} (meq/l)	Mg^{2+} (meq/l)	Na^{+} (meq/l)	K^{+} (meq/l)	Cl^{-} (meq/l)	HCO_3^{-} (meq/l)	SO_4^{2-} (meq/l)	NO_3^{-} (meq/l)	(A/B)*100
ESI 5	Esiama	0.10	0.92	0.60	0.05	0.45	0.44	0.31	0.05	14.51
ANKONEW 1	Ankobra newsite	0.32	0.78	0.78	0.03	0.34	1.00	0.14	0.01	12.18
AMP 5	Ampin	0.27	0.33	0.52	0.04	0.11	1.20	0.00	0.01	-6.61
NKR 6	Nkroful	0.92	0.39	1.22	0.03	0.68	0.72	0.53	0.03	13.52
NEWN 1	New Nzulazu	0.06	0.08	0.28	0.02	0.17	0.16	0.00	0.01	11.61
TIEKO 1	Tiekobo	0.04	0.05	0.16	0.02	0.11	0.16	0.05	0.00	-8.76
BOB 4	Bobrama	0.12	1.42	1.34	0.03	1.18	1.20	0.10	0.01	7.91
NEWN 2	New Nzulazu	0.88	0.68	0.70	0.07	0.06	2.20	0.15	0.01	-1.68
BONY 1	Bonyere	0.18	0.25	1.15	0.16	0.51	1.00	0.10	0.00	3.64
KAMG 1	Kamgbunli	1.91	2.97	1.13	0.05	0.90	3.00	0.88	0.00	11.67
ALU 2	Aluku	0.32	0.29	1.97	0.28	1.64	0.16	0.74	0.02	5.89
ATW 2	Atwinbanso	0.04	0.18	0.75	0.05	0.62	0.04	0.22	0.01	6.94
ASEM1	Asemko	0.20	0.44	0.72	0.02	0.23	0.98	0.00	0.01	6.42
SAL 5	Salman	2.40	1.32	0.74	0.02	0.11	3.60	0.38	0.01	4.46
Azulen 3	Azeneluno	1.00	1.98	1.50	0.08	0.39	1.40	3.45	0.01	-7.00
ALUK 1	Aluku	0.28	0.15	0.52	0.01	0.34	0.20	0.16	0.02	14.47
ALAB 2	Alabokazo	0.69	0.55	0.23	0.01	0.96	0.80	0.07	0.01	-10.87
KAM 2	Kamgbunli	0.48	0.70	0.36	0.02	0.34	0.56	0.39	0.01	9.66
NEWAN 2	New Ankasa	0.32	0.37	0.51	0.03	0.96	0.40	0.17	0.02	-11.69
TELEKO 2	Telekobokaso	0.84	0.56	1.42	0.03	0.56	2.00	0.63	0.00	-5.71

Appendix 19: Available cations and anion data with their ionic balances for the boreholes sampled in 2017(Continuation)

Sample ID	Sampling Location	Ca^{2+} (meq/l)	Mg^{2+} (meq/l)	Na^{+} (meq/l)	K^{+} (meq/l)	Cl^{-} (meq/l)	HCO_3^{-} (meq/l)	SO_4^{2-} (meq/l)	NO_3^{-} (meq/l)	(A/B)*100
ALAB 1	Alabokazo	0.19	0.70	0.96	0.09	0.62	1.80	0.00	0.02	-11.47
AWIA 1	Awiafotu junction	0.40	0.93	0.44	0.02	0.51	0.56	0.26	0.00	14.63
AZULEN 2	Azulenenuo	0.75	0.88	1.00	0.04	0.62	1.80	0.05	0.02	3.37
SAL 3	Salman	0.32	0.54	1.49	0.04	0.85	0.98	0.00	0.07	11.57
SAN 2	Sanzule	0.14	0.54	2.14	0.06	0.85	0.44	0.97	0.01	12.16
NGELEK 1	Ngelekazo	1.01	0.19	0.64	0.02	0.11	0.32	1.12	0.02	8.58
EIK 2	Eikwe	0.27	1.78	0.56	0.11	0.23	1.08	1.43	0.02	-0.74
NGELEK 2	Ngelekazo	0.53	0.07	0.66	0.08	0.34	0.32	0.62	0.00	2.20
SAN 3	Sanzule	0.68	1.53	0.57	0.07	0.34	1.24	1.09	0.03	2.75
KRIS 1	Krisan	0.12	0.30	1.97	0.17	0.68	0.40	1.56	0.00	-1.55
NGELEK 2	Ngelekpolley	0.53	0.19	1.04	0.19	0.45	0.44	1.40	0.02	-8.68
BA 1	Baku	0.14	1.18	1.36	0.08	0.56	0.92	1.48	0.00	-3.77
KEEG 1	Keegan	0.41	0.76	2.46	0.25	0.34	1.20	1.46	0.03	12.47
ASEM 2	Asemda	0.36	0.43	2.18	0.17	0.79	0.60	1.62	0.02	1.88
TWENE 2	Twenen	0.05	0.43	1.50	0.03	0.62	0.40	1.47	0.02	-10.74
NGE 1	Ngelekyi	0.58	0.02	0.74	0.08	0.34	0.04	1.40	0.00	-11.61

Appendix 20: Lithological Logs of the Boreholes Drilled Across the Lower Tano River Basin

	HEISA ENGINEERING COMPANY LIMITED				
	DRILLING LOG SHEET				
	North	West			
LOCATION GPS	5.06432	2.9435		AIRLIFT YIELD	100 l/min
REGION	Western	DISTRICT: Jomoro		COMMUNITY	Alomatouape
BH DEPTH	20m	DATE STARTED: 5/06/14		DATE COMPLETED	5/6/2014
DEPTH		GEOLOGICAL FORMATION			
1		Brownish coarse grained sand	1		
2			2		
3			3		
4			4		
5			5		
6			6		
7		Yellowish coarse grained sand	7		
8			8		
9			9		
10			10		
11			11		
12			12		
13			13		
14			14		
15			15		
16			16		
17		Brownish fine sand	17		
18			18		
19			19		
20			20		
21			21		
22			22		
23			23		
24			24		
25			25		
26			26		
27			27		
28			28		
29			29		
30			30		
31			31		
32			32		
33			33		
34			34		
35			35		
36			36		
37			37		
38			38		
39			39		
40			40		
41			41		
42			42		
43			43		
44			44		
45			45		
46			46		
47			47		
48			48		
49			49		
50			50		

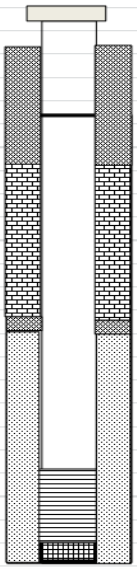

Plain PVC
Slotted PVC
Bail Plug
Gravel Pack
Grout Seal
Back fill

Appendix 20: Lithological Logs of the Boreholes Drilled Across the Lower Tano River Basin (Continuation)

	HEISA ENGINEERING COMPANY LIMITED				
	DRILLING LOG SHEET				
	North	**West**			
LOCATION GPS	5.07096	2.99782		**AIRLIFT YIELD**	200 l/min
REGION	Western	**DISTRICT:** Jomoro		**COMMUNITY**	Mpeasem
BH DEPTH	20m	**DATE STARTED:** 6/06/14		**DATE COMPLETED**	7/6/2014
DEPTH		**GEOLOGICAL FORMATION**			
1		Brownish coarse grained sand	1		
2			2		
3			3		
4			4		
5		Light brownish coarse grained sand	5		
6			6		
7			7		
8			8		
9		Yellowish fine sand	9		
10			10		
11			11		
12			12		
13			13		
14			14		
15			15		
16			16		Plain PVC
17		Brownish fine sand + clay	17		Slotted PVC
18			18		Bail Plug
19			19		Gravel Pack
20			20		Grout Seal
21			21		Back fill
22			22		
23			23		
24			24		
25			25		
26			26		
27			27		
28			28		
29			29		
30			30		
31			31		
32			32		
33			33		
34			34		
35			35		
36			36		
37			37		
38			38		
39			39		
40			40		
41			41		
42			42		
43			43		
44			44		
45			45		
46			46		
47			47		
48			48		
49			49		
50			50		

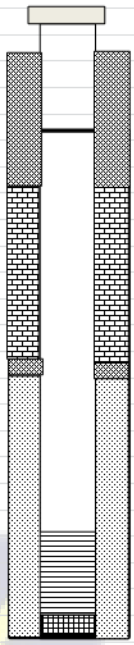

Appendix 20: Lithological Logs of the Boreholes Drilled Across the Lower Tano River Basin(Continuation)

	HEISA ENGINEERING COMPANY LIMITED				
	DRILLING LOG SHEET				
	North	**West**			
LOCATION GPS	5.07755	3.02855		**AIRLIFT YIELD**	200 l/min
REGION	Western	**DISTRICT:** Jomoro		**COMMUNITY**	Mangyea
BH DEPTH	20m	**DATE STARTED:** 9/07/14		**DATE COMPLETED**	10/7/2014
DEPTH		**GEOLOGICAL FORMATION**			
1		Greyish coarse grained sand	1		
2			2		
3			3		
4			4		
5		Yellowish coarse grained sand	5		
6			6		
7			7		
8			8		
9		Greyish fine sand + clay	9		
10			10		
11			11		
12			12		
13			13		
14			14		
15			15		
16			16		
17		Dark greyish sand + clay	17		
18			18		
19			19		
20			20		
21			21		
22			22		
23			23		
24			24		
25			25		
26			26		
27			27		
28			28		
29			29		
30			30		
31			31		
32			32		
33			33		
34			34		
35			35		
36			36		
37			37		
38			38		
39			39		
40			40		
41			41		
42			42		
43			43		
44			44		
45			45		
46			46		
47			47		
48			48		
49			49		
50			50		

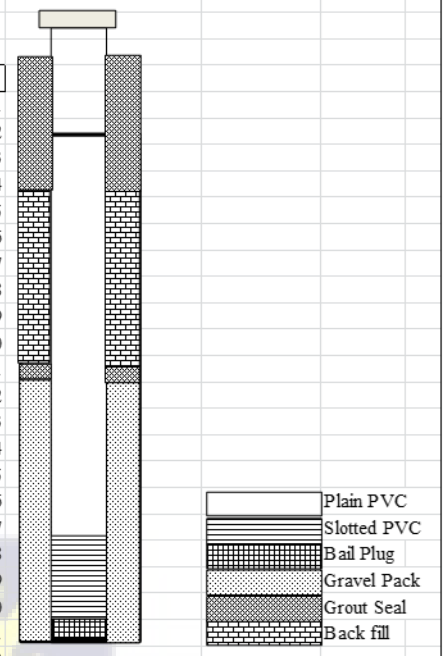

Appendix 20: Lithological Logs of the Boreholes Drilled Across the Lower Tano River Basin (Continuation)

	HEISA ENGINEERING COMPANY LIMITED				
	DRILLING LOG SHEET				
	North	**West**			
LOCATION GPS	4.91546	2.29158	**AIRLIFT YIELD**	300 l/min	
REGION	Western	**DISTRICT:** Ellembele	**COMMUNITY**	Asanda 1	
BH DEPTH	24m	**DATE STARTED:**19/07/14	**DATE COMPLETED**	19/7/2014	

DEPTH		**GEOLOGICAL FORMATION**	
1			1
2		Brownish coarse grained sand	2
3			3
4			4
5		Yellowish coarse grained sand + clay + conglomerates	5
6			6
7			7
8			8
9			9
10			10
11			11
12			12
13			13
14		Reddish clay	14
15			15
16			16
17			17
18			18
19			19
20		Dark greyish clay	20
21			21
22			22
23			23
24			24
25			25
26			26
27			27
28			28
29			29
30			30
31			31
32			32
33			33
34			34
35			35
36			36
37			37
38			38
39			39
40			40
41			41
42			42
43			43
44			44
45			45
46			46
47			47
48			48
49			49
50			50

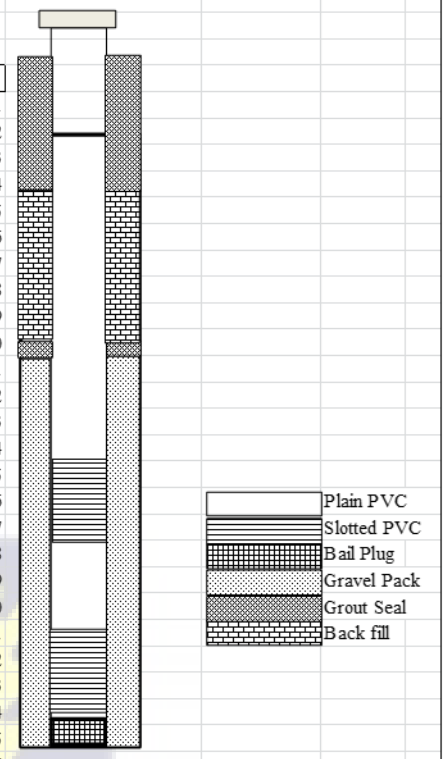

Appendix 20: Lithological Logs of the Boreholes Drilled Across the Lower Tano River Basin (Continuation)

	HEISA ENGINEERING COMPANY LIMITED				
	DRILLING LOG SHEET				
	North	**West**			
LOCATION GPS	4.91425	2.2863	**AIRLIFT YIELD**	300 l/min	
REGION	Western	**DISTRICT:** Ellembele	**COMMUNITY**	Asanda 2	
BH DEPTH	26m	**DATE STARTED:**23/07/14	**DATE COMPLETED**	23/7/2014	

DEPTH		**GEOLOGICAL FORMATION**	
1			1
2		Brownish coarse grained sand	2
3			3
4			4
5		Yellowish coarse grained sand + clay	5
6			6
7			7
8			8
9			9
10			10
11			11
12			12
13			13
14			14
15			15
16			16
17			17
18			18
19		Greyish coarse grained sand + Quartz	19
20			20
21			21
22			22
23			23
24		Dark greyish clay	24
25			25
26			26
27			27
28			28
29			29
30			30
31			31
32			32
33			33
34			34
35			35
36			36
37			37
38			38
39			39
40			40
41			41
42			42
43			43
44			44
45			45
46			46
47			47
48			48
49			49
50			50

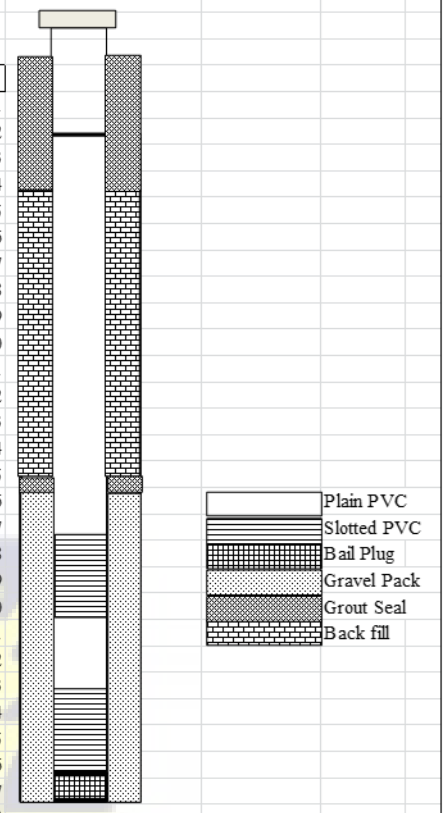

Appendix 20: Lithological Logs of the Boreholes Drilled Across the Lower Tano River Basin

	HEISA ENGINEERING COMPANY LIMITED				
	DRILLING LOG SHEET				
	North	**West**			
LOCATION GPS	4.97656	2.41541		**AIRLIFT YIELD**	90 l/min
REGION	Western	**DISTRICT:** Ellembele		**COMMUNITY**	Kangbunli
BH DEPTH	45m	**DATE STARTED:** 24/07/14		**DATE COMPLETED**	24/7/2014

DEPTH		**GEOLOGICAL FORMATION**	
1			1
2		Brownish clay	2
3			3
4			4
5		Reddish clay + sand	5
6			6
7			7
8			8
9		Brownish clay + sand	9
10			10
11			11
12			12
13			13
14			14
15		Greyish phyllites	15
16			16
17		Light greenish phyllites	17
18			18
19		Greyish phyllites	19
20			20
21			21
22			22
23			23
24		Dark greyish phyllites	24
25			25
26			26
27			27
28			28
29			29
30			30
31			31
32			32
33			33
34			34
35			35
36			36
37			37
38			38
39			39
40			40
41			41
42			42
43			43
44			44
45			45
46			46
47			47
48			48
49			49
50			50

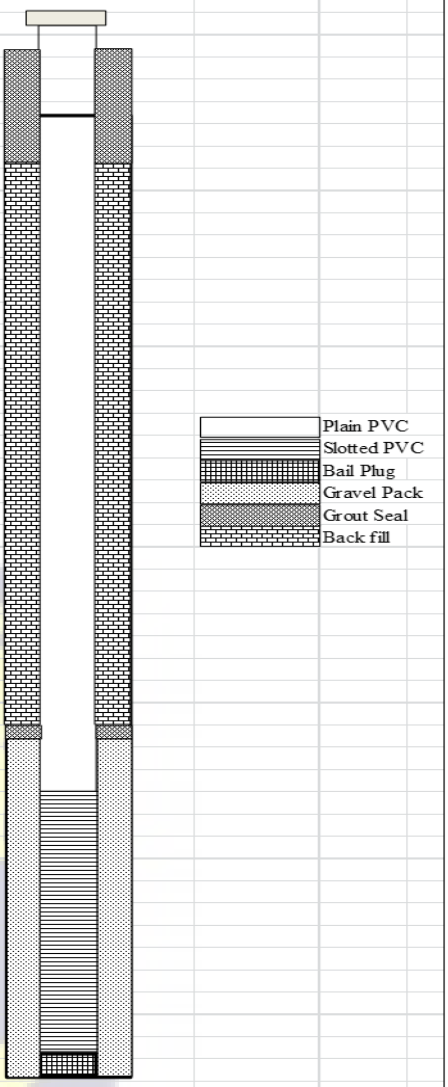

Appendix 21: **Fe^{2+}/SO_4^{2-} ratio data for the boreholes drilled in 2013 within the Lower Tano river Basin.**

Towns	latitude	longitude	Fe^{2+}	SO_4^{2+}	Fe^{2+}/SO_4^{2-}
Alumatoape	5.06432	-2.9435	0.00	4.97	0.00
Mpeasem	5.07096	-2.99782	0.39	6.09	0.06
Kamgbunli	4.97656	-2.41541	0.47	6.09	0.08
Elubo	5.28333	-2.76667	0.04	5.06	0.01
Bobrama	4.923303	-2.31477	0.01	6.31	0.00
Akanko	5.002748	-2.2372	0.30	11.00	0.03
Gwira ampansie	5.085727	-2.21155	0.32	4.19	0.08
Ndatiem	4.890833	-2.205	0.00	8.00	0.00
Ayisakro	4.89283	-2.21284	0.00	6.91	0.00
Kegyina	4.91667	-2.13333	0.00	4.11	0.00
Nyamebekyere	5.2	-2.4333	0.00	9.04	0.00
Akonu	4.83502	-2.20599	0.00	6.02	0.00
Ellanda Wharf	5.116	-2.733	0.21	10.00	0.02
Gwira Aiyinase	5.04476	-2.14201	0.01	7.00	0.00
Sanzule	4.96305	-2.4549	0.00	4.61	0.00
Nyamebekyere	5.21094	-2.43261	0.52	6.81	0.08
Samenye	5.08333	-2.55	0.00	10.00	0.00
Domiabra	5.15	-2.3	0.00	7.05	0.00
Sowudazem	5.05175	-2.88052	0.00	4.00	0.00
Alapoke	5.0127	-2.466	0.00	7.21	0.00
Aniwafutu	5.16213	-2.68665	0.22	7.00	0.03
Ankyernin	4.86833	-2.24139	0.02	0.01	2.00
Fawoman	5.347301	-2.71136	0.08	9.00	0.01
Dadwen	4.90286	-2.16061	0.37	10.00	0.04
Akpendue	5.01667	-2.45	0.00	7.01	0.00
Obengkrom			0.00	7.19	0.00
Cocoatown	5.31952	-2.73677	0.00	6.14	0.00
Kutukrom	5.298	-2.203	0.28	11.00	0.03
Ghana Nungua	5.35	-2.7667	0.00	6.01	0.00
Ankajeri	4.99812	-2.22773	0.00	5.13	0.00

Appendix 22: **Fe^{2+}/SO_4^{2-} ratio data for boreholes drilled from 2014 to 2015 within the Lower Tano river Basin.**

Sample Location	Latitude	Longitude	Fe^{2+}	SO_4^{2-}	Fe^{2+}/SO_4^{2-}
Newtown	5.08956	-3.09263	0.30	17.00	0.02
Effasu	5.08291	-3.04876	0.30	6.00	0.05
Mangyea	5.07755	-3.02855	5.00	BDL	
Mpeasem	5.07096	-2.99782	0.20	1.00	0.20
Alumatuape	5.06432	-2.9435	0.20	2.00	0.10
Jawey	5.06369	-2.93488	0.40	2.00	0.20
Annor Adjaye SHS	5.02144	-2.71708	0.00	6.00	0.00
Allengenzule	5.0098	-2.68806	0.00	4.00	0.00
Agyeza	5.01104	-2.69478	0.30	33.00	0.01
Ehoaka	5.02567	-2.68519	0.20	15.00	0.01
Ehoaka	5.02567	-2.68519	0.30	15.00	0.02
Twenen	5.0065	-2.67694	1.80	11.00	0.16
Kengen	5.00228	-2.64697	0.60	1.00	0.60
Elloyin	4.99467	-2.62214	0.20	8.00	0.03
Kangbunli	4.97656	-2.41541	0.20	9.00	0.02
Azuleleounu	4.94913	-2.3782	0.00	8.00	0.00
Asanda(1)	4.91546	-2.29158	0.10	10.00	0.01
Asanda (2)	4.91425	-2.2863	0.30	2.00	0.15

Appendix 23: Fe^{2+} /SO_4^{2-} ratio data for hand dug wells sampled in 2016 within the Lower Tano river Basin.

fCommunity	Latitude(˚N)	Longitude(˚W)	Fe^{2+}	SO_4^{2-}	Fe^{2+}/SO_4^{2-}	Community	Latitude(˚N)	Longitude(˚W)	Fe^{2+}	SO_4^{2-}	Fe^{2+}/SO_4^{2-}
Esiama	4.9344	-2.33813	0.33	39.62	0.01	Aniwa	4.9233	-2.32594	0.26	80.49	0.00
Nkroful	4.98655	-2.32747	8.74	149.51	0.06	Esiama	4.93219	-2.34206	0.12	28.44	0.00
Kikam	4.92662	-2.32500	0.86	59.23	0.01	Elubo	5.29211	-2.77604	0.57	147.21	0.00
Kikam	4.92529	-2.32464	0.52	72.85	0.01	Asanta	4.91073	-2.29116	0.47	58.74	0.01
Aniwa	4.93604	-2.35132	0.27	29.52	0.01	Ankobra	4.90062	-2.27150	0.50	42.26	0.01
Kikam	4.92585	-2.32154	0.19	47.17	0.00	Esiama	4.93607	-2.35018	0.67	75.30	0.01
Ampain	4.95799	-2.39705	0.01	10.45	0.00	Esiama	4.93521	-2.34561	0.53	53.25	0.01
Asanta	4.90925	-2.28399	0.16	21.48	0.01	Nkroful	4.98629	-2.32675	0.58	147.76	0.00
Nkroful	4.9545	-2.33259	0.14	21.87	0.01	Esiama	4.93604	-2.35132	1.01	148.16	0.01
Kikam	4.92629	-2.32084	0.11	40.30	0.00	Gyegyekrom	5.22398	-2.72766	2.71	15.28	0.18
Bomuakpole	4.99964	-2.33299	0.15	40.66	0.00	Elubo	5.28919	-2.77933	0.93	57.26	0.02
Kikam	4.92601	-2.32429	0.27	64.23	0.00	Azulenloanu	4.94966	-2.37797	0.33	21.97	0.01
Ankobra	4.90094	-2.27204	0.36	47.38	0.01	Half Assin(1)	5.05041	-2.88695	0.06	53.93	0.00
Asanta	4.91254	-2.29152	0.24	37.07	0.01	Bobrama	4.91499	-2.29979		7.00	0.00
gyegyEKROM	5.22464	-2.72497	0.14	20.40	0.01	Asanta	4.91105	-2.29195	0.06	87.38	0.00

Kikam	4.92884	-2.32364	0.18	22.56	0.01	Sanwoma	4.90392	-2.27359	0.31	6.23	0.05
Asanta	4.91587	-2.29252	0.12	62.46	0.00	Bobrama	4.91781	-2.29679	0.03	45.25	0.00
Esiama	4.94086	-2.34531	0.46	58.64	0.01	Ankobra (3)	4.90124	-2.2707	0.04	45.89	0.00

Appendix 24: Fe^{2+} /SO_4^{2-} ratio data for boreholes sampled in 2016 within the Lower Tano river Basin.

Community	Latitude(˚N)	Longitude(˚W)	Fe^{2+}	SO_4^{2-}	Fe^{2+}/SO_4^{2-}	Community	Latitude(˚N)	Longitude(˚W)	Fe^{2+}	SO_4^{2-}	Fe^{2+}/SO_4^{2-}
Salman(3)	5.00087	-2.22071	2.58	36.58	0.07	Telekobokaso	4.98707	-2.32713	0.17	66.28	0.00
Kamgbuli	4.98212	-2.41549	6.22	121.36	0.05	Aluku	4.99479	-2.26450	0.12	48.74	0.00
Kamgbuli	4.97767	-2.41583	3.78	25.24	0.15	Esiama	4.93708	-2.34753	0.04	1.58	0.03
Asemko	4.92277	-2.31524	0.14	46.28	0.00	Ankobra newsite	4.90565	-2.27132	1.46	40.70	0.04
Ampaim	4.95724	-2.40086	0.05	17.76	0.00	Sanwoma	4.90395	-2.27412	0.63	3.64	0.17
Aniwa	4.99158	-2.32870	1.17	30.30	0.04	Old Kablasuazo	5.027914	-2.773563	0.00	45.40	0.00
Nkroful	4.95619	-2.33067	0.04	18.20	0.00	Azulenloa	4.94894	-2.37827	9.85	1.48	6.66
Sanwoma	4.90604	-2.27475	0.08	9.50	0.01	Azuleno	4.94827	-2.38005	0.24	67.07	0.00
Aluku	4.99554	-2.26439	0.17	144.96	0.00	Fante new site	5.18559	-2.68215	3.93	38.64	0.10
Awiebo	5.03249	-2.44930	0.09	4.26	0.02	Elubo	5.29322	-2.77609	0.07	65.08	0.00
Esiama	4.93109	-2.34287	0.08	44.91	0.00	Bomuakpole(1)	4.99989	-2.33273	1.36	5.60	0.24
Ampain	4.95673	-2.40156	0.98	148.16	0.01	NyanZinli(1)	4.96455	-2.41607	0.17	10.01	0.02
Salman	5.00452	-2.22655	0.05	21.97	0.00	Atwibanso(1)	5.04212	-2.84168	1.79	11.54	0.15
Nkroful	4.97647	-2.32104	1.84	44.72	0.04	New Nzulezu(1)	5.09191	-2.57354	0.00	10.29	0.00
Bobrama	4.91557	-2.30108	0.07	42.17	0.00	NEW Ankasa	5.19929	-2.69873	0.00	39.32	0.00
Bomuakpole	5.00052	-2.33228	0.76	47.56	0.02	Bonyere	5.01905	-2.72693	0.04	25.70	0.00
Sanwoma	4.90566	-2.27330	0.91	0.23	4.02	Atwibaso(2)	5.04154	-2.84074	0.01	18.34	0.00
Alabokazo	4.9948	-2.43112	0.20	62.79	0.00	Awiafoto	5.16214	-2.68664	41.98	20.79	2.02

Aluku (1)	4.997	-2.26425	0.05	4.80	0.01	Aniwafuto(chips)	5.16436	-2.68576	0.06	27.95	0.00
Alabokazo	4.99548	-2.43462	0.04	6.15	0.01	New Nzulezu(2)	5.09097	-2.57487	0.32	16.50	0.02
Asanta(6)	4.91073	-2.29116	0.16	12.95	0.01	Tiekobo 1	5.05328	-2.69204	BDL	23.83	BDL
Salaman(1)	4.99815	-2.2779	47.42	25.01	1.90	Bobrama	4.91497	-2.29765	0.02	29.03	0.00

Appendix 25: Fe^{2+} /SO_4^{2-} ratio data for hand dug wells sampled in 2017 within the Lower Tano river Basin.

Community	Latitude(˚N)	Longitude(˚W)	Fe	SO	Fe/SO	Community	Latitude(˚N)	Longitude(˚W)	Fe	SO	Fe/SO
Nkroful (5)	4.94362	-2.34148		6.56	0.00	Asemda	4.98893	-2.53825	0.1472	46.60	0.00
Aluku 3	4.99472	-2.26495	0.02	29.34	0.00	Gyegyekrom(2)	5.22475	-2.72503	0.02149	18.96	0.00
Kikam 1	4.92572	-2.32163	0.11	1.80	0.06	Esiama 4	4.93525	-2.34557	0.3096	13.44	0.02
Nkroful (2)	4.96518	-2.32432	BDL	BDL	BDL	Ampaim (4)	4.94765	-2.37477	BDL	BDL	BDL
Esiama 8	4.93602	-2.35132	0.37	20.00	0.02	Eikwe	4.9641	-2.47050	0.2805	68.61	0.00
Elubo (5)	5.29075	-2.77642	0.06	8.16	0.01	Atuabo	4.98172	-2.55733	0.3033	48.52	0.01
Kikam 2	4.927	-2.32365	0.09	BDL	BDL	Benyin	4.98743	-2.58693	0.6054	49.67	0.01
Half Assin	5.05047	-2.88690	0.06	8.03	0.01	Esiama 7	4.93607	-2.35018	0.2236	92.56	0.00
Bomuakpole(1)	4.99963	-2.33297	BDL	13.28	BDL	Gyegyekrom(1)	5.22397	-2.72767	BDL	0.49	BDL
Nkroful(3)	4.96425	-2.32393	BDL	8.36	BDL	bobrama(2)	4.91482	-2.29978	BDL	12.95	BDL
Kikam (3)	4.9265	-2.32498	0.2073	46.23	0.00	Elubo(1)	5.28915	-2.77917	0.2869	46.96	0.01
Kikam (7)	4.92832	-2.32653	0.03468	1.74	0.02	Kikam	4.92885	-2.32460	0.06027	97.76	0.00
Elubo(5)	5.29387	-2.77643	BDL	8.16	BDL	Kikam (5)	4.92887	-2.32362	0.02421	27.87	0.00
Nkroful(1)	4.96638	-2.32527	0.2168	77.36	0.00	Azuleno(1)	4.9497	-2.37797	BDL	BDL	BDL
Aniwa(2)	4.98707	-2.32712	0.05197	36.07	0.00	Aniwa(1)	4.98655	-2.32747	BDL	36.56	BDL

Appendix 26: Fe^{2+} /SO_4^{2-} ratio data for Boreholes sampled in 2017 within the Lower Tano river Basin.

Community	Latitude(˚N)	Longitude(˚W)	Fe^{2+}	SO_4^{2-}	Fe^{2+}/SO_4^{2-}	Community	Latitude(˚N)	Longitude(˚W)	Fe^{2+}	SO_4^{2-}	Fe^{2+}/SO_4^{2-}
Sanzule(1)	4.96523	-2.45497	BDL	39.91		Aluku 2	4.99477	-2.26457	BDL	35.36	
Nyaniba	4.94373	-2.34152	0.15	65.08	0.00	Atwinbanso (2)	5.04155	-2.84072	BDL	10.49	
Ampaim(5)	4.95667	-2.40162	0.04	6.56	0.01	Asemko(1)	4.92278	-2.31527	0.28	0.00	
Atwinbanso(1)	5.0421	-2.84163	BDL	0.00		Salman 5	5.00088	-2.22070	0.04	18.16	0.00
Elubo (2)	5.29315	-2.77600	0.01	0.0	0.00	Azeneluno 3	4.94827	-2.38005	BDL	165.76	
Awiefoto	5.16213	-2.68665	BDL	0.00		Aluku 1	4.99697	-2.26427	0.03	7.76	0.00
Esiama (6)	4.93705	-2.34757	0.14	142.16	0.00	Alabokazo 2	4.99483	-2.43112	0.02	3.44	0.01
Old Kablazuaso	5.02812	-2.77367	0.01	0.33	0.03	Kamgbunli 2	4.98212	-2.41548	BDL	18.56	
Fante New Town(2)	5.18602	-2.68060	0.01	16.16	0.00	Ankasa 2	5.19878	-2.69985	0.07	8.36	0.01
half Assin SHS	5.05462	-2.87702	BDL	27.05		Telekobokaso(2)	4.97647	-2.32103	BDL	30.33	
Salman 2	4.99812	-2.22773	BDL	0.00		Alabokazo 1	4.99548	-2.43460	BDL	0.00	
Salman 1	4.99588	-2.22602	0.05	1.97	0.02	Awiafotu junction	5.17885	-2.67742	0.01	12.62	0.00
Esiama (1)	4.93485	-2.33815	0.10	12.62	0.01	Azulenenuo 2	4.94893	-2.37828	0.00	2.62	0.00
Azuleno (2)	4.94857	-2.38005	0.04	165.76	0.00	Salman 3	4.9983	-2.22575	0.10	0.00	103.90
Bomuakpolley	4.99158	-2.32867	BDL	0.00		Sanzule(2)	4.96305	-2.45490	0.10	46.56	0.00
Salman(3)	5.00152	-2.22655	BDL	10.16		Ngelekazo(kerrela hotel)	4.99107	-2.60290	0.09	53.61	0.00
Nkroful(4)	4.95625	-2.33073	BDL	0.00		Eikwe(2)	4.96878	-2.47097	0.10	68.61	0.00
Esiama(5)	4.93623	-2.34815	0.01	14.96	0.00	Ngelekazo(2)	4.99123	-2.60715	0.20	30.00	0.01
Ankobra newsite	4.90605	-2.27475	BDL	6.89		sanzule (3)	4.96128	-2.45525	0.06	52.46	0.00
Ampin	4.9583	-2.39888	0.04	0.00	0.00	Krisan(1)	4.96312	-2.46242	0.12	74.84	0.00
Nkroful (6)	4.944	-2.34132	BDL	25.36		ngelekpolley(2)	4.96728	-2.48238	0.11	67.30	0.00
New Nzulazu	5.09192	-2.57355	BDL	0.00		Baku	4.97165	-2.50010	0.14	71.23	0.00
Tiekobo (1)	5.05327	-2.69207	BDL	2.46		Keegan(1)	4.99907	-2.63940	0.21	70.25	0.00
Bobrama(4)	4.91557	-2.30108	0.07	4.75	0.01	Asemda	4.98817	-2.54078	0.19	77.95	0.00
New Nzulazu(2)	5.09097	-2.57483	BDL	7.36		Twenen(2)	5.0081	-2.67930	0.11	70.50	0.00
Bonyere	5.01908	-2.72690	0.17	4.92	0.03	Ngelekyi	4.96935	-2.49282	0.14	67.30	0.00
Kamgbunli	4.97768	-2.41582	0.00	42.46	0.00						

Appendix 27 Statistical summary of Chemical indices for the boreholes (Sampled years: 2013 and 2014 to 2015)

		2013			2014-2015			
Parameters	*WQI*	*MH%*	WQI	SAR	Na%	RSC (meq/L)	MH%	PI%
Number of samples	30	30	18	18	18	18	18	18
Mean	7.15	35.96	130.04	1.17	41.15	-0.42	27.60	82.82
Standard Error	3.22	1.57	19.46	0.26	4.63	0.05	3.48	4.28
Median	0.10	39.46	93.99	0.94	43.41	-0.38	26.94	85.02
Mode	N/A	18.46	N/A	N/A	N/A	N/A	N/A	N/A
Standard Deviation	17.66	8.61	82.57	1.12	19.63	0.23	14.77	18.15
Sample Variance	311.86	74.21	6817.76	1.25	385.20	0.05	218.04	329.34
Kurtosis	6.54	-0.55	-0.60	9.98	-0.47	-0.22	-1.25	-0.77
Skewness	2.70	-0.70	0.74	2.85	-0.48	-0.43	-0.03	-0.58
Range	67.87	28.98	262.89	5.03	67.10	0.85	43.74	56.27
Minimum	0.00	18.46	26.64	0.11	4.47	-0.90	5.77	49.26
Maximum	67.87	47.45	289.52	5.14	71.57	-0.05	49.51	105.53
Sum	214.45	1078.88	2340.80	21.00	740.71	-7.57	496.82	1490.69
Confidence Level (95.0%)	6.59	3.22	41.06	0.56	9.76	0.11	7.34	9.02

Appendix 28 Statistical summary of Chemical indices for the hand dug wells (Sampled years: 2016 and 2017)

		2016							2017			
Parameters	*WQI*	*SAR*	*Na%*	*RSC (mg/L)*	*MH%*	*PI%*	WQI	SAR	Na%	RSC (mg/L)	MH%	PI%
Number of samples	36	36	36	36	36	36	30	30	30	30	30	30
Mean	1376.58	2.86	62.19	-0.66	27.28	87.75	59.48	1.97	55.33	-0.11	33.98	93.64
Standard Error	706.37	0.45	2.65	0.16	3.18	3.67	8.22	0.20	2.30	0.18	3.08	4.93
Median	43.76	2.21	63.16	-0.51	24.16	85.73	41.06	1.72	58.09	0.03	32.21	90.71
Mode	N/A	N/A	N/A	N/A	N/A	N/A	N/A	1.33	46.97	N/A	25.52	N/A
Standard Deviation	4238.24	2.72	15.88	0.95	19.07	22.02	45.04	1.08	12.60	1.01	16.88	26.99
Sample Variance	17962637.16	7.41	252.32	0.90	363.85	485.07	2028.31	1.17	158.68	1.02	285.02	728.20
Kurtosis	16.50	12.76	-0.17	2.32	-0.41	0.35	-0.10	1.10	-0.39	0.69	1.00	5.92
Skewness	4.04	3.33	0.10	-0.91	0.65	0.70	1.01	1.12	-0.43	-0.41	0.81	1.78
Range	21310.22	14.61	66.56	4.84	69.93	90.00	162.88	4.48	51.55	4.49	78.48	144.87
Minimum	-0.01	0.51	29.82	-3.51	2.48	47.55	-0.04	0.65	29.27	-2.57	2.95	49.98
Maximum	21310.21	15.12	96.38	1.33	72.41	137.56	162.84	5.12	80.82	1.92	81.44	194.85
Sum	49556.79	103.07	2238.80	-23.73	982.13	3158.94	1784.51	58.96	1659.96	-3.25	1019.32	2809.23
Confidence Level (95.0%)	1434.01	0.92	5.37	0.32	6.45	7.45	16.82	0.40	4.70	0.38	6.30	10.08

Appendix 29 Statistical summary of Chemical indices for the Boreholes (Sampled years: 2016 and 2017)

		2016							2017			
Parameters	*WQI*	*SAR*	*Na%*	*RSC (mg/L)*	*MH%*	*PI%*	WQI	SAR	Na%	RSC (mg/L)	MH%	PI%
Number of samples	44	44	44	44	44	44	54	54	54	54	54	54
Mean	681.07	1.94	55.57	-0.36	38.10	91.93	12266.82	1.69	53.91	-0.17	56.10	103.40
Standard Error	210.33	0.22	3.11	0.11	3.40	4.48	3956.58	0.15	2.64	0.08	2.98	4.72
Median	36.32	1.58	54.21	-0.33	39.37	91.69	71.54	1.34	55.19	-0.11	57.09	97.69
Mode	N/A	N/A	N/A	N/A	N/A	N/A	N/A	N/A	N/A	N/A	N/A	N/A
Standard Deviation	1395.14	1.44	20.60	0.73	22.52	29.73	29074.81	1.10	19.19	0.59	21.73	34.36
Sample Variance	1946426.11	2.07	424.23	0.53	507.20	883.72	845344447.23	1.21	368.19	0.35	472.16	1180.45
Kurtosis	5.65	1.81	-0.83	-0.38	-0.44	-0.65	18.95	0.60	-0.83	0.96	-0.28	2.13

Skewness	2.48	1.47	-0.17	0.06	0.26	0.27	4.07	1.13	-0.25	-0.62	-0.46	1.19
Range	5684.42	5.79	75.36	3.24	85.66	118.00	172996.74	4.73	72.94	2.92	89.40	176.06
Minimum	-0.01	0.28	15.26	-1.93	4.37	39.92	6.44	0.29	16.21	-1.88	2.75	47.68
Maximum	5684.41	6.07	90.63	1.30	90.03	157.92	173003.17	5.02	89.15	1.05	92.15	223.74
Sum	29966.94	85.18	2445.23	-16.01	1676.49	4045.09	662408.30	89.45	2857.08	-9.09	2973.10	5480.20
Confidence Level (95.0%)	424.16	0.44	6.26	0.22	6.85	9.04	7935.89	0.30	5.29	0.16	5.99	9.47

Appendix 30 Calculated chloro-alkaline indices (Schoeller, 1965) for the boreholes drilled from 2014 to 2015

Sample Id	Location	Na^+	Cl^-	K^+	Cl^-	HCO_3^-	SO_4^{2-}	NO_3^-	Na +K	Na + K/Cl	CA1 - 1	Na + K/SO	CAI- 2
NB1	Newtown	6.79	6.32	0.35	6.32	2.65	0.35	0	7.14	1.13	5.19	20.16	-11.19
NB2	Effasu	0.58	0.56	0.07	0.56	0.62	0.12	0	0.65	1.15	-0.60	5.16	-3.98
NB3	Mangyea	0.60	0.74	0.03	0.74	0.51	0.00	0	0.63	0.85	-0.11	0.00	1.25
NB4	Mpeasem	0.49	0.99	0.04	0.99	1.23	0.02	0	0.53	0.54	0.45	25.45	-23.23
NB5	Alumatuape	0.32	0.28	0.02	0.28	0.33	0.04	0	0.34	1.20	-0.92	8.12	-7.51
NB6	Jawey	0.24	0.24	0.07	0.24	0.82	0.04	0	0.31	1.31	-1.07	7.45	-6.39
NB7	Annor Adjaye SHS	0.52	0.50	0.04	0.50	0.59	0.12	0	0.57	1.14	-0.64	4.53	-3.44
NB8	Allengenzule	0.71	0.71	0.01	0.71	0.25	0.08	0	0.72	1.01	-0.29	8.63	-7.67
NB9	Agyeza	0.99	0.85	0.15	0.85	0.43	0.69	0	1.15	1.35	-0.51	1.67	-0.39
NB10	Ehoaka	0.13	0.16	0.02	0.16	2.65	0.31	0	0.15	0.99	-0.83	0.49	2.32
NB11	Ehoaka	0.13	0.16	0.02	0.16	2.59	0.31	0	0.16	1.02	-0.86	0.51	2.24
NB12	Twenen	0.75	1.02	0.04	1.02	0.31	0.23	0	0.80	0.78	0.23	3.48	-2.15
NB13	Kengen	0.43	0.64	0.01	0.64	0.10	0.02	0	0.44	0.69	-0.05	21.30	-20.56
NB14	Elloyin	0.82	0.88	0.03	0.88	0.08	0.17	0	0.85	0.96	-0.08	5.11	-4.14
NB15	Kangbunli	0.94	0.72	0.07	0.72	2.80	0.19	0	1.01	1.41	-0.69	5.40	-1.87
NB16	Azuleleounu	0.63	0.65	0.05	0.65	0.59	0.17	0	0.68	1.06	-0.41	4.09	-2.86

NB17	Asanda	0.85	0.76	0.23	0.76	0.54	0.21	0	1.08	1.41	-0.65	5.19	-3.88
NB18	Asanda	0.33	0.30	0.01	0.30	0.49	0.04	0	0.34	1.13	-0.82	8.17	-7.37

All values are in meq/L and NB =New drilled borehole

Appendix 31 Calculated chloro-alkaline indices (Schoeller, 1965) for the hand dug wells sampled in 2016.

Sample number	Community	Na^+	Cl^-	K^+	HCO_3^-	SO_4^{2-}	NO_3^-	$Na^+ + K^+$	$Na^+ + K^+ / Cl^-$	CAI-1	$Na^+ + K^+ / SO_4^{2-}$	CAI - 2
HDW1	Esiama	1.43	0.90	0.01	1.00	0.82	0.01	1.44	1.60	-1.43	1.75	0.16
HDW2	Nkroful	5.44	2.20	1.46	0.60	3.11	0.02	6.90	3.14	-2.91	2.22	0.61
HDW3	Kikam	3.12	2.65	0.70	0.80	1.23	0.17	3.83	1.44	-0.26	3.11	0.51
HDW4	Kikam	3.76	2.88	1.06	0.80	1.52	0.03	4.82	1.68	-1.00	3.18	0.53
HDW5	Aniwa	1.02	0.56	0.27	0.20	0.61	0.02	1.28	2.28	-1.26	2.09	-1.30
HDW6	Kikam	1.14	0.85	0.17	0.20	0.98	0.09	1.31	1.54	-1.21	1.33	-0.19
HDW7	Ampain	0.23	0.51	0.02	0.08	0.22	0.01	0.24	0.48	0.26	1.11	-0.52
HDW8	Asanta	1.87	0.62	0.16	1.97	0.45	0.02	2.03	3.26	-1.80	4.53	-1.92
HDW9	Nkroful	0.78	0.45	0.15	0.40	0.46	0.02	0.93	2.07	-0.54	2.05	-1.18
HDW10	Kikam	1.78	1.18	0.19	0.84	0.84	0.02	1.97	1.66	-1.50	2.35	-0.30
HDW11	Bomuakpole	1.33	0.62	0.02	0.08	0.85	0.02	1.35	2.18	-1.84	1.60	-0.88
HDW12	Kikam	1.94	1.47	0.58	0.40	1.34	0.04	2.52	1.72	-0.76	1.88	0.02
HDW13	Ankobra	4.25	4.85	0.20	0.32	0.99	0.03	4.45	0.92	-0.47	4.51	0.69
HDW14	Asanta	0.85	0.79	0.06	0.36	0.77	0.02	0.90	1.14	-0.58	1.17	0.00
HDW15	Gyegyekrom	0.31	0.17	0.01	0.48	0.42	0.02	0.32	1.89	-1.10	0.75	-0.08
HDW16	Kikam	1.38	2.09	0.27	0.16	0.47	0.01	1.65	0.79	0.11	3.51	-1.26
HDW17	Asanta	0.92	1.13	0.04	0.20	1.30	0.02	0.96	0.85	0.67	0.74	0.60
HDW18	Esiama	2.96	1.86	0.55	0.20	1.22	0.04	3.51	1.89	-1.49	2.88	-0.77
HDW19	Aniwa	1.26	0.23	0.20	0.20	1.68	0.00	1.46	6.46	-6.12	0.87	-0.44
HDW20	Esiama	0.85	0.45	0.04	0.12	0.59	0.02	0.89	1.97	-0.95	1.50	-0.91
HDW21	Elubo	3.57	2.37	2.09	0.24	3.07	0.18	5.66	2.39	-1.66	1.85	0.94

HDW22	Asanta	2.98	1.64	0.73	1.20	1.22	0.03	3.71	2.27	-2.15	3.03	-0.17
HDW23	Ankobra	2.78	1.75	0.06	0.92	0.88	0.01	2.84	1.62	-0.61	3.22	-0.54
HDW24	Esiama	4.88	3.27	0.88	2.80	1.57	0.16	5.77	1.76	-0.35	3.68	2.55
HDW25	Esiama	0.93	0.62	0.13	1.00	1.11	0.02	1.06	1.71	-1.25	0.95	0.69
HDW26	Nkroful	1.47	0.51	0.25	0.24	3.08	0.01	1.72	3.39	-1.42	0.56	0.20
HDW27	Esiama	2.32	1.64	0.62	0.68	3.08	0.02	2.94	1.80	-1.29	0.95	1.38
HDW28	Gyegyekrom	0.66	0.39	0.01	0.12	0.32	0.01	0.67	1.68	-1.01	2.09	-1.57
HDW29	Elubo	0.99	0.62	0.27	0.76	1.19	0.01	1.27	2.04	-1.42	1.06	0.33
HDW30	Azulenloanu	0.99	0.56	0.06	0.28	0.46	0.01	1.05	1.85	-0.73	2.29	-1.44
HDW31	Half Assin	1.25	0.68	0.22	0.48	1.12	0.01	1.47	2.17	-1.94	1.31	-0.15
HDW32	Bobrama	0.95	0.56	0.02	0.40	0.15	0.02	0.96	1.71	-0.53	6.62	-5.63
HDW33	Asanta	2.09	1.07	0.52	1.00	1.82	0.01	2.61	2.44	-2.04	1.44	0.64
HDW34	Sanwoma	0.98	0.56	0.05	0.82	0.13	0.01	1.03	1.82	-1.14	7.92	-6.53
HDW35	Bobrama	2.78	1.13	0.02	1.47	0.94	0.04	2.80	2.48	-2.20	2.97	-0.33
HDW36	Ankobra (3)	4.20	4.68	0.37	1.04	0.96	0.08	4.56	0.97	-0.81	4.78	1.02

All values are in meq/L and HDW = Hand dug well

Appendix 32 Calculated chloro-alkaline indices (Schoeller, 1965) for the Boreholes sampled in 2016.

Sample Id	Sample Location	Ca^{2+}	Mg^{2+}	Na^{+}	K^{+}	Cl^{-}	HCO_3^{-}	SO_4^{2-}	NO_3^{-}	$Na^{+} + K^{+}$	$Na^{+} + K^{+}/Cl^{-}$	CA-1	$Na^{+} + K^{+}/SO_4^{2-}$	CA-2
BH 1	Salman	1.53	0.16	1.68	0.08	0.17	3.00	0.76	0.01	1.76	10.42	-10.25	2.32	0.86
BH 2	Kamgbuli	1.44	0.12	0.94	0.04	0.23	0.40	2.53	0.03	0.97	4.30	-4.08	0.38	0.27
BH 3	Kamgbuli	1.08	0.61	0.30	0.01	1.18	0.60	0.53	0.00	0.31	0.26	0.92	0.59	1.20
BH 4	Asemko	0.34	0.30	1.63	0.40	0.68	0.80	0.96	0.02	2.02	2.99	-2.31	2.10	-0.61
BH 5	Ampaim	0.31	0.54	1.22	0.21	1.02	0.44	0.37	0.01	1.43	1.41	-0.39	3.87	-2.41
BH 6	Aniwa	0.08	0.26	1.22	0.02	0.34	0.24	0.63	0.03	1.24	3.67	-3.33	1.97	-1.36
BH 7	Nkroful	0.21	0.17	1.98	0.05	0.73	1.20	0.38	0.02	2.03	2.77	-2.04	5.37	-3.42
BH 8	Sanwoma	0.56	0.04	1.47	0.04	1.47	0.44	0.20	0.03	1.51	1.03	0.44	7.63	-5.70
BH 9	Aluku	0.56	0.20	3.75	0.25	1.52	0.12	3.02	0.01	4.01	2.63	-1.11	1.33	0.32
BH 10	Awiebo	0.21	0.31	0.59	0.04	0.17	1.00	0.09	0.01	0.63	3.72	-3.55	7.09	-5.91

BH 11	Esiama	0.47	0.21	0.69	0.05	0.34	0.24	0.94	0.02	0.74	2.18	-1.84	0.79	-0.19
BH 12	Ampain	1.20	0.48	2.81	0.40	0.96	0.28	3.08	0.01	3.21	3.34	-2.39	1.04	0.21
BH 13	Salman	0.28	0.21	0.34	0.01	0.45	0.04	0.46	0.03	0.35	0.77	-0.32	0.76	-0.24
BH 14	Nkroful	1.63	0.33	1.52	0.03	0.56	1.24	0.93	0.03	1.55	2.76	-2.19	1.67	0.16
BH 15	Bobrama	0.11	1.03	1.29	0.04	0.79	0.44	0.88	0.04	1.33	1.68	-0.89	1.51	-0.24
BH 16	Bomuakpole	0.64	0.38	0.81	0.02	0.90	0.20	0.99	0.01	0.82	0.91	-0.01	0.83	0.28
BH 17	Sanwoma	0.41	0.52	0.62	0.03	1.52	0.48	0.00	0.00	0.66	0.43	1.09	139.91	-137.91
BH 18	Alabokazo	0.78	0.55	0.23	0.01	0.39	0.28	1.31	0.01	0.24	0.60	-0.21	0.18	0.50
BH 19	Aluku	0.25	0.10	1.01	0.03	0.34	0.98	0.10	0.00	1.04	3.07	-2.73	10.40	-9.07
BH 20	Alabokazo	0.16	0.53	0.86	0.08	1.02	0.44	0.13	0.02	0.94	0.93	0.09	7.34	-5.86
BH 21	Asanta(6)	0.78	0.25	1.31	0.22	0.73	1.20	0.27	0.03	1.53	2.09	-1.35	5.68	-3.72
BH 23	Salaman	0.18	0.14	0.31	0.01	0.11	0.08	0.52	0.02	0.32	2.84	-2.73	0.62	-0.40
BH 24	Telekobokaso	0.85	0.39	1.27	0.02	1.02	0.04	1.38	0.01	1.29	1.27	-0.26	0.94	0.13
BH 25	Aluku	0.49	0.21	1.79	0.26	1.41	0.12	1.01	0.02	2.05	1.45	-0.04	2.02	-0.47
BH 26	Esiama	0.12	0.13	0.65	0.04	0.45	0.60	0.03	0.01	0.69	1.53	-1.08	20.99	-19.93
BH 27	Ankobra newsite	2.90	0.20	1.49	0.10	1.97	1.52	0.85	0.00	1.58	0.80	1.17	1.87	1.63
BH 28	Sanwoma	1.87	0.10	1.24	0.08	0.51	2.95	0.08	0.02	1.32	2.59	-2.09	17.38	-13.91
BH 29	Old Kablasuazo	0.08	0.08	1.49	0.01	0.68	0.20	0.95	0.01	1.50	2.22	-1.54	1.59	-0.70
BH 30	Azulenloa	0.48	0.09	0.81	0.02	0.62	0.40	0.03	0.01	0.83	1.33	-0.71	26.79	-25.77
BH 31	Azuleno	0.78	1.35	1.29	0.07	1.13	0.20	1.40	0.01	1.36	1.21	-0.08	0.97	0.36
BH 32	Fante new site	0.70	0.79	0.37	0.08	0.23	0.36	0.80	0.02	0.45	1.98	-1.76	0.56	0.05
BH 33	Elubo	0.47	0.45	2.11	0.20	1.18	0.12	1.36	0.01	2.31	1.95	-0.77	1.71	-0.40
BH 34	Bomuakpole	0.79	0.73	1.17	0.02	0.39	1.97	0.12	0.02	1.19	3.02	-2.62	10.23	-7.85
BH 35	NyanZinli	0.68	0.03	1.10	0.44	0.68	0.80	0.21	0.00	1.53	2.26	-1.59	7.35	-5.87
BH 36	Atwibanso	0.09	0.11	0.52	0.01	0.28	0.16	0.24	0.02	0.53	1.86	-1.58	2.19	-1.73
BH 37	New Nzulezu	0.18	0.07	0.16	0.01	0.17	0.08	0.21	0.01	0.17	1.03	-0.86	0.81	-0.56
BH 38	NEW Ankasa	1.24	0.06	0.40	0.02	0.28	0.28	0.82	0.01	0.42	1.51	-1.22	0.52	0.05
BH 39	Bonyere	0.18	0.17	2.49	0.17	1.41	0.84	0.54	0.04	2.66	1.89	-0.48	4.97	-2.68
BH 40	Atwibaso	0.03	0.14	1.25	0.02	0.56	0.20	0.38	0.01	1.27	2.25	-1.69	3.32	-2.55
BH 41	Awiafoto	0.94	0.67	0.35	0.09	0.56	0.68	0.43	0.04	0.44	0.77	-0.21	1.01	0.28
BH 42	Aniwafuto(chips)	0.15	0.17	0.70	0.14	0.17	0.60	0.58	0.03	0.84	4.95	-4.79	1.44	-0.65
BH 43	New Nzulezu	1.11	0.54	0.63	0.06	2.37	0.08	0.34	0.07	0.69	0.29	2.08	2.00	0.53
BH 44	Tiekobo 1	0.31	0.01	0.80	0.09	0.11	0.28	0.50	0.01	0.90	7.97	-7.86	1.81	-1.41
BH 45	Bobrama	0.93	0.23	1.05	0.01	1.13	0.12	0.60	0.01	1.06	0.94	0.19	1.75	-0.50

All values are in meq/L and BH = Boreholes

Appendix 33 Calculated chloro-alkaline indices (Schoeller, 1965) for the hand dug wells sampled in 2017.

Sample Id	Community	Ca^{2+}	Mg^{2+}	Na^{+}	K^{+}	Cl^{-}	HCO_3^{-}	SO_4^{2-}	NO_3^{-}	$Na^{+}+K^{+}$	$Na^{+} + K^{+}/Cl^{-}$	CAI-1	$Na^{+} + K^{+}/SO_4^{2-}$	CAI-2
HDW1	Nkroful (5)	0.31	0.11	0.80	0.03	0.68	0.24	0.14	0.01	0.82	1.22	-0.54	8.93	-8.00
HDW2	Aluku 3	0.53	0.49	1.96	0.19	1.64	0.28	0.61	0.01	2.15	1.32	0.32	2.15	-0.23
HDW3	Kikam 1	1.30	0.49	1.61	0.19	0.56	3.00	0.04	0.01	1.80	3.20	-2.64	85.21	-81.64
HDW4	Nkroful (2)	0.24	0.06	0.53	0.02	0.51	0.20	0.00	0.01	0.55	1.08	-0.57	0.00	0.72
HDW5	Esiama 8	3.60	1.05	1.76	0.53	3.38	2.08	0.42	0.00	2.30	0.68	2.70	1.63	3.84
HDW6	Elubo (5)	0.46	0.57	3.69	0.68	3.78	0.20	0.17	0.05	4.37	1.16	2.62	6.81	-2.78
HDW7	Kikam 2	1.06	0.48	1.61	0.47	1.30	1.80	0.00	0.01	2.08	1.60	-0.31	0.00	3.11
HDW8	Half Assin	0.79	0.13	0.47	0.09	0.73	0.30	0.17	0.01	0.56	0.77	-0.03	4.57	-3.54
HDW9	Bomuakpole(1)	1.12	0.38	1.16	0.18	1.52	1.20	0.28	0.02	1.33	0.88	0.65	3.17	-0.43
HDW10	Nkroful(3)	0.56	0.33	1.15	0.15	0.45	1.00	0.17	0.03	1.30	2.89	-2.44	16.61	-15.12
HDW11	Kikam (3)	2.30	0.58	3.14	0.82	2.14	4.80	0.96	0.02	3.96	1.85	0.30	1.92	5.04
HDW12	Kikam (7)	0.66	0.36	1.03	0.30	2.26	0.28	0.04	0.02	1.32	0.59	1.67	16.25	-13.69
HDW13	Elubo(5)	1.76	0.05	3.18	0.21	3.78	0.04	0.17	0.05	3.39	0.90	2.88	5.28	-1.41
HDW14	Nkroful(1)	2.47	1.24	4.79	1.02	1.58	3.80	1.61	0.02	5.81	3.68	-2.10	2.28	3.11
HDW15	Aniwa(2)	1.12	0.38	1.16	0.18	0.73	2.00	0.75	0.01	1.33	1.82	-1.09	2.42	0.32
HDW16	Asemda	0.24	1.07	0.80	0.13	0.11	1.47	0.97	0.02	0.92	8.17	-8.06	8.43	-6.82
HDW17	Gyegyekrom(2)	0.52	0.12	0.37	0.02	0.17	0.32	0.39	0.02	0.39	2.29	-2.12	5.80	-5.29
HDW18	esiama 4	3.25	0.83	1.48	0.21	0.90	5.79	0.28	0.01	1.69	1.87	-0.97	6.68	0.02
HDW19	Ampaim (4)	0.18	0.10	0.36	0.04	0.56	0.24	0.00	0.01	0.40	0.71	-0.15	0.00	0.81
HDW20	Eikwe	1.22	0.66	3.78	0.28	1.52	2.89	1.43	0.04	4.06	2.67	-1.15	1.87	2.58
HDW21	Atuabo	1.05	0.79	2.12	0.12	0.11	2.00	1.01	0.02	2.24	19.84	-19.73	19.64	-17.51
HDW22	Benyin	2.98	1.16	3.50	0.28	2.99	1.96	1.03	0.00	3.78	1.26	1.73	1.22	3.73
HDW23	Esiama 7	2.47	0.78	4.47	0.87	0.73	4.00	1.93	0.02	5.34	7.29	-6.55	3.78	0.97
HDW24	Gyegyekrom(1)	0.07	0.13	0.26	0.02	0.11	0.40	0.01	0.00	0.28	2.46	-2.34	239.92	-239.40
HDW25	bobrama(2)	0.41	0.56	1.58	0.51	1.30	0.80	0.27	0.01	2.08	1.61	-0.31	5.96	-3.85
HDW26	Elubo(1)	2.06	0.24	0.83	0.36	0.68	1.00	0.98	0.06	1.19	1.75	-1.08	1.79	-0.06
HDW27	Kikam	0.85	0.51	1.25	0.18	0.79	0.60	2.04	0.02	1.43	1.81	-1.02	0.89	0.52
HDW28	Kikam (5)	0.48	0.37	1.77	0.21	1.41	1.60	0.58	0.01	1.97	1.40	0.01	2.41	0.61
HDW29	Azuleno(1)	0.35	0.39	1.07	0.08	0.56	0.98	0.00	0.01	1.15	2.03	-1.47	0.00	1.56
HDW30	Aniwa(1)	0.39	0.27	1.03	0.23	0.39	1.00	0.76	0.01	1.25	3.18	-2.78	4.17	-2.77

All values are in meq/L and HDW = hand dug well

Appendix 34 Calculated chloro-alkaline indices (Schoeller, 1965) for the Boreholes sampled in 2017.

Sample Id	Location	Ca^{2+}	Mg^{2+}	Na^{+}	K^{+}	Cl^{-}	HCO_3^{-}	SO_4^{2-}	NO_3^{-}	$Na^{+} + K^{+}$	$Na^{+} + K^{+} /Cl^{-}$	CAI - 1	$Na^{+} + K^{+} / SO_4^{2-}$	CAI-2
BH1	Sanzule	0.08	0.08	0.82	0.06	0.23	0.16	0.83	0.01	0.87	3.87	-3.65	4.66	-4.27
BH2	Nyaniba	0.42	0.36	2.01	0.04	1.07	0.32	1.36	0.005	2.05	1.91	-0.84	1.41	-0.01
BH3	Ampaim	0.15	0.65	0.92	0.07	0.85	0.52	0.14	0.00	0.99	1.17	-0.33	8.60	-7.23
BH4	Atwinbanso	0.06	0.17	0.64	0.04	0.56	0.40	0.00	0.004	0.68	1.20	-0.63	0.00	0.97
BH5	Elubo	0.32	0.59	1.96	0.19	1.58	0.80	0.000	0.02	2.15	1.36	0.22	0.00	2.40
BH6	Awiefoto	0.14	0.14	0.42	0.13	0.17	0.80	0.00	0.03	0.55	3.23	-3.06	0.00	0.99
BH7	Esiama	1.59	0.78	3.73	0.94	2.54	1.40	2.96	0.03	4.66	1.84	0.70	0.62	3.35
BH8	Old Kablazuaso	0.05	0.14	0.48	0.01	0.56	0.24	0.01	0.01	0.49	0.87	-0.31	127.95	-127.14
BH9	Fante New Town	0.57	0.16	0.85	0.15	0.23	0.96	0.34	0.02	1.01	4.46	-4.23	13.25	-12.05
BH10	Half Assin SHS	0.16	0.04	1.60	0.07	0.90	0.20	0.56	0.00	1.66	1.84	-0.94	3.27	-2.17
BH11	Salman	0.15	0.22	0.33	0.00	0.17	0.66	0.00	0.00	0.33	1.97	-1.80	0.00	0.82
BH12	Salman	0.68	0.77	0.73	0.01	0.17	1.80	0.04	0.00	0.74	4.38	-4.21	106.85	-104.88
BH13	Esiama	1.35	0.40	2.39	0.07	1.30	2.80	0.26	0.02	2.46	1.90	-0.60	7.22	-3.11
BH14	Azuleno	1.00	1.90	1.50	0.08	0.39	1.40	3.45	0.01	1.59	4.02	-3.63	1.17	0.64
BH15	Bomuakpolley	0.11	0.41	0.58	0.02	0.34	1.15	0.00	0.00	0.60	1.77	-1.43	0.00	1.49
BH16	Salman	0.24	0.28	0.35	0.01	0.11	0.44	0.21	0.02	0.36	3.19	-3.08	15.09	-14.52
BH17	Nkroful	0.18	0.22	0.63	0.03	0.56	0.44	0.00	0.01	0.66	1.17	-0.61	0.00	1.01
BH18	Esiama	0.10	0.92	0.60	0.05	0.45	0.44	0.31	0.05	0.65	1.45	-1.00	4.65	-3.71
BH19	Ankobra newsite	0.32	0.78	0.78	0.03	0.34	1.00	0.14	0.01	0.81	2.39	-2.05	16.68	-15.33
BH20	Ampin	0.27	0.33	0.52	0.04	0.11	1.20	0.00	0.01	0.56	4.99	-4.87	0.00	1.32
BH21	Nkroful	0.92	0.39	1.22	0.03	0.68	0.72	0.53	0.03	1.25	1.85	-1.17	3.50	-2.08
BH22	New Nzulazu	0.06	0.08	0.28	0.02	0.17	0.16	0.00	0.01	0.30	1.78	-1.61	0.00	0.34
BH23	Tiekobo	0.04	0.05	0.16	0.02	0.11	0.16	0.05	0.00	0.18	1.59	-1.48	31.02	-30.75
BH24	Bobrama	0.12	1.42	1.34	0.03	1.18	1.20	0.10	0.01	1.37	1.16	0.02	11.72	-9.33
BH25	New Nzulazu	0.88	0.68	0.70	0.07	0.06	2.20	0.15	0.01	0.77	13.69	-13.63	89.35	-87.09
BH26	Bonyere	0.18	0.25	1.15	0.16	0.51	1.00	0.10	0.00	1.31	2.58	-2.07	25.20	-23.69
BH27	Kamgbunli	1.91	2.97	1.13	0.05	0.90	3.00	0.88	0.00	1.18	1.31	-0.40	1.48	2.43
BH28	Aluku	0.32	0.29	1.97	0.28	1.64	0.16	0.74	0.02	2.25	1.38	0.26	1.87	-0.06
BH29	Atwinbanso	0.04	0.18	0.75	0.05	0.62	0.04	0.22	0.01	0.80	1.28	-0.66	5.87	-5.20
BH30	Asemko	0.20	0.44	0.72	0.02	0.23	0.98	0.00	0.01	0.74	3.28	-3.06	0.00	1.21
BH31	Salman	2.40	1.32	0.74	0.02	0.11	3.60	0.38	0.01	0.76	6.75	-6.64	17.86	-14.14
BH32	Azeneluno	1.00	1.98	1.50	0.08	0.39	1.40	3.45	0.01	1.59	4.02	-3.63	1.17	0.64
BH33	Aluku	0.28	0.15	0.52	0.01	0.34	0.20	0.16	0.02	0.53	1.58	-1.24	9.76	-9.20

BH34	Alabokazo	0.69	0.55	0.23	0.01	0.96	0.80	0.07	0.01	0.24	0.25	0.71	3.48	-1.72
BH35	Kamgbunli	0.48	0.70	0.36	0.02	0.34	0.56	0.39	0.01	0.38	1.13	-0.79	2.93	-2.03
BH36	Ankasa	0.32	0.37	0.51	0.03	0.96	0.40	0.17	0.02	0.54	0.56	0.40	3.23	-1.85
BH37	Telekobokaso	0.84	0.56	1.42	0.03	0.56	2.00	0.63	0.00	1.45	2.57	-2.01	4.08	-1.51
BH38	Alabokazo	0.19	0.70	0.96	0.09	0.62	1.80	0.00	0.02	1.05	1.69	-1.07	0.00	2.44
BH39	Awiafotu junction	0.40	0.93	0.44	0.02	0.51	0.56	0.26	0.00	0.46	0.90	-0.39	3.42	-2.35
BH40	Azulenenuo	0.75	0.88	1.00	0.04	0.62	1.80	0.05	0.02	1.04	1.68	-1.06	30.79	-28.35
BH41	Salman	0.32	0.54	1.49	0.04	0.85	0.98	0.00	0.07	1.53	1.81	-0.96	86861.05	-86859.16
BH42	Sanzule	0.14	0.54	2.14	0.06	0.85	0.44	0.97	0.01	2.21	2.61	-1.76	2.69	-1.39
BH43	Ngelekazo(kerrela hotel)	1.01	0.19	0.64	0.02	0.11	0.32	1.12	0.02	0.66	5.87	-5.76	5.26	-4.81
BH44	Eikwe	0.27	1.78	0.56	0.11	0.23	1.08	1.43	0.02	0.67	2.97	-2.74	2.08	-0.75
BH45	Ngelekazo	0.53	0.07	0.66	0.08	0.34	0.32	0.62	0.00	0.74	2.20	-1.86	3.52	-2.86
BH46	sanzule	0.68	1.53	0.57	0.07	0.34	1.24	1.09	0.03	0.64	1.90	-1.56	1.74	-0.13
BH47	Krisan	0.12	0.30	1.97	0.17	0.68	0.40	1.56	0.00	2.14	3.16	-2.48	2.03	-0.95
BH48	Ngelekpolley	0.53	0.19	1.04	0.19	0.45	0.44	1.40	0.02	1.23	2.72	-2.27	1.94	-1.03
BH49	Baku	0.14	1.18	1.36	0.08	0.56	0.92	1.48	0.00	1.43	2.54	-1.98	1.71	-0.23
BH50	Keegan	0.41	0.76	2.46	0.25	0.34	1.20	1.46	0.03	2.71	8.02	-7.68	5.48	-3.92
BH51	Asemda	0.36	0.43	2.18	0.17	0.79	0.60	1.62	0.02	2.35	2.98	-2.19	1.84	-0.43
BH52	Twenen	0.05	0.43	1.50	0.03	0.62	0.40	1.47	0.02	1.54	2.48	-1.86	1.69	-0.65
BH53	Ngelekyi	0.58	0.02	0.74	0.08	0.34	0.04	1.40	0.00	0.81	2.41	-2.07	1.72	-1.33

All values are in meq/L and BH = Boreholes

Appendix 35: Saturation indices computed for the sampled groundwater in the aquifer of the Apollonian formation and the aBirimian supergroup using using Phreeqc for Windows.

Sample number	Albite	Aragonite	Ca-Montmorillonite	Calcite	Chalcedony	Dolomite	Gibbsite	Gypsum	Halite	K-feldspar	K-Mica	Kaolinite	Quartz	SiO	Sy = syg-Sy k
1	-10.8	-3.1	-8.5	-3.0	-2.3	-5.5	0.2	-4.4	-7.4	-8.8	-2.8	-2.5	-1.8	-3.1	2.7
2	-6.4	-4.0	-2.4	-3.9	-0.5	-7.8	0.1	-3.5	-8.4	-5.4	0.5	0.9	-0.1	-1.4	-0.8
3	-6.3	-0.7	-2.8	-0.6	-1.6	-1.8	1.3	-2.5	-7.9	-4.9	4.0	1.1	-1.1	-2.4	0.2
4	-7.7	-2.4	-3.1	-2.2	-1.7	-4.1	1.5	-3.0	-8.8	-6.4	2.2	1.3	-1.2	-2.5	0.2

5	-4.0	-2.3	0.0	-2.2	-0.5	-4.5	0.9	-2.5	-7.4	-2.0	5.3	2.5	-0.1	-1.3	-1.6
6	0.0	-2.3		-2.2		-4.3	0.1	-2.6	-7.7						0.1
7	-6.3	-3.2	-2.4	-3.0	-0.6	-6.0	0.3	-4.4	-8.1	-4.4	1.8	0.9	-0.2	-1.5	-0.7
8	0.0	-1.8		-1.7	-2.3	-3.4		-2.2	-6.7				-1.9	-3.1	0.0
9	0.0	-3.1		-2.9			0.7		-8.4						0.7
10	-4.0	-3.3	1.5	-3.1	0.0	-6.7	0.9	-2.9	-8.9	-2.7	4.8	3.5	0.4	-0.8	-2.6
11	0.0	-1.0		-0.9		-2.4	0.4	-4.2	-8.1						0.4
12	-0.5	-2.6	6.2	-2.4	0.3	-5.7	2.4	-2.1	-7.4	0.1	10.4	7.1	0.8	-0.5	-4.7
13	-4.4	-3.3	0.5	-3.1	-0.2	-6.0	0.8	-3.5	-7.9	-3.2	4.1	2.9	0.2	-1.1	-2.0
14	0.0	-3.6		-3.5		-7.0	0.8	-4.2	-9.0						0.8
15	-8.7	-0.7	-4.6	-0.5	-2.3	-1.1	1.6	-2.5	-8.7	-7.7	1.2	0.4	-1.8	-3.1	1.2
16	-11.0	-5.3	-7.9	-5.2	-1.7	-9.8	-0.3	-5.7	-8.2	-10.3	-5.2	-2.3	-1.3	-2.5	2.0
17	-7.8	-3.3	-1.8	-3.1	-2.3	-5.1	3.0	-3.7	-8.2	-6.3	5.4	3.2	-1.9	-3.1	-0.1
18	0.0	-5.8		-5.6		-10.6	-1.2		-8.1						-1.2
19	-11.2	-4.8	-6.4	-4.7	-2.2	-8.9	1.2	-5.3	-9.1	-9.8	-1.8	-0.4	-1.8	-3.1	1.6
20	-8.2	-4.6	-3.7	-4.5	-0.9	-8.8	0.3		-8.0	-6.8	-0.6	0.5	-0.5	-1.7	-0.2
21	-2.1	0.0	2.9	0.1	-0.3	-0.2	1.8	-3.6	-7.5	-0.4	8.8	4.6	0.1	-1.2	-2.8
22	0.0	-2.3		-2.2		-4.3	0.1	-2.6	-7.7						0.1
23	-9.1	-4.4	-6.1	-4.2	-1.1	-8.9	-0.6		-8.2	-8.0	-3.6	-1.7	-0.6	-1.9	1.1
24	0.0	-1.2		-1.1		-2.2	0.9	-2.4	-6.8						0.9
25	0.0	-4.6		-4.4		-8.5	-0.1		-7.1						-0.1
26	-9.8	-3.9	-7.9	-3.8	-1.5	-7.5	-0.7	-2.8	-7.1	-8.3	-4.1	-2.7	-1.1	-2.3	2.0
27	-5.4	-4.1	0.0	-3.9	-0.3	-7.1	0.9		-7.9	-3.9	3.5	2.9	0.1	-1.1	-2.0
28	0.0	-3.7		-3.6		-7.0	0.5		-7.3						0.5
29	-3.8	-2.7	0.1	-2.6	0.3	-4.7	-0.2	-3.2	.8.28	-2.5	2.8	1.8	0.7	-0.6	-2.0
30	-4.1	-1.0	-0.7	-0.9	-0.5	-2.4	0.4	-4.2	-8.1	-2.3	4.2	1.6	0.0	-1.3	-1.2
31	0.0	-3.7		-3.5	-0.3	-6.3			-8.3				0.1	-1.1	0.0
32	-12.1	-5.7	-9.0	-5.6	-1.8	-10.9	-0.6		-8.9	-10.7	-6.2	-3.0	-1.4	-2.6	2.5
33	-6.5	-5.0	-2.2	-4.8	-0.3	-11.0	0.1	-2.9	-6.6	-5.2	0.6	1.1	0.1	-1.2	-1.1

34	-4.1	-2.8	0.6	-2.7	-0.2	-5.6	0.8	-2.4	-7.7	-2.4	4.9	2.9	0.2	-1.1	-2.1
35	-6.9	-3.9	-4.2	-3.8	-0.5	-7.5	-0.7	-2.8	-7.1	-5.3	-1.1	-0.7	-0.1	-1.3	0.0
36	0.0	-2.7		-2.5	-1.0	-4.7		-3.0	-8.5				-0.6	-1.8	0.0
37	-9.4	-3.7	-6.3	-3.6	-1.8	-7.0	0.4		-7.3	-7.7	-1.3	-1.1	-1.4	-2.6	1.5
38	-13.4	-6.5	-12.5	-6.4	-1.7	-11.9	-2.2	-4.2	-7.9	-12.1	-10.8	-6.0	-1.3	-2.5	3.9
39	-2.9	-3.3	2.4	-3.1	0.3	-6.0	0.8	-3.5	-7.9	-1.6	5.7	3.9	0.7	-0.5	-3.1
40	-11.4	-3.8	-8.7	-3.6	-1.9	-6.7	-0.3		-8.9	-10.7	-5.7	-2.8	-1.5	-2.8	2.5
41	-1.4	0.0	2.1	0.2	-0.4	0.4	1.4	-2.7	-6.0	-0.1	8.3	3.8	0.1	-1.2	-2.4
42	-2.8	-2.1	4.6	-2.0	-0.7	-4.9	3.2	-3.3	-8.1	-1.2	10.8	6.7	-0.3	-1.5	-3.5
43	-4.0	-3.0	3.1	-2.9	-0.7	-6.1	2.7		-8.0	-2.8	8.1	5.7	-0.3	-1.5	-3.0
44	-2.9	-1.1	3.3	-1.0	-0.5	-2.7	2.2	-3.7	-7.9	-1.4	8.6	5.2	0.0	-1.3	-3.0
45	-3.2	-3.0	4.3	-2.9	-0.6	-6.0	3.0	-4.0	-8.7	-1.8	9.7	6.4	-0.2	-1.4	-3.5
46	-3.9	-1.9	3.2	-1.7	-0.8	-4.1	2.8	-3.7	-8.9	-1.9	9.3	5.6	-0.4	-1.7	-2.8
47	-4.4	-2.9	2.3	-2.7	-0.8	-5.8	2.4	-3.3	-8.2	-2.9	7.5	5.0	-0.3	-1.6	-2.6
48	-5.1	-3.9	0.8	-3.7	-0.7	-7.5	1.8	-3.8	-7.9	-4.6	4.5	3.8	-0.3	-1.6	-2.0
49	-3.3	-2.5	3.6	-2.4	-0.6	-5.1	2.7	-2.4	-7.7	-1.5	9.5	5.9	-0.2	-1.5	-3.2
50	-4.7	-0.5	1.5	-0.3	-0.8	-1.2	2.0	-2.4	-9.3	-2.9	6.7	4.0	-0.4	-1.7	-2.0
51	-4.7	-0.5	1.5	-0.3	-0.8	-1.7	2.0	-2.4	-9.3	-2.9	6.7	4.0	-0.4	-1.7	-2.0
52	-2.9	-4.0	5.3	-3.8	-0.4	-7.6	3.3	-3.4	-7.7	-1.5	10.7	7.4	0.0	-1.3	-4.1
53	-5.5	-4.7	1.2	-4.5	-0.7	-9.2	2.0	-4.5	-8.2	-4.4	5.2	4.3	-0.3	-1.5	-2.3
54	-6.4	-4.8	-0.7	-4.7	-1.0	-9.2	1.7	-3.8	-7.8	-5.2	3.7	3.0	-0.6	-1.9	-1.3
55	-0.9	-0.8	5.5	-0.7	0.1	-1.4	2.3	-2.8	-7.8	0.5	10.6	6.5	0.6	-0.7	-4.2
56	-3.3	-2.9	3.2	-2.8	-0.3	-5.6	2.1	-3.1	-8.0	-1.8	8.1	5.3	0.1	-1.2	-3.2
57	-3.5	-2.1	2.4	-2.0	-0.7	-4.3	2.3	-3.1	-7.8	-1.5	8.7	4.8	-0.3	-1.6	-2.5
58	-3.6	-2.7	3.8	-2.6	-0.6	-5.7	2.7	-3.8	-8.6	-2.8	8.2	6.0	-0.1	-1.4	-3.3

Appendix 36: Publication And Conferences

1. Edjah, A. & Banoeng-Yakubo, Bruce & Akiti, T. & Stenni, Barbara & Dreossi, Giuliano & Doku-Amponsah, Kwabena. (2019). Characterization of water chemistry in some communities of the Lower Tano river basin, Ghana, West Africa. Arabian Journal of Geosciences. 12. 10.1007/s12517-019-4305-4.

2. Characterization of Surface Water and Groundwater Quality in the Lower Tano River Basin Using Statistical and Isotopic Approach. AAEdjah, Adwoba & ABStenni, Barbara & ACCozzi, Giulio & ADTuretta, Clara & AEDreossi, Giuliano & AFTetteh Akiti, Thomas & AGYidana, Sandow. AA (Department of Earth Science, University of Ghana Legon, Ghana West- Africa), AB(Department of Enviromental Sciences, Informatics and Statistics, Ca Foscari University of Venice, Italy), AC(Department of Enviromental Sciences, Informatics and Statistics, Ca Foscari University of Venic e, Italy), AD(Department of Enviromental Sciences, Informatics and Statistics, Ca Foscari University of Venice Italy), AE(Institute for the Dynamics of Environmental Processes, CNR, Venice, Italy), AF(Department of Nuclear Application and Techniques, Graduate School of Nuclear and Allied Sciences University of Ghana Legon), AG (Department of Earth Science, University of Ghana Legon, West - Africa). EGU General Assembly Conference Abstract, 2017/04/1, 447 https://ui.adsabs.harvard.edu/abs/2017EGUGA..19..447E.

Appendix 37: Contribution to knowledge

This study being the first detailed groundwater research in the Lower Tano River Basin has:

1. Contributed to the current hydrogeological knowledge on the Lower Tano River basin. This knowledge will contribute to a successful future groundwater study.
2. Successfully determined isotopic rainfall regression lines with equations $\delta^2 H = 7.69 \delta^{18} O + 11.68$ for the dry period and $\delta^2 H = 8\delta^{18}O + 11.31$ for the wet period. These two lines together with the local meteoric water line (Akiti,1986) could be used as reference lines for future research on aquifer recharge in the basin.
3. Provided a base line information on ages of the groundwater and recharge sources which will support groundwater management.